University of Naples Federico II
Department of Structures
for Engineering and Architecture

Roberto Tartaglia

SEISMIC PRE-QUALIFICATION OF EXTENDED STIFFENED BEAM-TO-COLUMN JOINTS

Ph.D. Thesis
XXIX Cycle (2014-2017)

Tutor:
Prof. Eng. R. Landolfo

Co-tutor:
PhD Eng. M. D'Aniello

Coordinator:
Prof. Eng. L. Rosati

Doctorate of Philosophy in
Structural Engineering, Geotechnical and Seismic Risk

fai cio che devi, accadrà quel che può

Table of Contents

Chapter I – Introduction

1 Motivation…………………………………………………...1

2 Objectives…………………………………………………5

References……………………………………………………...10

Chapter II – State of the art

Introduction………………………………………………….11

1 Bolts Behavior…...………………….…………………….14

2 T-stub Behavior….………………………………………18

3 Joint Behavior……………………………………….....25

3.1. Design criteria and experimental results…………….27

3.2. Analytical method…………………………………….43

3.3. Finite element models………………………………...48

References………………………………………………….....56

List of figures……………………………………………….....66

List of tables……………………………………………………...68

Chapter III – Normative background EC and AISC

Introduction……………………………………………...............69

1 European design procedure: EN1993-1-8…………….…70

1.1. Joint characterization………………………………...71

1.1.1. Stiffness classification…………………………71

1.1.2. Resistance classification………………………..73

1.2. Joint behavior………………………………………...75

1.2.1. Definition of components and their behavior…..75

1.2.2. Joint strength evaluation……………………….86

1.2.3. Joint stiffness valuation………………………..97

1.2.4. Rotational capacity……………………………..99

1.2.5. Moment rotation curve………………………..101

1.3. Criticisms of Eurocodes……………………………..102

2 American design procedure: AISC 358-16…………….110

2.1. Prequalification limit………………………………..112

2.2. Beam limitations..……………………………..115

2.3. Column limitations..…………………………...116

2.4. Column-beam relationship limitations……………...117

2.5. Continuity Plates……………………………….117

2.6. Bolts…………………………………………118

2.7. Connection detailing…………………………...118

2.8. Design procedure for the End-plate and bolt diameter…………………………………..123

2.9. Design procedure on the column side………………134

References……………………………………………143

List of figures………………………………………145

List of tables…………………………………………146

Chapter IV – Experimental tests on T-stub

Introduction……………………………………………...147

1 Tensile behavior of pre-loaded bolts…….…………..148

2 Investigated T-stub…………………….……………150

3 Experimental results……………………………………158

4 Discussion of results……………………………………171

References…………………………………………………174

List of figure………………………………………………174

List of tables………………………………………………176

Chapter V – Seismic qualification of extended stiffened joint

Introduction………………………………………………177

1 Design procedure proposed……………………………178

  1.1. Capacity design approach……………………..…….178

  1.2. Ductility criteria……………………………….………184

  1.3. Design assumptions for ES connection……………..189

    1.3.1. Design strength and stiffness of rib…………...190

    1.3.2. Influence of rib stiffeners on the effective length of equivalent T-stub…….………………….192

    1.3.3. Centre of compression and level arm………..198

1.3.4. Influence of rib stiffeners on the beam web in compression capacity…………….…………...200

1.3.5. Influence of the rib on the joint stiffness……..201

1.4. Design assumptions for column web panel…………204

1.4.1. Design shear force…………….………………204

1.4.2. Design shear strength…………….…………...206

1.5. Design of welds…………………….…………….………207

2 FEM Calibration…………….………………….…………212

2.1. Modelling assumptions……………………………..212

2.2. Validation of modelling assumptions………………..…219

3 Validation of design criteria by finite element analyses.225

3.1. Investigated beam-to-column assemblies…………..225

3.2. Comparison between current Eurocode and proposed design approach…………………………………….……240

3.3. Influence of the design overstrenght………………......243

3.4. Influence of rib on strength and stiffness…………...247

3.5. Position of compression center……………………..253

3.6. Active bolt rows……………………………….………258

3.7. Cyclic response……………………………….………260

3.8. Analytical prediction………………………….….…267

References…………………………………………….……..271

List of figures………………………………………….….…276

List of tables……………………………………….……..279

Chapter VI – Experimental test on beam-to column joint

Introduction…………………………………………….……281

1 Introduction of the experimental results…………….……281

1.1. Test setup…………………………………….………..282

1.1.1. Setup and transducers at University of Naples.284

1.1.2. Setup and transducers at University of Liege...287

1.2. Loading protocol……………………………….……..290

2 Coupon tests……………………………………….………292

3 Experimental results: extended stiffened joints………..296

3.1. ES1-TS-F-C2………………………………………...298

3.1.1. Calibration…………………………………..306

3.1.2. Strain gauge…………………………………311

3.2. ES1-TS-F-M………………………………………315

3.2.1. Calibration…………………………………..318

3.2.2. Strain gauge…………………………………319

3.3. ES1-TS-E-C1……………………………………...323

3.3.1. Calibration…………………………………..330

3.3.2. Strain gauge…………………………………334

3.4. ES2-TS-F-CA……………………………………..337

3.4.1. Calibration…………………………………..341

3.4.2. Strain gauge…………………………………344

3.5. ES2-TS-F-C2……………………………………...348

3.5.1. Calibration…………………………………..353

3.6. ES2-TS-E-C1……………………………………...357

3.6.1. Calibration……..…………………….……………363

3.6.2. Strain gauge…….……………….……….………366

3.7. ES2-TS-Esp-C……..……………….…………….…368

3.7.1. Calibration……..……………………………….…..372

3.7.2. Strain gauge…….……………….……….………375

3.8. ES3-TS-F-C1……..……………..…………….…...377

3.8.1. Calibration……..………………………….……..382

3.9. ES3-TS-F-C2……..……………..…………….…...386

3.9.1. Calibration……..……………………………….390

3.10. ES3-TS-F-M……..……………..…………….……394

3.10.1. Calibration……..………………………….……..396

3.11. ES3-TS-E-C1……..……………..…………….…...398

3.11.1. Calibration……..………………………….……402

3.12. ES3-TS-E-C2……..……………..…………….…...407

3.12.1. Calibration……..………………………….……..411

3.13. ES3-TS-Esp-C……..……………..…………….……414

3.13.1. Calibration……..…………….……….……..418

4 Results comparison and discussion……………….…...421

4.1. Experimental results comparison……………….…..421

4.2. Experimental analysis vs analytical and numerical prediction……..………….………………………..424

References……………………………….…………….…426

List of figures……..……………….………….…………427

List of tables……………………………….…….………439

Chapter VII – Parametric study

Introduction……………………………..……………..……441

1 Investigated parameters……………………………..442

2 Influence of variability of material yield strength……...446

3 Bolt row in the central axis of the connection…………466

4 Influence of rib geometry……….……………………..477

4.1. Rib stiffener contribution……………………..……….477

4.2. Thickness of rib stiffener…….……………………….482

4.3. Slope of rib stiffener…..…………………………..….497

References……..……………………….…………………..508

List of figures…….…………………….…………….…….509

List of tables……….………………………………..……..514

Chapter VIII – EJ vs AISC 358 design and performance approach

Introduction…….……………………..…………………..…….515

1 Differences between the Equaljoints design procedure and AISC 358……………………………………..………………516

1.1. Codes differences…………………………………...516

1.2. Structural design differences………………………..516

1.3. Connection design differences………………………523

2 MRF structures design according to US codes……......528

2.1. Designed structures…………………………………528

2.2. American and European designed joints..…………..536

3 Designed joint according to AISC 358………………...543

3.1. American vs European steel profile…………………543

3.2. American vs European joints behavior……………...548

3.3. Influence of mill imperfections……………………..557

4 Influence of the column details: presence of continuity plates and supplementary web plates…………………..568

References……………………………………………573

List of figures…………………………………………575

List of tables…………………………………………….578

Chapter IX – Conclusions

References…………………………………………….590

Annex

Introduction…………………………………………...591

Annex I Example of calculation……………………..592

1.1 Theoretical approach………………………….…..592

1.2 Resistance definition………….…………..………592

1.3 Stiffness definition…………..…………..…………624

1.4 Example of one bolt row joint configuration………...628

1.5 Example of two bolt rows joint configuration……….648

Annex II Coupon tests results…………………………...678

Annex III Rib Investigation……………………………...683

Annex IV Material investigation…………………………738

Annex V EJ vs AISC 358: additional results ……………775

References……………………………………………………779

List of figures…………………………………………………780

List of tables………………………………………………...781

CHAPTER I

Introduction

1 Motivation

Nowadays in Europe, EN 1993-1-8 [1] provides models to compute the strength and the stiffness of connections but no reliable analytical tools are available to predict the rotation capacity and the cyclic performance in relation to the connection typology. Furthermore, only EN1998-1-1 [2] provides design rules for joints in seismic areas, without offering any proper defined design procedure and pre-qualification criteria.

On the contrary, the approaches used in other countries with high seismic hazard are based on codified and easy-to-use design tools and procedures. In particular, on the basis of the widespread damage observed after the Northridge and Kobe earthquakes, North American practice is directed at prequalifying standard joints for seismic resistance.

In 1995, the US FEMA and the SAC joint venture initiated a comprehensive 6-year program of investigation, called FEMA/SAC program, to develop and evaluate guidelines for the inspection, evaluation, repair, rehabilitation, and construction of steel moment – frame structures (Mahin [3]).

The US research effort was directed to develop a specific standard (ANSI/AISC 358 [4]) containing design, detailing, fabrication and quality criteria for a set of selected types of connections, which should be prequalified for use with special moment frames (SMF) and intermediate moment frames (IMF).

While the American approach was more focused into the investigation of different joint geometry and configurations, the Japanese research placed greater emphasis in the improving of the mechanical steel behavior and in the welds details [5].

Japanese columns are usually made of cold formed steel tubes, and the shop welded connections are placed at short distance away from the face of the column. The critical point (or hot spot) of the Japanese welded connection is located at the tip of the flanges rather than at the center of the flange as noted in US connections. These differences limit the applicability of Japanese research results. Nevertheless, Japanese research suggests that the weld access holes details are important areas requiring further research consideration.

Unfortunately, American and Japanese design practice have ranges of steel sections clearly different from European design practice. Thus, the benefits of non-European research programs concerning pre-qualified moment resisting (MR) joints are not directly applicable. In light of these considerations, the design approach based on prequalification would certainly be of interest for the European market of steel constructions, especially if a simple and reliable design tool is considered.

In light of these considerations, the EQUALJOINTS research project (RFSR-CT-2013-00021) [6] aims at developing seismic prequalification procedures for a set of steel joints that are typically used in Europe. The project is coordinated by University of Naples and the consortium is formed by both academic and industrial partners. In particular: (i) University of Naples FEDERICO II - Italy, (ii) Université de Liege – Belgium, (iii) Universitatea Politehnica din Timişoara–Romania, (iv) Imperial College of Science, Technology and Medicine - UK (v)

Universidade de Coimbra - Portugal, (vi) Arcelormittal Belval & Differdange SA- Luxembourg and (vii) the European Convention for Constructional Steelwork Vereniging – Belgium.

2 Objectives

EQUALJOINTS’ aim is to provide pre-qualification criteria of a set of selected seismic resistant steel beam-to-column joints. In order to achieve this purpose, a large experimental program supported by theoretical and numerical analyses has been proposed. Both full-strength and partial-strength joints are examined for three types of bolted configurations and one welded “dog-bone” joint.

In this framework, the present thesis was conducted focusing on the pre-qualification of extended stiffened joints (ES).To this aim a thorough study on the up-to-date-technical literature and a critical revision of both the European and American actual design code was carried out. Furthermore, a large analytical and experimental study on the T-sub was performed in order to investigate the influence of bolt’s behavior on the failure mode ductility. Then, starting from the actual version of EN1993-1-8, a new design approach was proposed and validated against both numerical analyses and extensive experimental campaign. All the tests were then calibrated by means of finite element (FE) software and a comprehensive parametric study was carried out in order to investigate the influence of additional parameters such as the rib’s slope and thickness. Finally, the proposed design assumptions for the European design criteria were compared with the American prequalification procedure by means of parametric FE analyses.

The work organization and a short description of the chapters is reported hereinafter.

Chapter II: State of the art

A summary of the most important research results in the field of the extended stiffened and un-stiffened joints is pointed out; starting from novel research on the bolt characteristics, discussing about the importance of the T-Stub influence on the joint behavior. Finally, the results of recent studies and tests on both extended bolted connection are presented.

Chapter III – Normative background

The EN1993-1-8 [1] and the AISC358-16 [4] design procedure are reported and discussed with particular attention to the extended bolted connection. The Eurocode component method was thoroughly discussed and an example of its application on the un-stiffened connection is reported. The American standards, with particular regard to its prequalification limits and the design procedure for both stiffened and un-stiffened connection were pointed out.

Chapter IV – T-Stub behavior

The T-stub behavior was investigated with particular attention to the influence of the bolt type. Indeed, a set of 18 T-Stubs were designed and tested at University of Naples in order to investigate the ductility and failure mechanism under both monotonic and cyclic actions. The main design variables are: (i) the plate's thickness, (ii) the effective length and (iii) the type of preloadable bolts.

Chapter V – Seismic qualification

Design assumptions and procedure are proposed, starting from the component method (Chapter III), focusing on the most important requirements for seismic loading. Moreover, additional rules were introduced to cover some lacks in the European design codes (i.e. the influence of the stiffeners).

Starting from a set of MRF structures designed according to EN1993-1-1 [2] three beam-to column joint assemblies were selected; each assembly was designed as a full, equal and partial strength joint.

All the features of the proposed assumptions were confirmed by means of a FEM parametric analysis performed on models calibrated based on literature results.

Chapter VI – Experimental tests

Starting from the observations made in Chapter V and the designed joints, the results of the experimental campaign carried out at both University of Naples and University of Liege are presented and discussed. Moreover, the results of the FE calibration for each test are presented.

Chapter VII – Parametric study

To extend the observations on the results coming from the experimental campaign, a comprehensive parametric analysis was carried out. The yielding strength of end-plate material, the influence of an additional bolt row in the symmetry axis, the rib thickness and slope are some of the parameters investigated.

Chapter VIII – EJ vs AISC358 design and performance approach

The introduced design criteria and their effectiveness were also compared with the American design procedure. A set of structures were designed in line with the one defined in Chapter V but using US profiles and three beam-to-column assemblies were extracted to investigate full strength ES joints.

Chapter IX - Conclusions

The effectiveness of the proposed design criteria under seismic actions, the experimental results observed, the reliability of the calibration procedure, the parametric analysis results and the comparison with the American procedure are underlined and discussed.

Annex

All the results described in the thesis are summarized in the Annex, where two complete examples of application of the design assumptions are reported as well.

References

[1] EN 1993:1-8, Design of steel structures - Part 1-8: Design of joints. CEN 2005.

[2] EN 1998-1, Design of structures for earthquake resistance - Part 1: General rules, seismic actions and rules for buildings. CEN 2005.

[3] Mahin, A., Malley, J., Hamburger, R., (2002). Overview of the FEMA/SAC program for reduction of earthquake hazards in steel moment frame structures. Journal of constructional steel research, 58:511-528.

[4] ANSI/AISC 358-16 (2016). Prequalified Connections for Special and Intermediate Steel Moment Frames for Seismic Applications.

[5] Nakashima, M., Roeder, C.W., Maruoka, Y. (2000). Steel moment frame for earthquake in United States and Japan. Journal of structural engineering 126:861-868.

[6] EQUALJOINTS – European pre-QUALified steel JOINTS: RFSR-CT-2013-00021. Research Fund for Coal and Steel (RFCS) research programme.

CHAPTER II

State of the art

Introduction

Bolted connections can guarantee a stiff and resistant behavior providing at the same time sufficient ductility.

Nowadays, extended stiffened (ES) end-plate bolted connections are popular in the European steel construction industry and widely used in practice as moment-resistant joints in low and medium rise steel frames. Indeed, this type of connections are characterized by a limited use of welds i.e. solely shop welds of the end-plate and stiffeners to the beam, and then the end-plate-beam assembly is field-bolted to the column flange, thus shortening the construction time.

Bolted joints configurations allow the conception of both nominally pinned and full rigid joints by changing only the constructional details. Indeed, the possibility to change the number, the diameter and the bolt position, just as the end-plate thickness, the continuity plate, the additional web panel and the diagonal stiffeners, allows the designers to play with both the joint stiffness and resistance.

Furthermore, the economical aspect ponders significantly if taken into account; making holes (either using banks of drills or an automatic machine) and fastening on-site is relatively quick and cheaper with respect to welding processes.

On the contrary, regardless of the welding procedure, welds are more burdensome. Indeed, manual metal arc welding is time-consuming and labor intensive, while the automatic welding processes become capital intensive. Moreover, the inspections should be taken into account, considering that weld inspections by ultrasonic, radiographic or dye penetrant testing contribute to the increase of the constructional costs.

Therefore, it can be agreed that bolted connections, respect to the welded ones, represent an economical and performant alternative for seismic applications.

Finally, end-plate bolted joints have been the subject of extensive research in the last decades and many aspects related with the bolt, T stub, joint behavior and the effect of the joint in the steel frames, have been analyzed and agreed upon.

The main aim of this chapter is to review the literature results with particular regards to the design rules, experimental and numerical campaigns carried out and analytical methodologies for the prediction of the joint response.

1 Bolts Behavior

The behavior of the bolts significantly influences the joint response in terms of strength, stiffness and ductility.

With particular attention to the European market, EN1993:1-8 [1] and EN1998-1-1 [2], do not distinguish between the types of high-strength pre-loadable bolt assemblies available (intended as the system made up of bolt head, shank and nut).

However, the type of bolt assembly and its associated failure mode may severely affect the joint behavior in post-yield domain.

European standards for design (e.g. EN 1993 [3]) and fabrication (e.g. EN 1090 [5]) of structural steelwork allow the use of two categories of high strength bolts for structural applications: non-pre-loadable (ordinary) and pre-loadable (High Strength Friction Grip) bolts. In most of the cases, the non-preloaded structural grade 8.8 bolts are used, since they are more economical than pre-loadable fasteners. To the savings with the initial cost further cost reduction is added by the fact that since this bolt category is not to be tightened and no plastic strain is introduced in the threaded shank during the assembling process, the re-use of the fasteners is allowed.

Conversely, pre-loadable bolts should not be re-used after removal due to the large plastic deformations the threaded zone undergoes during tightening. Therefore, codes (i.e. EN 14399-3 [6] and EN 14399-4 [7]) provide requirements to be used for pre-loadable bolts, mainly due to the different properties of the standardized products available in the European market. The two most used bolt types are the British/French system HR (acronym of “High Resistance”) and the German system HV (German acronym of “Hochfeste Bolzen mit Vorspannung”, which in English means “high resistance bolts for pretension”).

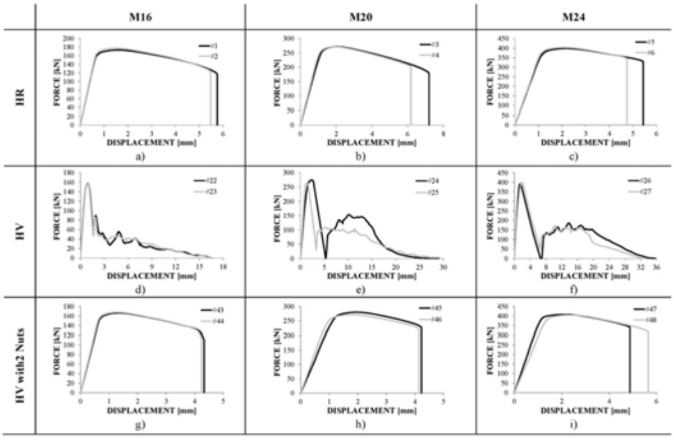

Figure 1-1 Force-displacement response curves for the monotonic tests. [8].

The main differences between these two classes were studied by D’Aniello et al [8] by means of a large experimental and numerical investigation. The Authors have investigated the most commonly used bolts for structural applications (HV and HR grade 10.9), performing both monotonic and cyclic tests.

The main outcome of this work is the recognition that these two bolt types have different failure modes. Indeed, results showed that HR type are characterized by shank necking failure, whereas nut stripping occurs for HV bolt assemblies (see Figure 1-1). Another interesting result was that by adding a second nut to an HV assembly the failure mode changes from nut stripping to shank necking. Moreover, for the calibration of the experimental results the Authors linearized the force-displacement curve in order to convert it in an equivalent true stress – true strain format, taking into account the different deformability contributions of the elements that constitute the bolt assembly. The true stress – true strain curves were normalized according to two different criteria to enable performing direct comparisons between bolt assemblies with different diameters. Both the inelastic deformation capacity and the existence of residual strength of bolt assemblies directly influences the capacity of equivalent T-Stub connections to develop mode 2 rather than mode 3 failure and the associated rotational capacity.

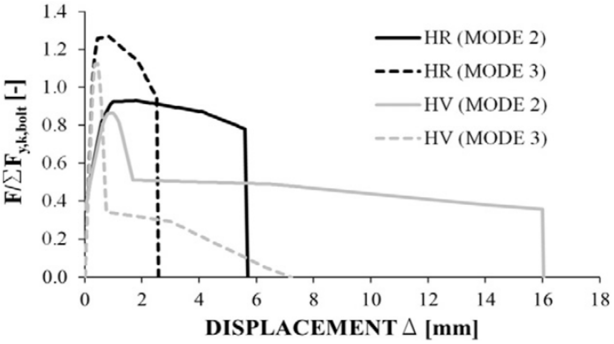

Figure 1-2 T-stub force-displacement response for the HR and HV type assemblies in modes 2 and 3 [8].

The influence of bolt assembly on bolted joints was discussed using a simple calculation example based on 2D analytical model of a T-stub (see Figure 1-2). The strength and analytical response curves of failure modes 2 and 3 were derived by taking into account the actual response curves of HR and HV bolt assemblies. This comparison showed that computing the T-stub failure mode based on nominal properties can be unsafe when HV assemblies are adopted. The design of bolted joints should take into account the bolt assembly type and the required rotation demand, in order to ensure that joint performance is consistent with specific requirements. With this regard, HV bolt assemblies can be suitable for joints that should behave as nominally pinned, whereas HR type assemblies are more appropriate for semi-rigid joints.

2 T-stub behaviour

The component method as it is implemented nowadays in design codes [1] relies heavily on the T-stub element. The starting point can be considered the analytical methodology proposed and experimentally verified by Zoetemeijer [9] in Netherlands in the 1970's. The goal was to characterize the behavior of the tensile region of a bolted connection under static loading conditions (see Figure 2-1).

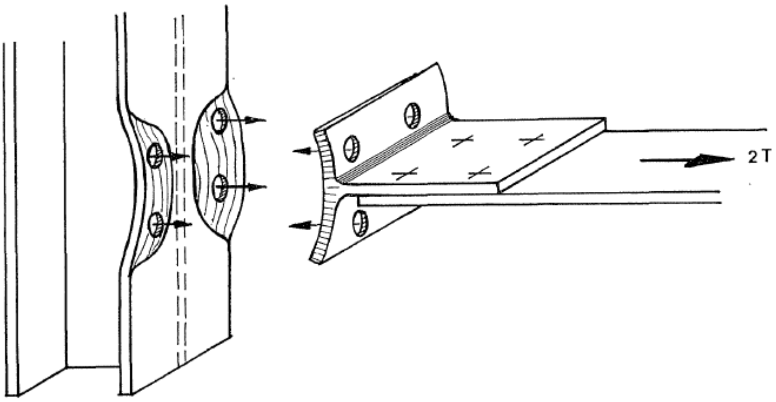

Figure 2-1: Bending of the column flange and T -stub flange at the tension side of a moment connection [9].

At that point, only two collapse mechanisms were considered (i.e. collapse governed by the bolts and by the flange, respectively) but the principle of using effective lengths to calculate the strength and stiffness of the bolted connections proved to give good results when compared with experimental results.

Ever since, significant effort of a number of research groups has culminated in the codification of the component method in the European code for the design of steel joints EN1993-1-8 [1].

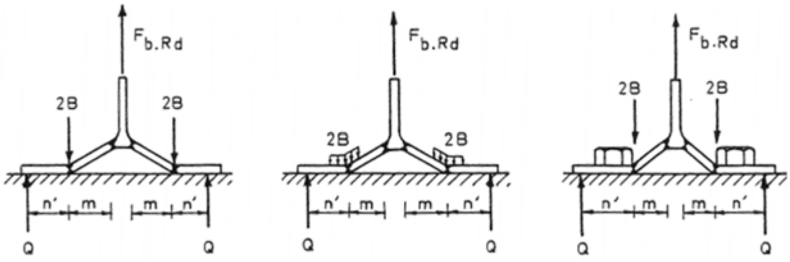

Figure 2-2 Taking into account the influence of the bolts on the plastic collapse of a T stub [10].

The turning point in this field was represented by the research carried out by Jaspart [10] as part of his doctoral work. The research includes aspects regarding both the joints themselves and their influence on the global behavior of the frames. Focusing on the work that concerned the joints, important developments related to the strength and stiffness of the column web panel and the deformability of the components were introduced. Different from previous work carried out by other researchers, the Author proposed simple purely theoretical formulas for the prediction of each connection component resistance and flexibility, eliminating thus the empirical aspects of foregoing methodologies (see Figure 2-2). These formulas allow the building of a bi-linear curve for each basic component and combined with the proposed column web panel characterization, a complete mechanical model (see Figure 2-3) that can closely predict the behavior of bolted joints was created.

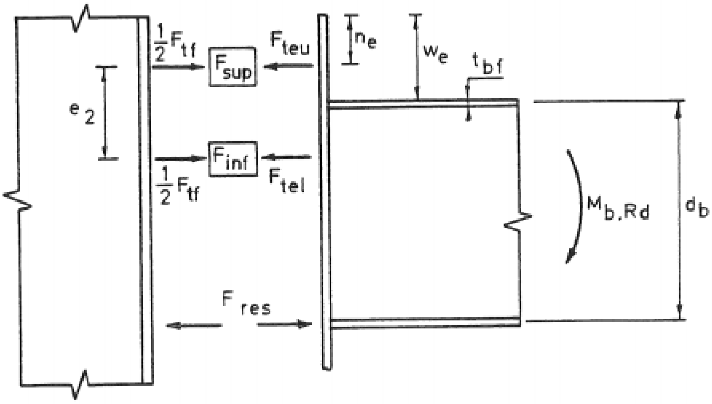

Figure 2-3 Forces in the bolt rows [10].

Piluso et al [11], [12] introduced the T-stub ductility concept and a theoretical model able to predict the deformation capacity of the T-stub. The Authors evaluated theoretically and demonstrated experimentally the importance of the failure mechanism for the inherent reserve of plastic deformation capacity. Furthermore, they demonstrated the strong correlation between ductility and plate thickness and distance between bolts and the T element web (see Figure 2-4).

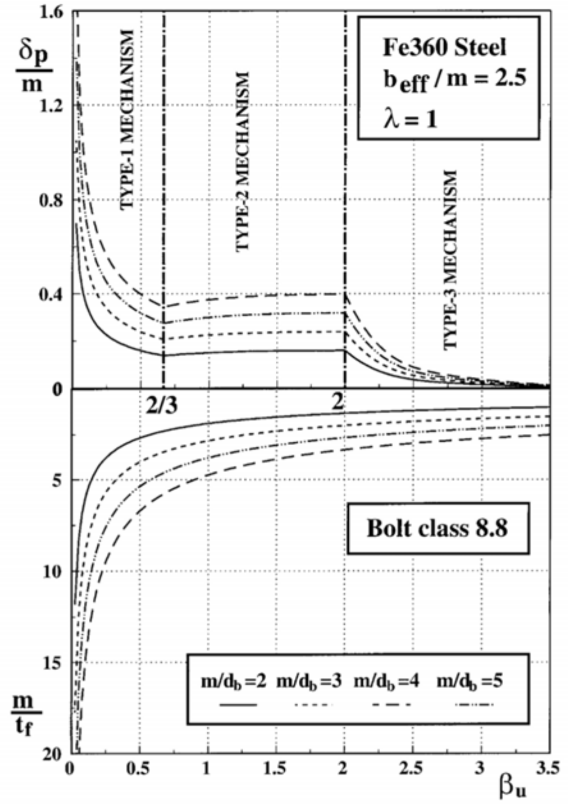

Figure 2-4: Plastic deformation capacity of single T element of bolted T-stubs [12].

This was one of the first steps made for the introduction of the concept of ductility as a major connection characteristic, along with strength and stiffness.

Experimental investigations carried out by Girao Coelho et al [13] on bolted end-plate connections confirm the previously mentioned dependency of the ductility with plate thickness, and studied other potential parameters influencing the deformation capacity (i.e. the end-plate steel grade) but also the joint strength and stiffness.

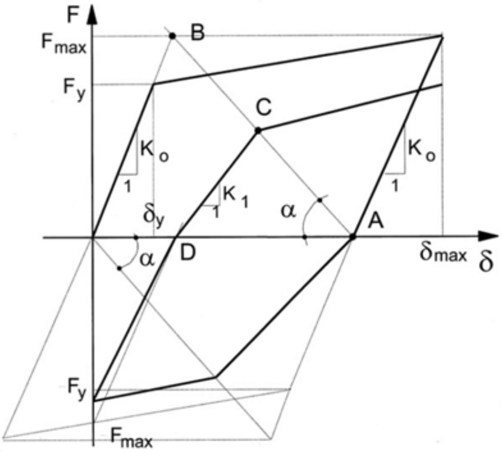

Figure 2-5: Cyclic model for type I mechanism [14].

The use of bolted end-plate joints in seismic areas required however a cyclic characterization of the T-stub behavior. To this aim, Piluso and Rizzano [14] and Latour et al. [15], [16] worked on the definition of a cyclic model (see Figure 2-5) able to characterize the T-stub and the joint behavior, respectively. The Authors of [14] validated the theoretical model on a set of T-stubs tested under monotonic and constant and variable amplitude cyclic loading, while in [15] and [16] the model was validated based on full scale joint tests.

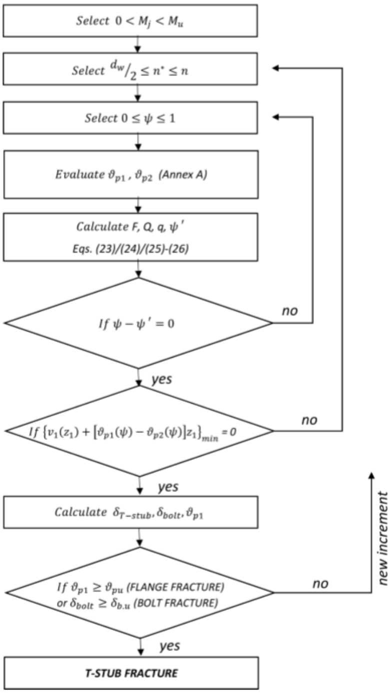

Figure 2-6 Flow chart for solving the system of equations [17].

In recent work, Francavilla et al. [17] showed advancements of the previously proposed analytical model and experimental results that validate the model presented (see Figure 2-6). The Authors argue that the component method as it is currently implemented in Eurocode 3 Part 1-8, lacks any specific rules for the prediction of the deformation capacity of joints.

As of now, there is no doubt on the crucial role the T-stub characteristics have on the overall bolted joint response, and it's therefore of paramount importance to properly understand and define this element before attempting to analyze the global joint behavior.

3 Joint behaviour

Bolted end-plate beam to column connections have been widely studied in the last fifty years. Design criteria have been developed by [18] that explained the behavior of end-plate connections by means of analogies with T-stubs. More recently, methods based on refined yield line analysis have been suggested, based on which the currently accepted design procedures of end-plate connections have been derived [23]. On the other hand, design methods based on finite element analysis have been also developed. In addition, considering the precision and accuracy of finite element analysis other studies that combine finite element methods and multivariable regression analysis of simulated data have been conducted.

ES joints can be designed to be both full or partial strength and either full or semi-rigid. The experimental and theoretical evidence showed that this type of joint can effectively behave as full strength. Conversely, a full rigid behavior could not be obtained in several cases. Therefore, ES bolted joints can be easily conceived as semi-rigid joints, which results in additional savings in the gravity load system [28]. Moreover, in moment resisting frames subjected to seismic loads the use of semi-rigid joints can lead to lighter structures thanks to lower design forces due to increase of fundamental periods related to the increase of lateral flexibility [29].

However, it can be argued that after Northridge and Kobe earthquakes semi-rigid connections have been considered as viable alternatives to welded connections for seismic resistant buildings, providing similar or superior seismic performance compared to full rigid connections [30]. Indeed, those seismic events showed that fully welded joints can be highly prone to premature brittle failure [30]. Having all the above in mind, a detailed overview of the research carried in the specific field of bolted beam to column extended end-plate joints is presented. The work has been subcategorized in function of the main tools used for the research work. Therefore, an initial section will present relevant experimental results and the design rules proposed by the researchers that carried out these investigations. The second section presents a short overview of the most relevant work of research groups that focused on providing engineers with simplified analytical methods but also updating and renewing the existing design procedures. Lastly, the third section is a summary of the FE investigations dealing with end-plate bolted joints available in the literature.

3.1 Design criteria and experimental results

Tsai and Popov [31] demonstrated already in the 1990s, how the extended stiffened joint is a viable alternative to the welded joint for moment resisting frames (MRF). The authors performed experimental and numerical investigations on joint configurations like presented in Figure 3-1.

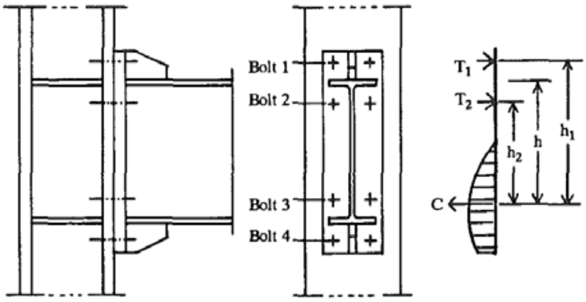

Figure 3-1 Bolt positioning and internal force distribution [31].

The results showed a very good behavior, with high capacity and stiffness and sufficient ductility of the joint, however the authors emphasized the need for further investigations on the cyclic behavior of this joint typology.

To this end, Korol et al [32] and Ghobarah et al. [33] performed at the beginning of 1990's two sets of tests with the aim to investigate the cyclic behavior of beam-to-column extended stiffened end plate joints. The overall behavior of the specimens has been examined and the behavior of their individual components (beam, column, connections, and panel zone) has been separately observed as well (see Figure 3-2). It was concluded that if properly designed and detailed, extended end-plate connections can be considered suitable for moment resisting frames also in high seismic intensity areas.

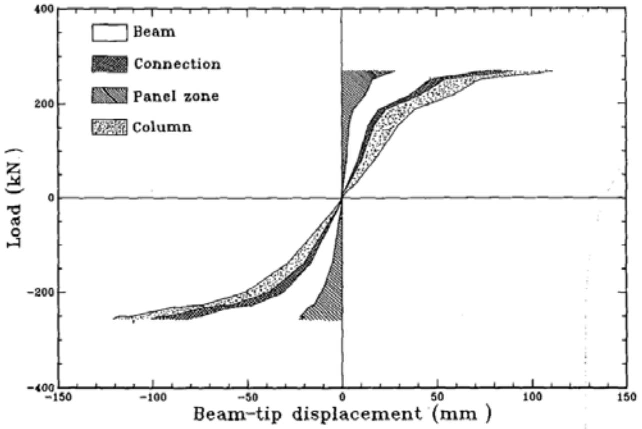

Figure 3-2 Contribution of Specimen Components to Beam-Tip Deflection (Specimen CC-3) [33].

More recently, in 2002, Sumner and Murray [34] published the first papers dealing with the prequalification of American steel connections within the framework of the SAC project.

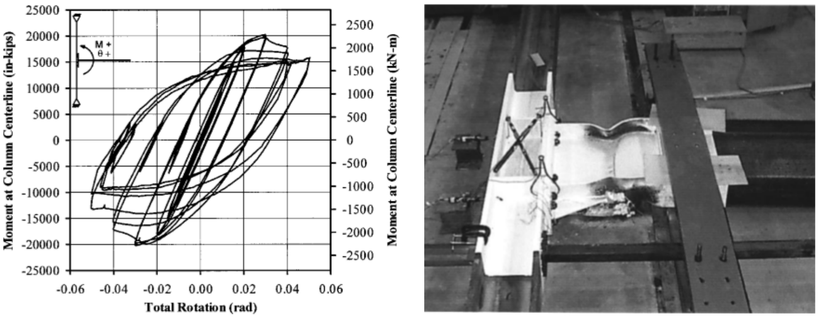

a) b)

Figure 3-3: Experimental results in terms of both moment rotation curve (a) and deformation (b) [34].

The results (see Figure 3-3) show that the end-plate connection can provide sufficient bending capacity to allow the concentration of all the plastic deformation in the beam. The Authors also highlighted the importance of the welds and their design. Their research is the base of the current joint pre-qualification procedure adopted in the American codes [36][1].

Moreover, some considerations regarding composite connections have been made. In particular, it was highlighted that these connections should be properly designed, given that the joint capacity increases considerably.

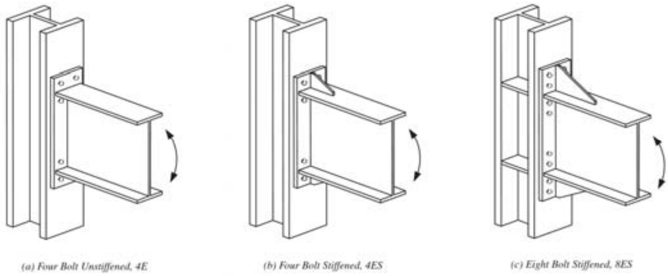

Figure 3-4 Extended end plate configurations [35].

Although the US prequalification venture has dedicated significant research to the stiffened extended end-plate joint, making it one of the main codified bolted solutions (see Figure 3-4) the European practice continued to focus on the unstiffened extended end-plate joint typology.

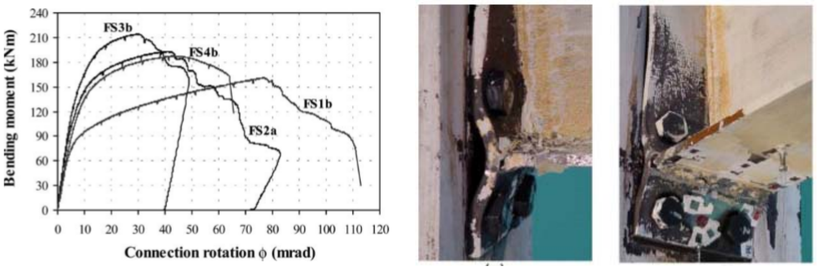

a) b)

*Figure 3-5: Experimental results in terms of Moment rotation curve (a) and deformation (b) [13].**Error! Reference source not found.***

A European experimental campaign for the assessment of the ductility of unstiffened end-plate connections has been performed by Girao Coelho et al. [13] in 2004 at the Delft University of

Technology. In order to investigate the behavior of this joint typology up to collapse, the specimens have been designed to induce the failure of the end-plate and/or bolts without development of the full beam plastic moment capacity.

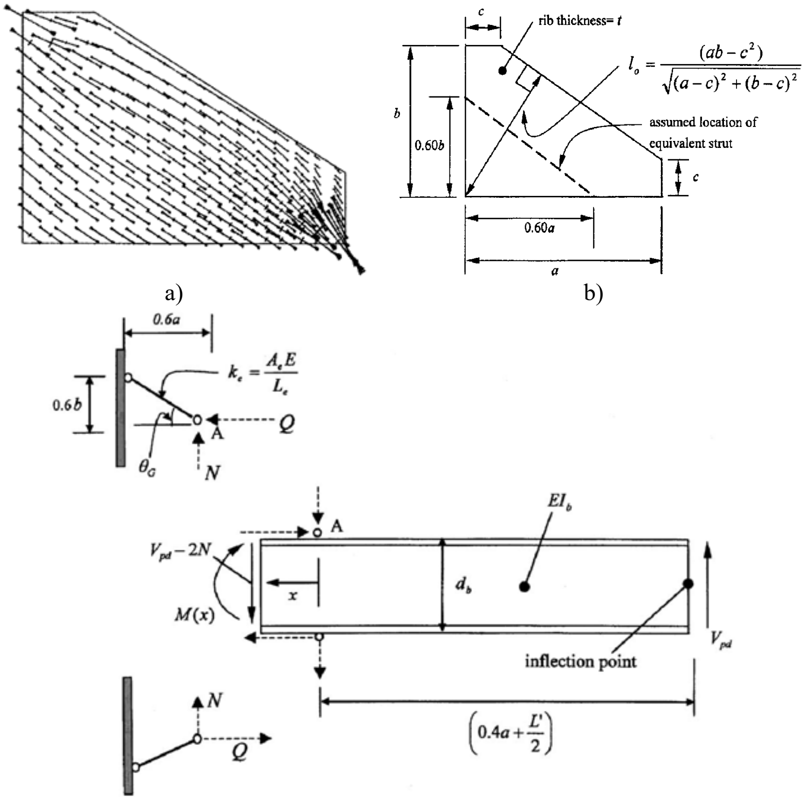

a) b)

c)

Figure 3-6: Rib internal actions distribution (a), equivalent strut model (b) and its action on the connected beam and column (c) [35].

The investigated parameters were the end-plate thickness and the steel grade of beams and plates. The test results (see Figure 3-5) showed that an increase in end-plate thickness leads to an improvement of the connection flexural strength and stiffness while the rotation capacity decreases. Except for the increase of stiffness, similar results were obtained by varying the end-plate steel grade.

The failure modes observed during the tests were the weld rupture in two specimens, nut stripping in four cases and bolt fracture in the remaining, which always occurred after significant yielding of the end plate and bolt bending.

For what concerns the behavior of welded joints stiffened by welded ribs, Lee et al [35],[38] observed that the classical beam theory does not provide good approximation of this connection response and that the internal force distribution in the rib could be modelled as a strut element in the rib diagonal. The Authors introduced a new mechanical model and step-by-step design procedure with the strut model proposed and represented in Figure 3-6.

On the basis of the theoretical results, an experimental campaign was conducted in order to validate the design procedure [35]. The main objectives were the investigation of the load migration in the rib and the development of strategies to avoid the plate brittle failure due to large stress concentration. A set of 4 experimental tests were conducted with the following joint characteristics:

1. RIB-NDB-AW: welded beam-to-column joint with the introduction of the rib stiffeners both on tension and compression side;
2. RIB-DB30-AW (2 specimens): the joints have the same characteristics of the previous one, but the beam has a section reduction of about 30%;
3. RIB-DB30-PE: the joint has the same characteristics of RIB-DB30-AW, but in this case the middle of the beam web (for almost 50% of the beam depth) was not welded to the column flange.

The results (see Figure 3-7) show a good joint capacity and ductility given that the specimens are able to reach the 4% of the chord rotation. Finally, from the experimental test results, the effectiveness of the analytical procedure and the identification of the strut model were validated.

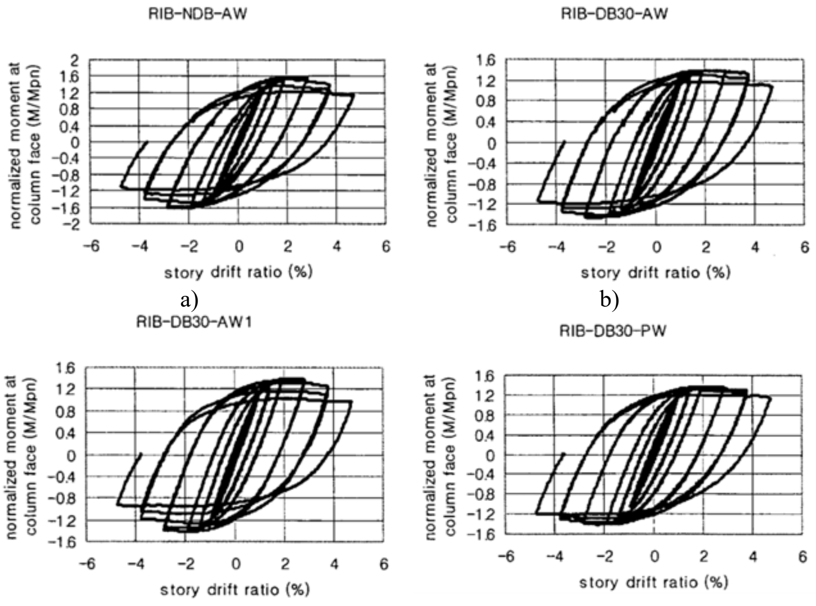

a) b) c) d)

Figure 3-7: Experimental moment rotation curve of: RIB-NDB-AW (a), RIB-DB30-AW (b), RIB-DB30-AW (c) and RIB-DB30-PE (d) [35].

The authors observed also that the mid-beam web can be detached from the column flange without losing the seismic capacity and avoiding the reverse shear action coming from the introduction of the ribs. Moreover, the beam trimming substantially decreases the cracks developed in the welds at the rib-beam interface, keeping the resistance almost the same.

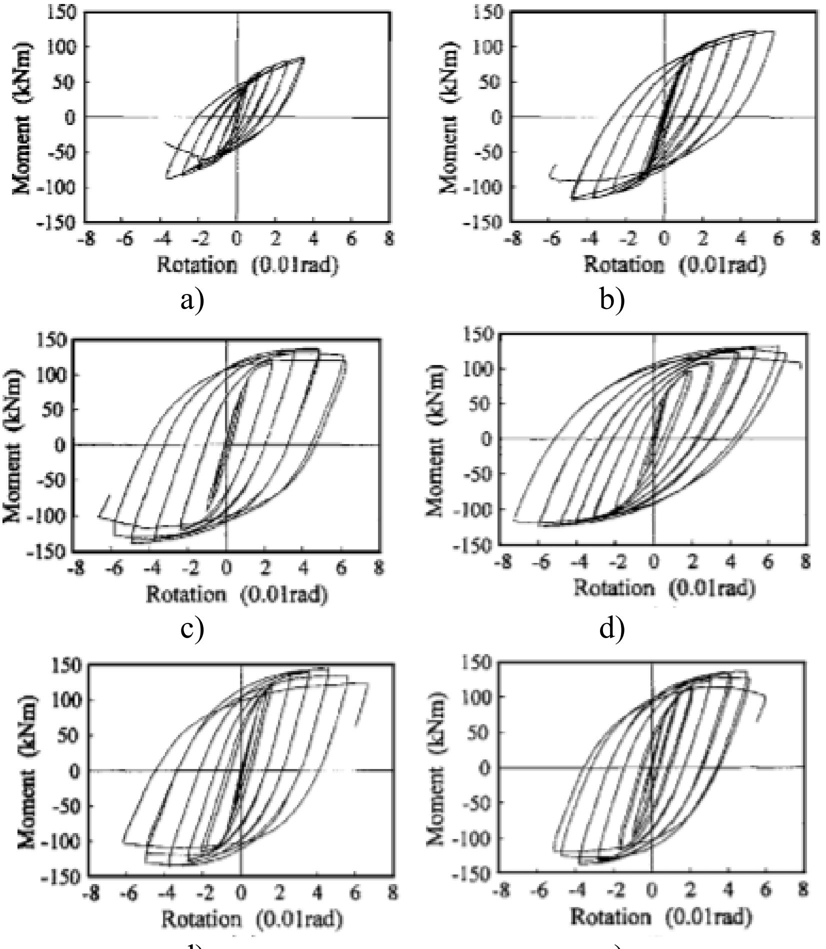

a) b)

c) d)

d) e)

Figure 3-8: Experimental results in terms of moment rotation curve [39].

In line with this research, Guo et al [39] investigated in 2006 the behavior of both stiffened and unstiffened joints under cyclic loading conditions. The Authors performed six tests (see Figure

3-8) and the results showed that all the specimens overcame the limit of 3% of rotation, but some substantial differences were observed between the stiffened and unstiffened joint. Indeed, the Authors highlighted the importance of the stiffeners not only to increase the load-carrying capacity and the joint elastic stiffness, but also with regards to the ductility.

In line with this conclusions Shi et al. [40], [41] confirmed the effectiveness of the extended end-plate connection in seismic areas. The Authors performed two series of full scale tests on steel beam-to-column end-plate connections specimens under both monotonic and cyclic loads. The results of the cyclic tests show that the extended stiffened joint can be used in steel moment frames due to their strength, stiffness, and the capacity to dissipate energy.

In Figure 3-9, results of some tested specimens are reported and it is possible to observe how the extended stiffened joints are able to ensure a ductile behavior. In [41] the specimens were designed to have different failures and as shown in Figure 3-9, function of the specimen's failure mode, different levels of ductility are observed. With particular attention to the joint ductility, it can be observed that EPC2 is the most brittle specimen, since the bolt failure governs the test; however all the joint assemblies overcame the limit of 4% of chord rotation

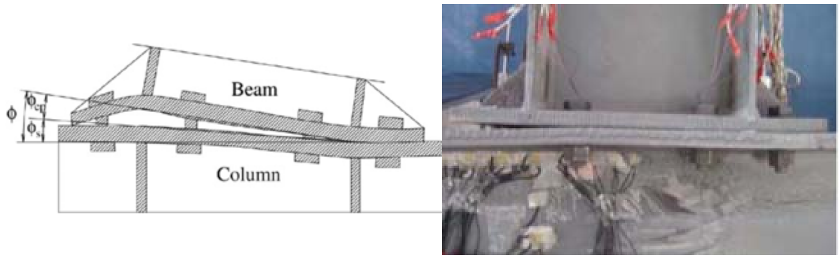

a) Definition of connection rotation b) Falure mode

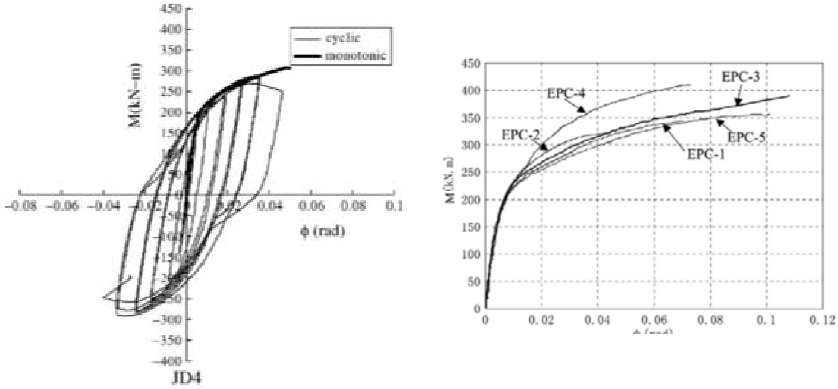

c) Cyclic vs. Monotonic curves d) Monotonic tests

Figure 3-9: Experimental results [41].

More recently, Abidelah et al [42] investigated for both extended (stiffened and unstiffened) and flush end-plate connection the main aspects of the tension and compression part that interfere with the definition of the joint response. To this aim an experimental campaign was conducted on eight beam-to-column assemblies and the results (see Figure 3-10) were compared with component method (EN1993-1-8) compliant predictions.

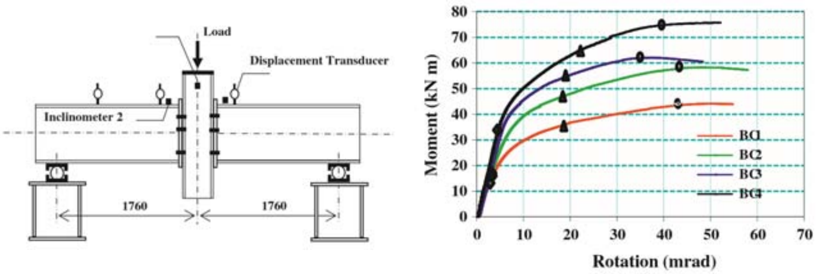

a) Experimental set-up b) Moment-rotation response curves

Figure 3-10: Experimental setup (a) and results (b) [42].

Moreover, the authors investigated three possible positions of the compression center, when the stiffener is placed both in tension and compression side. Figure 3-11 shows the three assumptions for the compression center: (i) placed in the beam flange (as prescribed by the EN1993-1-8), (ii) at the bottom edge of the rib or (iii) in the middle of the T-section composed by the beam flange and the stiffener.

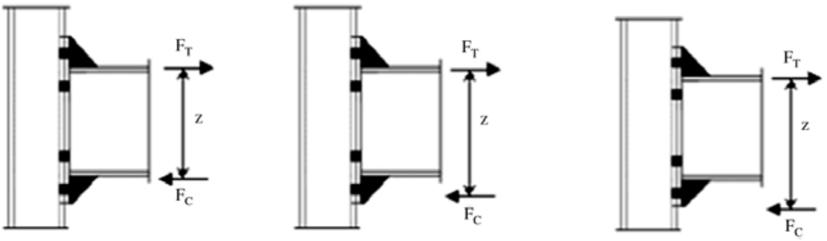

Figure 3-11: Three hypothesis on the compression center position [42].

The comparison between the experimental results and the analytical procedure shows that the second assumption captures more closely the resistance.

Finally, the Authors concluded that the presence of the rib stiffener on the tension side increases both the resistance and the joint stiffness, reducing the ductility but keeping however, the ultimate rotation large enough to ensure a ductile joint behavior.

In what concerns the compression side, it was demonstrated that the presence of the rib moves the position of the compression center from the middle of the beam flange to the centroid of the equivalent T-section.

Moreover, important considerations were highlighted with respect to the component method provisions. Indeed the EN1993-1-8 [1] provides a safe analytical model in terms of resistance, but not for the elastic stiffness that is in most cases overestimated.

Lin et al. [43] focused their research on the investigation of the seismic performance of an innovative constructional column solution. Even though the research is more focused on the column behavior, the presence of the extended beam-to-column connection leads to some interesting considerations, important also for this work. In particular, the test results show how, despite the balanced connection-beam failure, the joint is still able to exhibit good capacity and ductility (see Figure 3-12).

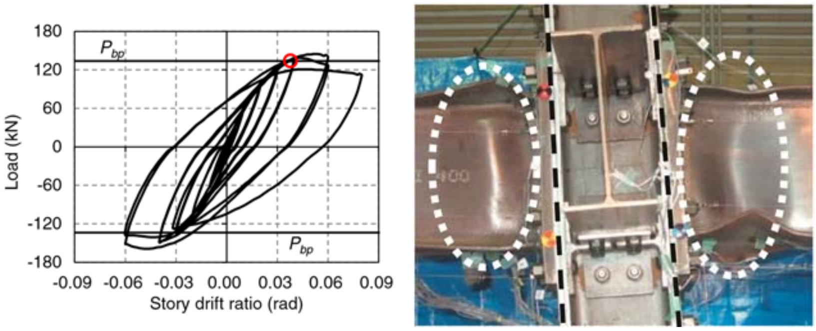

a) b)

Figure 3-12: Results of HTS joint in terms of moment rotation curve (a) and deformation (b) [43].

Moreover, the finite element model developed and calibrated based on the experimental results, was able to perfectly replicate the test results (see Figure 3-13).

The previous observations confirm two assumptions made for the current work: (i) a balanced damage distribution between the beam and connection can be achieved with good overall behavior of the assembly, and (ii) FE software are performant tools that can be used in order to conduct research work beyond the limits of experimental activities.

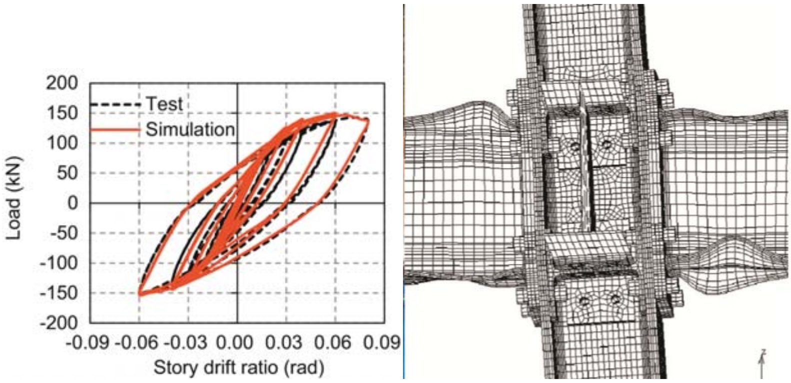

a) b)

Figure 3-13: FEM calibration results in terms of Moment rotation curve (a) and deformation (b) [43].

The behavior of stiffened end-plate moment connections under earthquake loading has been investigated. During the experimental tests the influence of the end-plate thickness, bolt diameter, end-plate stiffeners, and column stiffeners has been investigated. Tests clearly highlighted that in order to guarantee a ductile failure mode the damage should be concentrated into the extended end-plate.

*

In conclusion, analyzing existing results from literature, it can be recognized that both stiffened and unstiffened extended end-plate connections are able to perform with significant plastic rotational capacity and adequate strength and stiffness to be used in moment resisting frame in seismic zones.

Some open issues affecting the seismic behavior of connections result to still require investigation. These issues include:

- the effect of different steel grades of beams and columns on connection performance;
- the influence of stress concentration in the welds on low cycle fatigue;
- the role of panel zone yielding in shear on the connection behavior;
- the geometric parameters of the connection including beam depth, flange size and weld size;
- the strain rate and dynamic effects;
- the load and deformation history.

All the previous parameters affect the yield mechanism and failure mode which are the factors controlling both the resistance and the rotational capacity of the connection.

3.2 Analytical method

The work of Jaspart [10] has been fundamental for the development of the modern European code for the design of steel connections. As mentioned in the previous paragraph, the research included aspects related with joints and their influence on the global behavior of frames, with significant emphasis on the partial strength and semi-rigid aspects of bolted joints. The analytical method, based on the principle of effective lengths, for the prediction of each connection component resistance and flexibility was very straightforward and relatively easy to use while predicting with good accuracy the response of bolted joints.

Ever since, further proposals of improvements or additions to the codified component method have been suggested. In 2005 Mofid et al [44] proposed an analytical method to predict the extended end-plate connection behavior starting from the definition of the geometrical joint characteristics. With particular, regard to the unstiffened joint with four bolt rows, the Authors proposed a method substantially equal to the one of EN1993-1-8 but without providing any indication regarding the evaluation of the joint stiffness.

Maggi et al [45] investigated the behavior of bolted end-plate beam to column joints by means of experimental, numerical and analytical methods. One of the main conclusions drawn were that the component method give good approximations of the joint response for Failure modes 1 and 3 but as far as failure mode 2 is concerned, the method cannot model accurately the interaction between the bolts and the plates.

The necessity to define an analytical method capable to evaluate the bolted beam-to-column joint behavior was highlighted also by Aribert [46]. The Author provided an alternative procedure, in line with the EN1993-1-8, that is based on a sort of capacity design approach applied to the component method.

Latour et al 2011 [15], [16] introduced, starting from the component method approach, an analytical model able to predict the cyclic response of the beam-to-column bolted connection. The accuracy of the introduced method was validated against experimental tests performed by the authors and considering examples from literature.

Work aimed at the improvement of the vague EN1993-1-8 [1] requirements for joint ductility has been carried out by Da Silva et al. [47]. The Authors highlight the importance of the post-limit stiffness and limit displacement on the definition of a ductility limits. Based on test results, trial values were proposed as an initial approximation and then a ductility model able to predict the ‘‘yield’’ sequence of the components and a safe (lower bound) joint ductility index was used.

Regarding extended stiffened end-plate connections, the research of Lee et al. [35][38], Abidelah [42] and Shi et al [40][41] has solved many of the unknowns related with this joint typology and has provided valuable analytical concepts in order to fill the pre-existing code gap. This work has been already discussed in the previous paragraph, as it is correlated with experimental campaigns conducted by the Authors.

A different approach was taken by Terracciano et al [48], which proposed design charts that offer the possibility to quickly and easily establish joint configurations that can satisfy the structural performance requirements. The charts allow obtaining the joint stiffness, resistance and other characteristics function of the bolt diameter and end plate thickness, given the other joint characteristics. Furthermore the Authors proposed preliminary analytical equations for the calculation of stiffness and resistance of extended end-plate connections

Such charts that give the normalized stiffness, resistance (as described in EC3 [1]) , yield rotation and failure mode are presented in Figure 3-14 for HEM 280 column, IPE 550 beam, steel grade S275 and bolt grade 8.8.

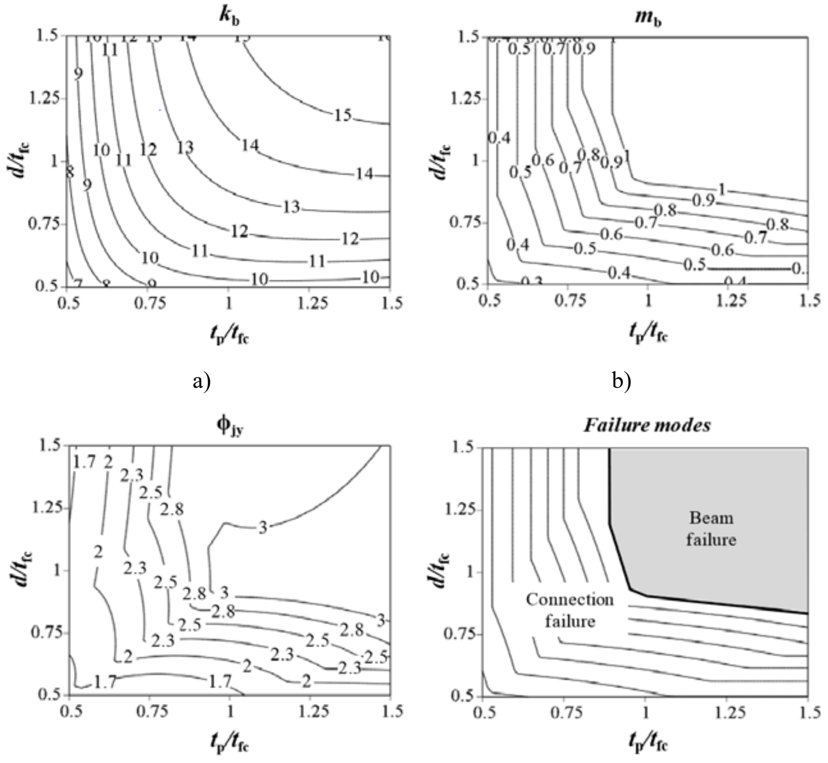

a) b)

c) d)

Figure 3-14 Normalized stiffness a), normalized resistance b), yield rotation c) and failure modes d) of extended end-plate connections [48].

In what concerns the simplified analytical expressions that resulted from the parametric study, comparison of the predictions, the numerical results and the component method showed difference of 7 and 10 % in terms of normalized moment resistance and stiffness, respectively (within the range of comparison between experimental and theoretical results).

When all is considered, it must be noted that the failure mode mechanism should be better defined, ensuring a clear differentiation between the partial, equal and full strength domain.

*

Simple yet accurate analytical tools for the design of steel bolted joints are a necessity. The component method as it is currently implemented in the Eurocode is a robust design procedure that has been tested along the years with good results, but it has also proved to have shortcomings and gaps. On the other hand, pre-qualification procedures, such as the one implemented in the US, has been proved a successful approach but not directly applicable to the European market.

3.3 Finite element models

Given the technological advances in the field of Finite Element Method (FEM) based software, numerical analyses of steel joints have become much easier to perform with more accurate results. The numerical modelling of the joints can be used also to overcome the lack of experimental results and to better comprehend local effects which are difficult to assess experimentally [49]. More important, FEAs are adequate for performing large parametric studies which can help us better understand the extent to which each parameter influences the behavior of the joint.

"Due to the high cost of steel connection materials, fabrication and testing; and since steel connection testing is a destructive test, it is important to predict the failure modes and connection behavior using finite element analysis" - Eldemerash 2012 [50] that calibrated using the software Anysis, the experimental tests carried out by Sumner et al (2000) [59].

The first FEM study in the steel joints field was performed by Bose et al. [51]**Error! Reference source not found.** that in 1990 investigated the behavior of the beam-to-column welded joint. After them, the FE models found a large diffusion in the steel joint research.

In 2011 Díaz et al. [49] summarized the most relevant numerical investigations carried out to the time.

With particular regard to the end-plate connection, Table 3.1 reports, in function of the time and the type of model introduced, the evolution of the FE models used for the joint investigation.

Table 3.1: Finite element models introduction in the steel joint field [49].

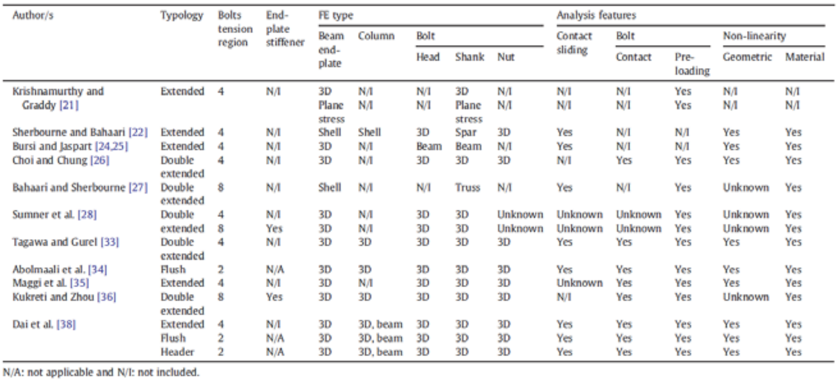

Author/s	Typology	Bolts tension region	End-plate stiffener	FE type					Analysis features				
				Beam end-plate	Column	Bolt			Contact sliding	Bolt		Non-linearity	
						Head	Shank	Nut		Contact	Pre-loading	Geometric	Material
Krishnamurthy and Graddy [21]	Extended	4	N/I	3D	N/I	N/I	3D	N/I	N/I	N/I	Yes	N/I	N/I
				Plane stress	N/I	N/I	Plane stress	N/I	N/I	N/I	Yes	N/I	N/I
Sherbourne and Bahaari [22]	Extended	4	N/I	Shell	Shell	3D	Spar	3D	Yes	N/I	N/I	Yes	Yes
Bursi and Jaspart [24,25]	Extended	4	N/I	3D	N/I	Beam	Beam	N/I	Yes	N/I	N/I	Yes	Yes
Choi and Chung [26]	Double extended	4	N/I	3D	N/I	3D	3D	3D	N/I	Yes	Yes	Yes	Yes
Bahaari and Sherbourne [27]	Double extended	8	N/I	Shell	N/I	N/I	Truss	N/I	Yes	N/I	Yes	Unknown	Yes
Sumner et al. [28]	Double extended	4	N/I	3D	N/I	3D	3D	Unknown	Unknown	Unknown	Yes	Unknown	Yes
		8	Yes	3D	N/I	3D	3D	Unknown	Unknown	Unknown	Yes	Unknown	Yes
Tagawa and Gurel [33]	Double extended	4	N/I	3D	3D	3D	3D	3D	Yes	Yes	Yes	Yes	Yes
Abolmaali et al. [34]	Flush	2	N/A	3D	3D	3D	3D	3D	Yes	Yes	Yes	Yes	Yes
Maggi et al. [35]	Extended	4	N/I	3D	N/I	3D	3D	3D	Unknown	Yes	Yes	Yes	Yes
Kukreti and Zhou [36]	Double extended	8	Yes	3D	3D	3D	3D	3D	N/I	Yes	Yes	Unknown	Yes
Dai et al. [38]	Extended	4	N/I	3D	3D, beam	3D	3D	3D	Yes	Yes	Yes	Yes	Yes
	Flush	2	N/A	3D	3D, beam	3D	3D	3D	Yes	Yes	Yes	Yes	Yes
	Header	2	N/A	3D	3D, beam	3D	3D	3D	Yes	Yes	Yes	Yes	Yes

N/A: not applicable and N/I: not included.

It can be observed how starting from Krishnamurthy [52] the models became more complex and able to predict the joint non-linearity. Moreover, the Author introduced a calibrated FEM model in Ansys to investigate the effectiveness of the modelling procedure. In particular, the FE model introduced is able to predict the joint failure mode while some problems can be observed with respect to both the resistance and stiffness prediction.

In 1998 also Bursi and Jaspar [53] introduced a 3D finite element model to study the behavior of the two type of bolted steel connections. The authors investigated the influence of the element type (i.e. C3D81, C3D8R) and the friction coefficient (i.e. 0, 0.25 or 0.50) on the moment rotation curve obtained from ABAQUS [54], by means of comparisons to experimental test results. Finally, the model introduced, considering the Richard-Abbott law (that allows the prediction of the imperfections) is able to predict the real joint behavior well (see Figure 3-15).

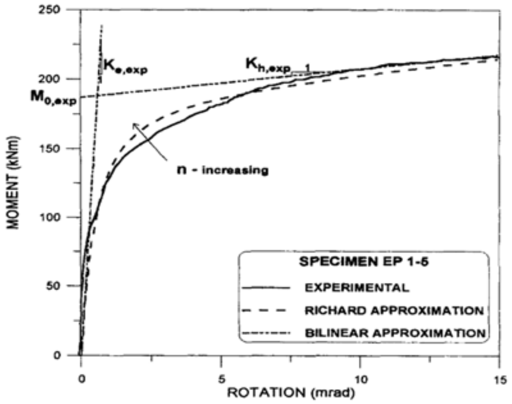

Figure 3-15: Experimental test against the FE model prevision in terms of Moment rotation curve [55].

In 2013 Wang et al [55] performed numerical analyses of experimental tests performed by Shi et al [40], Guo et al [39] and Yorgun et al [56], showing accurate predictions of the experimental results, speaking in terms of monotonic and hysteretic behavior and failure modes.

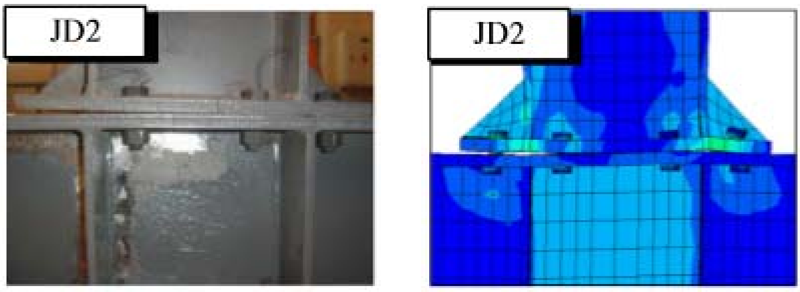

a) Experimental failure mode b) FE model failure mode

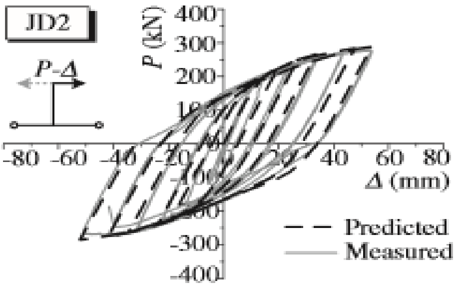

c) Cyclic response curves (numerical and experimental)

Figure 3-16 Experimental and numerical results comparison [55].

The Authors compared the behavior of three different beam to column joint typologies (welded, extended end plate and flush end plate), pointing out that extended end plate connections, if well configured, can achieve good hysteretic performance and thus become more suitable for use in seismic areas (the rib changes the failure mechanism, avoiding the brittle fracture in the welds). Figure 3-16 shows the hysteretic curves for the three joint typologies, where one can observe the strength and stiffness degradation due to pinching (visible for the extended end plate connections and severe for flush connection) and local buckling phenomena.

More recently, in 2013, Girao Coelho [57] presented the FEAs on the partial strength joint tested in 2004 [13]. The three-dimensional FEM is able to catch all the test results in terms of failure mode and joint resistance; indeed as showed in the test, the damage is confined in the end-plate. Moreover, starting from the calibrated model, the author performed a parametric analysis in order to investigate the beam depth influence on the rotational capacity.

Maggi et al [45] realised a FE parametric analysis on the beam-to-column extended end-plate connection, focusing on the influence of the end-plate and the bolts. The FE model was calibrated on the literature test performed at the São Carlos School of Engineering, Brazil. The monotonic experimental results show a very large joint ductility for all the investigated specimens, reaching rotational values up to 11% of the chord rotation (see Figure 3-17).

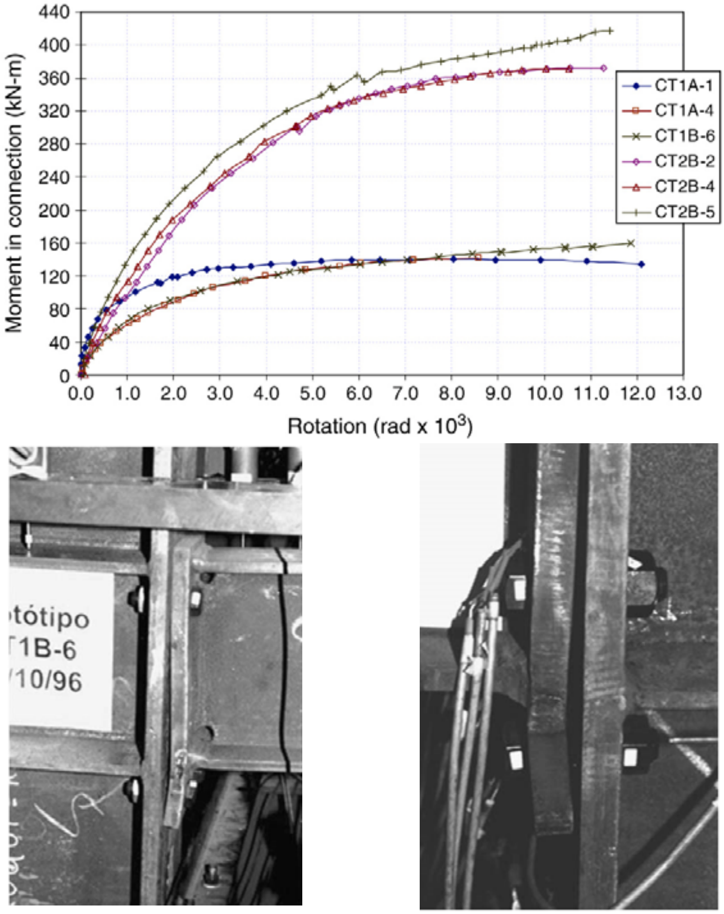

Figure 3-17 Experimental results [45].

Six experimental test were calibrated by FE models that show a good agreement in terms of both resistance and stiffness, while the models are not able to catch the failure mode when the mechanism is not clearly defined. Moreover, an investigation on the bolt row resistance for each line, with the T-stub sub-structuring was carried out.

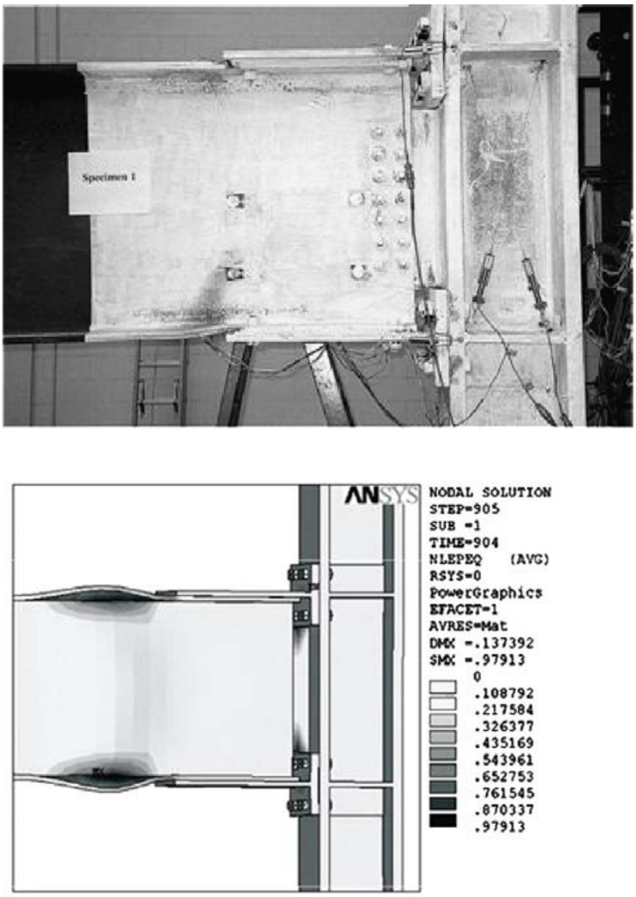

Figure 3-18 Experimental and numerical model comparison [58].

Gerami et al. [58] investigated the influence of the bolt arrangement on the moment capacity and on the failure mode of both end-plate and T-stub joint configurations (see Figure 3-18). The results of the performed numerical parametric study confirmed that although the bending moment capacity is not influenced, the distance between bolts and beam flange and web significantly influences the connection participation to the joint response, particularly for the T-stub connection. This is correlated with the pinching of the hysteretic loops when increasing the distance between bolts and beam and the contribution of dissipated energy. The authors concluded that the end-plate connection exhibits a better behavior and lower probability of failure with respect to the T-stub connection, and its use is recommended when cyclic loading conditions are expected.

*

FE software are a powerful tool that enables the engineer to better understand the joint behavior. However, due to economic concerns and also complexity in usage, this solution is not readily available for day-to-day design practice. The research community, on the other hand, can take full advantage of the potential capabilities and versatility of the numerical software.

References

[1] EN 1993:1–8, Design of Steel Structures - Part 1–8: Design of Joints. CEN, 2005.

[2] EN 1998-1, Design of Structures for Earthquake Resistance - Part 1: General Rules, Seismic Actions and Rules for Buildings. CEN, 2005.

[3] EN 1993:1–1, Design of Steel Structures - Part 1–1: General rules and rules for buildings. CEN, 2005.

[4] EN 1993-1-5, Design of Steel Structures - Part 1–5: Plated Structural Elements. CEN, 2005.

[5] EN 1090-1, Execution of steel structures and aluminum structures - Part 1: Requirements for conformity assessment of structural components. CEN, 2008.

[6] EN 14399-3, High strength structural bolting for preloading - Part 3: System HR - Hexagon bolt and nut assemblies. CEN, 2005.

[7] EN 14399-4, High strength structural bolting for preloading - Part 3: System HV - Hexagon bolt and nut assemblies. CEN, 2005.

[8] M. D'Aniello, D. Cassiano, R. Landolfo (2016). Monotonic and cyclic inelastic tensile response of European

preloadable gr10.9 bolt assemblies. Journal of Constructional Steel Research, 77–90.

[9] Zoetemeijer, P. (1974). A design method for the tension side of statically loaded, bolted beam-to-column connections. Heron, 20(1), 1-59.

[10] Jaspart, J.P (1991). Etude de la Semi-rigidite Des Noeuds Poutre-Colonne et son Influence sur la Resistance et la Stabilite des Ossature en Acier., Ph.D. Thesis; University of Liege, Liege, Belgium.

[11] V. Piluso, C. Faella and G. Rizzano (2001). Ultimate behavior of bolted t-stubs. I Theoretical model. Journal of. Structural Engineering, 127(6): 686-693.

[12] V. Piluso, C. Faella and G. Rizzano (2001). Ultimate behavior of bolted t-stubs. II Model validation. Journal of. Structural Engineering, 127(6): 694-704.

[13] A.M. Girao Coelho, F. S. K.Bijlaard, L. Simoes da Silva (2004). Experimental assessment of the ductility of extended end plate connections. Engineering Structures 26, 1185–1206.

[14] V. Piluso and G. Rizzano (2008). Experimental analysis and modelling of bolted T-stubs under cyclic loads. Journal of Constructional Steel Research, 64, 655–669.

[15] M. Latour, V. Piluso, G. Rizzano (2011). Cyclic Modeling of Bolted Beam-to-Column Connections: Component Approach. Journal of Earthquake Engineering, 15:537–563.

[16] M. Latour, V. Piluso, G. Rizzano (2001). Experimental Analysis of Bolted Steel Beam-to-Column Connections: Component Identification. Journal of Earthquake Engineering, 15:214–244.

[17] A. B. Francavilla, M. Latour,V. Piluso and G. Rizzano (2016). Bolted T-stubs: A refined model for flange and bolt fracture modes. Steel and Composite Structures, Vol. 20, No. 2, 267-293.

[18] Sherbourne, A. N. (1961). Bolted beam-to-column connections. Journal of Structural Engineering, 39(6), 203–210.

[19] Douty, R. T., and McGuire, W. F. (1965). High strength bolted moment connections. Journal of Constructional Steel Research, ASCE, 91(4), 101–128.

[20] Nair, R. S., Birkemoe, P. C., and Munse, W. H. (1974). High strength bolts subject to tension and prying. Journal of Structural Engineering. Div. ASCE, 100(2), 351–372.

[21] Mann, A. P., and Morris, L. J. (1979). Limit design of extended endplate connections. Journal of Structural Engineering, Div. ASCE, 105(3), 511–526.

[22] Agerskov H. (1977). Analysis of bolted connections subject to prying. Journal of Structural Engineering, Div. ASCE, 103(11): 2145–2163.

[23] Jaspart J.P. (1997). Contributions to recent advances in the field of steel joints – column bases and further configurations for beam-to-column joints and beam splices. Professorship Thesis, University of Liège.

[24] Bjorhovde R. (2004). Deformation considerations for connection performance and design. Proceedings of the Fifth International ECCS/AISC Workshop on Connections in Steel Structures: Innovative Steel Connections (Eds.: F.S.K. Bijlaard, A.M. Gresnigt and G.J. van der Vegte), Amsterdam, 11-20.

[25] Beg D., Zupanèiè E., Vayas I. (2004). On the rotation capacity of moment connections. Journal of Constructional Steel Research, 60, 601-620.

[26] Gioncu V., Mateescu G., Petcu D., Anastasiadis A. (2000). Prediction of available ductility by means of local plastic mechanism method: DUCTROT computer program.

Chapter 2.1 in Moment Resistant Connections of Steel Frames in Seismic Areas (Ed.: F Mazzolani), E&FN Spon, 95-146.

[27] Weynand K., Jaspart J.P., Steenhuis M. (1995). The stiffness model of revised Annex J of Eurocode 3. In: Proceedings of the Third International Workshop on Connections in Steel Structures III, Behaviour, Strength and Design (Eds.: R Bjorhovde, A Colson and R Zandonini), Trento, 441-452.

[28] Bjorhovde R., Colson A. (1991). Economy of semi-rigid frame design. in Connections in Steel Structures II: Behaviour, Strength and Design, Bjorhovde, R., Haaijer, G., and Stark, J.W.B (eds.), American Institute of Steel Construction, 418–430.

[29] Elnashai A., Elghazouli A.Y. (1994). Seismic behaviour of semi-rigid steel frames. Journal of Constructional Steel Research, 29, 149–174.

[30] Leon R.T. (1995). Seismic Performance of Bolted and Riveted Connections. Background Reports: Metallurgy, Fracture Mechanics, Welding, Moment Connections and Frame System Behavior, Report No SAC-95-09, FEMA-288 / March 1997, Federal Emergency Management Agency, Washington, DC.

[31] K-C. Tsai and E.P. Popov (1990). Cyclic behavior of end-plate moment connections. Journal of Structural Engineering, 116:2917-2930.

[32] R. M. Korol, A. Ghobarah and A. Osman (1990). Extended End-Plate Connections Under Cyclic Loading: Behaviour and Design. Journal Constructional of Steel Research, 16, 253-280.

[33] A. Ghobarah, R. M. Korol and A. Osman (1992). Cyclic behavior of extended end-plate joints. Journal of Structural Engineering, 118(5): 1333-1353.

[34] E. A. Sumner and T. M. Murray (2002). Behavior of Extended End-Plate Moment Connections Subject to Cyclic Loading. Journal of structural engineering, 128:4, 501-508.

[35] T. M. Murray, E. A. Sumner (2004). Extended End-Plate Moment Connections Seismic and Wind Applications Second Edition. American Institute of Steel Construction, Inc, April 2004.

[36] ANSI/AISC 358-16 (2016). Prequalified Connections for Special and Intermediate Steel Moment Frames for Seismic Applications.

[1] ANSI/AISC 341-10 (2010). Seismic Provisions for Structural Steel Buildings. American Institute of Steel Construction.

[37] C.-H. Lee, J.-H. Jung, M.-H. Oh, E.-S. Koo (2005) Experimental study of cyclic seismic behavior of steel moment connections reinforced with ribs. Journal of Structural Engineering, ASCE 131 (1), 108–118.

[38] C.-H. Lee (2002). Seismic design of rib-reinforced steel moment connections based on Equivalent Strut Model. Journal of Structural Engineering, ASCE 128 (9), 1121–1129.

[39] B. Guo, Q. Gu, F. Liu (2006). Experimental behavior of stiffened and unstiffened end-plate connections under cyclic loading, Journal of Structural Engineering, 132 (9), 1352–1357.

[40] Y. Shi, G. Shi, Y. Wang (2007). Experimental and theoretical analysis of the moment– rotation behaviour of stiffened extended end-plate connections”. Journal of Constructional Steel Research, 63, 1279–1293.

[41] G. Shi, Y. Shi, Y. Wang (2007). Behaviour of end-plate moment connections under earthquake loading”. Engineering. Structure. 29,703–716.

[42] A.Abidelah, A. Bouchaïr, D.E. Kerdal (2012). Experimental and analytical behavior of bolted end-plate connections with or without stiffeners. Journal of Constructional Steel Research, 76, 13–27.

[43] X. Lin, T. Okazaki, M. Nakashima (2014). Bolted beam-to-column connections for built-up columns constructed of H-SA700 steel Journal of Constructional Steel Research.

[44] M. Mofid, M.R.S Mohammad and M.S. McCabe (2005). Analytical approach on end plate connection: ultimate and yielding moment. Journal of Structural Engineering, 131:449-456.

[45] Y.I. Maggi, R.M. Gonçalves, R.T. Leon, L.F.L. Ribeiro (2005). Parametric analysis of steel bolted end plate connections using finite element modeling. Journal of Constructional Steel Research, 61, 689–708.

[46] J.M. Aribert (2012). Seismic design and strengthening of beam-to-column joints with bolted end plates. Stessa 2012, Mazzolani & Herrera (eds) Taylor & Francis Group, London, ISBN 978-0-415-62105-2.

[47] L. Simoes da Silva, A. Santiago, P. Vila Real (2002). Post-limit stiffness and ductility of end-plate beam-to-column steel joints. Computers and Structures, 80, 515–531.

[48] G. Terracciano, G. Della Corte, G. Di Lorenzo, R. Landolfo (2008). Simplified methods of analysis for end-plate beam-to-column joints.

[49] C. Díaz, M. Victoria, P. Martí, O. M. Querin, (2011). FE model of beam-to-column extended end-plate joints. Journal of Constructional Steel Research, 67, 1578–1590.

[50] Eldemrash Mohamed, Taher Abu-Lebdeh and Moayyad Al Nasra (2012). Finite Element Analysis of Large Capacity Endplate Steel Connections. Journal of Computer Science 8 (4): 482-493.

[51] Bose SK, McNeice GM, Sherbourne AN. (1972). Column webs in steel beam to column connexions. Part I: formulation and verification. Computers Structures, 2: 253–72

[52] Krishnamurthy N. (1978). A fresh look at bolted endplate behavior and design. Engineering Journal, 15(2), 39–49.

[53] O.S. Bursia, J.P. Jaspart (1998). Basic issues in the finite element simulation of extended end plate connections. Computers and Structures, 69, 361±382.

[54] Dassault Systèmes. Abaqus analysis 6.16 user's manual. Simula Inc. 2016.

[55] M Wang, Y Shi, Y Wang , G Shi (2013)Numerical Study on seismic behaviour of steel frame end plate connections. Journal of Constructional Steel Research, 90, 140–152.

[56] C. Yorgun, G. Bayramoglu, (2001). Cyclic tests for welded-plate sections with end-plate connections. Journal of Constructional Steel Research, 57(12):1309–20;

[57] A. M. Girao Coelho (2013).Rotation capacity of partial strength steel joints with three-dimensional finite element approach. Computers and Structures, 116, 88–97.

[58] M. Gerami, H. Saberi, V. Saberi, A: Saedi Daryanb (2011). Cyclic behavior of bolted connections with different arrangement of bolts. Journal of Constructional Steel Research, 67,690–705.

[59] Sumner EA, Mays TW, Murray TM. (2000) End-plate moment connections: test results and finite element method validation. 4th International Workshop on Connections in Steel Structures. 82–93.

List of figures

Figure 1-1 Force-displacement response curves for the monotonic tests. [8]. 15

Figure 1-2 T-stub force-displacement response for the HR and HV type assemblies in modes 2 and 3 [8]. 17

Figure 2-1: Bending of the column flange and T -stub flange at the tension side of a moment connection [9]. 18

Figure 2-2 Taking into account the influence of the bolts on the plastic collapse of a T stub [10]. 19

Figure 2-3 Forces in the bolt rows [10]. 20

Figure 2-4: Plastic deformation capacity of single T element of bolted T-stubs [12]...21

Figure 2-5: Cyclic model for type I mechanism [14]. 22

Figure 2-6 Flow chart for solving the system of equations [17].23

Figure 3-1 Bolt positioning and internal force distribution [31]. 27

Figure 3-2 Contribution of Specimen Components to Beam-Tip Deflection (Specimen CC-3) [33]............................28

Figure 3-3: Experimental results in terms of both moment rotation curve (a) and deformation (b) [34]. 29

Figure 3-4 Extended end plate configurations [35]. 30

Figure 3-5: Experimental results in terms of Moment rotation curve (a) and deformation (b) [13]......................... 30

Figure 3-6: Rib internal actions distribution (a), equivalent strut model (b) and its action on the connected beam and column (c) [35]. 31

Figure 3-7: Experimental moment rotation curve of: RIB-NDB-AW (a), RIB-DB30-AW (b), RIB-DB30-AW (c) and RIB-DB30-PE (d) [35]... 34

Figure 3-8: Experimental results in terms of moment rotation curve [40]. 35

Figure 3-9: Experimental results [42]. 37

Figure 3-10: Experimental setup (a) and results (b) [43]........... 38

Figure 3-11: Three hypothesis on the compression center position [43]. 38

Figure 3-12: Results of HTS joint in terms of moment rotation curve (a) and deformation (b) [44]......................... 40

Figure 3-13: FEM calibration results in terms of Moment rotation curve (a) and deformation (b) [44]......................... 41

Figure 3-14 Normalized stiffness a), normalized resistance b), yield rotation c) and failure modes d) of extended end-plate connections [49]. 46

Figure 3-15: Experimental test against the FE model prevision in terms of Moment rotation curve [56]. 50
Figure 3-16 Experimental and numerical results comparison [56]. 51
Figure 3-17 Experimental results [46]......................................53
Figure 3-18 Experimental and numerical model comparison [59]. 54

List of tables

Table 3.1: Finite element models introduction in the steel joint field [50]. 49

CHAPTER III

Normative background: EN1993-1-8 and AISC358-16

Introduction

Nowadays, in literature, there are several analytical methods to evaluate the beam-to-column joint behavior under seismic action (Chapter II). In the USA, after the Northridge earthquake (1994), a prequalification procedure was introduced by AISC358 [9]; contrariwise, in Europe, the joint behavior is studied using the component method (EN1993-1-8 [1]) and only few additional seismic requirements are presented in EN1998-1-1[2]. Differently from the American standard, the European codes do not provide a seismic prequalification procedure. The aim of this Chapter is to describe both design procedures, with particular focus on the limitations of the European regulations regarding the design of the extended end-plate bolted joint.

1 European design procedure: EN1993-1-8

EN1993-1-8 “gives the design methods for the design of joints subjected to predominantly static loading using steel grades S235, S275, S355 and S460” [1].

The joint characteristics influence the internal force distribution and stiffness of the overall structure; for this reasons its behavior should be accurately investigated.

To identify the joint effects on the structure three main cases can be studied: (i) simple, (ii) continuous and (iii) semi-continuous nodes. In the first case, the designers can consider that the joint does not transfer the bending moment, while in the second case the joint is able to transmit all the internal actions, which is the reason why they do not influence the structure’s behavior and can be neglected in analysis. Finally, in the case of semi-continuous nodes, the structure’s response is influenced by the joint and the extent of this influence should be investigated.

1.1 Joint characterization

1.1.1 Stiffness classification

A first step in the investigation of joints is the study of their stiffness; indeed according to EN1993-1-8 pr. 5.2.2 joints can be classified as: (i) rigid, (ii) nominally pinned and (iii) semi-rigid (the extended stiffened and un-stiffened beam-to-column joints fall within this last class). The joint classification according to stiffness is made by comparing the initial stiffness of the joint ($S_{j,ini}$) to the elastic stiffness of the connected beam (see Figure 1-1).

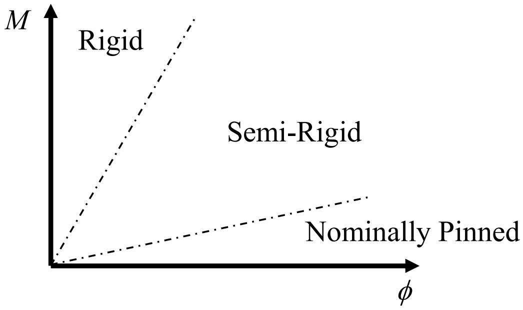

Figure 1-1: Joint classification in function of the stiffness [1].

Therefore, a joint is defined as *rigid* if its deformability does not influence the internal forces distribution and the global deformation of the frame; according to [1] this condition is fulfilled if:

$$S_{j,ini} \geq \frac{k_b E I_b}{L_b} \tag{1}$$

where: E is the steel elastic modulus, I_b is the beam moment of inertia and L_b is the beam length. k_b is a function of the steel structure considered and it is equal to 8 for dual structures where at least the 75% of the lateral force is carried by the bracing system, while it is equal to 25 for moment resisting frames (MRFs).

The joint can be defined as nominally pinned when its bending capacity is small enough to be neglected, sufficient rotational capacity is provided and the joint is designed to transfer only the shear forces.

$$S_{j,ini} \leq \frac{0.5 E I_b}{L_b} \tag{2}$$

A joint that does not satisfy the two limitations introduced can be classified as a partial rigid one.

$$\frac{0.5 E I_b}{L_b} \leq S_{j,ini} \leq \frac{k_b E I_b}{L_b} \tag{3}$$

1.1.2 Resistance classification

According to the EN1993-1-8 [1], joints can be classified also as a function of their strength by comparing their bending resistance ($M_{j,Rd}$) with the design moment resistance of the connected member [EN1993-1-8 pr 5.2.3]. In particular, three classes of joints can be defined: (i) full strength, (ii) nominally pinned or (iii) partial strength.

A joint can be defined as full strength when its capacity is larger than the weaker connected member. In this case, the joint would be able to transfer all the internal actions between the connected elements. According to EN1993-1-8 pr. 5.2.3.3 [1] a full strength joint should satisfy the limitations reported in Figure 1-2 where $M_{j,Rd}$ is the joint capacity, $M_{b,pl,Rd}$ is the beam capacity and $M_{c,pl,Rd}$ is the column bending resistance.

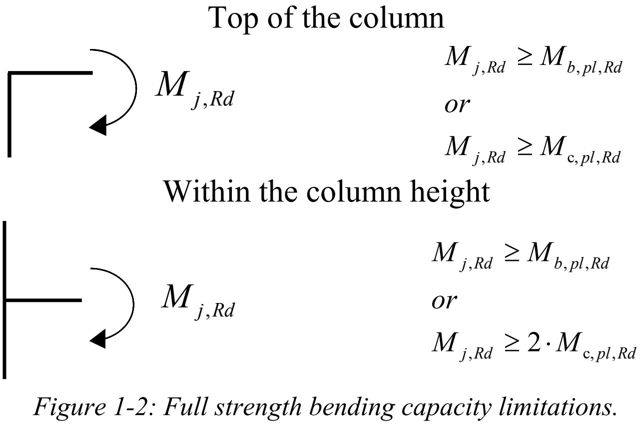

Top of the column

$$M_{j,Rd} \geq M_{b,pl,Rd}$$
or
$$M_{j,Rd} \geq M_{c,pl,Rd}$$

Within the column height

$$M_{j,Rd} \geq M_{b,pl,Rd}$$
or
$$M_{j,Rd} \geq 2 \cdot M_{c,pl,Rd}$$

Figure 1-2: Full strength bending capacity limitations.

A joint can be defined as nominally pinned when it is not able to resist bending moment. Moreover, this type of joint should guarantee the transfer of shear forces from one connected element to the other, also ensuring a proper level of rotational capacity. With particular regard to Figure 1-3, a joint can be classified as pinned when its bending capacity ($M_{\mathrm{j,Rd}}$) is smaller than 0.25 times the bending capacity of a full strength joint.

Finally, a joint can be defined as partial strength when its bending capacity does not respect either of the two limitations reported above.

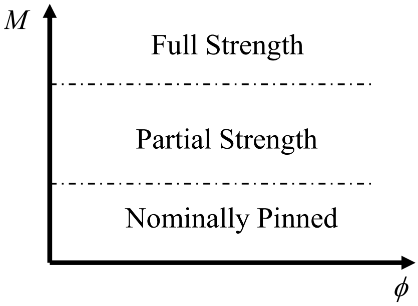

Figure 1-3: Joint strength classification [1].

1.2 Joint behavior

1.2.1 Definition of the components and their behavior

The component method implemented in EN1993:1-8 [1] allows predicting the joint flexural response both in terms of bending capacity ($M_{\mathrm{j,Rd}}$) and elastic stiffness ($S_{\mathrm{j,ini}}$).

This methodology consists in the identification of the sources of strength and deformability, which are generally known as joint components.

Each component influences both the joint strength and stiffness and will be modelled by an extensional spring characterized by an elastic perfectly plastic force-deformation (F-Δ) response (see Figure 1-4 a). Otherwise if the component influences only the joint resistance, it can be modelled by a rigid link considered with an infinite elastic stiffness and with a limited resistance (see Figure 1-4 b).

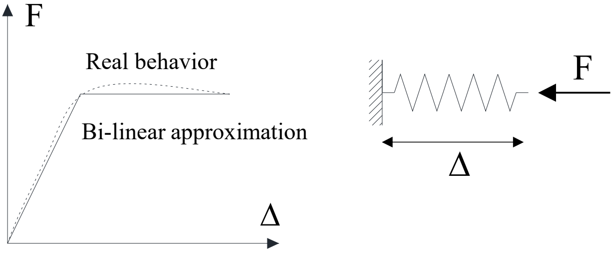

a)

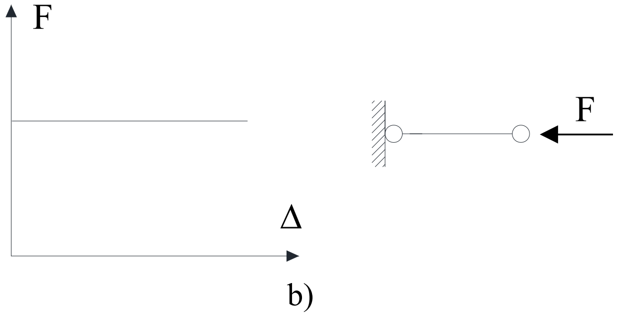

Figure 1-4: Basic components model: a) the spring element, b) the link element.

The main components in the case of bolted end-plate beam-to-column steel joints are depicted in Figure 1-5 and listed in Table 1.1.

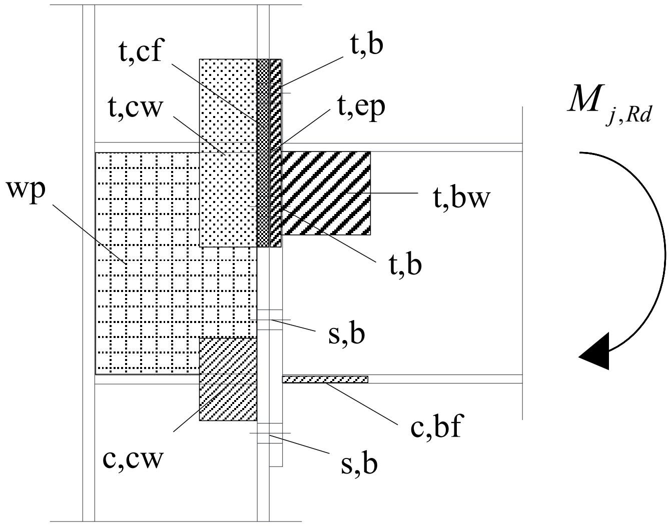

Figure 1-5: Main basic components of the extended beam-to-column joint.

Table 1.1: Description of the main basic components.

Zone	Label	Component
Tension	$t_{,b}$	Bolt in tension
	$t_{,ep}$	End-plate in bending
	$t_{,cf}$	Column flange in bending
	$t_{,bw}$	Beam web in tension
	$t_{,cw}$	Column web in tension
Shear	w_p	Column web panel in shear
Compression	$c_{,bf}$	Beam flange in compression
	$c_{,cw}$	Column web in compression
Shear	$s_{,b}$	Bolt in shear

The design resistance of the basic components in bolted extended end-plate joints (e.g. column flange in bending $t_{,cf}$, end-plate in bending $t_{,bf}$ and bolts in tension $t_{,b}$) are evaluated based on an equivalence with a T-stub. Therefore, the T-stub corresponds to two T elements connected at the level of their flanges by means of one or more bolt rows.

Indeed as shown in Figure 1-6 the column flange and end-plate in bending are evaluated by modelling equivalent T elements with the proper length. If there is more than one bolt row, the equivalent T element should be evaluated assuming that it works both alone and considering it as part of the group composed by all bolt lines. It results therefore, that the study of the equivalent T-stub strength is fundamental for the prediction of the joint response.

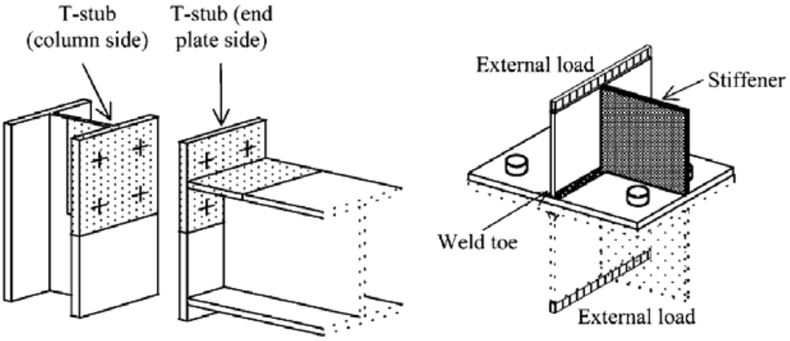

Figure 1-6: Equivalent T-stub in tension side [3].

The resistance of the T-stub can be calculated as the minimum of the corresponding three failure modes, as illustrated in Table 1.2, which are described as it follows:

- Mode 1 is characterized by the complete plasticization of the flange, whereas the bolts are not involved in the failure mechanism.
- Mode 2 is characterized by a combined mechanism of flange plasticization and failure of the bolts.
- Mode 3 is characterized by the failure of the bolts and it does not involve any plastic engagement of the T-stub flange.

Besides the obvious impact on the joint strength and stiffness, it can be anticipated that the T-stub behavior is fundamental also for the ductility of the system. The mechanical equivalence between the T-Stub and the corresponding element at bolt row level is obtained by means of the effective length (l_{eff}) which converts the real yield line patterns (both circular and non-circular) into an equivalent T-stub.

Depending on the geometry of the joint, different yield line patterns are possible, each of them characterized by an effective length of the equivalent T-stub. The shortest length corresponds to the minimum strength and is taken as the resistance of that bolt row. The bolt-to-stiffener distance (i.e. bolt to beam flange or web, or the rib stiffener, etc.) significantly influences the strength of the equivalent T-stub. In all cases, EC3 provides effective lengths of equivalent T-stubs for individual bolt rows and for bolt-rows as part of a group (i.e. see Figure 1-7).

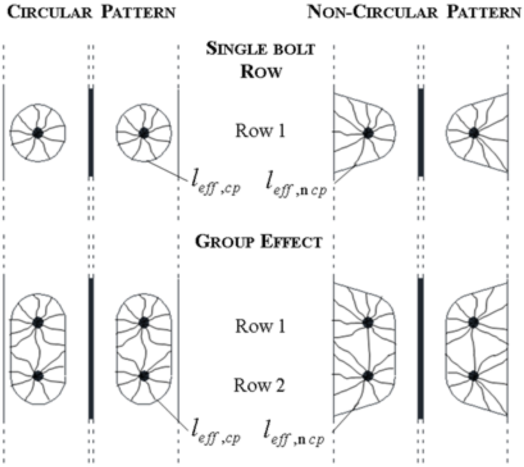

Figure 1-7: Yielding line distribution.

Table 1.2: T-stub failure mode and resistance.

<table>
<tr><th colspan="2">Failure mode 1</th></tr>
<tr><td>Failure mechanism</td><td>Resistance</td></tr>
<tr><td>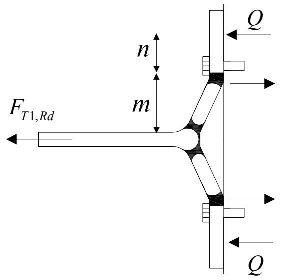
</td><td>$$F_{T1,Rd} = \frac{4M_{pl1,Rd}}{m}$$
where:
$M_{pl,1,Rd} = 0,25\Sigma\ell_{eff,1}\, t_{fc}^{\ 2} f_{y,fc} / \gamma_{M0}$
$m = (w/2 - t_{wc}/2 - 0.8r_c)$
L_{eff} are defined in EC3 in function of the T-stub geometry</td></tr>
<tr><th colspan="2">Failure mode 2</th></tr>
<tr><td>Failure mechanism</td><td>Resistance</td></tr>
<tr><td>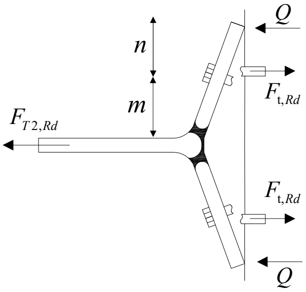
</td><td>$$F_{T2,Rd} = \frac{2M_{pl2,Rd} + n\sum F_{t,Rd}}{m+n}$$
where:
$M_{pl,2Rd} = 0,25\Sigma\ell_{eff,2}\, t_{fc}^{\ 2} f_{y,fc} / \gamma_{M0}$
$m = (w/2 - t_{wc}/2 - 0.8r_c)$
L_{eff} are defined in EC3 in function of the T-stub geometry</td></tr>
<tr><th colspan="2">Failure mode 3</th></tr>
<tr><td>Failure mechanism</td><td>Resistance</td></tr>
<tr><td>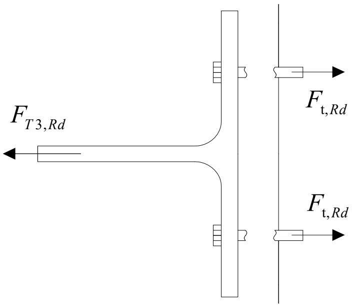
</td><td>$$F_{T3,Rd} = \sum F_{t,Rd}$$
where:
$$F_{t,Rd} = \frac{0.9 f_{ub} A_s}{\gamma_{M2}}$$</td></tr>
</table>

In order to also explain the resistance of other components, Table 1.3 presents the following components for the generic extended un-stiffened beam-to-column joint:

- column web panel in shear (w_p);
- column web panel in transversal compression ($c_{,cw}$);
- column web in tension ($t_{,cw}$);
- beam web in tension ($t_{,bw}$);
- beam flanges and web in compression ($c_{,bf}$).

Table 1.3: Joint components according to EN1993-1-8 [1].

Component	Details rules	References
Column web panel in shear (w_P)	$V_{wp,Rd} = \frac{0.9 A_{vc} f_{y,\mathrm{wc}}}{\sqrt{3}\gamma_{M0}} + V_{wp,\mathrm{add},Rd}$ $V_{wp,\mathrm{add},Rd} = \frac{4\ \mathrm{M}_{\mathrm{pl,fc,Rd}}}{d_s} \leq \frac{2\ \mathrm{M}_{\mathrm{pl,fc,Rd}} + \mathrm{M}_{\mathrm{pl,st,Rd}}}{d_s}$ where: $A_{vc} = A_c - 2b_c t_{fc} + (t_{wc} + 2r_c) t_{fc};$ $M_{\mathrm{pl,fc,Rd}}$ is the column design plastic moment resistance; $M_{\mathrm{pl,st,Rd}}$ is the continuity plate design plastic moment resistance; 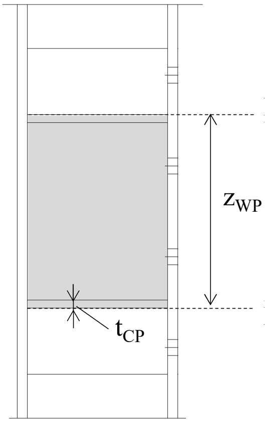 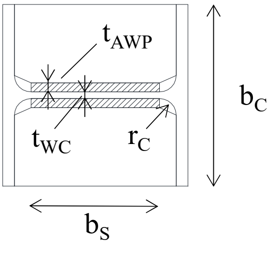	EN1993-1-8 pr.6.2.6.1

Component	Details rules	References
Column web in transversal compression ($c_{,cw}$)	The resistance of the column web and continuity plates may be computed with: $F_{wcc,Rd} = \frac{\omega k_{wc} b_{eff,c,cf} t_{wc} f_{y,wc}}{\gamma_{M0}} + \frac{A_{cp} f_{y,cp}}{\gamma_{M0}}$ where: $b_{eff,c,cf} = t_{fb} + \sqrt{2}(a_{w1} + a_{w2}) + 5(t_{fc} + r_c) + 2t_{ep}$ A_{cp} is the area of the continuity plates (both sides); The reduction factor k_{wc} taking into account the axial stress in the column web, given in 6.2.6.2(2) of EC3-1-8. The reduction factor ω is given by Table 6.3 in EC3-1-8; 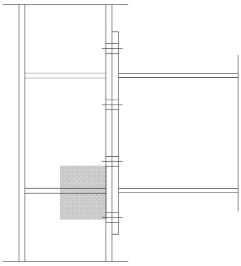 Note: if continuity plates are used, the reduction due to buckling of the column web under transverse compression can be neglected	EN1993-1-8 pr.6.2.6.2

Component	Details rules	References
Column web in tension ($t_{,cw}$)	$F_{wct,Rd} = \frac{\omega b_{eff,t,wc} t_{wc} f_{y,wc}}{\gamma_{M0}}$ The effective width $b_{eff,t,wc}$ of the column flange in tension should be taken as equal to the effective length of the equivalent T-stub representing the column flange in bending for an individual bolt-row or a bolt-group. 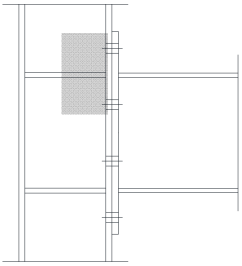 The reduction factor ω is given by Table 6.3 in EC3-1-8.	EN1993-1-8: pr. 6.2.6.3
Beam web in tension ($t_{,bw}$)	$F_{wbt,Rd} = b_{eff,t,wb} t_{wb} f_{y,wb} / \gamma_{M0}$ The effective width $b_{eff,t,wb}$ of the beam web in tension should be taken as equal to the effective length of the equivalent T-stub representing the end-plate in bending for an individual bolt-row or a bolt-group. 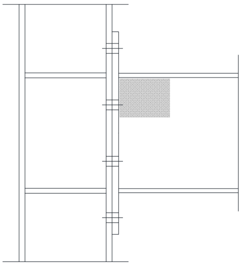	EN1993-1-8 pr. 6.2.6.8

Component	Details rules	References
Beam flanges and web in compression ($c_{,bf}$)	$F_{fbc,Rd} = M_{c,Rd}\, f_{y,b} \big/ (h - 0.5 t_{fb})$ - *h* is the depth of the connected beam; - $M_{c,Rd}$ is the design moment resistance of the beam plus the rib cross-section, reduced if necessary to allow for shear, see EN 1993-1-1. - t_{fb} is the flange thickness of the connected beam. 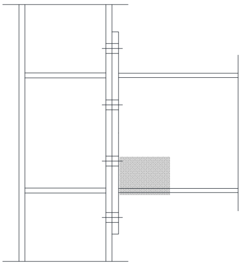	EN1993-1-8 pr. 6.2.6.7

1.2.2 Joint strength evaluation

Once all components that make up the joint are evaluated, a mechanical model is built.

On the tension-side, for each bolt row, all the components should be assembled in series, while on the compression side just one line is considered aligned with the compression center (see Figure 1-8). The center of compression, according to EN 1993-1-8 [1], is assumed in the mid-thickness of the beam compression flange.

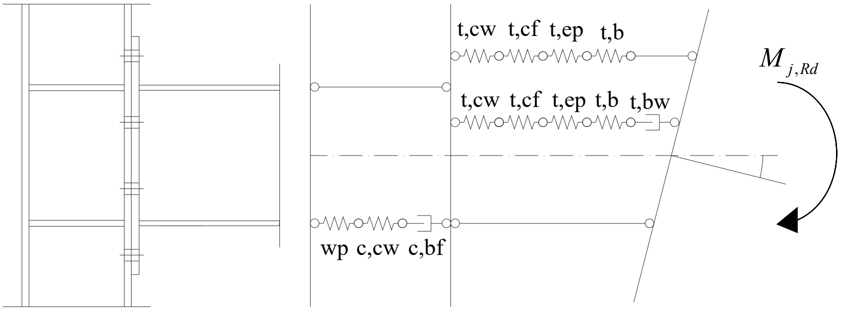

Figure 1-8: Combination of all the spring and the link.

Therefore, three distinct steps can be introduced to evaluate the joint bending capacity for the bolted moment resisting joint:

1. Calculating the resistance of each bolt row in the tension zone;
2. Checking if the total tension resistance can be achieved, as it may be limited by either the shear resistance of the column web

panel, or the resistance in compression (i.e. the beam flange in compression or the crushing or buckling of the column web).

3. Calculating the moment resistance $M_{j,Rd}$ as the sum of the tension forces multiplied by their respective lever arms, namely as follows.

$$M_{j,Rd} = \sum_r h_r F_{tr,Rd} \tag{4}$$

where $F_{tr,Rd}$ is the effective design tension resistance of bolt-row r; h_r is the distance from bolt-row r to the center of compression; r is the bolt row number.

Since the tension strength of a bolt-row may be limited by the effects of forces in other rows part of the group, the effective tension resistance of the bolt row individually is considered as a potential resistance. The final design tension resistance $F_{tr,Rd}$ for each bolt row should be determined in sequence, starting from the bolt row with the maximum lever arm up to the point when the equilibrium with the compressive strength is achieved. Moreover, the effective design tension resistance $F_{tr,Rd}$ at each bolt row in the tension zone should satisfy the following criterion:

$$F_{tr,Rd} = min(F_{t,fc,Rd}\,;\, F_{t,wc,Rd}\,;\, F_{t,ep,Rd}\,;\, F_{t,wb,Rd}\,) \tag{5}$$

where:

$F_{t,fc,Rd}$: is the column flange bending and bolt strength (6.2.6.4)

$F_{t,wc,Rd}$: is the resistance of column web in tension (6.2.6.3);

$F_{t,ep,Rd}$: is the end plate bending and bolt strength (6.2.6.5);

$F_{t,wb,Rd}$: is the resistance of beam web in tension (6.2.6.8).

In order to guarantee the internal equilibrium of plastic distribution of forces at each bolt-row the total design resistance should satisfy the following criterion:

$$\sum_r F_{tr,Rd} \leq min(V_{wp,Rd}; F_{c,wc,Rd}; F_{c,fb,Rd}) \qquad (6)$$

Where:

$V_{wp,Rd}$: is the column web panel strength;

$F_{c,wc,Rd}$: is the design resistance of the column web in compression;

$F_{c,fb,Rd}$: is the design resistance of the beam flange and web in compression.

In order to better clarify the resistance evaluation for all the bolt rows, an example of joint design procedure is introduced from Table 1.4 to Table 1.7.

The example is a classical extended un-stiffened joint typology with three bolt lines on the tension side, where neither continuity plates nor supplementary web plates are considered. The design procedure starts from the first bolt row and checks its tension resistance against the one on the compression side, proceeding then in order with the second and the third line, reaching the minimum between the maximum resistance in tension of all the lines and the maximum resistance in compression.

Therefore, the first step is to evaluate the resistance of the first bolt row considered alone. The active components on the tension side are the column web in tension, the column flange in bending and the end-plate in bending. The final line resistance that can be defined $F_{\mathrm{t,1,Rd}}$ is the minimum between the components on the tension side and the one on the compression side.

If the resistance of the first bolt row is governed by the compression side, it means that not all the tension resistance can be achieved. In this case, the second and the third bolt rows will be in elastic range or maybe not activated.

On the other hand, if the failure is governed by the spring in tension the second line is active as well and it should be checked.

Table 1.4: First bolt row line resistance evaluation.

First bolt row line resistance			
First bolt row alone	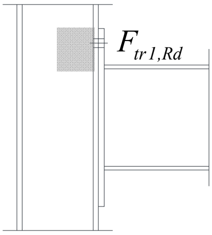	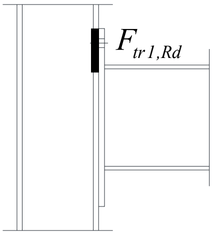	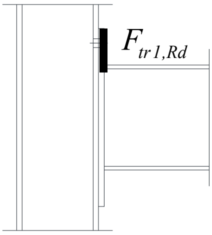
	Column web in tension	Column flange in bending	End-plate in bending
	$F_{tr1,Rd} \le F_{tr,cw,Rd}$	$F_{tr1,Rd} \le F_{tr,cf,Rd}$	$F_{tr1,Rd} \le F_{tr,ep,Rd}$
Compression and shear	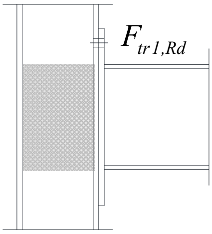	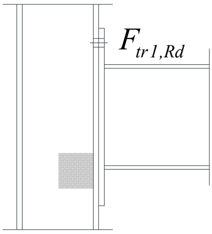	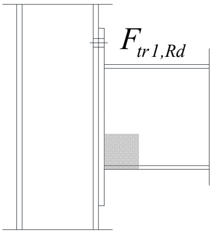
	Column web panel in shear	Column web in compression	Beam web in compression
	$F_{tr1,Rd} \le F_{wp,Rd}$	$F_{tr1,Rd} \le F_{c,cw,Rd}$	$F_{tr1,Rd} \le F_{c,bf,Rd}$
$F_{tr1,Rd} = min\left\{F_{t,cw,Rd}\,;F_{t,cf,Rd}\,;F_{t,ep,Rd}\,;F_{wp,Rd}\,;F_{c,cw,Rd}\,;F_{c,bf,Rd}\right\}$			

Moving on to the second bolt line, it is important to notice that, since in this example no continuity plates were introduced on the column side, in the calculation of the second bolt line, also the influence of the group effect should be taken into account.

The first step, as for the first bolt line, is to check the second row alone disregarding the possible group effect.

It is important to notice that since the second line is below the beam flange also the beam web in tension component should be taken into account.

To identify the group resistance (of the first and second bolt row on the column side), starting from the equivalent T-stub model explained above, different effective lengths should be introduced. Therefore, the resistance of the second bolt row line is the minimum between the resistance considering the second line alone and the one considering also the influence of the first row (for the tension side). On the compression side, the equilibrium should be verified considering also the resistance of the first line as reported in the last formulation of Table 1.5.

Table 1.5: Second bolt row line resistance.

Second bolt row line resistance		
Second bolt row alone	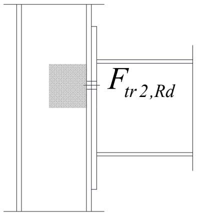	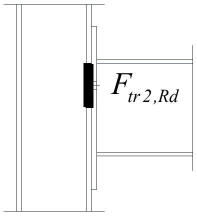
	Column web in tension	Column flange in bending
	$F_{tr2,Rd} \leq F_{tr,cw,Rd}$	$F_{tr2,Rd} \leq F_{tr,cf,Rd}$
	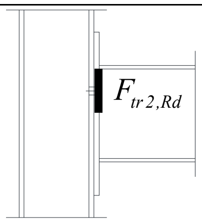	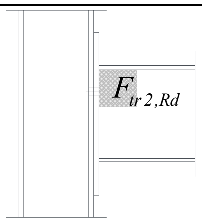
	End-plate in bending	Beam web in tension
	$F_{tr2,Rd} \leq F_{tr,ep,Rd}$	$F_{tr2,Rd} \leq F_{tr,bw,Rd}$
Group effect	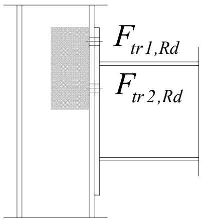	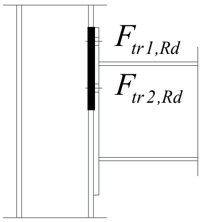
	Column web in tension	Column flange in bending
	$F_{tr1,Rd} + F_{tr2,Rd} \leq F_{tr,cw,Rd,(1+2)}$	$F_{tr1,Rd} + F_{tr2,Rd} \leq F_{tr,cf,Rd,(1+2)}$

<table>
<tr><th colspan="4">Second bolt row line resistance</th></tr>
<tr><td rowspan="3">Compression and shear</td><td>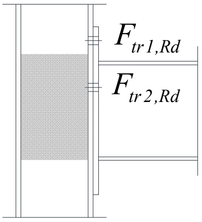 </td><td>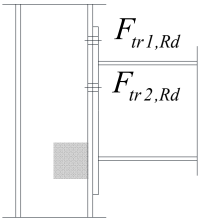 </td><td>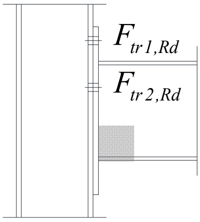 </td></tr>
<tr><td>Column web panel in shear</td><td>Column web in compression</td><td>Beam web in compression</td></tr>
<tr><td>$F_{tr1,Rd} + F_{tr2,Rd}$
$\leq F_{wp,Rd}$</td><td>$F_{tr1,Rd} + F_{tr2,Rd}$
$\leq F_{c,cw,Rd}$</td><td>$F_{tr1,Rd} + F_{tr2,Rd}$
$\leq F_{c,bf,Rd}$</td></tr>
<tr><td colspan="4">$$F_{tr2,Rd} = min \left\{ \begin{array}{l} F_{t,cw,Rd,(2)}; F_{t,cf,Rd,(2)}; F_{t,ep,Rd,(2)}; F_{t,bw,Rd,(2)} \\ F_{t,cw,Rd,(1+2)} - F_{tr1,Rd}; F_{t,cf,Rd,(1+2)} - F_{tr1,Rd} \\ F_{wp,Rd} - F_{tr1,Rd}; F_{c,cw,Rd} - F_{tr1,Rd}; F_{c,bf,Rd} - F_{tr1,Rd} \end{array} \right\}$$</td></tr>
</table>

As for the previous case, before checking the resistance of the third line, the failure mode of the second bolt row should be checked.

Indeed, if the compression component induced the failure, the third line would not be active, while if the resistance is governed by the tension side, regardless if the resistance comes from the line considered alone or as part of group, the third line will be active.

Table 1.6: Third bolt row line resistance (a).

<table>
<tr><th colspan="3">Third bolt row line resistance</th></tr>
<tr><td rowspan="6">Third bolt row alone</td><td>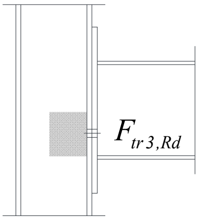 </td><td>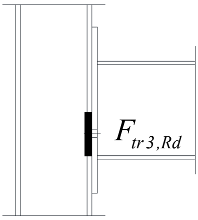 </td></tr>
<tr><td>Column web in tension</td><td>Column flange in bending</td></tr>
<tr><td>$F_{tr3,Rd} \leq F_{tr,cw,Rd,(3)}$</td><td>$F_{tr3,Rd} \leq F_{tr,cf,Rd,(3)}$</td></tr>
<tr><td>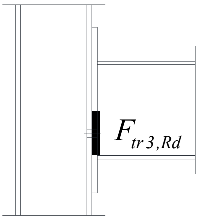 </td><td>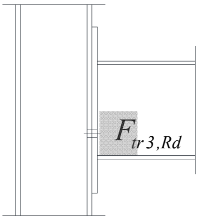 </td></tr>
<tr><td>End-plate in bending</td><td>Beam web in tension</td></tr>
<tr><td>$F_{tr3,Rd} \leq F_{tr,ep,Rd,(3)}$</td><td>$F_{tr3,Rd} \leq F_{tr,bw,Rd,(3)}$</td></tr>
<tr><td rowspan="3">Group effect 1+2</td><td>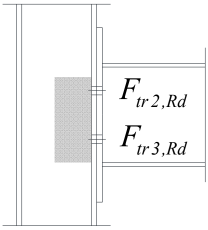 </td><td>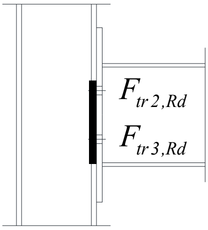 </td></tr>
<tr><td>Column web in tension</td><td>Column flange in bending</td></tr>
<tr><td>$F_{tr2,Rd} + F_{tr3,Rd} \leq F_{tr,cw,Rd,(2+3)}$</td><td>$F_{tr2,Rd} + F_{tr3,Rd} \leq F_{tr,cf,Rd,(2+3)}$</td></tr>
</table>

<table>
<tr><th colspan="3">Third bolt row line resistance</th></tr>
<tr><td rowspan="3">Group effect 1+2</td><td>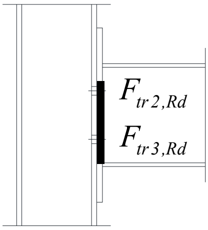 </td><td>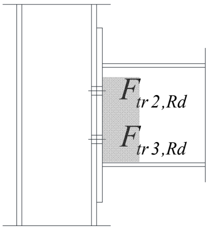 </td></tr>
<tr><td>End-plate in bending</td><td>Beam web in tension</td></tr>
<tr><td>$F_{tr2,Rd}+F_{tr3,Rd}\leq F_{tr,ep,Rd,(2+3)}$</td><td>$F_{tr2,Rd}+F_{tr3,Rd}\leq F_{t,bw,Rd,(2+3)}$</td></tr>
<tr><td rowspan="3">Group effect 1+2+3</td><td>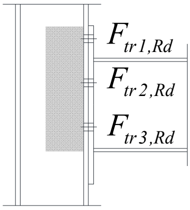 </td><td>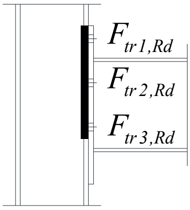 </td></tr>
<tr><td>Column web in tension</td><td>Column flange in bending</td></tr>
<tr><td>$F_{tr1,Rd}+F_{tr2,Rd}+F_{tr3,Rd}$
$\leq F_{tr,cw,Rd,(1+2+3)}$</td><td>$F_{tr1,Rd}+F_{tr2,Rd}+F_{tr3,Rd}$
$\leq F_{tr,cf,Rd,(1+2+3)}$</td></tr>
</table>

The resistance of the third bolt row in tension is reported in Table 1.6, where it should be noticed that on the column side two group effects are to be checked: (i) one made up by the second and third bolt rows, and (ii) the one made up considering also the first line. On the other hand, on the beam side just the group effect between the second and the third bolt row is verified. This difference is mainly due to the presence of a stiffener (in this case the beam flange) between the first and the second and third line.

Finally, Table 1.7 summarizes the third bolt row resistance that is the minimum between the tension resistances considering the line alone or as part of a group and the joint compression resistance.

Table 1.7: Third bolt row line resistance (b).

<table>
<tr><th colspan="4">Third bolt row line resistance</th></tr>
<tr><td rowspan="3">Compression and shear</td>
<td>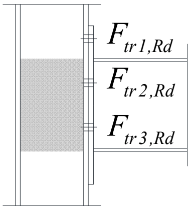 </td>
<td>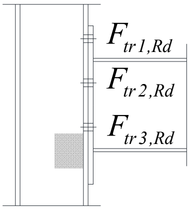 </td>
<td>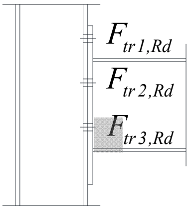 </td></tr>
<tr><td>Column web panel in shear</td><td>Column web in compression</td><td>Beam web in compression</td></tr>
<tr><td>$F_{tr\,1,Rd} + F_{tr\,2,Rd}$
$+F_{tr\,3,Rd} \leq F_{wp,Rd}$</td><td>$F_{tr\,1,Rd} + F_{tr\,2,Rd}$
$+F_{tr\,2,Rd} \leq F_{c,cw,Rd}$</td><td>$F_{tr\,1,Rd} + F_{tr\,2,Rd}$
$+F_{tr\,3,Rd} \leq F_{c,bf,Rd}$</td></tr>
<tr><td colspan="4">$$F_{tr\,3,Rd} = min\left\{\begin{array}{l} F_{t,cw,Rd,(3)}; F_{t,cf,Rd,(3)}; F_{t,ep,Rd,(3)}; F_{t,bw,Rd,(3)} \\ F_{t,cw,Rd,(2+3)} - F_{tr\,2,Rd}; F_{t,cf,Rd,(2+3)} - F_{tr\,2,Rd}; \\ F_{t,ep,Rd,(2+3)} - F_{tr\,2,Rd}; F_{t,bw,Rd,(2+3)} - F_{tr\,2,Rd}; \\ F_{t,cw,Rd,(1+2+3)} - F_{tr\,1,Rd} - F_{tr\,2,Rd}; \\ F_{t,cf,Rd,(1+2+3)} - F_{tr\,1,Rd} - F_{tr\,2,Rd}; \\ F_{wp,Rd} - F_{tr\,1,Rd} - F_{tr\,2,Rd}; F_{c,cw,Rd} - F_{tr\,1,Rd} - F_{tr\,2,Rd}; \\ F_{c,bf,Rd} - F_{tr\,1,Rd} - F_{tr\,2,Rd} \end{array}\right\}$$</td></tr>
</table>

1.2.3 Joint stiffness evaluation

EN1993-1-8 [1] provides criteria to predict the joint initial stiffness $S_{j,ini}$ starting from the flexibilities of all the joint basic components k_i as illustrated in Figure 1-9.

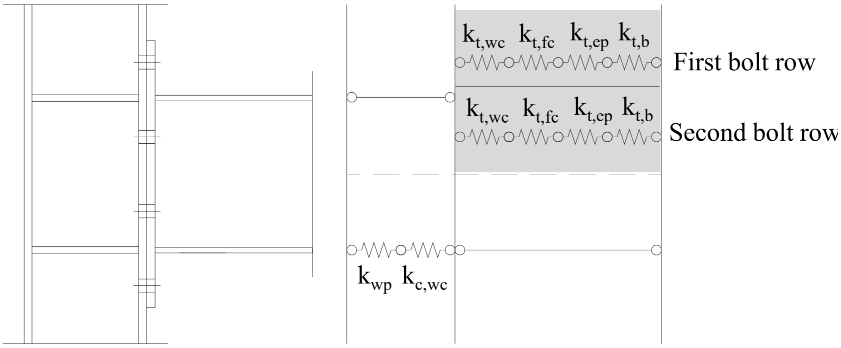

Figure 1-9: Basic component stiffness spring.

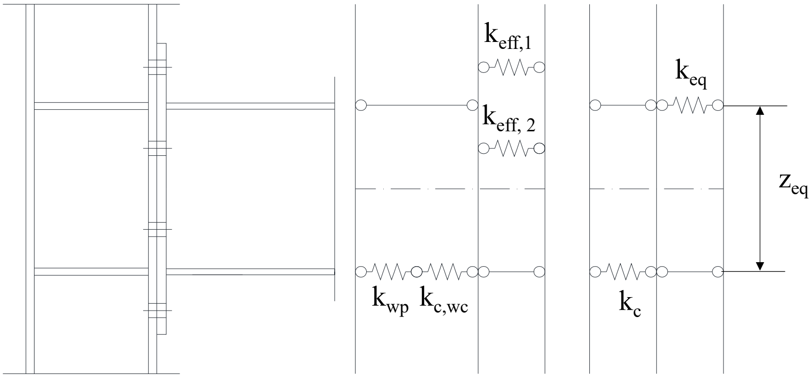

Figure 1-10: Effective and equivalent stiffness spring definition.

For each bolt-row all the contributions should be assembled in series and the effective stiffness coefficient $k_{\mathrm{eff,r}}$ for each bolt-row is to be evaluated by the formulation (see Figure 1-10):

$$k_{eff,r} = \frac{1}{\sum_i \frac{1}{k_{i,r}}} \tag{7}$$

where $k_{\mathrm{i,r}}$ is the stiffness coefficient of the generic bolt-row basic component. As a subsequent step, all the bolt-rows on the tension side will be assembled in parallel, as showed in Figure 1-10, and the equivalent stiffness coefficient on the tension side can be evaluated as:

$$k_{eq} = \frac{\sum_r k_{eff,r} \cdot h_r}{z_{eq}} \tag{8}$$

where h_{r} is the distance between the bolt row r and the center of compression and z_{eq} is the equivalent level arm defined as:

$$z_{eq} = \frac{\sum_r k_{eff,r} \cdot h_r^2}{\sum_r k_{eff,r} \cdot h_r} \tag{9}$$

Once the stiffness contribution on the tension side is defined, the initial joint stiffness can be evaluated as reported in the formulation:

$$S_{j,ini} = \frac{Ez_{eq}^{2}}{\mu \sum_i \frac{1}{k_i}} = \frac{Ez_{eq}^{2}}{\mu \left(\frac{1}{k_c} + \frac{1}{k_{eq}} \right)} \tag{10}$$

where E is the steel Young modulus; k_i is the stiffness coefficient for basic joint component i; z is the lever arm; μ is a stiffness ratio that depends on the ratio of the applied moment ($M_\mathrm{j,Ed}$) to the moment resistance ($M_\mathrm{j,Rd}$) of the joint, as reported hereinafter:

$$\mu = 1 \qquad if \qquad M_{j,Ed} \leq 2/3M_{j,Rd}$$

$$\mu = (1.5M_{j,Ed} / M_{j,Rd})^{\psi} \qquad if \qquad 2/3M_{j,Rd} \leq M_{j,Ed} \leq M_{j,Rd}$$

$$\psi : \quad EN1993-1-8 \quad table \quad 6.8$$

1.2.4 Rotational capacity

The rotational capacity is one of the most important characteristic of the beam-to-column joints due to its paramount influence on the overall structural response.

In this context it is important to understand and define the concept of ductility. At the joint level, the ductility, or as it is often called rotational capacity, can be defined as the ratio between the ultimate and the yielding rotation.

As a function of the designed joint typology, different limitations for ductility are introduced: for a full strength joint the rotational capacity verification can be neglected if the bending joint capacity ($M_{j,Rd}$) is at least 1.2 times larger than the connected beam capacity ($M_{pl,Rd}$). However, in order to avoid the local brittle failure (i.e. cracks in the welds or bolt failure) and according to the EN1998-1-1 [2], the joints should be designed to remain in elastic range.

On the other hand, partial strength joints should possess enough rotational capacity and be able to secure the development of all the plastic hinges in the structure. Therefore, an estimation of the joint rotational capacity is needed for the partial strength joint, as reported in EN1993-1-8 [1]. Two main scenarios are introduced by the code: (i) the column web panel in shear governs the limit state or (ii) the column flange/end-plate in bending yields.

In the first case, when it is the column web panel component that governs the failure, enough rotational capacity is ensured if:

$$h_W / t_W \leq 69\varepsilon \qquad (11)$$

Where h_w is the column web panel height, t_w is its thickness and ε is equal to the square root of 235/f_y.

Another possible solution, to guarantee sufficient rotational capacity to the joint, is to verify that both the following limitations are respected:

- The joint failure mode is governed by the column flange or by the end plate in bending;
- The thickness of the component that governs the failure satisfies:

$$t \leq 0.36d\sqrt{f_{ub} / f_y} \tag{12}$$

Where d is the bolt diameter, f_u is the bolt yielding stress and f_y is the plate yielding stress.

1.2.5 Moment rotation curve

The moment rotation curve of a joint (see Figure 1-11) is characterized by the following features: the joint bending capacity ($M_{j,Rd}$), the initial elastic stiffness ($S_{j,ini}$) and the rotational capacity (ϕ_{Cd}).

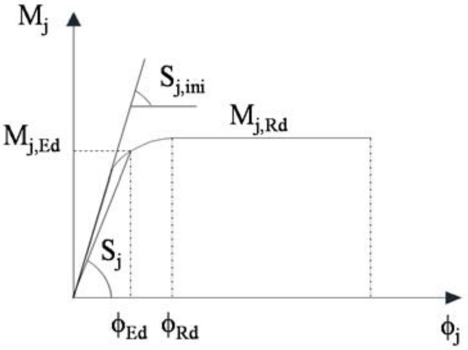

Figure 1-11: Design moment rotation characteristic for joint [1].

1.3 Criticisms of Eurocodes

The overview of EN1993-1-8 [1] procedure for the prediction of joint behavior, briefly summarized in the previous paragraph, needs some further considerations on the connection, the beam belonging to the joint and the column panel zone.

With particular regard to the extended stiffened joint, EN1993:1-8 does not provide adequate provisions to account for the influence of the rib stiffeners from the point of view both strength and stiffness. Moreover, specific provisions for the seismic design of joints are missing. Hereinafter the main criticisms of the Component method are briefly discussed:

1. EC3 assumes a priori a plastic distribution of forces at each bolt-row. However, since some components (e.g. the bolts) could provide insufficient ductility to guarantee the activation of the plastic strength of the other bolt-rows, the internal distribution of forces in the connection zone varies with the rotation level and it could differ from the one calculated. Therefore, in order to overcome this inconsistency, two possible approaches can be alternatively followed: (i) to correlate the calculated joint strength (and the relevant internal force distribution) with specified levels of joint rotation; (ii) to provide design criteria to guarantee the

formation of ductile mechanisms at each bolt-row having sufficient ductility to allow developing the plastic distribution of forces. The latter approach is the most effective, from the point of view of design, and it will be discussed in the following paragraph.

2. According to the Eurocodes the joints can be designed either as full-strength or partial-strength, with respect to the connected beam. These two different performance objectives may significantly modify the dissipative behavior of seismic resistant MRFs. Indeed, in the case of full strength joints, plastic hinges should form in the beams, while in the case of partial strength joints the plastic deformation should concentrate in the connection.

The full strength design strategy calls for the joint to guarantee a larger flexural overstrength with respect of the connected beams. Unfortunately, owing to the variability of steel strength and to the post-yield flexural overstrength of steel beams, these connections cannot have enough overstrength.

Indeed, in EN 1998-1-1 [2], the minimum required joint overstrength is equal to $1.1\times\gamma_{ov}\times M_{b,pl,Rd}$ (being $M_{b,pl,Rd}$ the beam plastic moment and γ_{ov} the ratio between the mean over the characteristic yield stress, generally assumed equal to 1.25) and it could be largely overcome in many cases.

3. Concerning partial strength joints, EN1998-1-1 [2] requires joints to have sufficient rotational capacity to guarantee the formation of a global mechanism.

The joint rotational response depends on the deformation behavior of each component constituting the joint (e.g. end-plate in bending, beam in tension, panel zone, bolts, etc.). Therefore, EN 1993 Part 1-8 expects the partial strength joints to have sufficient monotonic rotation capacity if designed in such a manner to concentrate the plastic deformations in those components capable of providing high ductility (e.g. the end-plate in bending), while the brittle components (such as bolts and welds) should behave elastically.

This criterion is sufficient for joints designed for gravity and wind loads. Regarding the seismic loading, EC8 refers to EC3 for the design and verification of members and connections and in case of semi-rigid and/or partial strength dissipative joints requires the following:

- the joints should have a rotational capacity consistent with the global deformations;

- members framing into the joints should behave in a stable manner at the ultimate limit state;
- the effect of joint deformation on global drift should be taken into account using either nonlinear static pushover analysis or non-linear dynamic time history analysis.

In addition, the joint should guarantee a rotational capacity at least equal to 0.035 rad for high ductility class (DCH) structures and 0.025 rad for medium ductility class (DCM) structures (provided that the design was conducted using a behavior coefficient q larger than 2). The cyclic rotation capacity should be ensured with a strength and stiffness degradation not greater than 20%. Finally, the column web panel shear deformation contribution should be less than 30% of the total rotational capacity.

Since no requirements and rules are provided to obtain this type of performance, EC8 requires design supported by specific experimental testing, resulting in impractical solutions within the typical time and budget constraints of real-life projects. As an alternative to design supported by testing, the code allows using analytical approaches based on experimental studies or prescribes to find existing data on experimental tests performed on similar connections in literature. It is clear that this procedure is unfeasible from the designer's point of view.

4. EC3 assumes perfectly plastic strength of the basic components, while disregarding the random variability of steel yield stress. These assumptions may lead to a flawed prediction of the joint failure mode. In particular the steel hardening could increase the ultimate strength corresponding to the potential mechanism thus activating undesirable failure modes (e.g. the hardening of the end-plate bending in a mode 1 could activate the bolt resistance; the beam hardening could activate the plastic strength of the connection, etc.). Moreover, the variability of yield stress could modify the joint ultimate strength; thus changing the weakest part and the expected failure mechanism. These considerations clearly highlight that it is difficult to guarantee both actual full strength behavior and appropriate ductility, in the case of partial strength joints.

5. The characterization of equivalent T-Stubs and corresponding effective lengths are not clearly provided for the connection’s bolt rows above the beam flange, when stiffeners are introduced. Indeed, the EC3 explicitly refers to extended unstiffened end-plate joints. Since no specific rules are provided, this implies that the designer has two alternatives: (i) assuming the effective lengths of the bolt rows of the column flange adjacent to a stiffener; (ii)

assuming the effective lengths of bolt row below the tension flange of the beam. These options may lead to an erroneous calculation of the strength of those bolt rows. Therefore, the future version of the EC3 should specify the appropriate yield line patterns for these bolt-rows. With this regard, a viable example is given by the Green Book P398 [4], which is based on the English BS EN 1993:1-8 and its UK National Annex, that gives more comprehensive and detailed rules to calculate yield line patterns.

6. According to EN1993:1-8 the shear strength of the column web panel should be calculated as the sum of the column web shear strength ($V_{\mathrm{wp,Rd}}$) and the additional shear strength ($V_{\mathrm{wp,add,Rd}}$) provided by the formation of local kinks in the column flanges. This requisite allows plastic deformation of the column web panel which are acceptable at ultimate limit states, for non-seismic conditions, and for seismic applications as well, for cases where dissipative joints are considered. Indeed, EN1998-1 [2] accepts that the column web panel shear deformation could contribute up to 30% of the plastic rotation capacity of the joint. However, this requirement is in opposition with the "strong column–weak beam" design philosophy, in which case full strength joints are assumed aiming to enforce plastic hinges in the beams, preserve the

columns integrity and minimize the residual interstorey drifts as well. The shear overstrength ($V_{\mathrm{wp,add,Rd}}$) should be neglected if the design purpose is to guarantee damage-free columns, because the column flange contribution is fully reached when the panel zone is in the post-yield range at a distortion about 4 times the yield rotation of web panel. Moreover, allowing the web panel to develop $V_{\mathrm{wp,add,Rd}}$ may lead to considerable post-earthquake residual deformations for deep columns, that correspond to large repairing costs. With this regard, it is clear that, in most cases, the column web should be strengthened by means of supplementary steel plates in order to increase the web area. However, it could be difficult to fulfil this aim following the requirements of EN1993:1-8. Indeed, according to Clause 6.2.6.1(6) in EN1993:1-8, the thickness of the supplementary web plate should be smaller than or equal to the column web thickness, neglecting any increase of the shear area for thicker plates regardless of whether a supplementary web plate is added on the other side of the column web. Cyclic tests carried out by Ciutina and Dubina [5] showed that the shear strength of the panel zone resistance increases proportionally to the shear area. Hence, the shear area can be increased by the total section of the supplementary plates. Moreover, the web panel strengthened by means of supplementary web plates proves to be very stable with good ductility and rotational capacity greater than 0.035 rad, value considered to guarantee the “high ductility” behavior required in EC8.

7. In EN1993:1-8, for extended end-plate connections the center of compression force transferred to the connection is assumed to be in line with the center of the compression flange of the beam. However, owing to the presence of the end-plate stiffener a larger lever arm is expected for ES connections, similarly to the case of haunched connections. The lever arm assumed by EN1993:1-8 may lead to over-conservative designs both for full and partial strength joints. Indeed, the smaller is the lever arm, the larger should be the strength of the basic component at each bolt-row. In the former case. this assumption solely leads to an increase of the constructional costs, in the latter case the design performance is not guaranteed and undesired plastic mechanisms might be activated (e.g. the column flexural strength). On the other hand, a larger lever arm might lead to smaller shear forces acting in the column web panel, with beneficial effects in terms of costs if supplementary web plates are necessary.

2 American design procedure: AISC358-16

In the USA, after the Northridge earthquake, recommendations for seismic design of extended stiffened bolted beam-to-column joints were developed within the SAC project and published as a series of FEMA documents [6]-[7] and then incorporated into the AISC358 [8] and AISC341 [9].

These seismic provisions require that beam-to-column connections should be designed with sufficient strength to guarantee the formation of plastic hinges into the beams and located close to the protruding part of the connection away from the column face. This design philosophy leads to having a strong column, a strong connection, and a weak beam [9] and it is introduced for both special (SMF) and intermediate (IMF) steel moment resisting frames in seismic applications.

To this aim, AISC358-16 specifies: (i) design, (ii) fabrication detailing and (iii) quality criteria, for connections that will be prequalified in accordance with the AISC Seismic Provisions for Structural Steel Buildings [9].

Connections can be considered as prequalified only when both their design and fabrication meet all the requirements and the rules described in the code. With particular regard to both stiffened and unstiffened extended bolted end-plate connections AISC358-16 (chapter 6) introduces three types of joint configurations: (i) un-stiffened four-bolt configuration (4E), (ii) stiffened four-bolt configuration (4ES) and (iii) stiffened eight-bolt configuration (8ES) (see Figure 2-1).

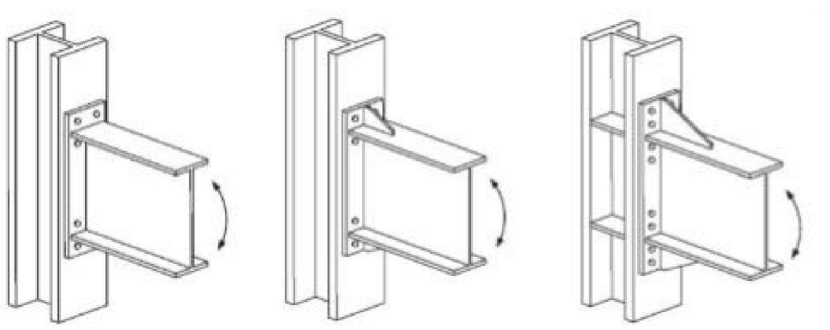

Figure 2-1: Extended, stiffened and un-stiffened, end-plate configuration: a) un-stiffened for bolt configuration (4E), b) stiffened for bolt configuration (4ES) and c) stiffened eight-bolt configuration (8ES) [8].

For each type of connection, the design procedure leads to a strong connection able to concentrate all the plastic demand in the connected beam.

Before starting the discussion on the American approach, two aspects have to be clarified: (i) the distinction between "connection" and "joint" is not clearly addressed in the American code with respect to the Eurocode, where the joint is defined as the combination of the connection and the column web panel; (ii) all the symbols in the following tables are according to the AISC358-16 nomenclature, and they can be different from the ones reported for the Eurocode and introduced in the previous paragraphs.

2.1 Prequalification limits

The limitations on joint geometry are summarized in Table 2.1 and in Figure 2-2 where for all three possible joint typologies the definition of the most important geometrical parameters are pointed out.

These ranges are related to the features of the joints tested within the SAC project.

Table 2.1: Parametric limit for prequalification (AISC358-16 table 6.1 [8]).

Parameter	Four-Bolt Unstiffened (4E)		Four-Bolt Stiffened (4ES)		Eight-Bolt Stiffened (8ES)	
	Max. in. (mm)	Min. in. (mm)	Max. in. (mm)	Min. in. (mm)	Max. in. (mm)	Min. in. (mm)
t_{bf}	3/4 (19)	3/6 (10)	3/4 (19)	3/8 (10)	1 (25)	9/10 (14)
b_{bf}	9 1/4 (235)	6 (152)	9 (229)	6 (152)	12 1/4 (331)	7 1/2 (190)
d	55 (1400)	13 3/4 (349)	24 (610)	13 3/4 (349)	36 (914)	18 (457)
t_p	2 1/4 (57)	½ (13)	1 1/2 (38)	1/2 (13)	2 1/2 (64)	¾ (19)
b_p	10 3/4 (273)	7 (178)	10 3/4 (273)	7 (178)	15 (381)	9 (229)
g	6 (152)	4 (102)	6 (152)	3 1/4 (83)	6 (152)	5 (127)
p_{fi}, p_{fo}	4 1/2 (114)	1 1/2 (38)	5 1/2 (140)	1 ¾ (44)	2 (51)	1 5/8 (41)
p_b	-	-	-	-	3 3/4 (95)	3 ½ (89)

Where: b_{bf}: is the beam flange width, b_p is the end-plate width, d is the connected beam depth, g is the horizontal distance between the bolts, p_b is the vertical distance between the inner and the outer bolts row (for the 8ES joint configuration), p_{fi} is the vertical distance between the beam flange and the nearest inside bolt row;

p_{fo} is the vertical distance between the beam flange and the nearest outside bolt row, t_{bf} the beam flange thickness and t_p the end-plate thickness.

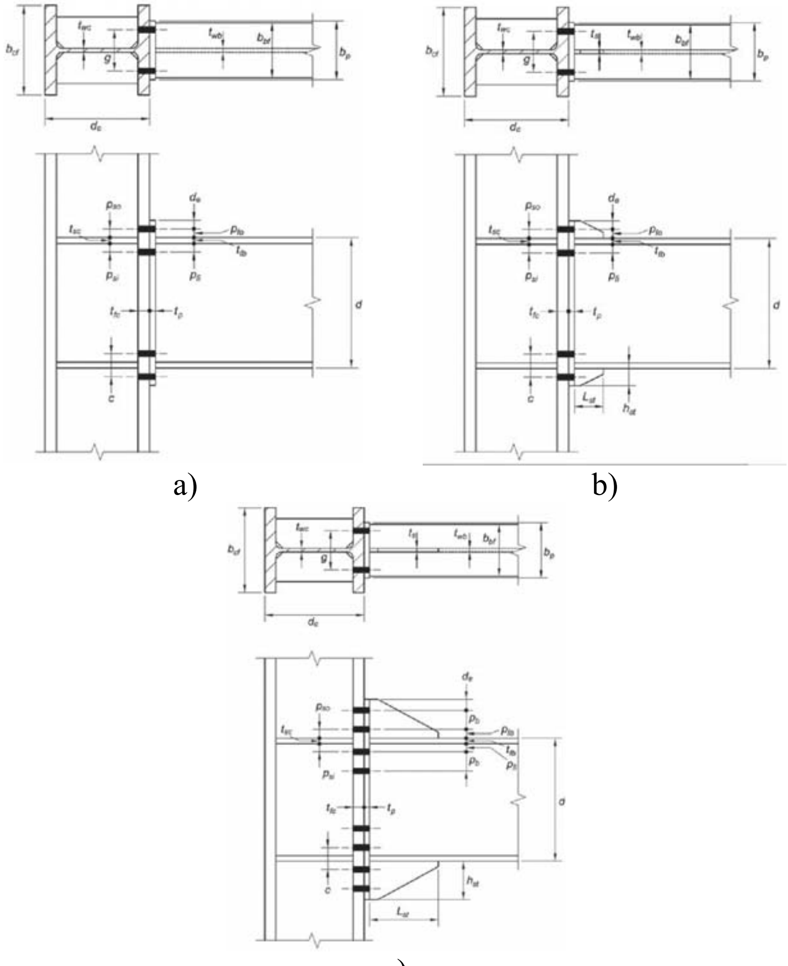

a) b)

c)

Figure 2-2: Geometrical dimensions of joints: 4E (a), 4ES (b), 8ES (c) [8].

2.2 Beam limitations

“Beams shall be rolled wide-flange or built-up I-shaped members conforming to the requirements Table 2.1.

At moment-connected ends of welded built-up sections, within at least the depth of beam or 3 times the width of flange, whichever is less, the beam web and flanges shall be connected using either a complete-joint-penetration (CJP) groove weld or a pair of fillet welds each having a size 75% of the beam web thickness but not less than 1/4 in. (6 mm). For the remainder of the beam, the weld size shall not be less than that required to accomplish shear transfer from the web to the flanges” AISC358-16 [144].

The beam geometry in terms of depth (d) and in terms of flange thickness should meet the table prescriptions; moreover, no limitations are provided on the weight per foot.

From the structural point of view, in order to limit the demand to the joint in terms of stiffness, two limitations are reported in terms of span-to-depth ratio: (i) 7 (or greater) for SMF and (ii) 5 (or greater) for IMF.

Moreover, both the lateral bracing system and the width-to-thickness ratio (between flanges and web) should conform to the AISC Seismic Prevision [AISC341-10 [9]].

Another important parameter to define is the protected zone that plays a central role in the definition of the system behavior. Indeed, this distance measured from the column face is introduced to ensure that the joint behavior is governed by the steel solution only without any appreciable influence of the concrete slab.

In line with this proposal, AISC358-16 gives two ways to define the protected zone in function of the joint typology (stiffened and unstiffened). For unstiffened connections (4E) the protected zone should be equal to the smaller between a distance equal to the depth of the beam, and three times the beam flange width.

Contrariwise, for stiffened connections (4ES and 8ES) the portion of beam from the column face, considered as protected zone, should be the lesser between: (i) the end of the rib stiffeners plus one-half the beam depth and (ii) three times the beam flange width.

2.3 Column limitations

The column depth, in case of: (i) rolled shape profile, (ii) built-up wide-flange columns and (iii) cruciform flanged columns, should not exceed the depth relative to a W36 (W920) steel profile.

Given their application in seismic zones, the column should be classified as a ductile element. Therefore, AISC358-16 limits the allowed columns in function of their width-to-thickness ratio according to AISC Seismic prevision [ASIC341-10 Chapter D, D1-4 [9]].

No limitations are imposed on either the column flange thickness or on the weight per foot.

Moreover, it is important to note that only if the end plate is bolted on the column flange and not on the web side, the joint can be considered as prequalified.

2.4 Column-beam relationship limitation

The beam-to-column limitations, both in terms of the column web panel zone properties and in terms of column-beam moment ratio, should conform to the AISC Seismic Provision [9]. For instance, in the case of Special moment frames (SMF) the internal hierarchy between the column and the beam capacity should be verified [AISC341-10 Chapter E, E3-4 [9]].

2.5 Continuity Plates

The continuity plates can be introduced to increase the column flange bending resistance, changing the yielding path or to meet some local verifications both in tension and in compression.

Therefore, the necessity of continuity plates will be investigated in Table 2.3 where all column design requirements are summarized. The requirements regarding the continuity plate welds have to be in accordance with the AISC Seismic Provisions [for IMF and SMF respectively ASIC341-10 Chapter E, E3-6f], except for continuity plates of thickness less than or equal to 3/8 in. (10 mm), where double-sided fillet welds are allowed.

2.6 Bolts

All bolts should be preloadable high-strength bolts according to ASTM A325/A325M, A490/A490M, F1852 or F2280. All information about the installation requirements and their quality control are reported in the AISC Seismic Provisions [AISC341-10 [9]].

2.7 Connection detailing

AISC358-16 provides important limitations for the connection geometry and welds; and in particular for: (i) Gauge dimension, (ii) Pitch and Row Spacing, (iii) End-plate width, (iv) Rib stiffeners, (v) finger shims, (vi) Composite slab detailing and (vii) welding details.

1. The gauge (g) maximum dimension is limited to the beam width.

2. The minimum pitch distance is equal to the bolt diameter plus 1/2 in. (13 mm) for bolts up to 1 in. (25 mm) diameter, and to the bolt diameter plus 3/4 in. (19 mm) for larger diameter bolts.

The pitch distances, p_{fi} and p_{fo}, are the distances from the face of the beam flange to the centerline of the nearer bolt row.

The pitch distances, p_{si} and p_{so}, are the distances from the face of the continuity plate to the centerline of the nearer bolt row.

The spacing, p_b, is the distance between the inner and outer row of bolts in an 8ES end-plate moment connection. The spacing of the bolt rows shall be at least 22/3 times the bolt diameter.

3. The end–plate width should be at least equal to or larger than the connected beam flange width; in line with this limitation, the effective end-plate width should not be greater than the connected beam flange thickness plus 1 in. (25 mm).

4. Also AISC358-16 introduces a limitation on the minimum stiffener (also called rib) length and fixes its maximum inclination at 30°:

$$L_{st} = \frac{h_{st}}{tan\,30°} \quad (1) \qquad (13)$$

where L_{st} is the rib base and h_{st} is the rib height, evaluated from the end-plate edge to the beam flange.

Moreover, both on the beam flange and on the end-plate side, the stiffener plates should end, with landings approximately 1 in. (25 mm) long as reported in Figure 2-3.

According to AISC358-16 par 6.9: "The stiffener shall be clipped where it meets the beam flange and end-plate to provide clearance between the stiffener and the beam flange weld".

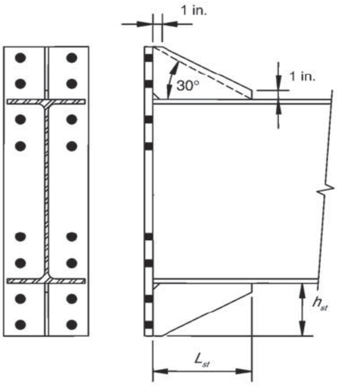

Figure 2-3: End-plate stiffener layout and geometry for 8ES connection configuration [8].

In order to impose a resistance hierarchy between the beam web and the rib stiffeners AISC358-16 requires that, when the beam and end-plate stiffeners have the same material strengths, the rib thickness should be greater than, or equal to, the beam web thickness. However, if the two elements have a different material the rib thickness should be greater than or equal to the beam thickness times the ratio between their material strengths [pr.6.9].

This limitation is also reported in the end-plate and bolt design procedure at step 10.

5. The use of finger shims (see Figure 2-4) at the top and/or bottom of the connection and on either one or both sides is permitted, but subjected to the limitations of the RCSC Specifications [8].

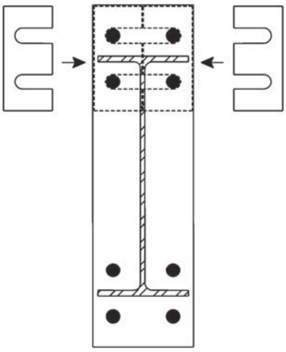

Figure 2-4: Finger shims [8].

6. In addition to the protected zone limitations (for the intermediate moment resisting frames IMF), from the column face, for a distance equal to $1^{1/2}$ times the depth of the beam, no welded shear stud connectors should be placed on the beam flange.

7. AISC358-16 also introduces limitations and indications on the weld that should be used in function of the connected elements (pr. 6.9-7 [8]). Therefore, for the bolted end-plate connection, in

line with the expected stress distribution, different type of welds are required. Between the beam flange and the end-plate, given the expected high stress concentration, CJP groove welds are required. Along this line, also the welds between both beam flange and end-plate with the rib stiffeners should be CJP groove welds. Only in the case the rib is equal to or thinner than 3/8in. (10mm) fillet welds (designed to develop the rib capacity) are allowed.

Moreover, since the stress demand is smaller at the level of the beam web and end-plate, either fillet welds (designed to allow the development of the full beam web tension resistance) or the CJP groove weld can be used. Full depth PJP groove welds are permitted where Back-gouging of the root is not required in the flange directly above and below the beam web for a length equal to $1.5k_1$.

Finally, due to their brittle failure, the weld access hole should not be used.

2.8 Design procedure for the End-plate and bolt diameter

The design procedure is structured in two macro-steps; the first one is the design of the end-plate and bolts, while the second is focused on the column design but without any prescription for the column web panel where AISC358-16 refers to the Seismic Provisions [9].

In the end-plate and bolt design step, twelve sub-steps can be identified having the main aim to define the bolt diameter, the end-plate thickness, and also the local action (F_{fu}.). F_{fu} represents the equivalent force (both in terms of compression and tension) coming from the design moment applied to the connection respect to the internal lever arm (it will be further discussed in the following tables).

Before starting with the design procedure it is important to define both the resistance factor and the beam bending plastic capacity. Indeed, AISC358-16 pr.2.4 [8], defines the value of the resistance factor ϕ_d (equal to 1) for ductile and ϕ_n (equal to 0.9) for non-ductile limit states respectively. These values will be introduced in the design procedure and the equation to evaluate the probable maximum moment that is a fundamental parameter for all the joint design:

$$M_{pr} = C_{pr} R_y F_y Z_e \qquad (14)$$

where R_y is the ratio between the expected yield stress to the specified minimum yield stress F_y. The plastic section modulus (that correspond to the W_{pl} in Eurocode symbols definition) is Z_e. C_{pr} is a factor that takes into account the peak of the connection strength (i.e. material hardening, local resistance) and it can be evaluated as:

$$C_{pr} = \frac{F_y + F_u}{2F_y} \leq 1.2 \qquad (15)$$

Once M_{pr} is defined, the design procedure can start with the first step, which is focused on the definition of the required bending moment at column face (M_f). Therefore, once the connection requirements are checked, it is possible to define the required bolt diameter and the end-plate thickness (steps 3 and 5 respectively). Once all the geometrical dimensions are defined, the local force F_{fu} (step 7) is evaluated in order to verify the local resistances of the connection components.

This equivalent force plays a central role in the local verifications and will also be introduced in the column design phase to verify the column flange in bending, the column web welding, the column web buckling and the column web crippling.

The complete design procedure is described in the following, focusing the attention on the meaning of each step; moreover, the column web design, according to AISC341 [9] and AISC360 [10] is presented.

Table 2.2: Macro-step 1 [8].

End-plate and bolt diameter design	
Step 1	Determination of the connected member size and evaluation of the Moment at the column face
	$M_f = M_{pr} + V_u + S_h$ where: M_{pr} is the maximum probable moment at the plastic hinge S_h is the distance from the column face to the plastic hinge V_u is the shear force at the end of the beam: $V_u = \frac{2M_{pr}}{L_h} + V_{gravity}$ b_f is the beam flange width; d is the connection depth; L_h is the distance between plastic hinge locations; L_{st} is the rib stiffeners length; t_p is the end-plate thickness; $V_{gravity}$ is the shear force resulting from: $1.2D + f_1 L + 0.2S$ D are the dead loads; L are the live loads; f_1 is a load factor from the applicable building code for live loads, but not less than 0.5; S is the seismic demand.
Step 2	The second step is concerned with the selection of both the connection configuration (4E, 4ES and 8ES) and the preliminary joint geometrical dimensions (g, p_{fi}, p_{fo}, p_b, h_i, etc) that will be verified later on in the design procedure.

End-plate and bolt diameter design	
Step 3	Determination of the required bolt diameter
	In function of the joint configuration defined in step 2, two formulations are presented to evaluate the bolt diameter required: ➢ 4E and 4ES: $d_{b,req} = \sqrt{\dfrac{2M_f}{\pi F_{nt}(h_0 + h_1)}}$ ➢ 8ES: $d_{b,req} = \sqrt{\dfrac{2M_f}{\pi F_{nt}(h_1 + h_2 + h_3 + h_4)}}$ where: F_{nt} is the nominal bolt tensile strength; h_0 is distance from the beam compression flange centerline to the centerline of the *i*th tension bolt row; h_i is the distance from the beam compression flange centerline to the tension-side outer bolt row. 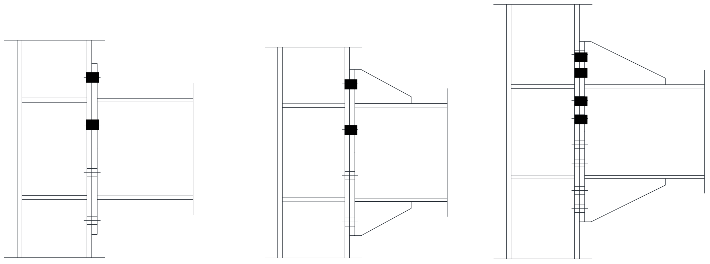 4E 4ES 8ES The formulation is obtained considering the plate as infinitely elastic and with a linear force distribution
Step 4	Define an equivalent bolt diameter according to the minimum requirement obtained in step 3

<table>
<tr><th colspan="2">End-plate and bolt diameter design</th></tr>
<tr><td rowspan="2">Step 5</td><td>Determinate the required end-plate thickness</td></tr>
<tr><td>The definition of the end-plate resistance is function of the yielding path distribution on the plate, therefore it strongly depends on the joints configuration.

$$t_{b,req} = \sqrt{\frac{1.11M_f}{F_{yp}Y_p}}$$

where:
F_{yp} is is the specified end-plate minimum yielding stress;
Y_p is end-plate yield line mechanism parameter (see Figure 2-5).

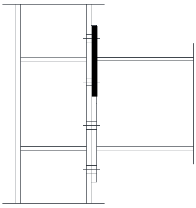
4E

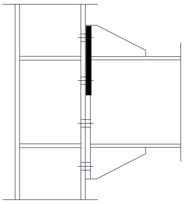
4ES

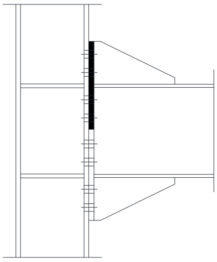
8ES</td></tr>
</table>

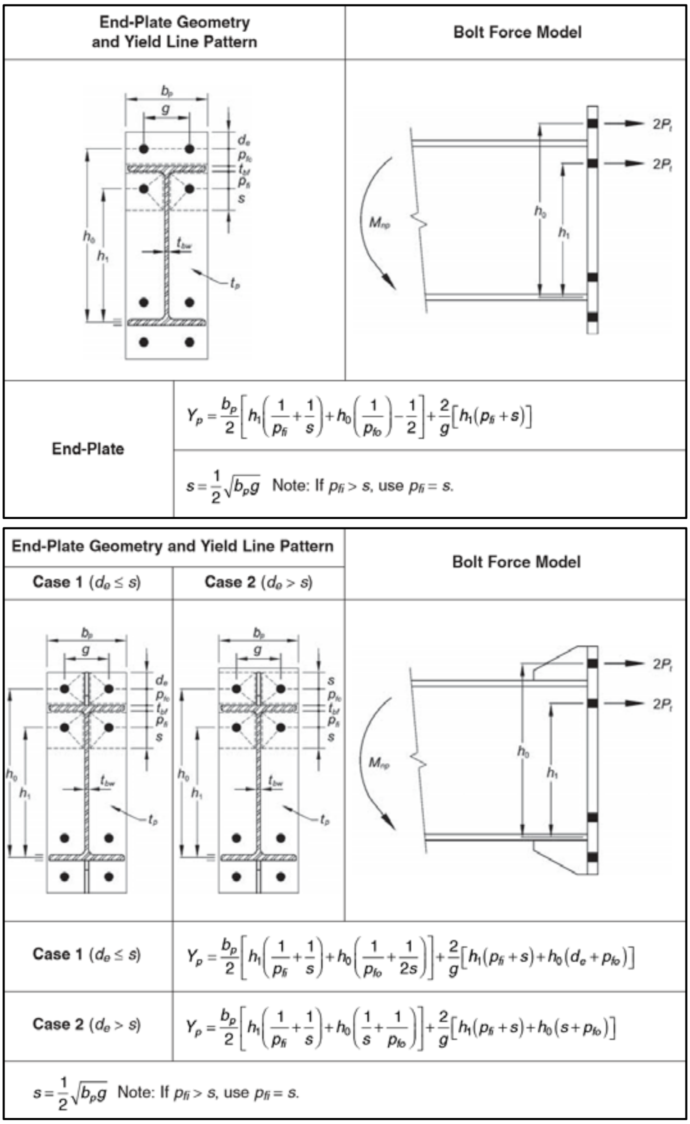

End-Plate Geometry and Yield Line Pattern	Bolt Force Model
End-Plate	$Y_p = \frac{b_p}{2}\left[h_1\left(\frac{1}{p_{fi}}+\frac{1}{s}\right)+h_0\left(\frac{1}{p_{fo}}\right)-\frac{1}{2}\right]+\frac{2}{g}\left[h_1\left(p_{fi}+s\right)\right]$
	$s=\frac{1}{2}\sqrt{b_p g}$ Note: If $p_{fi}>s$, use $p_{fi}=s$.

End-Plate Geometry and Yield Line Pattern		Bolt Force Model
Case 1 ($d_e \leq s$)	**Case 2** ($d_e > s$)	
Case 1 ($d_e \leq s$)	$Y_p = \frac{b_p}{2}\left[h_1\left(\frac{1}{p_{fi}}+\frac{1}{s}\right)+h_0\left(\frac{1}{p_{fo}}+\frac{1}{2s}\right)\right]+\frac{2}{g}\left[h_1\left(p_{fi}+s\right)+h_0\left(d_e+p_{fo}\right)\right]$	
Case 2 ($d_e > s$)	$Y_p = \frac{b_p}{2}\left[h_1\left(\frac{1}{p_{fi}}+\frac{1}{s}\right)+h_0\left(\frac{1}{s}+\frac{1}{p_{fo}}\right)\right]+\frac{2}{g}\left[h_1\left(p_{fi}+s\right)+h_0\left(s+p_{fo}\right)\right]$	
$s=\frac{1}{2}\sqrt{b_p g}$ Note: If $p_{fi}>s$, use $p_{fi}=s$.		

Figure 2-5: Yield line mechanism parameter [8] for the 4E and 4ES joint configurations.

End-plate and bolt diameter design	
Step 6	Define the end-plate thickness according to the minimum requirement defined in step 5
Step 7	Definition of the F_{fu} F_{fu} is the transversal force that will be introduced to verify all the compression and tension local actions: $F_{fu} = \sqrt{\frac{M_f}{d - t_{bf}}}$ where d is the beam depth and t_{bf} is the beam flange thickness. 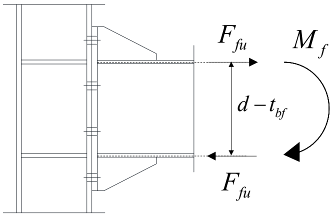
Step 8	Shear yielding failure Verification of the shear resistance respect the tension action F_{fu} (just for 4E joint configuration): $F_{fu} / 2 \leq R_n = 0.6 F_{yp} b_p t_p$ where b_p is the end-plate width to be not greater than the beam flange width. 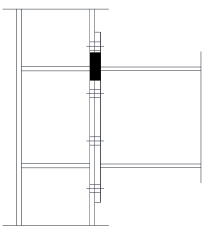 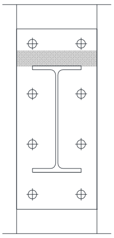

End-plate and bolt diameter design

Step 9

Shear rupture of the extended portion of the end-plate

Verification of the shear of the extended portion of the end-plate (just for 4E joint configuration):

$$F_{fu} / 2 \leq R_n = 0.6 F_{up} A_n$$

where:

F_{up} is the specified end-plate minimum tensile stress;
d_b is the bolt diameter;
A_n is the end-plate net area:

- In terms of in^2 $A_n = t_p \left[b_p - 2(d_b + 1/8) \right]$
- In terms of mm^2 $A_n = t_p \left[b_p - 2(d_b + 3) \right]$

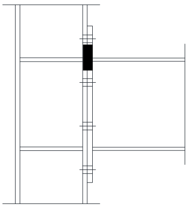

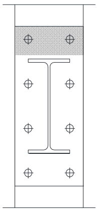

Step 10

Stiffeners verification

For both 4ES and 8ES the rib geometry should be verified; two verification are introduced in this step: (i) on the thickness and (ii) against the buckling phenomena.

Strength check (i.e. thickness verification)

$$t_s \geq t_{bw} \left(\frac{F_{yb}}{F_{ys}} \right)$$

where:

t_{bw} is the beam web thickness;
t_s is the rib thickness;
F_{yb} is the specified beam minimum tensile stress;
F_{ys} is the specified stiffener minimum tensile stress.

End-plate and bolt diameter design	
Step 10	Stiffeners verifications
	Buckling check (i.e. slenderness verification) $\frac{h_{st}}{t_s} \le 0.56\sqrt{\frac{E}{F_{ys}}}$ Where h_{st} is the rib height defined as reported in figure, all the welds prescriptions are already reported in the prequalification limit paragraph 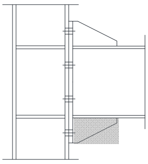 4ES 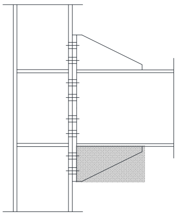 8ES
Step 11	Connection shear rupture
	The connection shear rupture is related to the bolt on the compression side, therefore: $V_u \le R_n = (n_b) F_{nv} A_b$ where: n_b is the number of bolt on the compression side; A_b is the bolt nominal gross area; F_{nv} is the bolt nominal shear strength; V_u is the shear force at the beam end. 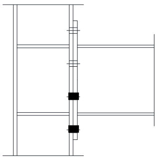 4E 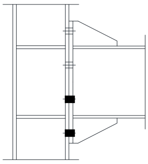 4ES 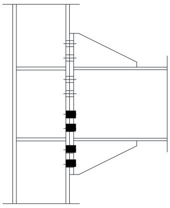 8ES

<table>
<tr><th colspan="2">End-plate and bolt diameter design</th></tr>
<tr><td rowspan="2">Step 12</td><td>Bolt bearing/tear out failure</td></tr>
<tr><td>The bearing/tear-out failure that can affect both the column and the end-plate can be verified with :
$$V_u \le R_n = (n_i) r_{ni} + (n_0) r_{no}$$
where:
n_i is the number of inner bolts;
n_o is the number of outer bolts;
r_{ni} is: $r_{ni} = 1.2 L_c t F_u < 2.4 d_b t F_u$
r_{no} is: $r_{n0} = 1.2 L_c t F_u < 2.4 d_b t F_u$
L_c is the clear distance, in the force direction, between edge of the adjacent hole or edge of material;
F_u is the specified end-plate minimum tensile stress;
d_b is the bolt diameter;
t is the end-plate or column flange thickness.</td></tr>
</table>

2.9 Design procedure on the column side

In the following tables, all the design steps of the column side macro-step are reported and explained:

Table 2.3 : Column-side design steps.

Column-side design	
Step 1	Check the column flange for the flexural yielding
	The column flange thickness should be verified to check if it meets the minimum thickness required by: $$t_{cf} \geq \sqrt{\frac{1.11M_f}{F_{yc}Y_c}}$$ where: F_{yc} is the specified column flange minimum tensile stress; Y_c is the column flange yield mechanism; t_{cf} is the column flange thickness. 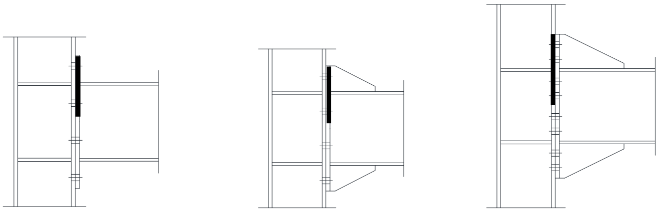 4E 4ES 8ES If a greater value of thickness is required two approaches can be followed: (i) increase the column size or (ii) introduce the continuity plates. Indeed, introducing the stiffeners, the yielding mechanism (Y_c) will change, increasing the column resistance.

Column-side design	
Step 2	Required stiffeners force
	The column flange flexural design strength is: $M_{cf} = F_{yc} Y_c t_{cf}^2$ where: Y_c is the unstiffened column yield mechanism. Therefore if the continuity plates are required to increase the column bending capacity, the relative force required of the stiffeners is evaluate by: $R_n = \frac{M_{cf}}{(d - t_{bf})}$ 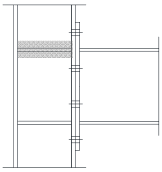 4E 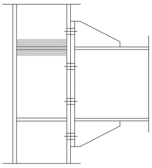 4ES 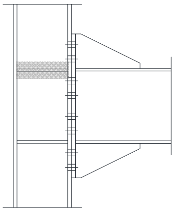 8ES

<table>
<tr><th colspan="2">Column-side design</th></tr>
<tr><td rowspan="2">Step 3</td><td>Local web column</td></tr>
<tr><td>$F_{fu} \le R_n = C_t(6k_c + t_{bf} + 2t_p)F_{yc}t_{cw}$
where:
C_t is 0.5, if the distance from the column top to the top beam flange face is less than the column depth, otherwise is 1;
F_{yc} is the specified column web yielding stress;
k_c is the distance from the outer column flange to the web fillet weld toe;
t_{cw} is the column web thickness.</td></tr>
<tr><td rowspan="2">Step 4</td><td>Unstiffened column web buckling</td></tr>
<tr><td>The position of the compression center is located at the centerline of the beam flange; indeed a local column web panel buckling verification is needed.
➢ If F_{uf} is applied at a distance greater than $d_c/2$ from the end of the column:
$F_{fu} \le R_n = \dfrac{24t_{cw}^3\sqrt{EF_{yc}}}{h}$
➢ If F_{uf} is applied at a distance less than $d_c/2$ from the end of the column:
$F_{fu} \le R_n = \dfrac{12t_{cw}^3\sqrt{EF_{yc}}}{h}$
where h is the clear distance between flanges minus the fillet weld</td></tr>
</table>

<table>
<tr><th colspan="2">Column-side design</th></tr>
<tr><td rowspan="2">Step 5</td><td>Column web crippling</td></tr>
<tr><td>

$$F_{fu} \leq R_n$$

If F_{fu} is at a distance greater than or equal to $d_c/2$ from the end of the column:

$$R_n = 0.8t_{cw}^3\left[1+3\left(\frac{N}{d_c}\right)\left(\frac{t_{cw}}{t_{cf}}\right)^{1.5}\right]\sqrt{\frac{EF_{yc}t_{cf}}{t_{cw}}}$$

If F_{fu} is at a distance less than $d_c/2$ from the end of the column:

- If $N/d_c \leq 0.2$

$$R_n = 0.4t_{cw}^3\left[1+3\left(\frac{N}{d_c}\right)\left(\frac{t_{cw}}{t_{cf}}\right)^{1.5}\right]\sqrt{\frac{EF_{yc}t_{cf}}{t_{cw}}}$$

- If $N/d_c > 0.2$

$$R_n = 0.4t_{cw}^3\left[1+\left(\frac{4N}{d_c}-0.2\right)\left(\frac{t_{cw}}{t_{cf}}\right)^{1.5}\right]\sqrt{\frac{EF_{yc}t_{cf}}{t_{cw}}}$$

where:
N is: $N = b_f + 2w + 2t_p$;
d_c is the column overall depth;
t_p is the end-plate thickness.

</td></tr>
</table>

<table>
<tr><th colspan="2">Column-side design</th></tr>
<tr><td rowspan="2">Step 6</td><td>Required strength for the continuity plate</td></tr>
<tr><td>If stiffener plates are required for any of the column limit states described, the required stiffener strength is:
$$F_{su} = F_{fu} - min(R_n)$$
where Fsu is the minimum design strength for:
➢ Column flange bending (step 2);
➢ Column web welding (step 3);
➢ Column web buckling (step4);
➢ Column web crippling (step 5).</td></tr>
<tr><td>Step 7</td><td>Check the column web panel in accordance with the prequalification limits section.</td></tr>
</table>

The AISC358 design procedure provides all the steps to evaluate and verify the connection geometry, but more information are needed to design the column web panel. Indeed, [8] redirects to the AISC Seismic provision and to AISC360 [10] for the definition of the column web panel behavior; in the following all of these prescriptions are summarized.

Moreover, it should be noted that the AISC360 [10] verification regards just the column web panel, but due to local action the column flange local buckling should also be verified.

Table 2.4: AISC 341 [9] column verifications.

Column-side design	
AISC360 – J10 – 1	Flange local buckling
	Flange local buckling $R_n = 6.25 F_y t_f^2$ where: F_{yf} is the specified column flange yielding stress; t_f is the thickness of the loaded flange.
AISC360 – J10 – 2	Web local yielding
	When the concentrated force is applied at a distance from the profile end which is greater than its depth d: $R_n = F_{yw} t_w (5k + l_b)$ When the concentrated force is applied at a distance from the profile end which is equal or less than its depth d: $R_n = F_{yw} t_w (2.5k + l_b)$ where: F_{yw} is the specified column flange yielding stress; k is the distance from outer face of the flange to the web toe of the fillet; l_b is the bearing length; t_w is the web thickness.

Column-side design	
AISC360 – J10 – 3	Web local crippling
	When the concentrated compressive force to be resisted is applied at a distance from the member end that is greater than or equal to d/2 $R_n = 0.8t_w^2\left[1+3\left(\frac{l_b}{d}\right)\left(\frac{t_w}{t_f}\right)^{1.5}\right]\sqrt{\frac{EF_{yw}t_f}{t_w}}$ $R_n = 0.4t_w^2\left[1+3\left(\frac{l_b}{d}\right)\left(\frac{t_w}{t_f}\right)^{1.5}\right]\sqrt{\frac{EF_{yw}t_f}{t_w}}$ $R_n = 0.4t_w^2\left[1+3\left(\frac{4l_b}{d}-0.2\right)\left(\frac{t_w}{t_f}\right)^{1.5}\right]\sqrt{\frac{EF_{yw}t_f}{t_w}}$ where: F_{yf} is the specified column flange yielding stress; t_f is the loaded flange.
AISC360 – J10 – 5	Web compression buckling
	$R_n = \frac{24t_w^3\sqrt{EF_{yw}}}{h}$ where: F_{yf} is the specified column flange yielding stress; t_f is the loaded flange.

Column-side design	
AISC360 – J10 – 6	Web panel in shear
	When the effect of the panel zone is not considered in the frame stability: If $P_r \leq 0.4P_c$ $R_n = 0.6F_y d_c t_w$ If $P_r > 0.4P_c$ $R_n = 0.6F_y d_c t_w \left(1.4 - \frac{P_r}{P_c} \right)$ When the effect of the panel zone is considered in the frame stability: If $P_r \leq 0.75P_c$ $R_n = 0.6F_y d_c t_w \left(1 + \frac{3b_{cf} t_{cf}^2}{d_b d_c t_w} \right)$ If $P_r > 0.75P_c$ $R_n = 0.6F_y d_c t_w \left(1 + \frac{3b_{cf} t_{cf}^2}{d_b d_c t_w} \right) \left(1.9 - \frac{1.2\,P_r}{P_c} \right)$ where: F_{yf} is the specified column flange yielding stress; A_g is the gross cross-sectional area of member; b_{cf} is the column flange width; d_b is the beam depth; d_c is the column depth; F_y is the specified column web yielding stress; $P_y = F_y A_g$, axial yield strength of the column; t_{cf} is the column flange thickness; t_w = column web thickness;

In the case one or more of the previous verifications are not satisfied, transversal stiffeners (continuity plates) or doubler plates should be used; except for the first case, where in order to avoid the flange buckling only the transversal stiffener can be introduced.

Moreover, AISC360-16 [10] provides the following limitations for the doubler plate introduction:

- Doubler plates required for compression strength shall be designed in accordance with the requirements of Chapter E [10];
- Doubler plates required for tensile strength shall be designed in accordance with the requirements of Chapter D [10];
- Doubler plates required for shear strength shall be designed in accordance with the provisions of Chapter G [10];
- Doubler plates shall comply with the following additional requirements: (i) the thickness and extent of the doubler plate shall provide the additional material necessary to equal or exceed the strength requirements; (ii) the doubler plate shall be welded to develop the proportion of the total force transmitted to the doubler plate.

References

[1] EN 1993:1-8, Design of steel structures - Part 1-8: Design of joints. CEN 2005.

[2] EN 1998-1, Design of structures for earthquake resistance - Part 1: General rules, seismic actions and rules for buildings. CEN 2005.

[3] Girao Coelho A. M., da Silva L. S., Bijlaard F.S.K . (2004). Experimental assessment of the ductility of extended end plate connections. Engineering Structures 26, 1185–1206.

[4] Joints in Steel Construction: Moment-Resisting Joints to Eurocode 3 (P398). Edited by The Steel Construction Institute and The British Constructional Steelwork Association, 2013, ISBN 978-1-85-942209-0.

[5] Ciutina A. L., Dubina D. (2008). Column Web Stiffening of Steel Beam-to-Column Joints Subjected to Seismic Actions. Journal of Structural Engineering, 134(3), 505–510.

[6] FEMA (2000a), FEMA-350, Recommended Seismic Design Criteria for New Steel Moment Frame Buildings, Federal Emergency Management Agency, Washington, DC.

[7] FEMA (2000b), FEMA-353, Recommended Specifications and Quality Assurance Guidelines for Steel Moment Frame

Construction for Seismic Applications, Federal Emergency Management Agency, Washington, DC.

[8] ANSI/AISC 358-16 (2016). Prequalified Connections for Special and Intermediate Steel Moment Frames for Seismic Applications.

[9] ANSI/AISC 341-10 (2010). Seismic Provisions for Structural Steel Buildings. American Institute of Steel Construction.

[10] ANSI/AISC 360-16 (2016). Specification for Structural Steel Buildings. American Institute of Steel Construction.

List of figures

Figure 1-1: Joint classification in function of the stiffness [1]. . 71
Figure 1-2: Full strength bending capacity limitations. 73
Figure 1-3: Joint strength classification [1]. 74
Figure 1-4: Basic components model: a) the spring element, b) the link element. 76
Figure 1-5: Main basic components of the extended beam-to-column joint. 76
Figure 1-6: Equivalent T-stub in tension side [3]. 78
Figure 1-7: Yielding line distribution. 79
Figure 1-8: Combination of all the spring and the link............. 86
Figure 1-9: Basic component stiffness spring........................... 97
Figure 1-10: Effective and equivalent stiffness spring definition. 97
Figure 1-11: Design moment rotation characteristic for joint [1]. 101
Figure 2-1: Extended, stiffened and un-stiffened, end-plate configuration: a) un-stiffened for bolt configuration (4E), b) stiffened for bolt configuration (4ES) and c) stiffened eight-bolt configuration (8ES) [8]. 111

Figure 2-2: Geometrical dimensions of joints: 4E (a), 4ES (b), 8ES (c) [8]. 114
Figure 2-3: End-plate stiffener layout and geometry for 8ES connection configuration [8]. 120
Figure 2-4: Finger shims [8]. 121
Figure 2-5: Yield line mechanism parameter [8] for the 4E and 4ES joint configurations. 129

List of tables

Table 1.1: Description of the main basic components....77
Table 1.2: T-stub failure mode and resistance....80
Table 1.3: Joint components according to EN1993-1-8 [1]. 82
Table 1.4: First bolt row line resistance evaluation....90
Table 1.5: Second bolt row line resistance. 92
Table 1.6: Third bolt row line resistance (a). 94
Table 1.7: Third bolt row line resistance (b). 96
Table 2.1: Parametric limit for prequalification (AISC358-16 table 6.1 [8]). 113
Table 2.2: Macro-step 1 [8]. 126
Table 2.3 : Column-side design steps. 134
Table 2.4: AISC 341 [9] column verifications. 139

CHAPTER IV

Experimental tests on the T-stub

Introduction

The bolt behavior can strongly influence the joint stiffness and strength and, especially in seismic zones, it plays a fundamental role in the definition of the joint ductility. As anticipated in Chapter II, EN1993-1-8 [1] allows the use of both HV and HR without making any distinction between them. Conversely, as shown by D'Aniello et al. [2], these two types of pre-loadable bolts are characterized by different ultimate tensile response. Therefore, the aim of this chapter is to investigate the influence of the type of pre-loadable bolt on the behavior of T-stub connections designed for mode 2 and 3. To this end, sixteen experimental tests were performed.

1 Tensile Behavior of pre-loadable bolts

As discussed in Chapter II, HV and HR bolts show different behavior under tensile action. The failure of HR bolts occurs in the shank and it has lower displacement capacity than HV assemblies that fail for nut stripping.

D’Aniello et al [2] investigated the HV and HR bolts failure mode in case of a pure axial load (see Figure 1-1). Figure 1-2 depicts the two different failure modes and relevant response curves of HV and HR bolts.

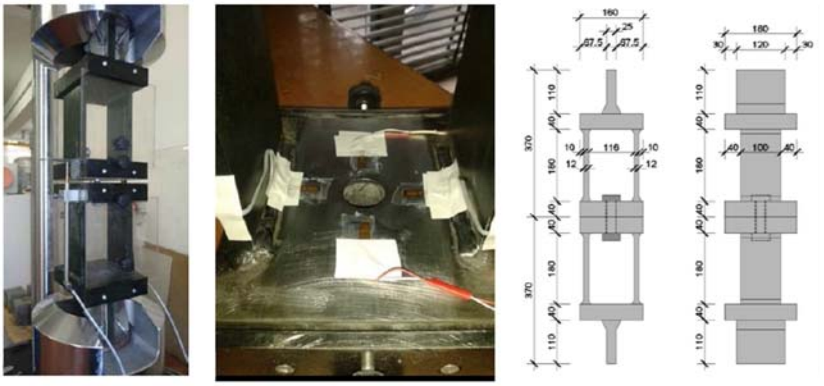

Figure 1-1: Bolts investigation UNINA setup [2].

Due to the nut stripping, the post-peak response of HV bolts has a saw-teeth profile corresponding to the failure of the threads. Contrariwise, HR bolts show a different force displacement curve; once reached the maximum value of deformation (around 6mm) the bolts present a brittle failure (in the shank) without showing any reserve of resistance.

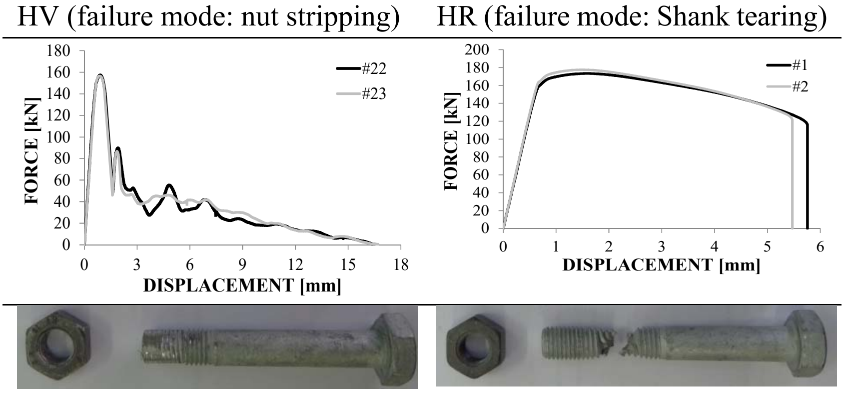
HV (failure mode: nut stripping) HR (failure mode: Shank tearing)

Figure 1-2: HV and HR bolts failure mode under monotonic load [2].

2 Investigated T-stub

The influence of the bolt failure on the T-stub behavior is a function of its design performance. Therefore, as anticipated in Chapter III, the theory recognizes three T-stub failure modes, in function of the ratio between the bolts and the plate resistance (see Figure 2-1):

- Mode 1 – characterized by the complete plasticization of the plate, whereas the bolts are not involved in the failure mechanism.
- Mode 2 – characterized by a combined mechanism of plate plasticization and failure of the bolts.
- Mode 3 - characterized by the failure of the bolts and it does not involve any plastic engagement of the T-stub flange.

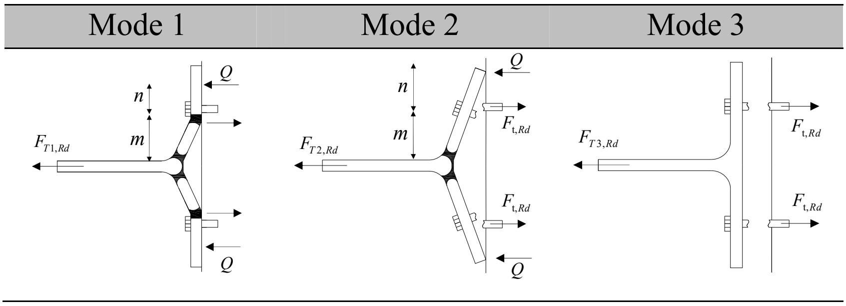

Figure 2-1: T-Stub failure mode

Moreover, the T-stub behavior can be summarized on the η-β plane as reported in Figure 2-2.

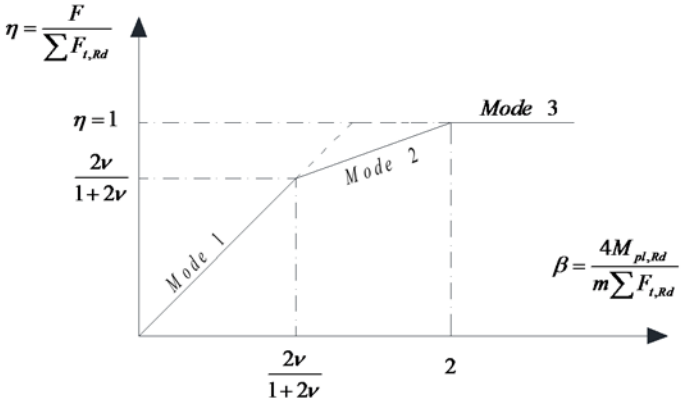

Figure 2-2: T-Stub resistance and corresponding mechanism according to EN1993:1-8 [1]

Where β is the ratio between the flexural strength of the connected plate ($M_{pl,Rd}$), and the axial strength of the bolts ($F_{t,Rd}$) and η, the ratio reported in the vertical axis, is the ratio between the T-stub strength (F) over $F_{t,Rd}$. As it can be observed, the strength for mode 1, in case of non-circular patterns depends on the ratio $v = n/m$, where m is the distance between the bolt axis and the connected plate and the transversal one, and n is the minimum of the distance between the plate edge and the bolts axis or $1.25m$. Therefore, the three main regions identified in the graph correspond to the three T-stub failure modes.

Moreover, also the development of the prying force can influence the T-stub behavior.

Starting from the observations above, the T-stub specimens were designed to consider all possible failure modes (mode 1, 2 and 3). Moreover, the influence of the prying force was also investigated by considering two different T-stub configurations: (1) Short, considering *e* equal to the minimum value according to EN1993-1-8 [1] and (2) Long, with *e* assumed as the maximum value equal to 2.5*m* (see Figure 2-3).

All T-stub geometries and characteristics are summarized and described in Table 2.1, Figure 2-4 and Figure 2 5.

For each investigated parameter (bolts type and activation of the prying force) four specimens were designed and tested, changing the connected plate thickness in order to investigate all the possible failure modes. In particular, for the first T-stub configuration (with short flange) the tested connected plates are equal to 8, 12, 15 and 20mm (see Figure 2-6) corresponding respectively to a failure mode 1, a failure mode 2 close to mode 1, mode 2 close to mode 3 and mode 3. Analogously, the second configuration (with longer connected plate) was designed to develop all three failure modes by varying the connected plate thickness from a minimum of 10 mm (corresponding to a failure mode 1) to a maximum of 20mm (corresponding to a mode 3).

Table 2.1: T-stub specimens' characteristics.

Label	Configuration	Bolt type	Plate tickness	Failure mode
	[S or L]	[HV or HR]	[mm]	[1, 2 or 3]
T-S-HV-8	S	HV	8	1
T-S-HV-12	S	HV	12	2 cl 1
T-S-HV-15	S	HV	15	2 cl 3
T-S-HV-20	S	HV	20	3
T-S-HR-8	S	HR	8	1
T-S-HR-12	S	HR	12	2 cl 1
T-S-HR-15	S	HR	15	2 cl 3
T-S-HR-20	S	HR	20	3
T-L-HV-10	L	HV	10	1
T-L-HV-12	L	HV	12	2 cl 1
T-L-HV-15	L	HV	15	2 cl 3
T-L-HV-20	L	HV	20	3
T-L-HR-10	L	HR	10	1
T-L-HR-12	L	HR	12	2 cl 1
T-L-HR-15	L	HR	15	2 cl 3
T-L-HR-20	L	HR	20	3

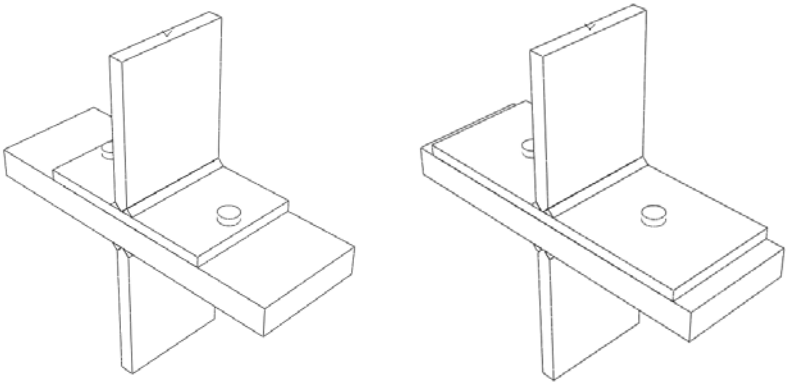

Configuration 1 (short connected plate) Configuration 2 (long connected plate)

Figure 2-3: T-stub configurations.

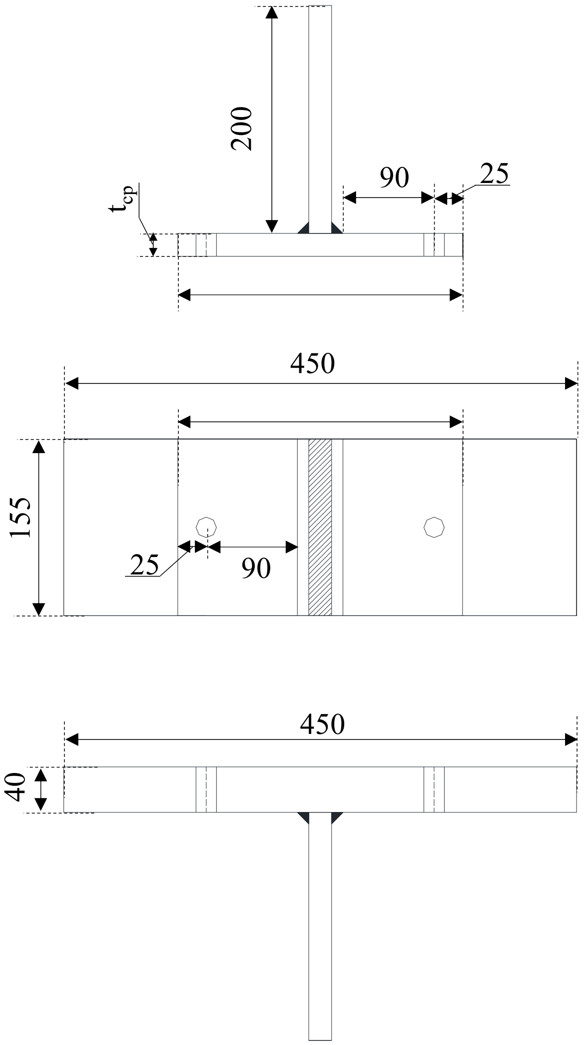

Figure 2-4: Configuration 1(short connected plate) geometrical characteristics.

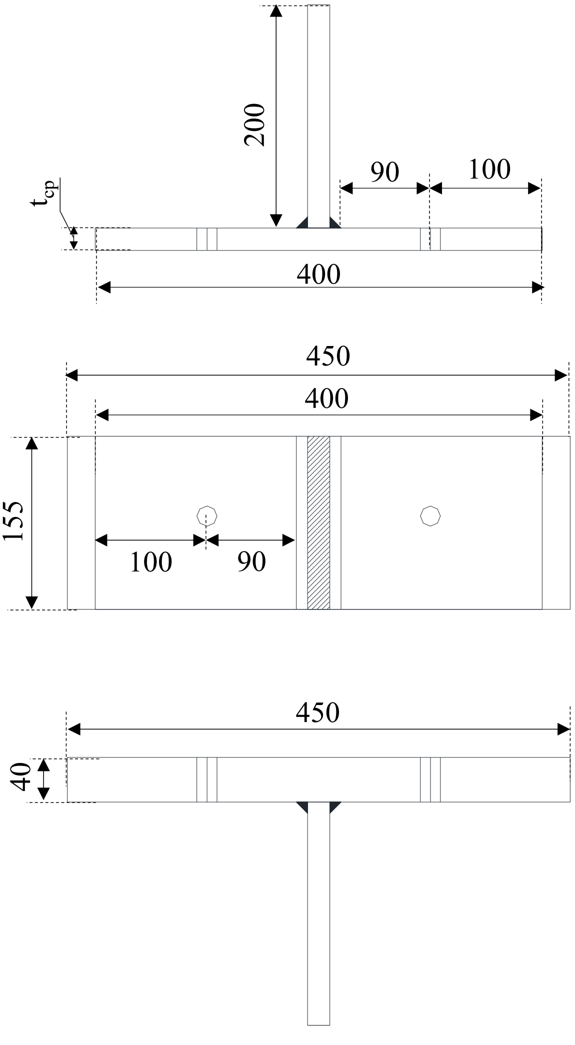

Figure 2-5: Configuration 2 (long connected plate) geometrical characteristics.

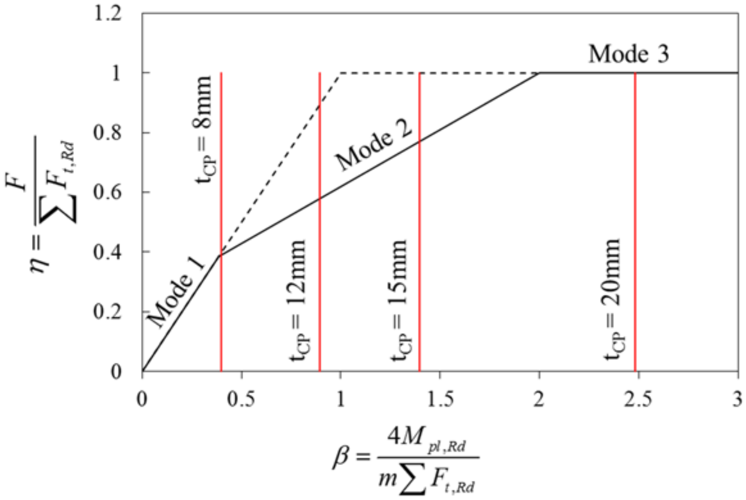
Configuration 1 (short connected plate)

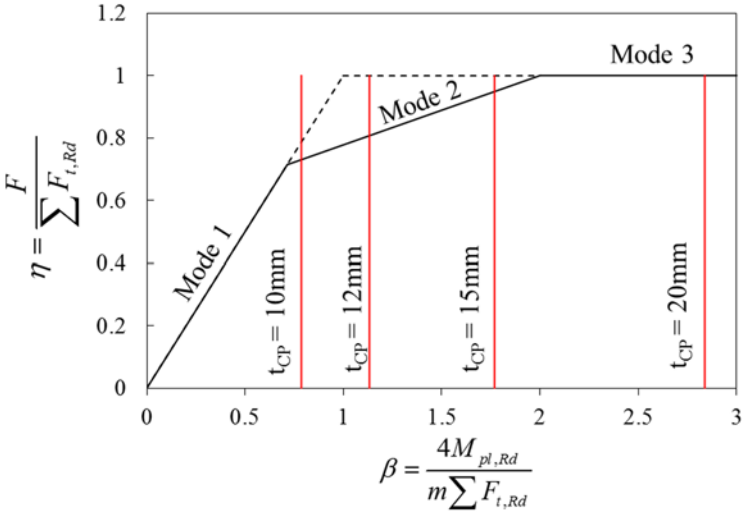
Configuration 2 (long connected plate)

Figure 2-6: T-stub configuration 1 and 2: design performance

3 Experimental results

All experimental results are reported from Figure 3-3 to Figure 3-10 in terms of force displacement curves, T-stub and bolt failure modes.

As a general observation and in line with the design assumptions, it can be observed that increasing the thickness of the connected plate, the specimens' resistance increases and the failure moves from the plates to the bolts. Conversely, going from a mode 1 to a mode 3 the T-stub ductility decreases.

When a mode 1, or mode 2 close to mode 1 is observed (T-S-HV/HR-8, T-S-HV/HR-12, T-L-HV/HR-10 and T-L-HV/HR-12), the largest part of the plastic deformation is concentrated in the connected plate with the activation of all four plastic hinges, while just for high level of displacement, the bolt failure can be observed.

For instance, with particular regard to T-L-HR-10, three stages can be identified in the force displacement curve (see Figure 3-2).

Stage 1: the specimen remains in elastic range. This lasts up to the activation of the four plastic hinge in the connected plate.

Stage 2: starting with the activation of the four plastic hinges, the stiffness decreases with respect to the elastic one but the resistance continues to increase due to the hardening developing in the hinges.

Stage 3: the stiffness increases due to membrane action developing in the plate.

Indeed, when large displacements are reached, the connected plate segments in between the plastic hinges, transfer the forces from the bolts as normal action (see Figure 3-2). Therefore, differently from the first two stages, where the bolts are mainly subjected to tensile action, with the development of the catenary action in the plate, the bolts undergo also shear and bending actions.

These considerations are confirmed by the observation of the bolts failure mode (see Figure 3-1); indeed, it can be recognize that due to the bending actions, the bolt fracture occurs in the shank with an inclination of about 40°. This type of failure mode can be observed for all the specimens designed to show a mode 1 or a mode 2 close to a mode 1 failure, independently from the configuration (short or long T-stub) and from the type of bolts used.

The T-S-HV/HR-15, T-S-HV/HR-20, T-L-HV/HR-15 and T-L-HV/HR-20 specimens are designed to show a failure mode 3 or a mode 2 close to mode 3. As it can be observed, independently from the T-stub configuration (short or long) the plastic demand is more concentrated in the bolts, leading to the expected T-stub failure mode.

Figure 3-1: T-L-HR-10 bolts failure mode.

Comparing for instance, the results of T-S-HV-15 and T-S-HR-15 is possible to observe a slight difference in the force displacement curve due to the influence on the failure mode of the bolts behaviour.

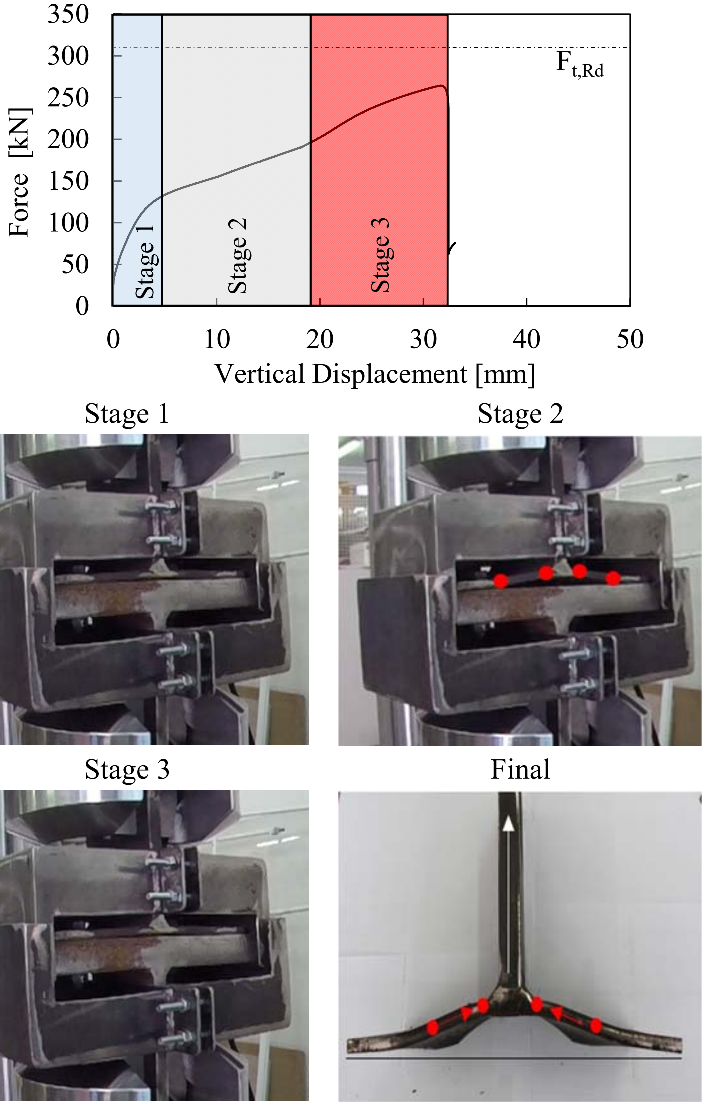

Figure 3-2: Results of T-L-HR-10-HR in terms of force displacement curve and plastic deformation develop

Indeed in this case, the HR bolts crack in the shank with an immediate loss of capacity, while the HV configuration show an initial loss of capacity (comparable with the HR bolts), due to the nut stripping and a subsequent capacity re-load. At the end of this re-loading branch the fracture occurs in the bolt shank.

Both specimens show a failure mode 2, with a small plastic demand in the connected plate and almost all the energy dissipation in the bolts. In line with this, it can be observed that the failure mode is influenced by the type of bolt. The results confirm the nut stripping phenomena that characterizes the HV bolts failure, with a re-loading branch in the latter part of the test, while the HR bolts exhibit a less ductile failure i.e. the rupture in the bolt shank.

A more conclusive example of the difference between the bolt failure modes is showed in the T-S-20 and T-L-20 specimens designed to develop a failure mode 3. In these cases, the differences between the bolts are clear from the failure mode exhibited, but no appreciable differences can be pointed out from the force-displacement curve.

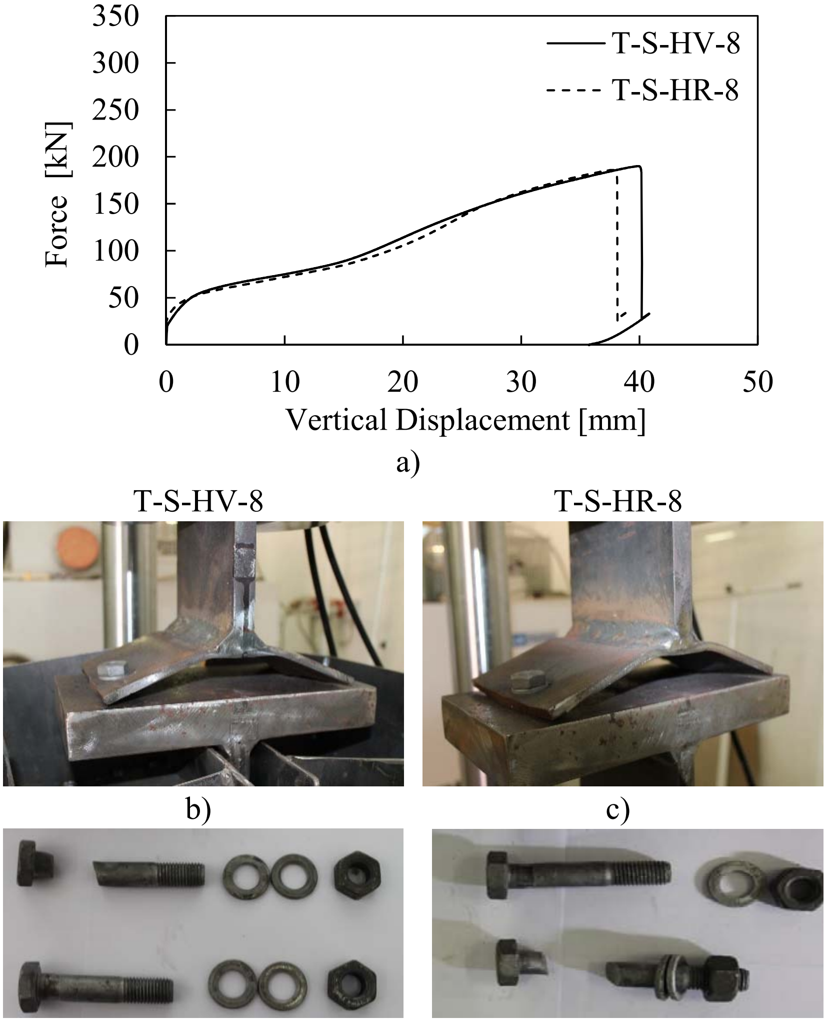

a)

b)

c)

d)

e)

Figure 3-3: Results of T-S-HV and HR with a connected plate equal to 8mm in terms of: Force displacement curve (a) and failure mode (b-e).

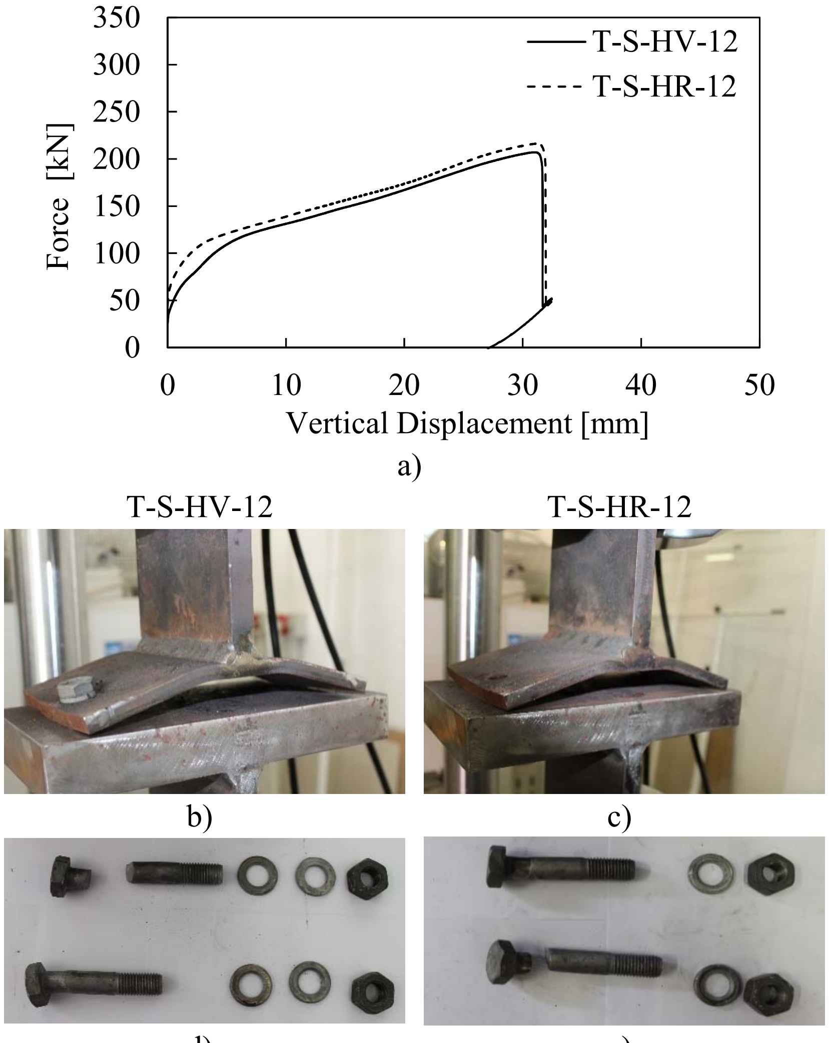

a)

T-S-HV-12 T-S-HR-12

b) c)

d) e)

Figure 3-4: Results of T-S-HV and HR with a connected plate equal to 12mm in terms of: Force displacement curve (a) and failure mode (b-e).

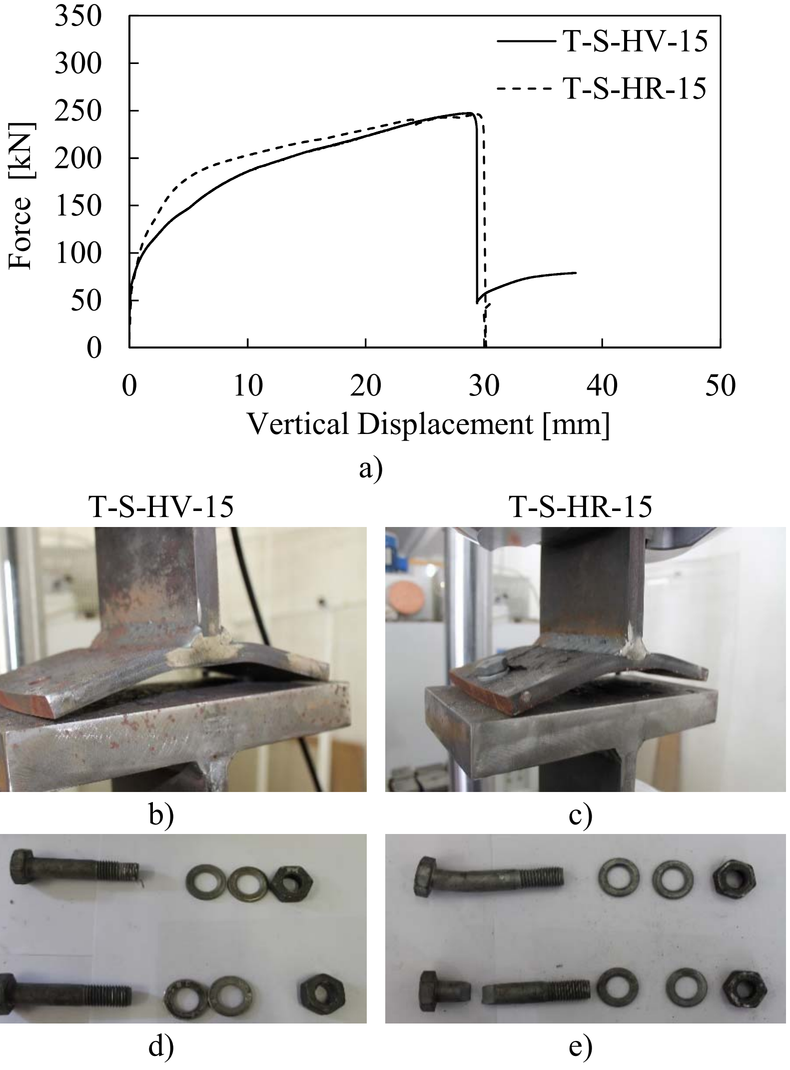

Figure 3-5: Results of T-S-HV and HR with a connected plate equal to 15mm in terms of: Force displacement curve (a) and failure mode (b-e).

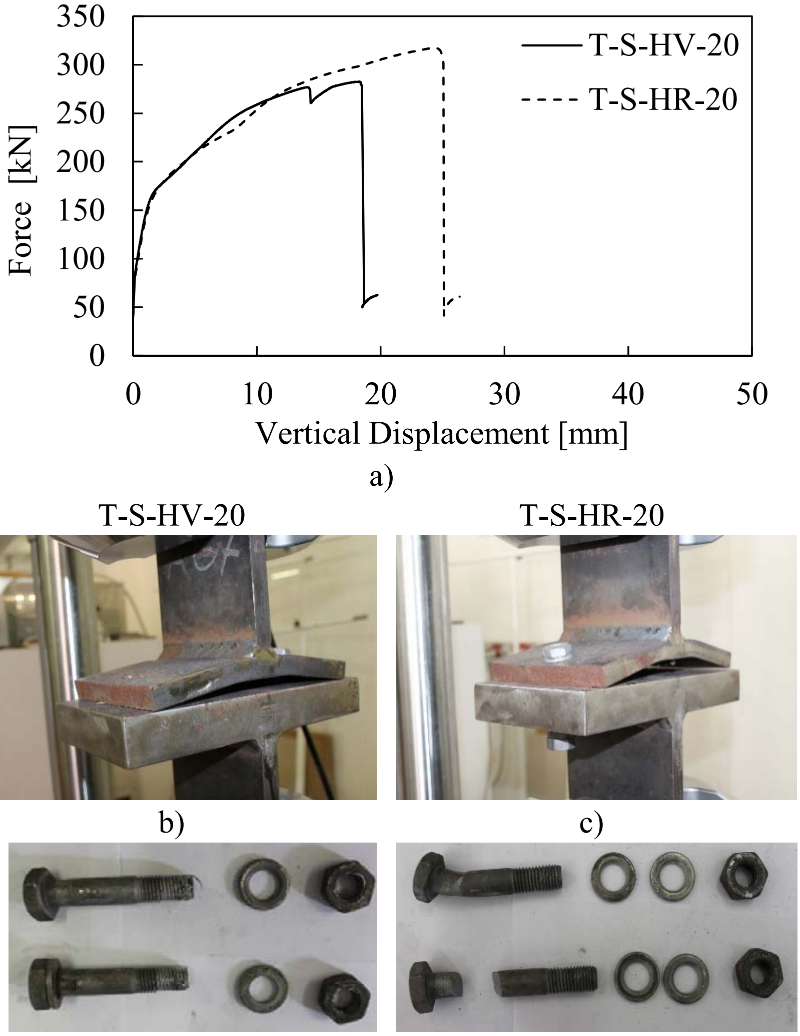

a)

b)

c)

d)

e)

Figure 3-6: Results of T-S-HV and HR with a connected plate equal to 20mm in terms of: Force displacement curve (a) and failure mode (b-e).

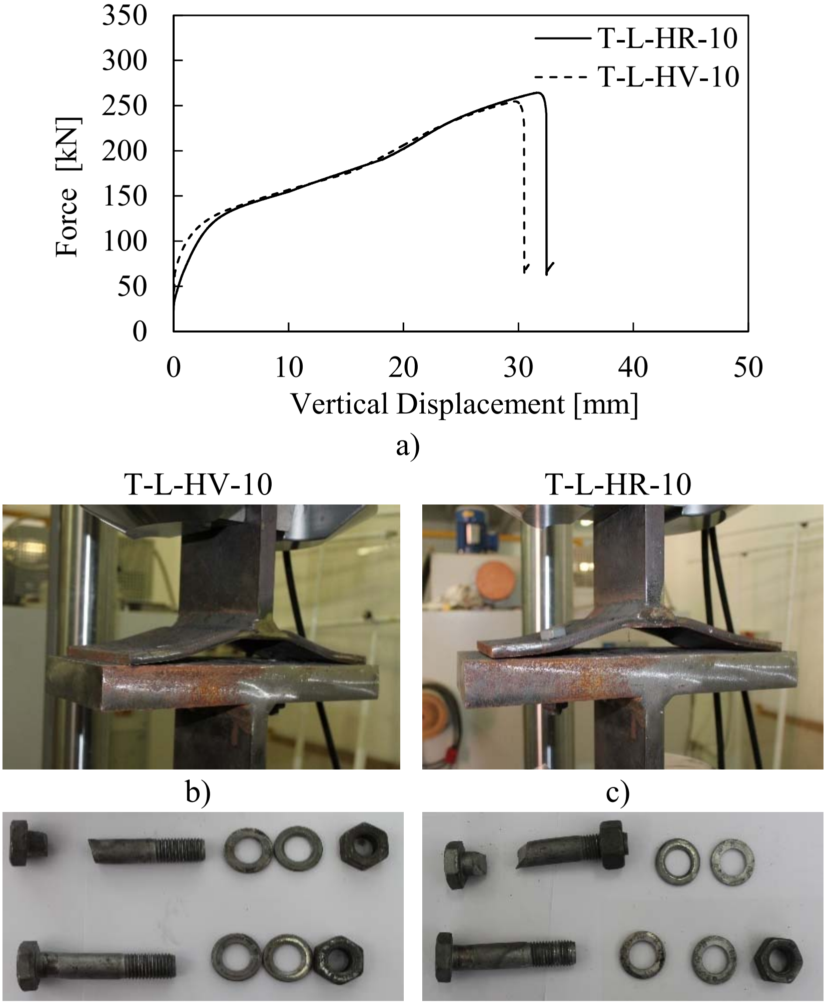

a)

b) c)

d) e)

Figure 3-7: Results of T-L-HV and HR with a connected plate equal to 10mm in terms of: Force displacement curve (a) and failure mode (b-e).

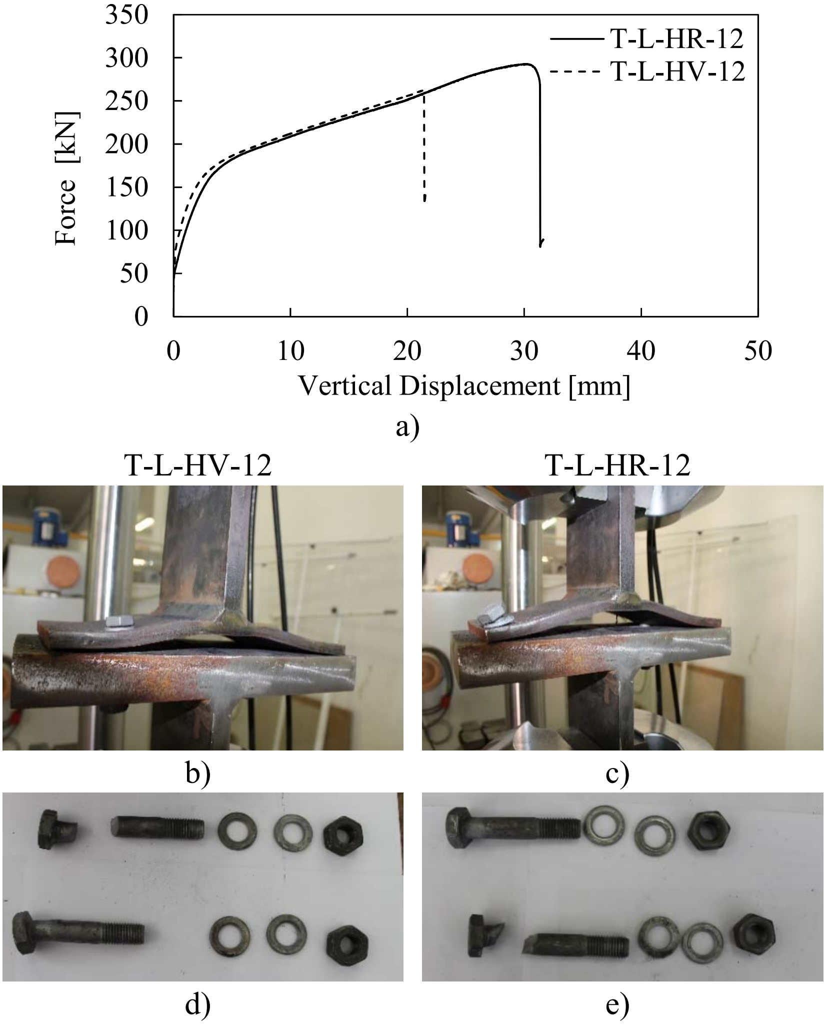

Figure 3-8: Results of T-L-HV and HR with a connected plate equal to 12mm in terms of: Force displacement curve (a) and failure mode (b-e).

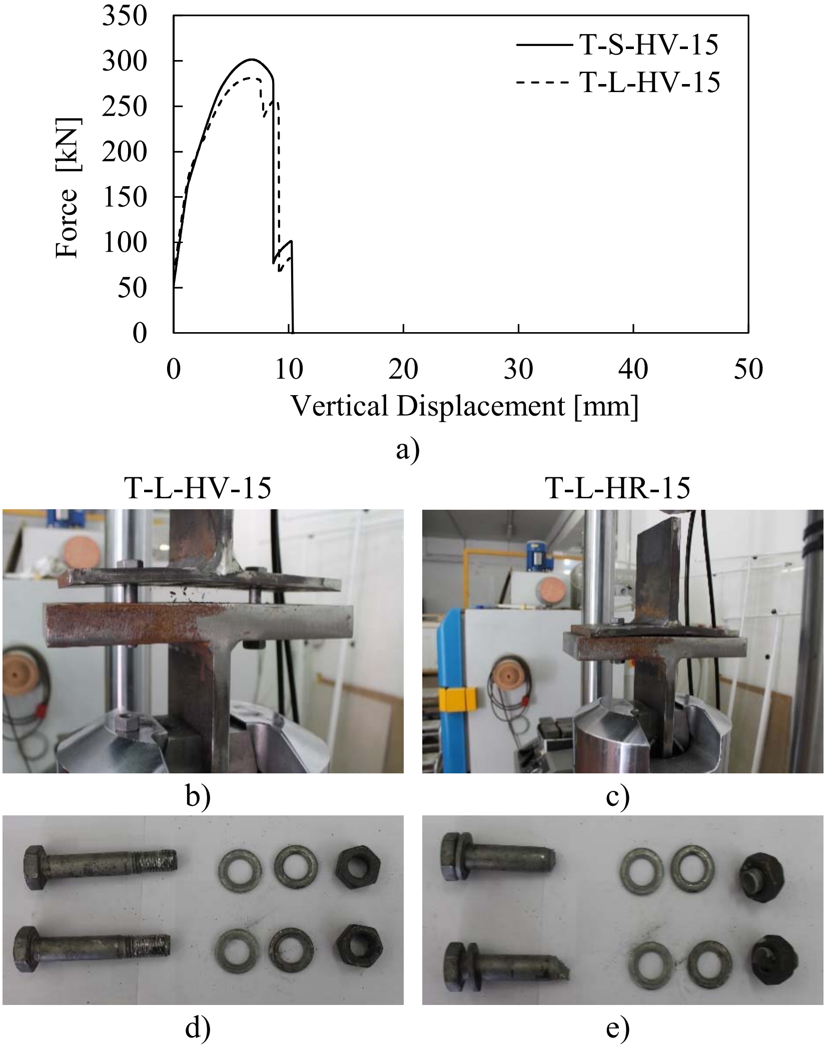

Figure 3-9: Results of T-L-HV and HR with a connected plate equal to 15mm in terms of: Force displacement curve (a) and failure mode (b-e).

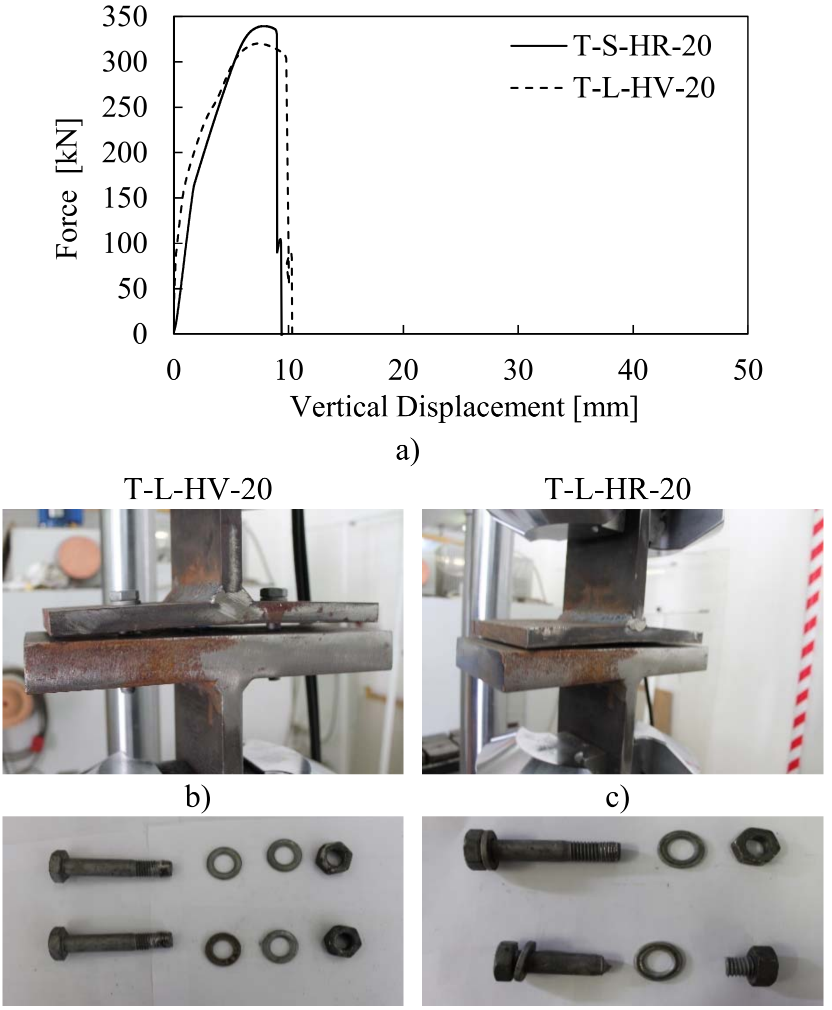

a)

b) c)

d) e)

Figure 3-10: Results of T-L-HV and HR with a connected plate equal to 20mm in terms of: Force displacement curve (a) and failure mode (b-e).

4 Discussion of results

From the analysis of the experimental results it can be observed that if either mode 1 or mode 2 close to 1 is ensured, the type of bolts and the developing of the prying forces do not influence the T-stub failure mode and in particular their ductility. Indeed, for value of connected plate equal to 8 and 10mm (or 10 and 12 for the second configuration) for both HR and HV bolts, the ultimate failure after the formation of the plastic hinges in the plate appear in the bolt shank due to a combination of shear and axial force in the bolts (see Figure 4-1).

	HV Bolts	HR Bolts
T-S-8		
T-S-12		

Figure 4-1: Bolts failure mode when a mode 1 or 2 close to mode 1 develop.

Contrariwise, when the connected pate is thick enough to move the failure mode from mode 1 to mode 3, in function of the bolts type, two failure mode can be recognized (see Figure 4-2); this difference influence slight also the force displacement curve.

In line with the results observed by D'Aniello et al. [2] the HR show a failure in the bolts shank, while a nut stripping can be observed when the HV bolts are tested. In these cases indeed the axial actions on the bolts plays a central role in the definition of the ultimate resistance, and although in the bolts can be observed still a plastic deformation due to the bending and the shear, these actions play a less important role with respect to the axial force.

	HV Bolts	HR Bolts
T-S-15		
T-S-20		
T-L-15		
T-L-20		

Figure 4-2: Bolts failure mode when a mode 3 or 2 close to mode 3 develop.

References

[1] EN 1993:1-8, Design of steel structures - Part 1-8: Design of joints. CEN 2005.

[2] M. D'Aniello, D. Cassiano, R. Landolfo (2016). Monotonic and cyclic inelastic tensile response of European preloadable gr10.9 bolt assemblies. Journal of Constructional Steel Research, 124, 77–90.

List of figures

Figure 1-1: Bolts investigation UNINA setup [2]. 148
Figure 1-2: HV and HR bolts failure mode under monotonic load [2]..149
Figure 2-1: T-Stub failure mode 150
Figure 2-2: T-Stub resistance and corresponding mechanism according to EN1993:1-8 [2] 151
Figure 2-3: T-stub configurations. 154
Figure 2-4: Configuration 1(short connected plate) geometrical characteristics. 155

Figure 2-5: Configuration 2 (long connected plate) geometrical characteristics.. 156
Figure 2-6: T-stub configuration 1 and 2: design performance 157
Figure 3-1: T-L-HR-10 bolts failure mode............................. 160
Figure 3-2: Results of T-L-HR-10-HR in terms of force displacement curve and plastic deformation develop 161
Figure 3-3: Results of T-S-HV and HR with a connected plate equal to 8mm in terms of: Force displacement curve (a) and failure mode (b-e). 163
Figure 3-4: Results of T-S-HV and HR with a connected plate equal to 12mm in terms of: Force displacement curve (a) and failure mode (b-e). 164
Figure 3-5: Results of T-S-HV and HR with a connected plate equal to 15mm in terms of: Force displacement curve (a) and failure mode (b-e). 165
Figure 3-6: Results of T-S-HV and HR with a connected plate equal to 20mm in terms of: Force displacement curve (a) and failure mode (b-e). 166
Figure 3-7: Results of T-L-HV and HR with a connected plate equal to 10mm in terms of: Force displacement curve (a) and failure mode (b-e). 167

Figure 3-8: Results of T-L-HV and HR with a connected plate equal to 12mm in terms of: Force displacement curve (a) and failure mode (b-e)......................................168
Figure 3-9: Results of T-L-HV and HR with a connected plate equal to 15mm in terms of: Force displacement curve (a) and failure mode (b-e)......................................169
Figure 3-10: Results of T-L-HV and HR with a connected plate equal to 20mm in terms of: Force displacement curve (a) and failure mode (b-e)......................................170
Figure 4-1: Bolts failure mode when a mode 1 or 2 close to mode 1 develop..172
Figure 4-2: Bolts failure mode when a mode 3 or 2 close to mode 3 develop..173

List of tables

Table 2.1: T-stub specimens' characteristics............................153

CHAPTER V

Seismic qualification of extended stiffened joint

Introduction

The component method provide a good analytical solution to design the beam-to-column joints under predominantly static loading, but specific provisions for seismic design are missing.

Therefore, starting from the component method main criticism (described in Chapter III) the aim of this Chapter is to introduce updated requirements to seismic design extended stiffened joints in the framework of EN1993-1-8 [1].

On the base of these new assumptions, a set of three beam-to-column joints are designed (ES1, ES2 and ES3) and their behavior are investigated by means of parametric FE analyses.

1 Design procedure proposed

1.1 Capacity design approach

According to EC8 [1], the seismic design of steel structures is based on the concept of dissipative structures, where specific zones should be able to develop plastic deformation in order to dissipate the seismic energy. On the contrary, the non-dissipative parts should behave elastically under seismic action in order to avoid brittle collapse.

The hierarchy of the resistances is the fundamental principle allowing this performance by detailing non-dissipative zones to resist the full plastic strength of the related dissipative members.

The proposed design criteria extend this philosophy to the joints, by establishing a hierarchy among the strengths of macro-components (e.g. the column web panel, the connection, and the beam described in Figure 1-1), and their sub-components (e.g. endplate, bolts, welds, etc.), as well.

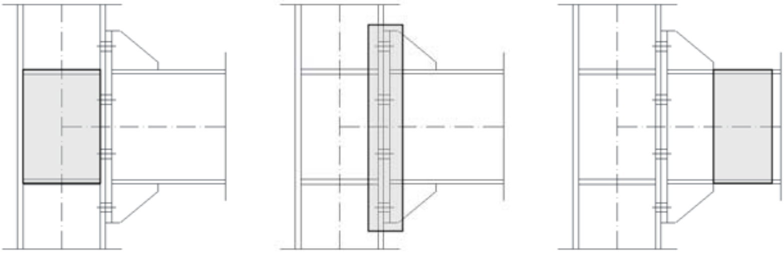

Figure 1-1: Plastic regions for the examined performance design objectives: a) full strength, b) equal strength and c) partial strength joints.

Each macro-component is individually designed according to specific assumptions and then simply capacity design criteria are applied. Therefore, three different design objectives were defined comparing the joint (i.e. web panel and connection) strength to the beam flexural resistance, namely: (i) full strength, (ii) equal strength and (iii) partial strength joints.

Full strength joints are designed to guarantee the formation of all plastic deformations into the beam, which is consistent with EC8 strong column-weak beam capacity design rules. Equal strength joints are characterized by the contemporary yielding of all macro-components (i.e. connection, web panel and beam). Partial strength joints are designed to develop the plastic deformation only in the joint.

It should be also noted that both EC3 [2] and EC8 [1] do not consider the case of equal strength joint, which is proposed in this study as an intermediate performance level.

Moreover, EN1998-1-1 (pr. 6.6.1) define as general role that plastic deformations should be avoided in the column; in line with this principle for all the designed criteria investigated an additional specification can be introduced. Indeed, as already discussed, since the joint is defined as the sum of the column web panel and the connection, Equal and Partial strength joints can be designed to show a strong, a balance or a weak column web panel respect to the dissipative zone.

Therefore, an Equal strength joint can be designed to show both the damage evolution in the joint and in the beam (balance web panel) or just in the connection and in the beam (strong web panel). Likewise, a Partial strength joint can be designed to show the damage only in the column or in the connection (weak or strong column web panel respectively) or both on the connection and in the column web panel (balance column web panel).

The capacity design rules to obtain the required joint behavior can be guaranteed by satisfying the following inequalities:

- Full strength joint:

$$M_f = \min(M_{wp,Rd}, M_{\mathrm{j},Rd}) \geq M_{\mathrm{j,E}d} = \alpha \cdot (M_{\mathrm{B},Rd} + V_{B,Ed} \cdot s_h) \quad (1)$$

- Equal and Partial (for strong, balance and weak web panel respectively):

$$M_{wp,Rd} > M_{\mathrm{j},Rd} \geq M_{\mathrm{j,E}d} = \alpha \cdot (M_{\mathrm{B},Rd} + V_{B,Ed} \cdot s_h) \quad (2)$$

$$M_{wp,Rd} = M_{\mathrm{j},Rd} \geq M_{\mathrm{j,E}d} = \alpha \cdot (M_{\mathrm{B},Rd} + V_{B,Ed} \cdot s_h) \quad (3)$$

$$M_{\mathrm{j},Rd} \geq M_{wp,Rd} \geq M_{\mathrm{j,E}d} = \alpha \cdot (M_{\mathrm{B},Rd} + V_{B,Ed} \cdot s_h) \quad (4)$$

where:

M_f is the design moment at the column face;

$M_{wp,Rd}$ is the flexural strength corresponding to the strength of column web-panel:

$$M_{wp,Rd} = V_{wp,Rd} \cdot z_{wp} \quad (5)$$

$V_{wp,Rd}$ is the shear resistance of the column web panel;

z_{wp} is the internal level arm;

$M_{j,Rd}$ is the flexural strength of the connection zone;

$M_{j,Ed}$ is the design bending moment at the column face;

α depends on the design performance level. It is equal to $\gamma_{sh} \times \gamma_{ov}$ for the full strength joints, while equal to 1 for equal strength joints and smaller than 1 for partial strength joints. In this thesis to limit the lower bound of α in order to avoid excessive damage concentration in the connection zone, the strength ratio is assumed equal to 0.8, which corresponds to the lower bound limit to qualify the strength of joints in special moment resisting frames according to AISC341-10[5].

$M_{B,Rd}$ is the plastic flexural strength of the connected beam;

s_h is the distance between the column face and the tip of the rib stiffener;

$V_{B,Ed}$ is the shear force corresponding to the occurring of the plastic hinge in the connected beam; it is given by:

$$V_{B,Ed} = V_{B,Ed,M} + V_{B,Ed,G} \qquad (6)$$

Where:

$V_{B,Ed,M}$ is the shear force due to the formation of plastic hinges at both beam ends, spaced by the length L_h and calculated as:

$$V_{B,Ed,M} = \frac{2 \cdot M_{B,rd}}{L_h} \qquad (7)$$

$V_{B,Ed,G}$ is the contribution due to the gravity loads; it should be noted that this amount does not account for the distance between the column face and plastic hinge e L_h is the approximate distance between plastic hinges;

γ_{ov} is overstrength factor due to the material randomness, depending on the steel grade. In this paper it is assumed equal to 1.25, as recommended by EC8 [1];

γ_{sh} is the strain hardening factor corresponding to the ratio between the ultimate over the plastic moment of the beam.

In EN1993:1-8 this overstrength ratio is assumed equal to 1.2 for full strength joints, while contradictorily EN1998-1 assumes a value equal to 1.1. The late Italian code OPCM 3274 [6] overcame this contradiction by providing the flexural overstrength (s) using the formulation suggested by Mazzolani and Piluso [7] and [8]. More recently this formulation has been updated by D'Aniello et al. [9], as follows:

$$s = \frac{1}{C_1 + C_2\lambda_f^2 + C_3\lambda_w^2 + C_4\frac{b_f}{L_v} + C_5\frac{E}{E_h} + C_6\frac{\varepsilon_h}{\varepsilon_y}} \tag{8}$$

being λ_f the beam flange slenderness, λ_w the web slenderness, b_f the flange width, L_v the shear length, E the elastic modulus, E_h is the hardening modulus, ε_h the strain corresponding to the beginning of hardening and ε_y the first yielding strain, and finally the coefficients C_i are reported in [9].

Based on the main findings obtained by [9] to [11] it can be argued that *s* factor ranges within 1.15-1.3 for European profiles commonly used for beams (e.g. IPE and HEA).

On the other hand, US prequalification procedure (i.e. AISC358-16 [12]) assumes the following:

$$\gamma_{sh,AISC} = \frac{f_y + f_u}{2 \cdot f_y} \leq 1.20 \qquad (9)$$

Based on the characteristic yield and ultimate strength of European mild carbon steel grades, γ_{sh}, AISC can be assumed equal to 1.20 for European applications. Anyway, as it should be noted, the strain hardening factors given by Eqs. (8) and (9) are generally larger than 1.1, which is the value recommended by EC8 [1]. Therefore, in the present study γ_{sh} factor is conservatively assumed as the maximum between those calculated by Eq. (8) and Eq. (9).

1.2 Ductility criterion

Strength, stiffness and ductility are strictly related to the components of the joint, which fall on two categories, i.e. ductile and brittle. Therefore, the joint ductility depends on the type of failure mode and the corresponding plastic deformation capacity of the activated components (as anticipated in Chapter III).

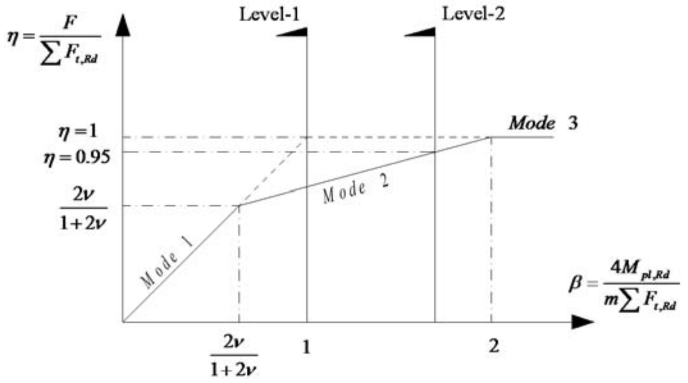

Figure 1-2: T-Stub resistance and corresponding mechanism according to EN1993:1-8 [2].

Moreover, the joint ductility is also strictly dependent on the ductility of the equivalent T-stubs at each bolt row in tension, whose behavior deserves some considerations. Figure 1-2 concisely depicts the dependency of failure mode on geometric properties and end-plate to bolt strength ratio [13]. Indeed, in abscissa it is reported β that is the ratio between the flexural strength of the plates, or column flanges, ($M_{pl,Rd}$) and the axial strength of the bolts ($F_{t,Rd}$), while the vertical axis reports the ratio η between the T-stub strength (F) over $F_{t,Rd}$. As it can be observed, the strength for mode 1 in case of non-circular pattern depends on the ratio $\nu = n/m$, where m is the distance between the bolt axis and the flange-to-web expected location of the plastic hinge, and n is the minimum of the distance between the edge of the flange and the bolts axis or 1.25m.

Therefore, in line with EC3, in order to avoid brittle collapse (i.e. mode 3) two possible ductility criteria can be adopted, namely:

Level-1: $\beta \leq 1$ this condition imposes either a failure mode I or failure mode II (but very close to mode I), which provide very high ductility.

Level-2: $\beta < 2$ and $\eta \leq 0.95$, this condition imposes a failure mode II with limited ductility, but avoiding brittle failure.

It should be noted that the level of ductility to be guaranteed depends on the design performance objectives. Indeed, it is crucial providing the larger ductility for Equal and Partial strength, less for Full strength joints. Moreover, as also anticipated in Chapter III, according to the EN1993-1-8, the joint rotation capacity should be checked if M_{jrd} is less than 1.2 $M_{B,pl,rd}$.

Otherwise two alternative ways can be pursued: 1) performing experimental tests; 2) controlling the thickness t of either end-plate or column flange, provided that the joint design moment resistance is governed by those components, which should satisfy the following inequality:

$$t \leq 0.36d\sqrt{\frac{f_{ub}}{f_y}} \tag{10}$$

where *d* is the nominal bolt diameter, f_y is the yield strength of the relevant basic component and f_{ub} is the bolt ultimate strength.

Eq. (10) theoretically complies with the ductility Level-1 depicted in Figure 1-2. Indeed, it is based on the assumption that bolted joints have sufficient rotation capacity if the resistance of each individual bolt ($F_{t,Rd}$) is greater than the resistance ($F_{p,Rd}$) of the connected plates (end-plate or column flange) in order to prevent premature failure of the bolts. The EN1993-1-8 design resistance of a bolt in tension is given as follows:

$$F_{t,Rd} = \frac{0.9 A_s f_{ub}}{\gamma_{M2}} \tag{11}$$

where *As* is the tensile stress area of the bolt and γ_{M2} is the relevant partial safety factor (recommended equal to 1.25).

In addition, according to the EN 1993-1-8, the maximum design resistance of a plate occurs in the case of a circular mechanism, which leads calculating the following strength:

$$F_{p,Rd} = \frac{\pi t^2 f_y}{\gamma_{M0}} \tag{12}$$

where t is the plate thickness and γ_{M0} is the relevant partial safety factor (recommended equal to 1).

As it can be easily recognized Eqs. (11 and 12) assume perfectly plastic behavior of steel plates. However, in light of the considerations previously discussed, the ductility Level-1 for seismic resistant Partial strength joints should be expressed accounting for both the random variability of plate material and its relevant strain hardening, so that the following inequality can be used:

$$F_{t,Rd} \geq \gamma \cdot F_{p,Rd} = \gamma_{ov} \cdot \gamma_{sh} \cdot F_{p,Rd} \tag{13}$$

The overstrength factor γ in Eq. (13) can be taken equal to 1.5, since the Eurocode recommended value for γ_{ov} is equal to 1.25, the value for γ_{sh} is equal to 1.2 for European mild carbon steel. Thus rearranging the inequality Eq. (13) with Eq. (11 and 12), the ductility condition accounting for capacity design criteria can be expressed as following (where the recommended partial safety factor γ_{M0} is equal to 1.0):

$$t \leq \frac{0.42 \cdot d}{\sqrt{\gamma_{ov} \cdot \gamma_{sh}}} \cdot \sqrt{\frac{\gamma_{\mathrm{M0}} \cdot f_{ub}}{\gamma_{\mathrm{M2}} \cdot f_y}} = 0.30 \cdot d \cdot \sqrt{\frac{f_{ub}}{f_y}} \tag{14}$$

Regarding full and equal strength joints, even though either no or poor ductility should be respectively exploited, a local hierarchy criterion is advisable in order to avoid undesirable failure mode in the brittle components due to material variability. Hence, in line with ductility Level-2, the strength of bolts should satisfy the following inequality:

$$F_{t,Rd} \geq \gamma_{ov} \cdot F_{p,Rd} \tag{15}$$

It is important to highlight that all criteria previously described require that failure of welds has to be unquestionably avoided, because of their brittle collapse mechanism.

1.3 Design assumptions for ES connection

The connection zone includes the bolt rows belonging to end-plate, the column flange and the rib stiffeners.

Differently from the component method implemented in EN1993:1-8 [1], where all bolt rows in tension are rigorously obtained by imposing the equilibrium with compression internal resultant, the number of active bolt-rows in tension has been assumed a-priori as shown in Figure 1-3, because the contribution of lower rows is generally negligible under pure bending condition [14].

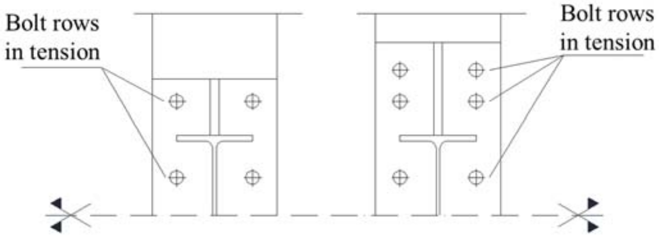

Figure 1-3: Assumed position of bolt rows in tension.

Moreover, since the presence of the rib stiffener is not properly addressed by EC3, some specific requirements are accounted for. With this regard, analytical and semi-empirical formulations given by literature and validated by numerical simulations are assumed to design and verify the joints investigated in this study, as described and discussed hereinafter.

1.3.1 Design strength and stiffness of rib

The design strength and stiffness of rib are assumed on the basis of the equivalent truss model provided by Lee [15] (see Figure 1-4). The Equivalent strut area of the rib, A_e, is defined as follows:

$$A_e = \eta \cdot h_e \cdot t \tag{16}$$

Where: η is defined as equivalent strut area factor, whose recommended value for practical design purposes is 1.5, *t* is the rib thickness and h_e is the width perpendicular to the strut line (see Figure 1-4a) and it is defined as:

$$h_e = \frac{ab - c^2}{\sqrt{(a-c)^2 + (b-c)^2}} \tag{17}$$

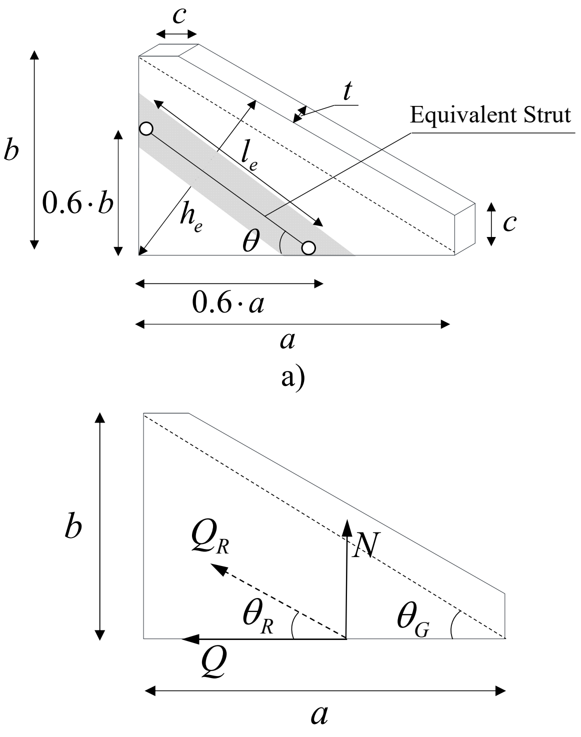

a)

b)

Figure 1-4: Geometry of rib stiffener (a) and forces developing at beam/column-to-rib interface according to [63].

The design forces acting on the rib stiffeners at the beam/column-to-rib interface (see Figure 1-4b) should be evaluated as follows:

$$N = \left(\frac{b}{a} \right) \cdot Q \tag{18}$$

$$Q = \frac{\dfrac{ad_b \cdot (0.21a + 0.51L^{'})}{I_b}}{\dfrac{1}{\eta} \cdot \dfrac{0.6\sqrt{a^2 + b^2}\sqrt{(a-c)^2 + (b-c)^2}}{(ab - c^2) \cdot \mathrm{t}} + \dfrac{(0.81b + 0.13d_b)(ad_b)}{I_b}} \cdot V_{B,Ed} \tag{19}$$

Being *a*, *b* and the dimensions of rib plate as shown in Figure 1-4, while d_b and I_b are the depth and second moment of area of the beam, respectively. $V_{B,Ed}$ is the design shear force acting in the beam at the intersection with the rib stiffener, which can be computed according to Eq. (6).

1.3.2 Influence of rib stiffeners on effective lengths of equivalent t-stub

The rib stiffener influences the shape of T-Stub mechanisms, which also depend on the number of bolt rows (see Figure 1-3) due to possible occurrence of group effect. Therefore, the assumptions made by EN1993:1-8 [2] for the effective lengths of the end-plate bolt rows above the beam flange in tension are not appropriate.

In this work two configurations with either one (1br) or two (2br) bolt rows placed above the beam flange are addressed (see Figure 1-5)

In the former case, the effective length is assumed as that for the stiffened column flange, being the influence of beam flange similar to that provided by continuity plates, but considering the presence of the free edge on the end-plate. In the second case, due to the group effect the effective length is computed as given by the Green Book P398 [3]. Both for circular and non-circular pattern the effective length are summarized, in Table 1.1 for the one bolt row configuration and from Table 1.2 to Table 1.4 for two bolts row above the beam flange. In the latter case, the results are reported for the first and the second bolt row line considering the lines both as alone and as part of a group.

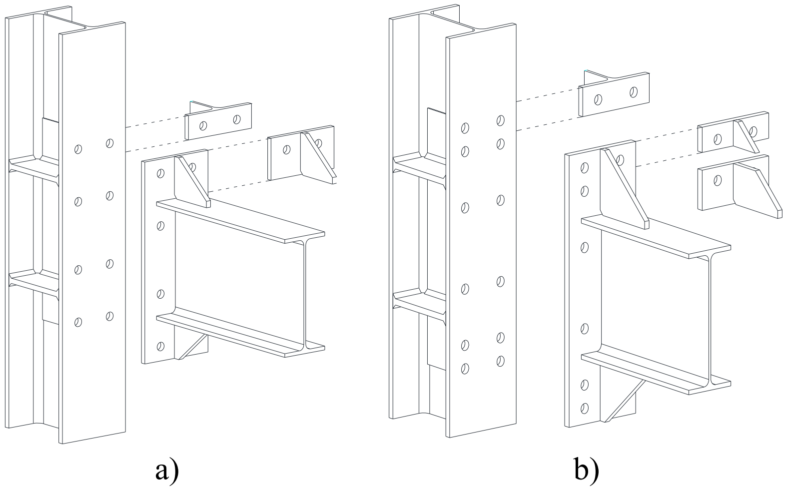

Figure 1-5: Equivalent T-Stub for ES joints: the cases with one (a) and two (b) bolt rows above the beam flange in tension.

Table 1.1: Effective length for the first line of 1br configuration.

Circular patterns	Non-circular patterns
$l_{eff,cp} = 2\pi m$	$l_{eff,nc} = \alpha m-(2m+0.625e)+e_x$
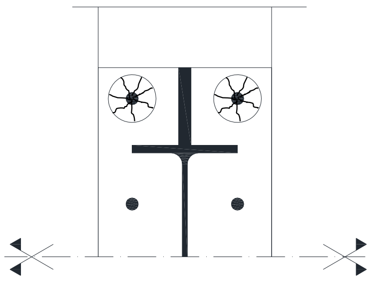	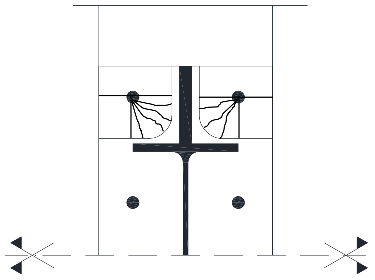
$l_{eff,cp} = \pi m+2e_x$	$l_{eff,nc} = 2m+0.625e+e_x$
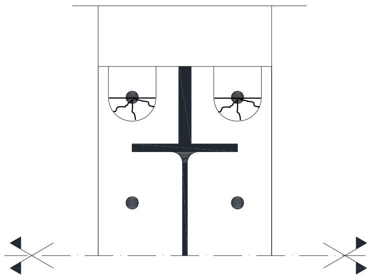	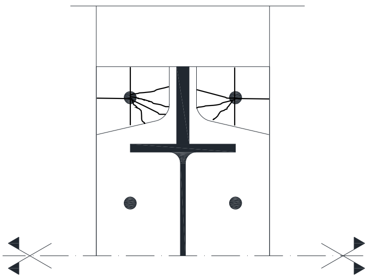
Dimension definition	$l_{eff,nc} = 4m+1.25e$
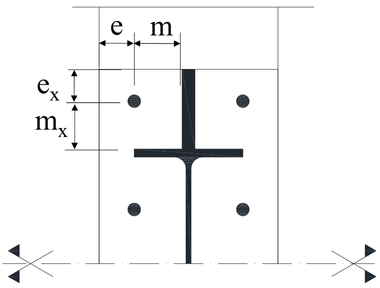	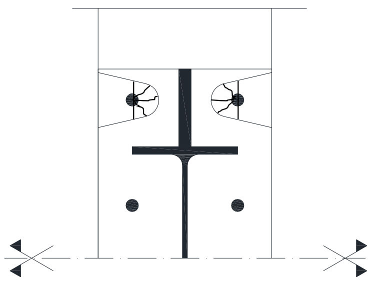

Table 1.2: Effective length for the first line of 2br configuration.

<table>
<tr><th>Circular patterns</th><th>Non-circular patterns</th></tr>
<tr><td>$l_{eff,cp} = 2\pi m$</td><td>$l_{eff,nc} = 2m+0.625e+e_1$</td></tr>
<tr><td>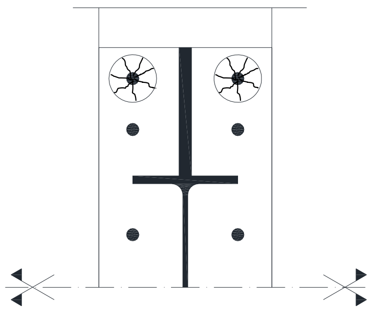</td><td>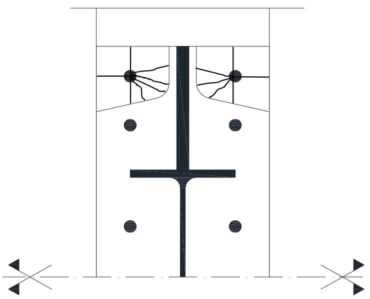</td></tr>
<tr><td>$l_{eff,cp} = \pi m+2e_1$</td><td>$l_{eff,nc} = 4m+1.25e$</td></tr>
<tr><td>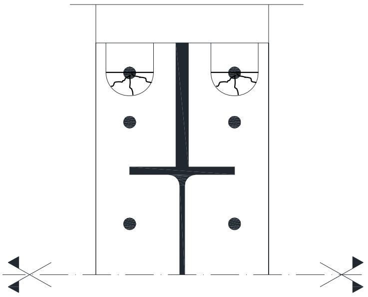</td><td>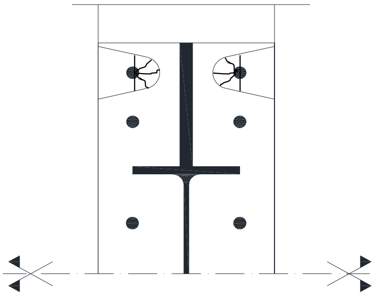</td></tr>
<tr><td colspan="2">Dimensions definition</td></tr>
<tr><td colspan="2">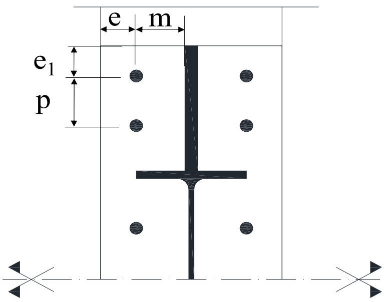
</td></tr>
</table>

Table 1.3: Effective length for the first line (considered as part of group) of 2br configuration.

Circular patterns	Non-circular patterns
$l_{eff,cp}$ = πm+p	$l_{eff,nc}$ = 2m+0.625e+0.5p
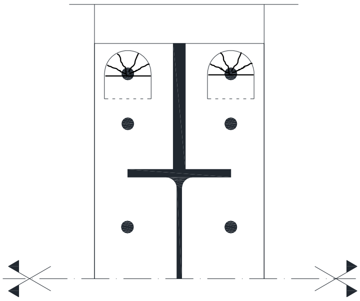	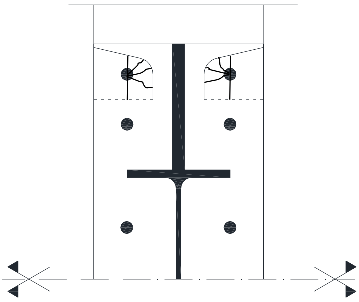
$l_{eff,cp}$ = 2e$_1$+p	$l_{eff,nc}$ = e$_1$+0.5p
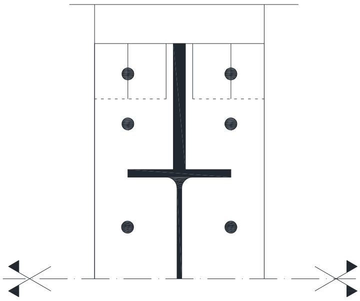	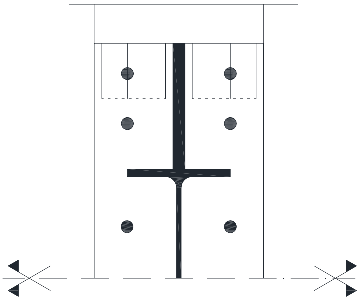

Table 1.4: Effective length for the second line of 2br configuration.

<table>
<tr><th>Circular patterns</th><th>Non-circular patterns</th></tr>
<tr><td>$l_{eff,cp} = 2\pi m$</td><td>$l_{eff,nc} = \alpha m$</td></tr>
<tr><td>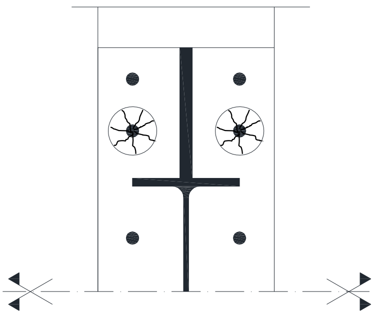</td><td>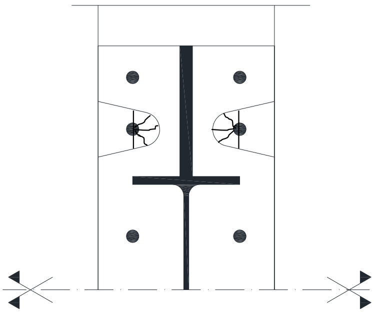</td></tr>
<tr><td colspan="2">Group Effect – Second bolt row line</td></tr>
<tr><td>$l_{eff,cp} = \pi m+p$</td><td>$l_{eff,nc} = 0.5p+\alpha m-(2m+0.625e)$</td></tr>
<tr><td>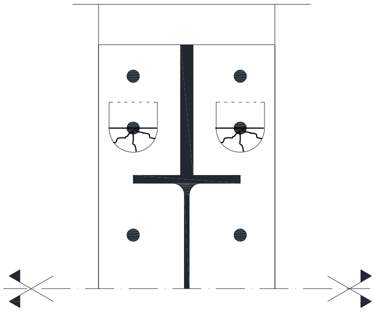</td><td>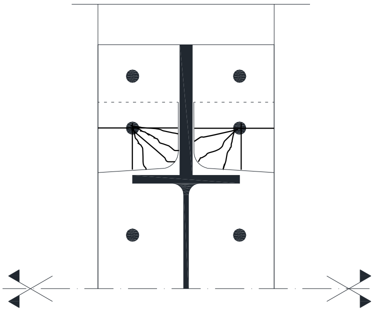</td></tr>
<tr><td colspan="2">$l_{eff,cp} = \pi m+p$</td></tr>
<tr><td colspan="2">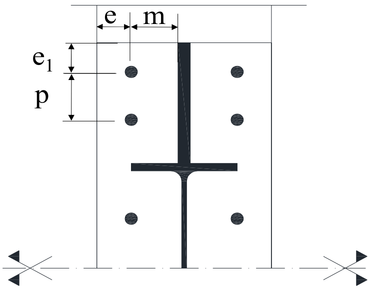
 </td></tr>
</table>

1.3.3 Centre of compression and lever arm

The appropriate evaluation of position of center of compression and the corresponding lever arm z has a great importance to calculate the joint bending strength. For end-plate joints covered by EN 1993-1-8 provisions, the compression center is located in the middle of thickness of beam flange. Anyway, experimental and numerical results on bolted ES joints carried out by Abidelah et al. [16] showed that the compression center is generally shifted below the position assumed by EC3, and approximately located at the centroid of the "T" section made of the rib stiffener and the beam flange. The numerical and experimental results on welded joints with rib stiffeners obtained by [15], [17] highlighted that bending from beam to column is mainly transferred by a full truss mechanism rather than the classical beam theory, where the rib behaves as an inclined strut as shown in Figure 1-4.

It is clear that the position of center of compression varies with the joint rotation demand due to the formation of plastic modes with different engagement of each joint component. However, tests on welded joints carried out by Lee et al. [17] showed that up to interstorey drift ratios equal to 5% the strut model for rib is effective, with center of compression shifted at 0.6 times the rib height (see Figure 1-6a) that differ from the results obtained by

Abidelah et al.[16]. Therefore, in order to verify their accuracy, both assumptions were numerically investigated.

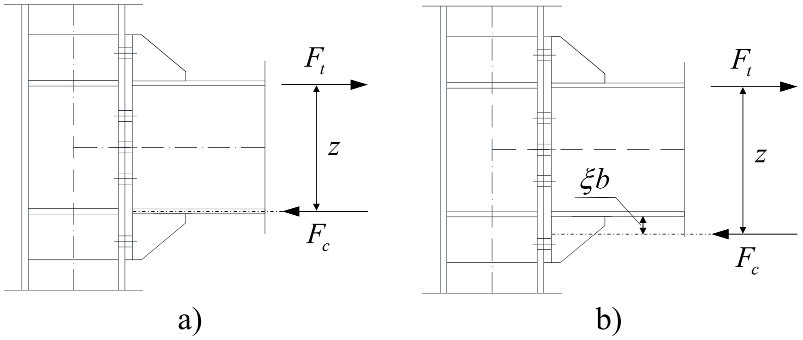

Figure 1-6: Centre of compression and lever arm: a) EC3:1-8 for end-plate connections; b) shifted position due to strut mechanism into the rib stiffener.

1.3.4 Influence of rib stiffeners on the beam web in compression capacity

According to EN1993-1-8, the design compression forces acting on beam web component is given by the following:

$$F_{c,fb,Rd} = \frac{M_{b,Rd}}{d_b - t_{fb}} \tag{20}$$

where $M_{b,Rd}$ is the bending moment capacity of the transverse section of the beam, d_b is the beam height and t_{fb} is the beam flange thickness. Eq. (20) is conceived for extended unstiffened end-plate connections, where the maximum bending moment corresponds to the plastic strength of the beam $M_{b,Rd}$. In case of ES joints the maximum bending moment $M_{j,Ed}$, given by Eq. (1 to 4), is larger than $M_{b,Rd}$. On the other hand, the lever arm z for ES joints is deeper due to rib strut mechanism. Therefore, the compression forces acting on beam web component can be more rationally obtained as follows:

$$F_{c,fb,Rd} = \frac{M_{j,Ed}}{z} = \frac{M_{j,Ed}}{d_b + \xi b - 0.5t_{fb}} \tag{21}$$

Where ξb is the position of the compression center as shown in Figure 1-7.

1.3.5 Influence of rib on joint stiffness

The ribs should be accounted for the evaluation of joint stiffness, as well, because they behave as additional mechanical components.

Figure 1-7 shows the proposed mechanical model for strength and stiffness calculation of ES joints, which assemblies the axial springs corresponding to each joint component.

Indeed, as introduced in Chapter III, springs and struts are used to model the behavior of each joint component. Two different components could be introduced to model the rib both on tension and compression side. Indeed, in the first case, the presence of the rib influences the yielding line pattern, thus modifying the effective length and the corresponding strength and stiffness on the end-plate side. Hence, the contribution to the stiffness provided by the rib can be taken into account as follows:

$$k_5 = \frac{0.9 l_{eff} t_p^3}{m^3} \tag{22}$$

where k_5 is the stiffness coefficient for the end-plate in bending (according to EN1993-1-8 table 6.11), t_p is the end-plate thickness, m is a geometrical distance described in Chapter III and l_{eff} is the effective length of the equivalent T-stub.

Moreover, in the components definition, should be also introduced a strut element (without the elastic stiffness, but only with a resistance limit) to consider the own rib resistance to the tension action.

On the compression side, the presence of the rib can be modelled by means of an elastic-plastic spring in parallel with the resultant of the other compression components (see Figure 1-7). Hence, the rib stiffness coefficient compliant to [15] can be expressed as follows:

$$c_{Rib} = \frac{A_e}{L_e} \cdot \cos\left(\arctan\left(\frac{b}{a} \right) \right) \qquad (23)$$

Where A_e is the equivalent area of the strut (see Eq. 16), L_e is the equivalent length of the strut (see Figure 1-4a), while a and b are the sides of rib (see Figure 1-4a).

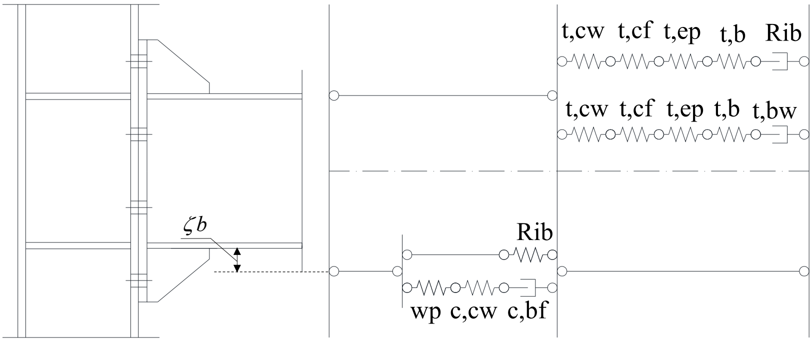

Figure 1-7: Proposed mechanical model for stiffness calculation for ES joints.

1.4 Design assumptions for column web panel

1.4.1 Design shear force

As discussed previously, the rib strut mechanism theoretically corresponds to enlarge the lever arm z_{wp}. As a consequence, the web panel zone involved by the bending transfer mechanism is deeper, which implies reducing the shear forces acting on the column web panel as respect to those developing in unstiffened joints (see Figure 1-8). Therefore, on the basis of the structural scheme reported in Figure 1-9, the design shear force can be estimated as follows:

$$V_{wp,Ed} = \frac{\sum M_{j,Ed}}{z_{wp}} - V_c \qquad (24)$$

Where $\Sigma M_{j,Ed}$ is the sum of bending moments in the beam at the column face; z_{wp} is the distance between the middle of the continuity plate corresponding to the beam flange in tension and the position of center of compression into the connection; V_c is the shear force in the column.

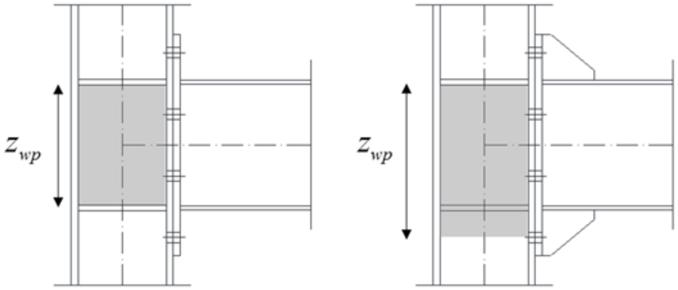

Figure 1-8: Influence of the rib stiffener on column web panel area.

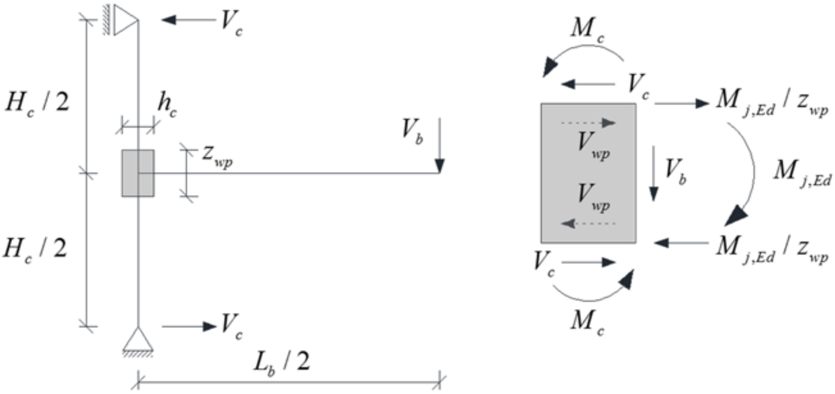

Figure 1-9: Evaluation of shear design force on the column web panel.

1.4.2 Design shear strength

The design plastic shear strength $V_{wp,Rd}$ of column web panel computed according to EN1993-1-8 is given by the following:

$$V_{wp,\mathrm{R}d} = \frac{0.9 \cdot A_v \cdot f_y}{\sqrt{3} \cdot \gamma_{M0}} + V_{wp,add,Rd} \qquad (25)$$

where $V_{wp,add,Rd}$ is the contribution to the web panel shear resistance due to the plastic hinges, which can be developed in the column flanges or continuity plates.

The $V_{wp,add,Rd}$ contribution should be neglected for joint designed to have a strong web panel and where the column should behave in elastic range. As a consequence, additional web plates are necessary in several cases to satisfy the strength requirement. With this regard, in light of experimental results carried out by [4] and the numerical outcomes described hereinafter, it is disregarded the limitation imposed by EC3:1-8 at clause 6.2.6.1(6) for maximum thickness of supplementary web plates. Hence, the resisting shear area A_v is assumed as the sum of column shear area $A_{v,c}$ and the gross area of additional web plates $A_{v,p}$.

Contrariwise, the $V_{wp,add,Rd}$ contribution should be taken into account when the joint is designed with a balance resistance between the connection and the column web panel; in this case indeed, for both equal and partial strength also the column web panel is involved in the plastic range. This consideration is even more true when, the joints are designed considering a weak web panel approach; indeed in this scenario the plastic deformation is balance or totally concentrated (respectively for equal and partial strength) in the column web panel.

In any case for full strength joint the $V_{wp,add,Rd}$ contribution should not be considered since independently from the weaker component i.e. connection or column web panel, only the beam will be involved in the plastic range.

Another aspect needing some remarks is the depth of additional web plates. Indeed, being z_{wp} larger than the beam depth it is assumed the depth of end-plate as minimum depth for these supplementary plates. This assumption should guarantee that the shear resisting area is sufficiently far from the heat affected zone of horizontal fillet welds connecting the plate to the column web panel.

1.5 Design of welds

All design considerations discussed in the previous paragraph require that the failure of welds should be avoided in any case. Apart from the calculation of strength that should comply with

EN1993:1-8 [2], the joint details should be conceived by adopting the most appropriate type of weld depending on the component that must be connected and its relevant plastic engagement. Unfortunately, the current version of EN1993:1-8 does not provide specific details for seismic resistant joints. Hence, the designer is free to select the type of weld base material and details that are nominally able to withstand the design forces, but this approach does not guarantee the fulfilment of the design performance. On the contrary, US practice based on qualification procedure given by AISC358-16 [12] avoids any subjective choice by imposing specific details to guarantee the design objectives. In light of this observation, it is reasonable to extend the main types of weld details given by AISC358-16 to European ES joints. Thereby, three types of weld details, as summarized in Table 1.5, are adopted for the ES joints examined in the parametric study described and discussed hereinafter, namely: fillet weld (FW), plug weld (PW), and full penetration weld (FPW).

Table 1.5: Welds type prescribed in function of the in function of the design criteria [5].

Welded Elements	Joint strength Full	Equal	Partial
Beam flange to End-plate (bf-ep)	FPW	FPW	FPW
Beam web to End-plate (bw-ep)	FPW	FPW	FW
Continuity plates to column (cp-c)	FW	FW	FPW
Rib to End-plate (r-ep)	FPW	FPW	FPW
Rib to Beam flange (r-bf)	FPW	FPW	FPW
Supp. web plates to Column (Swp-c)	FPW+PW	FPW+PW	FPW+PW

In particular, as recommended by AISC358, FPWs are considered for rib stiffeners, because of the large stress concentration and strain demand developing by the rib strut mechanism. FPWs are also used for beam flange to end-plate splices with reinforcing fillet welds according to AISC358-16 provisions. This choice is crucial to ensure the appropriate T-Stub mechanism in the connection zone where the larger demand is expected. On the other hand, beam web to end-plate welds can be FWs, since lesser concentration of stress and relevant strain demand is expected.

Full Penetration welds	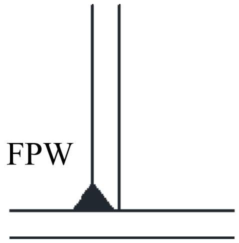	Introduced for: bf-ep (for all the design criteria)
Full Penetration welds	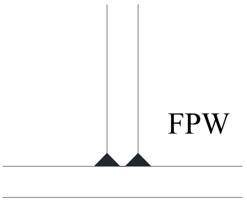	Introduced for: bw-ep (full and equal strength) cp-c (only partial strength) r-ep (for all the design criteria) r-bf (for all the design criteria)
Filled weld	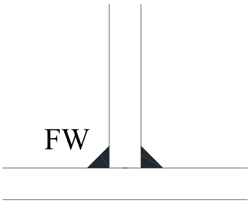	Introduced for: bw-ep (for the partial strength) cp-c (for full equal strength)
Full Penetration welds	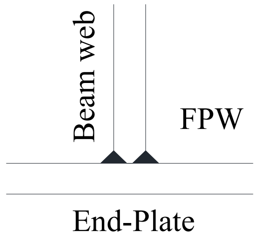	Introduced for: Supplementary web plate to column (for all the design criteria)

Figure 1-10: Type of welds introduced.

On the contrary, if the contribution $V_{wp,add,Rd}$ is accounted for (e.g. for partial strength joints), FPWs should be used in order to avoid brittle failure due to their large plastic engagements.

Finally, consistently to the experimental outcomes by [4], FPWs are considered for connecting the vertical edges of additional web plates to the column and PWs to prevent the buckling or separation of the lapped parts.

2 FEM Calibration and validation

2.1 Modelling assumptions

Finite element analyses (FEAs) were carried out using ABAQUS 6.16 [18]. Both material and geometrical nonlinearities were considered.

As indicated by [19], the element C3D8I (i.e. 8-node linear brick, incompatible mode) is adopted for discretizing all parts constituting the joint, e.g. beams, columns, welds and bolts. This element is selected because it is more effective than C3D8R (i.e. 8-node linear brick, reduced integration) to avoid shear locking phenomenon, which might significantly affect the initial stiffness of joint. The structured meshing technique is assigned to obtain regular shape for elements, especially for those elements discretizing rounded parts, e.g. bolt shanks, bolt head and nuts (see Figure 2-1). The boundary conditions are in accordance with the sub-structuring shown in Figure 2-2, which is consistent with the distribution of internal forces under lateral loads. The bending moment at the mid span of the beam and the column is zero, and the midpoint of the beam and the column under lateral loads is the inflection point with null bending moment and shear force different from zero.

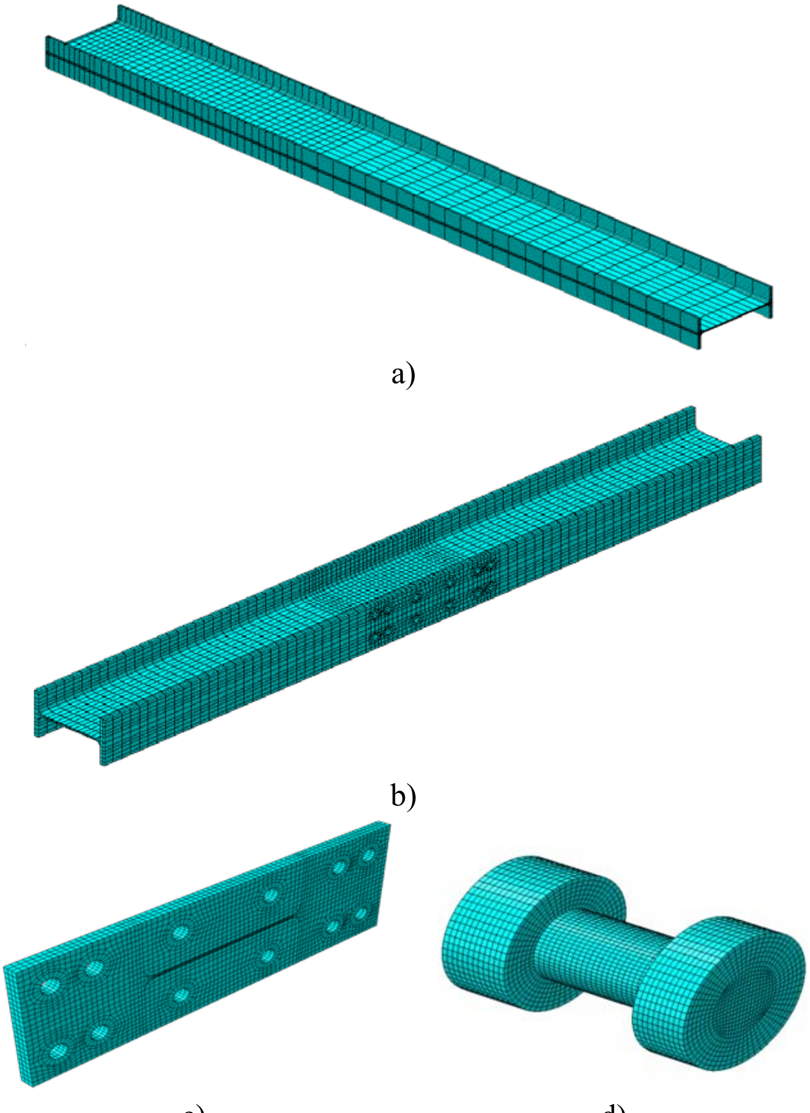

a)

b)

c) d)

Figure 2-1: Element mesh: beam (a), column (b), end-plate (c) and bolts (d).

Torsional restraints out of the length of plastic hinge are also introduced in order to simulate the restraining conditions imposed by the slab. The spacing of lateral torsional restraints is assumed equal to the lateral-torsional stable length segment according to EN 1993-1, clause 6.3.5.3.

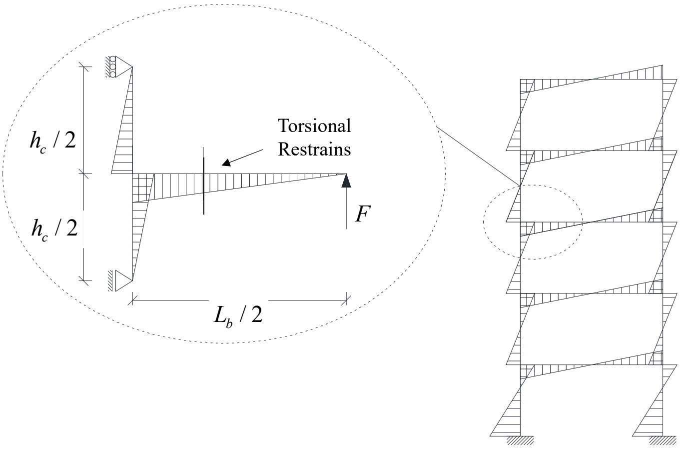

Figure 2-2: Sub-structuring and boundary conditions for FEAs of ES joints.

Contacts are modelled to simulate the interactions between the following surfaces (see Figure 2-3): (i) contact between end plate and column flange; (ii) contact between bolt nuts and the surfaces of end plate and column flange; and (iii) contact between bolt shanks and holes of both end plate and column flange.

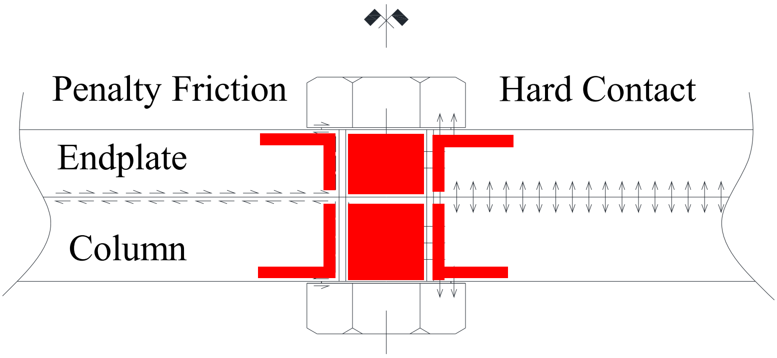

Figure 2-3: Abaqus Contact definition.

Both normal and tangent contacts are considered. The former is formulated with "Hard contact" law that simulates the unilateral contact in the normal direction of the interface between the extended end-plate and the column flange, namely the possible opening of the connected parts. The latter depicts the contribution of the friction to the shear strength of the interface and it is implemented using "Coulomb friction" and a slip coefficient equal to 0.3. This value corresponds to the case of surfaces cleaned by wire-brushing with loose rust removed according to EN1993:1-8 that is the finishing level more commonly adopted in ordinary European practice for building unless specified differently.

The geometrical imperfections in the beam are accounted for (as recommended in EN1993:1-5 [20]) by imposing the deformed shape of the critical buckling modes consistent with the overall lateral-torsional mechanism. In accordance with the European normative (EN 10034 [21]) the amplitude of the imperfections is equal to 80% of the geometric fabrication tolerances. Therefore, according to [21], two configurations of the out of square geometrical imperfections can be used i.e. with coincident flanges or not (see Figure 2-4).

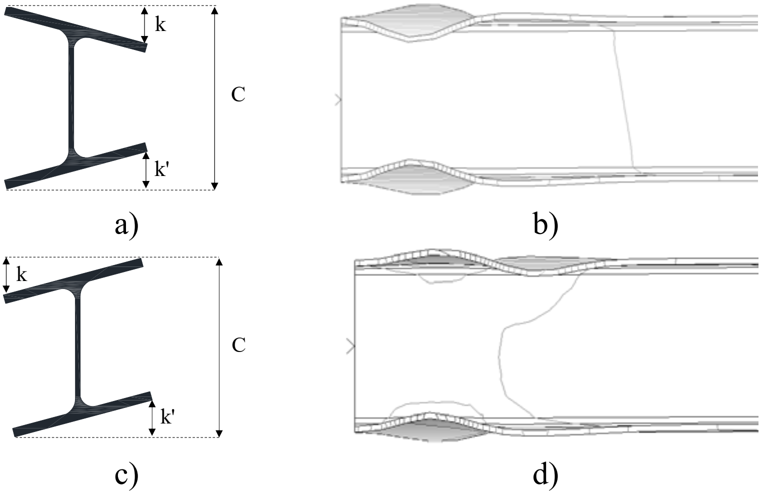

a) b)

c) d)

Figure 2-4: Example of the geometrical imperfections on the beam flanges: a) and b) coincident flange, c) and d) not coincident flange.

In order to investigate, which is the most demanding configuration, two FEM analysis on a cantilever beam, subject to a concentrated force in the extremity, were performed (see Figure 2-5).

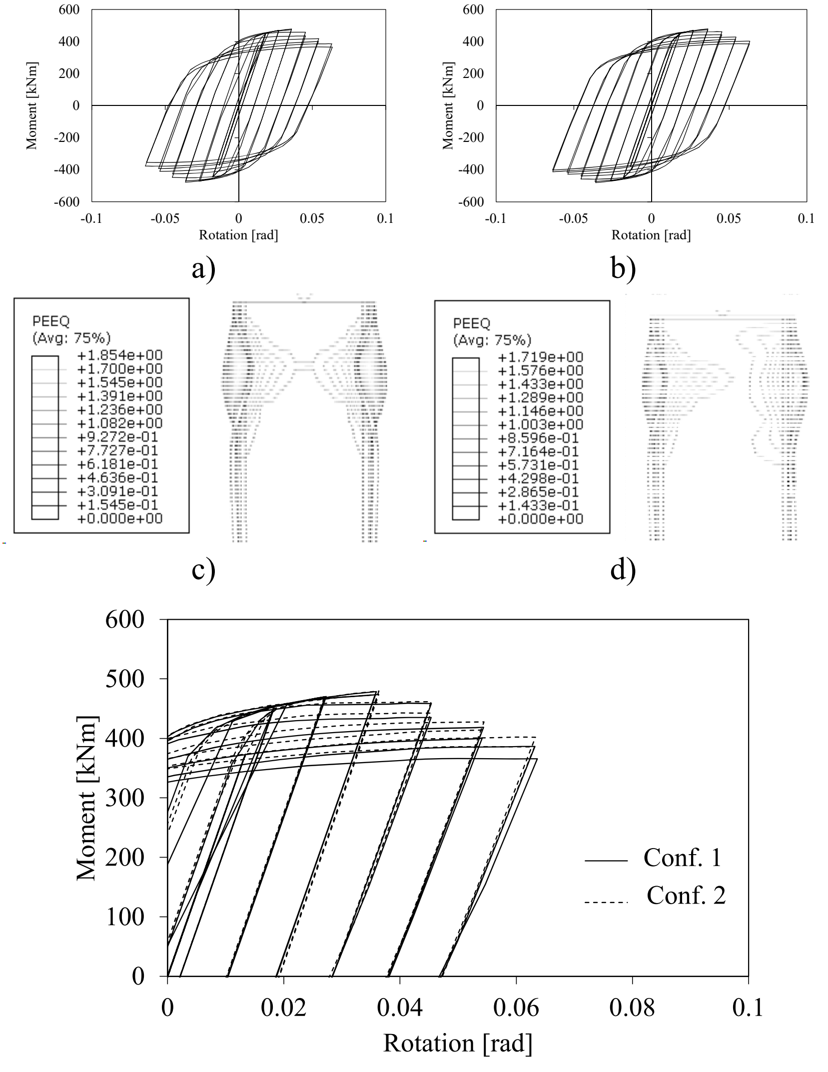

Figure 2-5: Investigation on the imperfection on post-peak strength: a), b), e) in terms of moment rotation curve and c), d) in terms of PEEQ deformation.

Analyzing the results, no significant differences can be pointed out from the comparison of the moment-rotation curves up to 5% of chord rotation, while the PEEQ distribution shows slightly larger values when the beam flange waves are coincident. Therefore, for a conservative approach, coincident buckling waves were modelled in the following analyses.

The clamping force simulating the tightening of bolts was evaluated according to EN1993:1-8 and applied in the middle face of bolt shanks using “Bolt Load” command.

S355 grade with average yield stress estimated as 1.25f_y according to EN1998-1 is assumed for beams, column and plates constituting the joints. Steel yielding is modelled by means of the Von Misess yield criteria. Plastic hardening was represented using both nonlinear kinematic and isotropic hardening law on the basis of the data provided by Dutta et al. [22]. The material constituting high strength bolts is modelled as described by Swanson and Leon [23], which discretize the bolt force–displacement curve by means of a piecewise multilinear relationship, which simulate the elastic response, the yielding and the bolt behavior after the plastic state up to failure. This force-displacement relationship is converted into equivalent stress–strain law, and subsequently expressed in terms of true stress–logarithmic strain curve.

In order to simulate the failure of bolts, the ductile damage in tension option is used with a value of the ultimate strain equal to 0.05. Latour et al. [24] highlighted that the adoption of 0.05 for the ultimate strain is a lower limit (if compared to the ultimate elongation given by EN ISO 898-1 [26]) that does not impair the generality of the results. Indeed, the value of the bolt ultimate strain affects only the ductility of equivalent T-stub if activated, while the resistance is not influenced by the ultimate strain.

An elastic-perfectly plastic stress-strain relationship is assumed for the material simulating the welds, with yield stress equal to 460MPa corresponding to an electrode grade A46 (as given by EN ISO 2560 [25])

Finally, both rib-to-end plate and rib-to-beam flange complete penetration groove welds between the rib and the end plate and all remaining fillet welds are geometrically modelled. The continuity is obtained by introducing an internal restrain tying the surfaces between the weld and the connected region.

2.2 Validation of modelling assumptions

The FEM assumptions are validated against the experimental tests carried out by Shi et al. [27], which tested a set of five ES joints in order to investigate the influence of end-plate geometry and the bolts on failure mechanism under pure bending moment. It should be noted that only the material properties (namely yield strength for steel plates and bolts) and the presence of torsional restraints of the validated models differ from those used in the numerical study presented hereinafter, owing to the need to be consistent with the experimental setup adopted by [27].

The comparison between numerical and experimental results is reported both in terms of joint moment rotation curves and distribution of PEEQ. The latter represents the equivalent plastic strain, and it can be used to show the concentration of plastic deformation and to represent a measure of local ductility and fracture tendency of the material, as well. PEEQ corresponds to the second invariant of the plastic strain tensor and is function of the plastic strain components in the direction specified by i and j, according to the following:

$$PEEQ = \sqrt{\frac{2}{3}\varepsilon_{ij}^{p} \cdot \varepsilon_{ji}^{p}} \qquad (26)$$

As it can be observed from Figure 2-6, the FEA predictions accurately match experimental response curves and failure modes.

EPC1	Test results	PEEQ
	 EPC-1	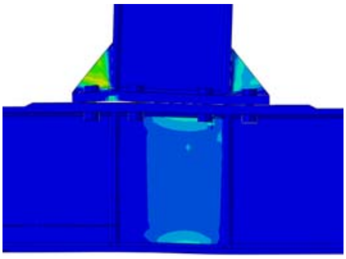
	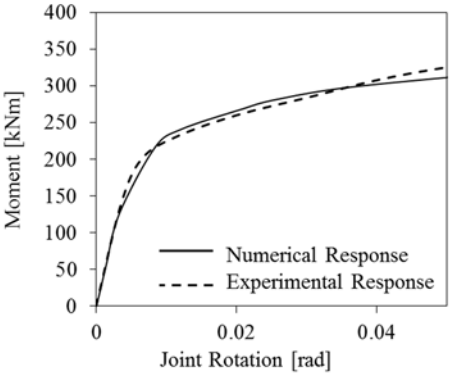	
EPC2	Test results	PEEQ
	 EPC-2	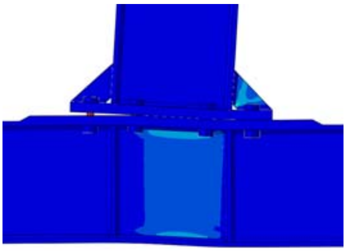

<table>
<tr><td rowspan="2">EPC2</td><td colspan="2">Moment Rotation curve</td></tr>
<tr><td colspan="2">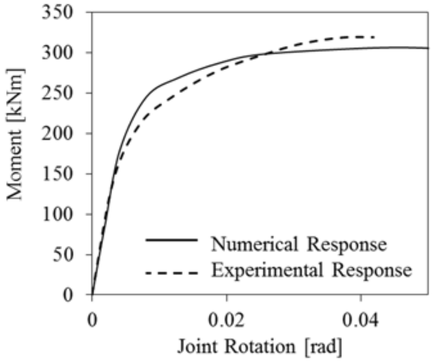
</td></tr>
<tr><td rowspan="4">EPC3</td><td>Test results</td><td>PEEQ</td></tr>
<tr><td>
EPC-3</td><td>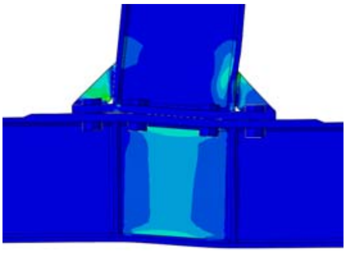</td></tr>
<tr><td colspan="2">Moment Rotation curve</td></tr>
<tr><td colspan="2">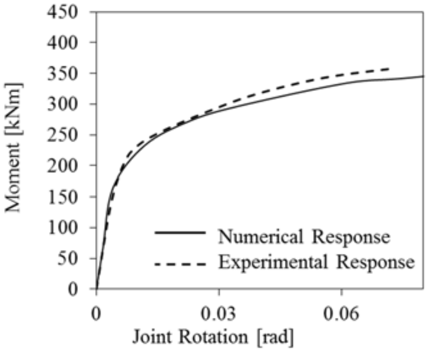
</td></tr>
</table>

<table>
<tr><td rowspan="4">EPC4</td><td>Test results</td><td>PEEQ</td></tr>
<tr><td>
EPC-4</td><td>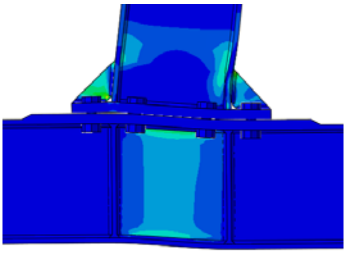</td></tr>
<tr><td colspan="2">Moment Rotation curve</td></tr>
<tr><td colspan="2">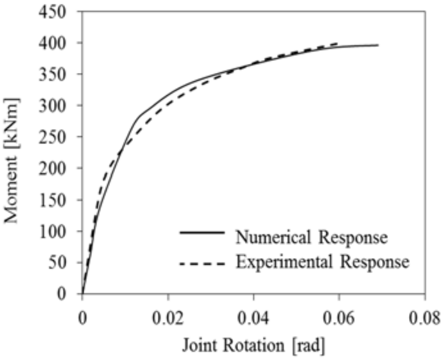
</td></tr>
<tr><td rowspan="2">EPC5</td><td>Test results</td><td>PEEQ</td></tr>
<tr><td>
EPC-5</td><td>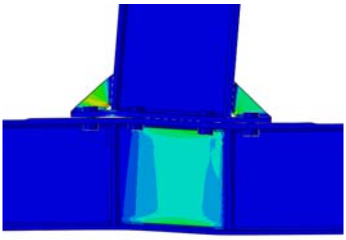</td></tr>
</table>

EPC5	Moment Rotation curve
	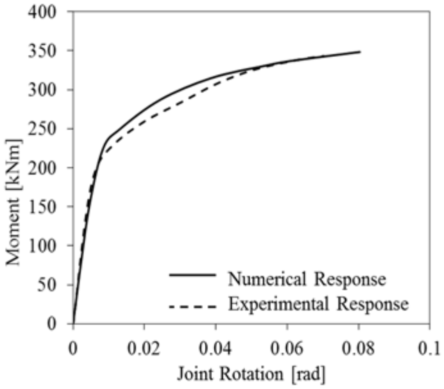

Figure 2-6: Experimental tests by Shi et al. [27] vs. finite element simulations.

3 Validation of design criteria by finite element analyses

3.1 Investigated beam-to-column assemblies

The effectiveness of design criteria discussed is investigated by means of parametric monotonic and cyclic FEAs on a set of beam-to-column assemblies. The dimensions of beam and columns are extracted from an ensemble of low and medium-rise Moment Resisting Frames (MRFs) designed according to EN 1998-1 [1] (see Figure 3-1).

The MRF structure have a square plane with 3×6m and 3×8m spans in both directions, the first story was considered at 4.5m from the ground floor while the interstory height equal to 3.5 m (Figure 3-1 a and b).

Two building heights were considered with 3 and 6 stories. Two MRFs systems are placed in x direction for all the structures length while in y direction, just in the middle spam are placed four MRF systems (Figure 3-2)

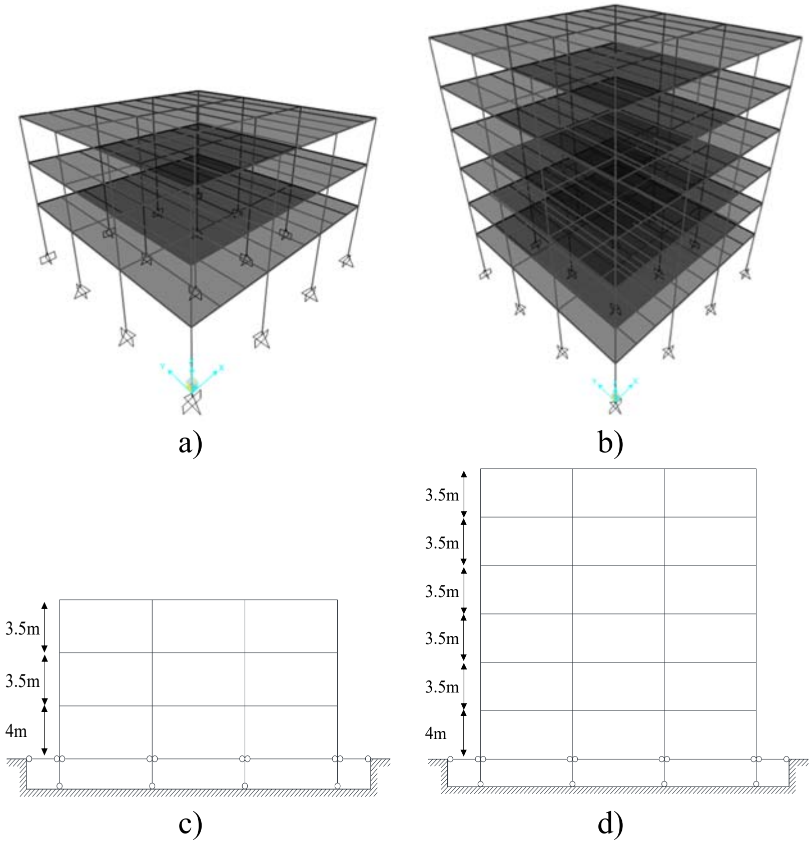

Figure 3-1: MRFs structures designed according to EN1998-1-1 [1]: SAP models (a and b) and longitudinal view (c and d).

The dead load were assumed equal to 5.5 kN/m^2 and live load equal to 3kN/m^2; in addition, according to European practice, two seismicity levels were assumed (i.e. PGA equal to 0.25g and 0.35g). Therefore, eight structures were designed (see Table 3.1), and all the results are summarize from Table 3.2 to Table 3.17.

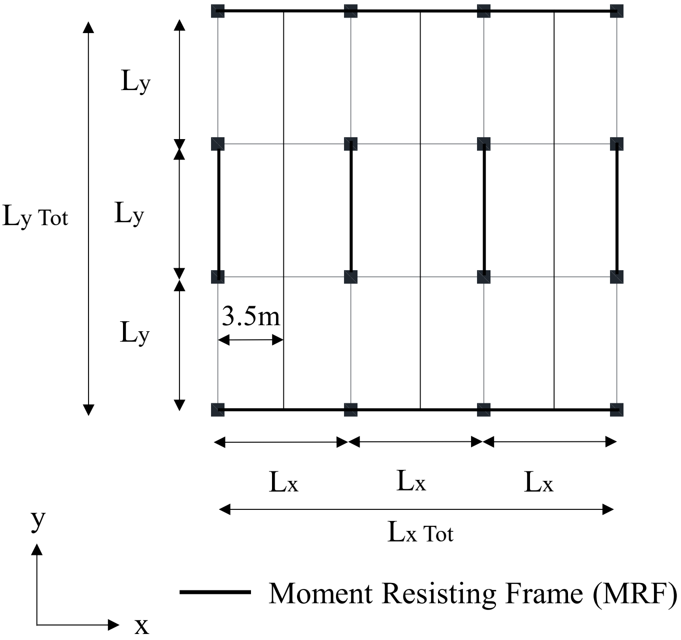

Figure 3-2: MRFs Structures in plane.

Table 3.1: MRFs structures designed.

Labels	Floor [m]	Spam [-]	Length [m]	Seismicity level [g]
M-3-3-6-0.25	3	3	6	0.25
M-3-3-6-0.35	3	3	6	0.35
M-3-3-8-0.25	3	3	8	0.25
M-3-3-8-0.35	3	3	8	0.35
M-6-3-6-0.25	6	3	6	0.25
M-6-3-6-0.35	6	3	6	0.35
M-6-3-8-0.25	6	3	8	0.25
M-6-3-8-0.35	6	3	8	0.35

For all the designed structures, the omega value (Ω) was reported since it is an important parameter that represent the maximum differences between the beams plastic moment capacity and their internal actions under seismic combination loads.

Moreover, since in almost all the design structures, the most restrictive verification was the inter-storey drift limitation, the displacements both in terms of absolute value and in terms of inter-storey drift are reported. Indeed according to EN1993-1-8 (pr. 4.4.3.2), the displacement between the stories (*dr*) should be limited in function of the introduced non-structural elements behavior. In the designed structures a ductile elements were hypothesized and the 0.075 limit was introduced.

Moreover, the second order (P-Delta) effect were verify and the θ (inter-storey drift sensitivity coefficient) values are reported in all the tables. As expected, since the MRF lateral deformability, in almost in all the cases θ value is between 0.1 and 0.2, and in this case the secondary order effects can be approximately take into account by multiplying the seismic action effect by α (according to EN1993-1-8 pr. 44.2.2), where α is equal to 1/(1-θ).

Table 3.2: M-3-3-6-0.25 geometry characteristics.

Floor	Columns		Beams		Spam Length	Interstory
	External	Internal	External	Internal	[m]	[m]
I	HE300B	HE400B	IPE450	IPE450	6	4.5
II	HE280B	HE340B	IPE360	IPE360		3.5
III	HE280B	HE340B	IPE330	IPE330		3.5

Table 3.3: M-3-3-6-0.25 design results.

Floor	Omega	θ	α	Lateral Displacemnts	
	[-]	[%]	[-]	[m]	[%]
I	2.83	5.66%	1.06	0.050	0.56%
II		6.35%	1.07	0.052	0.75%
III		4.71%	1.05	0.043	0.62%

Table 3.4: M-3-3-6-0.35 geometry characteristics.

Floor	Columns		Beams		Spam Length	Interstory
	External	Internal	External	Internal	[m]	[m]
I	HE400B	HE550B	IPE500	IPE500	6	4.5
II	HE340B	HE550B	IPE450	IPE450		3.5
III	HE340B	HE500B	IPE450	IPE450		3.5

Table 3.5: M-3-3-6-0.35 design characteristics.

Floor	Omega	θ	α	Lateral Displacements	
	[-]	[%]	[-]	[m]	[%]
I	3.24	2.95%	1.03	0.053	0.59%
II		3.22%	1.03	0.053	0.76%
III		2.12%	1.02	0.040	0.57%

Table 3.6: M-3-3-8-0.25 geometry characteristics.

Floor	Columns		Beams		Spam Length	Interstory
	External	Internal	External	Internal	[m]	[m]
I	HE450B	HE550B	IPE500	IPE500		4.5
II	HE450B	HE550B	IPE500	IPE500	8	3.5
III	HE400B	HE500B	IPE500	IPE500		3.5

Table 3.7: M-3-3-8-0.25 design characteristics.

Floor	Omega	θ	α	Lateral Displacements	
	[-]	[%]	[-]	[m]	[%]
I		5.5%	1.06	0.0508	0.56%
II	2.60	5.7%	1.06	0.0493	0.70%
III		3.5%	1.04	0.0356	0.51%

Table 3.8: M-3-3-8-0.35 geometry characteristics.

Floor	Columns		Beams		Spam Length	Interstory
	External	Internal	External	Internal	[m]	[m]
I	HE550B	HE650M	IPE600	IPE600		4.5
II	HE500B	HE650B	IPE600	IPE600	8	3.5
III	HE500B	HE650B	IPE500	IPE500		3.5

Table 3.9: M-3-3-8-0.35 design characteristics.

Floor	Omega	θ	α	Lateral Displacements	
	[-]	[%]	[-]	[m]	[%]
I		2.99%	1.03	0.052	0.56%
II	2.95	3.36%	1.03	0.054	0.75%
III		2.35%	1.02	0.043	0.61%

Table 3.10: M-6-3-6-0.25 geometry characteristics.

Floor	Columns		Beams		Spam lentgh	Interstory
	External	Internal	External	Internal	[m]	[m]
I	HE500B	HE550B	IPE550	IPE550	6	4.5
II	HE500B	HE550B	IPE550	IPE550		3.5
III	HE450B	HE500B	IPE500	IPE500		3.5
IV	HE450B	HE500B	IPE450	IPE450		3.5
V	HE400B	HE450B	IPE400	IPE400		3.5
VI	HE400B	HE450B	IPE360	IPE360		3.5

Table 3.11: M-6-3-6-0.25 design characteristics.

Floor	Omega	θ	α	Lateral Displacements	
	[-]	[%]	[-]	[m]	[%]
I	3.59	4.67%	1.05	0.034	0.38%
II		5.46%	1.06	0.035	0.49%
III		5.30%	1.06	0.037	0.53%
IV		4.95%	1.05	0.037	0.53%
V		4.55%	1.05	0.037	0.53%
VI		3.45%	1.04	0.030	0.42%

Table 3.12: M-6-3-6-0.35 geomwtry characteristics.

Floor	Columns		Beams		Spam lentgh	Interstory
	External	Internal	External	Internal	[m]	[m]
I	HE550B	HE650B	IPE600	IPE600	6	4.5
II	HE550B	HE650B	IPE600	IPE600		3.5
III	HE500B	HE600B	IPE550	IPE550		3.5
IV	HE500B	HE600B	IPE500	IPE500		3.5
V	HE450B	HE550B	IPE500	IPE500		3.5
VI	HE450B	HE550B	IPE360	IPE360		3.5

Table 3.13: M-6-3-6-0.35 design characteristics.

Floor	Omega	θ	α	Lateral Displaements	
	[-]	[%]	[-]	[m]	[%]
I	3.86	2.35%	1.02	0.028	0.31%
II		2.78%	1.03	0.029	0.42%
III		2.70%	1.03	0.031	0.44%
IV		2.48%	1.03	0.031	0.44%
V		2.10%	1.02	0.028	0.40%
VI		1.64%	1.02	0.023	0.32%

Table 3.14: M-6-3-8-0.25 geometry characteristics.

Floor	Columns		Beams		Spam lentgh	Interstory
	External	Internal	External	Internal	[m]	[m]
I	HE600M	HE650M	IPE600	IPE600	8	4.5
II	HE600M	HE650M	IPE600	IPE600		3.5
III	HE550M	HE600M	IPE600	IPE600		3.5
IV	HE550M	HE600M	IPE550	IPE550		3.5
V	HE500M	HE550M	IPE550	IPE550		3.5
VI	HE500M	HE550M	IPE500	IPE500		3.5

Table 3.15: M-6-3-8-0.25 design characteristics.

Floor	Omega	θ	α	Lateral Displacements	
	[-]	[%]	[-]	[m]	[%]
I	3.44	4.38%	1.05	0.038	0.42%
II		5.88%	1.06	0.045	0.64%
III		5.36%	1.06	0.045	0.64%
IV		4.53%	1.05	0.041	0.59%
V		3.60%	1.04	0.035	0.50%
VI		2.46%	1.03	0.025	0.36%

Table 3.16: M-6-3-8-0.35 geomerty characteristics.

Floor	Columns		Beams		Spam lentgh	Interstory
	External	Internal	External	Internal	[m]	[m]
I	HE650M	HE800M	IPE750x173	IPE750x173	8	4.5
II	HE650M	HE800M	IPE750x173	IPE750x173		3.5
III	HE600M	HE700M	IPEO600	IPEO600		3.5
IV	HE600M	HE700M	IPEO600	IPEO600		3.5
V	HE550M	HE600M	IPE550	IPE550		3.5
VI	HE550M	HE600M	IPE500	IPE500		3.5

Table 3.17: M-6-3-8-0.35 design characteristics.

Floor	Omega	θ	α	Lateral Displacements	
	[-]	[%]	[-]	[m]	[%]
I	3.38	2.32%	1.02	0.037	0.41%
II		2.97%	1.03	0.041	0.59%
III		3.08%	1.03	0.046	0.66%
IV		2.84%	1.03	0.046	0.66%
V		2.51%	1.03	0.043	0.61%
VI		1.97%	1.02	0.036	0.51%

From the designed structures, three beam-to-column configurations were selected for the numerical investigations, which are the following:

- ES1: IPE360 – HEB 280;
- ES2: IPE450 – HEB 340;
- ES3: IPE600 – HEB 500.

Three levels of design performance are considered: (i) full, (ii) equal (with strong column web panel) and (iii) partial strength (with balance column web panel).

For full strength joints it is investigated the influence of design overstrength (i.e. accounting for both randomness of yield strength and strain hardening) on joint response. Furthermore, the ultimate capacity and the relevant failure modes of full strength joints are examined by performing analyses assuming a fictitiously elastic behavior of the beam (i.e. no plasticity for the material of beams). In order to investigate the influence of the rib stiffeners on the strength and stiffness of joints, each assembly is also analyzed with and without rib at the same other geometrical and mechanical properties. In addition, another set of 9 joints strictly designed according to both EC3 and EC8 requirements (e.g. effective lengths, end-plate thickness, column web panel strength and lever arm calculated as given by EN1993:1-8, and overstrength as given by EN1998-1) to fulfil the three design objectives (namely full, equal and partial strength) were analyzed in order to outline the differences with the proposed criteria.

Finally, 30 joints were designed and investigate. Twelve full strength joint (four for each assembly) were designed according to: (i) Standard EN19931-1-8 procedure (EC), (ii) new design procedure with the compression center position according to Lee (Lee), (iii) new design procedure with the compression center position according to Abidelah (Ab) and (iv) new design procedure with the overstrength factor according to EN1998-1-1 (EC8). Nine Equal and Partial strength joints (three for each assembly) were designed according to: (i) Standard EN19931-1-8 procedure (EC), (ii) new design procedure with the compression center position according to Lee (Lee) and (iii) new design procedure with the compression center position according to Abidelah (Ab).

It should be noted that S355 is assumed for all steel elements (i.e both members and plates), grade S460 (see EN ISO 2560 [25]) for welds and high strength grade 10.9 pre-loadable bolts (see EN ISO 898-1 [26]).

All the geometrical properties are explained in Figure 3-3 and reported from Table 3.18 to Table 3.20.

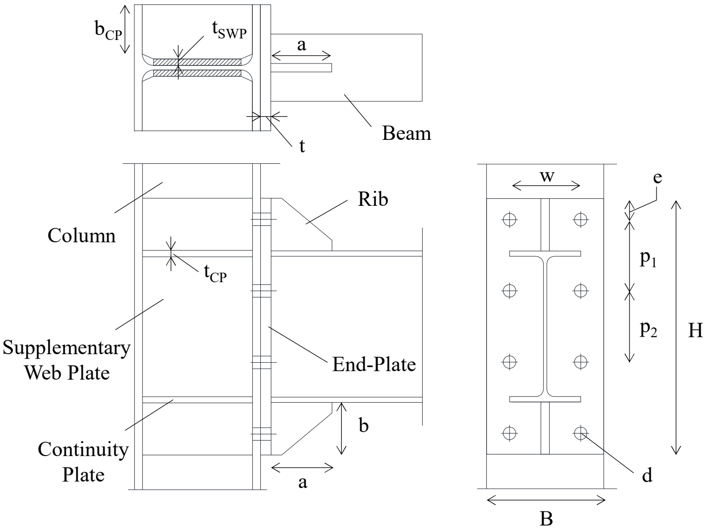

Figure 3-3: Main geometrical details of ES joints reported in Table 4.

Each joint is analyzed under both monotonic and AISC341-10 [5] loading protocol. The numerical results are post-processed for total chord rotations ranging between 1% and 4%, in order to characterize thoroughly the joint performance into the range of expected demand according to AISC341 [5] and EN1998-1 [1]. Moreover, all contributions to chord rotation are examined, namely web panel distortion, connection, beam and column rotations, respectively. The results shown in the following refer to both (i) total chord rotation, and (ii) joint rotation, which is rotation of the connection and the contribution of the web panel, neglecting the contribution of beam and columns.

Table 3.18: ES1 joints geometrical characteristics.

Joint ID	Design Criteria	Comp. center	End-Plate			Bolt spacing					CP	Additional web plate	
			H	B	t	d	e	w	p1	p2	t_{CP}	Side	t_{SWP}
			mm	mm	mm	mm	mm	mm	mm	mm	mm	-	mm
ES1-F-EC	F(1.1γov)	EC	760	260	25	30	50	150	80	155	14	2	14
ES1-F-C1	F(γshγov)	Lee	760	260	25	30	50	160	75	160	14	2	8
ES1-F-C2	F(γshγov)	AB	760	260	25	30	50	150	75	160	14	2	8
ES1-F-BE	F(γshγov)+BE	Lee	760	260	25	30	50	160	75	160	14	2	8
ES1-F-EC8,ov	F(1.1γov)	Lee	760	260	18	30	50	170	70	165	14	2	8
ES1-F-EC8,ov-BE	F(1.1γov)+BE	Lee	760	260	18	30	50	170	70	165	14	2	8
ES1-F_NR	F(γshγov)	Lee	760	260	25	30	50	160	75	160	14	2	8
ES1-E-EC	E	EC	600	280	20	30	50	160	160	180	14	2	8
ES1-E-C1	E	Lee	600	280	18	27	50	170	160	180	14	1	8
ES1-E-C2	E	Ab	600	280	18	27	50	160	160	180	14	1	8
ES1-E_NR	E	Lee	600	280	18	27	50	170	160	180	14	1	8
ES1-P08-EC	P08	EC	600	280	18	27	50	170	160	180	14	1	8
ES1-P08-C1	P08	Lee	600	280	16	27	50	170	160	180	14	-	-
ES1-P08-C2	P08	Ab	600	280	16	27	50	160	160	180	14	-	-
ES1-P08_NR	P08	Lee	600	280	16	27	50	170	160	180	14	-	-

Table 3.19: ES2 joints geometrical characteristics.

Joint ID	Design Criteria	Comp center	End-Plate			Bolt spacing					CP	Additional web plate	
			H	B	t	d	e	w	p1	p2	t_{CP}	Side	t_{SWP}
			mm	mm	mm	mm	mm	mm	mm	mm	mm	-	mm
ES2-F-EC	F(1.1γov)	EC	870	280	25	30	50	160	90	155	15	2	16
ES2-F-C1	F(γshγov)	Lee	870	280	25	30	50	160	75	180	15	2	10
ES2-F-C2	F(γshγov)	AB	870	280	25	30	50	150	75	180	15	2	10
ES2-F-BE	F(γshγov)+BE	Lee	870	280	25	30	50	160	75	180	15	2	10
ES2-F-EC8,ov	F(1.1γov)	Lee	870	280	22	30	50	170	70	190	15	2	10
ES2-F-EC8,ov-BE	F(1.1γov)+BE	Lee	870	280	22	30	50	170	70	190	15	2	10
ES2-F_NR	F(γshγov)	Lee	870	280	25	30	50	160	75	180	15	2	10
ES2-E-C1	E	EC	770	300	25	30	55	170	200	260	15	2	8
ES2-E-C1	E	Lee	770	300	20	30	55	170	200	260	15	1	8
ES2-E-C2	E	Ab	770	300	20	30	55	160	200	260	15	1	8
ES2-E_NR	E	Lee	770	300	20	30	55	170	200	260	15	1	8
ES2-P08-EC	P08	EC	770	300	18	30	55	160	200	260	15	1	12
ES2-P08-C1	P08	Lee	770	300	18	30	55	170	200	260	15	-	-
ES2-P08-C2	P08	Ab	770	300	18	30	55	160	200	260	15	-	-
ES2-P08_NR	P08	Lee	770	300	18	30	55	170	200	260	15	-	-

Table 3.20: ES3 joints geometrical characteristics.

Joint ID	Design Criteria	Comp Centre	End-Plate			Bolt spacing					CP	Additional web plate	
			H	B	t	d	e	w	p1	p2°	t_{CP}	Side	t_{SWP}
			mm	mm	mm	mm	mm	mm	mm	mm	mm	-	mm
ES3-F-EC	F(1.1γov)	EC	1100	280	30	36	50	170	115	190	20	2	16
ES3-F-C1	F(γshγov)	Lee	1100	280	30	36	55	170	95	210	20	2	15
ES3-F-C2	F(γshγov)	AB	1100	280	30	36	55	160	95	210	20	2	15
ES3-F-BE	F(γshγov)+BE	Lee	1100	300	30	36	55	170	95	210	20	2	15
ES3-F-EC8,ov	F(1.1γov)	Lee	1100	280	28	36	55	170	90	230	20	2	15
ES3-F-EC8,ov-BE	F(1.1γov)+BE	Lee	1100	280	28	36	55	170	90	230	20	2	15
ES3-F_NR	F(γshγov)	Lee	1100	300	30	36	55	170	95	210	20	2	15
ES3-E-EC	E	EC	1100	300	25	36	55	170	95	210	20	1	15
ES3-E-C1	E	Lee	1100	300	22	36	55	170	95	210	20	1	15
ES3-E-C2	E	Ab	1100	300	22	36	55	160	95	210	20	1	15
ES3-E_NR	E	Lee	1100	300	22	36	55	170	95	210	20	1	15
ES3-P08-C1	P08	EC	1100	300	22	36	55	170	95	210	20	1	15
ES3-P08-C1	P08	Lee	1100	300	20	36	55	170	95	210	20	-	-
ES3-P08-C2	P08	Ab	1100	300	20	36	55	160	95	210	20	-	-
ES3-P08_NR	P08	Lee	1100	300	20	36	55	170	95	210	20	-	-

3.2 Comparison between current Eurocode and proposed design approach

The comparison between the geometrical properties reported from Table 3.18 to Table 3.20 clearly shows that the both Eurocode complaint joints and those designed according to the proposed approach have similar dimensions, but with heavy details (e.g. the thickness of plates) for Eurocode compliant joints. The comparison of response curves shown in Figure 3-4 for all joints assemblies, alternatively designed according to both approaches, clearly highlights that the overall performance does not exhibit appreciable variation for full strength joints, while both equal and partial strength joints designed according to EC3 are characterized by larger flexural strength. This feature can be explained considering that EC3 assumes the center of compression in the middle of beam flange in compression, thus underestimating the lever arm. Hence, to fulfil the strength requirement it is necessary to overdesign the strength at each bolt-row, thus indirectly counterbalancing the rough estimation of the lever arm. Even though unconsciously, this feature is still consistent with the design objective. Figure 3-5 shows both the Von Mises stress and PEEQ distribution at chord rotation equal to 4% for full strength joints. It is interesting to note that Eurocode-compliant joints have higher concentration of plasticity in the bolts than the cases designed according to proposed approach, where a higher concentration of plasticity in the beam flange is observed. This result highlights the effectiveness of the additional design requirement expressed by Eq. 18.

Even for equal and partial strength joints, small differences in terms of overall response between Eurocode and proposed criteria can be observed. Anyway, joints designed according to Eurocodes are characterized by slightly larger strength and lesser plastic engagement than those designed according to the proposed approach, once more due to the larger thickness of connection components. This issue is also confirmed by plastic strain demand at different levels of joint rotation.

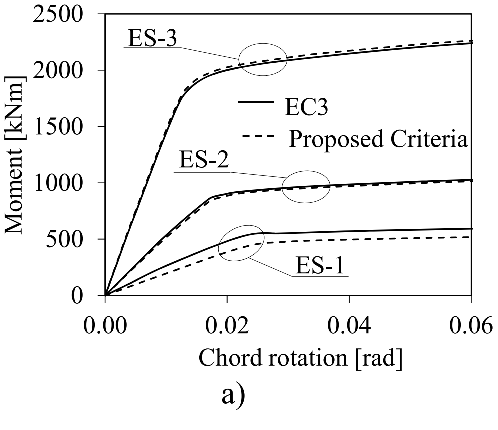

a)

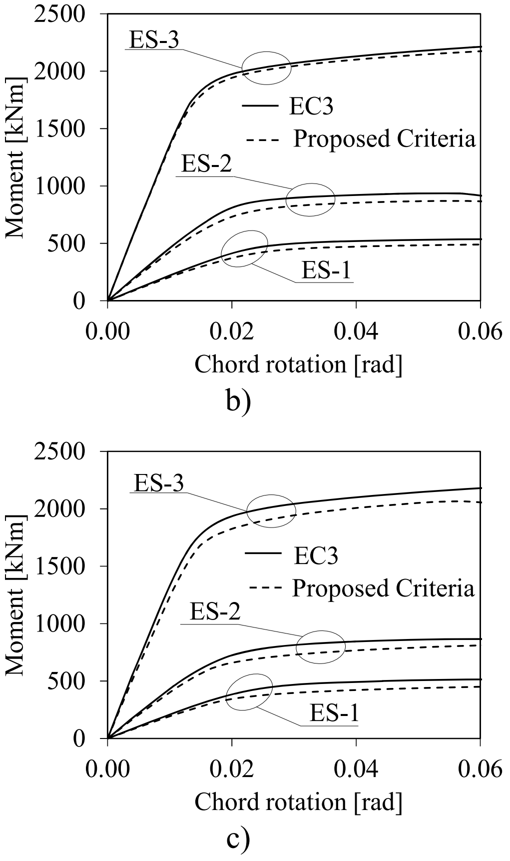

Figure 3-4: Moment-rotation response curves: Eurocode vs. proposed design criteria for full (a), equal (b) and partial (c) strength joints.

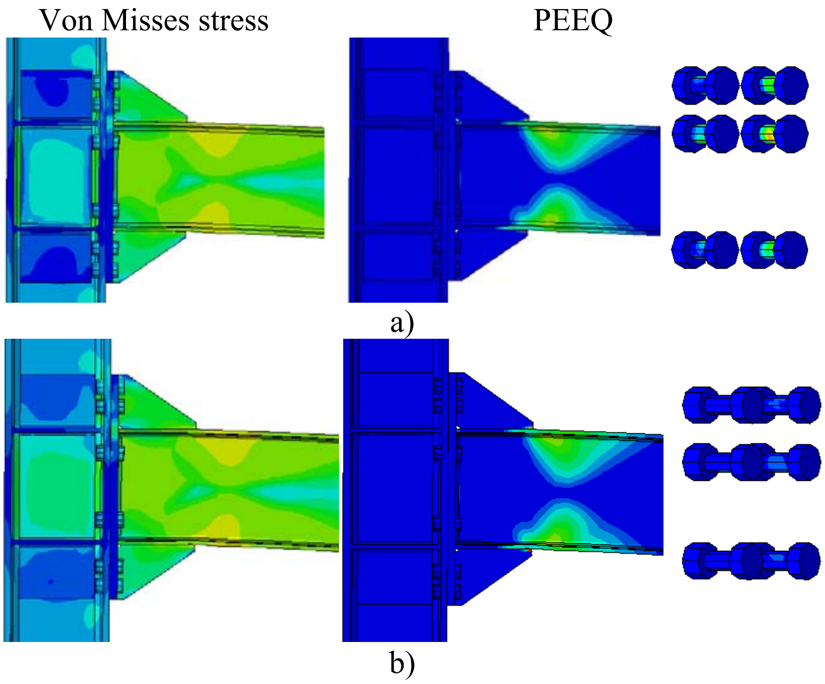

Figure 3-5: Von Misses stress and PEEQ distribution: Eurocode (a) vs. proposed (b) design approach.

3.3 Influence of the design overstrength

In order to evaluate the influence of the design overstrength to guarantee full strength joints, two sets of joints are designed according to the proposed criteria (see Table 4), considering alternatively two different overstrength factors: (i) $\gamma_{sh}\times\gamma_{o}V \geq 1.2\times1.25 = 1.50$ (being γ_{sh} = max{γsh, AISC, s}); (ii) 1.1×γov =

1.1×1.25 = 1.375, which is the overstrength factor recommended by EC8.

As shown in Table 3.18 to Table 3.20, the geometries are similar, but using EC8 overstrength thinner end plates can be obtained.

Since the response is analogous for all beam-to-column assemblies, for briefness sake the results are shown hereinafter for the set of joints with intermediate beam depth (i.e. ES2 joints). Figure 3-6 shows the flexural response and the shape of plastic mode of this couple of full strength joints. The differences in terms of both strength and stiffness of total chord rotation are negligible (see Figure 3-6 a). However, focusing only on the joint response curve extracted from the total chord rotation (see Figure 3-6 b), it is evident that joints designed assuming EC8 overstrength factor exhibit plastic deformations larger than those experienced by the stronger joint. This finding is also better clarified by comparing the PEEQ distributions for the former (see Figure 3-6 c, d) and second case (see Figure 3-6 e, f), which start developing for chord rotations larger than 2%.

The joint designed with the proposed overstrength mainly exhibits beam plasticization with negligible plastic strains for the other elements.

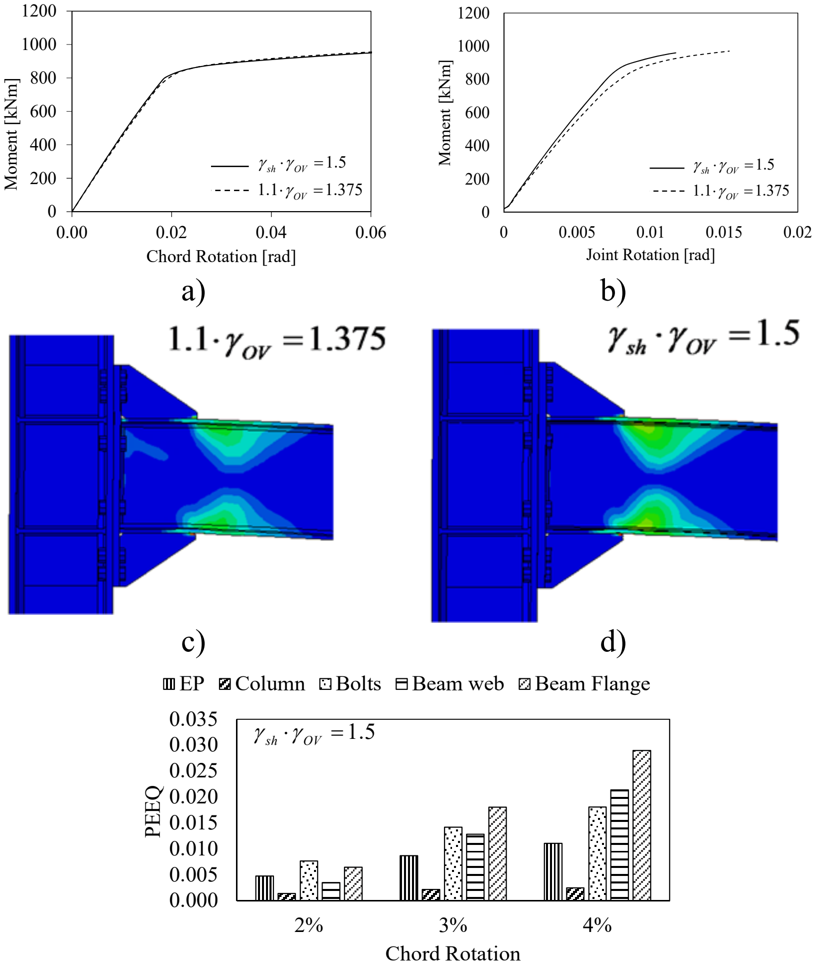
1200
1000
800
600
400
200
0
Moment [kNm]
0.00
0.02
0.04
0.06
Chord Rotation [rad]
$\gamma_{sh} \cdot \gamma_{OV} = 1.5$
$1.1 \cdot \gamma_{OV} = 1.375$
0
0.005
0.01
0.015
0.02
Joint Rotation [rad]
$1.1 \cdot \gamma_{OV} = 1.375$
$\gamma_{sh} \cdot \gamma_{OV} = 1.5$
▥ EP
▨ Column
⊡ Bolts
⊟ Beam web
▧ Beam Flange
0.035
0.030
0.025
0.020
0.015
0.010
0.005
0.000
PEEQ
2%
3%
4%
Chord Rotation

a) b)

c) d)

e)

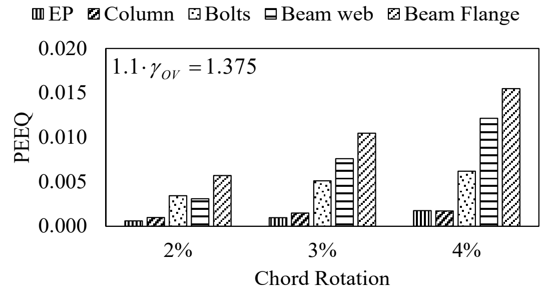

f)

Figure 3-6: Results of the overstrenght investigation in terms of: (a) Moment chord rotation, (b) Moment joint rotation, (c and d) PEEQ distribution and (e and f) PEEQ in evolution at 2%, 3% and 4% of chord rotation.

In order to characterize the ultimate capacity and the relevant failure mode of full strength joints, beams are also fictitiously modelled with a perfectly elastic behavior. This assumption allows shifting the formation of plastic mechanism from beam to the joint. The results of these analyses confirm the larger strength (i.e. about 10% more) of the joints designed using the proposed overstrength factor (see Figure 3-7).

3.4 Influence of Rib on strength and stiffness

In order to highlight the influence of rib stiffeners on strength and stiffness of extended end-plate joints, all beam-to-column assemblies are analyzed with and without ribs.

Figure 3-8 and Figure 3-9 show the yield line pattern achieved at chord rotation equal to 4% for the case with one and two bolt rows above the beam flange in tension, respectively.

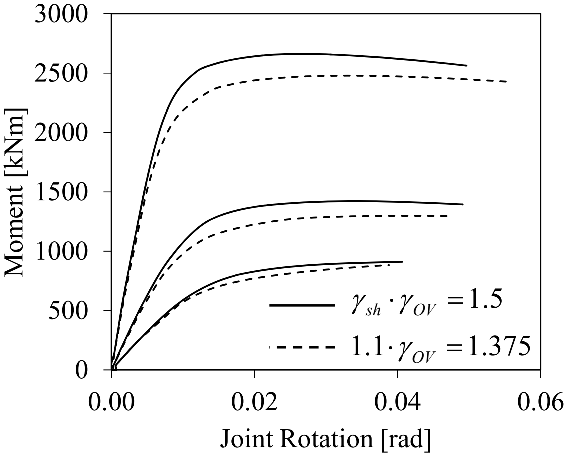

Figure 3-7: Flexural response of full strength joints assuming indefinite elastic behavior for beams.

The equivalent T-Stub above beam flange in tension of the unstiffened joint with one bolt rows up is characterized by beam-type mode (see Figure 3-8 a), while the yield line pattern of the corresponding stiffened joint is different (see Figure 3-8 b).

Indeed, in the latter case the yield lines are mainly bounded by the rib and the beam flange, as well, forming a X-shape that involves a 3D mechanism, consistent with the circular yield line.

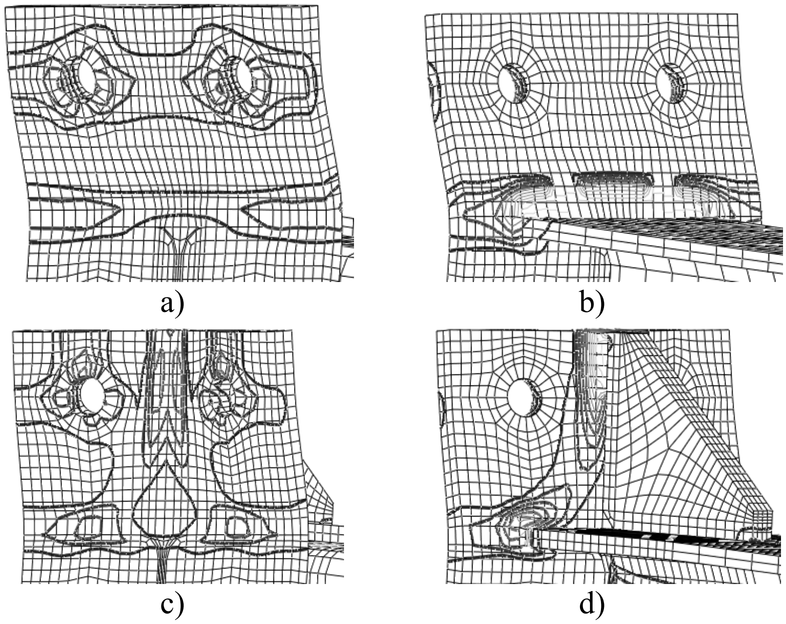
a) b)
c) d)

Figure 3-8: Yield lines for one bolt row up configuration: a) Unstiffened and b) Stiffened joints.

The cases with two bolt rows up configurations show analogous response. Once more, the T-Stub mechanisms and the relevant group effect for unstiffened end-plate joint are consistent with the EC3 predictions (see Figure 3-9 a). While the plastic mode of the corresponding stiffened joint is significantly different (see Figure 3-9 b).

Even in this case, the circular yield line is restrained by the rib and beam flange, but no group effect can be recognized.

Figure 3-10 shows the response curves for full (F), equal (E) and partial (P) strength joints with both extended stiffened (i.e. ES1, ES2 and ES3) and unstiffened (i.e. E1, E2 and E3) configuration up to a total chord rotation equal to 0.06 rad.

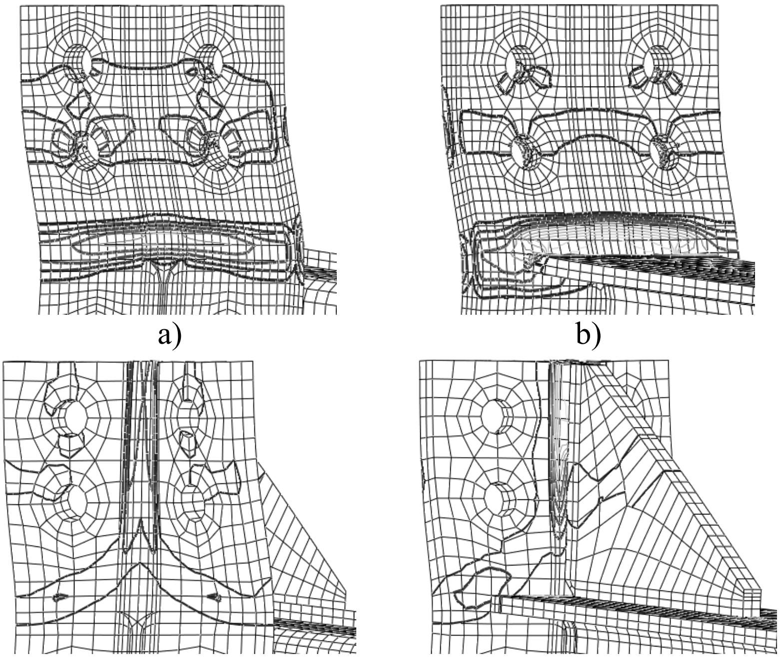

a) b)

c) d)

Figure 3-9: Yield lines for tow bolt rows up configuration: a) Unstiffened and b) Stiffened joints.

The plots confirm that all full strength ES joints behave in elastic range, while the corresponding unstiffened joints are characterized by plastic engagement even though lower than equal and partial unstiffened joints. As reported in Table 3.21, the rib increases both stiffness (from 8% to 42%) and strength (from 14% to 83%) of joints. These results confirm the need to properly account for the rib contribution as an additional component in analytical modelling.

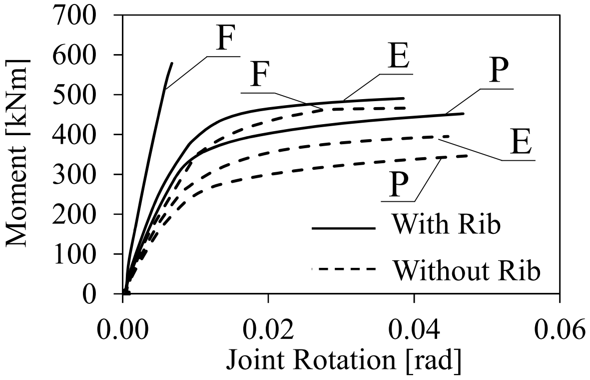

a)

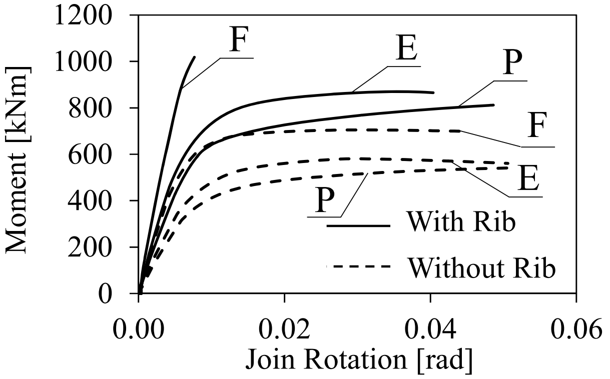

b)

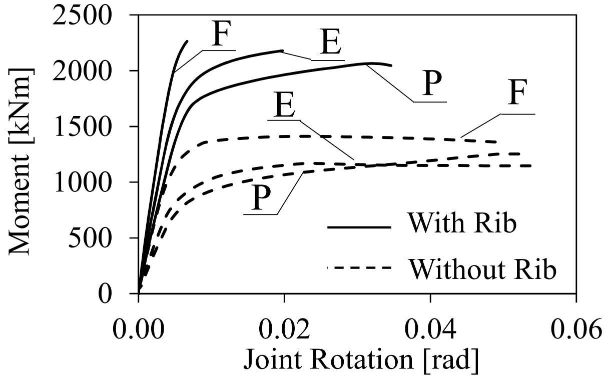

c)

Figure 3-10: The influence of the rib stiffener on moment-joint rotation response curve; a) ES1 vs. E1, b)ES2 vs. E2 and c)ES3 vs. E3 joints.

Table 3.21: Stiffened vs Unstiffened joint: Strength and Stiffness.

Joint assembly	Joint Perf.	Conf.	Stiff.	Increase stiff ratio	Res.	Increase Res. ratio	Beam Stiff	Beam Stiff. ratio
[-]	[-]	[-]	[kNm]	[-]	[kNm]	[-]	[kNm]	[-]
ES1-F	F	R	97297	2.25	578	1.24	5239	19
ES1-F_NR	F	WR	43243		466			8
ES1-E	E	R	54054	1.43	490	1.24		10
ES1-E_NR	E	WR	37838		395			7
ES1-P	P	R	45946	1.37	452	1.31		9
ES1-P_NR	P	WR	33514		346			6
ES2-F	F	R	167568	1.59	1018	1.44	10993	15
ES2-F_NR	F	WR	105405		705			10
ES2-E	E	R	116216	1.67	870	1.50		11
ES2-E_NR	E	WR	69730		581			6
ES2-P	P	R	90811	1.56	812	1.50		8
ES2-P_NR	P	WR	58378		541			5
ES3-F	F	R	497297	1.67	2264	1.60	30694	16
ES3-F_NR	F	WR	297297		1411			10
ES3-E	E	R	378378	1.75	2179	1.86		12
ES3-E_NR	E	WR	216216		1169			7
ES3-P	P	R	297297	1.83	2066	1.65		10
ES3-P_NR	P	WR	162162		1253			5

3.5 Position of compression center

The position (ξb) of center of compression is derived from FEAs by integrating the contact pressure between the end-plate and the column face. In order to verify the accuracy of design assumptions proposed by Lee [15] and Abidelah et al. [16], two sets of joints are designed (see Table 3.19 Table 3.20 for details about the geometrical properties) and analyzed. As shown in Figure 3-11, the contact area between end-plate and the column face varies with the imposed rotation and it differs with the design joint strength. This result implies that also the position ξb and the relevant neutral axis depth in plastic range depend on the level of rotation demand.

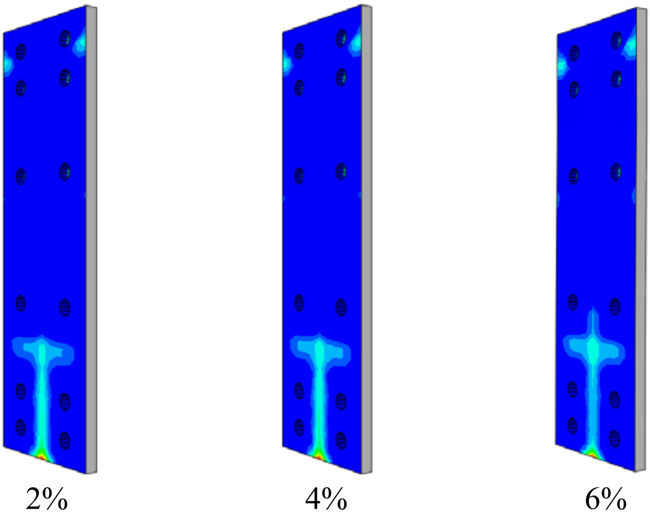
2% 4% 6%

ES2-F-C2

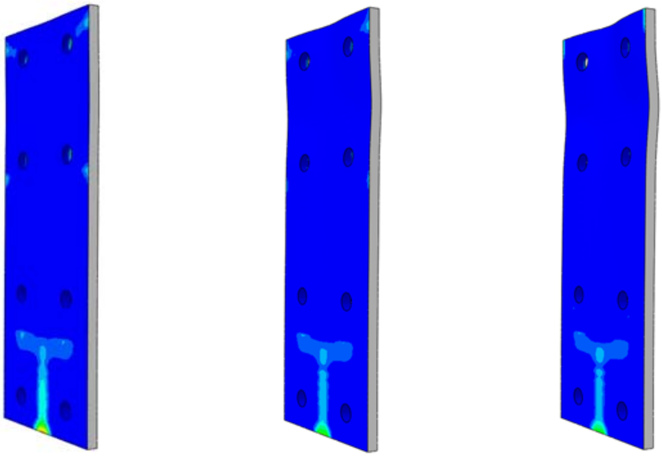

2% 4% 6%

ES2-E-C2

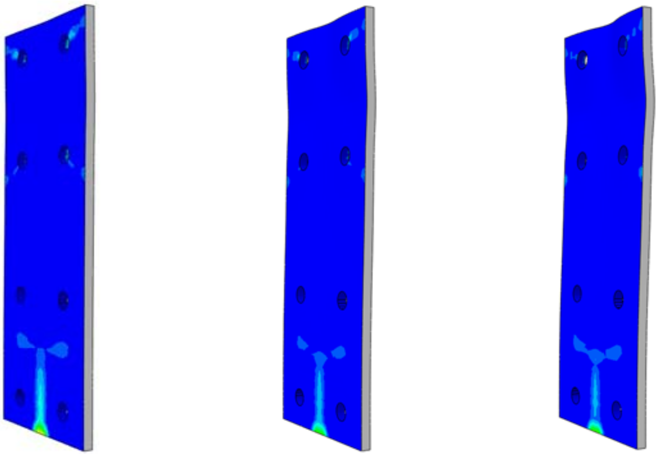

2% 4% 6%

ES2-P-C2

Figure 3-11: Evolution of contact pressure between end-plate and column face with chord rotation.

Figure 3-12 clearly shows the relationship between ξb and the imposed chord rotation for all beam-to-column assemblies. It is worth noting that up to chord rotation equal to 4% the actual position of ξb ranges within 0.6b and the centroid of the T compressed zone (i.e. the rib stiffener and the beam flange) for all examined cases and generally reduces at increasing rotations. Hence, the pure strut model given by [15] is not conservative for ES bolted joints. Conversely, assuming the center of compression into the centroid of the T compressed zone as [16] is conservative in all cases even though it leads to overestimate the joint resistance for equal and partial strength joints, being the lever arm deeper than that assumed according to [16].

This feature depends on the different contributions of both strut and beam mechanisms. In weaker connections, the occurrence of failure modes at upper bolt rows causes the gap opening between the end-plate and the column face, which activate the strut mechanism that is the only possible to guarantee the force transmission from beam to column. On the contrary, in full strength joints no gap opening can be recognized, thus the bending actions are mainly transferred by beam-type mechanism that is consistent with the hypothesis of ξb located into the center of T-section made of rib and beam flange [16]. In light of the obtained results it is advisable to design ES joints assuming the position of center of compression according to [16].

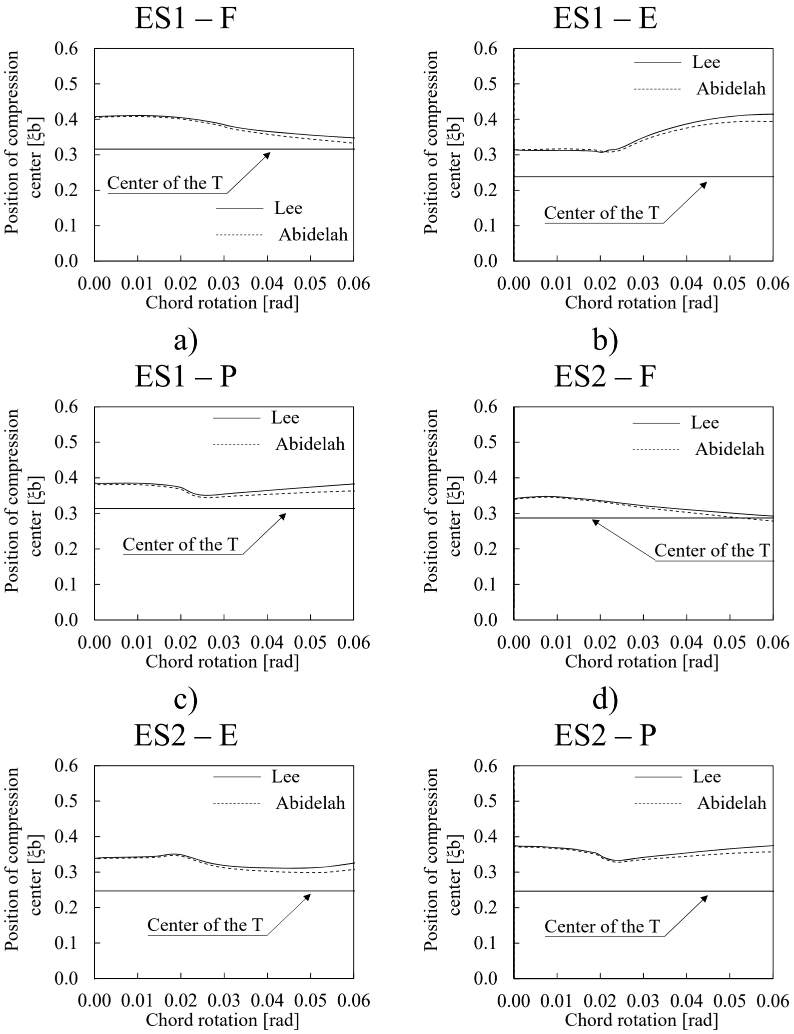

a) b) c) d) e) f)

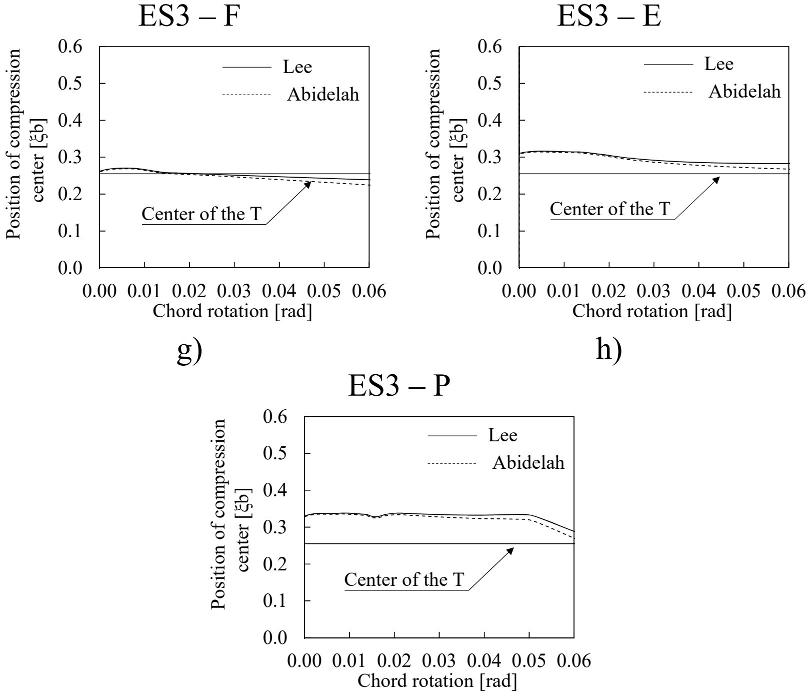

g) h)

i)

Figure 3-12: Position of compression center (ξb) vs chord rotation considering both the Lee [15]position of the compression center and Abidelah;[16] for: a) ES1 – F, b) ES1 – E, c) ES1 – P, d) ES2 – F, e) ES2 – E, f) ES2 – P, g) ES3 – F, h) ES3 – E, and i) ES3 – P.

3.6 Active bolt rows

According to EN1993:1-8 , all bolt rows above the beam flange in compression can be potentially in tension and their contribution should be considered equal to their plastic resistance unless group effect is activated and up to the equilibrium with compression strength is reached. On the contrary, in the present study the number of active bolts rows is fixed a-priori, considering in compression those lines below the horizontal symmetry axis of the connection as shown in Figure 1-3.

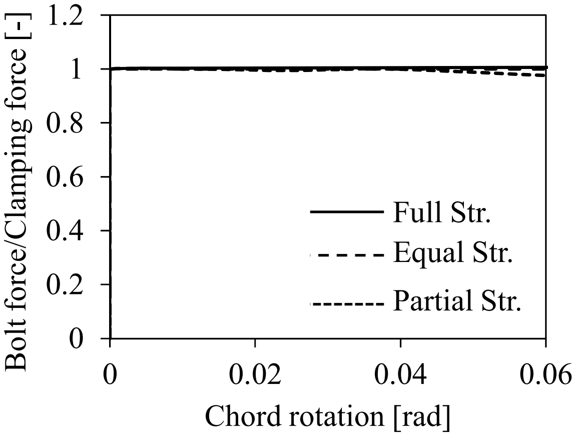

a)

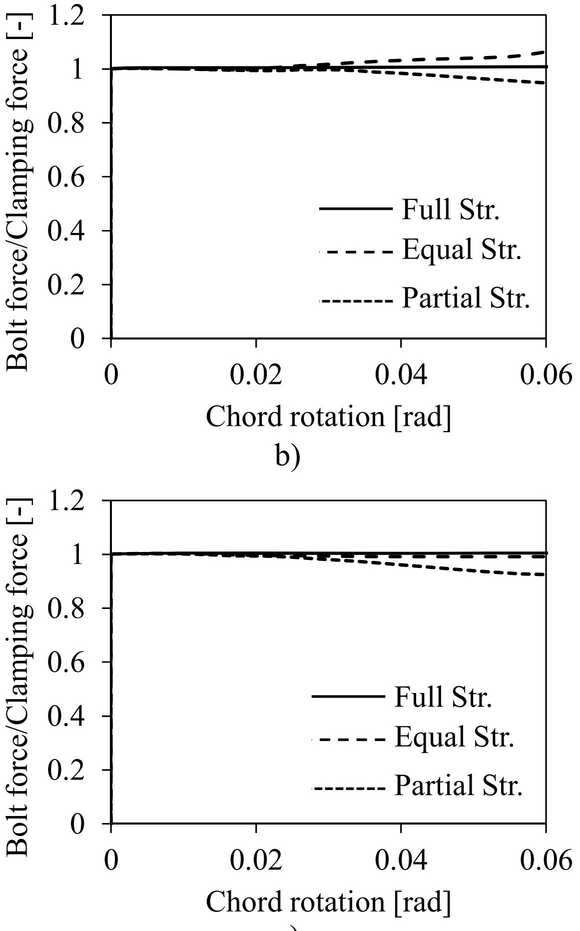

Figure 3-13: Evolution of axial force in the bolts above the beam flange in compression for full, equal and partial strength joints designed with ξb according to[16]: a) ES1, b) ES2, c) ES3 assemblies.

The results from FEAs confirm the effectiveness of this assumption for all assemblies. With references to the joints designed with ξb according to [16], Figure 3-13 shows the evolution of axial forces developing into the bolts above the beam flange in compression, normalized by the clamping force assumed equal to the value recommended by EN1993:1-9, where no appreciably variations can be observed. This implies that the proposed assumption is reasonable within chord rotation equal to 4%.

3.7 Cyclic response

Figure 3-14 summarizes the cyclic performance of full, equal and partial strength joints for the three beam-to-column assemblies designed according to the proposed procedure using with ξb as given by [16]. All these cases experience satisfactory and stable loops, guaranteeing a good energy dissipation capacity and plastic rotation capacity larger than 4%, with strength degradation lower than 80% of the nominal flexural strength, thus satisfying the requirements of AISC341.

It is interesting to note that all partial and equal strength joints do not show appreciable strength degradation, while full strength joints suffer the effect of cyclic actions. This difference is mainly due to the role of imperfections that affect the performance of the beam at large plastic strain. Indeed, in partial and equal strength joints the beams are less engaged in plastic range, thus the overall response mostly depends on mechanical components of the connections and panel zone. On the contrary, in case of full strength joints the response mainly depends on the beam. With this regard, it should be observed that having assumed geometric imperfections equal to the 80% of the maximum fabrication tolerances, as recommended by EN1993:1-5 [20], is a very severe hypothesis that conservatively penalizes the estimated rotation capacity of the analyzed joints.

The pinching of hysteretic loops is solely recognizable for some of equal and partial strength joints, since it depends on the development of the gap opening between the end-plate and column flange in the tension zone of the connection. This phenomenon reduces the energy dissipation capacity of the joints.

ES1	Full Strength	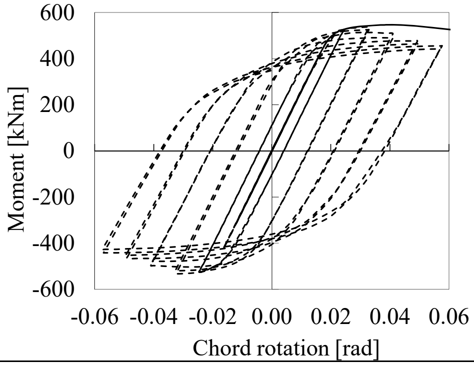
	Equal Strength	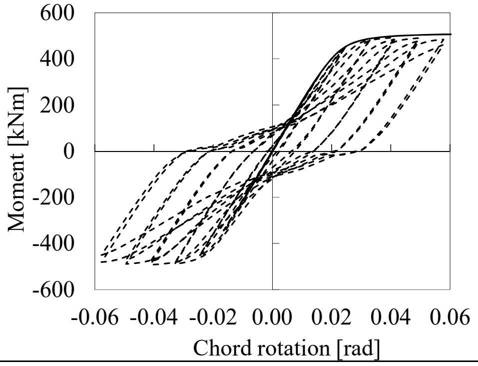
	Partial Strength	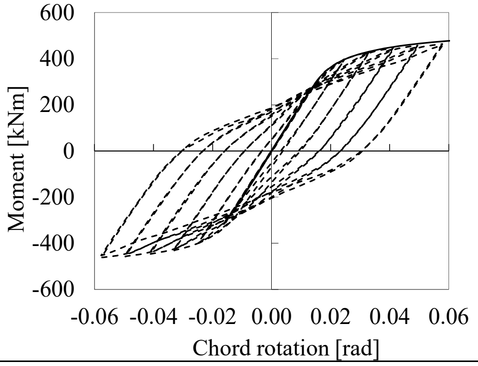

<table>
<tr>
<td rowspan="3">ES2</td>
<td>Full Strength</td>
<td>
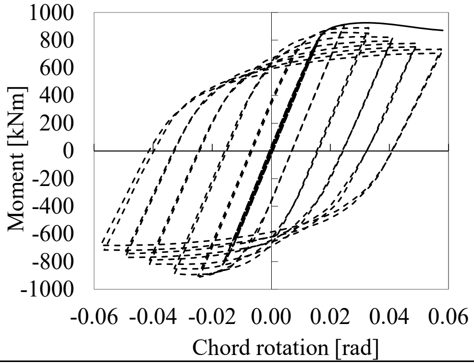

</td>
</tr>
<tr>
<td>Equal Strength</td>
<td>
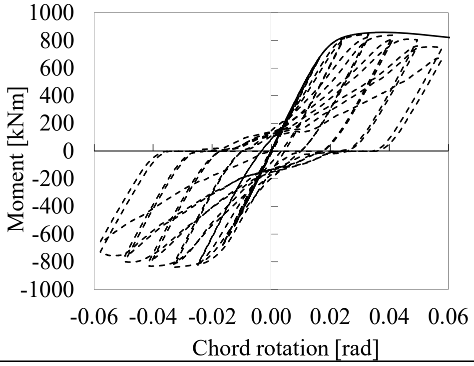

</td>
</tr>
<tr>
<td>Partial Strength</td>
<td>
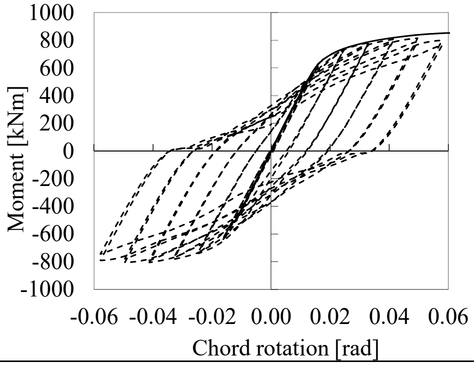

</td>
</tr>
</table>

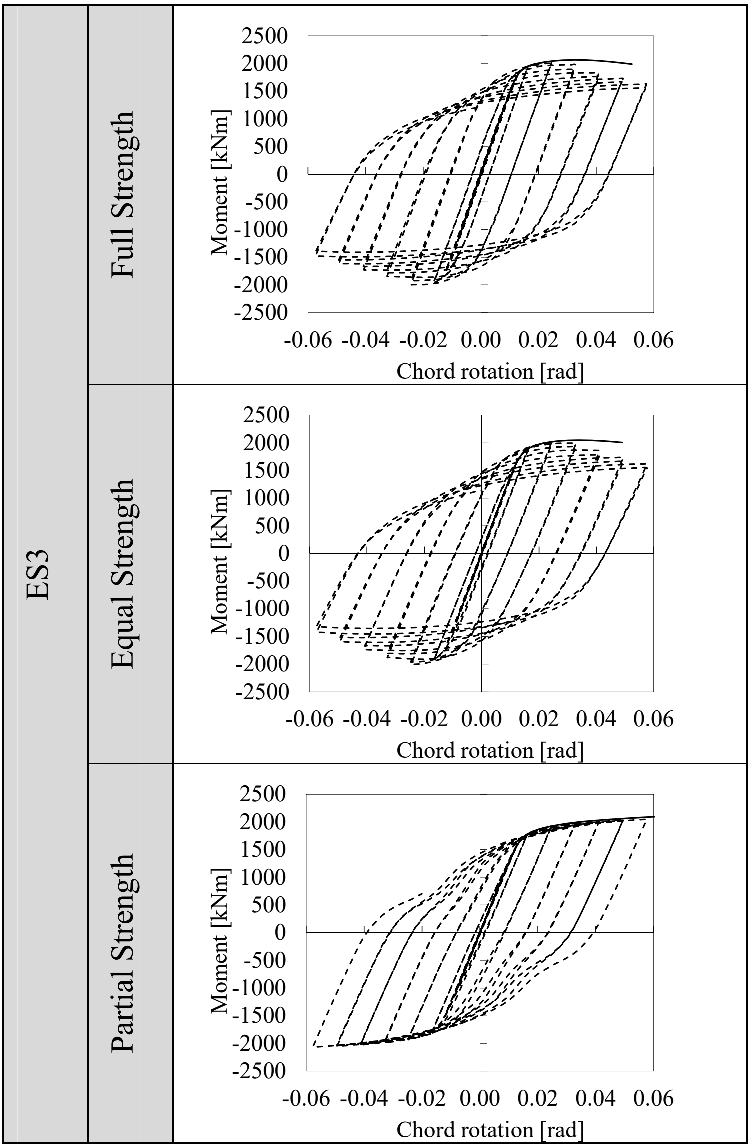

Figure 3-14: Hysteretic response of ES joints.

In order to highlight such effect, the dissipated energy (DE) cumulated per cycle (i.e. calculated as the sum of the areas enclosed by each hysteretic loop) is normalized to the energy cumulated up to 0.04 rad of chord rotation by full strength joints ($DE_{0.04Full}$). Figure 3-15 shows the comparison of the normalized cumulated energy ($DE/ DE_{0.04Full}$) for the three joint assemblies. As expected, equal and partial strength joints dissipate lesser energy than full strength joints, even though the differences reduce with increasing of the dimension of beam-column assemblies. However, it is interesting to observe that for all assemblies partial strength joints provide energy dissipation capacity (i.e. about 50% of $DE_{0.04Full}$) larger than equal strength joints (i.e. about 40% of $DE_{0.04Full}$). This feature depends on the type of experienced failure mode. Indeed, in partial strength joints the plastic deformations are mainly concentrated into the end-plate, while equal strength joints show damage concentration into bolts with limited plastic deformations in the end-plate. Some plastic deformations also develop in the compression zone of the beams, due to strut behavior of the rib. However, the differences in the damage pattern are consistent with the design criterion for equivalent T-stubs of the connections. Indeed, mode 2 was assumed for equal strength, while mode 1 was considered for partial strength joints.

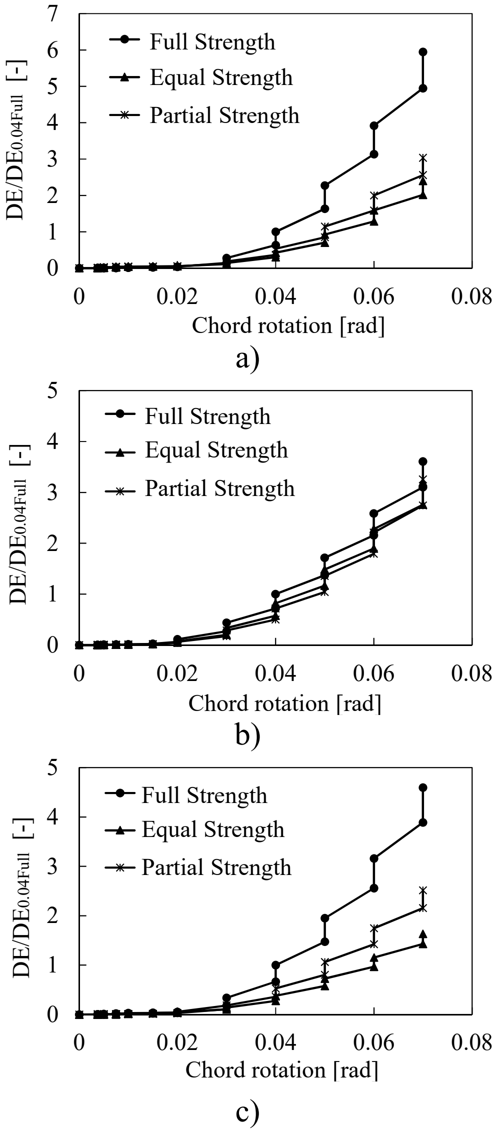

Figure 3-15: Normalized energy dissipation capacity of a) ES1, b) ES2 and c) ES3 joint assemblies.

3.8 Analytical prediction

The analytical prediction is based on the mechanical model shown in previous paragraph (see Figure 1-7). The comparison between analytical and FEA response curves are depicted in Figure 3-16, with this regard the simulated response of full strength joints is obtained assuming perfectly elastic behavior of the beam in order to obtain the ultimate response of the joint.

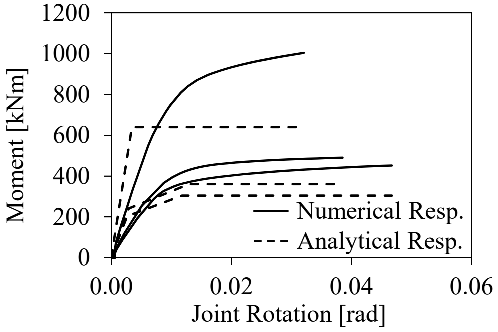

a)

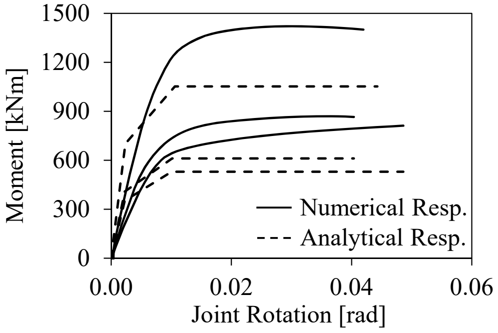

b)

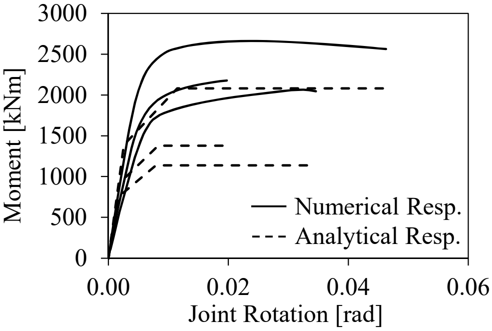

c)

Figure 3-16: Analytical vs. FEA response curves of ES1 (a), ES2 (b) and ES3 (c) assemblies.

The failure modes predicted by analytical models are confirmed by FEAs. Indeed, the equivalent T-stubs in partial strength joints are characterized by mode 1, while mode 2 is the failure mechanism for bolt rows of both equal and full strength joints. The comparison between calculated strength and FEA prediction shows that the analytical resistance satisfactory corresponds to the simulated yield strength (i.e. the knee of the simulated response curve). It is trivial to recognize that the differences in terms of ultimate resistance in Figure 3-16 are due to the simplified assumptions of mechanical model that disregards the hardening of each component. Hence, the effective lengths given by the Green Book [3] are adequate to predict the yield strength of the ES connections.

For what concerns the stiffness, Table 3.22 shows the comparison between the stiffness calculated according to EN1993:1-8 (i.e. disregarding the presence of rib) and that obtained assuming the mechanical model shown in Figure 1-7. As it can be observed both mechanical models substantially overestimate the initial stiffness obtained from finite element simulations even though this inconsistency reduces for joints with deeper beams (i.e. ES3 group). This result is in line with literature [16],[28],[31], and it may be explained by the limits of EC3 model to account for the flexural stiffness of the bolts and the actual distribution of prying forces and contact areas.

Table 3.22: Analytical vs. FE prediction of joint stiffness.

Joint assembly	Design performance level	Stiffness according to EC3:1-8 neglecting Rib ($S_{j,ini,NR}$)	Stiffness according to model in Figure 3-16 ($S_{j,ini,R}$)	Stiffness from FEA	$S_{j,ini,NR}$ / $S_{j,ini,FEM}$	$S_{j,ini,R}$ / $S_{j,ini,FEM}$
ES1	Full strength	205026	386185	97297	2.1	4.0
	Equal strength	85050	134653	54054	1.6	2.5
	Partial strength	64367	108586	45945	1.4	2.4
ES2	Full strength	349953	637971	167567	2.1	3.8
	Equal strength	170107	287588	116216	1.5	2.5
	Partial strength	129801	233531	90810	1.4	2.6
ES3	Full strength	829587	1317391	497297	1.7	2.6
	Equal strength	602828	1043786	378378	1.6	2.8
	Partial strength	384905	785567	297297	1.3	2.6

CHAPTER V

References

[1] EN 1998-1, Design of structures for earthquake resistance - Part 1: General rules, seismic actions and rules for buildings. CEN 2005.

[2] EN 1993:1-8, Design of steel structures - Part 1-8: Design of joints. CEN 2005.

[3] Joints in Steel Construction: Moment-Resisting Joints to Eurocode 3 (P398). Edited by The Steel Construction Institute and The British Constructional Steelwork Association, 2013, ISBN 978-1-85-942209-0.

[4] Ciutina A. L., Dubina D. (2008). Column Web Stiffening of Steel Beam-to-Column Joints Subjected to Seismic Actions. Journal of Structural Engineering, 134(3), 505–510.

[5] ANSI/AISC 341-10 (2010). Seismic Provisions for Structural Steel Buildings. American Institute of Steel Construction.

[6] O.P.C.M. 3274 20 March 2003 (2003) Initial items on the general criteria for seismic zonation of the National territory and seismic code (in Italian). G.U.R.I. n.72 DEL 08/05/2003.

[7] Mazzolani FM, Piluso V. (1992). Member behavioural classes of steel beams and beam-columns. Proc. of First State of the ArtWorkshop, COST, Strasbourg, 517-29.

[8] Mazzolani FM, Piluso V. (1996) Theory and design of seismic resistant steel frames. London: E & FN Spon an imprint of Chapman & Hall.

[9] D'Aniello M., Landolfo R., Piluso V., Rizzano G. (2012). Ultimate Behaviour of Steel Beams under Non-Uniform Bending. Journal of Constructional Steel Research, 78, 144–158.

[10] Güneyisi E.M., D'Aniello M., Landolfo R., Mermerdaş K. (2013). A novel formulation of the flexural overstrength factor for steel beams. Journal of Constructional Steel Research, 90, 60-71

[11] Güneyisi E.M., D'Aniello M., Landolfo R., Mermerdaş K. (2014). Prediction of the flexural overstrength factor for steel beams using artificial neural network. Steel and Composite Structures, 17(3), 215-236.

[12] ANSI/AISC 358-16 (2016). Prequalified Connections for Special and Intermediate Steel Moment Frames for Seismic Applications.

[13] Jaspart J.P. (1997). Contributions to recent advances in the field of steel joints – column bases and further configurations for beam-to-column joints and beam splices. Professorship Thesis, University of Liège.

[14] Tartaglia R., D'Aniello M. (2017). Nonlinear performance of extended stiffened end plate bolted beam-to-column joints subjected to column removal. The Open Civil Engineering Journal.

[15] Lee C-H. (2002). Seismic Design of Rib-Reinforced Steel Moment Connections based on Equivalent Strut Model. Journal o Structural Engineering, ASCE, 128(9), 1121-1129.

[16] Abidelah A., Bouchaïr A., Kerdal D.E. (2012). Experimental and analytical behavior of bolted end-plate connections with or without stiffeners. Journal of Constructional Steel Research, 76, 13–27.

[17] Lee C.-H. Jung J.-H., Oh M.-H., Koo E-S. (2005). Experimental Study of Cyclic Seismic Behavior of Steel Moment Connections Reinforced with Ribs. Journal of Structural Engineering, ASCE, 131(1), 108-118

[18] Dassault Systèmes. Abaqus analysis 6.16 user's manual. Simula Inc.; 2016

[19] Wang M., Y Shi, Y Wang, G Shi (2013). Numerical Study on seismic behaviour of steel frame end plate connections. Journal of Constructional Steel Research, 90,140-152.

[20] EN 1993-1-5, Design of steel structures - Part 1-5: Plated structural elements. CEN 2005.

[21] EN 10034. Structural steel I and H sections: Tolerances on shape and dimensions. CEN 1993.

[22] Dutta A., Dhar S., Acharyya S.K., (2010). Material characterization of SS 316 in low-cycle fatigue loading. Journal of Materials Science, 45(7), 1782-1789.

[23] Swanson J. A., Leon R. (2001). Stiffness modelling of bolted t-stub connection components. Journal of Structural Engineering, ASCE , 127(5), 498-505.

[24] Latour M., Rizzano G., Santiago A., da Silva L. (2014). Experimental analysis and mechanical modeling of T-stubs with four bolts per row. Journal of Constructional Steel Research, 101, 158–174.

[25] EN ISO 2560. Welding consumables - Covered electrodes for manual metal arc welding of non-alloy and fine grain steels – Classification, CEN 2009.

[26] EN ISO 898-1. Mechanical properties of fasteners made of carbon steel and alloy steel - Part 1:Bolts, screws and studs, CEN 1999.

[27] Shi Y., Shi G., Wang Y. (2007). Experimental and theoretical analysis of the moment- rotation behaviour of stiffened extended end-plate connections. Journal of Constructional Steel Research, 63, 1279-1293.

[28] Girao Coelho A. M., da Silva L. S., Bijlaard F.S.K . (2004). Experimental assessment of the ductility of extended end plate connections. Engineering Structures 26, 1185–1206.

[29] Díaz C., Victoria M., Martí P., Querin O.M. (2011). FE model of beam-to-column extended end-plate joints. Journal of Constructional Steel Research, 67, 1578–1590.

[30] Giusy Terracciano. (2013). Yield and ultimate rotations of beam-to-column end-plate connections. PhD Thesis, University of Naples Federico II.

[31] Reinosa J.M., Loureiro A., Gutierrez R., Lopez M. (2015). Analytical plate approach for the axial stiffness prediction of stiffened angle cleats. Journal of Constructional Steel Research, 106, 77–88.

[32] CSI, "SAP2000 Integrated Software for Structural Analysis and Design," Computers and Structures Inc., Berkeley, California.

List of figures

Figure 1-1: Plastic regions for the examined performance design objectives: a) full strength, b) equal strength and c) partial strength joints... 179

Figure 1-2: T-Stub resistance and corresponding mechanism according to EN1993:1-8 [2]. 185

Figure 1-3: Assumed position of bolt rows in tension............ 190

Figure 1-4: Geometry of rib stiffener (a) and forces developing at beam/column-to-rib interface according to [63]... 191

Figure 1-5: Equivalent T-Stub for ES joints: the cases with one (a) and two (b) bolt rows above the beam flange in tension.. 193

Figure 1-6: Centre of compression and lever arm: a) EC3:1-8 for end-plate connections; b) shifted position due to strut mechanism into the rib stiffener. 199

Figure 1-7: Proposed mechanical model for stiffness calculation for ES joints. 203

Figure 1-8: Influence of the rib stiffener on column web panel area.. 205

Figure 1-9: Evaluation of shear design force on the column web panel.. 205

Figure 1-10: Type of welds introduced.................................. 210

Figure 2-1: Element mesh: beam (a), column (b), end-plate (c) and bolts (d)... 213

Figure 2-2: Sub-structuring and boundary conditions for FEAs of ES joints.. 214

Figure 2-3: Abaqus Contact definition. 215

Figure 2-4: Example of the geometrical imperfections on the beam flanges: a) and b) coincident flange, c) and d) not coincident flange..216

Figure 2-5: Investigation on the imperfection on post-peak strength: a), b), e) in terms of moment rotation curve and c), d) in terms of PEEQ deformation. 217

Figure 2-6: Experimental tests by Shi et al. [27] vs. finite element simulations...224

Figure 3-1: MRFs structures designed according to EN1998-1-1 [1]: SAP models (a and b) and longitudinal view (c and d). 226

Figure 3-2: MRFs Structures in plane. 227

Figure 3-3: Main geometrical details of ES joints reported in Table 4. 236

Figure 3-4: Moment-rotation response curves: Eurocode vs. proposed design criteria for full (a), equal (b) and partial (c) strength joints.......................................242

Figure 3-5: Von Misses stress and PEEQ distribution: Eurocode (a) vs. proposed (b) design approach.....................243

Figure 3-6: Results of the overstrenght investigation in terms of: (a) Moment chord rotation, (b) Moment joint rotation, (c and d) PEEQ distribution and (e and f) PEEQ in evolution at 2%, 3% and 4% of chord rotation......246

Figure 3-7: Flexural response of full strength joints assuming indefinite elastic behavior for beams.....................247

Figure 3-8: Yield lines for one bolt row up configuration: a) Unstiffened and b) Stiffened joints. 248

Figure 3-9: Yield lines for tow bolt rows up configuration: a) Unstiffened and b) Stiffened joints. 249

Figure 3-10: The influence of the rib stiffener on moment-joint rotation response curve; a) ES1 vs. E1, b)ES2 vs. E2 and c)ES3 vs. E3 joints. 251

Figure 3-11: Evolution of contact pressure between end-plate and column face with chord rotation. 254

Figure 3-12: Position of compression center (ξb) vs chord rotation considering both the Lee [15]position of the compression center and Abidelah;[16] for: a) ES1 – F, b) ES1 – E, c) ES1 – P, d) ES2 – F, e) ES2 – E, f) ES2 – P, g) ES3 – F, h) ES3 – E, and i) ES3 – P.......... 257

Figure 3-13: Evolution of axial force in the bolts above the beam flange in compression for full, equal and partial strength joints designed with ξb according to[16]: a) ES1, b) ES2, c) ES3 assemblies........................... 259

Figure 3-14: Hysteretic response of ES joints. 264

Figure 3-15: Normalized energy dissipation capacity of a) ES1, b) ES2 and c) ES3 joint assemblies........................... 266

Figure 3-16: Analytical vs. FEA response curves of ES1 (a), ES2 (b) and ES3 (c) assemblies................................... 268

List of tables

Table 1.1: Effective length for the first line of 1br configuration. 194

Table 1.2: Effective length for the first line of 2br configuration. 195

Table 1.3: Effective length for the first line (considered as part of group) of 2br configuration. 196

Table 1.4: Effective length for the second line of 2br configuration...197

Table 1.6: Welds type prescribed in function of the in function of the design criteria [5]...209

Table 3.1: MRFs structures designed......................................227

Table 3.2: M-3-3-6-0.25 geometry characteristics...................229

Table 3.3: M-3-3-6-0.25 design results....................................229

Table 3.4: M-3-3-6-0.35 geometry characteristics...................229

Table 3.5: M-3-3-6-0.35 design characteristics........................229

Table 3.6: M-3-3-8-0.25 geometry characteristics...................230

Table 3.7: M-3-3-8-0.25 design characteristics........................230

Table 3.8: M-3-3-8-0.35 geometry characteristics...................230

Table 3.9: M-3-3-8-0.35 design characteristics........................230

Table 3.10: M-6-3-6-0.25 geometry characteristics.................231

Table 3.11: M-6-3-6-0.25 design characteristics......................231

Table 3.12: M-6-3-6-0.35 geomwtry characteristics................231

Table 3.13: M-6-3-6-0.35 design characteristics. 232

Table 3.14: M-6-3-8-0.25 geometry characteristics. 232

Table 3.15: M-6-3-8-0.25 design characteristics. 232

Table 3.16: M-6-3-8-0.35 geomerty characteristics. 233

Table 3.17: M-6-3-8-0.35 design characteristics. 233

Table 3.18: ES1 joints geometrical characteristics. 237

Table 3.19: ES2 joints geometrical characteristics. 238

Table 3.20: ES3 joints geometrical characteristics. 239

Table 3.21: Stiffened vs Unstiffened joint: Strength and Stiffness. 252

Table 3.22: Analytical vs. FE prediction of joint stiffness. 270

CHAPTER VI

Experimental tests on Beam-to-Column joints

Introduction

In the Equaljoint research project a set of 24 specimens (see Table 1.1) are tested at University of Naples (UNINA) and University of Liege (ULg) both on T (with one primary beam) and X (with two primary beams) extended stiffened joints. Within this large experimental campain a set of 13 tests are object of this thesis; therefore in this chapter only the results of extended stiffened joint for the T configuration will be presented.

To identify the real meccanical joint charateristics also a large number of coupon tests were performed and in the following reported.

1 Introduction of the experimental results

In the framework of the Equaljoints project [1] the tests were performed on both full and equal strength joints, under monotonic and cyclic loads. Moreover, also the influence of the loading protocol and the shot pinning effect on the welds were investigated.

Three T type beam-to-column assemblies were tested: (i) ES1 (beam IPE360 and column HEB280), (ii) ES2 (beam IPE450 and column HEB340) and (iii) ES3 (beam IPE600 and column HEB500).

All extended stiffened joints where designed at University of Naples in order to investigate both the full and equal strength design criteria. The first two assemblies (ES1 and ES2) were tested at University of Naples Federico II, while ES3 joints were tested at University of Liege.

The joints are designed according to the proposed design procedure described in Chapter V, where the compression center was assumed in the center of the equivalent T in compression (according to the Abdallah [6] assumptions).

All profiles and plates are S355, while in the design phase bolts 10.9 were considered.

Table 1.1: Experimental test on extended stiffened joint within the Equaljoints research program [1].

Group	Connection type	Joint configuration	Connection strength	Loading protocol	Beam/column depth		
					1	2	3
1	ES	TS	F	M	ES1-TS-F-M*	ES2-TS-F-CA*	ES3-TS-F-M*
	ES	TS	F	C1	ES1-TS-F-C1*	ES2-TS-F-C1*	ES3-TS-F-C1*
	ES	TS	F	C2	ES1-TS-F-C2	ES2-TS-F-C2	ES3-TS-F-C2*
2	ES	TS	E	C1	ES1-TS-E-C1*	ES2-TS-E-C1*	ES3-TS-E-C1*
	ES	TS	E	C2	ES1-TS-E-C2	ES2-TS-E-C2	ES3-TS-E-C2*
	ES	TS	Esp	C	ES1-TS-Esp-C	ES2-TS-Esp-C*	ES3-TS-Esp-C*
3	ES	XB	E	C1	ES1-XB-E-C1	ES2-XB-E-C1	ES3-XB-E-C1
	ES	XB	E	C2	ES1-XB-E-C2	ES2-XB-E-C2	ES3-XB-E-C2

*Experimental results object of this thesis

CHAPTER VI

1.1 Test setup

In the following the designed test setups used both by the University of Naples and University of Liege, in the experimental activities, are presented.

1.1.1 Setup and transducers at University of Naples

The test setup of University of Naples is presented in Figure 1-1; it is suitable for both internal and external joints. The connections are tested horizontally; the size of specimens are 3.75m for both columns and beams.

The column ends have been designed to be pinned and restrained with cylindrical hinges placed at a distance of 3.4m; additional restraints have been provided in order to avoid lateral-torsional buckling in the beams. Stiffeners have been provided at the beam extremity where the two actuators are located.

The jack capacity was verified considering a possible over-strength of the material i.e. the ultimate strength for the S355 steel was assumed to be 1,25×510 N/mm^2. With respect to the deformation requirement, a rotation of about 60-70mrad at the joint level could be reached during the tests.

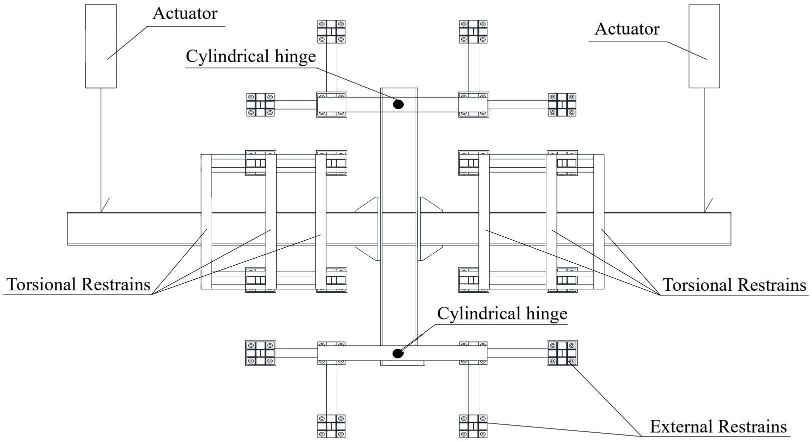

Figure 1-1: Set-up at University of Naples.

To record the specimens deformation and their displacements during the tests, both displacement transducer (LVDT) and strain gauge (SG) were used; in particular, in Figure 1-2, all the transducer locations are shown. With this distribution of LVDT, the key deformations, that are necessary to characterize the joint behavior, can be derived; in detail:

- Transducers 1 and 2 have been located at the cylindrical hinges in order to measure the column rigid rotation;
- Transducers 3 and 4 have been located along the column length in order to evaluate the displacement due to the column elastic rotation;

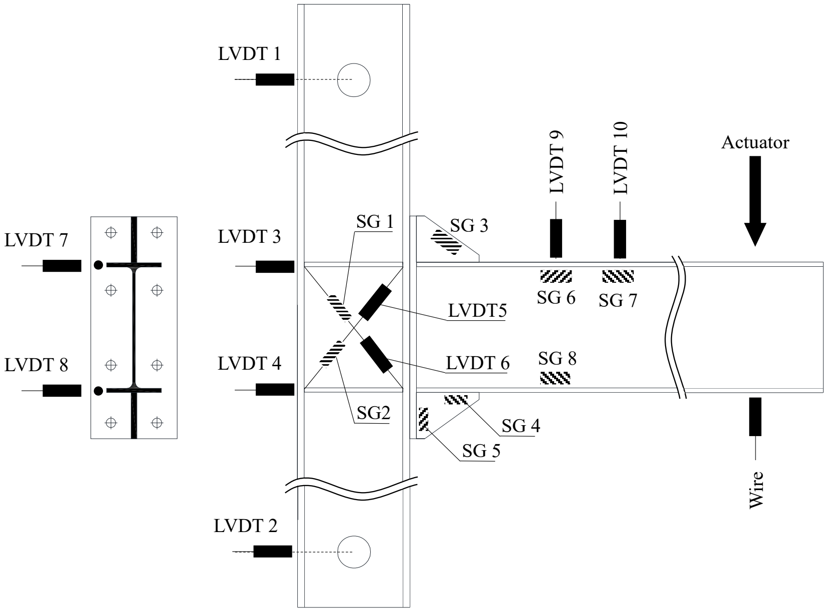

Figure 1-2: Instrumentation introduced by the University of Naples.

- The panel zone rotation is given by transducers 5-6 diagonally fixed on the panel at the level of continuity plates
- The joint rotation is measured by transducers 7-8 fixed at the end plate.
- Transducers 9-10 are located in the beam zone where the plastic hinge is expected in order to measure potential plastic rotation of the beam.
- In order to measure the girder displacements, a wire transducers has been located at beam ends.

The strain-gauge transducers were applied to verify the components local deformation. Therefore eight strain gauge were used for each test and placed as illustrated in Figure 1-2; in particular: (i) two transducers in the column web panel, (ii) three transducers in the internal part of the beam flange and (iii) three transducers on the ribs (two on the stiffeners base and height and on the diagonal direction).

1.1.2 Setup and transducers at University of Liege

Figure 1-3 gives a general view of the test setup for the double sided specimens (i.e. internal beam-to-column joints) used at the University of Liège. The system is placed in a horizontal plane, parallel to the strong floor of the lab. The total beam length is equal to 5.5m and the column height is equal to 3.5m. The column is fixed by a hinge with no lateral displacements allowed at one end, and by a hinge with only the axial displacement allowed at the other. The loads are applied at the beam ends through two identical hydraulic jacks with a capacity of 1000kN both compression and tension and with a stroke equal to ±200 mm (i.e. 400 mm in total).

Lateral bracings are used to avoid the out-of-plane displacement/instability of the specimens during the tests. In case of single sided specimens (i.e. external beam-to-column joints), the same setup is used with only one jack.

To ensure the failure of the specimens before the attainment of the jack capacity, the potential material over-strength has been considered by amplifying the nominal ultimate strength of the steel, hence the design ultimate strength is 1,25*510 N/mm^2. With respect to the deformation requirements, a rotation of about 50-60mrad at the joint level could be reached during the tests.

Displacement transducers used for the recording of the deformation of the tested specimens in ULg and their locations are shown in Figure 1-4.

Therefore, also in this case, with this distribution of displacement transducers, the key deformations that are necessary to characterize the joint behavior can be derived; in detail:

- Displacement of the load point: D1;
- Rigid displacements of the column ends: D2, D3 and D4
- Rotation of the plastic hinge (at the beam level): D5, D6, D7 and D8;
- Rotation of the connection zone: D7, D8, D9 and D10;
- Deformation in shear of the web panel: D11 and D12.

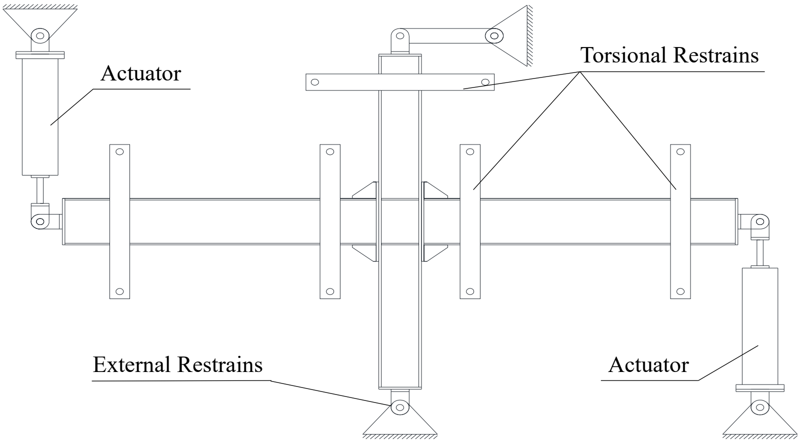

Figure 1-3: Set-up at University of Liege.

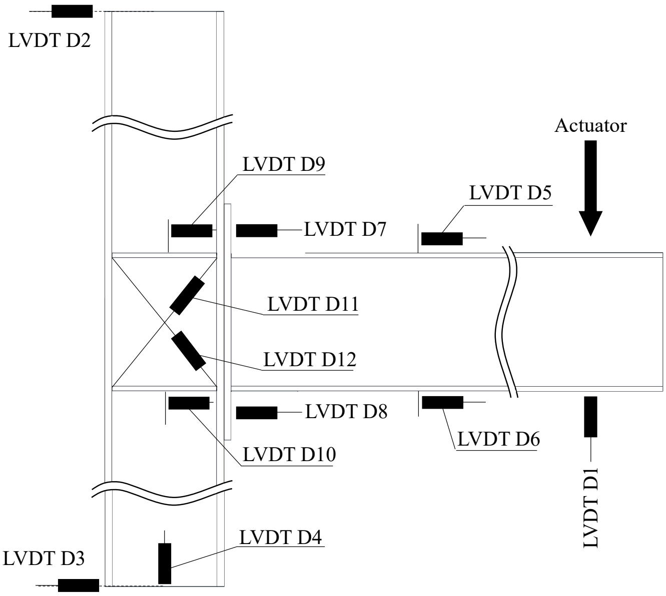

Figure 1-4: Instrumentation introduced by the University of Liege.

1.2 Loading protocol

As anticipated both monotonic and cyclic loading protocols were used; with regard to the cyclic tests two loading protocols were applied: (i) AISC341-10 [3] and the (ii) Equaljoints [1] cyclic protocols.

AISC341 loading protocol (Figure 1-5 a) is in accordance with the American prescriptions, i.e. for each displacement level applied, three cycles are performed, up to the fifth step, after which just two cycles are performed. EJ loading procedure was developed within the research project in order to propose innovative loading protocols able to ask a similar energy demand from the joint, but by means of a more rapid loading procedure (Figure 1-5 b). To compare the protocols demands in terms of dissipated energy, the two loading protocol were compared function of the internal energy ask to the specimens.

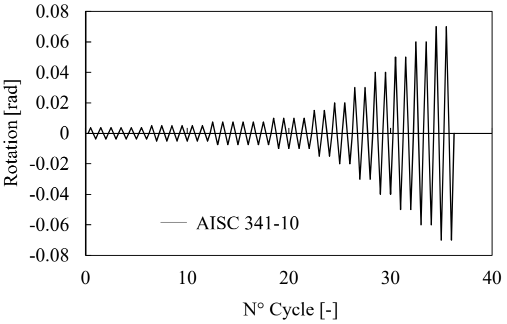

a)

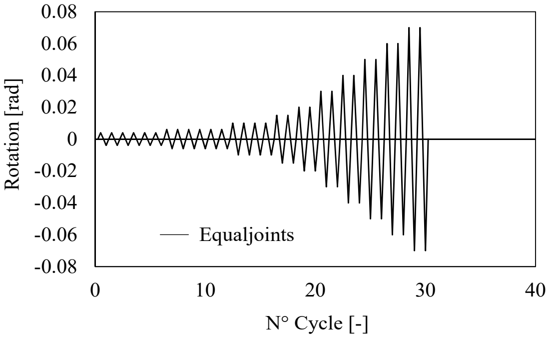

b)

Figure 1-5: AISC341-10 [3] (a) and Equaljoints [1] (b) loading protocol.

As reported in Figure 1-6, AISC341 is a little bit more demanding respect to the EJ, that on the other hand, is quicker given the lower number of cycles in the small displacements range.

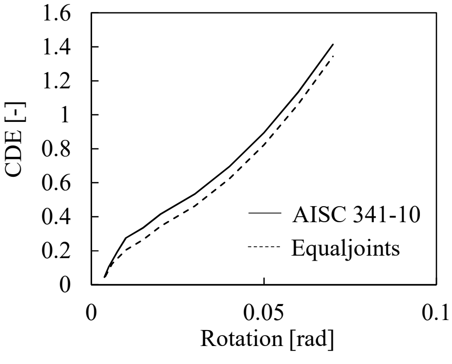

Figure 1-6: Cumulated energy for:AISC341-10 [3] and EqualJoint loading protocol [1].

2 Coupon tests

The material characteristics can play a central role in the joint behavior, for this reason, at University of Naples and at University of Liege, a set of 66 coupon tests were performed on specimens taken from the column, the beam and the plate used in the experimental campaign. The results of all the tests are reported in the Annex while in the following an average for each column, beam and plate is showed (see Table 2.1).

Table 2.1: Coupon test results.

Profile	Coupon position	f_y N/mm²	f_u N/mm²	E N/mm²	Elongation %
IPE 600	web	461.9	506.2	207135	33.0
	flange	475.8	552.2	184153	35.5
IPE 450	web	425.6	516.2	205049	30.7
	flange	410.9	517.1	205981	32.9
IPE 360	web	395.7	511.0	197845	32.1
	flange	381.2	518.2	190581	30.3
HEB 280	web	383.6	497.5	191785	27.0
	flange	387.0	502.8	193520	31.1
HEB 340	web	420.2	497.7	203647	32.0
	flange	486.2	565.8	226153	29.5
HEB 500	web	436.2	501.0	214817	34.6
	flange	435.1	552.4	217079	34.7
HEB 650	web	441.5	484.5	203220	36.2
	flange	409.1	509.1	211573	38.8
Plates	t_{ep} 15mm	459.2	567.3	209001	33.8
	t_{ep} 18mm	417.9	551.7	196202	33.4
	t_{ep} 20mm	509.3	563.4	211253	20.6
	t_{ep} 25mm	459.8	589.8	216028	32.9
	t_{ep} 30mm	344.5	485.6	205849	41.3

An example of the importance of the coupon test use to understand the joint behavior is represented by comparing the results of IPE 450 flange 3 with IPE 450 flange 4 reported in the Annex. The first coupon was extracted from the beam flange of the ES2-TS-F-CA, while the second one coming from the beam flange of the ES2-TS-F-C2 assembly.

Figure 2-1 show a substantial differences in terms of the yielding strength (around 16%) between the two specimens extracted. Therefore, the joint capacity, especially in case of full strength, will show a large difference in terms of bending capacity (as will be highlight later in this Chapter).

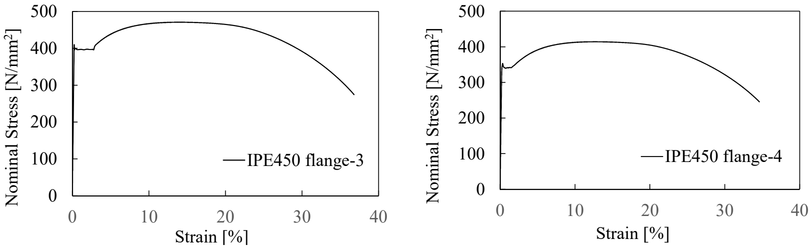

a) b)

Figure 2-1: Coupon test results of the IPE450 from the ES2-TS-F-CA (a) and ES2-TS-F-C2 (b).

For reason of brevity only few pictures of the coupon tests campaign are showed in Figure 2-2; in particular: the MTS machine setup and an example of coupon test experimental result.

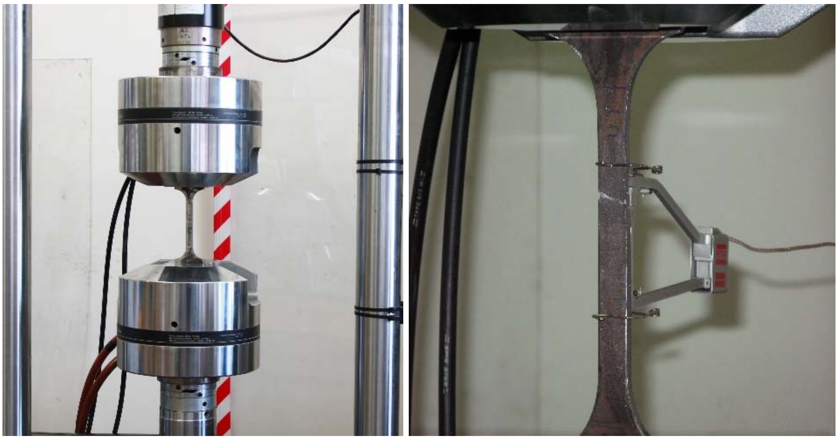

a) b)

Figure 2-2: University of Naples coupon test setup (a) and an example of the coupon test experimental results (b).

The stress-strain relationship for the plate are showed in Figure 2-3. All the others results are reported in the Annex.

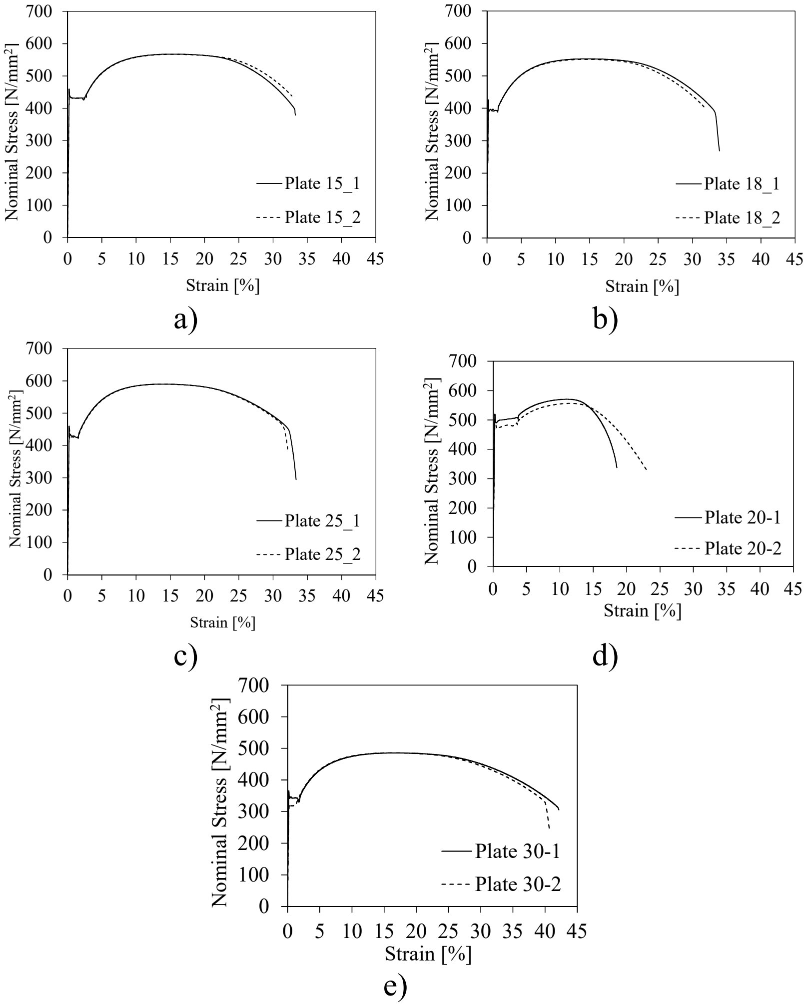

Figure 2-3: Stress-strain curve of plate with a thickness of: 15mm (a), 18mm (b), 25mm (c), 20mm (d) and 30mm (e).

3 Experimental results: extended stiffened joints

The extended stiffened joint were designed at University of Naples according to the innovative assumptions introduced in Chapter V. As already show in the previous chapter, ES1 and ES2 full strength joints were designed considering a two bolts rows above the beam flange, while just one row was introduced in case of equal strength joint. Conversely, for ES3 joints, both equal and full strength joints have a two bolts row above the beam. All the joints characteristics were reported in Table 3.1 and Figure 3-1

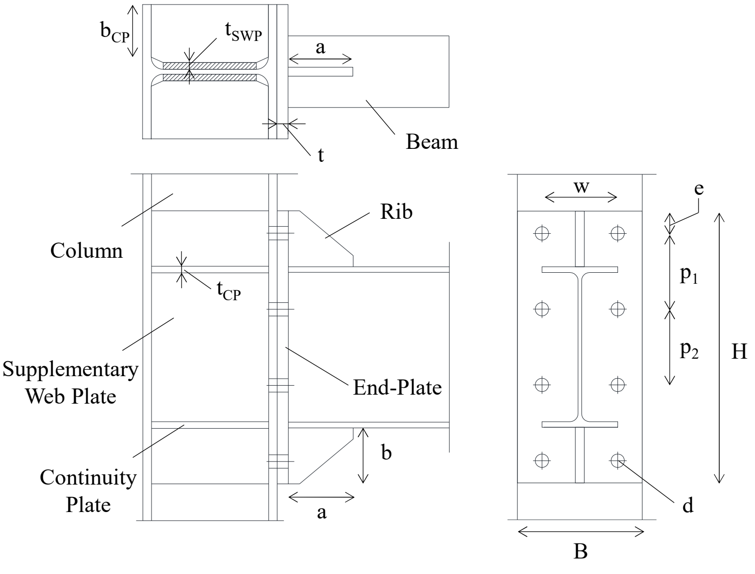

Figure 3-1: Main geometrical details of ES joints reported in Table 4.

Table 3.1: Tested specimens geometrical characteristics.

Joint ID	Design Criteria	Compression center	End-Plate			Bolt spacing					CP	Additional web plate	
			H mm	B mm	t mm	d mm	e mm	w mm	p1 mm	p2 mm	t_{CP} mm	Side -	t_{SWP} mm
ES1-F-C1	F	Abidelah	760	260	25	30	50	150	75	160	14	2	8
ES1-E-C1	E	Abidelah	600	280	18	27	50	160	160	180	14	1	8
ES2-F-C1	F	Abidelah	870	280	25	30	50	150	75	180	15	2	10
ES2-E-C1	E	Abidelah	770	300	20	30	55	160	200	260	15	1	8
ES3-F-C1	F	Abidelah	1100	280	30	36	55	160	95	210	20	2	15
ES3-E-C1	E	Abidelah	1100	300	22	36	55	160	95	210	20	1	15

CHAPTER VI

3.1 ES1-TS-F-C2

ES1–TS–F–C2 is a cyclic test on the smaller beam-to-column assembly (the beam is an IPE360 and the column an HEB280). The joint is designed as full strength, therefore all the plastic damage is assumed to be concentrated in the beam, leaving the rest of the joint in elastic range.

The AISC341 [3] loading protocol was applied with an increase of rotation demand up to 7%. The test was executed with no observable fracture after the first two cycles at 7%, as seen in the pictures taken and in the moment rotation curve (see Figure 3-3). Therefore, the assembly was subjected to subsequent cycles at constant rotation (7%) up to the crack formation and propagation in the beam flange.

Analyzing the behavior of the joint in terms of strength, it can be observed that the moment-chord rotation curve shows an increasing trend up to 5% of rotation (see Table 3.2) after which point the joint resistance decreases significantly due to the buckling of the beam flanges. The joint show a bending capacity at 4% rotation larger than 80% of the beam flexural capacity, hence the joint can be classified as full strength (according to AISC358 [4]).

Table 3.2: ES1-TS-F-C2 - Experimental results.

Joint		ES1-TS-F-C2	
Design Criteria		Full strength	
Elastic Stiffness		22856	[kNm]
0.8 M_{pl}		361.8	[kNm]
$M_{j,Rd}$	4%	505.97	[kNm]
	-4%	-529.05	[kNm]
	Max (5%)	526.16	[kNm]
	Min -(5%)	-557.86	[kNm]
Dissipated energy	4%	122	[kNm]
	5%	233	[-]
	6%	385	[-]
	7%	527	[-]

Moving from the global to the local response of the joint, the rotational contribution of each macro-component is evaluated in order to investigate the degree of participation of each individual component to the chord rotation (see Figure 3-4 from *a* to *d*). Indeed, the curves show that almost all the chord rotation is developed by the beam and the contribution of the connection and column web panel is negligible. This further confirms the hypothesis made in the design process, validating the failure by the formation of the plastic hinge at the beam extremity with the concentration of the demand in the beam flanges, leaving the other joint components in the elastic range.

For instance, to confirm this statement, just for this test and the one performed on the same beam-to-column assembly, but designed as equal strength (ES1-TS-E-C), the bolt deformation are plotted.

Figure 3-2 shows the elastic deformation of two bolts extracted respectively form the first and second bolt row lines.

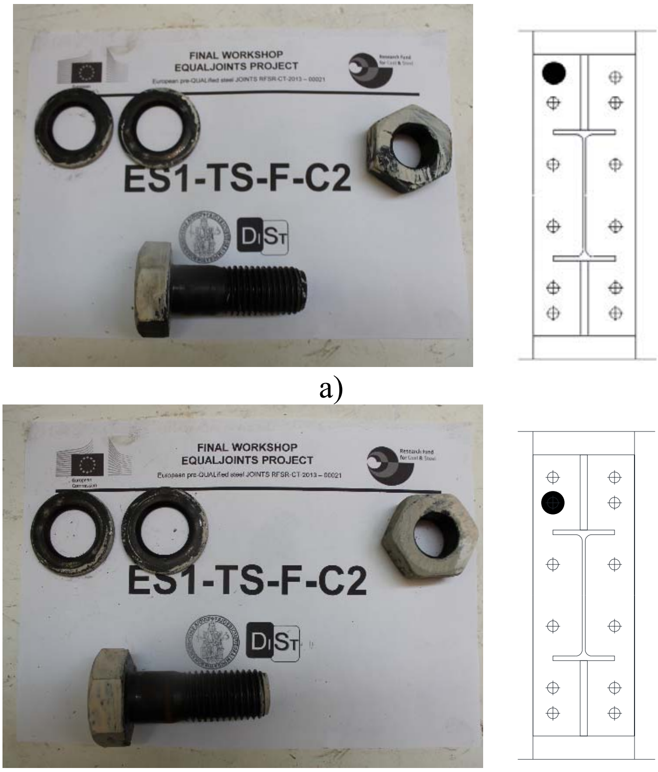

a)

b)

Figure 3-2: Bolts deformation from first (a) and from the second (b) bolt row.

It can be observed that just small plastic deformation on the threaded part are visible; these deformation coming from the clamping force applied in the assembly phase, while no plastic deformation due to the applied displacement can be pointed out. Hence, the ductility criteria introduced in Chapter V find a good validation since no plastic deformation is observed in bolts the remains perfectly elastic.

The bolts behavior observed in this case can be easily generalized for all the beam-to-column full strength joints investigated; hence, for reason of brevity, in the next paragraph will not be plotted.

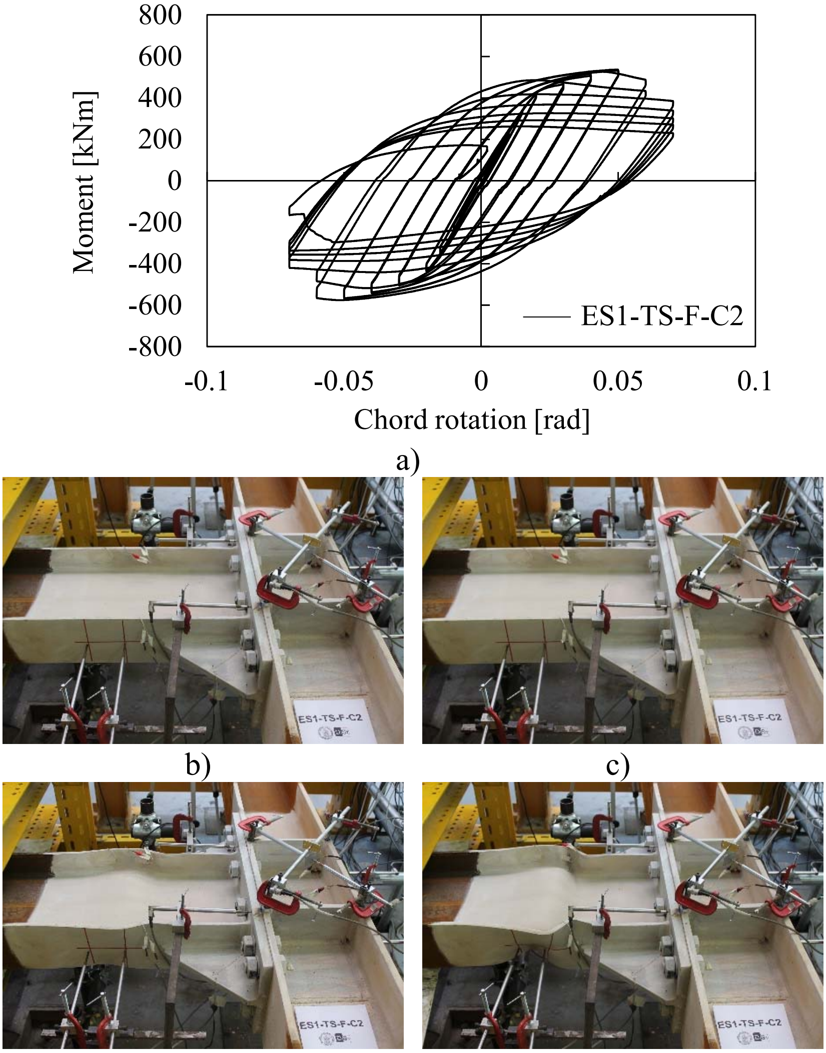

a)

b) c)

d) e)

Figure 3-3: Moment chord rotation (a), joint configuration: initial (b), at 2% (c), at 4% (d) and at 6% (e) of chord rotation.

Apart from strength and stiffness, another important aspect related to the joint characterization is the ductility. The ductility represents a crucial characteristic of a joint with respect to its seismic behavior and it is directly correlated with the energy dissipation capacity. For this reason, Figure 3-5 *b* shows the cumulated dissipated energy normalized to the one at 4% function of the chord rotation. According to this diagram, the investigated joint is able to dissipate up to five times the energy measured at 4%, reaching rotation levels of 7%. This demonstrates the strong ductility of the joint that is mainly provided through the inelastic deformation of the steel beam.

Moreover, the large deformation capacity of the joint is visible also from the shape of the cycles at 4%, 5%, 6% and 7% (see Figure 3-4 from *e* to *h*) and the corresponding energy dissipated for each of the mentioned cycles (see Table 3.2). As showed, increasing the joint rotation the damage on the beam increases with a consequential reduction of stiffness.

It should be noted that in accordance with the loading protocol applied, for each rotational level, two cycles are performed and no appreciable differences can be observed in the pair of moment rotation curves.

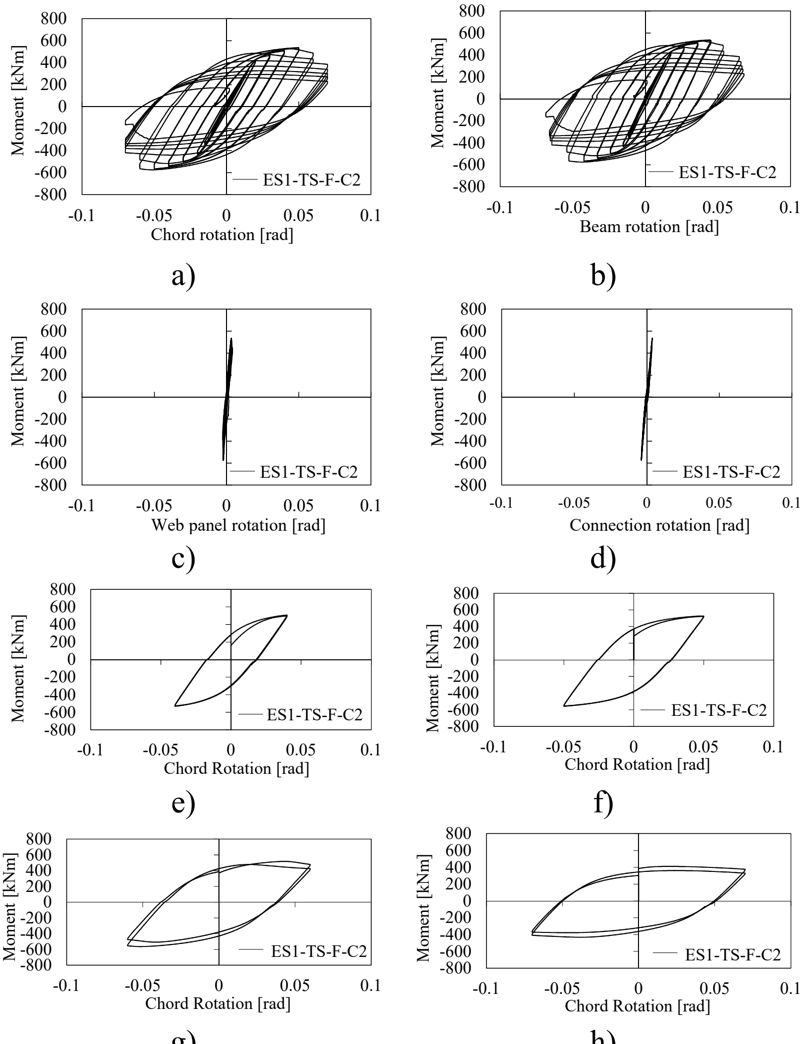

Figure 3-4: Moment chord rotation (a, e, f, g and h), beam rotation (b), column web panel rotation (c) and connection rotation (d).

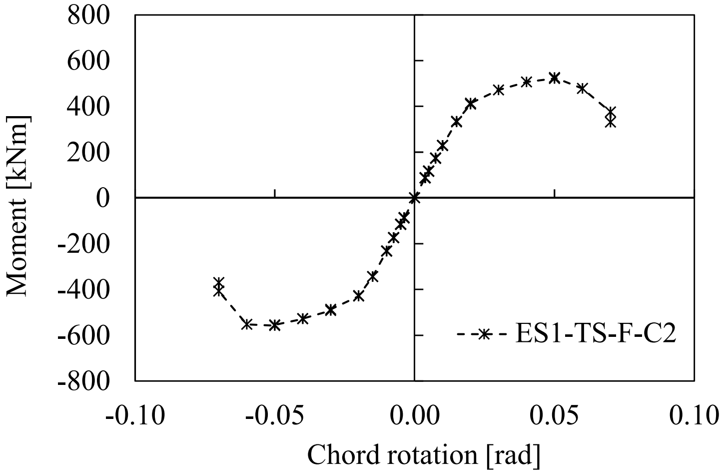

a)

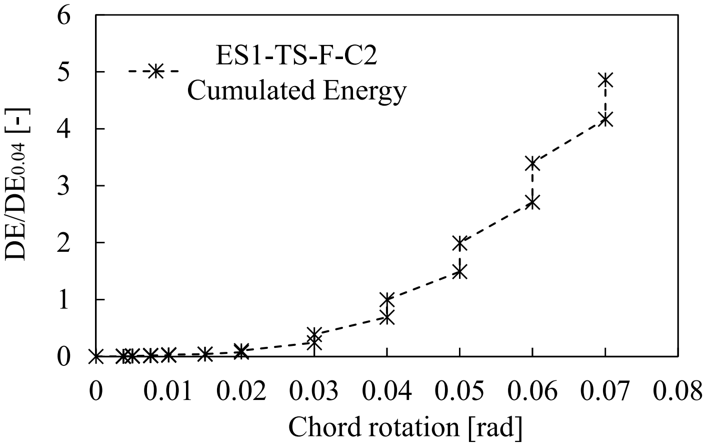

b)

Figure 3-5: Experimental test backbone curve (a) and cumulated energy respect to the 4% rotation (b).

3.1.1 Calibration

The joint was modelled using Abaqus 6.14 [5] FE software in order to confirm the global response and failure mode, and get further insight on aspects of detail that might have not been measured during the experiment. The model was built in line with all the specifications described in the previous Chapter V using the results of the coupon tests in order to define the material properties. For the sake of accuracy, the geometrical imperfections were accounted for by performing a preliminary buckling analysis and considering the relevant buckling shapes.

The results are presented in Figure 3-6 *a* in terms of moment rotation curve of the numerical model together and the backbone curve. Another relevant result is the cumulated energy curve plotted in Figure 3-6 *b* that serves for the comparison of the energy dissipated by the real joint and the model. Starting from the backbone curves (see Figure 3-7 *b*) it is possible to underline the FE model's ability to catch both the elastic stiffness and the test resistance.

Moreover, no significant differences can be pointed out comparing the results in terms of global moment rotation curve (see Figure 3-7 *a*), indeed both the cycle shapes and pinching effect are comparable. In addition, the cumulated energy is almost the same – the FE model shows around 5 times the dissipated energy with respect to the 4% rotation which is consistent with the experimentally measured values.

The calibrated model is also able to catch test failure mode; Figure 3-8 shows that the beam exhibits a decidedly good behavior up to the manifestation of flange instability. The software is also able to predict the zone where the fracture will be reached showing a large concentration of plastic deformation with the same shape observed during the tests (see Figure 3-8 c and d). Despite this accuracy, since the material fracture was not explicitly modelled in the software, the failure of the numerical model is associated with the last point of the backbone curve that corresponds to the flange fracture. This assumption is made due to the strong descending trend of the curve.

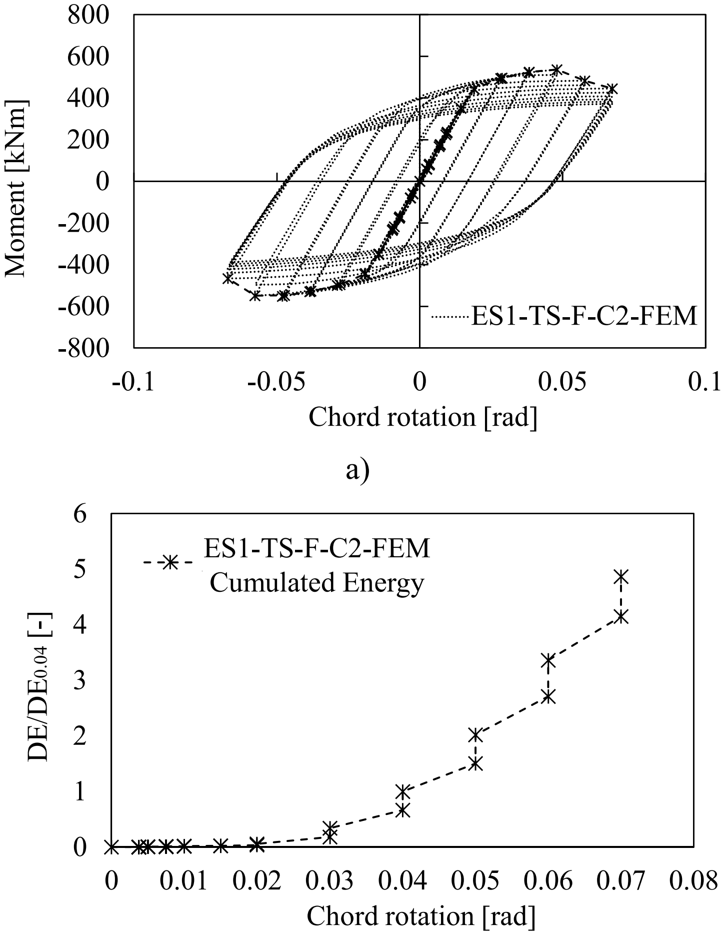

a)

b)

Figure 3-6: FEM: FEM Moment rotation curve (a) and cumulated energy respect to the 4% rotation (b).

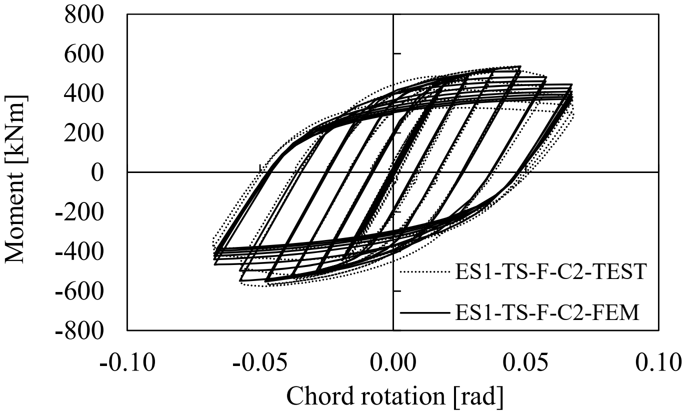

a)

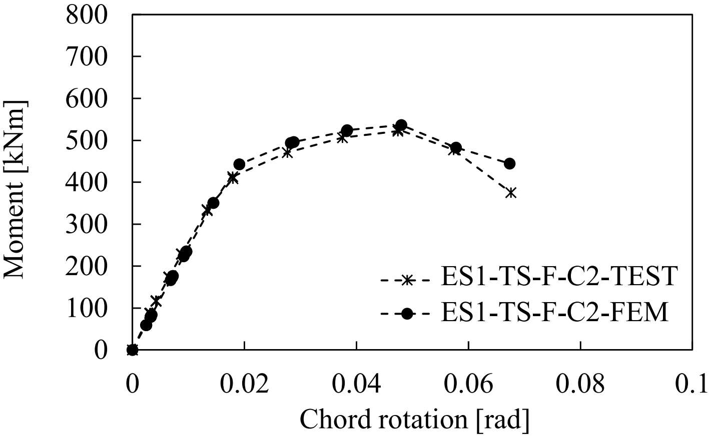

b)

Figure 3-7: Experimental result against the FEM prevision both in terms of cyclic (a) and Back bone curve (b).

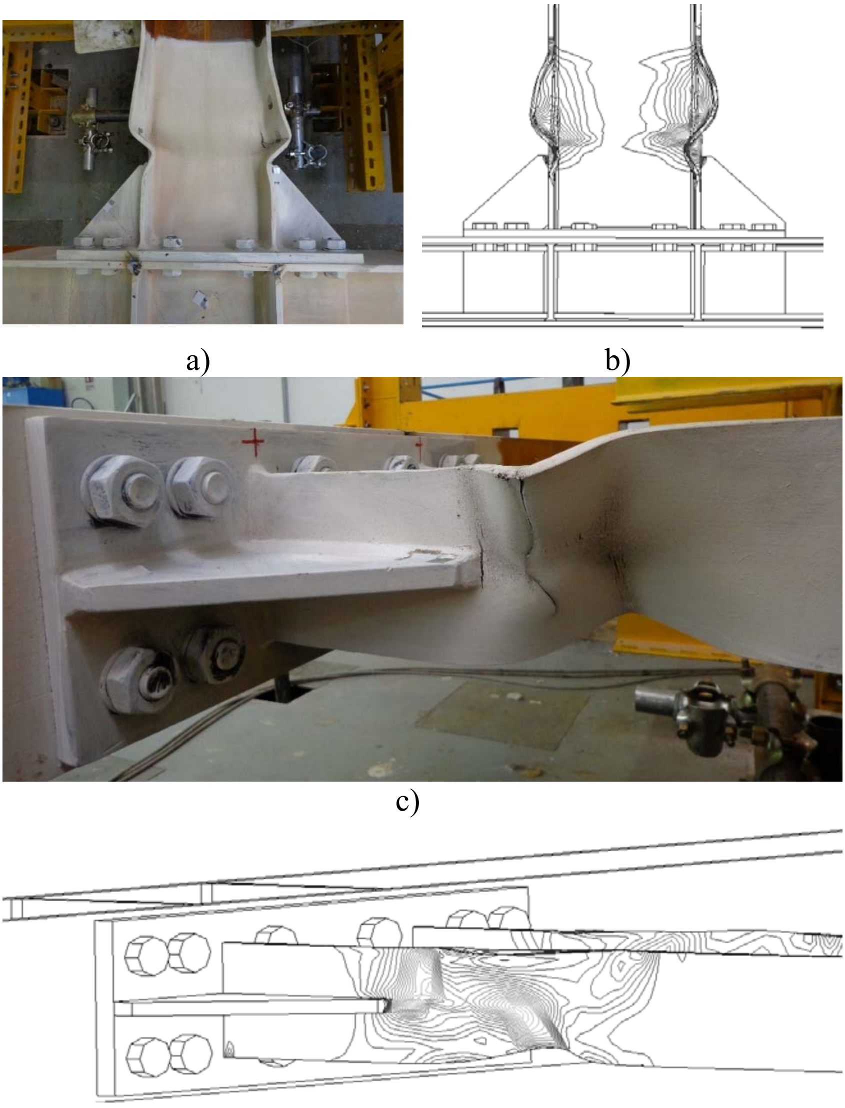

a) b)

c)

d)

Figure 3-8: Failure mode: Experimental (a and c) against FEM PEEQ distribution (b and d).

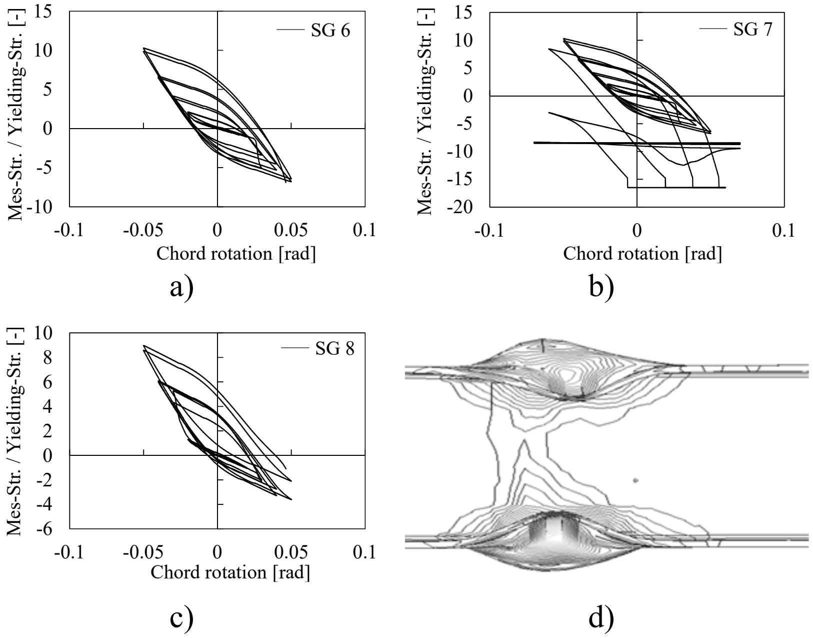

Figure 3-9 Strain gauge measurements (a, b and c) FEM plastic hinge (d).

3.1.2 Strain Gauge

The local deformation of the joint was monitored using strain-gauges and the results recorded by the devices are hereby reported. The devices were placed in areas of the specimen that are considered as representative, and for a full strength joint one of these areas is represented by the beam flange where three devices are placed. In Figure 3-9 *a*, *b* and *c* the strain-gauge measurements on the beam flanges are reported with respect to the material yielding deformation (evaluated by the coupon tests). Figure 3-9 *d* shows the plastic deformation of the beam flanges, which was measured to be reaching values of ten times the yielding strain.

The strain-gauge placed on the column web panel (as reported in Figure 3-10 *a* and *b*) shows that no local deformation overcomes the limit of the yielding strain which is additional confirmation that the column web panel remains in elastic range. The same evidence is confirmed by the lack of visible plastic deformation in Figure 3-10 *c* and the interpretation of the FE model that does not show any yielding line on the column web panel (see Figure 3-10 *d*).

The strain-gauge placed on the ribs (as reported in Figure 3-11) shows that also the stiffeners are in elastic range. Indeed Figure 3-11 *a* and *b* shows that on the rib no plastic deformation are reached and the same response can be observed from the device placed on the rib diagonal (see Figure 3-11 *c*). The lectures from these instruments are visually validated by Figure 3-11 e and *f*, where no plastic deformation can be observed.

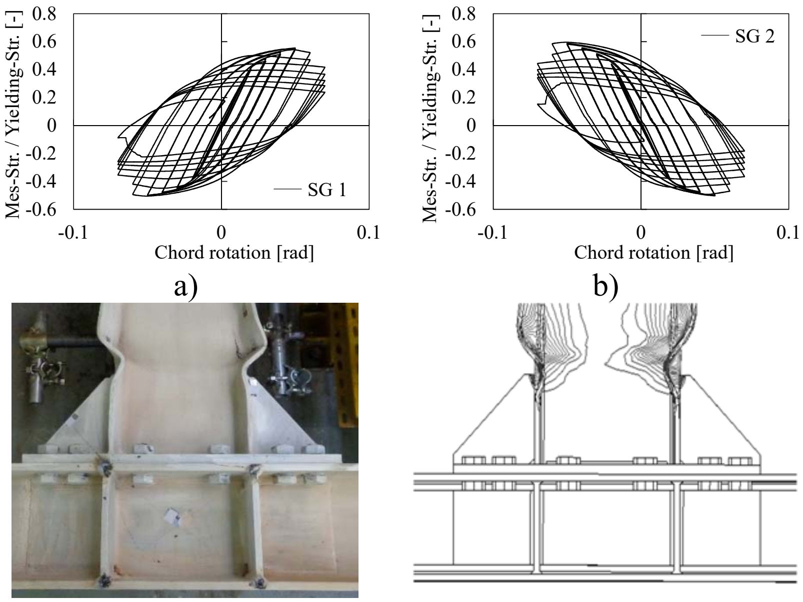

a) b)

c) d)

Figure 3-10: Column web panel deformation in terms of: strain-gauge measurements (a and b), experimental test (c) and FEM yielding line distribution (d).

However, small cracks in the welds and plastic deformation at the ribs extremities can be observed, where also the FE model shows plastic strain concentration. This section represents the limit between the connection and the beam and therefore, large values of internal forces are concentrated. Furthermore, the ribs work also as restrains, preventing the propagation of the beam flange deformation and instability phenomena.

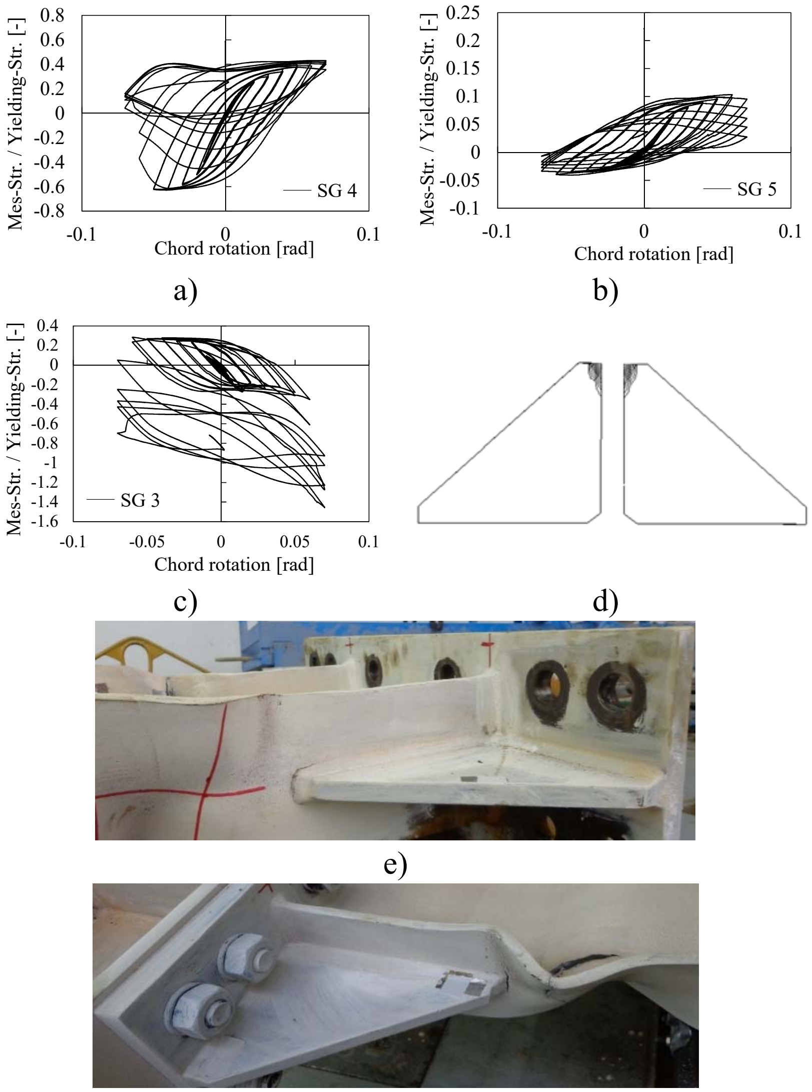

a) b)

c) d)

e)

f)

Figure 3-11: Strain gauge measurements on the ribs (a, b and c) PEEQ on the ribs (d) detailed view of the tested ribs (e and f).

3.2 ES1-TS-F-M

The ES1–TS–F–M is a monotonic test performed on the smaller beam-to-column assembly (i.e. the beam is an IPE360 and the column an HEB280). The joint is designed as full strength, and it is subjected to monotonic load, increasing displacement up to 35mm in order to reach a chord rotation equal to 10%.

The moment rotation curve (see Figure 3-12 a) shows the maximum joint capacity is around 580kNm. This value is slightly larger than the one measured in the cyclic test and the reason can be assumed to be the geometrical imperfection. Indeed, since for the monotonic test the ductility demand on the joint is appreciably smaller with respect to the one in the cyclic test, the beam flange buckling is less evident and does not influence the joint capacity, allowing the development of a larger hardening with a consequential larger joint capacity.

Figure 3-12 from *b* to *e* shows several stages of the test, starting with the initial one going through 4%, 10% and finally, the last stage after unloading.

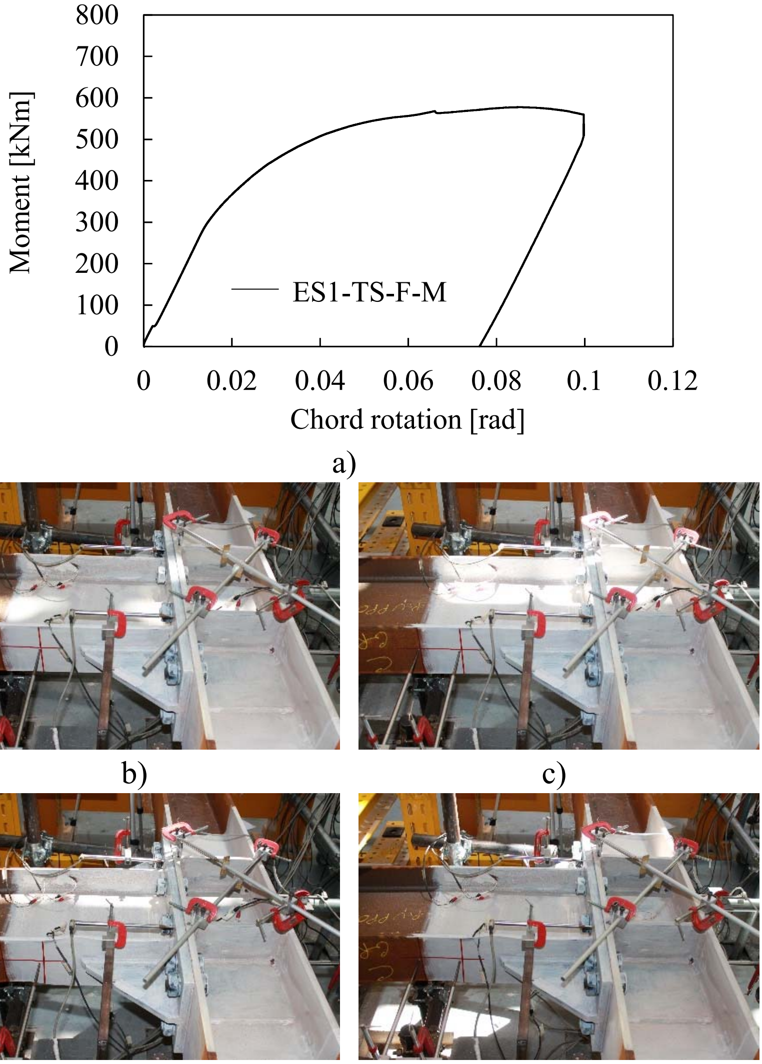

a)

b)

c)

d)

e)

Figure 3-12: Moment chord rotation (a), joint configuration: initial (b), at 2% (c), at 4% (d) and at 6% (e) of chord rotation.

The macro-component rotational contributions depicted in Figure 3-13, confirm the effectiveness of the designed joint. As already showed in the previous test, all the chord rotation is developed by the beam and both the column web panel and the connection remain in elastic range providing negligible contribution to the total joint rotation.

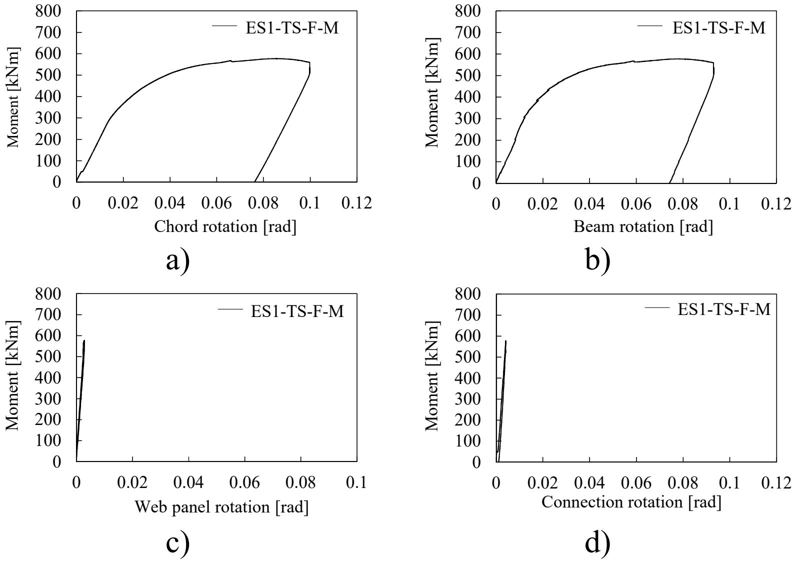

a) b)

c) d)

Figure 3-13: Moment chord rotation (a), beam rotation (b), column web panel rotation (c) and connection rotation (d).

3.2.1 Calibration

The numerical calibration for this test was made starting from the same model introduced in the previous paragraph by changing both the material properties, in accordance with the coupon test results, and the loading action.

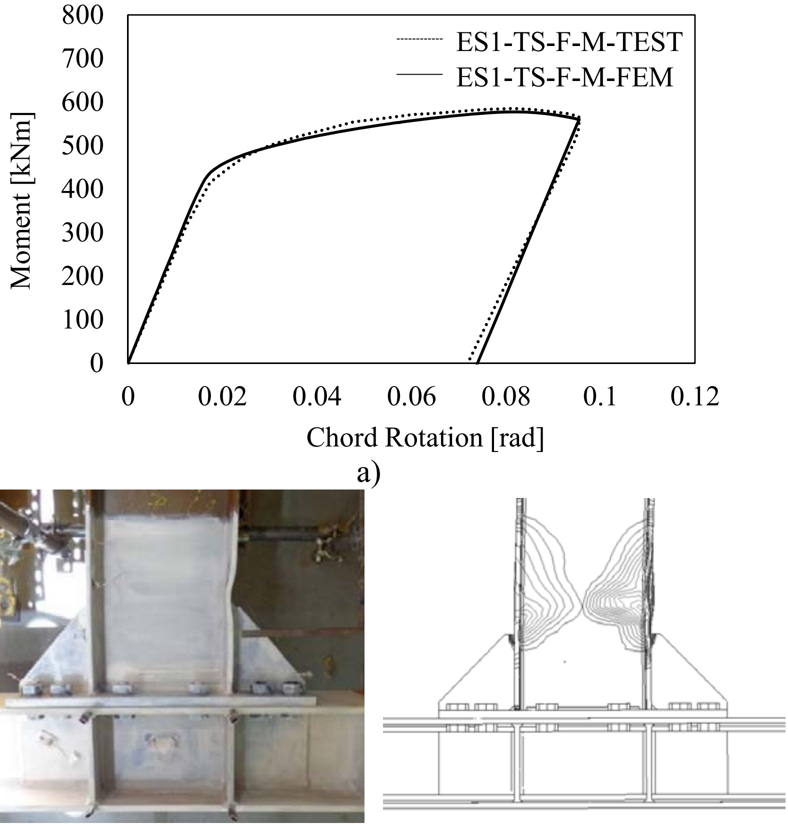

a)

b) c)

Figure 3-14: Experimental result against the FEM prevision both in terms of moment rotation curve (a) and failure mode (b and c).

The FE model is able to accurately predict the test response; as reported in Figure 3-14 *a* both the elastic stiffness and the maximum joint resistance are calibrated.

The unloading branch at the end of the test and the joint failure mode are closely reproduced by the software. Furthermore, perfect agreement of the deformed shape is reported in Figure 3-14 *b* and *c* that show the plastic deformation observed during the test and the PEEQ distribution, respectively. The only difference that can be observed between the experimental and FE model results is the yielding knee that could be caused by the different material characteristics.

3.2.2 Strain gauge

Strain-gauges are placed in the column web panel and on the ribs. As showed in the previous paragraph for ES1-TS-F-C2 specimen, the results are presented in terms of normalized strain curves (the measured one divided by the yielding strain evaluated experimentally) and plastic deformation.

Perfectly in line with the design assumption and the rotational contribution depicted in Figure 3-13 *c*, the curves of the devices on the column web panel show that the maximum normalized strains range between 0.5 and 0.6 (Figure 3-15 *a* and *b*) meaning the column web panel is in elastic range.

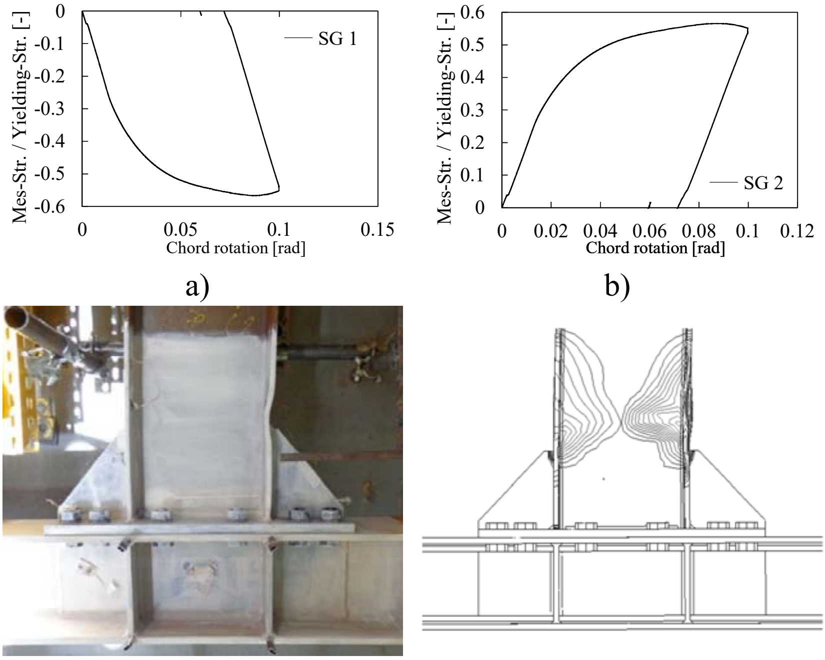

a) b)

c) d)

Figure 3-15 Web panel strain gauges results: normalized strain versus chord rotation (a and b) plastic deformation of the tested specimen (c) PEEQ distribution on the FE model (d).

These results are confirmed by examining the tested specimen, i.e. the experimental test shows no damage in the column (see Figure 3-15 *c*) and from the PEEQ distribution in the FE model (see Figure 3-15 *d*) that shows no concentration out of the beam area.

The experimental results of the devices on the ribs reveal that both stiffeners are in the elastic range (see Figure 3-16 *a* and *b*), however, the FE model reveals traces of plastic deformation on the named parts. This difference is probably caused by the strain-gauge positioning. Indeed, on the compression side, the device is placed on the diagonal and it is far from the damage concentration zone. On the tension side, the device placed on the rib base is close to the plastic zone, but it reads just on the stiffener while the deformations are concentrated at the beam-rib weld interface.

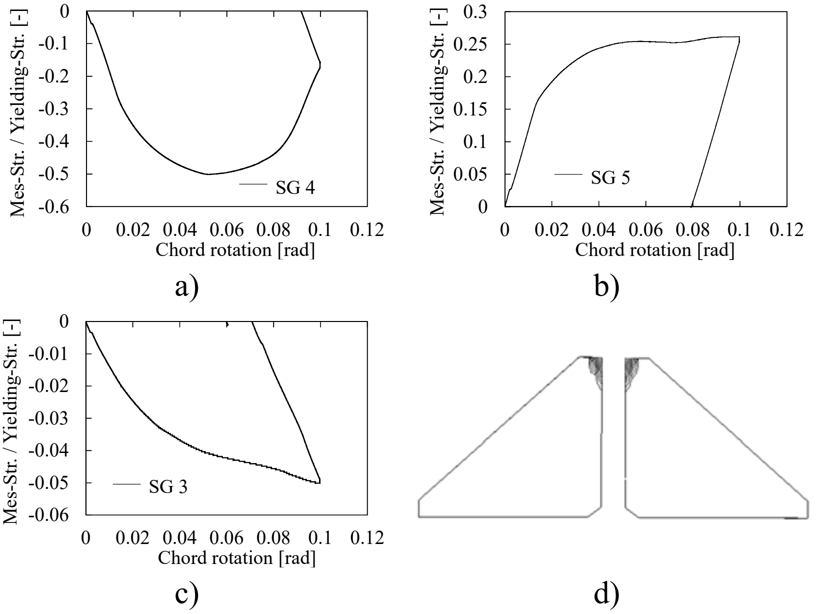

a) b)

c) d)

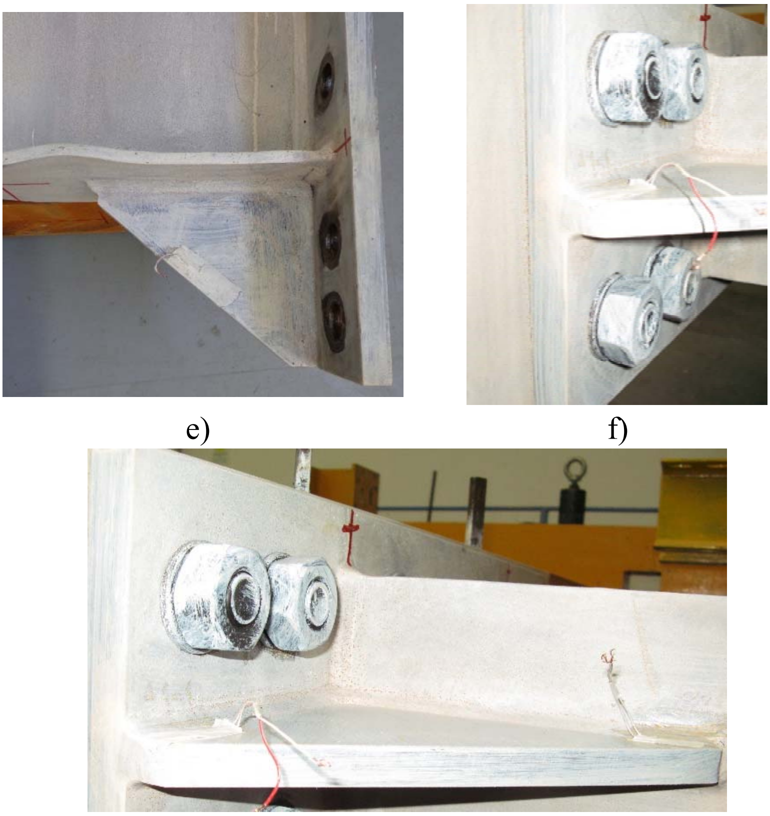

e)

f)

g)

Figure 3-16: Rib strain gauges results: normalized strain versus chord rotation (a, b and c), PEEQ distribution on the FE model (d), plastic deformation of the tested specimen (e, f and g).

3.3 ES1-TS-E-C1

ES1–TS–E–C1 is a cyclic test on the same beam-to column assembly seen in the previous paragraphs (i.e. the beam is an IPE360 and the column HEB280) and designed as an equal strength joint. The joint is indeed designed to show a balanced damage distribution between the beam and the connection while the column web panel should remain in elastic range.

The joint behavior can be divided in two parts: in the first, the plate yields and the beam behaves elastically with the plate gap opening and the correlated activation of the T-Stub on the tension side. Increasing the rotational demand, the steel plate starts to develop hardening with a consequential increase of its resistance. This represents the second step, i.e. the damage moves from the plate towards the beam. As it can be observed from Figure 3-18, once the yielding starts to develop in the beam, the buckling of the flanges occurs, directing the failure in the beam.

Table 3.3 summarizes the test results and it can be observed that at 4% rotation the bending demand in the joint is closer to the beam capacity (440kNm). The flexural capacity increases up to 6%, where the failure mechanism moves from the plate to the beam and the flange instability leads to a reduction of the joint capacity.

This aspect is also evident from the plotted rotational contributions of all the macro-components (see Figure 3-19). Indeed, compared with the full strength joint in the previous paragraph, the connection rotational contribution plays a central role in the chord rotation definition. The failure mode involves also the connection, not only the beam, and for this reason, important considerations on the joint ductility are needed. In particular, the plastic demand is concentrated mainly in the end-plate, and activates the equivalent T-stub in the tension side showing a failure mode 2 close to mode 1 (in accordance with the design requirements). Moreover, this evidence is also confirmed by the bolts plastic deformation (see Figure 3-17); indeed differently from the ones show for full strength (ES1-TS-F-C2), in case of equal strength joint part of plastic deformation is also concentrated in the bolts despite if the failure mode is close to the mode 1.

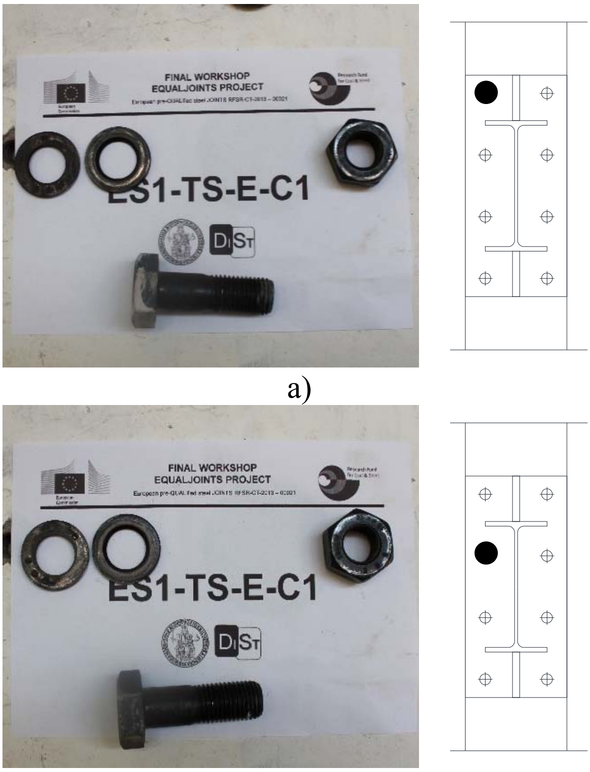

a)

b)

Figure 3-17: Bolts deformation from first (a) and from the second (b) bolt row.

Further investigations aim to identify the ductility level of this type of failure and compare it to the full strength joints. To this end, Table 3.3 and Figure 3-19 report the amount of dissipated energy and the shape of the two cycles at 4%, 5%, 6% and 7% chord rotation. It can be easily recognized how the cycle area increases with the increase of applied rotation without showing an evident cyclic degradation (as also confirmed by the cycle's shape).

In order to understand the joint ductility level, it is interesting to observe also the results in Figure 3-20, where the cumulated energy is reported function of the chord rotation. It is clear how the energy at 7% is almost 5.5 times the cumulated energy at 4% rotation. This evidence confirms that an equal strength joint, whose plastic demand is concentrated not just in the beam, but also in the connection (especially in the end-plate), can provide a good behavior in terms of ductility.

Table 3.3: ES1-TS-E-C1 test results.

Joint		ES1-TS-E-C1	
Design Criteria		Equal strength	
Elastic Stiffness		19090	[kNm]
0.8 M_{pl}		361.8	[kNm]
$M_{j,Rd}$	4%	464.58	[kNm]
	-4%	-476.54	[kNm]
	Max (6%)	498.73	[kNm]
	Min (-6%)	-514.95	[kNm]
Dissipated energy	4%	78	[kNm]
	5%	153	[-]
	6%	259	[-]
	7%	400	[-]

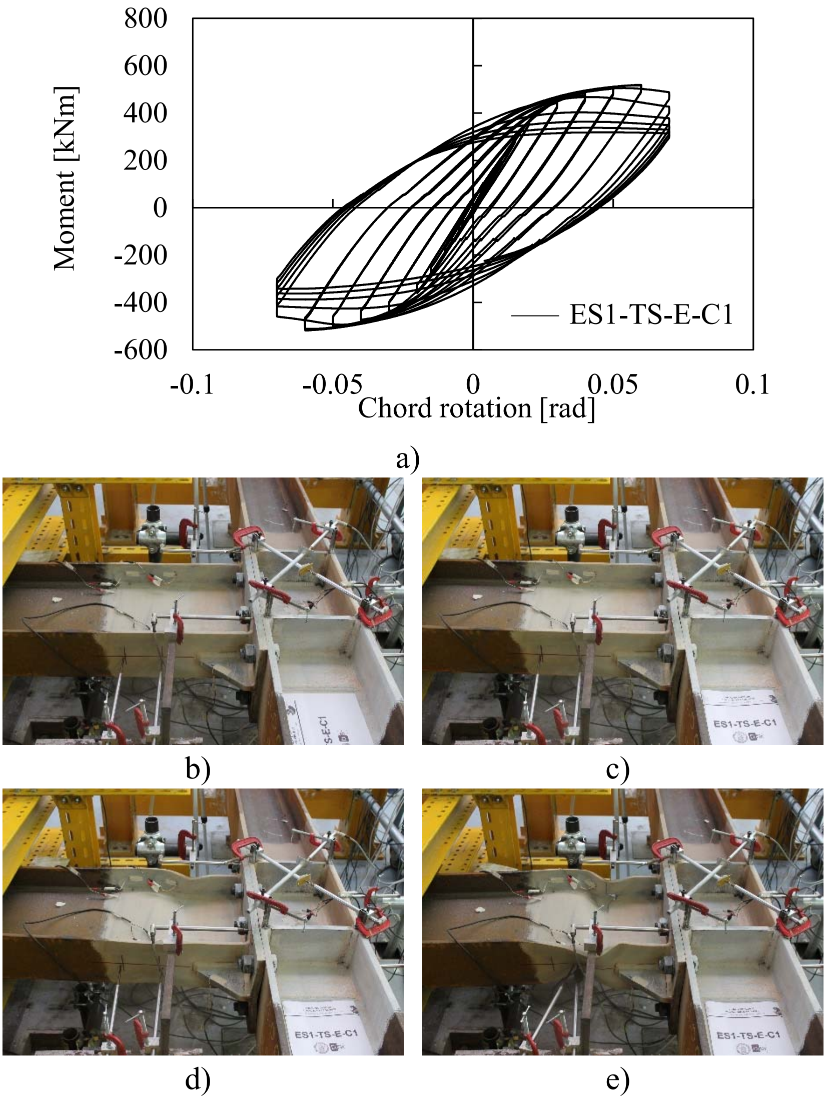

Figure 3-18: Moment chord rotation (a), joint configuration: initial (b), at 2% (c), at 4% (d) and at 6% (e) of chord rotation.

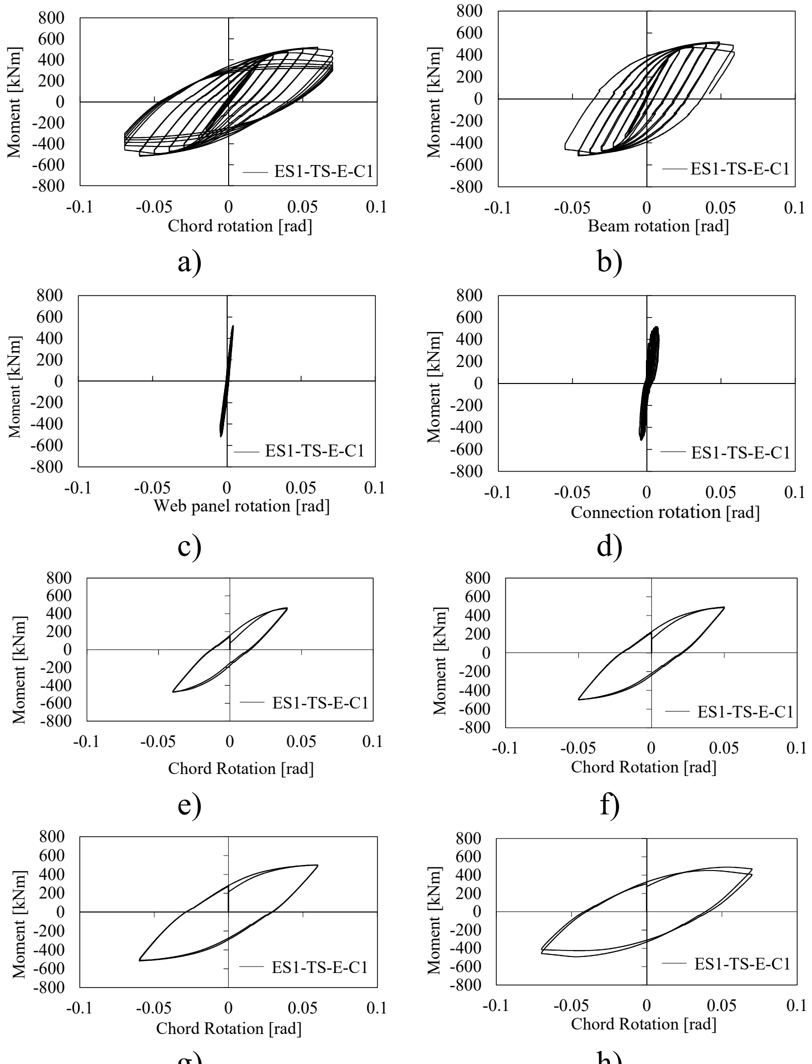

a) b) c) d) e) f) g) h)

Figure 3-19: Moment chord rotation (a, e, f, g and h), beam rotation (b), column web panel rotation (c) and connection rotation (d).

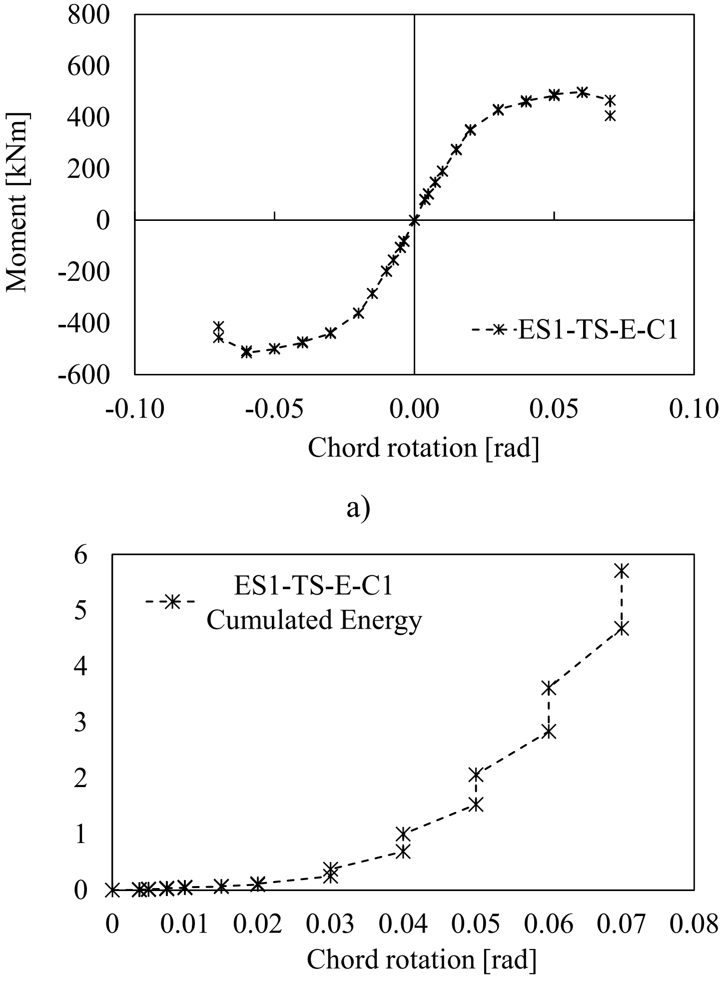

a)

b)

Figure 3-20: Experimental test backbone curve (a) and cumulated energy respect to the 4% rotation.

3.3.1 Calibration

As showed for the previous assembly, also in this case a FE model was built (see Figure 3-21) in order to calibrate the experimental results.

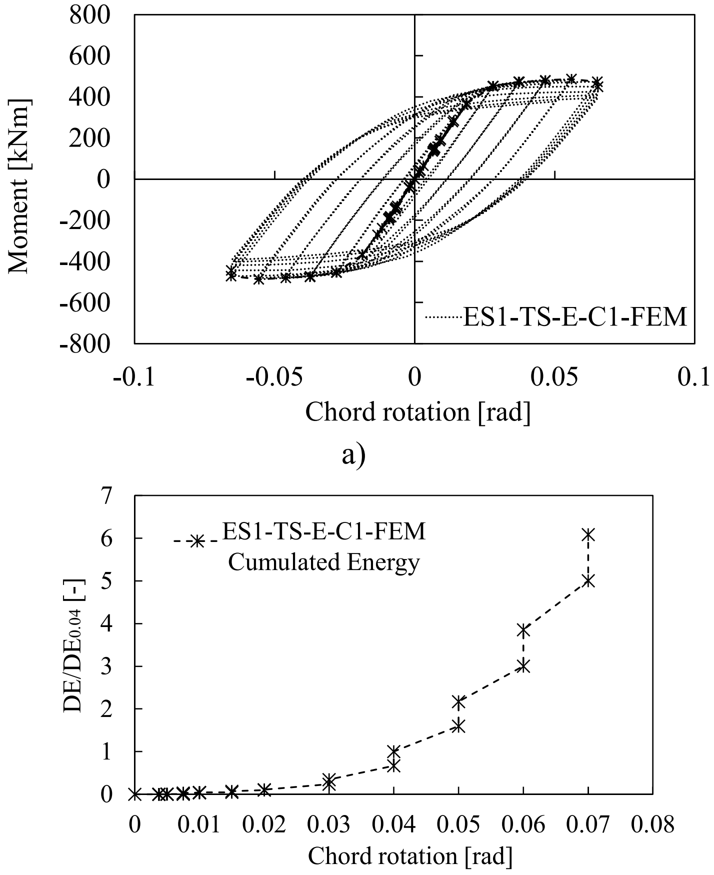

a)

b)

Figure 3-21: FEM: (a) Moment rotation curve and (b) cumulated energy respect to the 4% rotation.

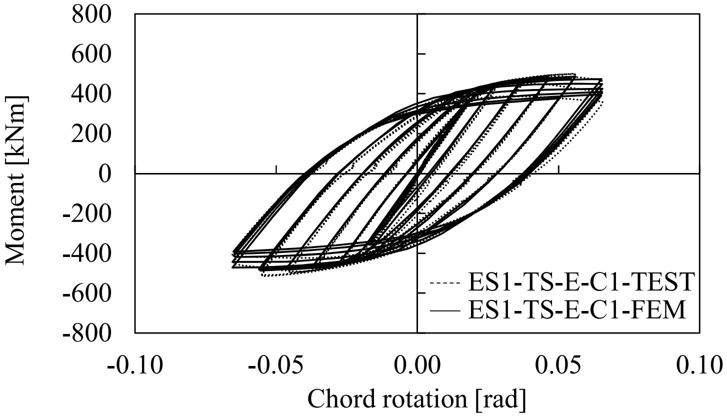

a)

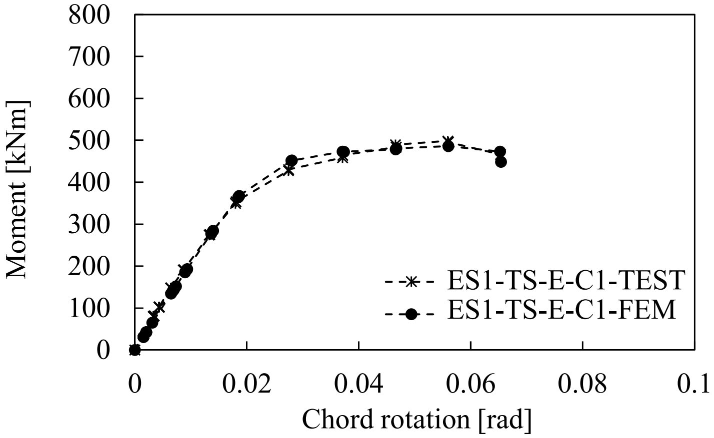

b)

Figure 3-22: Experimental result against the FEM prevision both in terms of cyclic (a) and Back bone curve (b).

A perfect agreement can be pointed out from the comparison of both the cyclic and backbone curve (see Figure 3-22). The Abaqus model is indeed able to predict both the elastic stiffness and the joint resistance. Moreover, the curve degradation caused by the buckling of the beam flanges, is also well calibrated. The FE model is able to reproduce the damage propagation and failure mode, i.e. large plastic demand in the end-plate with residual gap opening (see Figure 3-23) and the beam failure due to the buckling of the flanges is observed, exactly as seen in the experimental test. For this case, the distribution of the displacement is plotted as well. In Figure 3-23 f) it is evident how the experimentally measured displacements are perfectly matched by the FE analysis.

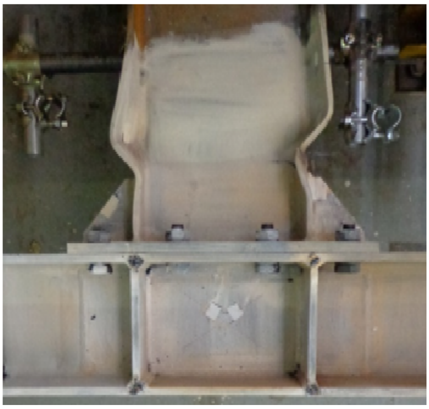

a)

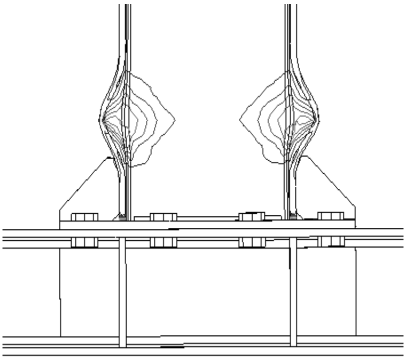

b)

c)

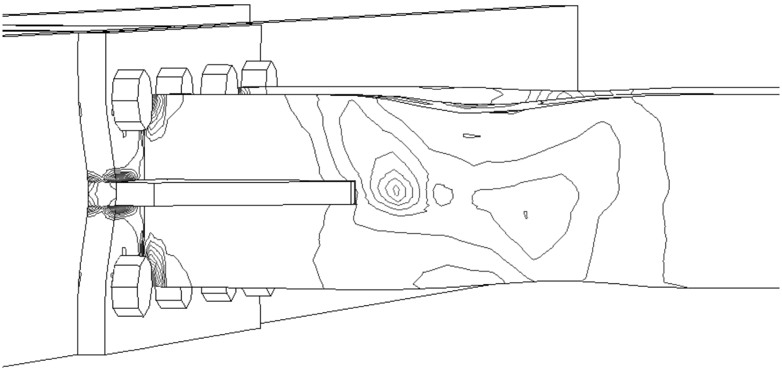

d)

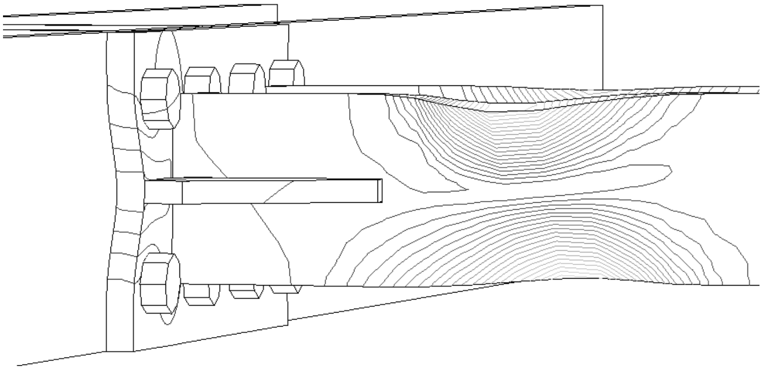

f)

Figure 3-23: Failure mode: Experimental (a and c) against FEM PEEQ distribution (b and d) and FEM displacements magnitude (f).

3.3.2 Strain gauge

The strain-gauge measurements (see Figure 3-24 *a* and *b*) on the column confirms an elastic behavior of the web panel, despite the fact that some small plastic deformations can be noticed for high values of rotation. Indeed, the FE model as well (see Figure 3-24 *d*) shows small concentration of PEEQ in the web panel, while no appreciable deformation can be observed in the experimental specimens (see Figure 3-24 *c*).

The device on the ribs' base and height (see Figure 3-25 *a*, *b* and *c*) do not show significant engagement in plastic range, while some plastic deformation can be observed in the rib on the diagonal. This is believed to be caused by the activation of the T-stub on the tension side.

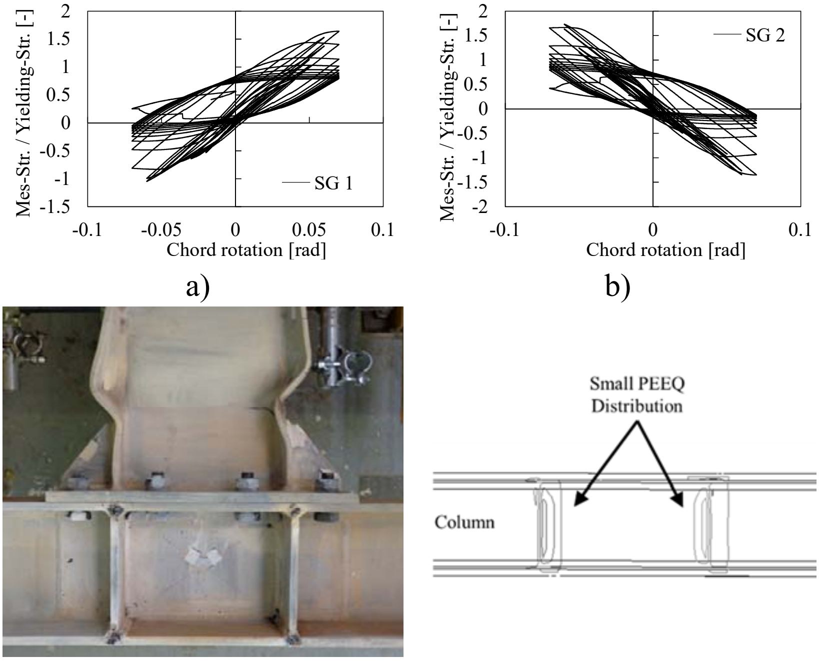

a) b)

c) d)

Figure 3-24 Web panel strain gauges results: normalized strain versus chord rotation (a and b) plastic deformation of the tested specimen (c) PEEQ distribution on the FE model (d).

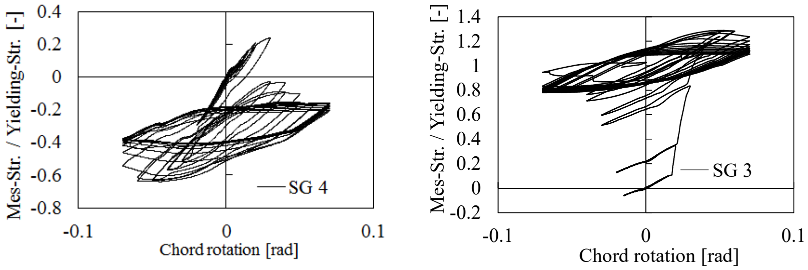

a) b)

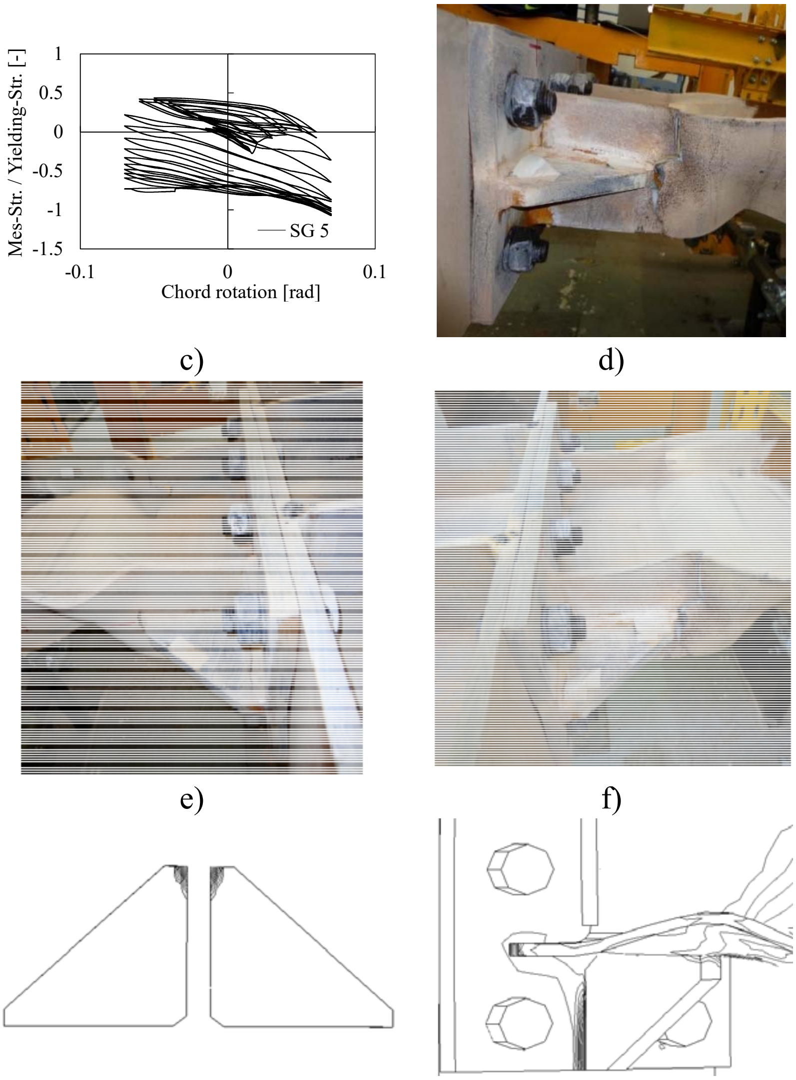

c) d)

e) f)

g) h)

Figure 3-25: Rib strain gauges results: normalized strain versus chord rotation (a, b and c), plastic deformation of the tested specimen (d, e and f) and PEEQ distribution on the FE model (g and h).

3.4 ES2–TS–F–CA

ES2–TS–F–CA is a cyclic test on the IPE 450 beam and HEB340 column assembly. The joint is designed as full strength and the Equaljoint [1] loading protocol was applied.

The moment-rotation curve (Figure 3-26 *a*) shows an increasing bending capacity up to 5% rotation (see Table 3.4), after which the geometric imperfection on the beam flanges reduces the joint capacity. In line with the previous full strength tests, also in this case, the plastic demand is concentrated at the beam extremity, and no appreciable plastic deformation can be observed in other components of the joint. The rotational contribution (Figure 3-27 *b*, *c* and *d*) confirm the failure mode observed, showing a small rotational contribution of both the column web panel and the connection with most of the chord rotation developed by the beam.

Table 3.4: ES2-TS-F-CA test results.

Joint		ES2-TS-F-CA	
Design Criteria		Full strength	
Elastic Stiffenes		41717.5	[kNm]
0.8 M_{pl}		604.14	[kNm]
$M_{j,Rd}$	4%	971.06	[kNm]
	-4%	-993.95	[kNm]
	Max (5%)	1021.9	[kNm]
	Min (-5%)	-1030.2	[kNm]
Dissipated energy	4%	184	[kNm]
	5%	377	[-]
	6%	645	[-]
	7%	876	[-]

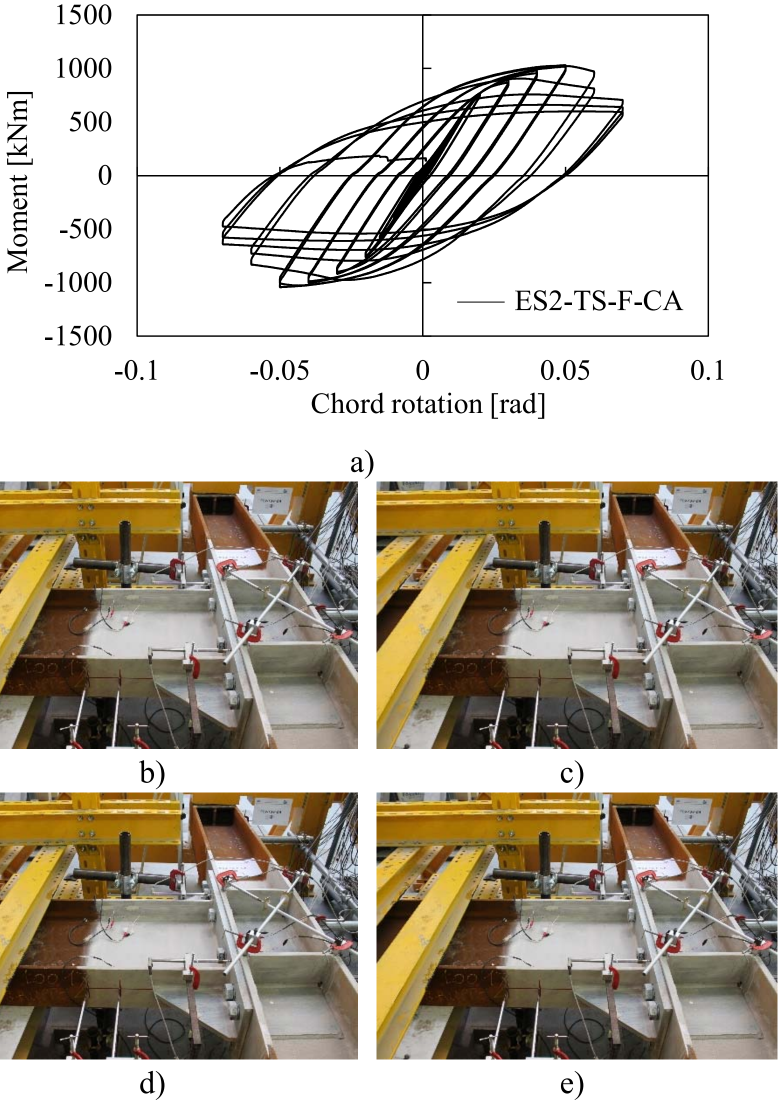

a)

b)

c)

d)

e)

Figure 3-26: Moment chord rotation (a), joint configuration: initial (b), at 2% (c), at 4% (d) and at 6% (e) of chord rotation.

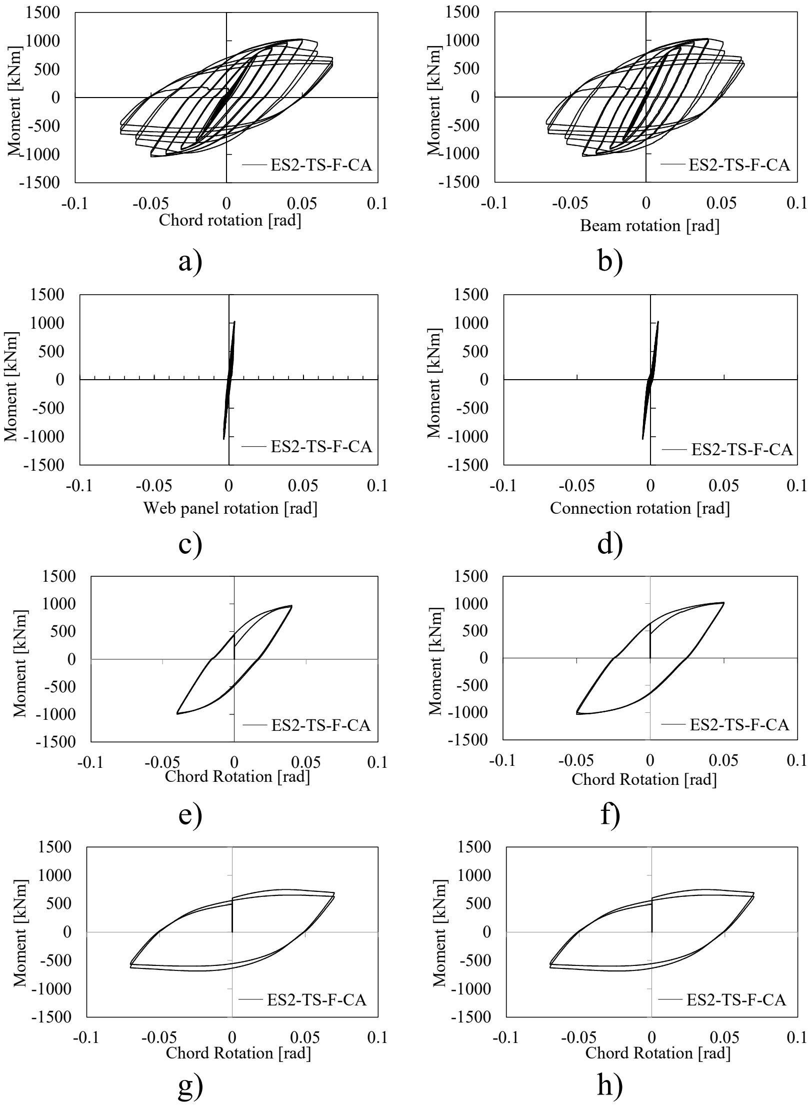

Figure 3-27: Moment chord rotation (a, e, f, g and h), beam rotation (b), column web panel rotation (c) and connection rotation (d).

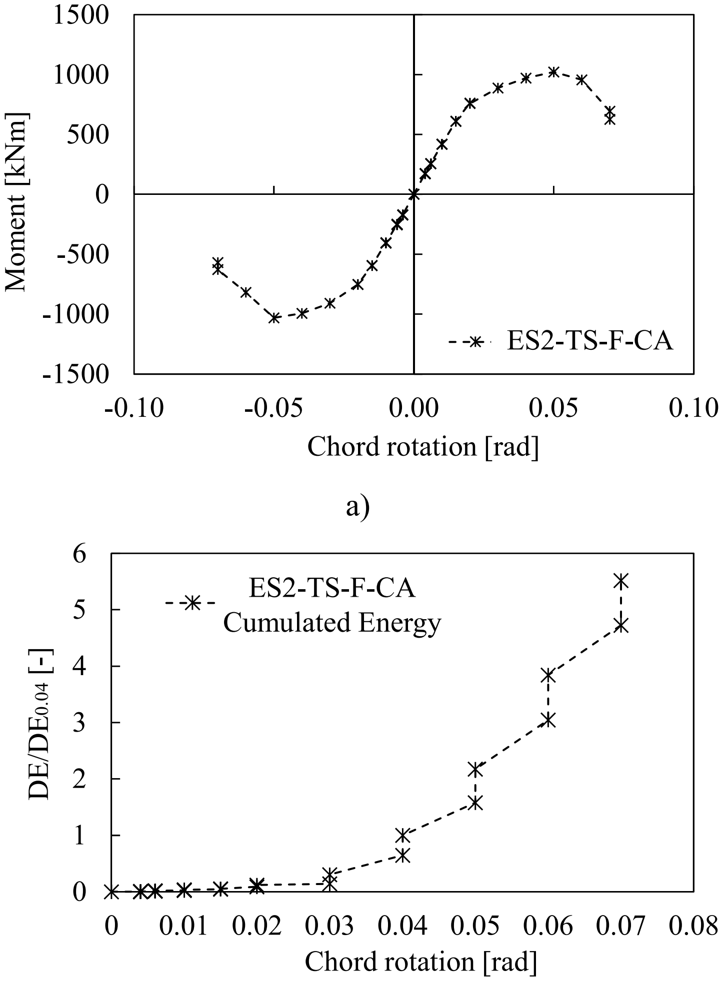

a)

b)

Figure 3-28: Experimental test backbone curve (a) and cumulated energy respect to the 4% rotation.

The beam flange geometric imperfections do not influence just the joint bending capacity, but due to the decrease of both stiffness and resistance, they influence also the dissipated energy (see Figure 3-28). The cycles' shape and their respective area determine the joint ductility which actually represents the energy dissipated by the plastic deformation of the joint.

In this test, despite the significant effects of imperfections, with increasing chord rotation, the cycles provide increasing dissipative capacity, as seen in Figure 3-27 *e*, *f*, *g* and *h* and also in Table 3.4. The cumulated energy is also reported in function of the chord rotation (see Figure 3-28 *b*), where at 7% the cumulated energy is around 5.5 time the energy at 4%. This proves the high joint ductility, i.e. the joint is able to dissipate more than 5 times the energy required for the upper limit of qualification (4%).

3.4.1 Calibration

The FE model is able to replicate the test results in terms of elastic stiffness, resistance (see Figure 3-30) and failure mode (see Figure 3-31). Moreover, the beam degradation is well caught by modelling the geometric imperfections on the beam.

Some differences between the FEM results and the test can be observed on the shape of the moment-rotation curve (see Figure 3-29). In this case, it is indeed possible to observe how the FE model shows more important pinching effects that reduce the area of the cycles.

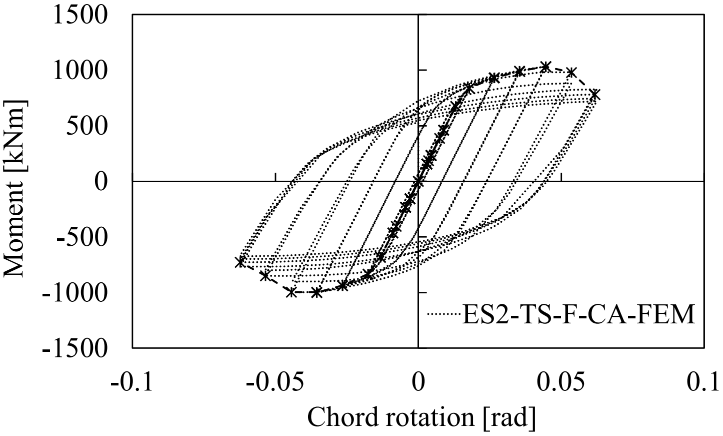

a)

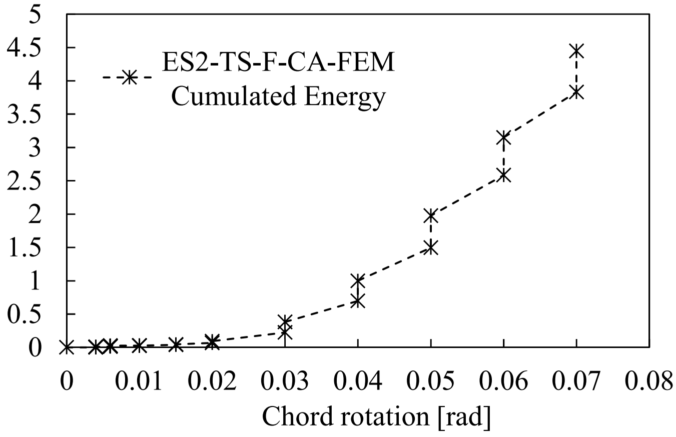

b)

Figure 3-29: FEM: (a) Moment rotation curve and (b) cumulated energy respect to the 4% rotation.

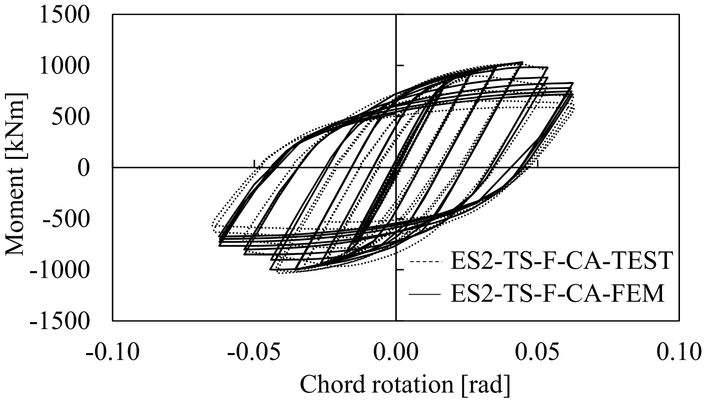

a)

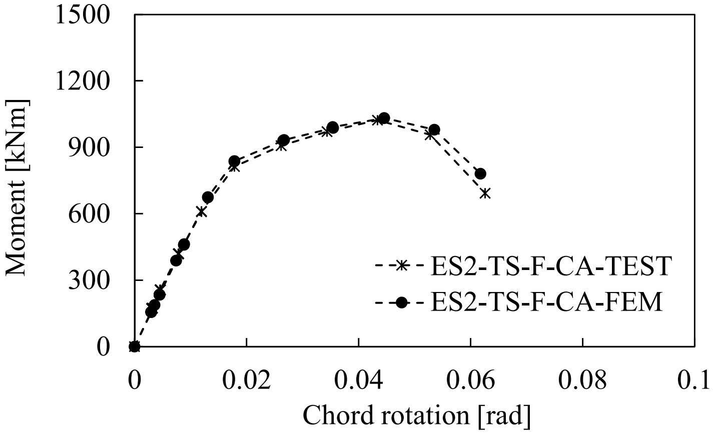

b)

Figure 3-30: Experimental result against the FEM prevision both in terms of cyclic (a) and Back bone curve (b).

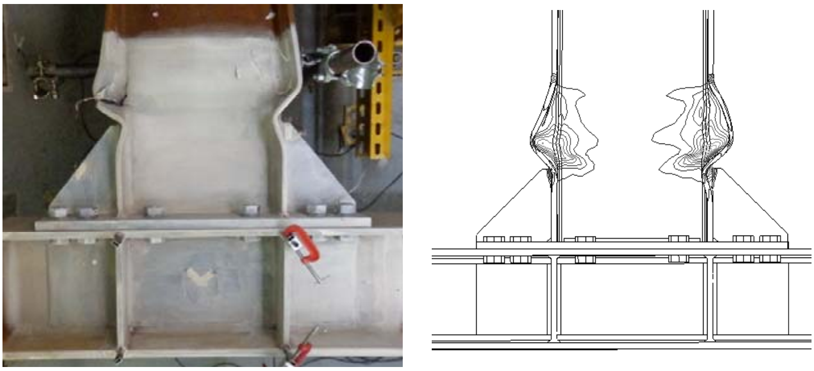

a) b)

Figure 3-31: Failure mode: Experimental (a and c) against FEM PEEQ distribution (b and d).

This difference is also confirmed in terms of cumulated energy, i.e. at 7% of rotation the dissipated energy DE on $DE_{0.04}$ is almost 4.5, compared to 5.5% evaluate in the experimental test. Finally, the differences between the software and the experimental results show a good agreement and the text can be considered calibrated.

3.4.2 Strain-gauge

The strain-gauges on the web panel (see Figure 3-32 *a* and *b*) confirms that no plastic deformation are attained in the column. Moreover, yield line distributions from the test results (see Figure 3-32 *c*) and from the FE model (see Figure 3-32 *d*) show that the column web panel remains in elastic range.

The device placed on the rib height (see Figure 3-33 a) does not report any plastic deformation as also confirmed from the picture of both the test specimens and the FEA results (see Figure 3-33 c, *d*, *e* and *f*).

The same observation can be made for the device placed on the other rib on the diagonal section; also, this device does not show any overcoming of the ratio between the measured and the yielding strain (see Figure 3-33 b). To be observed how the device SG 3 rotates around the zero axis for small rotational values but with the increasing rotation is shifted to another position at about 0.35 (see Figure 3-33 b). This is caused by a rigid movement of the device during the test.

Finally, the device placed on the rib base did not read anything up to the end of the test due to fracture and yielding on the rib base that compromised its functionality.

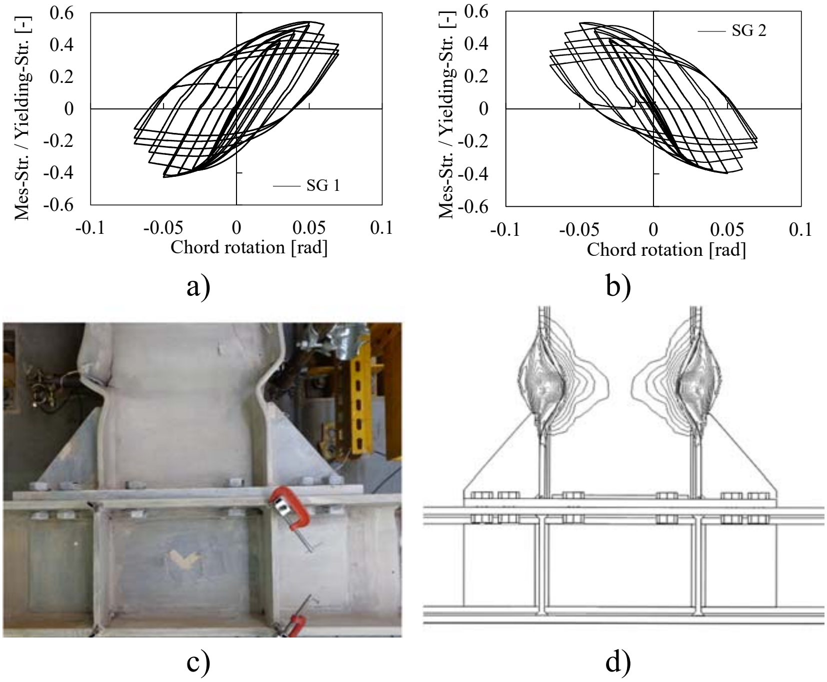

a) b)

c) d)

Figure 3-32 Web panel strain gauges results: normalized strain versus chord rotation (a and b) plastic deformation of the tested specimen (c) PEEQ distribution on the FE model (d).

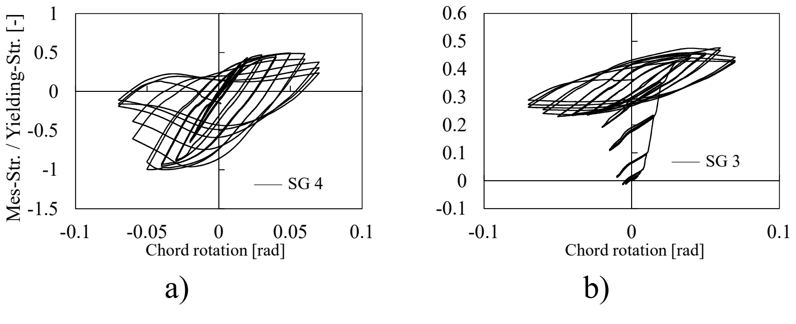

a) b)

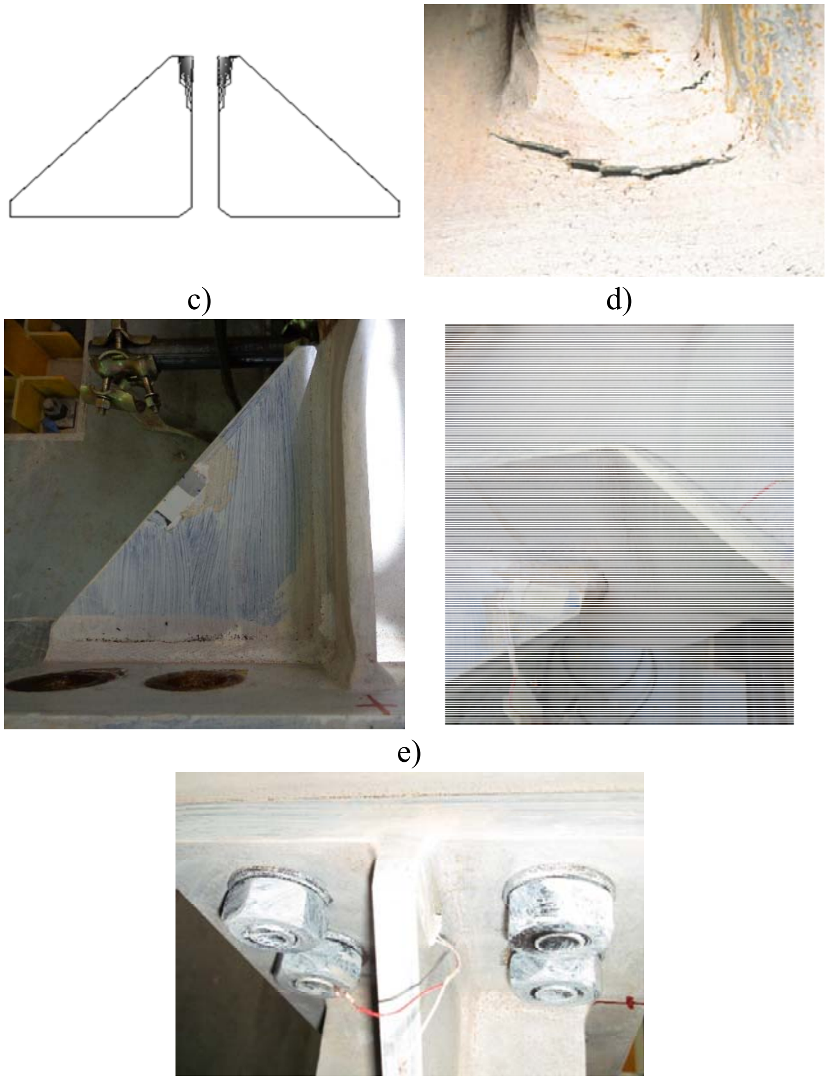

c) d)

e)

f)

Figure 3-33: *Rib strain gauges results: normalized strain versus chord rotation (a and b), PEEQ distribution on the FE model (c) and plastic deformation of the tested specimen (d, e and f).*

3.5 ES2–TS–F–C2

ES1–TS–F–C2 is a cyclic test with the same geometrical characteristics reported in the previous test (ES2-TS-F-CA) with the sole change of the loading protocol used, i.e. the AISC341 [3]. Therefore the differences between the two loading protocol could be pointed out; with particular attention to the joint performance in terms of capacity degradation and dissipated energy.

Hence, the joint also in this case is designed as a full strength one, meaning that all the plastic deformation is expected in the connected beam. Indeed, the experimental test validated the assumptions made in the design process and the failure mode is well matched (see Figure 3-34). The moment-rotation curve (see Figure 3-34 *a*) shows also the respective degradation of the capacity due to the material and mechanical imperfections.

Despite the similar global behavior with respect to the previous investigated joint, some differences are to be pointed out. The joint's elastic stiffness is indeed comparable, but some interesting differences can be observed from the resistance point of view (see Table 3.4 and Table 3.5).

In particular, this joint reaches a smaller value of bending moment (i.e. at 4% rotation the ES2-TS-F-CA showed a capacity 17% larger than for the current joint). This difference in terms of resistance is not caused by the loading protocol applied but by the beam material characteristics.

Indeed, by checking the coupon test results (see Figure 2-1), it can be noticed that the yielding strength of the ES2-CA material is almost 15%larger than that of the ES2-C2.

Perfectly in accordance with the other full strength joints investigated, also in this case the study of the macro-component rotational contribution (see Figure 3-35 *b*, *c*, and *d*) confirms that almost all the chord rotation is due to the beam rotation, while the column web panel and the connection bring very small contributions.

Table 3.5: ES2-TS-F-C2 test result.

Joint		ES2-TS-F-C2	
Design Criteria		Full strength	
Elastic Stiffness		45077.1	[kNm]
0.8 M_{pl}		604.14	[kNm]
$M_{j,Rd}$	4%	846.41	[kNm]
	-4%	-876.86	[kNm]
	Max (5%)	859.5691	[kNm]
	Min (-4%)	-876.86	[kNm]
Dissipated energy	4%	318	[kNm]
	5%	529	[-]
	6%	740	[-]
	7%	934	[-]

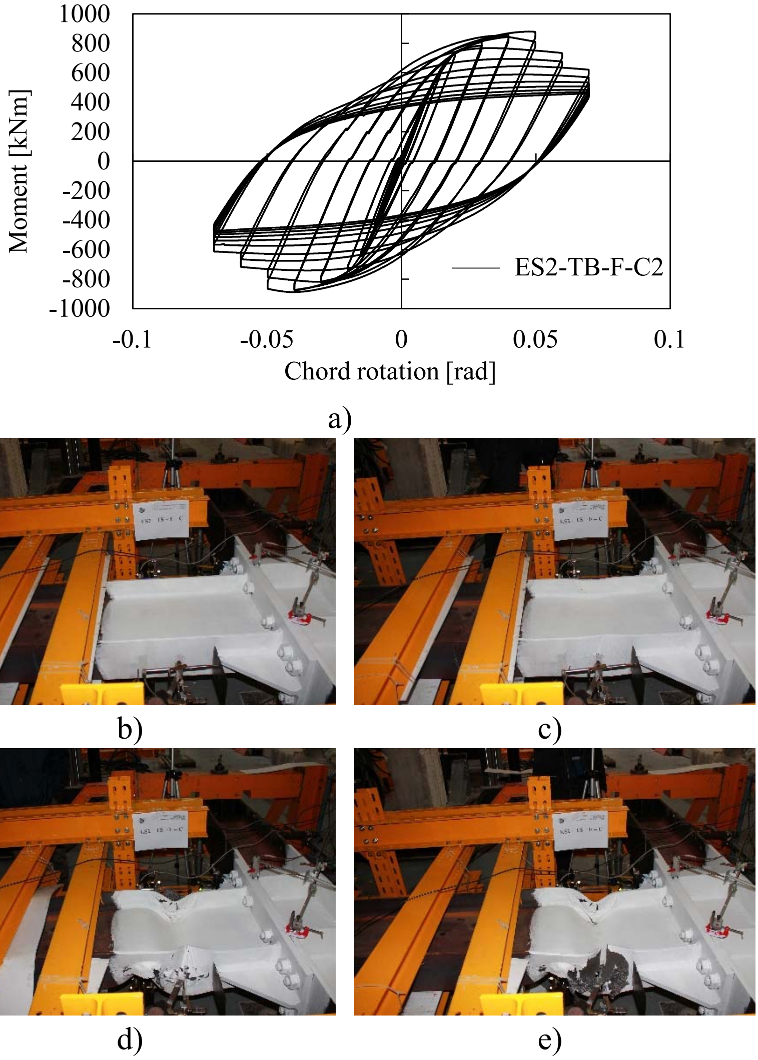

a)

b)

c)

d)

e)

Figure 3-34: Moment chord rotation (a), joint configuration: initial (b), at 2% (c), at 4% (d) and at 6% (e) of chord rotation.

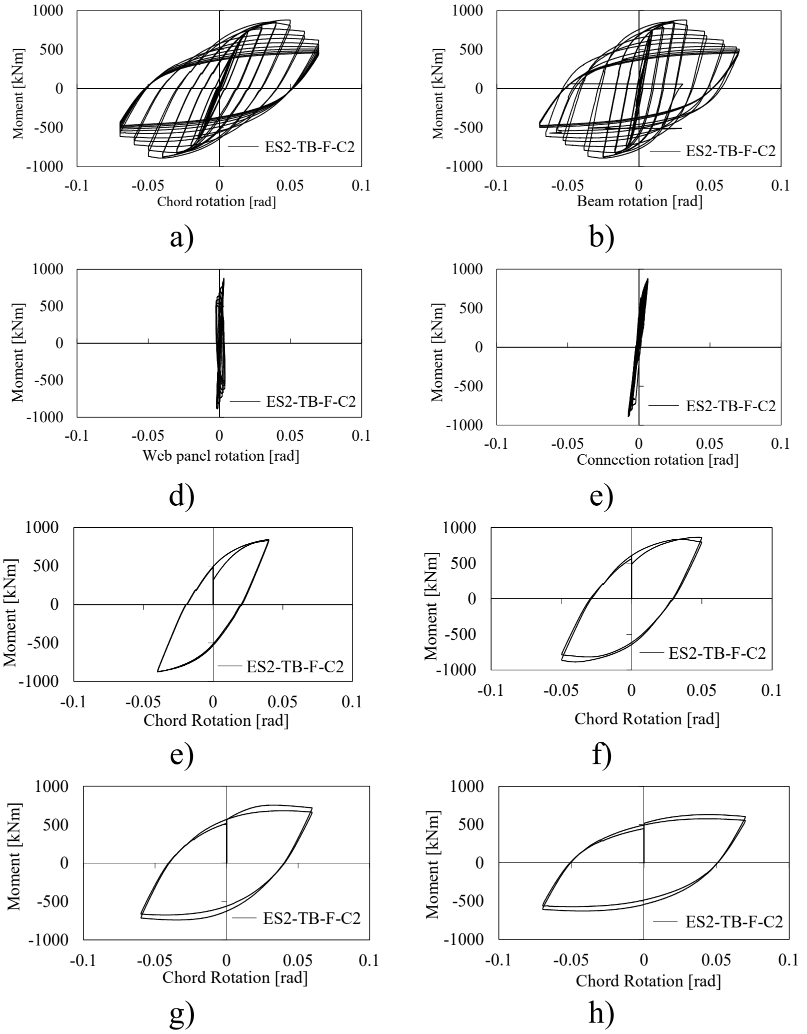

Figure 3-35: Moment chord rotation (a, e, f, g and h), beam rotation (b), column web panel rotation (c) and connection rotation (d).

The dissipated energy, both in terms of moment rotation cycles and in terms of the ratio between the cumulated energy at 7% and at 4% rotation (see Figure 3-36), confirm that this joint dissipates less energy with respect to the one tested considering the EJ loading protocol.

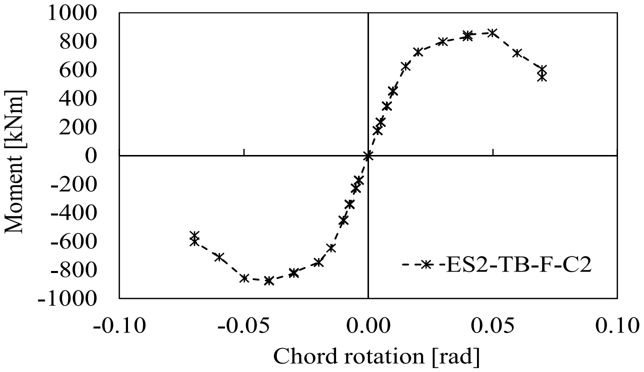

a)

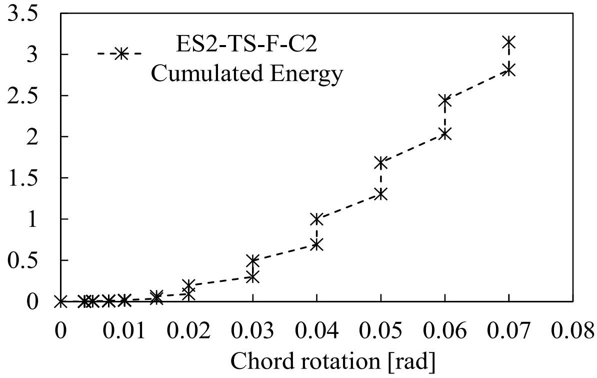

b)

Figure 3-36: Experimental test backbone curve (a) and cumulated energy respect to the 4% rotation.

3.5.1 Calibration

The FE calibration was done on the same model used in the previous paragraph, changing the material characteristics and the loading protocol assigned.

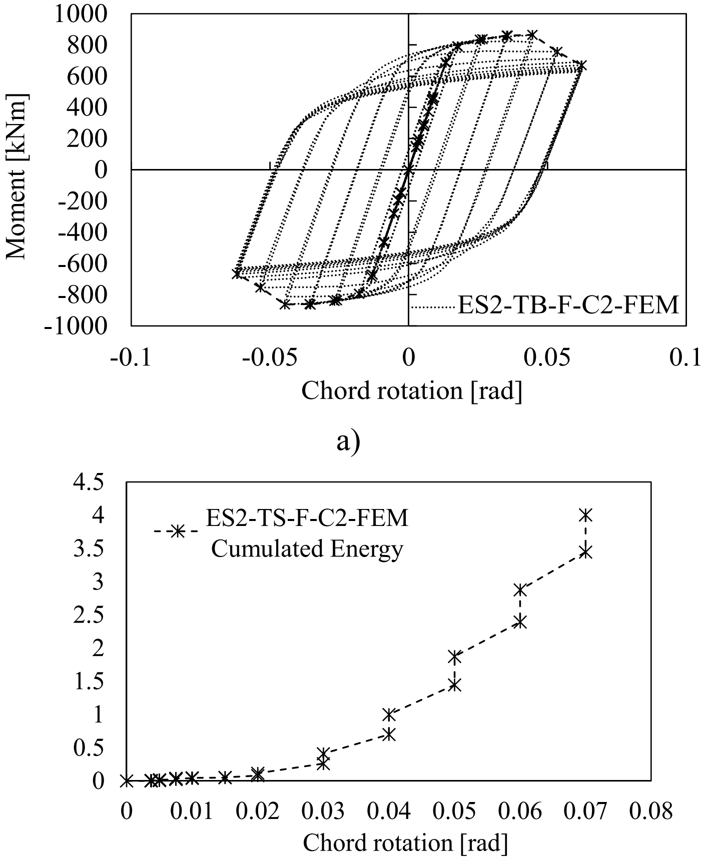

a)

b)

Figure 3-37: FEM: (a) Moment rotation curve and (b) cumulated energy respect to the 4% rotation.

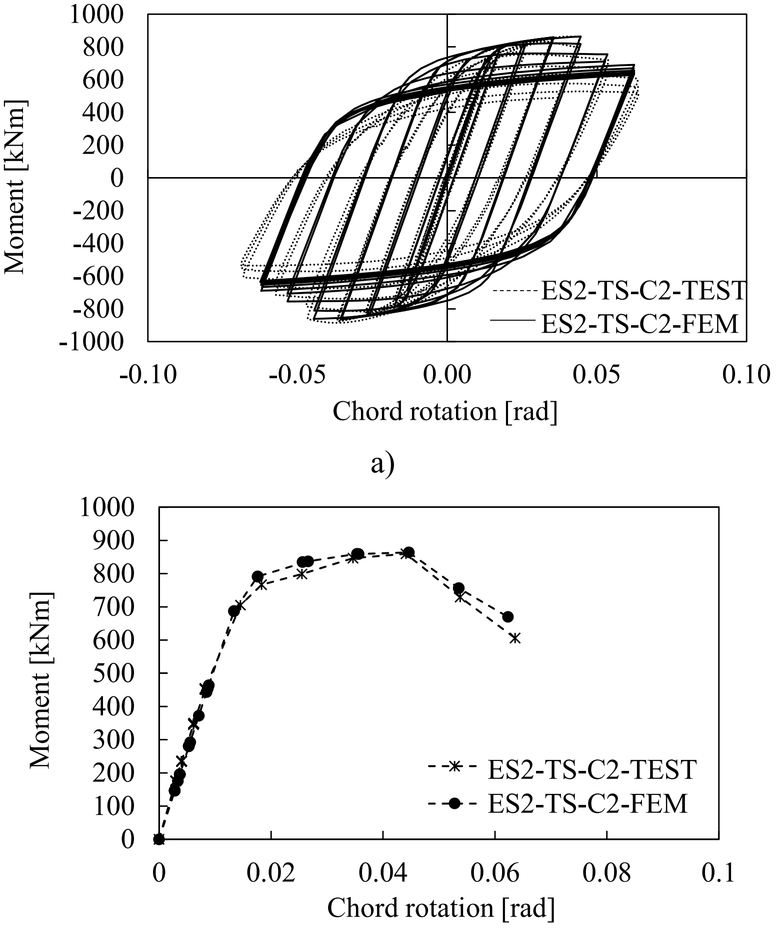

a)

b)

Figure 3-38: Experimental result against the FEM prevision both in terms of cyclic (a) and Back bone curve (b).

Owing to the different material characteristics, the cumulated energy dissipated by the model is smaller with respect to the same model presented in the previous chapter.

The backbone curve comparison (see Figure 3-38 *b*) shows a good agreement between the FEA and the test both in terms of elastic stiffness and resistance; while some differences can be underlined from the complete cyclic curve comparison (see Figure 3-38 *a*). Indeed, in this case, the numerical model is not able to perfectly reproduce the test stiffness degradation, which influences the cumulative energy dissipated. Therefore, some differences can be observed by comparing the cumulated energy measured for the test and the FE model, respectively (see Figure 3-38 *a* and Figure 3-37 *b*).

Furthermore, the failure mode and the plastic strain distribution on the experimental specimen (see Figure 3-39) is well calibrated by the PEEQ distribution. Indeed, even the plastic engagement of the ribs is well interpreted by the yielding line distribution on area of the welds between the beam and the ribs.

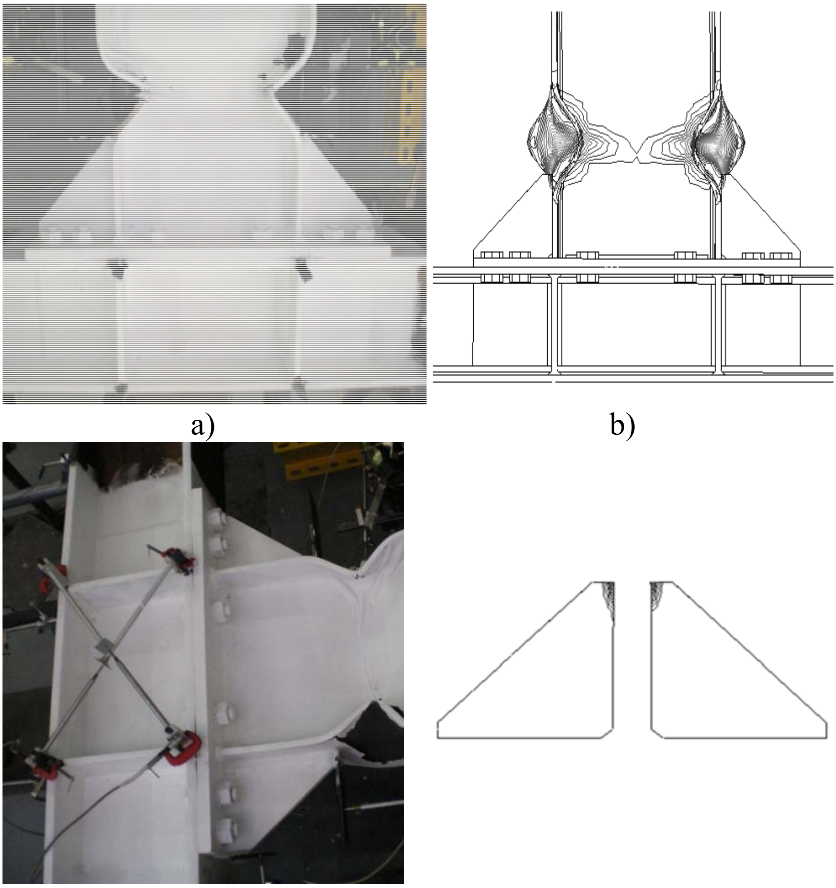

a) b)

c) d)

Figure 3-39: Failure mode: Experimental (a and c) against FEA PEEQ distribution (b and d).

3.6 ES2–TS–E–C1

ES2–TS–E–C1 is a cyclic test of the ES2 beam to column assembly (beam IPE450 and column HEB340), considering the AISC341 [3] loading protocol.

The joint is designed as equal strength, having the expected plastic deformation evenly distributed between the connection and the beam. The experimental results show that the joint bending capacity increases up to 7% rotation (see Figure 3-40 *a*) value beyond which fracture occurs in the beam flange (as also confirmed by Table 3.6). Contrary to what was observed in the case of full strength joints, no beam flange buckling occurred. This is confirmed as well by the moment rotation curve, where a clear stiffness decrease is not visible.

Table 3.6: ES2-TS-E-C1.

Joint		ES2-TS-E-C1	
Design Criteria		Equal strength	
Elastic Stiffenes		37067	[kNm]
0.8 M_{pl}		604.14	[kNm]
$M_{j,Rd}$	4%	812.12	[kNm]
	-4%	-857.96	[kNm]
	Max (7%)	897.192	[kNm]
	Min (-6%)	-914.67	[kNm]
Dissipated energy	4%	156	[kNm]
	5%	284	[-]
	6%	459	[-]
	7%	103	[-]

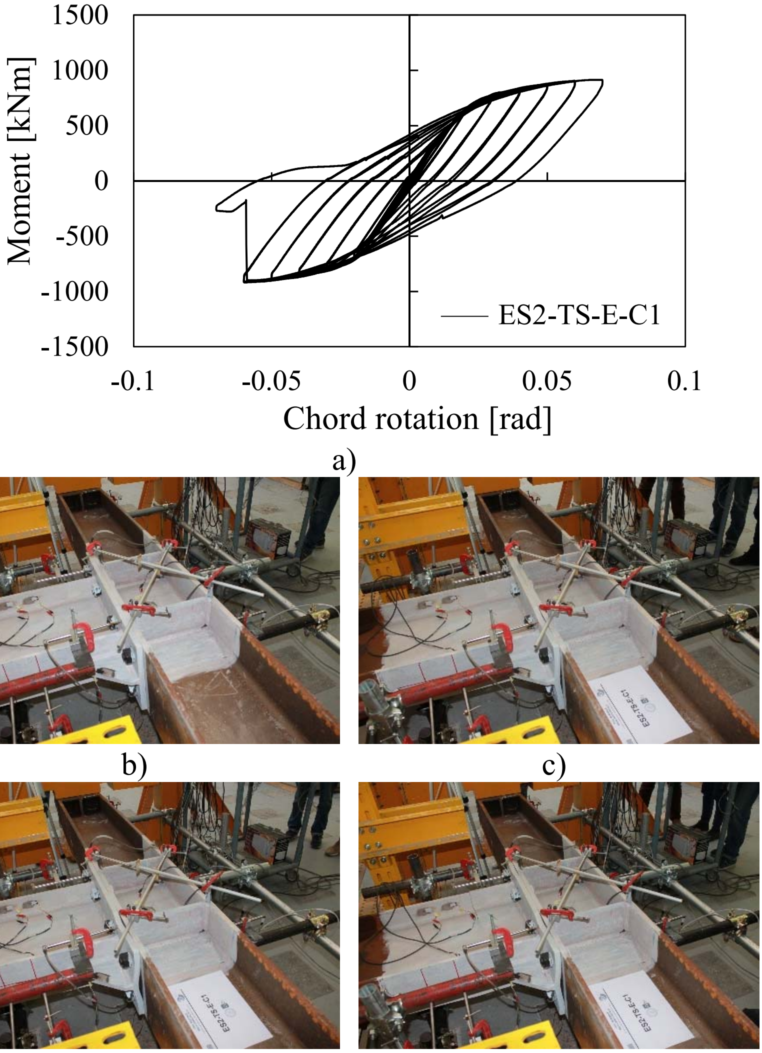

a)

b)

c)

d)

e)

Figure 3-40: Moment chord rotation (a), joint configuration: initial (b), at 2% (c), at 4% (d) and at 6% (e) of chord rotation.

On a global level, observing the joint test evolution up to a rotation of 6% (see Figure 3-40 from *b* to *e*) the activation of the equivalent T-stub in tension and the plastic demand concentrated in the plate are visible. Afterwards, a small plastic deformation is observed in the beam in the first cycle at 7% when the fracture occurs without the development of local buckling of the flanges.

Looking more into detail, the large engagement of the connection is apparent from the macro-component rotation contribution (see Figure 3-41 *b*, *c* and *d*). The gap opening caused by the plate's plastic deformation contributes to the global joint rotation reducing the rotational demand on the beam, perfectly in agreement with the hypothesis introduced in the design phase. Nevertheless, the column has a very small rotational contribution (see Figure 3-41 *c*) given that the joint was designed assuming a strong column web panel.

As seen for ES1-TS-E-C1, also in this case the joint shows a high level of inherent ductility, being able to reach up to 7% of rotation without significant decrease of stiffness.

Looking at the area described by independent cycles at 4%, 5%, 6% and 7% of rotation (see Figure 3-41 from *e* to *h*), which is a measure of the energy dissipated, an increasing trend can be observed for increasing values of chord rotation (see Table 3.6).

Further evaluations of the cumulated dissipated energy of the joint shows an ultimate value of four times the energy dissipated at 4% of rotation.

As opposed to the full strength joint, in this case, all the plastic demand is concentrated in the connection therefore, the joint ductility depends on the failure mode of the equivalent T-stub in the tension side. In Figure 3-40 *c*, *d* and *e* a failure mode 2, close to mode 1 can be distinguished, with most of the plastic deformation concentrated in the plate and limited plastic deformation in the bolts.

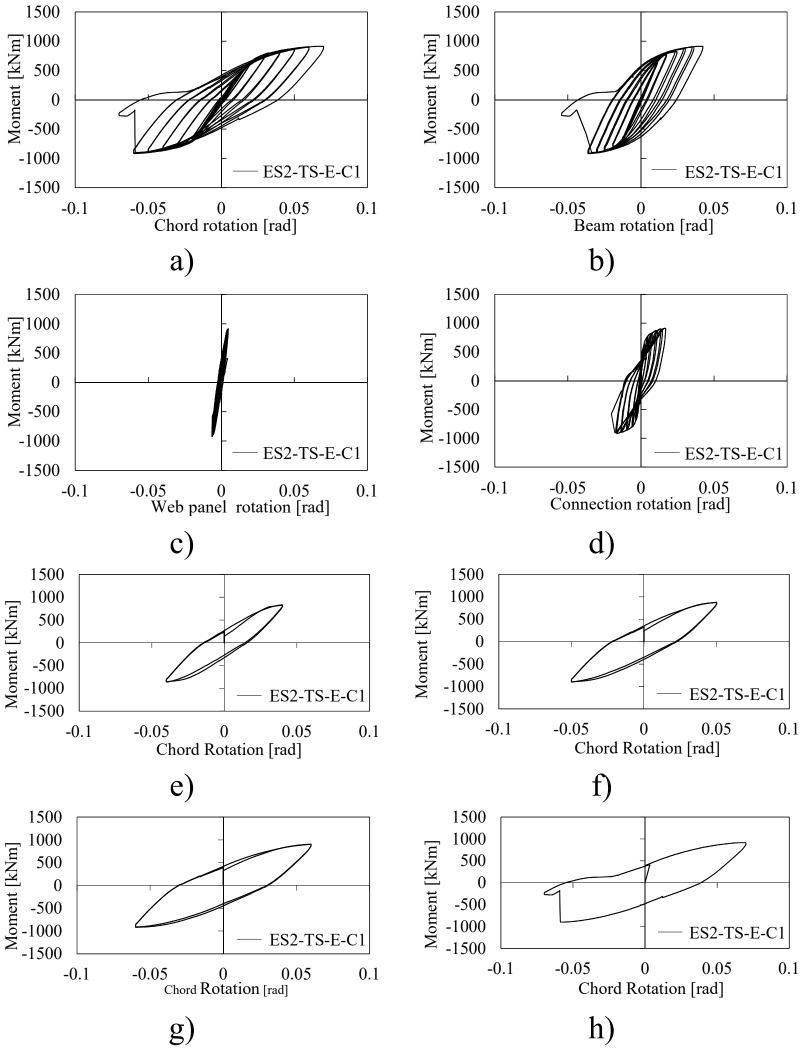

Figure 3-41: Moment chord rotation (a, e, f, g and h), beam rotation (b), column web panel rotation (c) and connection rotation (d).

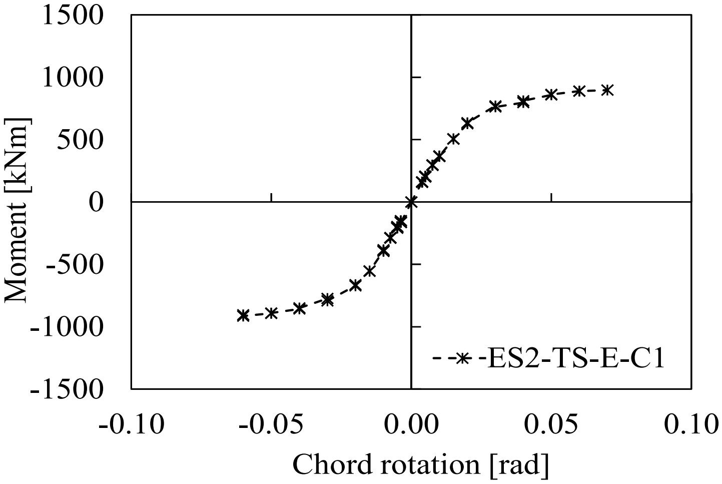

a)

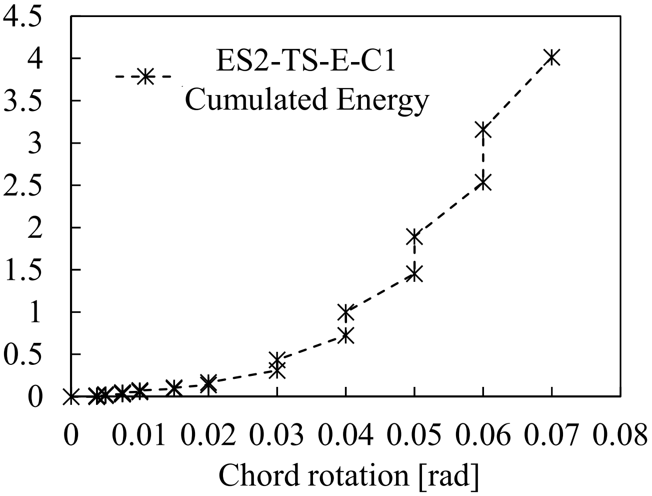

b)

Figure 3-42: Experimental test backbone curve (a) and cumulated energy respect to the 4% rotation.

3.6.1 Calibration

The results of FEM calibration of the ES2–TS–E–C1 (see Figure 3-43, Figure 3-44 and Figure 3-45) show a very good agreement between the test and the numerical prevision.

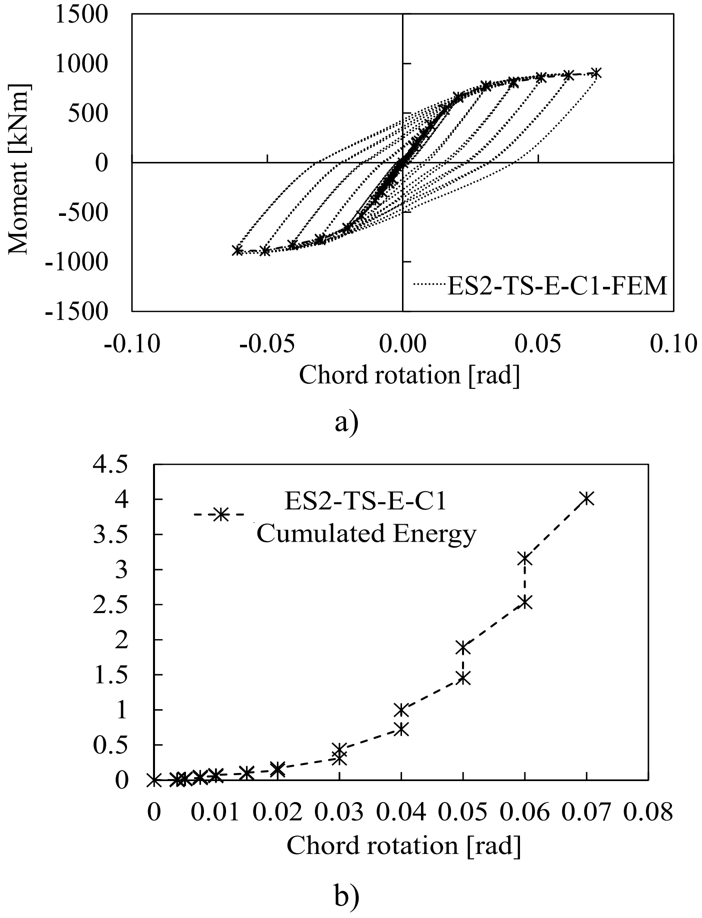

Figure 3-43: FEM: (a) Moment rotation curve and (b) cumulated energy respect to the 4% rotation.

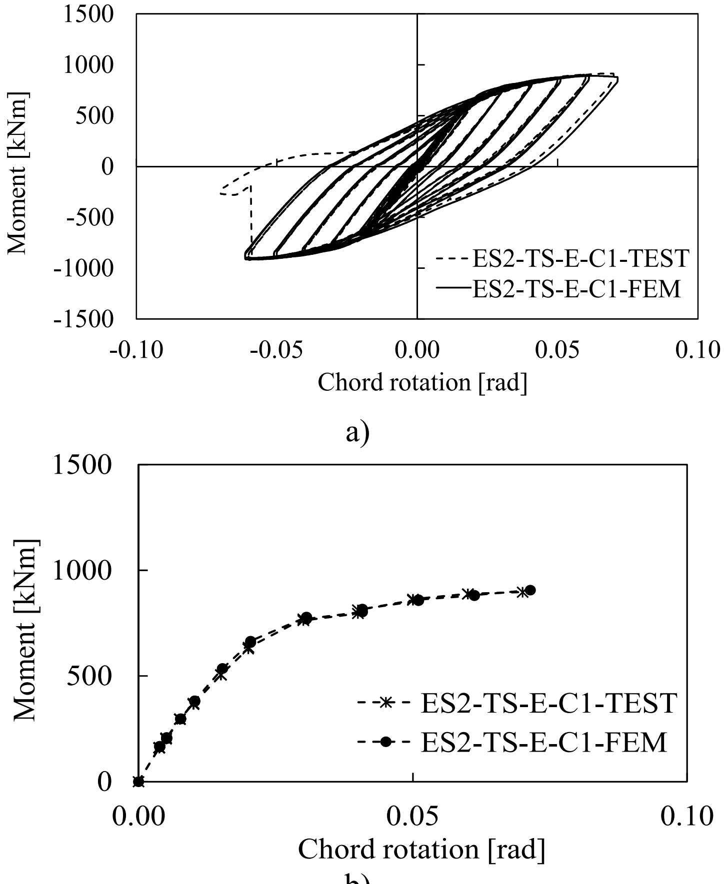

a)

b)

Figure 3-44: Experimental result against the FEM prevision both in terms of cyclic (a) and Back bone curve (b).

The type of the failure observed, differently from the ES1–TS–E–C1, does not include the beam flange with a consequent easier calibration procedure that does not need the beam geometrical imperfection modelling.

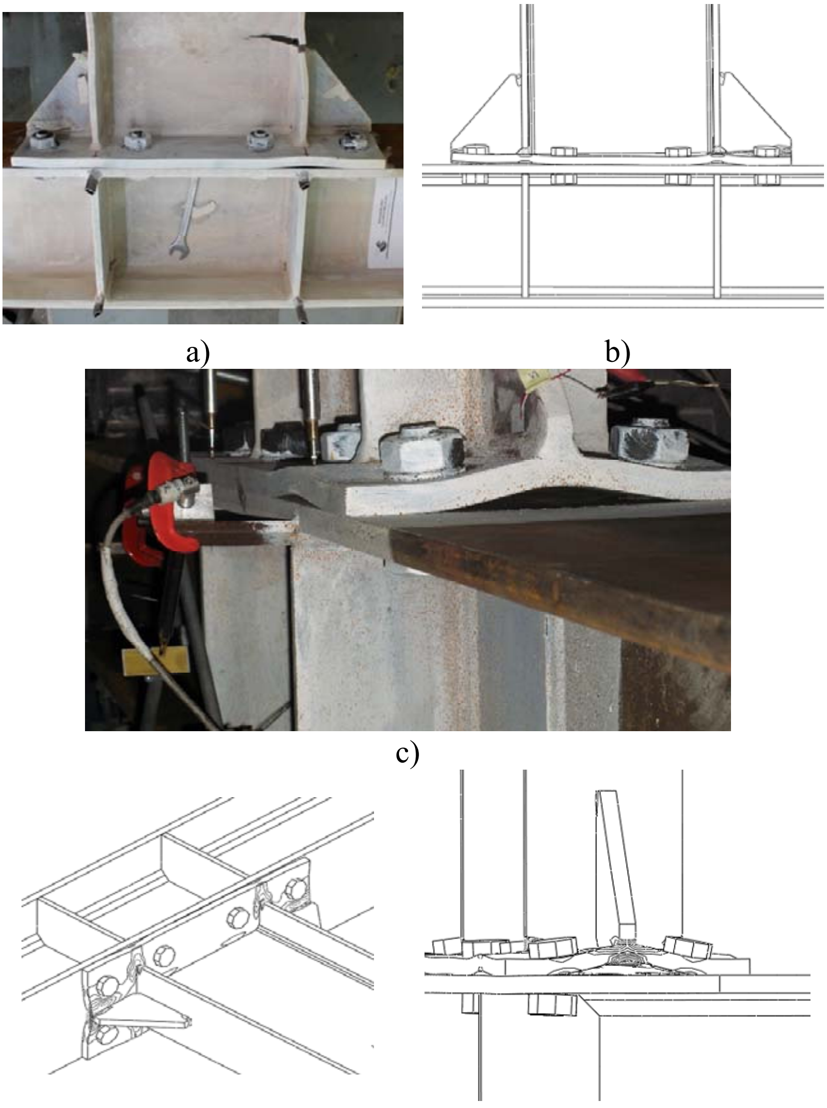

a) b)

c)

d) e)

Figure 3-45: Failure mode: Experimental (a and c) against FEM PEEQ distribution (b, d and e).

3.6.2 Strain gauge

The results of the strain-gauge on the column side confirm that the web panel is in elastic range, even though small plastic deformation can be observed in the device lecture and from the FE analysis (see Figure 3-46).

The device placed on the rib base reads no plastic deformation, but the result is biased given its position (see Figure 3-47). Plastic deformation are, however, measured on the rib diagonal where, due to the activation of the equivalent T-stub in tension, large stress concentrations occurred during the test.

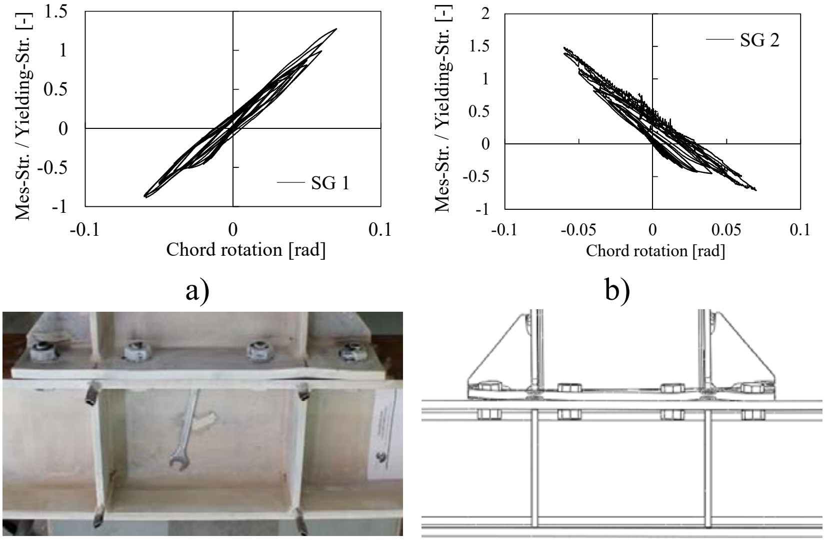

a) b)

c) d)

Figure 3-46: Plastic deformation on the column web panel: a and b) strain-gauge lecture, c) experimental test, d) FEM PEEQ distribution.

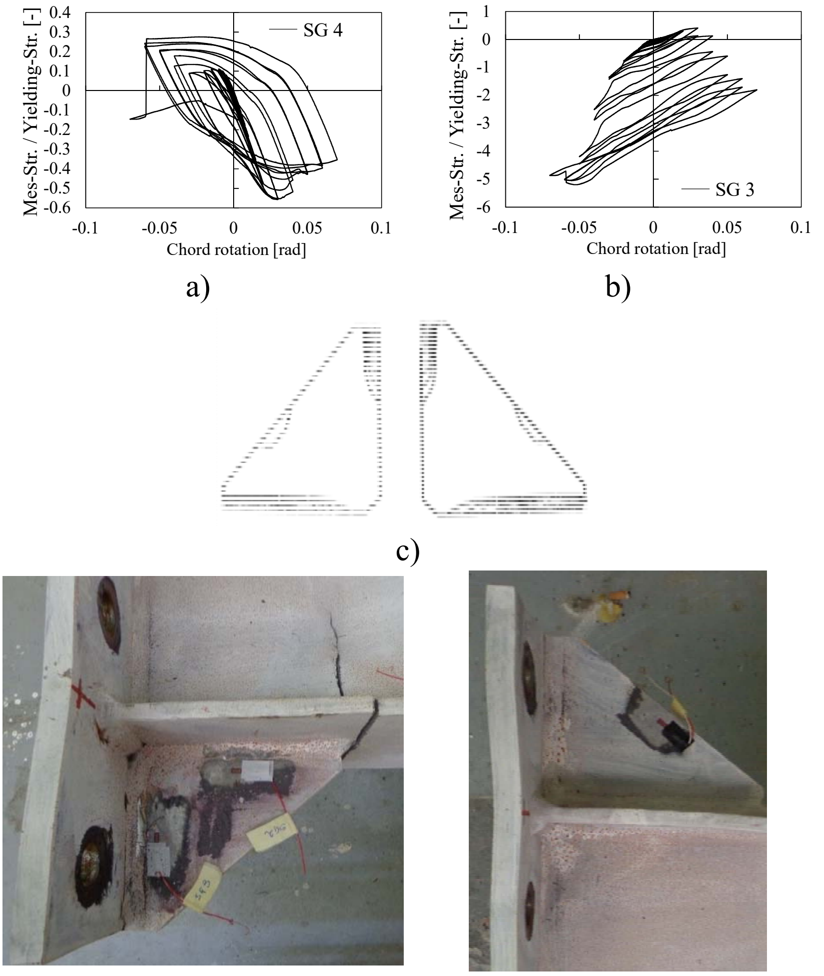

a)
b)
c)
d)
e)

Figure 3-47: Rib strain gauges results: normalized strain versus chord rotation (a and b), PEEQ distribution on the FE model (c) and plastic deformation of the tested specimen (d and e).

3.7 ES2–TS–ESP–C

A specimen geometrically identical with the previous, ES2–TS–Esp–C1 with the singular difference i.e. the welding technology used. The specimen has been tested in order to investigate the influence of the shot pinning technique used for the welding.

The test results (see Table 3.7) in terms of: i) elastic stiffness, ii) joint resistance and iii) failure mode are close to the ones obtained in the previous test (ES2-TS-E-C1). The shot-pinning indeed does not bring any improvement to the joint behavior. However, a minimal difference can be pointed out: the test shows that the joint performs half cycle more (see Figure 3-48) respect to the ES2-TS-E-C1 and therefore the fracture develops on the opposite flange.

Table 3.7: ES2-TS-ESP-C test results.

Joint		ES2-TS-E-C1	
Design Criteria		Equal strength	
Elastic Stiffenes		38189	[kNm]
0.8 M_{pl}		604.14	[kNm]
$M_{j,Rd}$	4%	817.09	[kNm]
	-4%	-861.7	[kNm]
	Max (6%)	882.096	[kNm]
	Min (-6%)	-908.62	[kNm]
Dissipated energy	4%	159	[kNm]
	5%	290	[-]
	6%	470	[-]
	7%	443	[-]

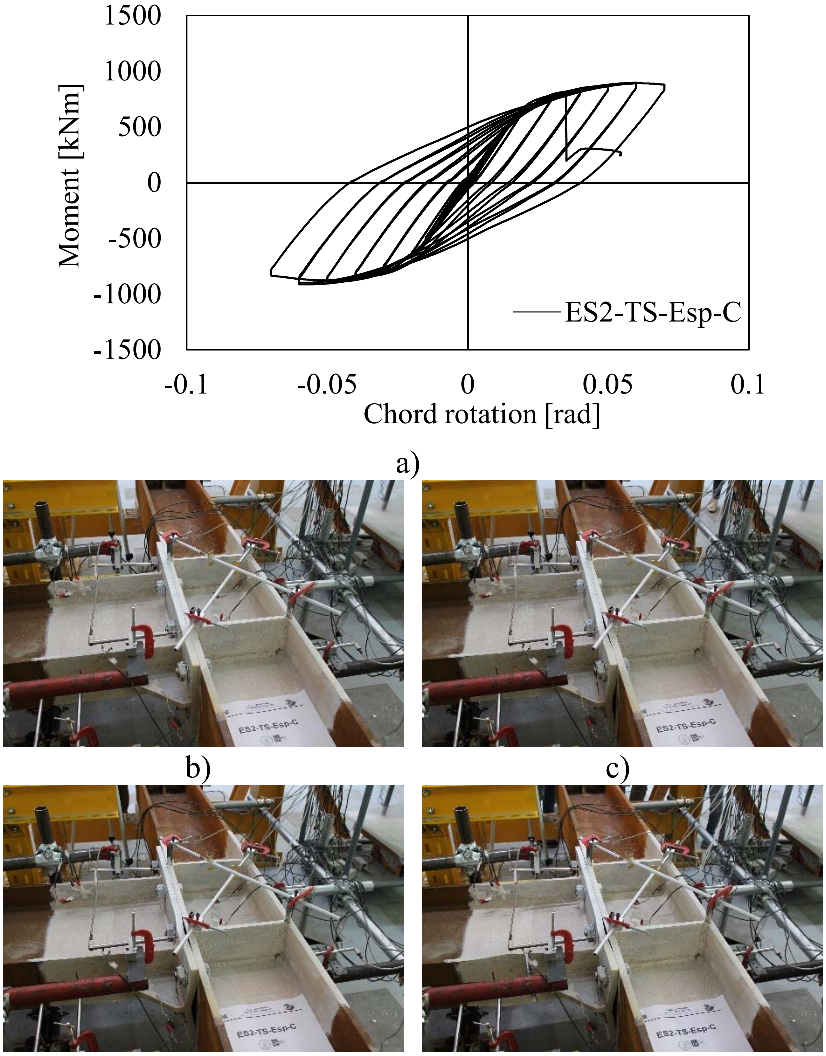

a)

b) c)

d) e)

Figure 3-48: Moment chord rotation (a), joint configuration: initial (b), at 2% (c), at 4% (d) and at 6% (e) of chord rotation.

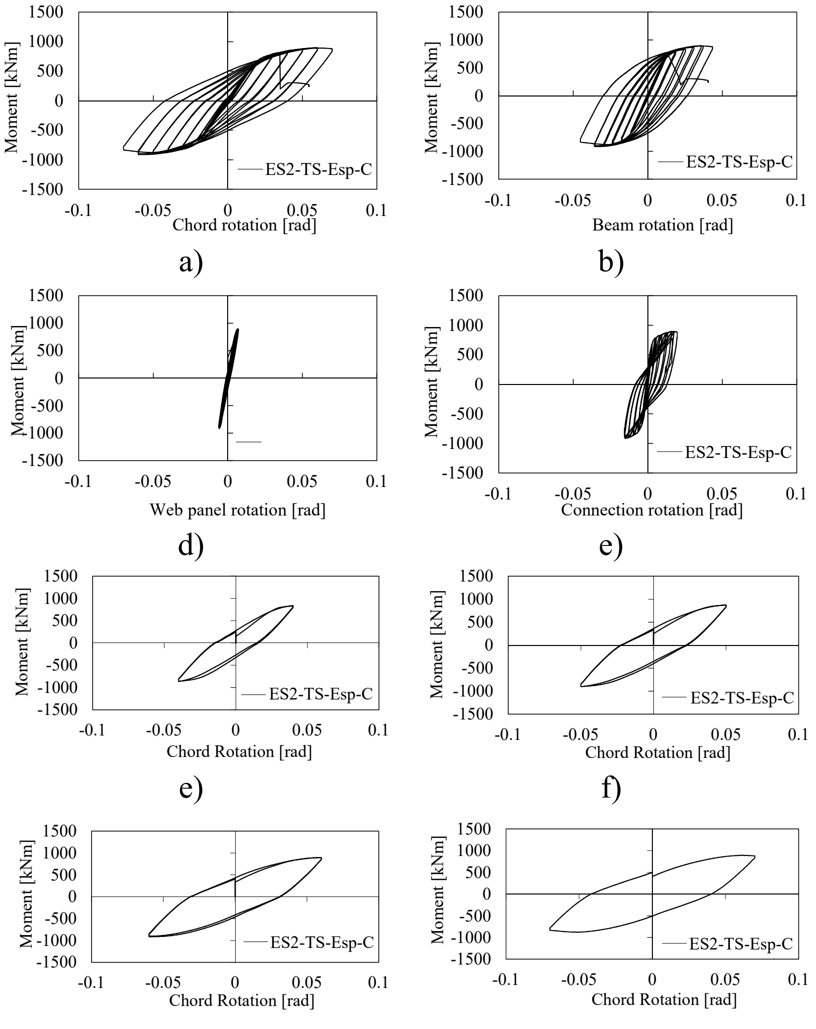

a) b)

d) e)

e) f)

g) h)

Figure 3-49: Moment chord rotation (a, e, f, g and h), beam rotation (b), column web panel rotation (c) and connection rotation (d).

All the other results: macro-component rotational contribution (see Figure 3-49 *a, b, c* and *d*), dissipated and cumulated energy (see Table 3.7 and Figure 3-50 *b*) are similar to the ones discussed for the previous test, with insignificant differences.

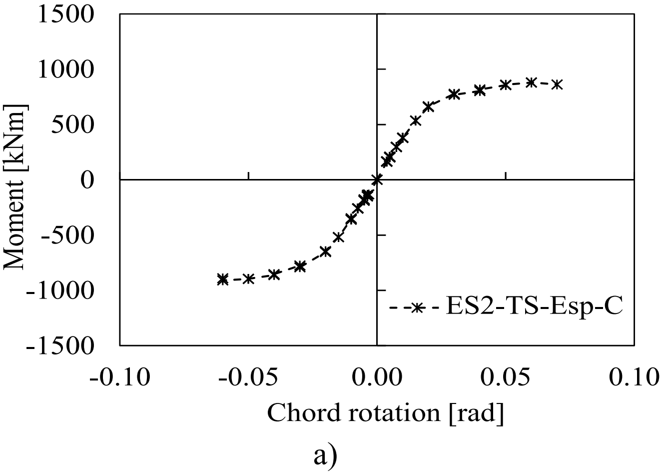

a)

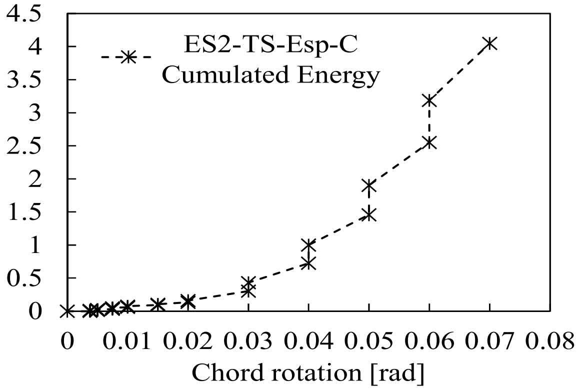

b)

Figure 3-50: Experimental test backbone curve (a) and cumulated energy respect to the 4% rotation.

3.7.1 Calibration

Since not appreciable differences can be pointed out with respect to the ES2–TS–E–C1, the same FE model was used for the calibration.

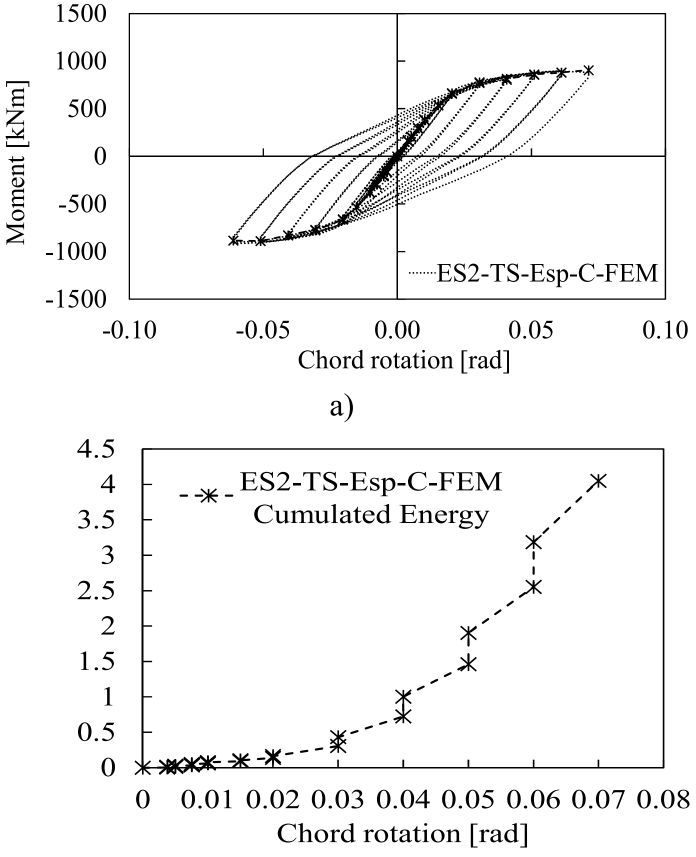

a)

b)

Figure 3-51: FEM: (a) Moment rotation curve and (b) cumulated energy respect to the 4% rotation.

In line with the results showed in the previous paragraph, also in this case a very good agreement, between the test and the numerical prevision, can be pointed out (see Figure 3-51, Figure 3-52 and Figure 3-53).

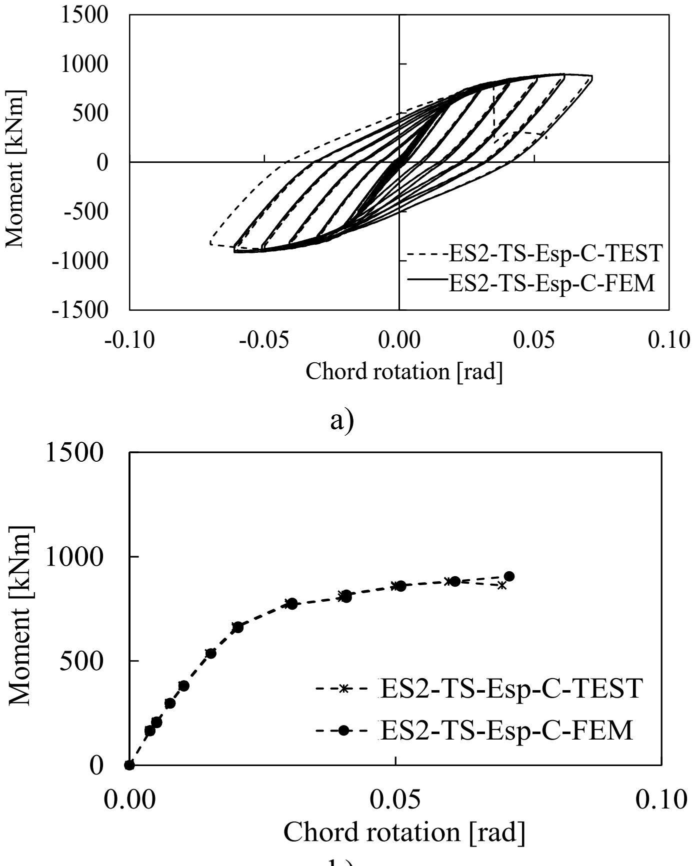

a)

b)

Figure 3-52: Experimental result against the FEM prevision both in terms of cyclic (a) and Back bone curve (b).

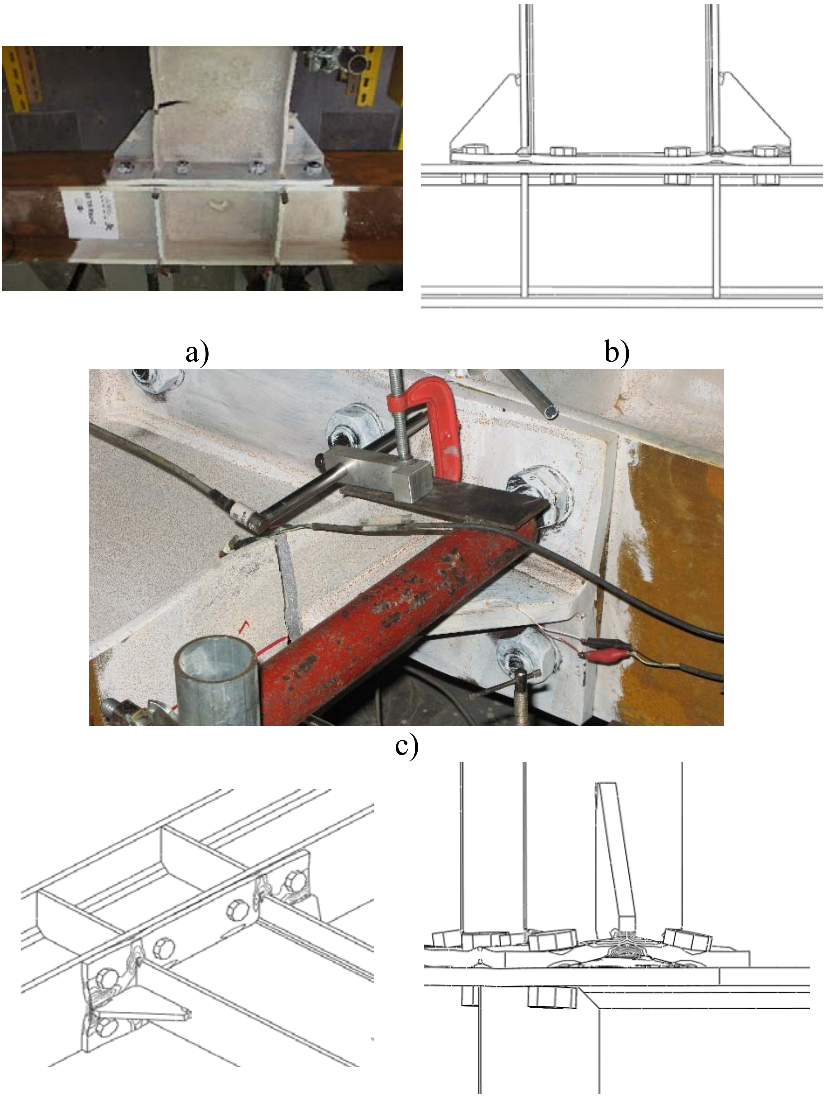

a) b)

c)

d) e)

Figure 3-53: Failure mode: Experimental (a and c) against FEM PEEQ distribution (b, d and e).

3.7.2 Strain gauge

As observed until now, also the strain-gauge measurements are perfectly in line with the results showed in the previous paragraph (ES2-TS-E-C1). Indeed, also for this test, no significant plastic deformation are showed in the column web panel (see Figure 3-54) and on the rib base and height (see Figure 3-55). On the other hand, due to the activation of the T-stub in tension local plastic deformation are registered on the ribs diagonal (see Figure 3-55).

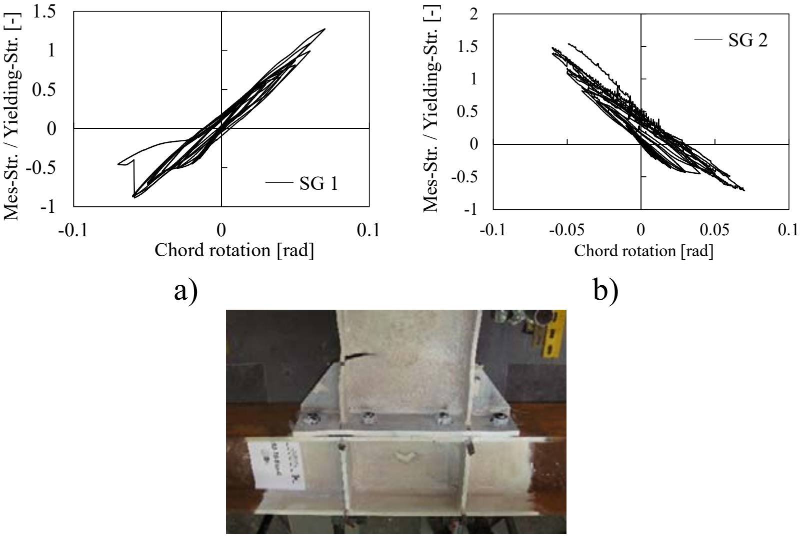

a) b)

c)

Figure 3-54: Column web panel plastic deformation: strain-gauge lecture (a and b), and experimental test observation (c).

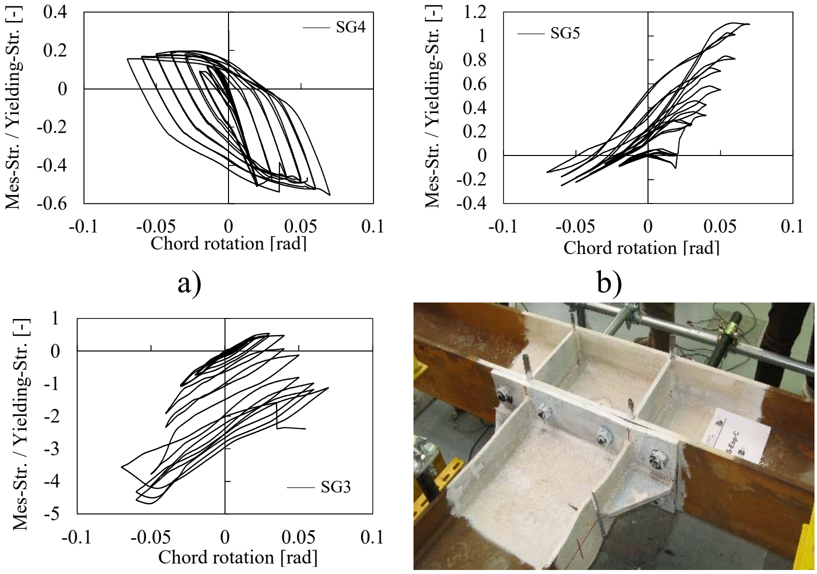

a) b)

c) d)

Figure 3-55: Rib strain gauges results: normalized strain versus chord rotation (a, b and c), and plastic deformation of the tested specimen (d).

The showed results also confirm the scientific repetitiveness, confirming once again the height performance, in terms of both resistance and ductility, of the equal strength joint.

3.8 ES3–TS–F–C1

ES3–TS–F–C1 is a cyclic test on the larger beam-to-column assembly (an IPE600 beam and a HEB500 column). The joint is designed as full strength and the AISC341 [3] loading protocol was applied. As all the ES3 assemblies, this joint was designed at the University of Naples, but the test was performed at University of Liege. The joint behaves as a full strength one, developing a stable hysteretic moment-rotation curve (see Figure 3-56 *a*) and reaching a bending capacity greater than the plastic resistance of the connected beam, thus directing the formation of the plastic hinge at its extremities (see Table 3.8 and Figure 3-56 *b* and *c*). A reduction of the bending capacity due to the beam geometrical imperfections is visible in the cyclic response curve.

Table 3.8: ES3-TS-F-C1 test results.

Joint		ES3-TS-F-C1	
Design Criteria		Full strength	
Elastic Stiffens		263848	[kNm]
0.8 M_{pl}		1246.9	[kNm]
$M_{j,Rd}$	4%	1956.61	[kNm]
	-4%	-1667.78	[kNm]
	Max (3%)	2202.2943	[kNm]
	Min (-2%)	-2065.4	[kNm]
Dissipated energy	4%	998	[kNm]
	5%	-	[-]
	6%	-	[-]
	7%	-	[-]

Differently from the tested joints previously presented, this test was stopped when the first micro-fracture appeared in the welds at the beam-rib interface.

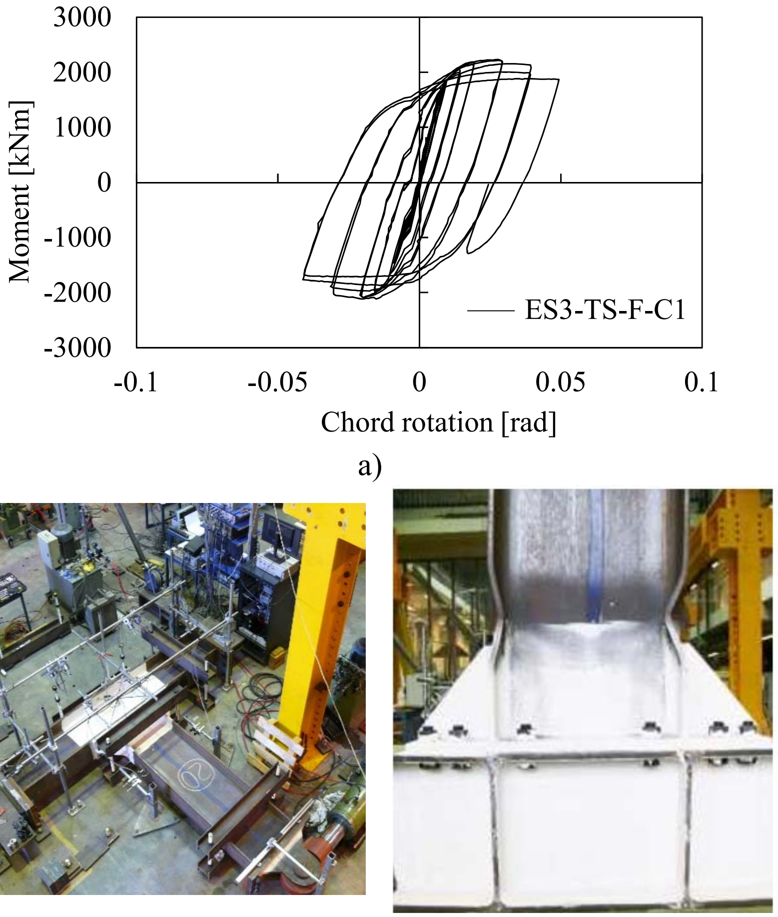

a)

b) c)

Figure 3-56: Moment chord rotation (a) and joint failure mode (b and c).

In spite of the interruption, the joint arrived up to a rotation of 4% and had a reduction in terms of resistance of less than 20% of the beam plastic capacity hence, in line with the AISC341-10 [3] prescriptions the joint can be considered pre-qualified.

More detailed, on a macro-component level, the contribution of the column web panel and connection in the total value of chord rotation is very small (see Figure 3-57 *c* and *d*) in agreement with what was observed until now in the full strength joints.

The dissipated energy was evaluated as well for this specimen (see Figure 3-57 and Figure 3-58). However, due to the test interruption, just the two cycles at 4% of rotation were plotted (see Figure 3-57 *e*).

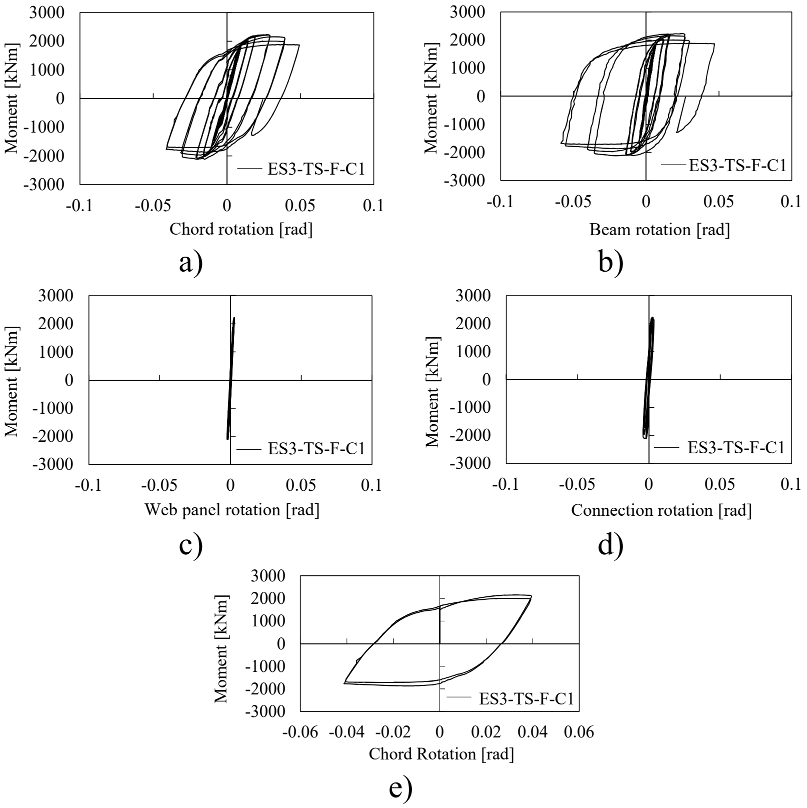

Figure 3-57: Moment chord rotation (a and e), beam rotation (b), column web panel rotation (c) and connection rotation (d).

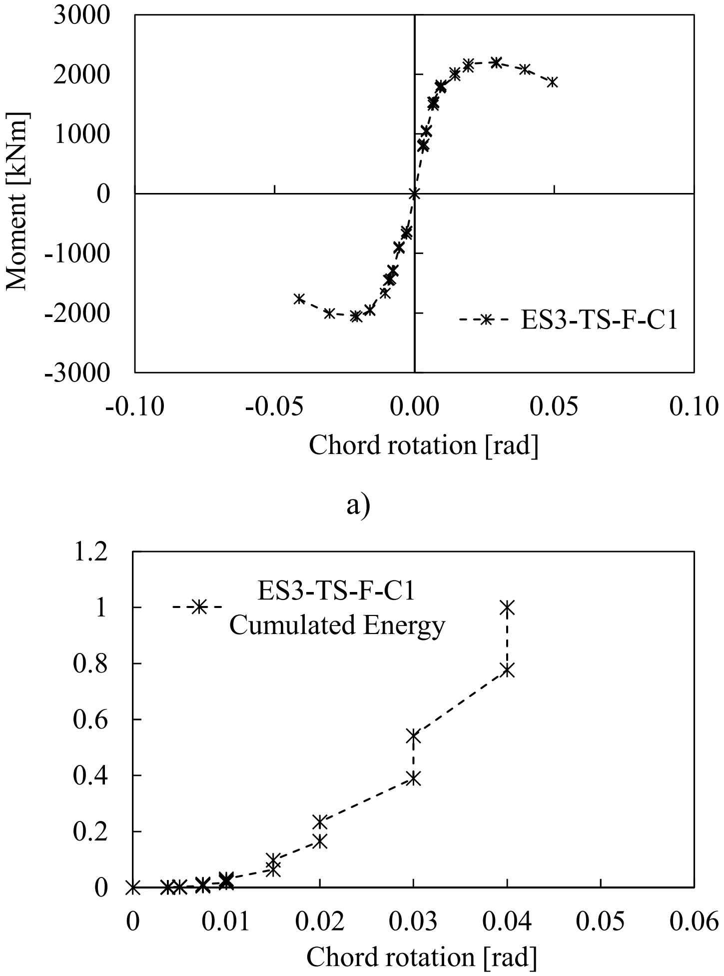

a)

b)

Figure 3-58: Experimental test backbone curve (a) and cumulated energy respect to the 4% rotation.

3.8.1 Calibration

The same modelling assumptions detailed in the previous chapter were applied for the ES3 joint, with the necessary model geometry adjustments (length of beam and column and torsional restrains position) in order to accommodate the different set up configuration used at University of Liege. Moreover, the loading protocol (displacement history) was extracted directly from the test since the different position of the displacement application point and the control point.

The FE model can perfectly replicate the joint response in terms of elastic stiffness and resistance as it can be observed from the overlapping of the backbone curves (see Figure 3-60 *b*). Furthermore, the strength degradation and the pinching effects are well reproduced by the FE software (see Figure 3-60 *a*). Likewise, the cumulated energy diagram (see Figure 3-59 *b*) shows good agreement with the experimental test (see Figure 3-58 *b*). In order to be compliant with the experimental test, the FE analysis was stopped at the end of the second 5% rotation cycle. For this reason, as it can be observed also from the moment rotation curve (see Figure 3-60 *a*), the numerical results show one and half cycle more with respect to the experimental curve.

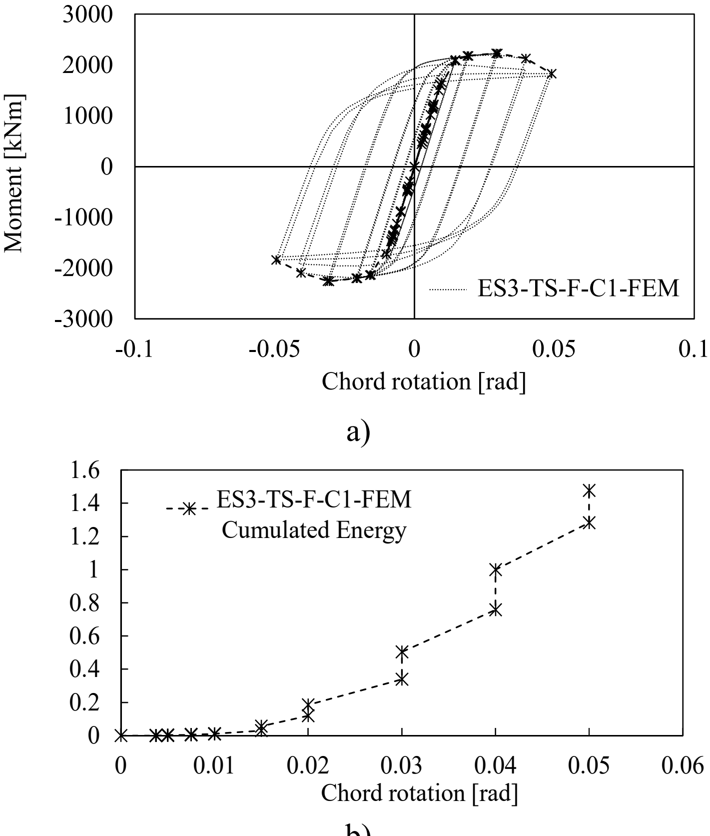

a)

b)

Figure 3-59: FEM: (a) Moment rotation curve and (b) cumulated energy respect to the 4% rotation.

The yield line distribution on the beam flange is in perfect agreement with the plastic deformation observed during the experimental test. The observation remains valid also for the ribs, with particular regard to the micro fractures observed at the level of the welds between the beam and the rib that correspond to the large concentration of PEEQ in the FE model (see Figure 3-61).

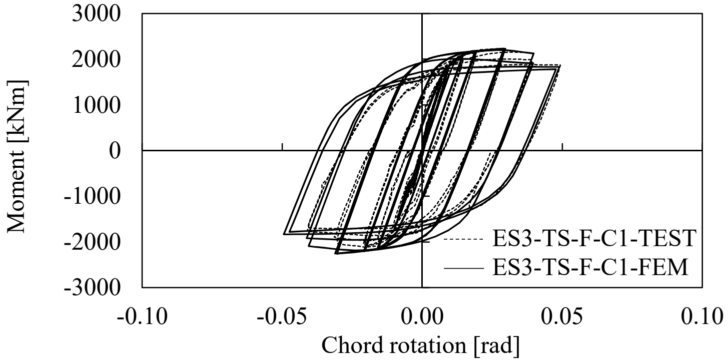

a)

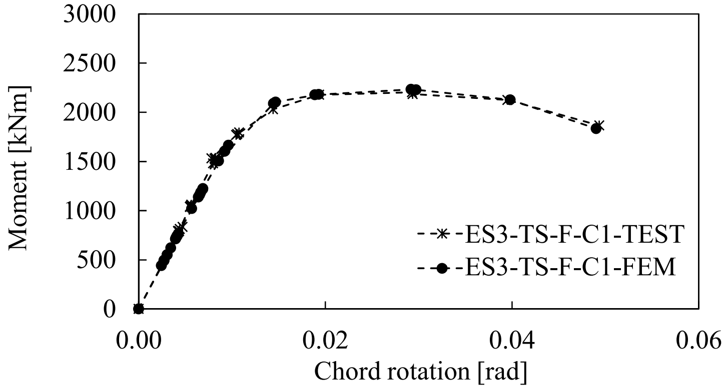

b)

Figure 3-60: Experimental result against the FEM prevision both in terms of cyclic (a) and Back bone curve (b).

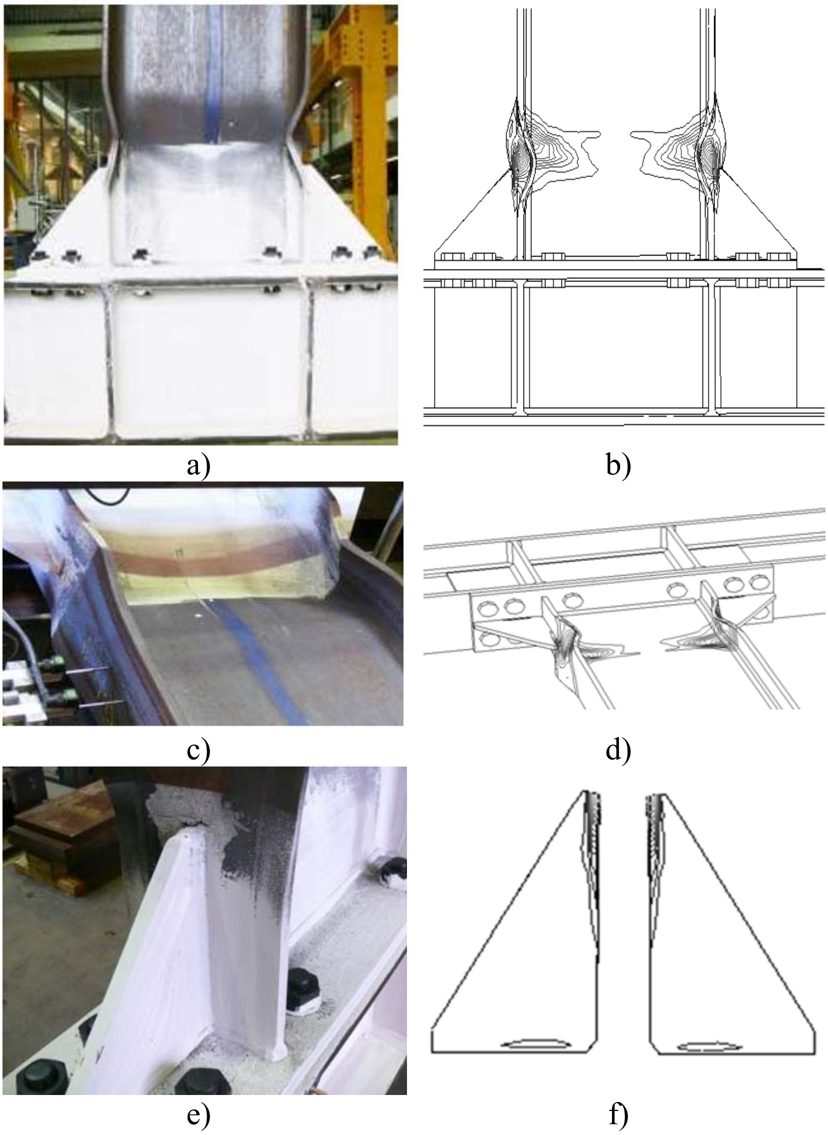
a) b)

c) d)

e) f)

Figure 3-61: Failure mode: Experimental (a, c and e) against FEM PEEQ distribution (b, d and f).

3.9 ES3–TS–F–C2

ES3–TS–F–C2 represents a cyclic test on the same joint tested in the previous paragraph without changing neither the geometry nor the loading protocol applied, in order to investigate the scientific redundancy. Moreover, also this test was stopped around 4% of rotation due to micro-fractures observed on the beam-rib welds (see Figure 3-67). The joint has a typical full strength behavior, with the formation of the plastic hinge in the beam (see Figure 3-62), leaving the other components elastically, as it can be observed from the rotational contributions of each macro component (see Figure 3-63).

Some differences can be pointed out in terms of elastic stiffness; indeed as reported in Table 3.9 there is a large differences with the results observed in the previous tests (ES3-TS-F-C1).

Table 3.9: ES3-TS-F-C2 test results.

Joint		ES3-TS-F-C2	
Design Criteria		Full strength	
Elastic Stiffens		148856	[kNm]
0.8 M_{pl}		1246.9	[kNm]
$M_{j,Rd}$	4%	1878.35	[kNm]
	-4%	-1381.22	[kNm]
	Max (3%)	2163.6648	[kNm]
	Min (-3%)	-2105.1	[kNm]
Dissipated energy	4%	800	[kNm]
	5%	-	[-]
	6%	-	[-]
	7%	-	[-]

In particular, it can be observed a decrease of stiffness from 263848 to 148856kNm. This large difference between the tests is due to some problem occurs after the first test on the experimental setup.

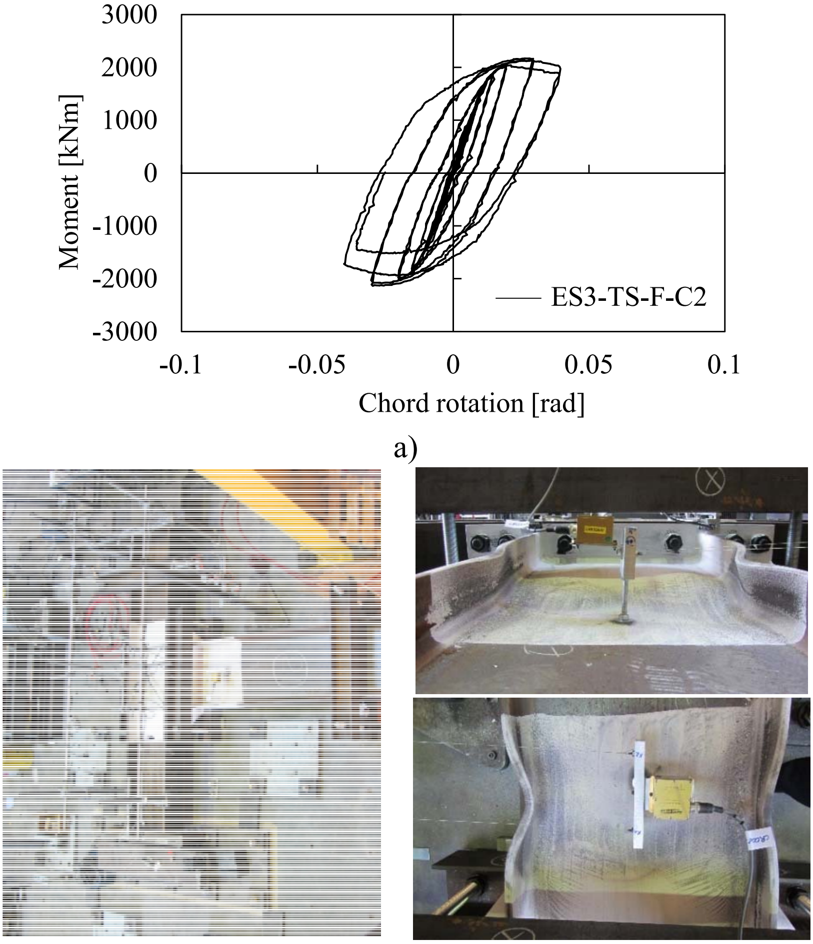

a)

b) c)

Figure 3-62: Moment chord rotation (a) and joint failure mode (b and c).

The differences of the elastic stiffness could be noted also observing the backbone curve and dissipated energy curves (see Figure 3-63 and Figure 3-64).

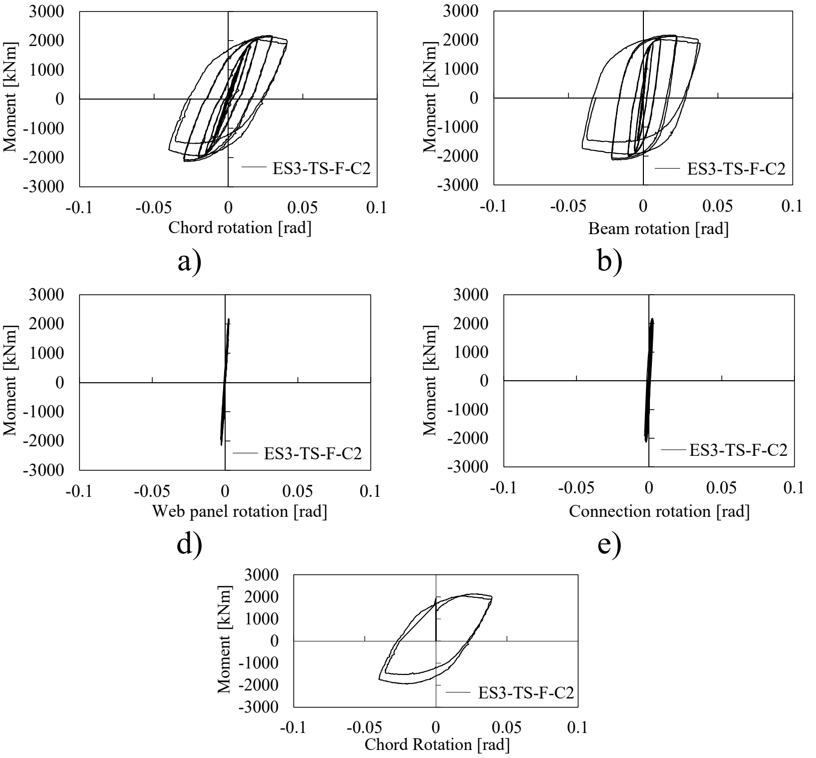

a) b)

d) e)

e)

Figure 3-63: Moment chord rotation (a, and e), beam rotation (b), column web panel rotation (c) and connection rotation (d).

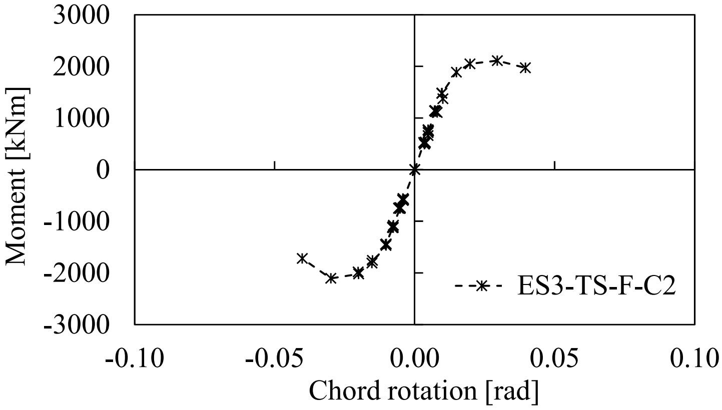

a)

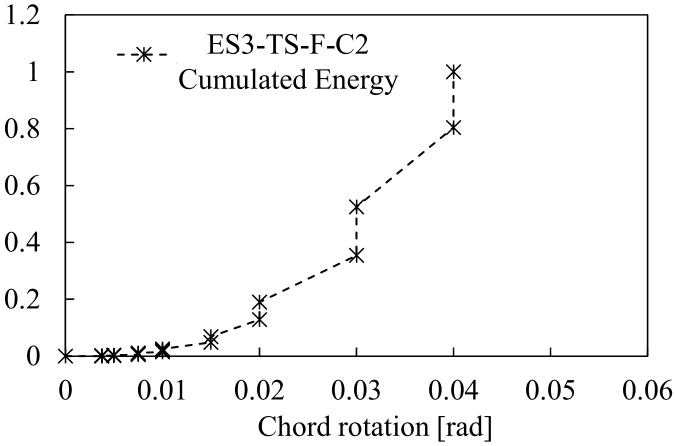

b)

Figure 3-64: Experimental test backbone curve (a) and cumulated energy respect to the 4% rotation.

3.9.1 Calibration

The FE model introduced in the calibration phase is the same introduced in the previous chapter for the ES3-TS-F-C1 joint, since there are not differences in terms of both geometries and loading protocol. Despite this, as anticipated substantial differences regarding the joints elastic stiffness can be pointed out. Since that problem is related to the setup stiffness, in the calibration phase an elastic spring was introduced to model the setup deformability. In this way indeed it is possible calibrate the tests response considering at the same time the movement of the setup.

Moreover, both the maximum resistance and the moment at 4% of chord rotation are slightly different with respect to the ES3-TS-F-C1 results. Indeed, ES3-TS-F-C2 show a smaller yielding resistance but, at the same time, a smaller geometrical imperfection on the beam flanges. Therefore, respect to the previous model in the ES3-TS-F-C2 model was decrease the yielding limit of the beam material (according to the coupon tests results) and a less amplification factor for the beam buckling wave was used. Finally, Figure 3-65, Figure 3-66 and Figure 3-67, show the comparison between the new FE model and the experimental results, where it can be notice that, the ultimate resistance, the elastic stiffness and the plastic damage are perfectly interpreted.

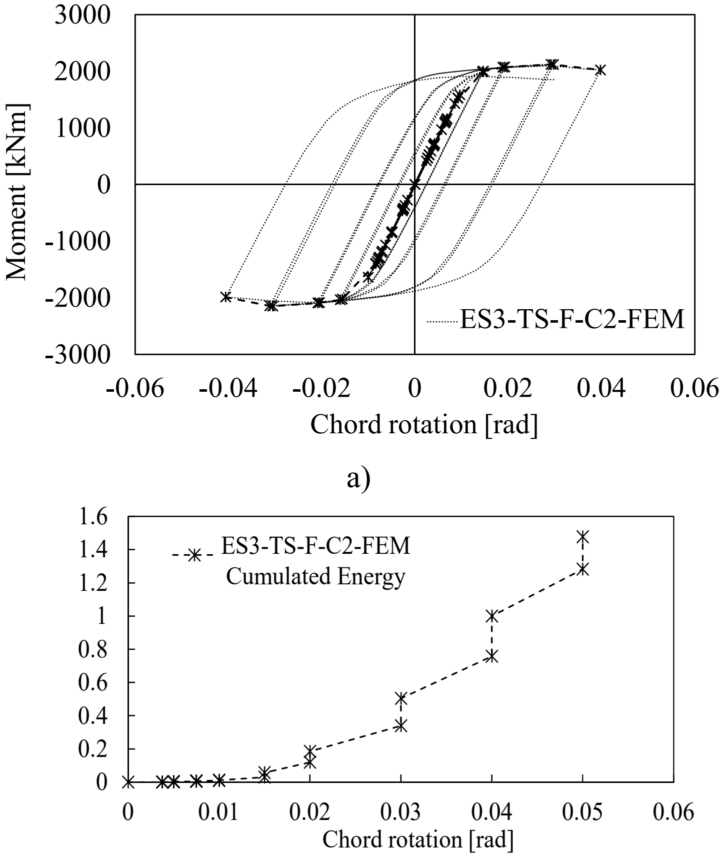

b)

Figure 3-65: FEM: (a) Moment rotation curve and (b) cumulated energy respect to the 4% rotation.

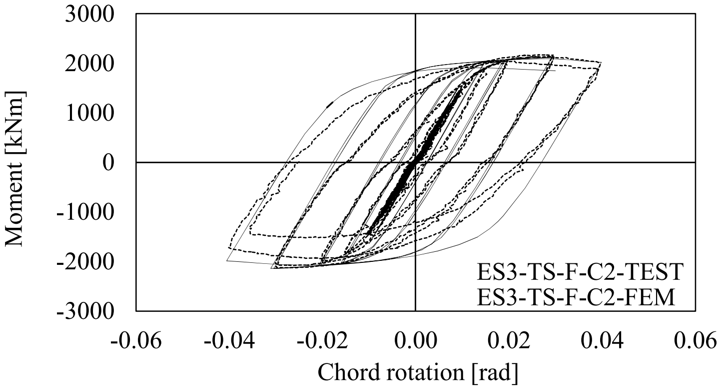

a)

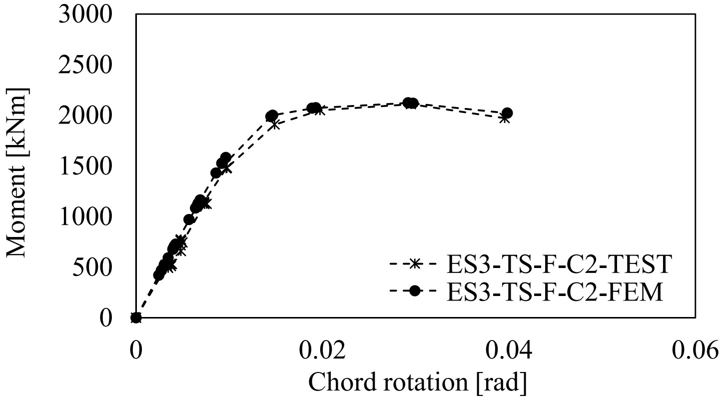

b)

Figure 3-66: Experimental result against the FEM prevision both in terms of cyclic (a) and Back bone curve (b).

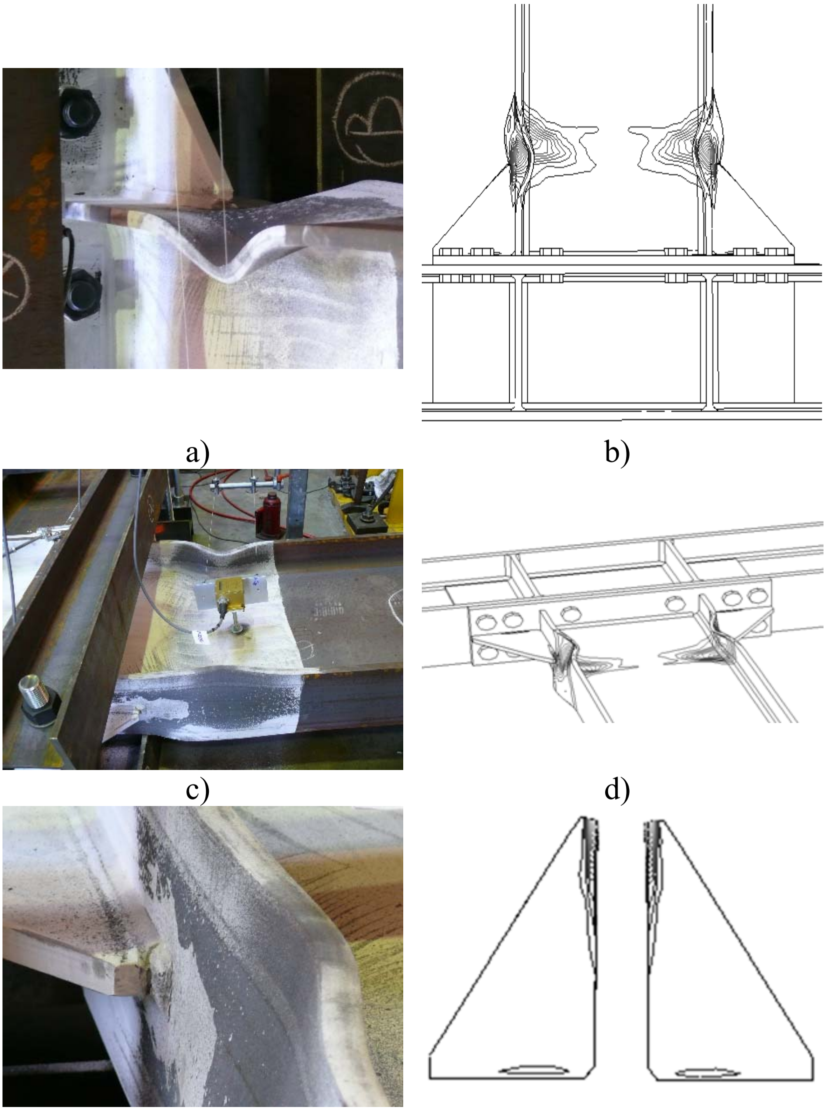

a) b)

c) d)

e) f)

Figure 3-67: Failure mode: Experimental (a, c and e) against FEM PEEQ distribution (b, d and f).

3.10 ES3–TS–F–M

The ES3–TS–F–M is a monotonic test performed on the same joint geometry reported in the previous two paragraphs (ES3-TS-F-C1 and ES3-TS-F-C2).

In order to properly investigate the joint ductility the maximum imposed rotation is 7%. On the moment rotation curve in Figure 3-69 *a,* the unloading and reloading steps are highlighted in order to define the correct joint elastic stiffness.

In terms of bending capacity, the trend is ascending up to a rotation of 5%, reaching a value of 2250kNm, after which the capacity decreases due to the buckling of the beam compression flange (see Figure 3-69 *b*). As already observed in ES3-TS-F-C2 test, also for the monotonic test there is a problem in the definition of the joint elastic stiffness due to some local deformation on the experimental setup.

The formation of the plastic hinge in the beam (see Figure 3-68 *b*) causes the concentration of the largest part of the rotational demand in the beam, perfectly in line with what observed until now for the full strength joints. The connection and column web panel remain in elastic range showing a small rotational participation in the joint response (see Figure 3-69 *c* and *d*).

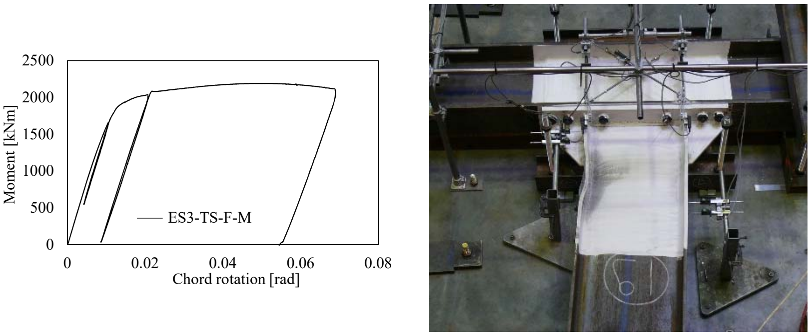

a) b)

Figure 3-68: Moment chord rotation (a) and joint failure mode (b).

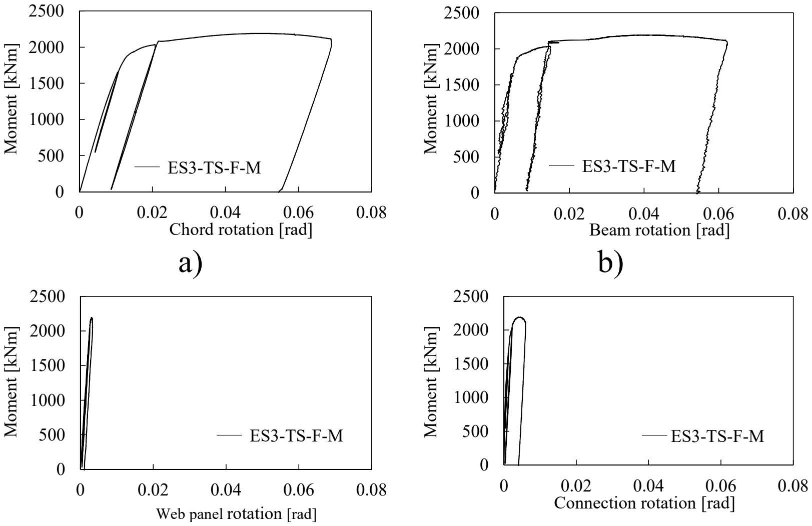

a) b)

c) d)

Figure 3-69: Moment chord rotation (a), beam rotation (b), column web panel rotation (c) and connection rotation (d).

3.10.1 Calibration

The FE calibration was made, starting from the same model, already developed for the ES3-TS-F-C2 tests, considering indeed the introduction of an elastic spring to take into account the setup deformability. Then, the material properties were changed according to the coupon test results.

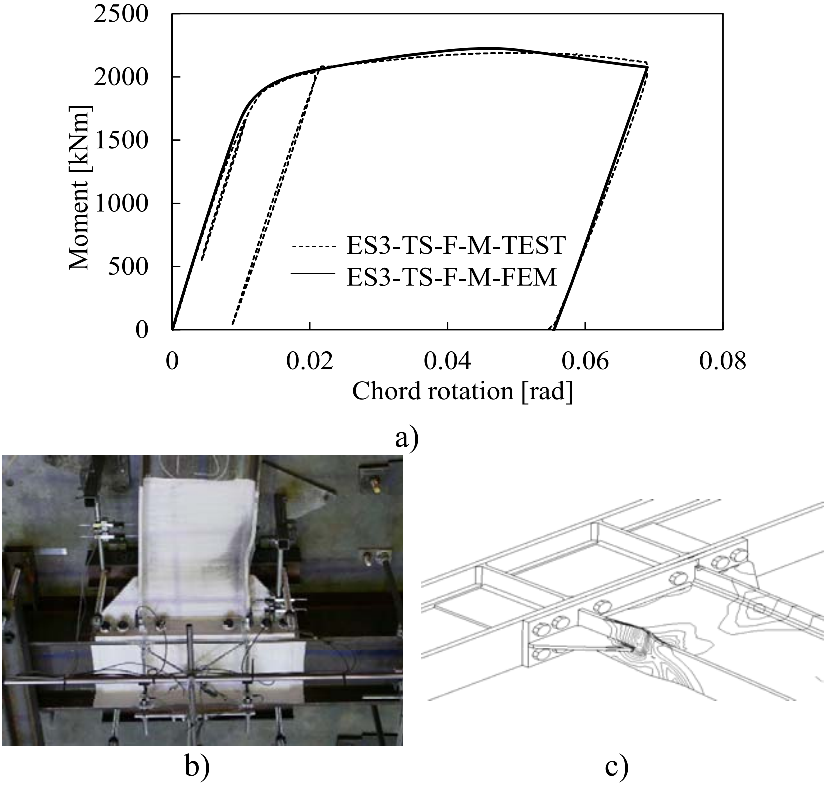

a)

b) c)

Figure 3-70: Experimental result against the FEM prevision both in terms of moment rotation curve (a), and failure mode (b and c).

Figure 3-70 shows good agreement between the experimental test and the numerical results, both in terms of moment rotation curve and in terms of the failure mode reached.

The elastic stiffness and the joint maximum resistance are perfectly calibrated, as is the yielding point transition. Moreover, the elastic unloading branch is perfect interpreted by the FE analysis.

The PEEQ distribution is perfectly in line with the plastic deformation measured during the test. The differences regarding the out of square imperfection introduced are insignificant.

The plastic deformation distribution in the FEA shows slightly larger values on the compressed beam flange, where the buckling wave is more evident. This difference, probably due to not perfect FE geometrical imperfection calibration, is marked also on the moment rotation curve, where it's possible to observe that, compared to the experimental results, the FE model shows a larger resistance decrease at a rotation of about 4.5%, while the test shows this decrease only at 5%.

Finally, it can be concluded that the proposed numerical model is able to predict the joint response with a high level of accuracy.

3.11 ES3–TS–E–C1

ES3–TS–E–C1 is a cyclic test on the equal strength joint of the largest beam to column assembly.

The equal strength joint, as already mentioned, should exhibit a uniform distribution of the plastic deformation between the connection and the beam, while the column web panel should remain in elastic range.

Table 3.10: ES3-TS-E-C1 test results.

Joint		ES3-TS-E-C1	
Design Criteria		Equal strength	
Elastic Stiffens		137217	[kNm]
0.8 M_{pl}		1246.9	[kNm]
$M_{j,Rd}$	4%	1941.97	[kNm]
	-4%	-1738.27	[kNm]
	Max (3%)	2120.36	[kNm]
	Min (-3%)	-2061.3	[kNm]
Dissipated energy	4%	751	[kNm]
	5%	-	[-]
	6%	-	[-]
	7%	-	[-]

As all the ES3-F tests, also in this case, the test was stopped at 5% of rotation due to micro cracks in the welds connecting the rib and the beam.

On a global level, the moment rotation curve (see Figure 3-71 *a*) shows increasing bending capacity up to a rotation of 3% (see Table 3.10), when the damage moves from the end-plate towards the beam. The geometric imperfections trigger the flange buckling (see Figure 3-71 *c*) redirecting the failure in the beam and thus causing the bending strength decrease.

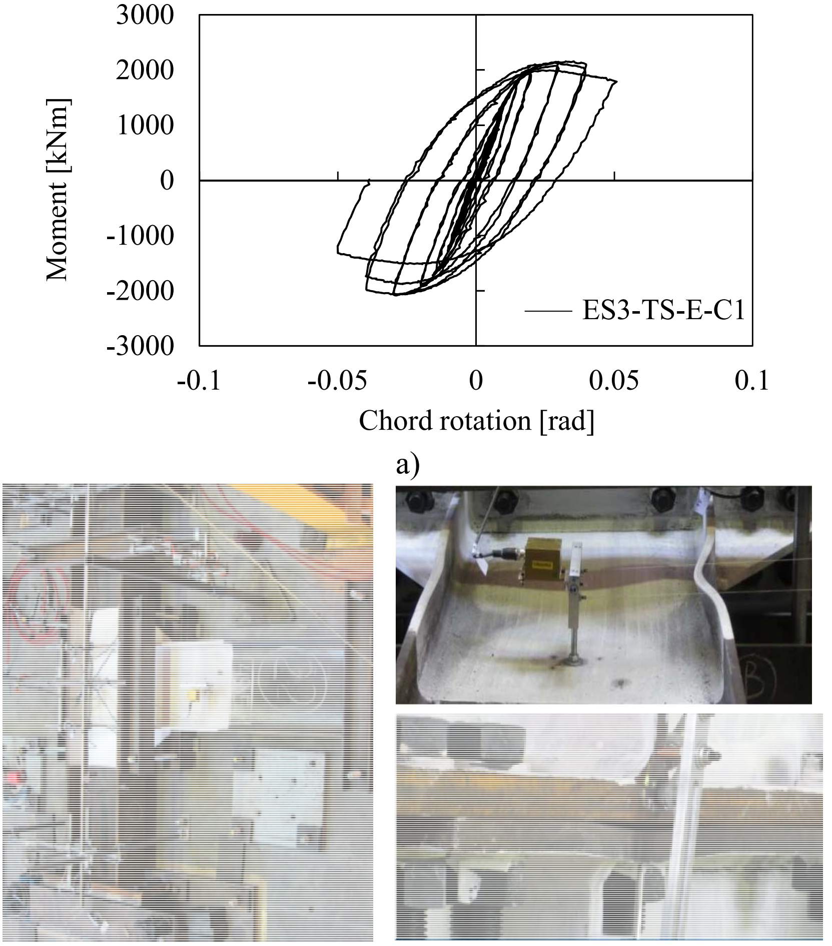

a)

b) c)

Figure 3-71: Moment chord rotation (a) and joint failure mode (b and c).

The participation of the connection on the failure mode is also confirmed by the macro-component rotational contribution (see Figure 3-72), where the rotation caused by the gap opening of the end plate plays a central role in the chord rotation definition.

In spite of the failure mode, the joint shows a good ductility because the connection's plastic deformation is mainly concentrated in the end-plate, leaving the bolts in elastic range.

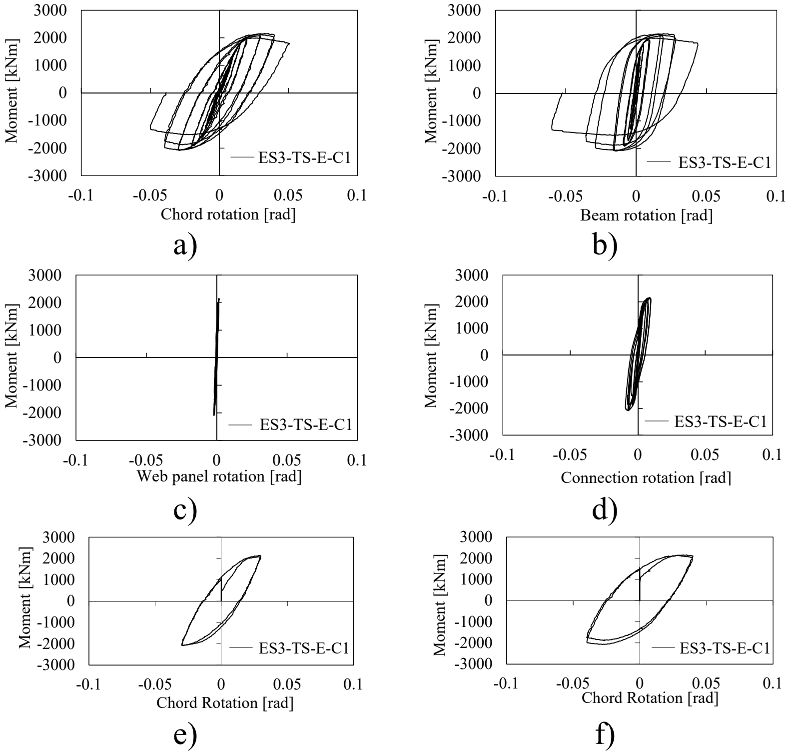

a) b) c) d) e) f)

Figure 3-72: Moment chord rotation (a, e and f), beam rotation (b), column web panel rotation (c) and connection rotation (d).

The high joint ductility is confirmed also by the shape of the cycle at 4% and 5% of rotation (see Figure 3-72 *e* and *f*) and from the cumulated energy diagram (see Figure 3-73 *b*).

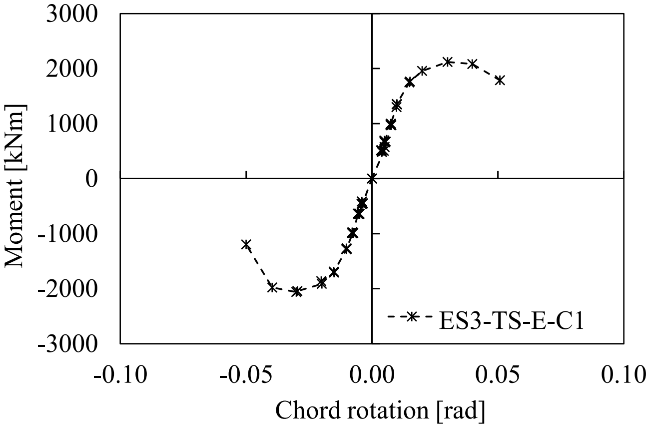

a)

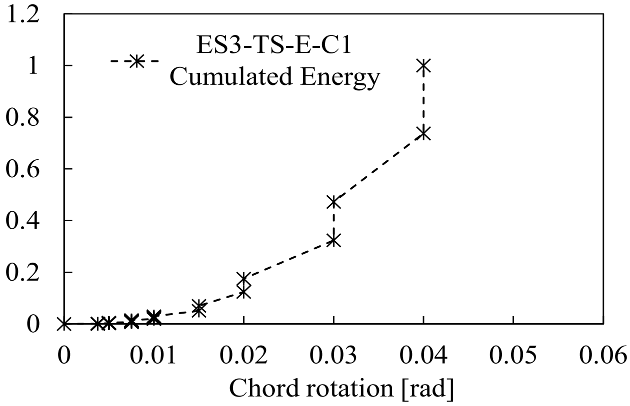

b)

Figure 3-73: Experimental test backbone curve (a) and cumulated energy respect to the 4% rotation.

3.11.1 Calibration

The results of the FEM calibration in terms of moment rotation curve and dissipated energy are reported in Figure 3-74 *a* and *b* respectively. As it can be observed, the Abaqus model is able to perfectly reproduce the elastic stiffness and the test resistance, considering also the decrease of bending capacity due to the activation of the geometrical imperfection on the beam side (see Figure 3-75).

Furthermore, the failure mode is well caught by the PEEQ distribution (see Figure 3-76 *a* and *b*); indeed, in line with the experimental results the FE model shows the plasticization of both the end-plate and the beam extremity. Moreover, also the presence of the residual gap opening is well interpreted by the FEM results (see Figure 3-77).

Figure 3-77 *b* show, the micro-fracture opening due to the large stress concentration leads in the rib-to-beam interface. In line with this feature, also the FE model show (see Figure 3-77 *a* and *c*) a large plastic demand at the rib extremities.

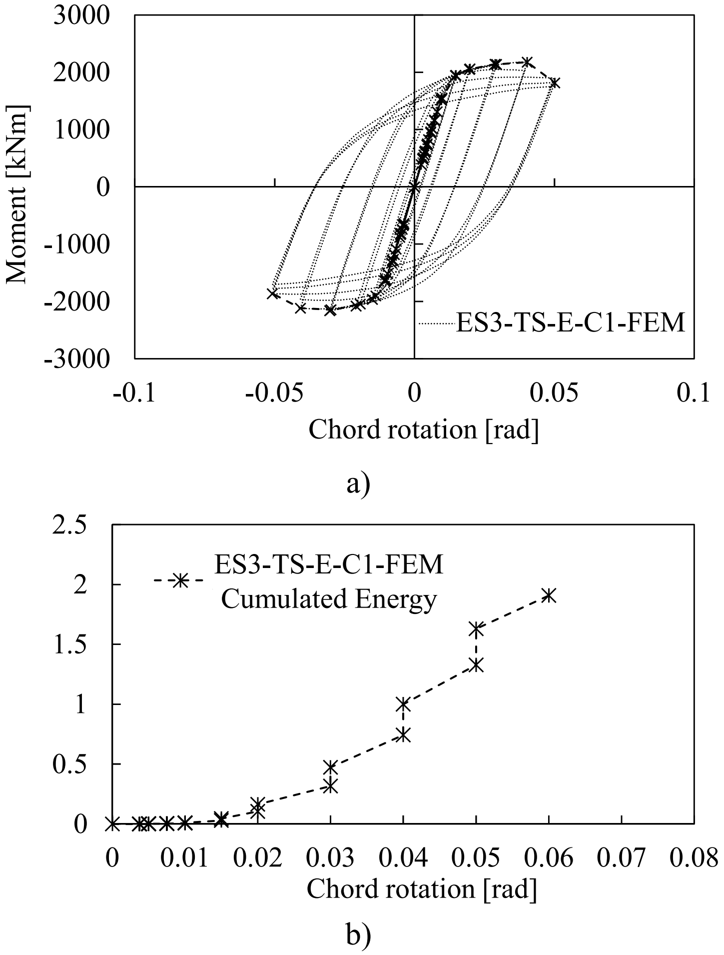

Figure 3-74: FEM: (a) Moment rotation curve and (b) cumulated energy respect to the 4% rotation.

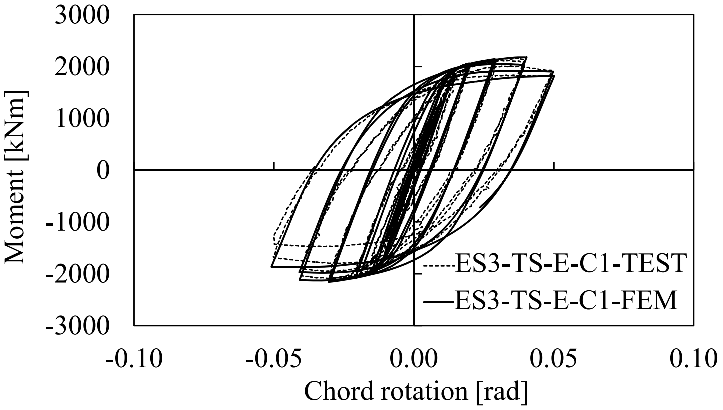

a)

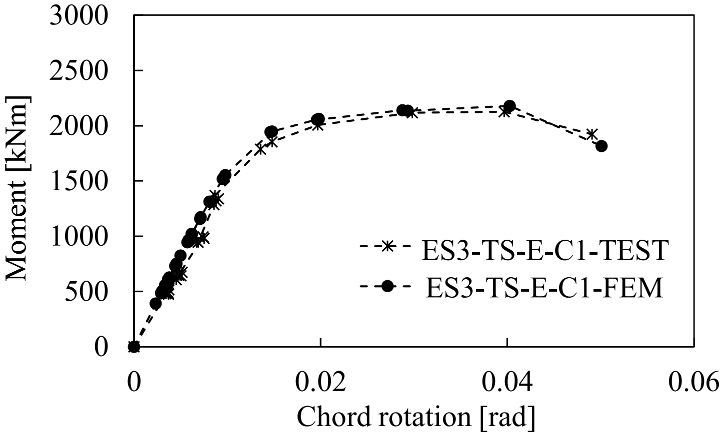

b)

Figure 3-75: Experimental result against the FEM prevision both in terms of cyclic (a) and Back bone curve (b).

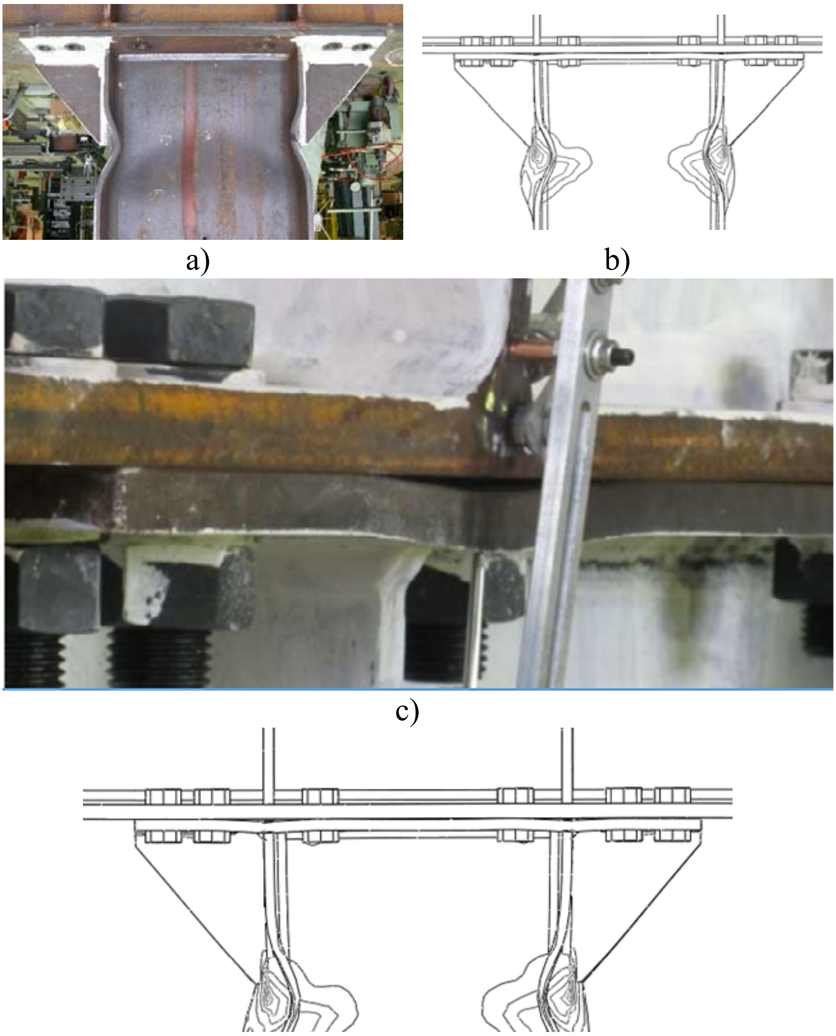
a) b)

c)

d)

Figure 3-76: Failure mode: Experimental (a and c) against FEM PEEQ distribution (b and d).

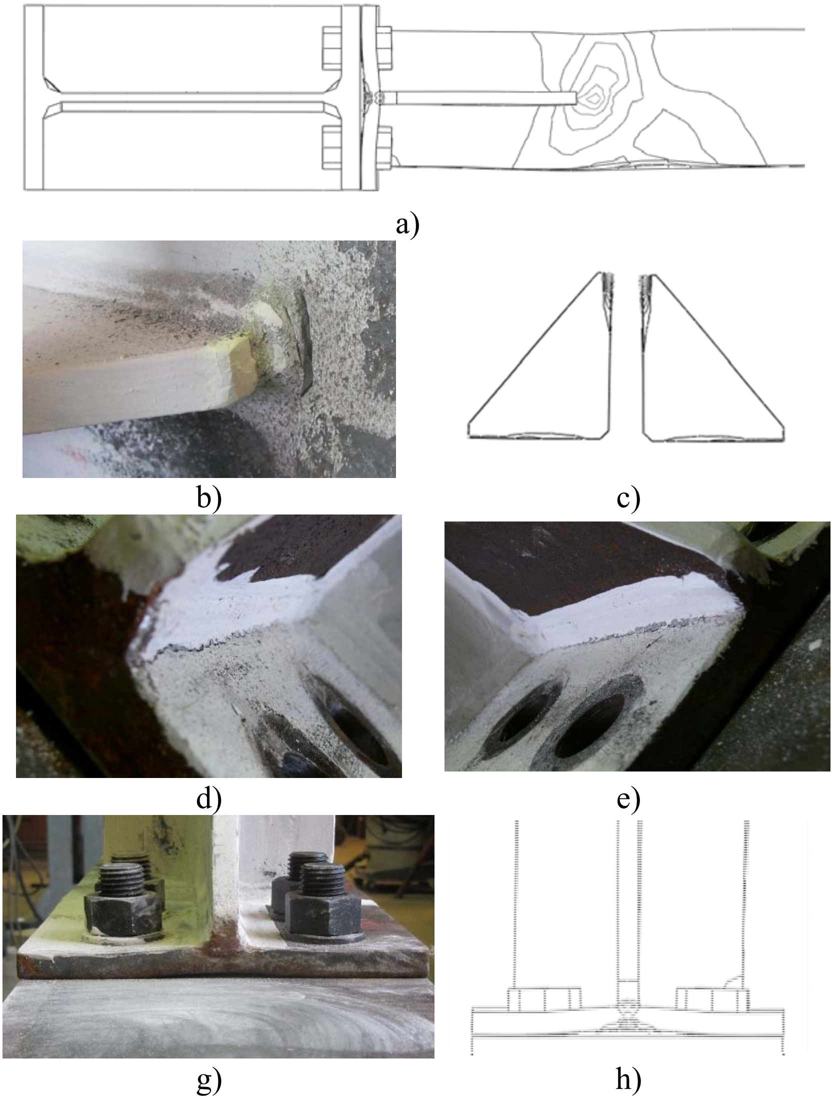

a)

b) c)

d) e)

g) h)

Figure 3-77: Failure mode: Experimental (b, d, e and g) against FEM PEEQ distribution (a, c and h).

3.12 ES3–TS–E–C2

The ES3-TS-E-C2 specimen show almost the same results (see Table 3.11) discussed in the previous paragraph. Indeed, also in this case the it can be observed a ductile failure mode (see Figure 3-78 and Figure 3-80) with a large concentration of the plastic deformation both on the end-plate and on the beam (see Figure 3-79). Moreover, as observed for ES3-TS-E-C1, there is an initial activation of the equivalent T-stub in tension on the end-plate and, due to the hardening developed in the plate, the subsequent plastic deformation in the beam. The only difference can be found in the rotational level achieved i.e. the ES3-TS-E-C2 arrives up to 5% of rotation without exhibiting any cracks in the welds.

Table 3.11: ES3-TS-E-C2 Test result.

Joint		ES3-TS-E-C2	
Design Criteria		Equal strength	
Elastic Stiffens		133831	[kNm]
0.8 M_{pl}		1246.9	[kNm]
$M_{j,Rd}$	4%	2085.29	[kNm]
	-4%	-1864.7	[kNm]
	Max (4%)	2127.0065	[kNm]
	Min (-3%)	-2095.2	[kNm]
Dissipated energy	4%	718	[kNm]
	5%	1137	[-]
	6%	-	[-]
	7%	-	[-]

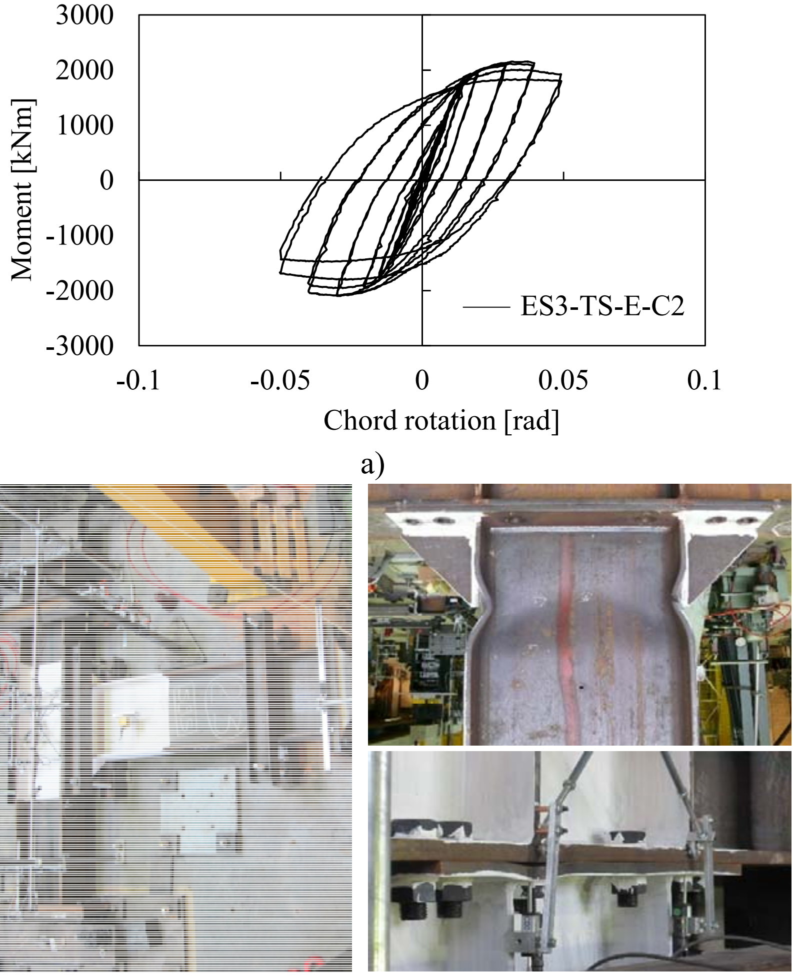

a)

b) c)

Figure 3-78: Moment chord rotation (a) and joint failure mode (b and c).

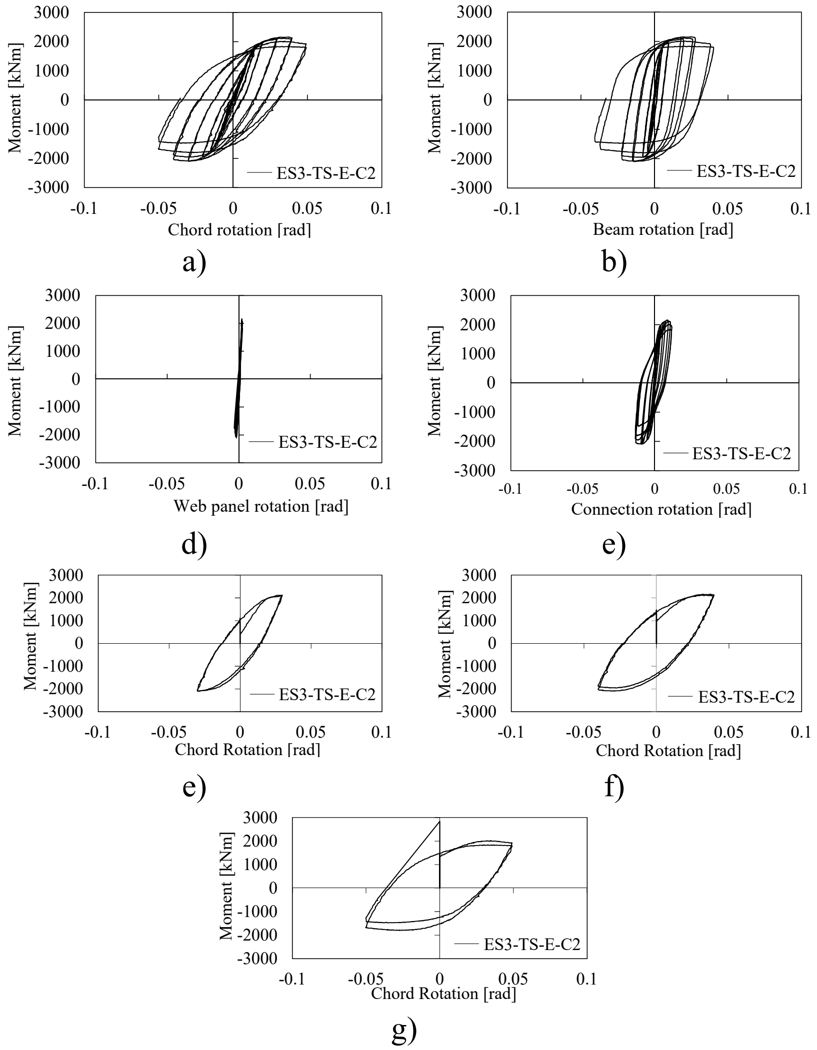

a) b)

d) e)

e) f)

g)

Figure 3-79: Moment chord rotation (a, e, f, and g), beam rotation (b), column web panel rotation (c) and connection rotation (d).

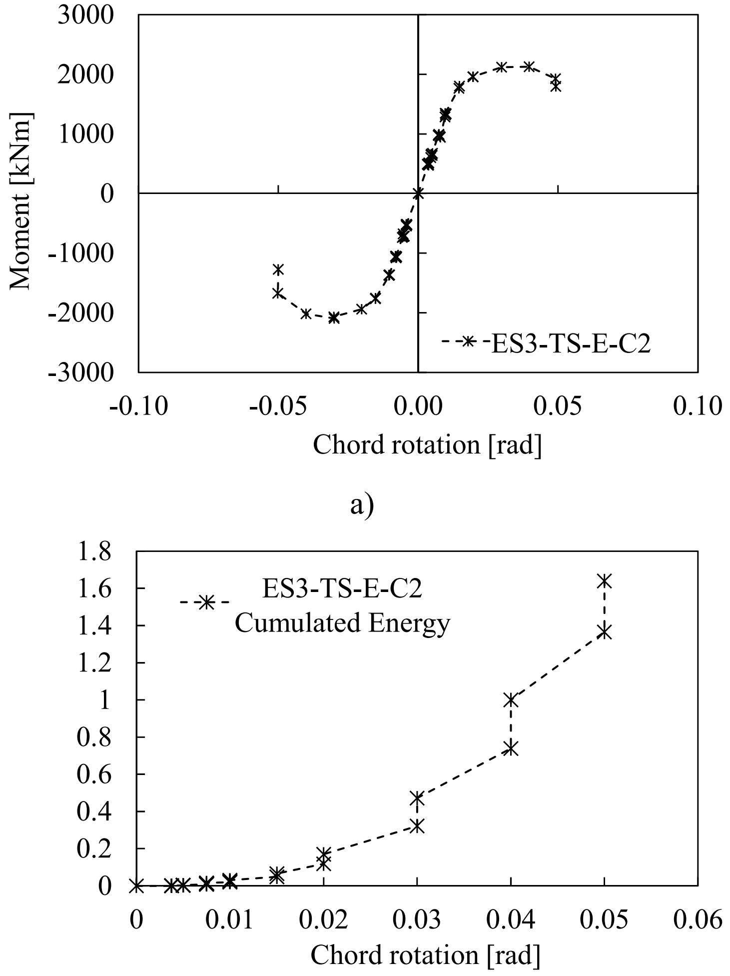

a)

b)

Figure 3-80: Experimental test backbone curve (a) and cumulated energy respect to the 4% rotation.

3.12.1 Calibration

The FE model used for the calibration (see Figure 3-81) of this tests is the same of the one introduced for the calibration of ES3-TS-F-C1.

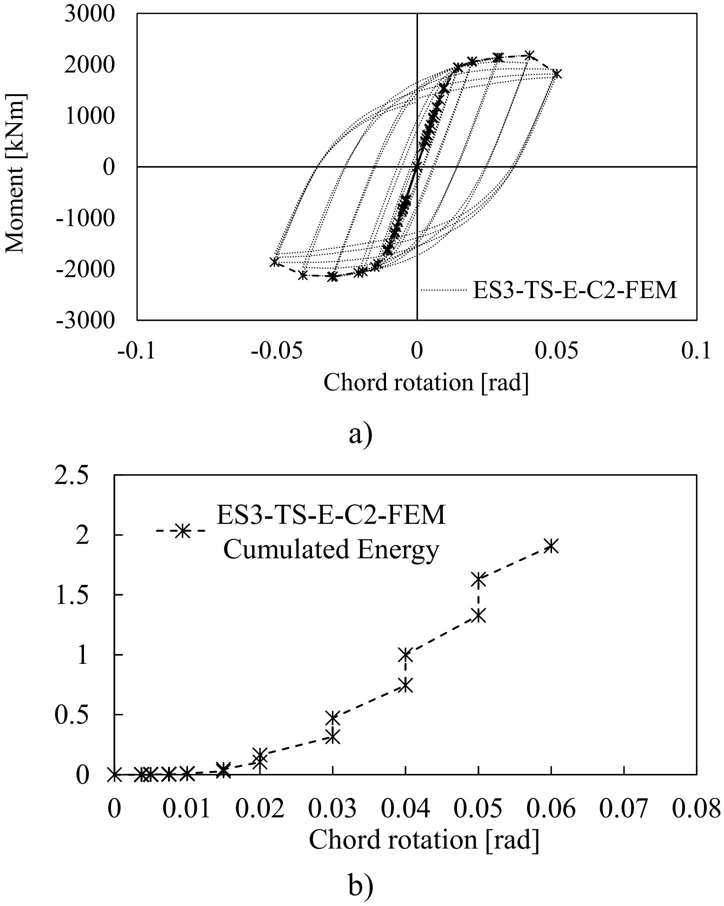

a)

b)

Figure 3-81: FEM: (a) Moment rotation curve and (b) cumulated energy respect to the 4% rotation.

The only differences are the geometrical imperfection of the beam that in this specimen are slightly larger with respect to the ES3-TS-E-C1 specimens. Although this difference the FE model is able to perfectly reproduce the experimental test results (see Figure 3-82 and Figure 3-83).

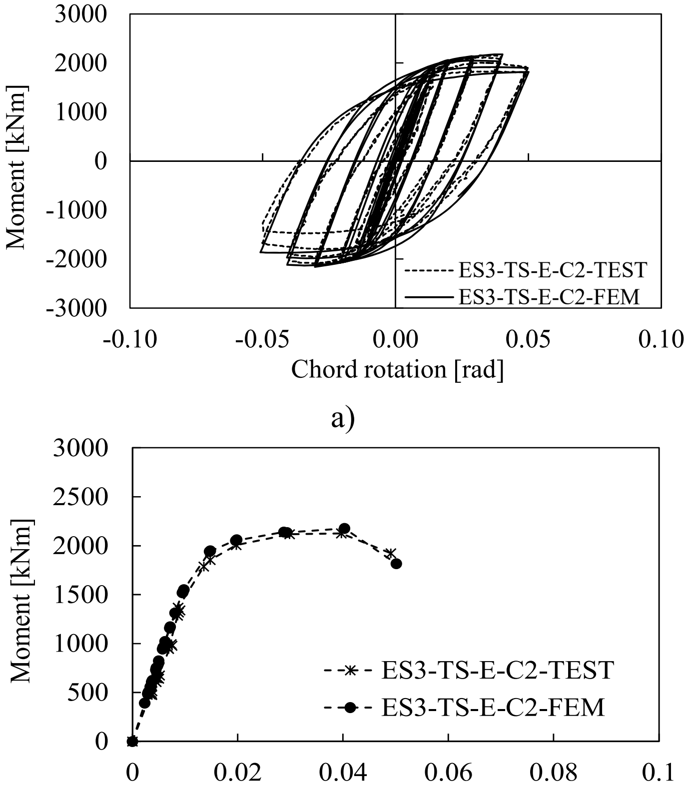

Figure 3-82: Experimental result against the FEM prevision both in terms of cyclic (a) and Back bone curve (b).

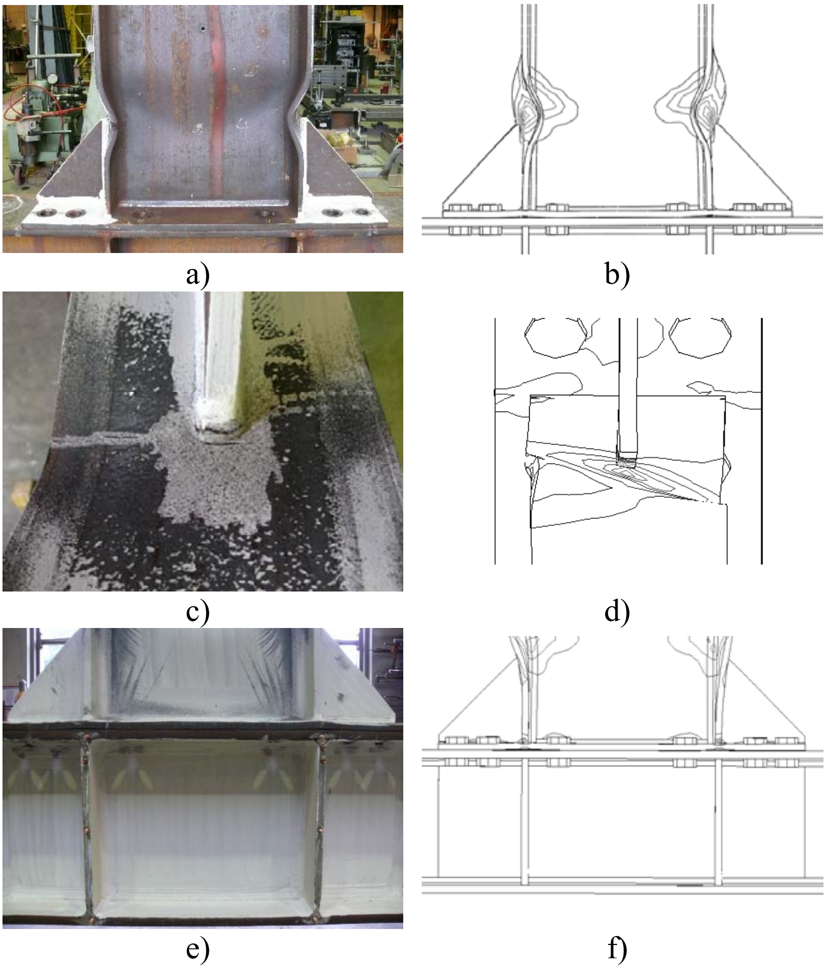

a) b)

c) d)

e) f)

Figure 3-83: Failure mode: Experimental (a, c and e) against FEM PEEQ distribution (b, d and f).

3.13 ES3–TS–Esp–C

The only differences between the ES3-TS-Esp-C and the previous two specimens is the welding technique; in this specimen indeed, the shot pinning technology was applied on the welds to improve their behavior.

As it can be observed from Table 3.12, Figure 3-84, Figure 3-85and Figure 3-86 the results, in terms of moment rotation curve, dissipated energy and failure mode, are perfectly in line with the one observed for the two specimens without the treatment on the welds shot. Indeed, as already observed for the ES2 equal strength joint, any substantial differences for the joint global behavior can be pointed out when the shot pinning is introduced.

Table 3.12: ES3-TS-E-C2 test result.

Joint		ES3-TS-Esp-C	
Design Criteria		Equal strength	
Elastic Stiffenes		134660	[kNm]
0.8 M_{pl}		1246.9	[kNm]
$M_{j,Rd}$	4%	1985.76	[kNm]
	-4%	-1739.92	[kNm]
	Max (4%)	2090.1	[kNm]
	Min (-3%)	-2082.6	[kNm]
Dissipated energy	4%	960	[kNm]
	5%	161	[-]
	6%	-	[-]
	7%	-	[-]

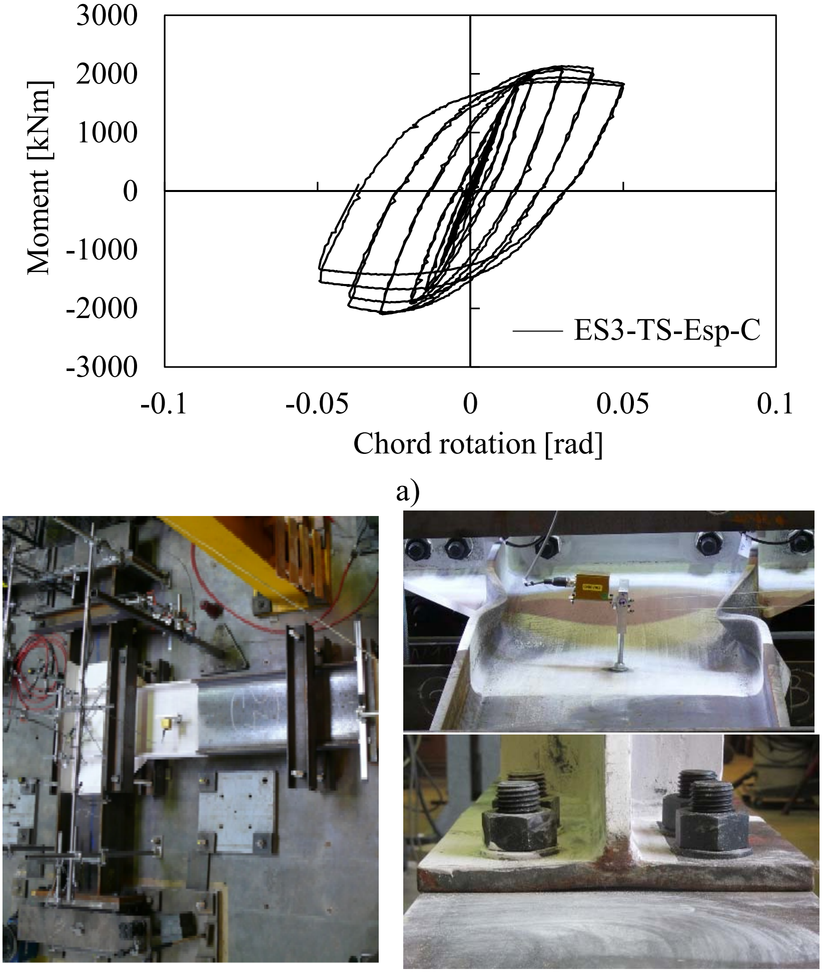

a)

c)

d)

Figure 3-84: Moment chord rotation (a) and joint failure mode (b and c).

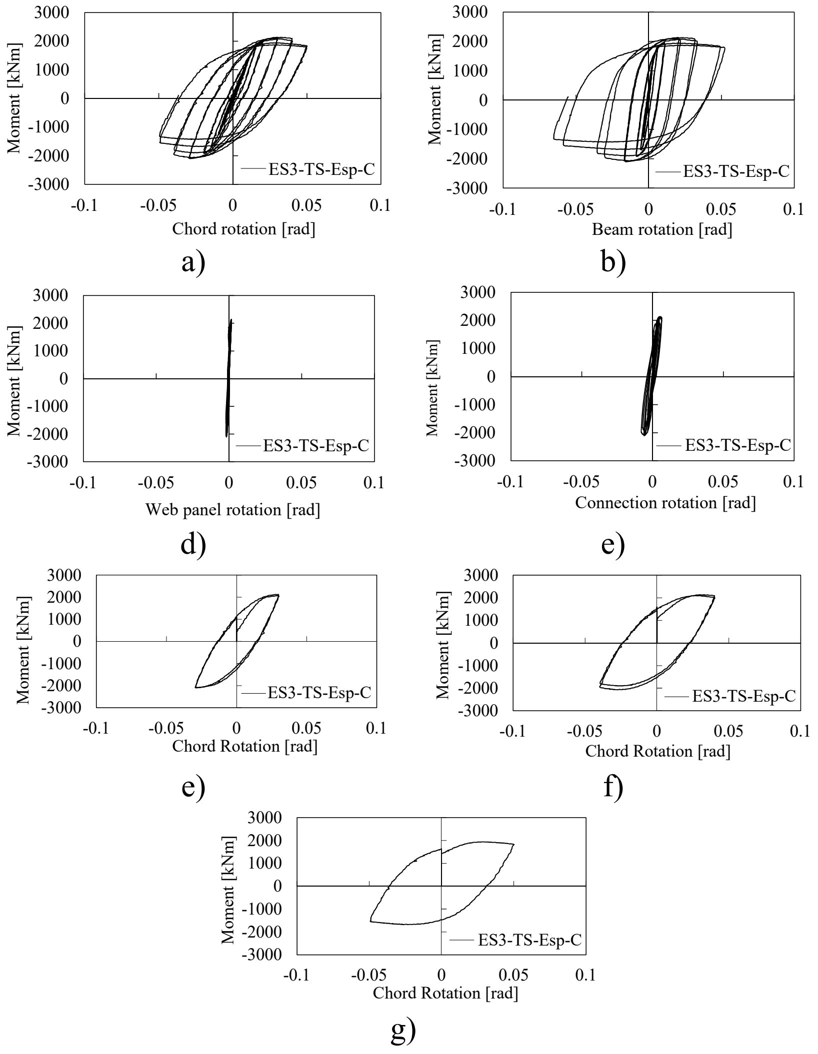

a) b)

d) e)

e) f)

g)

Figure 3-85: Moment chord rotation (a, e, f, and g), beam rotation (b), column web panel rotation (c) and connection rotation (d).

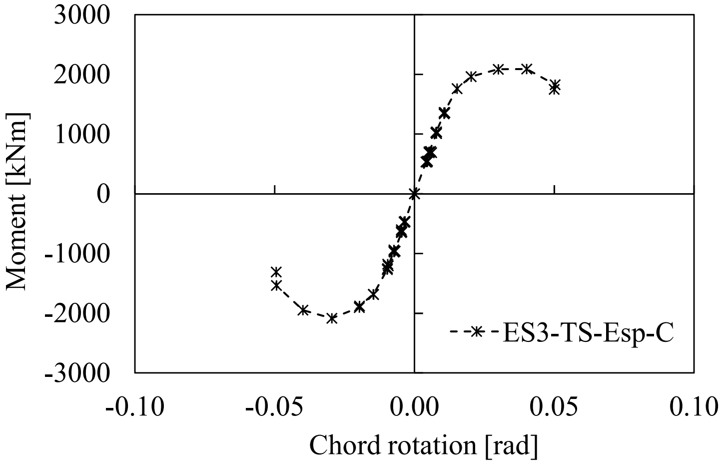

a)

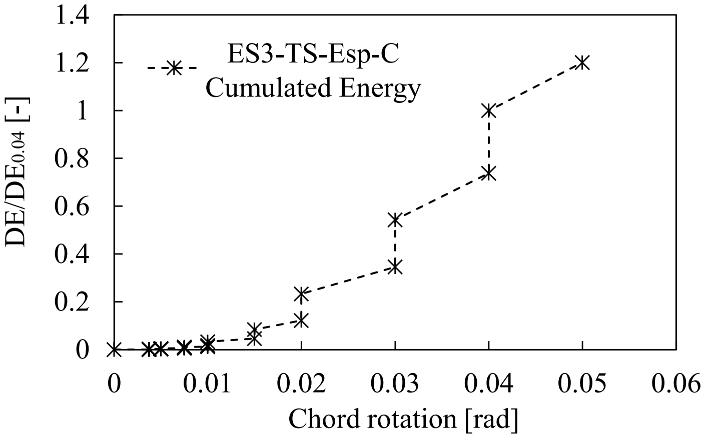

b)

Figure 3-86: Experimental test backbone curve (a) and cumulated energy respect to the 4% rotation.

3.13.1 Calibration

Since no appreciable differences can be pointed out with respect of the last two equal strength joints (ES3-TS-E-C1 and ES3-TS-E-C2), the same model described in the previous paragraph was introduced in the calibration phase.

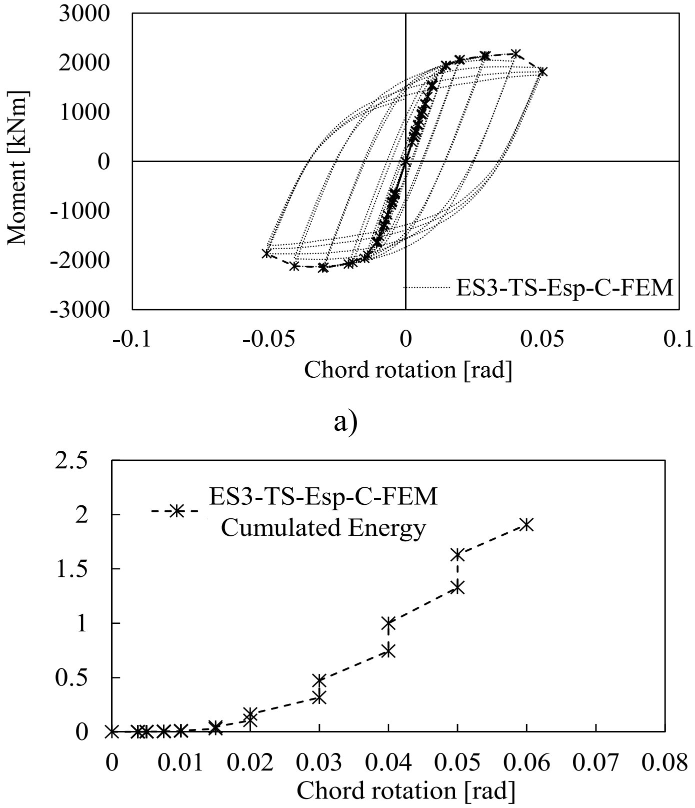

a)

b)

Figure 3-87: FEM: (a) Moment rotation curve and (b) cumulated energy respect to the 4% rotation.

Indeed, as it can be observed from the results reported in Figure 3-88 and Figure 3-89, the FE model is, also in this case, able to reproduce all the test features as the elastic stiffness, the resistance and the failure mode.

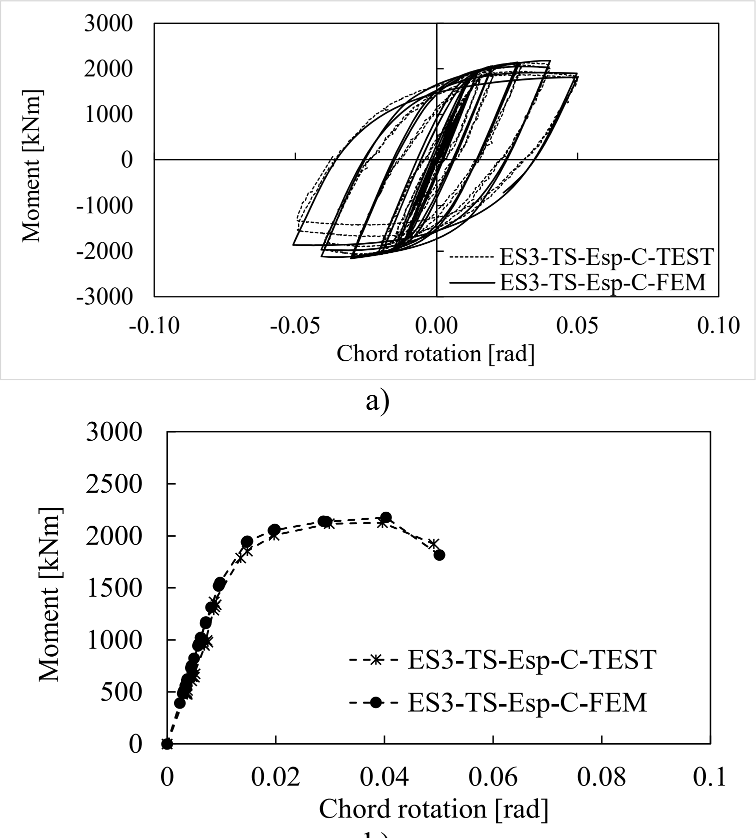

b)

Figure 3-88: Experimental result against the FEM prevision both in terms of cyclic (a) and Back bone curve (b).

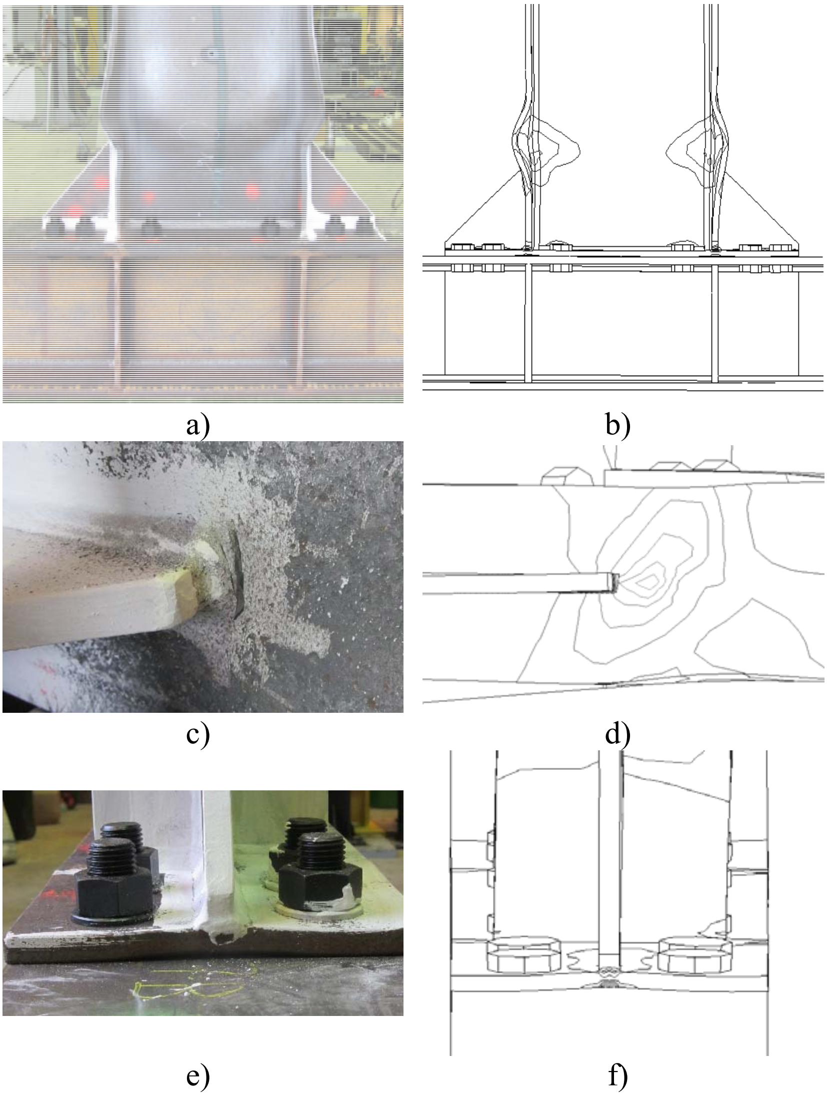

a) b) c) d) e) f)

Figure 3-89: Failure mode: Experimental (a, c and e) against FEM PEEQ distribution (b, d and f).

4 Results comparison and discussion

4.1 Experimental results comparison

The experimental results reported in the previous paragraph are hereinafter compared and discussed, focusing on: (i) the differences between the equal and the full strength joints behavior, (ii) the influence of the cyclic loading protocol applied and (iii) the effect of the shot pinning on the welds behavior.

The ES1-TS-F and ES1-TS-E assemblies (see Table 4.1 comparison a) show a difference of 10% (in terms of bending capacity) at 4% of rotation. This diversity decrease for higher value of rotations where, since the presence of the geometrical imperfections on the beam flange, the full strength show a resistance decrease, while the bending capacity in the equal strength joint increase almost constantly up to 5% of rotation. Moreover, since the different geometry and connection configuration (ES1-TS-F has two bolts row above the beam flange, while ES1-TS-E just one), also in terms of stiffness the joints show an important difference, in particular, as expected, the full strength is stiffer (20%) than the equal one.

The same trend can be observed also between ES2 assemblies (see Table 4.1 comparison d), where the differences, between the two performance levels (equal and full), are more evident.

Contrariwise, ES3 assembly show smaller differences between the full and the equal strength joints; indeed in this case, the equal strength joint behavior is more similar to the full strength one, showing just small plastic deformation in the connection, that are mainly concentrated in the beams.

Table 4.1: Differences between the experimental tests.

Test Specimens	Comparison	Stiffness	Resistance			
			4%	-4%	Max	Min
ES1-TS-F-C1 ES1-TS-E-C2	(a)	1.20	1.09	1.11	1.05	1.08
ES2-TS-F-C1 ES2-TS-F-C2	(b)	0.93	1.15	1.13	1.19	1.17
ES2-TS-E-C1 ES2-TS-Esp-C	(c)	0.99	0.99	1.00	1.02	1.01
ES2-TS-F-C1 ES2-TS-E-C1	(d)	1.13	1.20	1.16	1.14	1.13
ES3-TS-E-C1 ES3-TS-Esp-C	(e)	1.02	0.98	1.00	1.01	0.99
ES3-TS-F-C1 ES3-TS-E-C1	(f)	1.92	1.01	0.96	1.04	1.00

The influence of the loading protocol was also investigated for the full strength joints; therefore ES2-TS-F-C1 and ES2-TS-F-C2 were tested respectively according to the EqualJoints (see Figure 1-5 b) and the AISC341 (see Figure 1-5 a) loading protocol. No different between the joint stiffeness can be pointed out, while the strong difference in terms of bending capacity (see Table 4.1 comparison b and Figure 4-1 b) should not be attribuited to loading protocol, but, as already discussed in the previous paragraph, to the material characteristichs.

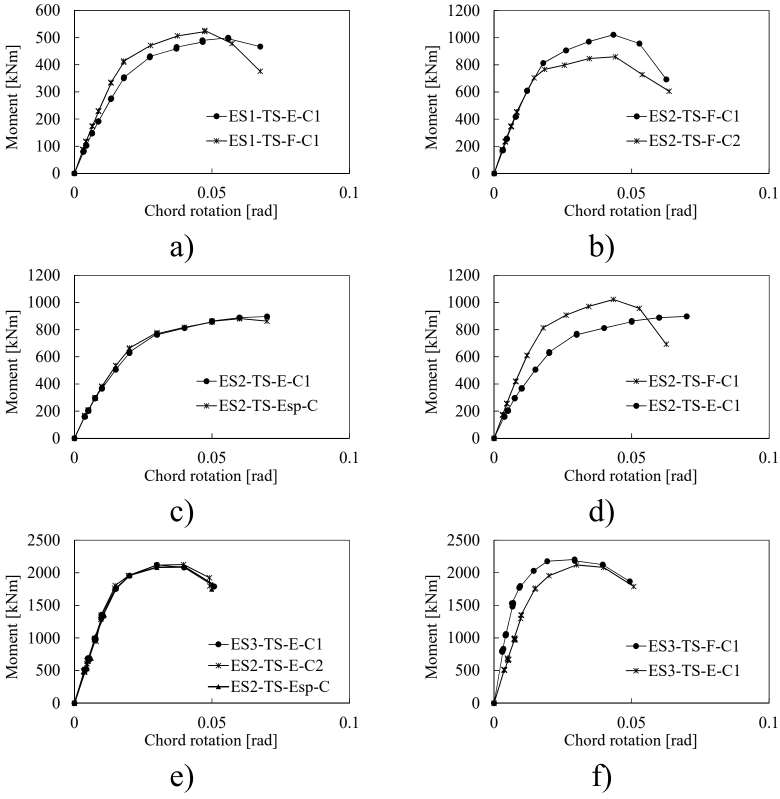

Figure 4-1: comparison between the experimental tests in terms of backbone curve for: (a) ES1-TS-F and ES1-TS-E, (b) ES2-TS-F-C1 and ES2-TS-F-C2, (c) ES2-TS-E-C1 and ES1-TS-Esp-C, (d) ES2-TS-F and ES2-TS-E, (e) ES3-TS-E-C1, ES3-TS-E-C2 and ES3-TS-Esp-C and (f) ES3-TS-F and ES3-TS-E.

Moreover, also the influence on the shot pinning, on the welds behavior, were investigated. As can be observed both from the ES2 and ES3 assembly (see Table 4.1 comparison c and e, and Figure 4-1 c and e) where no differences neighter in terms of stiffness, resistance and failure mode can be pointed out.

4.2 Experimental analysis vs Analytical and Numerical prediction

In the previous paragraph were observed how for all the tested joints, the failure mode was coherent with the hypothesis made in the design phase. In addition to those results, also the comparison, in terms of elastic stiffness, between the analytical model, the numerical prevision and the experimental results were pointed out. It should be notice that, since the analytical model predict the initial joint stiffness, from the tests results should be extrapolate only the contribution of the connection and the column web panel (as already done in Chapter V for the pre-test analysis).

Table 4.2 show, in accordance with the results in Chapter V how the mechanical model overestimate the initial joint stiffness, and at the same time, as already notice during the calibration phase, how the differences between the FEM and the experimental results are negligible.

Table 4.2: Elastic stiffness comparison between: the analytical model, the experimental tests and the numerical prediction.

Joint assembly		Stiffness according to model (Chapter VI) $S_{j,ini,R}$	Stiffness from Tests $S_{j,ini,EXP}$	Stiffness from FEA $S_{j,ini,FEM}$	$S_{j,ini,R}$ / $S_{j,ini,EXP}$	$S_{j,ini,R}$ / $S_{j,ini,FEM}$	$S_{j,ini,Exp}$ / $S_{j,ini,FEM}$
ES1	ES1-TS-F-C2	195916	113373	110617	1.73	1.77	1.02
	ES1-TS-F-M		111555	109819	1.76	1.78	1.02
	ES1-TS-E-C1	83281	60983	60162	1.37	1.38	1.01
ES2	ES2-TS-F-C1	306515	207922	203661	1.47	1.51	1.02
	ES2-TS-F-C2		186918	184659	1.64	1.66	1.01
	ES3-TS-E-C1	180360	126561	124351	1.43	1.45	1.02
	ES2-TS-Esp-C		126449		1.43		1.02
ES3	ES3-TS-F-C1	558679	523464	519675	1.07	1.08	1.01
	ES3-TS-F-C2		524253		1.07		1.01
	ES3-TS-E-C3	496352	487205	483945	1.02	1.03	1.01
	ES3-TS-E-C4		490804		1.01		1.01
	ES3-TS-E-C5		488871		1.02		1.01

*C*HAPTER *VI*

References

[1] EQUALJOINTS – European pre-QUALified steel JOINTS: RFSR-CT-2013-00021. Research Fund for Coal and Steel (RFCS) research programme.

[2] EN 1993:1-8, Design of steel structures - Part 1-8: Design of joints. CEN 2005.

[3] ANSI/AISC 341-10 (2010). Seismic Provisions for Structural Steel Buildings. American Institute of Steel Construction.

[4] ANSI/AISC 358-16 (2016). Prequalified Connections for Special and Intermediate Steel Moment Frames for Seismic Applications.

[5] Dassault Systèmes. Abaqus analysis 6.16 user’s manual. Simula Inc.; 2016.

[6] Abidelah A., Bouchaïr A., Kerdal D.E. (2012). Experimental and analytical behavior of bolted end-plate connections with or without stiffeners. Journal of Constructional Steel Research, 76, 13–27.

List of figures

Figure 1-1: Set-up at University of Naples. 285
Figure 1-2: Instrumentation introduced by the University of Naples. 286
Figure 1-3: Set-up at University of Liege. 289
Figure 1-4: Instrumentation introduced by the University of Liege. 289
Figure 1-5: AISC341-10 [3] (a) and Equaljoints [1] (b) loading protocol. 291
Figure 1-6: Cumulated energy for:AISC341-10 [3] and EqualJoint loading protocol [1]... 291
Figure 2-1: Coupon test results of the IPE450 from the ES2-TS-F-CA (a) and ES2-TS-F-C2 (b). 293
Figure 2-2: University of Naples coupon test setup (a) and an example of the coupon test experimental results (b). 294
Figure 2-3: Stress-strain curve of plate with a thickness of: 15mm (a), 18mm (b), 25mm (c), 20mm (d) and 30mm (e). 295
Figure 3-1: Main geometrical details of ES joints reported in Table 4... 296

Figure 3-2: Bolts deformation from first (a) and from the second (b) bolt row. 300

Figure 3-3: Moment chord rotation (a), joint configuration: initial (b), at 2% (c), at 4% (d) and at 6% (e) of chord rotation..302

Figure 3-4: Moment chord rotation (a, e, f, g and h), beam rotation (b), column web panel rotation (c) and connection rotation (d). 304

Figure 3-5: Experimental test backbone curve (a) and cumulated energy respect to the 4% rotation (b).....................305

Figure 3-6: FEM: FEM Moment rotation curve (a) and cumulated energy respect to the 4% rotation (b).....................308

Figure 3-7: Experimental result against the FEM prevision both in terms of cyclic (a) and Back bone curve (b)..........309

Figure 3-8: Failure mode: Experimental (a and c) against FEM PEEQ distribution (b and d). 310

Figure 3-9 Strain gauge measurements (a, b and c) plastic hinge (d)..311

Figure 3-10: Column web panel deformation in terms of: strain-gauge measurements (a and b), experimental test (c) and FEM yielding line distribution (d).................313

Figure 3-11: Strain gauge measurements on the ribs (a, b and c) PEEQ on the ribs (d) detailed view of the tested ribs (e and f). 314

Figure 3-12: Moment chord rotation (a), joint configuration: initial (b), at 2% (c), at 4% (d) and at 6% (e) of chord rotation. 316

Figure 3-13: Moment chord rotation (a), beam rotation (b), column web panel rotation (c) and connection rotation (d). 317

Figure 3-14: Experimental result against the FEM prevision both in terms of moment rotation curve (a) and failure mode (b and c). 318

Figure 3-15 Web panel strain gauges results: normalized strain versus chord rotation (a and b) plastic deformation of the tested specimen (c) PEEQ distribution on the FE model (d). 320

Figure 3-16: Rib strain gauges results: normalized strain versus chord rotation (a, b and c), PEEQ distribution on the FE model (d), plastic deformation of the tested specimen (e, f and g). 322

Figure 3-17: Bolts deformation from first (a) and from the second (b) bolt row. 325

Figure 3-18: Moment chord rotation (a), joint configuration: initial (b), at 2% (c), at 4% (d) and at 6% (e) of chord rotation..327

Figure 3-19: Moment chord rotation (a, e, f, g and h), beam rotation (b), column web panel rotation (c) and connection rotation (d)..328

Figure 3-20: Experimental test backbone curve (a) and cumulated energy respect to the 4% rotation. 329

Figure 3-21: FEM: (a) Moment rotation curve and (b) cumulated energy respect to the 4% rotation. 330

Figure 3-22: Experimental result against the FEM prevision both in terms of cyclic (a) and Back bone curve (b)......331

Figure 3-23: Failure mode: Experimental (a and c) against FEM PEEQ distribution (b and d) and FEM displacements magnitude (f). 334

Figure 3-24 Web panel strain gauges results: normalized strain versus chord rotation (a and b) plastic deformation of the tested specimen (c) PEEQ distribution on the FE model (d)...335

Figure 3-25: Rib strain gauges results: normalized strain versus chord rotation (a, b and c), plastic deformation of the tested specimen (d, e and f) and PEEQ distribution on the FE model (g and h).. 336

Figure 3-26: Moment chord rotation (a), joint configuration: initial (b), at 2% (c), at 4% (d) and at 6% (e) of chord rotation.. 338

Figure 3-27: Moment chord rotation (a, e, f, g and h), beam rotation (b), column web panel rotation (c) and connection rotation (d)... 339

Figure 3-28: Experimental test backbone curve (a) and cumulated energy respect to the 4% rotation......................... 340

Figure 3-29: FEM: (a) Moment rotation curve and (b) cumulated energy respect to the 4% rotation......................... 342

Figure 3-30: Experimental result against the FEM prevision both in terms of cyclic (a) and Back bone curve (b)..... 343

Figure 3-31: Failure mode: Experimental (a and c) against FEM PEEQ distribution (b and d)................................ 344

Figure 3-32 Web panel strain gauges results: normalized strain versus chord rotation (a and b) plastic deformation of the tested specimen (c) PEEQ distribution on the FE model (d).. 346

Figure 3-33: Rib strain gauges results: normalized strain versus chord rotation (a and b), PEEQ distribution on the FE model (c) and plastic deformation of the tested specimen (d, e and f)..347

Figure 3-34: Moment chord rotation (a), joint configuration: initial (b), at 2% (c), at 4% (d) and at 6% (e) of chord rotation...350

Figure 3-35: Moment chord rotation (a, e, f, g and h), beam rotation (b), column web panel rotation (c) and connection rotation (d)..351

Figure 3-36: Experimental test backbone curve (a) and cumulated energy respect to the 4% rotation. 352

Figure 3-37: FEM: (a) Moment rotation curve and (b) cumulated energy respect to the 4% rotation. 353

Figure 3-38: Experimental result against the FEM prevision both in terms of cyclic (a) and Back bone curve (b)......354

Figure 3-39: Failure mode: Experimental (a and c) against FEA PEEQ distribution (b and d). 356

Figure 3-40: Moment chord rotation (a), joint configuration: initial (b), at 2% (c), at 4% (d) and at 6% (e) of chord rotation...358

Figure 3-41: Moment chord rotation (a, e, f, g and h), beam rotation (b), column web panel rotation (c) and connection rotation (d)..361

Figure 3-42: Experimental test backbone curve (a) and cumulated energy respect to the 4% rotation......................... 362
Figure 3-43: FEM: (a) Moment rotation curve and (b) cumulated energy respect to the 4% rotation......................... 363
Figure 3-44: Experimental result against the FEM prevision both in terms of cyclic (a) and Back bone curve (b)..... 364
Figure 3-45: Failure mode: Experimental (a and c) against FEM PEEQ distribution (b, d and e)............................ 365
Figure 3-46: Plastic deformation on the column web panel: a and b) strain-gauge lecture, c) experimental test, d) FEM PEEQ distribution. 366
Figure 3-47: Rib strain gauges results: normalized strain versus chord rotation (a and b), PEEQ distribution on the FE model (c) and plastic deformation of the tested specimen (d and e). 367
Figure 3-48: Moment chord rotation (a), joint configuration: initial (b), at 2% (c), at 4% (d) and at 6% (e) of chord rotation. 369
Figure 3-49: Moment chord rotation (a, e, f, g and h), beam rotation (b), column web panel rotation (c) and connection rotation (d)....................................... 370

Figure 3-50: Experimental test backbone curve (a) and cumulated energy respect to the 4% rotation. 371
Figure 3-51: FEM: (a) Moment rotation curve and (b) cumulated energy respect to the 4% rotation. 372
Figure 3-52: Experimental result against the FEM prevision both in terms of cyclic (a) and Back bone curve (b)......373
Figure 3-53: Failure mode: Experimental (a and c) against FEM PEEQ distribution (b, d and e)..............................374
Figure 3-54: Column web panel plastic deformation: strain-gauge lecture (a and b), and experimental test observation (c)..375
Figure 3-55: Rib strain gauges results: normalized strain versus chord rotation (a, b and c), and plastic deformation of the tested specimen (d). 376
Figure 3-56: Moment chord rotation (a) and joint failure mode (b and c). 378
Figure 3-57: Moment chord rotation (a and e), beam rotation (b), column web panel rotation (c) and connection rotation (d)..380
Figure 3-58: Experimental test backbone curve (a) and cumulated energy respect to the 4% rotation. 381

Figure 3-59: FEM: (a) Moment rotation curve and (b) cumulated energy respect to the 4% rotation.......................... 383

Figure 3-60: Experimental result against the FEM prevision both in terms of cyclic (a) and Back bone curve (b)..... 384

Figure 3-61: Failure mode: Experimental (a, c and e) against FEM PEEQ distribution (b, d and f). 385

Figure 3-62: Moment chord rotation (a) and joint failure mode (b and c).. 387

Figure 3-63: Moment chord rotation (a, and e), beam rotation (b), column web panel rotation (c) and connection rotation (d).. 388

Figure 3-64: Experimental test backbone curve (a) and cumulated energy respect to the 4% rotation.......................... 389

Figure 3-65: FEM: (a) Moment rotation curve and (b) cumulated energy respect to the 4% rotation.......................... 391

Figure 3-66: Experimental result against the FEM prevision both in terms of cyclic (a) and Back bone curve (b)..... 392

Figure 3-67: Failure mode: Experimental (a, c and e) against FEM PEEQ distribution (b, d and f). 393

Figure 3-68: Moment chord rotation (a) and joint failure mode (b). 395

Figure 3-69: Moment chord rotation (a), beam rotation (b), column web panel rotation (c) and connection rotation (d)...395
Figure 3-70: Experimental result against the FEM prevision both in terms of moment rotation curve (a), and failure mode (b and c). 396
Figure 3-71: Moment chord rotation (a) and joint failure mode (b and c). 399
Figure 3-72: Moment chord rotation (a, e and f), beam rotation (b), column web panel rotation (c) and connection rotation (d)...400
Figure 3-73: Experimental test backbone curve (a) and cumulated energy respect to the 4% rotation. 401
Figure 3-74: FEM: (a) Moment rotation curve and (b) cumulated energy respect to the 4% rotation. 403
Figure 3-75: Experimental result against the FEM prevision both in terms of cyclic (a) and Back bone curve (b)......404
Figure 3-76: Failure mode: Experimental (a and c) against FEM PEEQ distribution (b and d). 405
Figure 3-77: Failure mode: Experimental (b, d, e and g) against FEM PEEQ distribution (a, c and h).....................406

Figure 3-78: Moment chord rotation (a) and joint failure mode (b and c). 408
Figure 3-79: Moment chord rotation (a, e, f, and g), beam rotation (b), column web panel rotation (c) and connection rotation (d). 409
Figure 3-80: Experimental test backbone curve (a) and cumulated energy respect to the 4% rotation. 410
Figure 3-81: FEM: (a) Moment rotation curve and (b) cumulated energy respect to the 4% rotation. 411
Figure 3-82: Experimental result against the FEM prevision both in terms of cyclic (a) and Back bone curve (b). 412
Figure 3-83: Failure mode: Experimental (a, c and e) against FEM PEEQ distribution (b, d and f). 413
Figure 3-84: Moment chord rotation (a) and joint failure mode (b and c). 415
Figure 3-85: Moment chord rotation (a, e, f, and g), beam rotation (b), column web panel rotation (c) and connection rotation (d). 416
Figure 3-86: Experimental test backbone curve (a) and cumulated energy respect to the 4% rotation. 417
Figure 3-87: FEM: (a) Moment rotation curve and (b) cumulated energy respect to the 4% rotation. 418

Figure 3-88: Experimental result against the FEM prevision both in terms of cyclic (a) and Back bone curve (b)......419

Figure 3-89: Failure mode: Experimental (a, c and e) against FEM PEEQ distribution (b, d and f). 420

Figure 4-1: comparison between the experimental tests in terms of backbone curve for: (a) ES1-TS-F and ES1-TS-E, (b) ES2-TS-F-C1 and ES2-TS-F-C2, (c) ES2-TS-E-C1 and ES1-TS-Esp-C, (d) ES2-TS-F and ES2-TS-E, (e) ES3-TS-E-C1, ES3-TS-E-C2 and ES3-TS-Esp-C and (f) ES3-TS-F and ES3-TS-E. 423

List of tables

Table 1.1: Experimental test on extended stiffened joint within the Equaljoints research program [1]. 283
Table 2.1: Coupon test results.. 292
Table 3.1: Tested specimens geometrical characteristics. 297
Table 3.2: ES1-TS-F-C2 - Experimental results..................... 299
Table 3.3: ES1-TS-E-C1 test results...................................... 326
Table 3.4: ES2-TS-F-CA test results. 337
Table 3.5: ES2-TS-F-C2 test result... 349
Table 3.6: ES2-TS-E-C1... 357
Table 3.7: ES2-TS-ESP-C test results. 368
Table 3.8: ES3-TS-F-C1 test results....................................... 377
Table 3.9: ES3-TS-F-C2 test results....................................... 386
Table 3.10: ES3-TS-E-C1 test results.................................... 398
Table 3.11: ES3-TS-E-C2 Test result.................................... 407
Table 3.12: ES3-TS-E-C2 test result. 414
Table 4.1: Differences between the experimental tests. 422
Table 4.2: Elastic stiffness comparison between: the analytical model, the experimental tests and the numerical prediction. 425

CHAPTER VII

Parametric Study

Introduction

In this Chapter, a comprehensive parametric study based on finite element simulations is presented. The modelling assumptions of FE models are validated in the previous Chapter. The investigated parameters are the influence of the variability of yield stress, the geometry of the connection, the geometry of the rib stiffener and the design performance level.

1 Investigated parameters

Starting from the ES1, ES2 and ES3 joints (designed and described in Chapter V), a wider range of assemblies were investigated by varying the following parameters:

- The yield strength variability ratio (being f_y the actual yield stress and $f_{y,d}$ the design yield stress of steel end-plate). This parameter was varied as 0.65, 0.77, 1.00 and 1.30 corresponding to steel grade S235, S275, S355, S460 assuming S355 with average yield stress equal to $\gamma_{ov}\times f_y$=443.75MPa (i.e. γ_{ov} =1.25 according to EC8 [16]) as reference material for RJs. In addition, both realistic and elastic-perfectly plastic stress-strain laws were considered for S355 in order to highlight the role of hardening on the joint response as respect to the analytical calculation of EC3:1-8.
- The influence of a further inner bolt row located in the center of the connection under both seismic and robustness scenario.
- The rib slope, considering two possible inclination 30° and 40°. Indeed, starting from the American practice (where

only rib with 30° are allowed in the prequalification procedure), the effect of a stocky rib was investigated.

- The rib thickness influence on the joint behavior starting from an unstiffened configuration (increasing the thickness of 5mm at time) up to a stocky rib with a thickness equal to 30mm.

The program of the parametric study is summarized in Table 1.1, Table 1.2 and in Figure 1-1. The mechanical response of the joints was evaluated under monotonic and cyclic loading, in order to simulate the effects alternatively induced by seismic action and column loss.

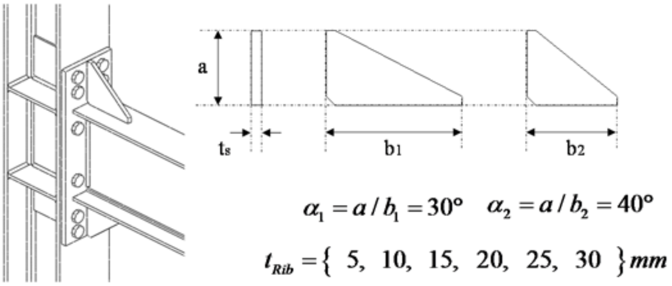

Figure 1-1: Investigated Rib parameters.

Table 1.1: Investigated variability of steel strength of the end-plate material.

Joint ID	Performance Level (*)	yield strength variability ratio $\bar{f} = f_y / f_{y,d}$				Bolt row in the center of the connection	
		$\bar{f} = 0.65$	$\bar{f} = 0.77$	$\bar{f} = 1$	$\bar{f} = 1.3$		
ES1-F	F	0.65	0.77	1.00	1.30	yes	no
ES1-E	E	0.65	0.77	1.00	1.30	yes	no
ES1-P	P	0.65	0.77	1.00	1.30	yes	no
ES2-F	F	0.65	0.77	1.00	1.30	yes	no
ES2-E	E	0.65	0.77	1.00	1.30	yes	no
ES2-P	P	0.65	0.77	1.00	1.30	yes	no
ES3-F	F	0.65	0.77	1.00	1.30	yes	no
ES3-E	E	0.65	0.77	1.00	1.30	yes	no
ES3-P	P	0.65	0.77	1.00	1.30	yes	no

* F = Full Strength Joint; E=Equal Strength Joint; P=Partial Strength Joint

Table 1.2: Investigated rib parameters.

Joint ID	Performance Level	Rib thickness						Rib slope	
		[mm]	[mm]	[mm]	[mm]	[mm]	[mm]	[°]	[°]
ES1-F	F	5	10	15	20	25	30	30°	40°
ES1-E	E	5	10	15	20	25	30	30°	40°
ES1-P	P	5	10	15	20	25	30	30°	40°
ES2-F	F	5	10	15	20	25	30	30°	40°
ES2-E	E	5	10	15	20	25	30	30°	40°
ES2-P	P	5	10	15	20	25	30	30°	40°
ES3-F	F	5	10	15	20	25	30	30°	40°
ES3-E	E	5	10	15	20	25	30	30°	40°
ES3-P	P	5	10	15	20	25	30	30°	40°

CHAPTER VII

---

2 Influence of variability of material yield strength

Figure 2-1 depicts the monotonic results, both in terms of chord and joint rotation, for the three beam-to-column assembly (i.e. ES1, ES2 and ES3) and for all examined performance levels (i.e. full, equal and partial strength).

In case of full strength joints (see Figure 2-1 a, Figure 2-2 a and Figure 2-3 a) no appreciable difference can be pointed out in terms of moment chord rotation curve, where for all the three assembly the curve are perfectly overlap except for the elastic-plastic material. Indeed, for this latter case since no hardening is taken into account the joint ultimate resistance is constant.

In order to focus the attention on the joint behavior, at 6% of the chord rotation, the contribution of the column web panel and connection were extrapolated. Therefore Figure 2-1 b, Figure 2-2 b and Figure 2-3 b show how perfectly in line with the chord rotation results, also the curve expressed in function of the joint rotation did not show considerable differences with respect to the end-plate yielding strength variation.

The only appreciable difference, for the full strength joints, can be found in the joint engagement respect to the whole rotational response. Indeed it is possible observe, with particular regard to the ES3-F assembly, increasing the yielding strength and thus the connection resistance, respect to the others component, the connection play a less important role in the whole joint rotation. In other words, the increasing the material strength, the connection is less engaged in the whole behavior definitions.

The same trend of results is more evident in the equal and partial strength results, where since the large engagement of the joint in the assembly replay, the yielding material influence is more evident both in terms of chord and joint rotation.

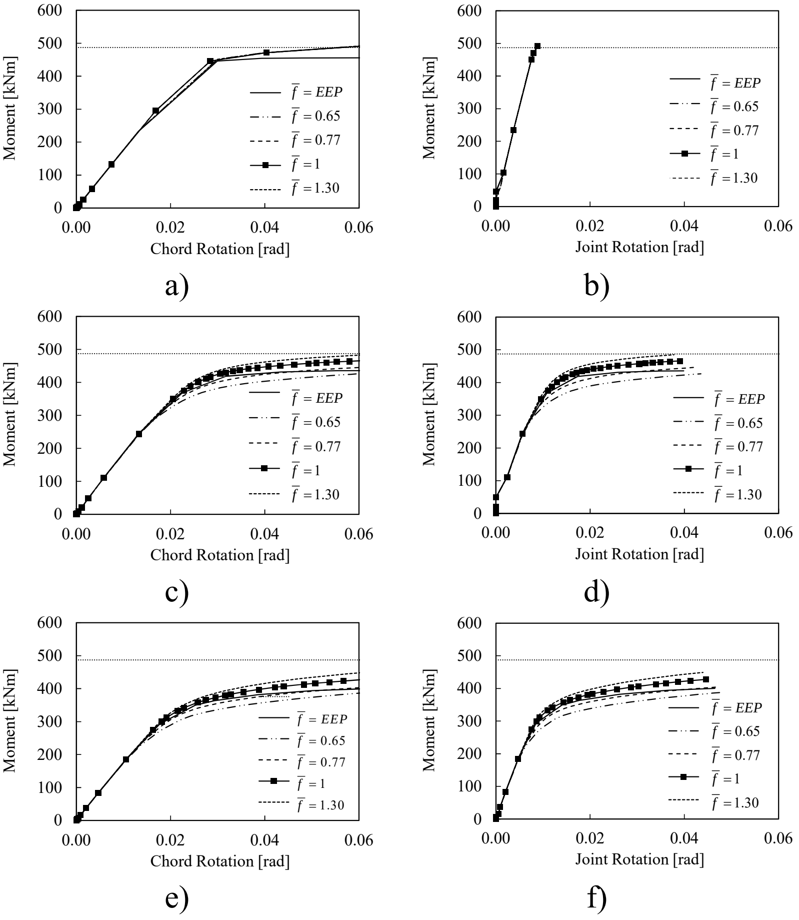

a) b)

c) d)

e) f)

Figure 2-1: Moment rotation curve of ES1 assembly designed as: full strength (a and b in terms of chord and joint rotation respectively), equal strength (c and d in terms of chord and joint rotation respectively) and partial strength e and f in terms of chord and joint rotation respectively).

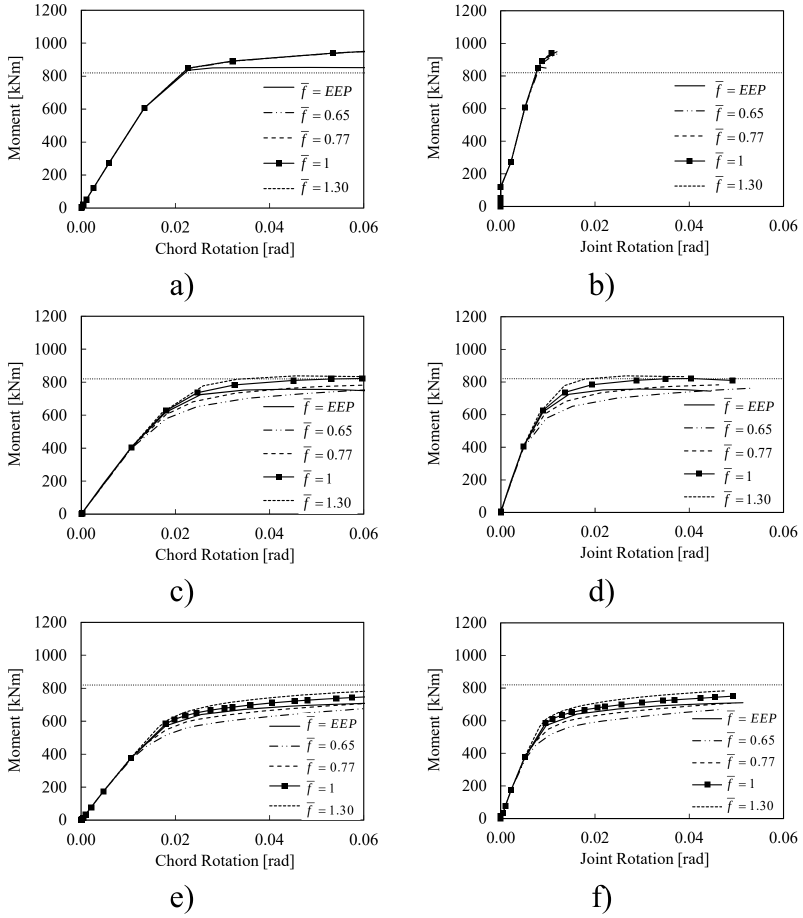

a) b)

c) d)

e) f)

Figure 2-2: Moment rotation curve of ES2 assembly designed as: full strength (a and b in terms of chord and joint rotation respectively), equal strength (c and d in terms of chord and joint rotation respectively) and partial strength e and f in terms of chord and joint rotation respectively).

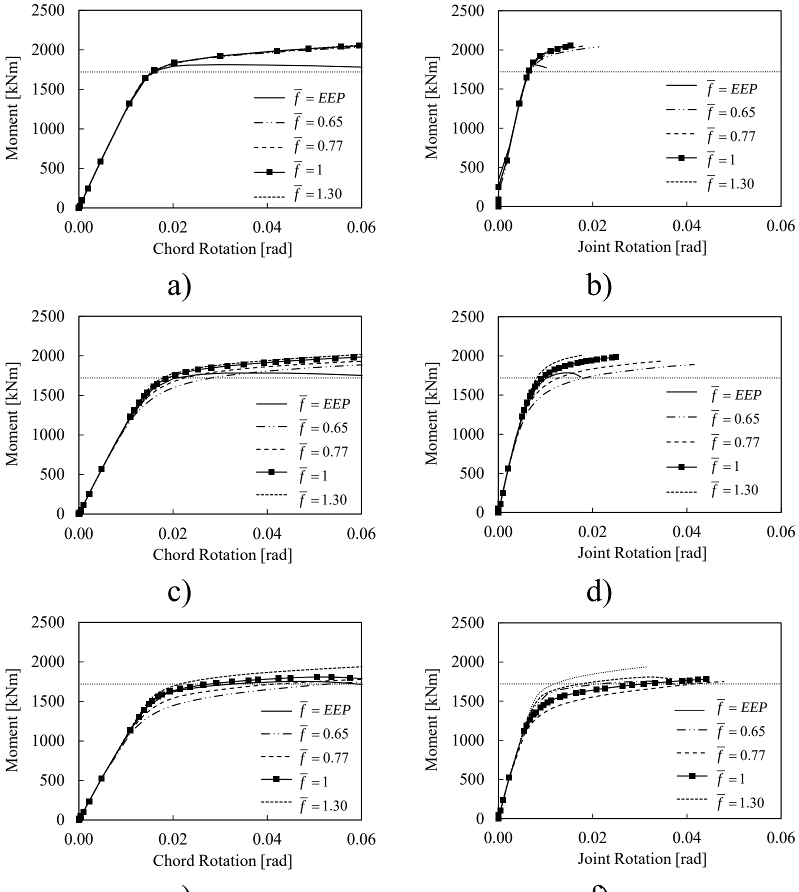

Figure 2-3: Moment rotation curve of ES1 assembly designed as: full strength (a and b in terms of chord and joint rotation respectively), equal strength (c and d in terms of chord and joint rotation respectively) and partial strength e and f in terms of chord and joint rotation respectively).

In case of ES3-P (see Figure 2-3 f), for instance, the increase of the joint engagement with the material strengthening is also confirmed by the PEEQ distribution in Figure 2-4.

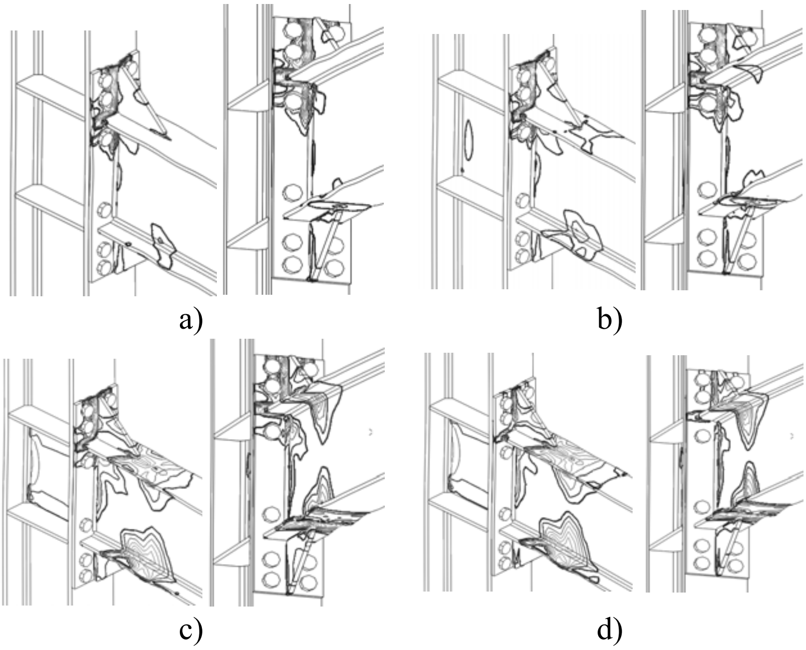

Figure 2-4: ES3-P PEEQ distribution changing the material yielding strength.

Finally, from the monotonic curve it possible to conclude that the end-plate material variability influence solely the joint bending capacity of the Equal and Partial joint, without showing significant variation for the full strength configurations. In the following (see Figure 2-5) also the histogram in function of the end-plate material confirm the previous results comparing the bending capacity variation at 4% of rotation.

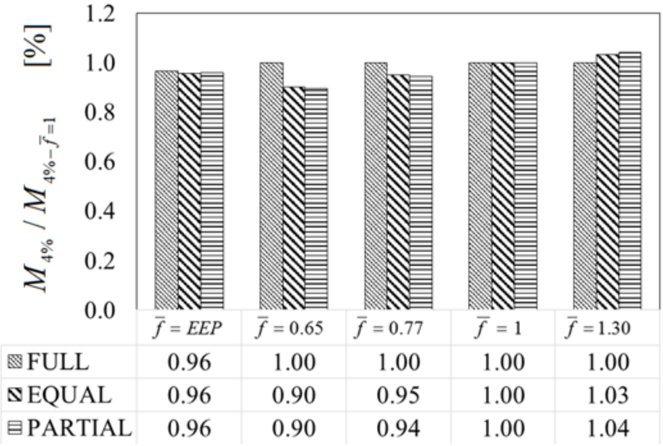

	$\bar{f} = EEP$	$\bar{f} = 0.65$	$\bar{f} = 0.77$	$\bar{f} = 1$	$\bar{f} = 1.30$
▨ FULL	0.96	1.00	1.00	1.00	1.00
⧅ EQUAL	0.96	0.90	0.95	1.00	1.03
⊟ PARTIAL	0.96	0.90	0.94	1.00	1.04

a)

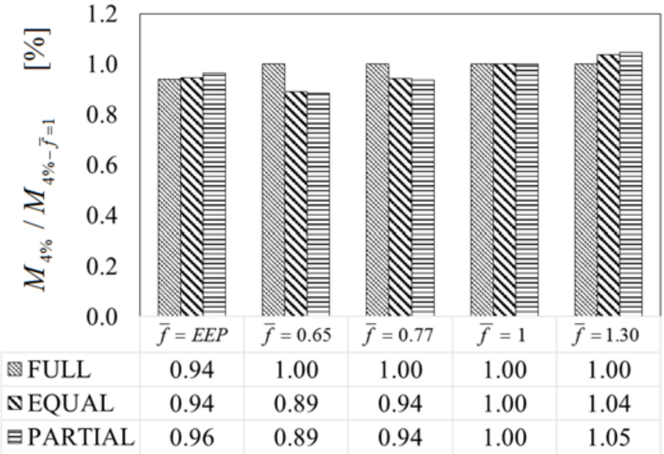

	$\bar{f} = EEP$	$\bar{f} = 0.65$	$\bar{f} = 0.77$	$\bar{f} = 1$	$\bar{f} = 1.30$
▨ FULL	0.94	1.00	1.00	1.00	1.00
⧅ EQUAL	0.94	0.89	0.94	1.00	1.04
⊟ PARTIAL	0.96	0.89	0.94	1.00	1.05

b)

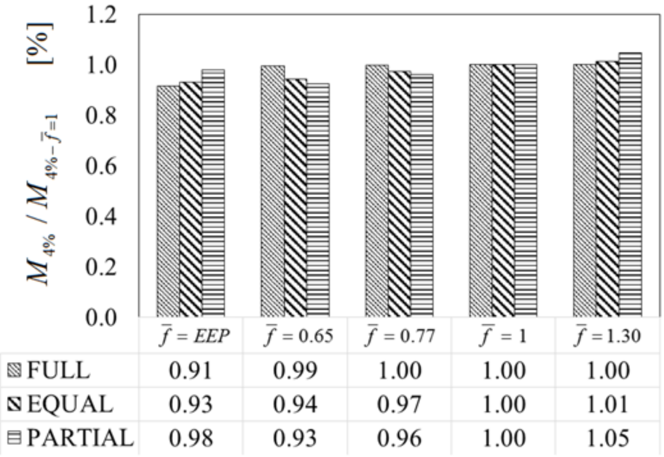

	$\bar{f} = EEP$	$\bar{f} = 0.65$	$\bar{f} = 0.77$	$\bar{f} = 1$	$\bar{f} = 1.30$
▩ FULL	0.91	0.99	1.00	1.00	1.00
▧ EQUAL	0.93	0.94	0.97	1.00	1.01
▤ PARTIAL	0.98	0.93	0.96	1.00	1.05

c)

Figure 2-5: Joint bending capacity in function of the performance design and the end-plate material variability for: ES1 (a), ES2 (b) and ES3 (c) joint configurations.

For the same investigation, as anticipated, also cyclic simulations were performed, since they allows quantifying the influence of end-plate material variability on the energy dissipation capacity of the joint.

For reason of brevity in the following only the results of the ES2 joint configuration are reported and discussed while all the others results are reported in the Annex. The cyclic moment rotation curve, the relative dissipated energy and the PEEQ distributions are hereinafter reported just for the ES2 designed as equal and partial strength for reason of brevity; all the others results are reported in the Annex. As already shown from the monotonic analyses, ES2-F are not really influenced by material variability; indeed as shown by the cyclic moment rotation curve, in all the case the curve shape is similar and the failure is due to the activation of the buckling waves on the bema flanges (see Figure 2-6). In line with this observation is also the distribution of the dissipated energy in the components; indeed it can be observed that almost for all the joints, all the plastic energy is concentrated at the beam extremities (see Figure 2-7).

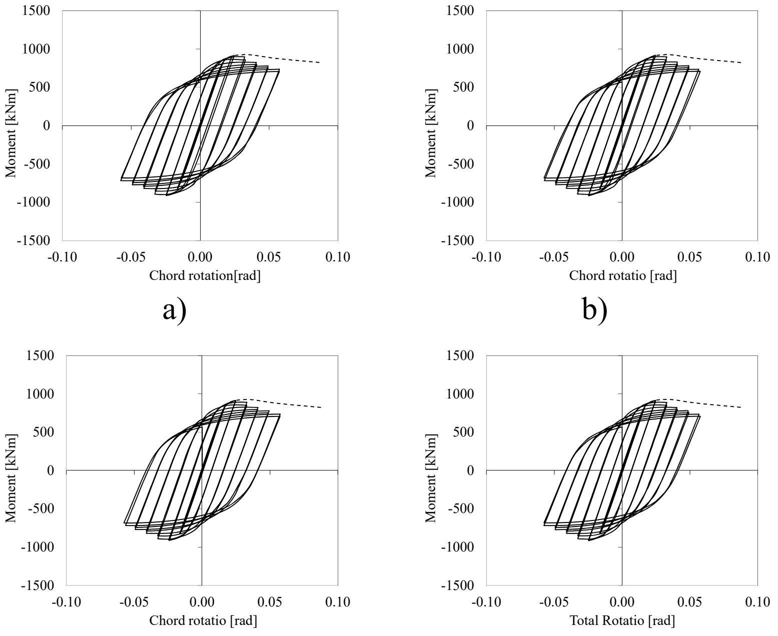

a) b)

c) d)

Figure 2-6: ES2-Full strength moment rotation curve changing the end-plate material.

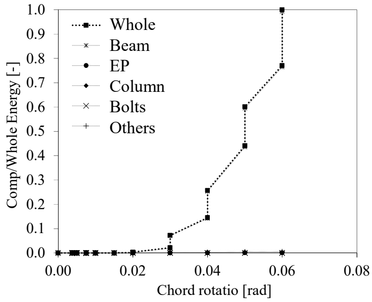
Whole
Beam
EP
Column
Bolts
Others
Comp/Whole Energy [-]
1.0
0.9
0.8
0.7
0.6
0.5
0.4
0.3
0.2
0.1
0.0
0.00
0.02
0.04
0.06
0.08
Chord rotatio [rad]

a)

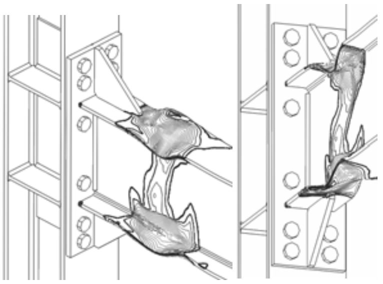

b)

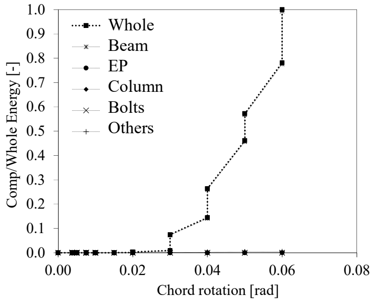
Whole
Beam
EP
Column
Bolts
Others
Comp/Whole Energy [-]
1.0
0.9
0.8
0.7
0.6
0.5
0.4
0.3
0.2
0.1
0.0
0.00
0.02
0.04
0.06
0.08
Chord rotation [rad]

c)

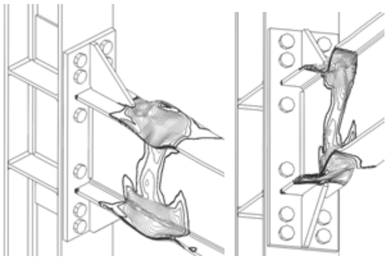

d)

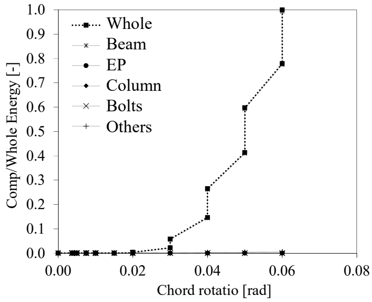
Whole
Beam
EP
Column
Bolts
Others
Comp/Whole Energy [-]
1.0
0.9
0.8
0.7
0.6
0.5
0.4
0.3
0.2
0.1
0.0
0.00
0.02
0.04
0.06
0.08
Chord rotatio [rad]

e)

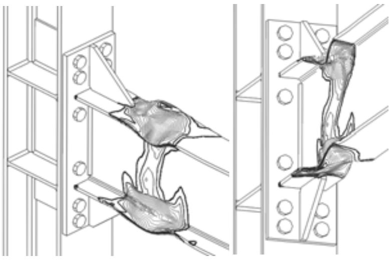

f)

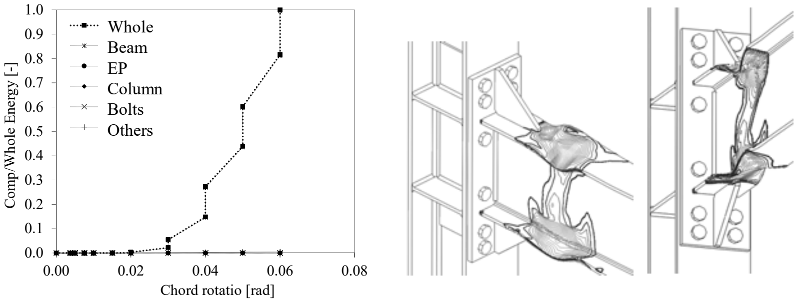

g) h)

Figure 2-7: ES2-Full strength joints dissipated energy for component (a, c, e, and g) and PEEQ distribution (b, d, g and h) for increasing material strengthening.

Different consideration can be done for the ES2-E; indeed in this case changing the end plate material, moment rotation curve change shape (see Figure 2-8). In particular, starting from the weakest material configuration, the cyclic curve presents series of resistance pick without the continuity with the following cycle. This behavior is mainly related to the end-plate since all the plastic deformation are concentrated. Increasing the material resistance the differences between the peak decrease, but conversely the pinching effect increase. Indeed, increasing the end-plate resistance the plastic deformation moves from the connected plate to the bolts and the beam. All these observations are confirmed by the PEEQ distribution and the dissipated energy for component reported in Figure 2-9. Indeed for the first material configuration (the weakest), all the plastic deformation is concentrated in the end-plate, while increasing the material yielding resistance the plastic deformation moves from the end-plate to the beam.

For $\overline{f} = 1$, the plastic deformation is well distributed between the beam and the connection (leaving the column web panel in elastic range). Therefore, increasing the yielding material strength, the dissipated energy is almost uniformly distribute between the end-plate, the bolts and the beam. In the last configuration, when the adopted material is 30% larger than the referring one, a large amount of dissipated energy and the relative PEEQ distribution are mainly concentrated in the connected beam (see Figure 2-9). Therefore as observed for ES2-E, the equal strength joint is able to ensure a balance resistance and hence an almost uniform plastic distribution between the connection and the beam. Moreover, the ductility limitation introduced in Chapter V ensure a ductile failure mode also for a joint with a material characteristics 35% less resistance than the design one

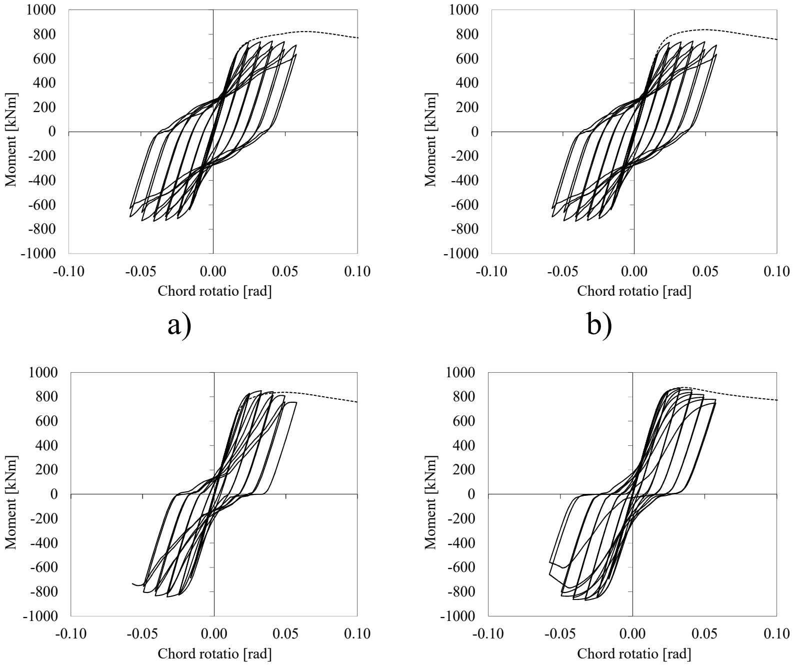

a) b)

c) d)

Figure 2-8: ES2-Equal strength moment rotation curve changing the end-plate material.

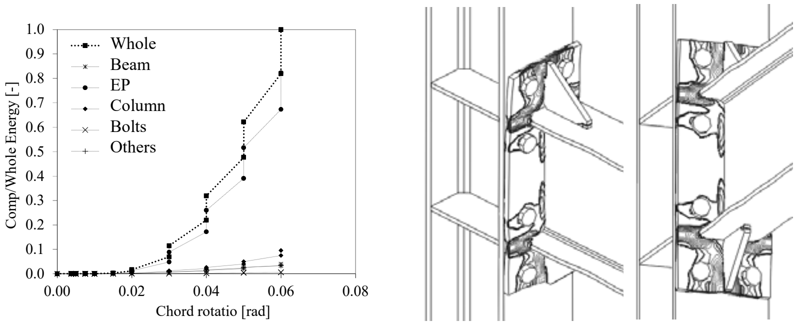

a) b)

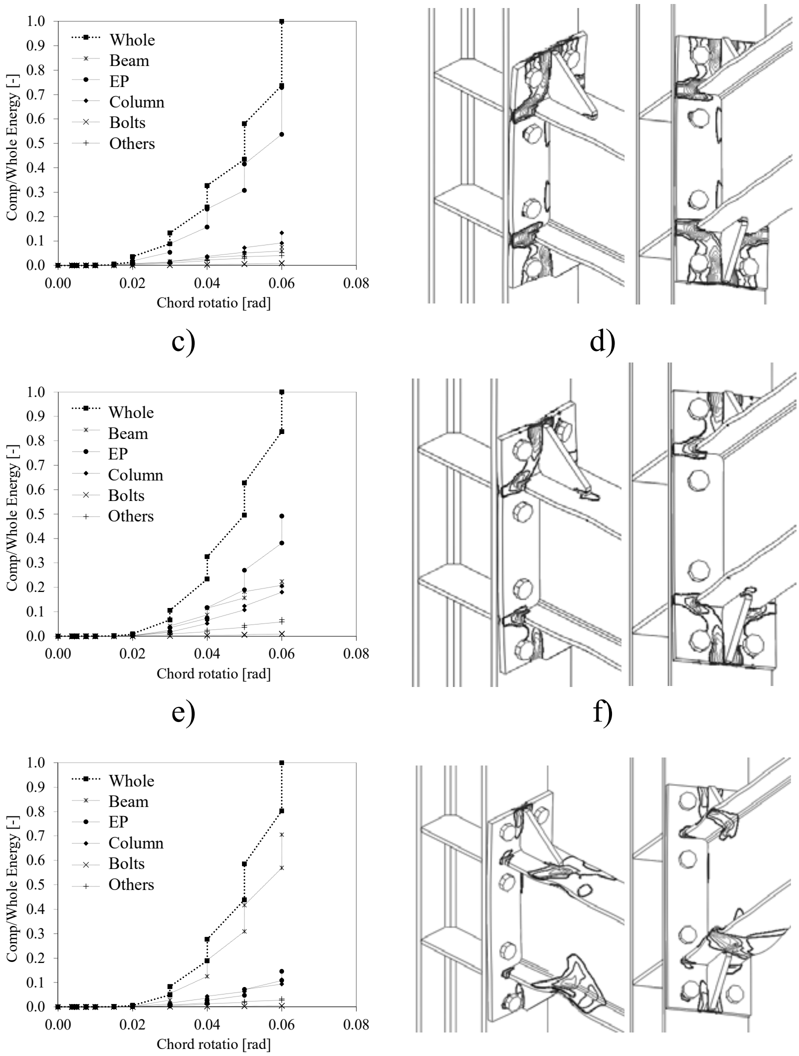

c) d)

e) f)

g) h)

Figure 2-9: ES2-Equal strength joints dissipated energy for component (a, c, e, and g) and PEEQ distribution (b, d, g and h) for increasing material strengthening.

The results of the partial strength joint ES2-P are in line with the previous one. Indeed, also in this case, changing the end-plate material, the plasticity distribution and the components involved in the failure mode change. Some differences can be observed from the moment rotation curve (see Figure 2-10) were increasing the material characteristics, a decrease of the pinching effect is observed. Thus also the dissipated energy as show in Figure 2-11 change; in particular has done before starting from the weak end-plate configuration to the more resistant it is possible observe the migration of the plastic deformation from the end plate, to the column web panel an then also to the beam.

In particular starting with the first configuration $\overline{f} = 0.65$, all plastic deformations are concentrated into the end-plate, while increasing its resistance also the column web panel is involved in plastic range (see Figure 2-11 c and d). $\overline{f} = 1$ configuration shows a balance situation where the plastic deformation are almost equally distributed between the column web panel and the end-plate, in line with the Partial strength joint with a balance column web panel design assumption. The last configuration $\overline{f} = 1.3$ show an increase of the plastic deformation in the column web panel, but at the same time also some PEEQ concentration on the beam (at the interface with the ribs). Moreover, in this case a small amount of energy was also concentrated in the bolts, that since the increase of the end-plate material resistance are working in plastic range showing a failure mode 2 and not 1 as they are designed to.

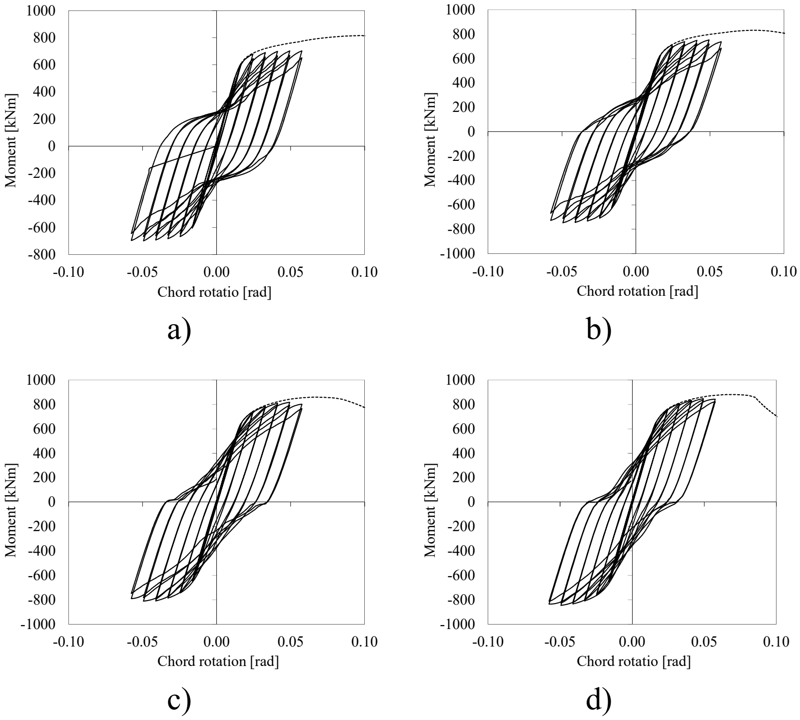

a) b)

c) d)

Figure 2-10: ES2-Partial strength moment rotation curve changing the end-plate material.

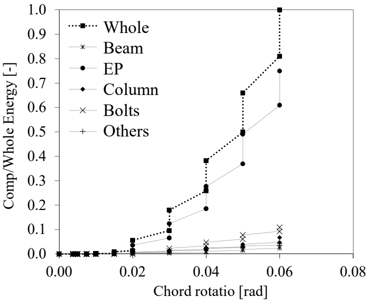
Comp/Whole Energy [-]
1.0
0.9
0.8
0.7
0.6
0.5
0.4
0.3
0.2
0.1
0.0
Whole
Beam
EP
Column
Bolts
Others
0.00
0.02
0.04
0.06
0.08
Chord rotatio [rad]

a)

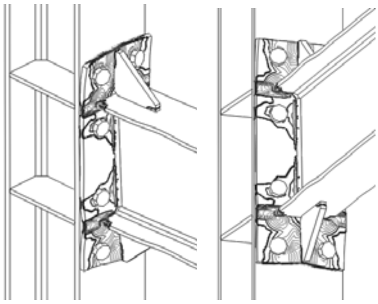

b)

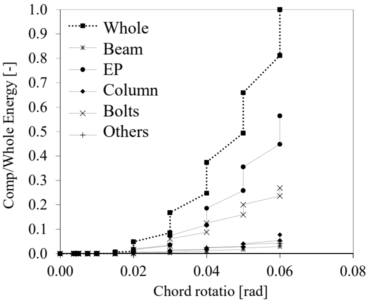
Comp/Whole Energy [-]
1.0
0.9
0.8
0.7
0.6
0.5
0.4
0.3
0.2
0.1
0.0
Whole
Beam
EP
Column
Bolts
Others
0.00
0.02
0.04
0.06
0.08
Chord rotatio [rad]

c)

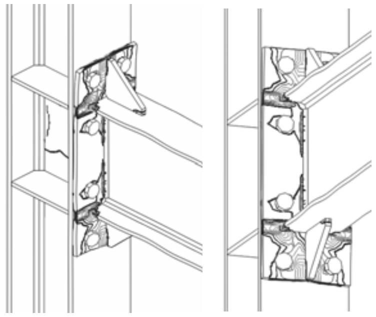

d)

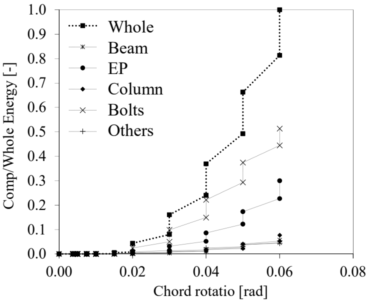
Comp/Whole Energy [-]
1.0
0.9
0.8
0.7
0.6
0.5
0.4
0.3
0.2
0.1
0.0
Whole
Beam
EP
Column
Bolts
Others
0.00
0.02
0.04
0.06
0.08
Chord rotatio [rad]

e)

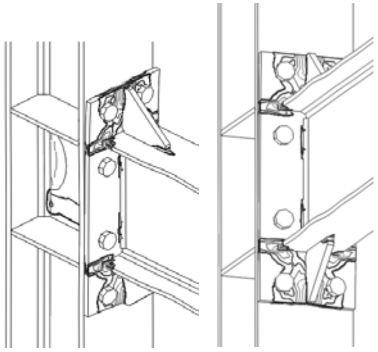

f)

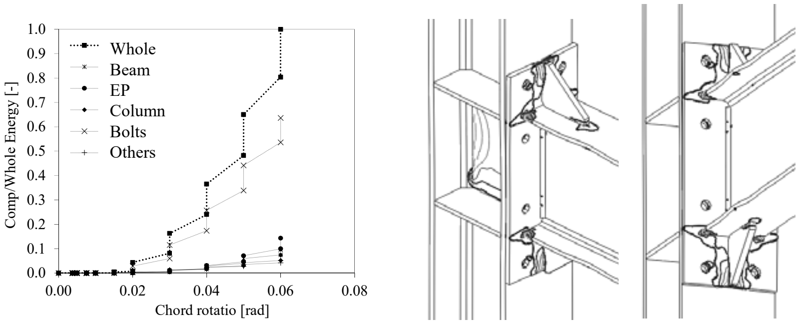

g) h)

Figure 2-11: ES2-Partail strength joints dissipated energy for component (a, c, e, and g) and PEEQ distribution (b, d, g and h) for increasing material strengthening.

Figure 2-12 reports the energy dissipated at 4% of chord rotation by each joint component per beam-to-column assembly.

Coherently with the response curves already discussed, full strength joints show that almost all internal energy dissipation is concentrated into the beam (about 98% for all specimens) independently from the end-plate material configuration.

As anticipated, both the equal and the partial strength joints behavior is more affected by the end-plate yielding variability; in particular the results introduced Figure 2-12 b and c highlight the migration at 4% of chord rotation of the plastic deformation from the end-plate to the others component with the material variability. In particular, for the equal strength joints it is possible to observe how the plastic deformation in the beam increase with the investigated configuration, and at the same time the plastic deformation decries in the end-plate. The same trend is confirmed also for the partial strength joint, where another important observation regards the dissipated energy by the column web panel that in the equal strength configuration is almost 0. Indeed, partial strength joint show an increase of the plastic deformation in the column web pane up to the configuration. After that a small decrease in the column can be observed since in this latter case the beam has a significant increase of plastic deformation.

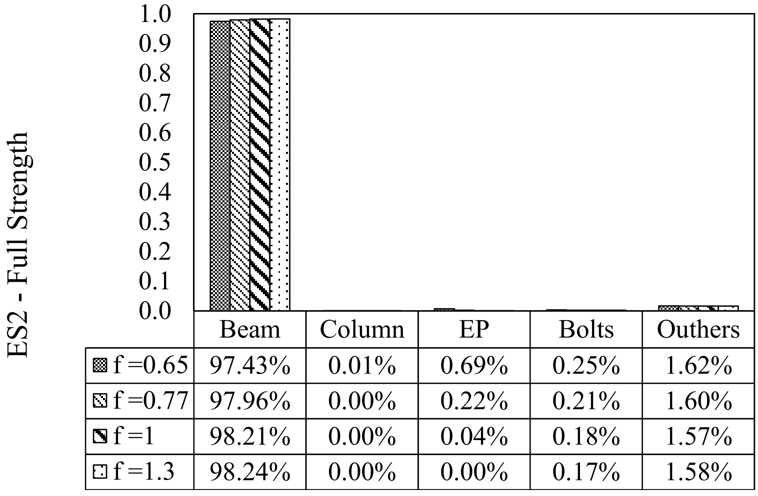

	Beam	Column	EP	Bolts	Outhers
▩ f =0.65	97.43%	0.01%	0.69%	0.25%	1.62%
▧ f =0.77	97.96%	0.00%	0.22%	0.21%	1.60%
◩ f =1	98.21%	0.00%	0.04%	0.18%	1.57%
⬚ f =1.3	98.24%	0.00%	0.00%	0.17%	1.58%

a)

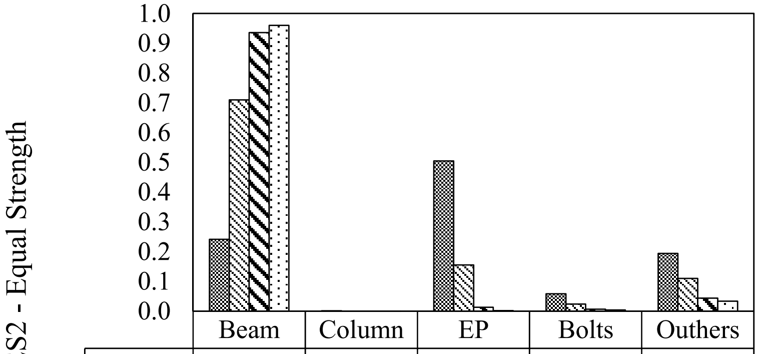

	Beam	Column	EP	Bolts	Outhers
▩ f =0.65	24.15%	0.14%	50.46%	5.80%	19.45%
▧ f =0.77	70.99%	0.08%	15.56%	2.38%	10.99%
◩ f =1	93.61%	0.01%	1.34%	0.64%	4.39%
⊡ f =1.3	95.97%	0.01%	0.19%	0.43%	3.41%

b)

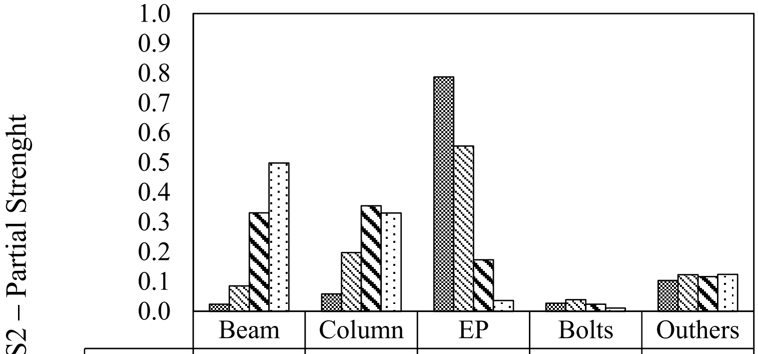

	Beam	Column	EP	Bolts	Outhers
▩ f =0.65	2.39%	5.85%	78.74%	2.68%	10.35%
▧ f =0.77	8.54%	19.75%	55.50%	3.89%	12.32%
◩ f =1	33.11%	35.48%	17.29%	2.44%	11.69%
⊡ f =1.3	49.85%	32.99%	3.59%	1.15%	12.43%

c)

Figure 2-12: Dissipated energy at 4% of rotation for: Full strength (a), equal strength (b) and Partial strength (c).

3 Bolt row in the central axis of the connection

As anticipated, the influence of an additional bolts row in the symmetry axis of the connection was investigated considering to possible scenario: (i) seismic actions and (ii) column loss.

Figure 3-1 shows (at 4% of the chord rotation) the contribution in terms of both resistance and elastic stiffness between the RJ and the joints with the additional bolt row in the middle of the connections (i.e. MBRJ). As it can be observed no appreciable differences can be pointed out as well as for the results of the cyclic analysis (see Figure 3-2 to Figure 3-4). The unique differences can be observed in case of partial strength joints. Indeed, ES2-P and ES3-P show a slightly larger dissipated energy when an additional bolt row is introduced. This evidence is due to the slightly increasing of the cycle's area due to a smaller gap opening between the two configurations (RJ and MBRJ).

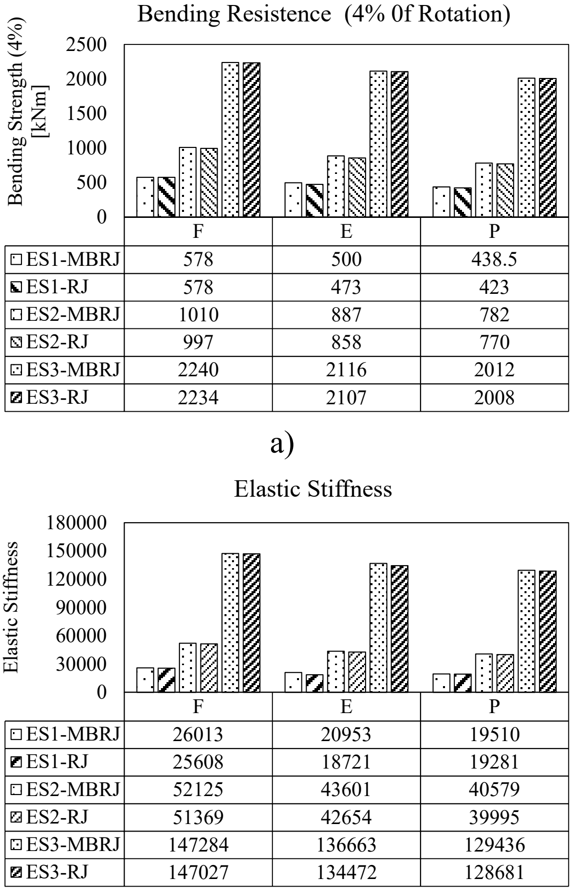

	F	E	P
□ ES1-MBRJ	578	500	438.5
▧ ES1-RJ	578	473	423
□ ES2-MBRJ	1010	887	782
▧ ES2-RJ	997	858	770
□ ES3-MBRJ	2240	2116	2012
▨ ES3-RJ	2234	2107	2008

a)

	F	E	P
□ ES1-MBRJ	26013	20953	19510
▨ ES1-RJ	25608	18721	19281
□ ES2-MBRJ	52125	43601	40579
▨ ES2-RJ	51369	42654	39995
□ ES3-MBRJ	147284	136663	129436
▨ ES3-RJ	147027	134472	128681

b)

Figure 3-1: Comparison between the bending capacity of the RJ and MBRJ joints in terms of : bending capacity (a) and elastic stiffeness (b).

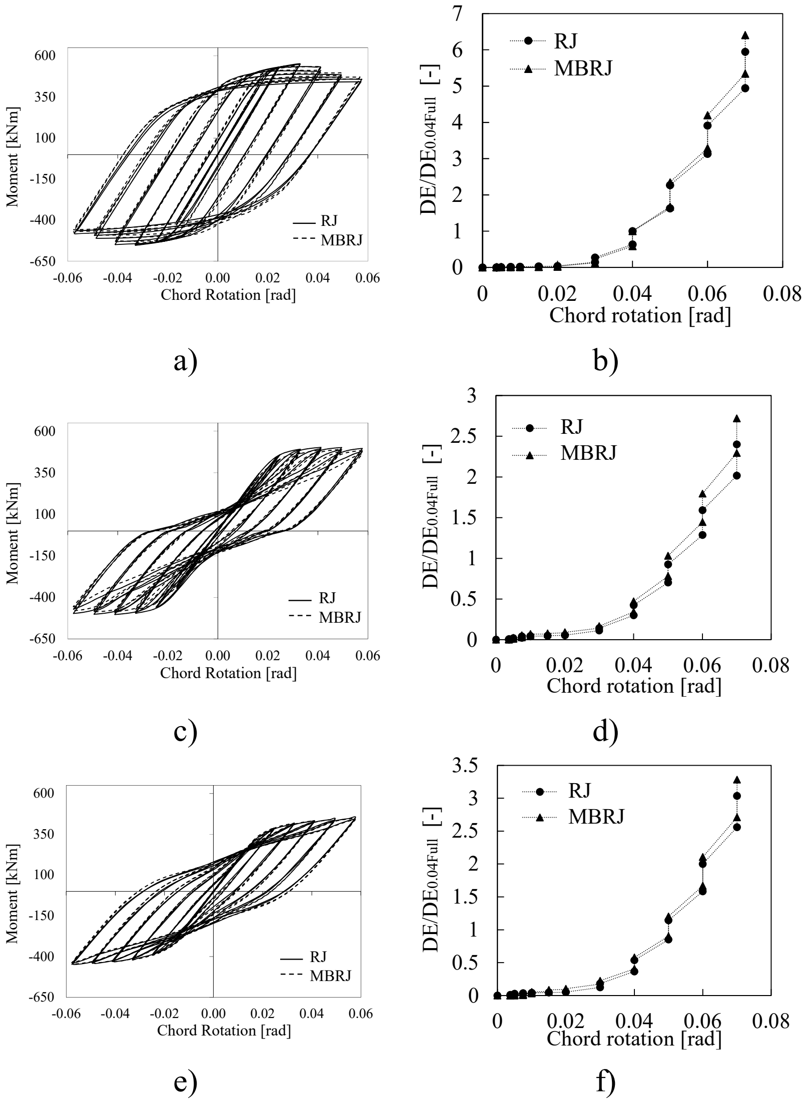

Figure 3-2: ES1 comparison between RJ and MBRJ in terms of moment rotation curve and dissipated energy ration respectively for Full, equal and partiacl strength joints.

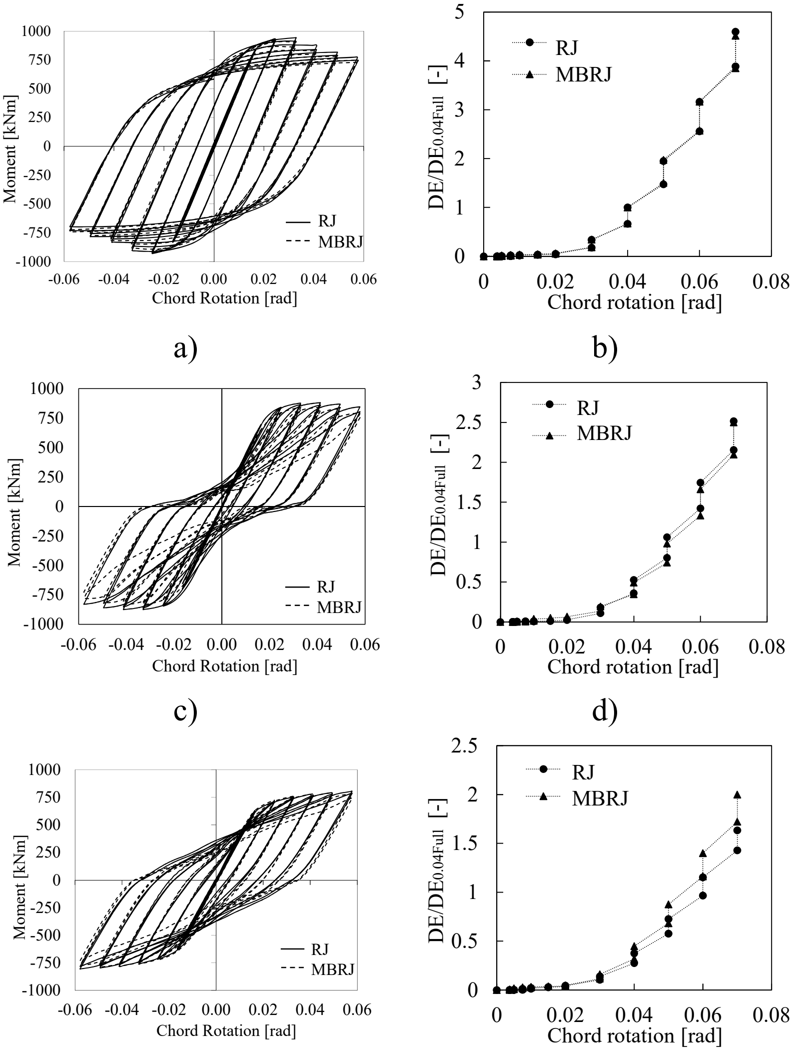

a) b)

c) d)

e) f)

Figure 3-3: ES2 comparison between RJ and MBRJ in terms of moment rotation curve and dissipated energy ration respectively for Full, equal and partiacl strength joints.

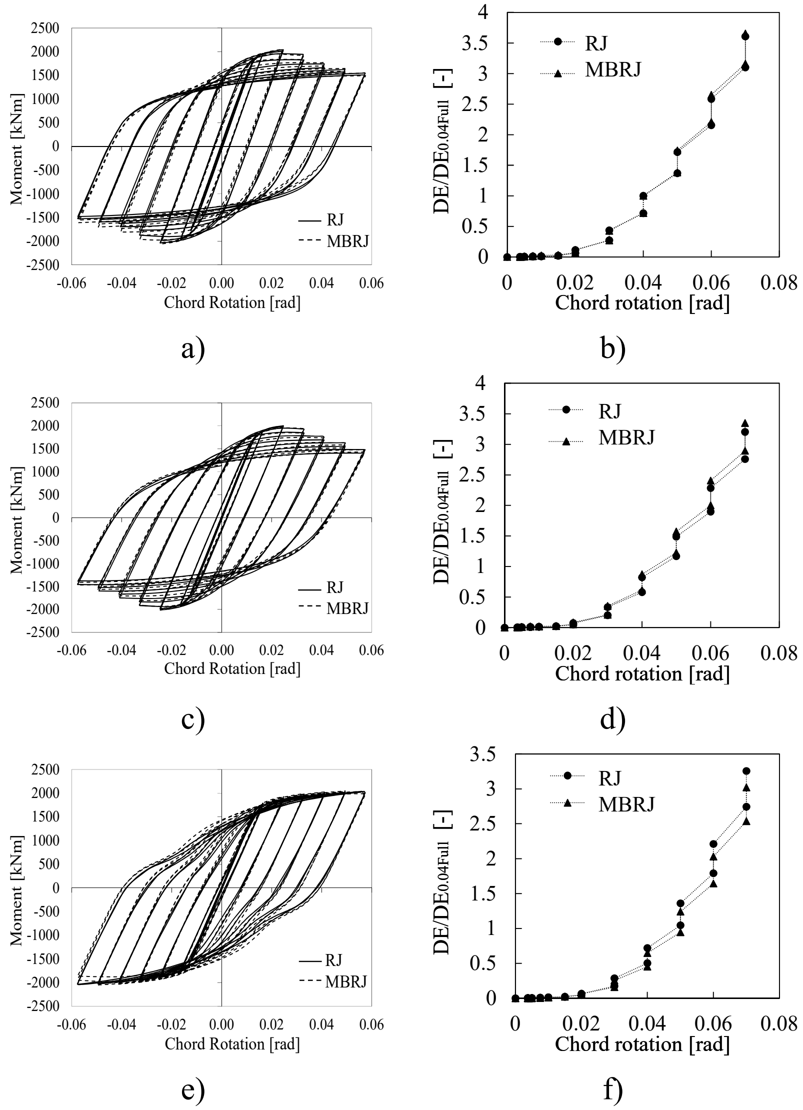

a) b)

c) d)

e) f)

Figure 3-4: ES3 comparison between RJ and MBRJ in terms of moment rotation curve and dissipated energy ration respectively for Full, equal and partiacl strength joints.

The differences between the ES2-P and ES3-P in terms of the dissipated energy, as anticipated, is due different cycle's area; the introduction of an additional bolt row decries the pinching effect at large value of rotation (see Figure 3-5).

However, the difference is small and can be neglected respect to the advantage to use one less bolt row in terms of both material and executional time costs.

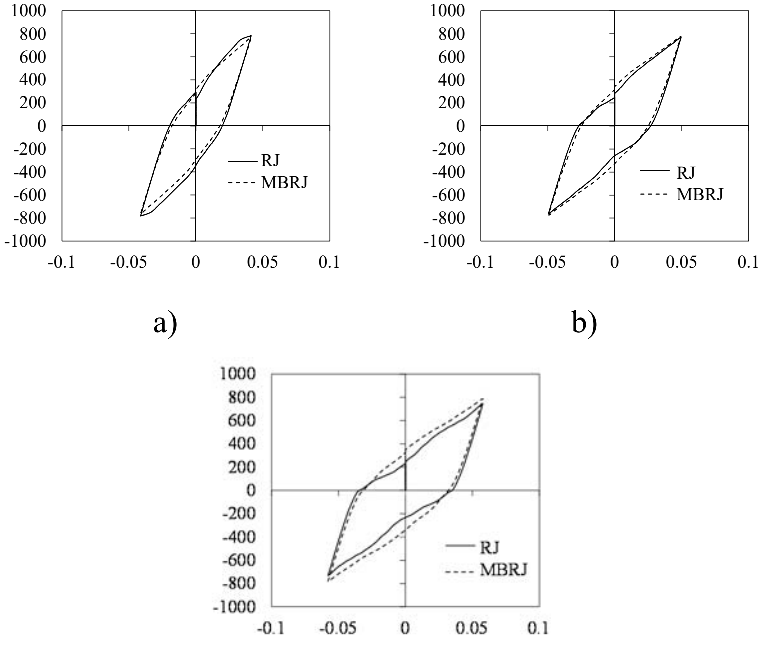

a)

b)

c)

Figure 3-5: Cycles shape comparison between RJ and MBRJ at: 5% (a), 6% (b) and 7% (c) of chord rotation.

Even though the presence of the additional bolt row is negligible for seismic actions, it is very important under column loss, where the joints are subjected to large rotation demand and significant values of bending moment and axial loads, developing due to the catenary action (see Figure 3-6).

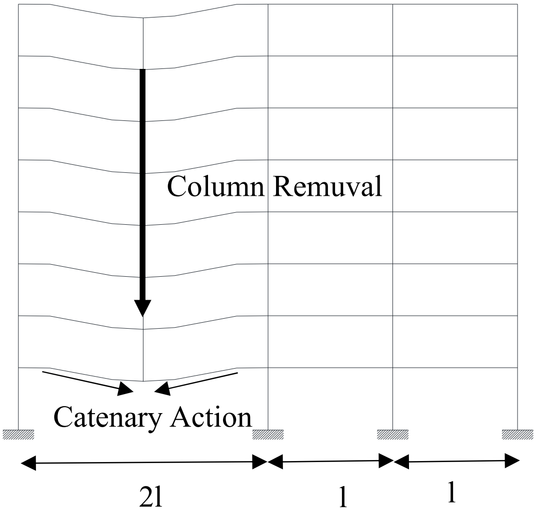

Figure 3-6: Column removal scenario.

Under column loss, the bending moment at column face calculated with the first order theory (Eq. (1)) does not correspond to the actual bending moment acting on connection, which also depends on the moment developed by the axial tensile force in large deformation.

$$M^{I} = V \cdot L_{b} / 2 \qquad (1)$$

Where V is the shear action at the middle section of the beam and L_b is its length. Hence, the bending moment on the connection can be calculated as follows:

$$M_{connection} = M^{I^{\circ}} + M^{II^{\circ}} = M^{I^{\circ}Order} - N_{Cat} \cdot \Delta \qquad (2)$$

Where N_{cat} is the normal action develop in the beam due to the catenary action, Δ is the vertical displacement.

Figure 3-7 shows the comparison between RJs and MBRJs in terms of first and second order bending moments and yield line pattern with the corresponding PEEQ indexes.

As expected, full strength joints show both similar response curves and plastic deformation pattern (see Figure 3-7). Moreover, the presence of additional bolt row allows developing the full plastic catenary action into the beam reducing the gap opening. The connection remains practically closed and follow the column deformations; indeed as it can be observed there is the formation plastic pattern from the upper column to the beam flange, with a develop of a plastic hinge (with a very low neutral axis is observed).

This failure mode is activated by the presence of catenary action developing into the beam. Indeed, the resultant of tensile strength in the connection is significantly larger than the resultant of compression forces.

Differently from the Full strength joint, in both Equal and Partial strength configuration the effectiveness of the additional bolt row is evident. Indeed, in these types of joints, the weaker component is the connection and increasing its axial strength is beneficial to resist catenary action and to improve the rotation capacity.

Figure 3-8 and Figure 3-9 clearly show that the increase in second order moment due to the presence of an additional bolt row is significant and proportional with the rotational level. Moreover, an additional difference, between the Full strength configuration and the Equal and Partial, is that in these latter cases the developing of the arc effect for low value of rotation (around 5%).

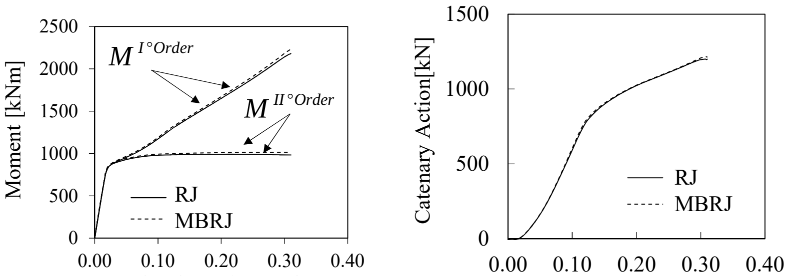

a) b)

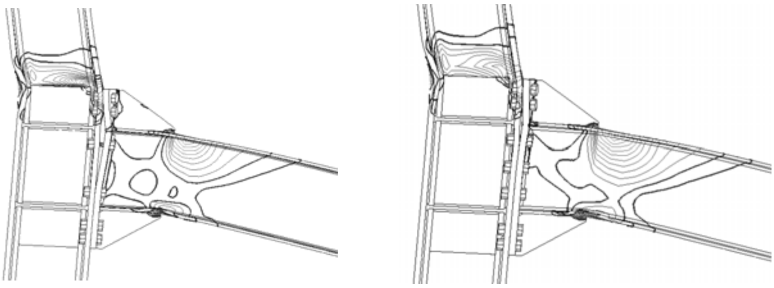

c) d)

Figure 3-7: ES2-F Comparison between RJ and MBRJ joint configuration in terms of: moment rotation curve (a), Normal action in the beam (b) and PEEQ distribution at 20% of rotation (c and d).

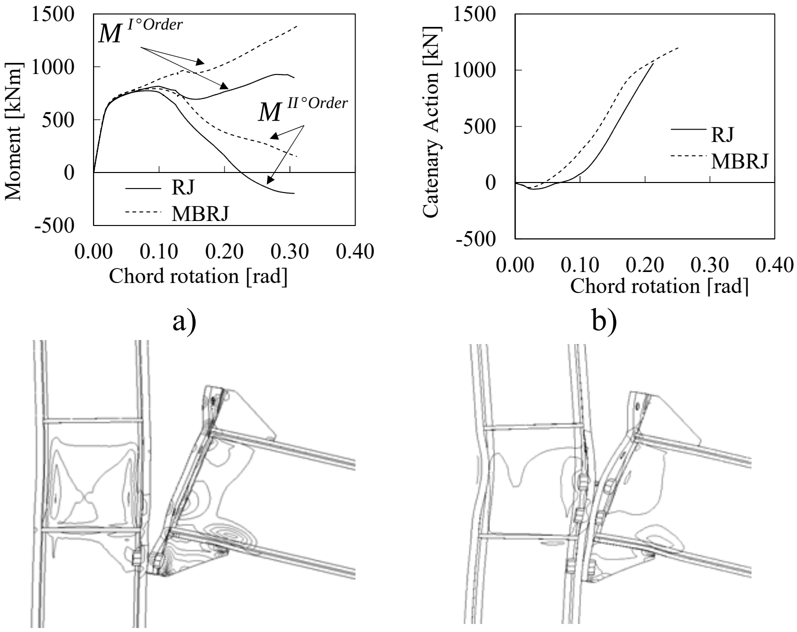

a) b)

c) d)

Figure 3-8: ES2-E Comparison between RJ and MBRJ joint configuration in terms of: moment rotation curve (a), Normal action in the beam (b) and PEEQ distribution at 20% of rotation (c and d).

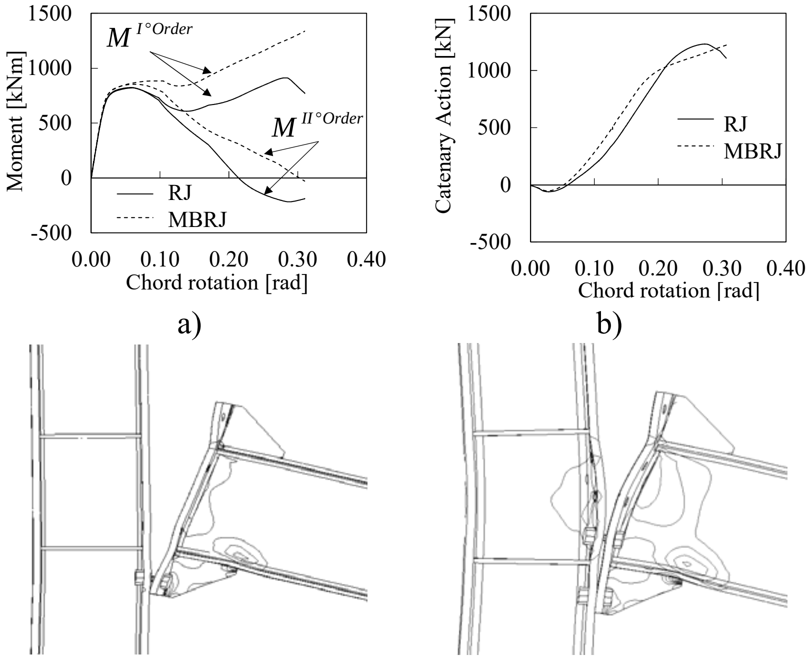

a) b)

c) d)

Figure 3-9: ES2-P Comparison between RJ and MBRJ joint configuration in terms of: moment rotation curve (a), Normal action in the beam (b) and PEEQ distribution at 20% of rotation (c and d).

4 Influence of Rib geometry

As anticipated in Chapter V, the rib stiffeners strongly influence the joint response both in terms of resistance and in terms of stiffness. Despite the significant advantages brought by these plates, the European [7] code does not give any prescription to regulate their use and provides no limitations regarding their application. Therefore, in this paragraph, starting from the consideration investigated in the previous chapter, aspect as the rib thickness and its slope will be presented and investigated by means of a broad parametric analysis.

All the beam-to-column assembly (ES1, ES2 and ES3) for all the design performance level are investigated as reported in Table 1.2.

4.1 Rib stiffener contribution

The first step of this analysis is investigate in in which terms the rib stiffener can modify the mechanical behavior of extended end-plate joints. Therefore, a set of beam-to-column joints have been analyzed considering four types of arrangements of the stiffeners: with rib stiffeners on both beam flanges (hereinafter identified as RS), unstiffened (U), with rib just on the tension side (RST) and with rib just on the compression side (RSC). The results of these analyses are compared in terms of: moment rotation curve, equivalent plastic strain (i.e. PEEQ) and distribution of contact pressure (i.e. CPRESS).

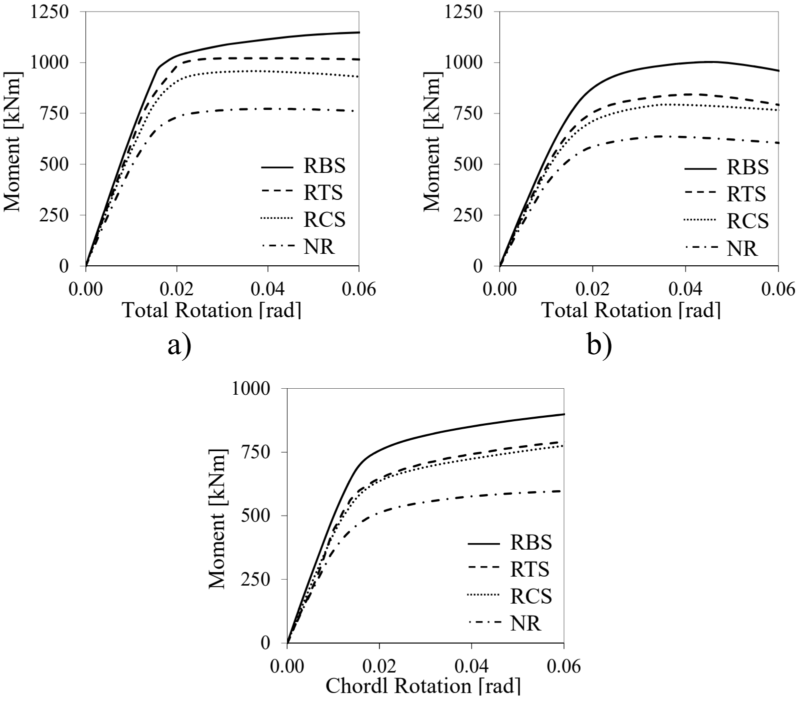

a) b)

c)

Figure 4-1: ES-2 Moment rotation curve: a) full strength, b) equal strength, c) partial strength and d) geometrical sketch.

Figure 4-1 shows the results for the ES-2 beam to column assembly for all the performance levels introduced. It can be observed the differences in terms of strength and stiffness between the stiffened and unstiffened joints.

However, it is not so distinguishable the difference between the models with just one stiffener, whether it is in the tension or in the compression side. In both cases, there is a comparable increase of resistance and stiffness with respect to the unstiffened joint; however, this increase is caused by two completely different mechanisms. In ES-2-RTS, the rib on the tension side influences the yielding line distribution and hence the resistance of each bolt row on tension side, while in the ES-2-RCS the resistance increases due to the lowering of the compression center and the relative increase of the internal level arm.

The arguments brought find confirmation in the yielding line distribution (see Figure 4-2). It is important to notice how the rib presence in the tension side strongly influence the activated T-Stub mechanism.

Figure 4-2c shows the distribution of the contact pressure (CPRESS) on the end-plate for RS-T and RS-C cases. As it can be observed the presence of the rib on compression side concentrates the contact forces within the projection of the rib area on the end-plate, namely out of the beam flange in compression. On the other hand, the presence of the rib in tension clearly highlights that the bolt rows above the beam flange in tension are more engaged than the one below, thus clarifying that the resultant of the tension resistance of the connection is located above the beam flange. These results confirm that the lever arm of the resultant of tension and compression strength of ES joints is larger than the beam depth.

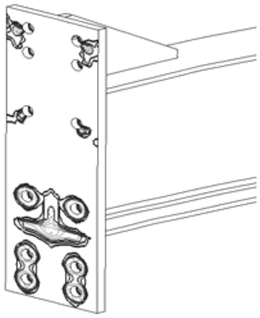

a)

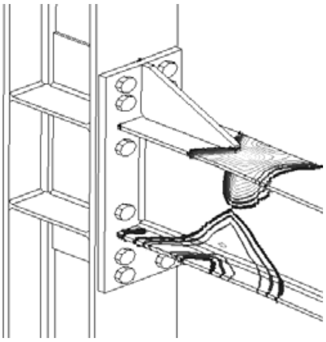

b)

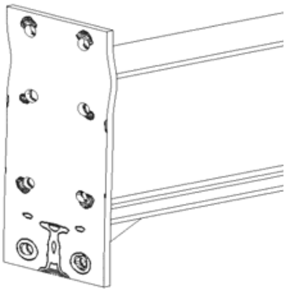

c)

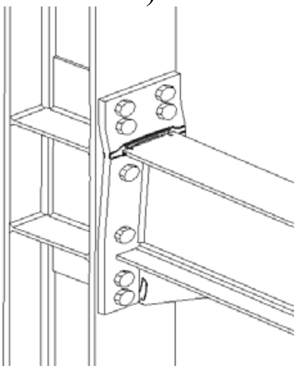

d)

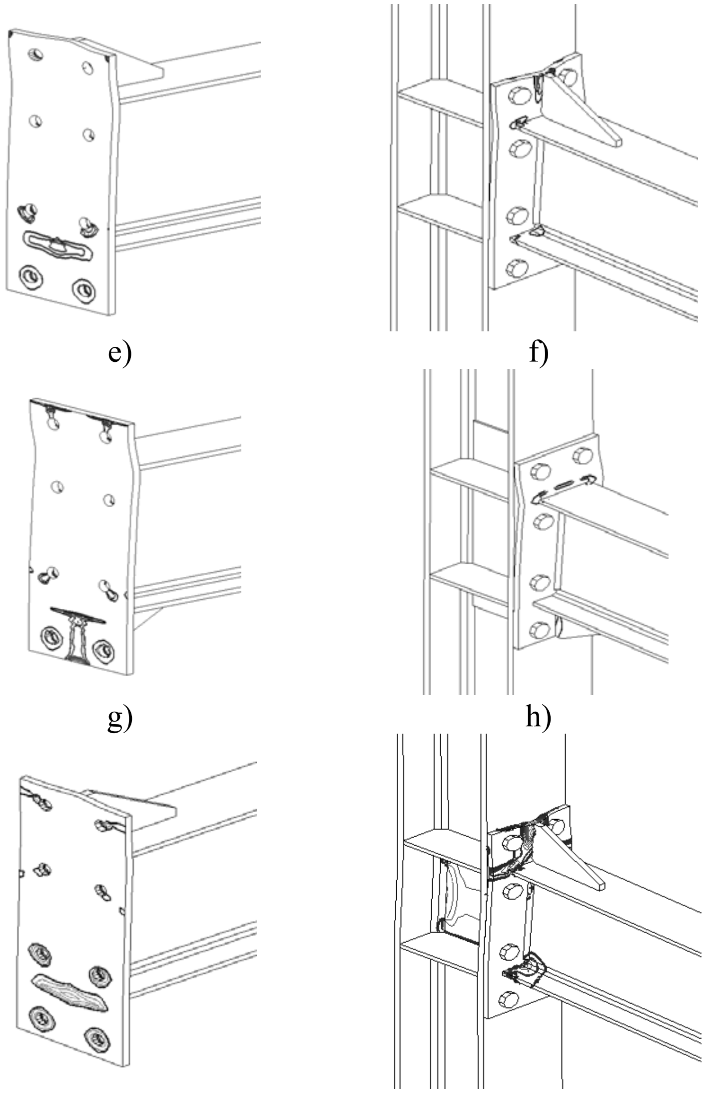

e) f)

g) h)

i) l)

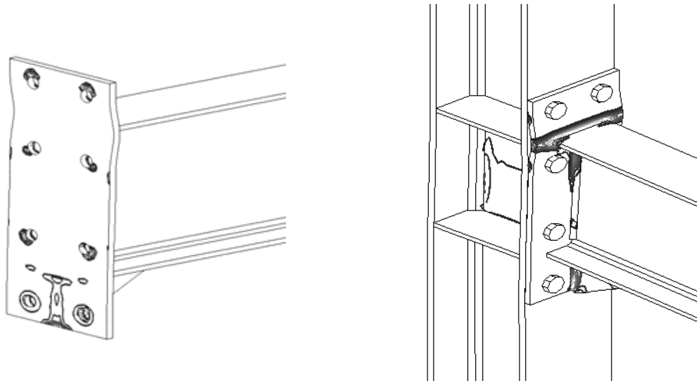
m) n)

Figure 4-2: Yielding line (PEEQ) and contact pressure (CPRESS) distribution.

4.2 Thickness of rib stiffener

Once the importance of the ribs has been clarified and the mechanisms that bring the changes in the joint behavior have been identified, it is important to determine to which extent the geometrical parameters (thickness and inclination) are determining the stiffeners' effectiveness.

As discussed, the European [7] code does not account for this kind of stiffeners, therefore no regulations could be found in the current code version. Nevertheless, some guidelines could be found in research studies and in the international steel codes framework. Indeed as anticipated in Chapter III, AISC 358 [4], in the prequalification procedures, introduces two important limitations on the rib thickness:

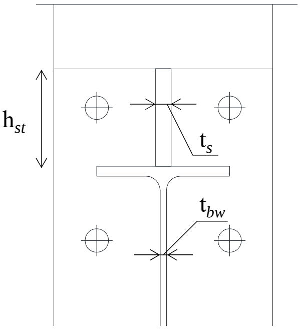

Figure 4-3: Rib and beam geometrical parameters.

$$\frac{h_{st}}{t_s} \geq 0.56 \cdot \sqrt{\frac{E}{F_{ys}}} \qquad (3)$$

$$t_s \geq t_{bw} \cdot \left(\frac{F_{yb}}{F_{ys}} \right) \qquad (4)$$

Where: h_{st} is rib height, t_s is rib thickness, E is steel elastic modulus, F_{ys} is rib steel yielding value and F_{yb} it is beam steel yielding value. According to the American code, the designers have to verify the rib against buckling and at the same time, it is imposed for the rib to have a greater thickness than the beam web (for the same steel properties). Both limitations have the same purpose to avoid rib buckling and keep the plates in elastic range to preserve their efficiency. Having in mind these considerations, the rib thickness was varied starting from a value of 5 mm up to 30 mm in the current parametric study. In order to investigate the rib's efficiency function of its thickness and at same time verify if the limitations introduced for the American configurations could be applied also for the European joints.

Therefore, for each investigated configurations the AISC358-16 [4] verification is carried out as well in order to compare the numerical results with the code prescriptions. Table 4.1 summarizes the analytical checks while Figure 4-4 show the results in terms of moment - joint rotation curve.

The rib thickness plays a central role in the global response of the joint assembly. The results in terms of moment joint rotation curves show a strong dependency of the ultimate resistance and joint plastic engagement with the rib thickness. This phenomenon is explained by the instability that occurs in the stiffening plates on the compression side.

The results presented in Figure 4-4 show how full strength joints, for values of rib thickness not meeting the buckling limitation, are strongly influenced by the value of the thickness. Meanwhile, when the thickness increases and overcomes the limit value (see Table 4.1), the joint's ultimate capacity remains constant.

For instance, ES1 models show a strong dependency with the rib thickness up to 10mm, value beyond which the joint resistance and stiffness are not affected regardless of the amount of plastic involvement of the connection. AISC regulations are in line with the new found results confirming that rib thickness values less than 15mm do not meet the requirements.

Table 4.1: AISC verifications for ribs thickness parametric analysis.

Joint ID	Beam	Rib		Ratio	AISC Prescriptions	
	t_{bw}	t_s	h_{st}		Thickness Eq. (4)	Buckling Eq. (3)
	mm	mm	mm	-		
ES1	8	0	200	0.0	-	-
		5	200	0.6	Not Satisfy	Buckling
		10	200	1.3	Satisfy	Buckling
		15	200	1.9	Satisfy	Verified
		20	200	2.5	Satisfy	Verified
		25	200	3.1	Satisfy	Verified
		30	200	3.8	Satisfy	Verified
ES2	9.4	0	210	0.0	-	-
		5	210	0.5	Not Satisfy	Buckling
		10	210	1.1	Satisfy	Buckling
		15	210	1.6	Satisfy	Buckling
		20	210	2.1	Satisfy	Verified
		25	210	2.7	Satisfy	Verified
		30	210	3.2	Satisfy	Verified
ES3	12	0	250	0.0	-	-
		5	250	0.4	Not Satisfy	Buckling
		10	250	0.8	Not Satisfy	Buckling
		15	250	1.3	Satisfy	Buckling
		20	250	1.7	Satisfy	Verified
		25	250	2.1	Satisfy	Verified
		30	250	2.5	Satisfy	Verified

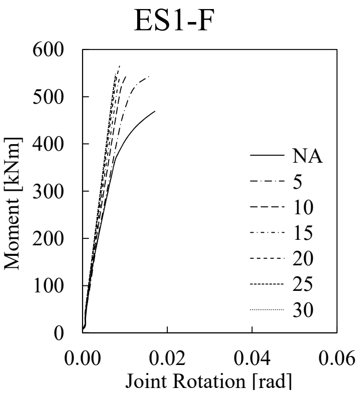
ES1-F
Moment [kNm]
600
500
400
300
200
100
0
0.00
0.02
0.04
0.06
Joint Rotation [rad]
NA
5
10
15
20
25
30

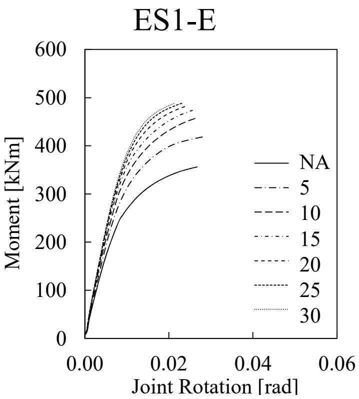
ES1-E
Moment [kNm]
600
500
400
300
200
100
0
0.00
0.02
0.04
0.06
Joint Rotation [rad]
NA
5
10
15
20
25
30

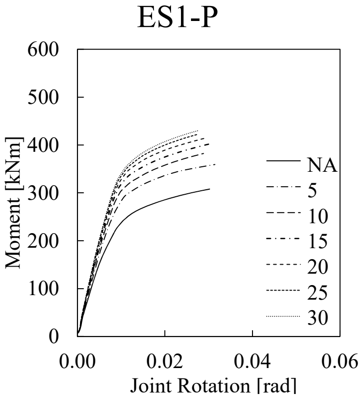
ES1-P
Moment [kNm]
600
500
400
300
200
100
0
0.00
0.02
0.04
0.06
Joint Rotation [rad]
NA
5
10
15
20
25
30

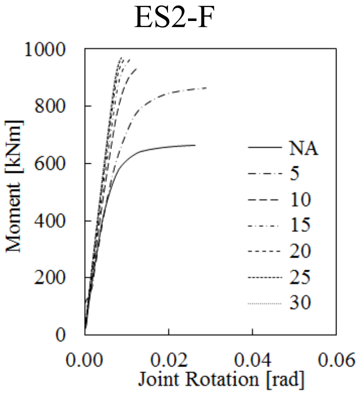
ES2-F
Moment [kNm]
1000
800
600
400
200
0
0.00
0.02
0.04
0.06
Joint Rotation [rad]
NA
5
10
15
20
25
30

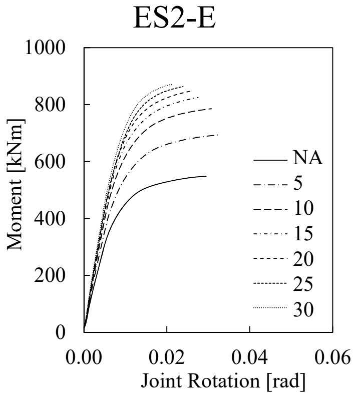
ES2-E
Moment [kNm]
1000
800
600
400
200
0
0.00
0.02
0.04
0.06
Joint Rotation [rad]
NA
5
10
15
20
25
30

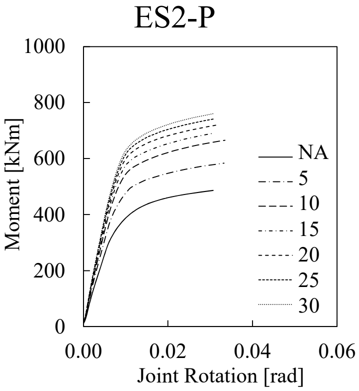
ES2-P
Moment [kNm]
1000
800
600
400
200
0
0.00
0.02
0.04
0.06
Joint Rotation [rad]
NA
5
10
15
20
25
30

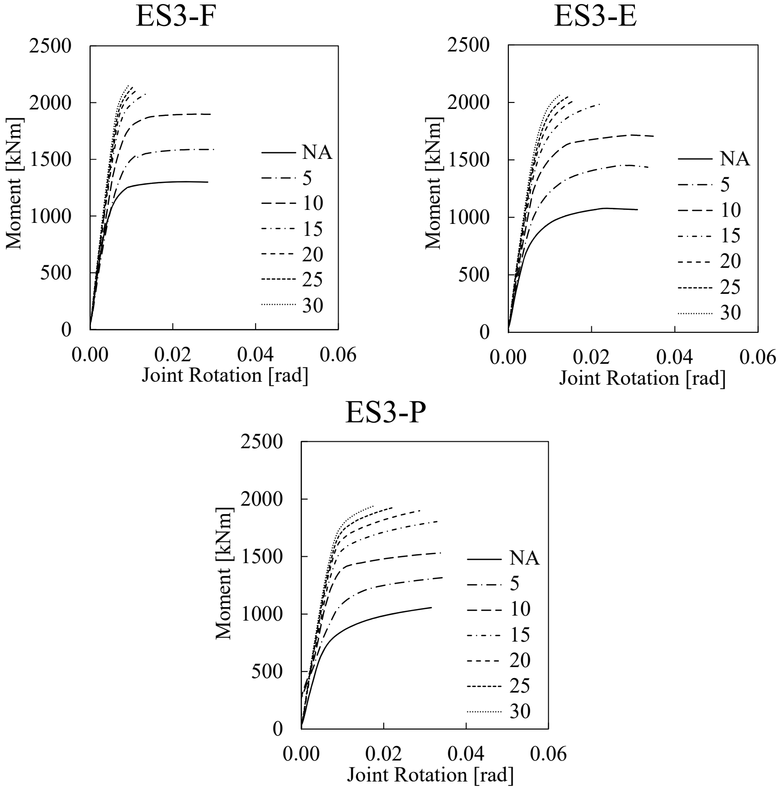

Figure 4-4: Moment joint rotation curves.

Since the large correlation between the connection and the joint behavior in case of equal and more for the partial strength joint it can be observed that, differently from the full strength joints, these joints show a larger variability of the bending capacity with the thickness increase, independently if the AISC358-16 [4] limitation are meet.

The results are also validated by the yielding line distribution reported in Figure 4-5. It is clear how increasing the rib thickness the yielding line distribution changes and migrates from the rib towards the beam, while remaining approximately unchanged in position for values of rib thickness larger than 10mm.

PEEQ distribution	CPRESS	PEEQ distribution	CPRESS
ES2 – F – NA		ES2 – F – 5mm	
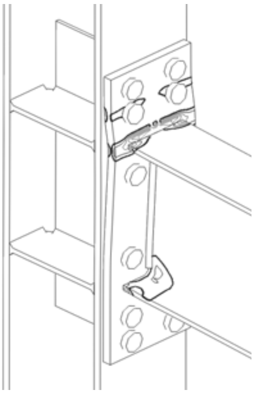	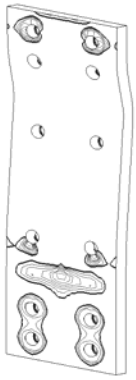	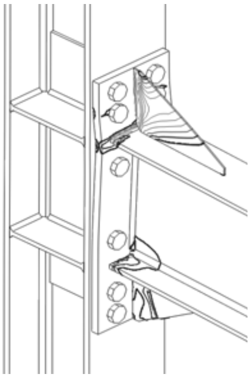	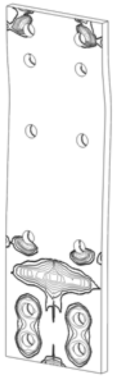
ES2 – F – 10mm		ES2 – F – 15mm	
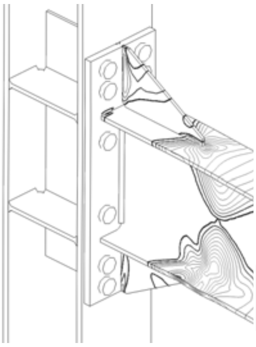		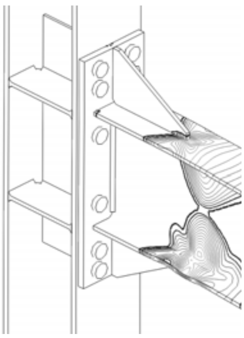	

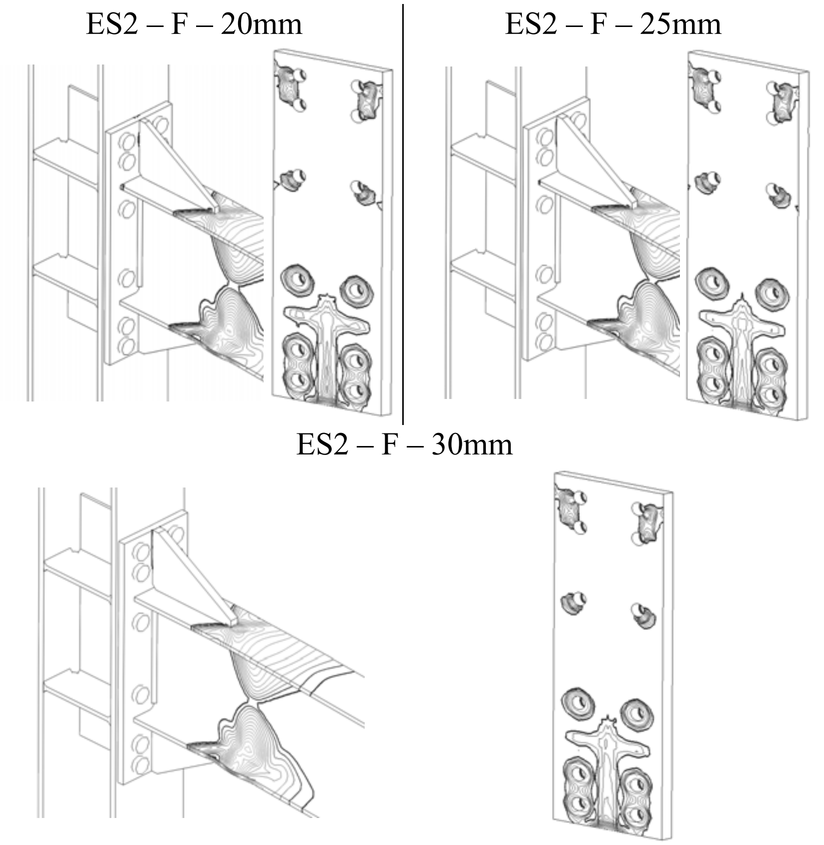

ES2 – F – 20mm

ES2 – F – 25mm

ES2 – F – 30mm

Figure 4-5: Results for various rib thicknesses a) Yielding line distribution and b) CPRESS distribution.

Moreover, as highlighted by Cermelj et al [5] the plastic demand can concentrate in the welds connecting the rib and the beam. This occurs particularly for the assemblies with intermediate rib thickness and it could activate a brittle failure as show by Guo et al [2]. These observations enforce the need for special attention to be paid to the welds design, execution and verification.

All these observations made on the yielding line evolution find confirmation also in the CPRESS distribution at the interface between end plate and column flange. Figure 4-5 shows the contact force on the end plate at 4% of the chord rotation, where due to an increase of the contact force above the compressed beam flange it follow a shifting of the compression center.

Moreover, for values of rib thickness that ensure the prevention of the buckling phenomena, the compression center should move from the compressed beam flange downwards, to a given position on the rib stiffener.

As anticipated in design phase (Chapter V) and here confirmed, the shifting of the compression center is very important in the joint resistance definition, affecting not only the internal lever arm and therefore the connection bending capacity, but also on the design of the web panel.

It is important to notice how the compression center position depends not only on the rib thickness but also on the rotational level reached. Therefore, the variation of the compression center position in function of the chord rotation (see Figure 4-6) was investigated changing the rib thickness; for reason of brevity hereinafter only the ES2 assembly results are reported.

In case of full strength configuration (see Figure 4-6 a), the joints with rib thickness equal to 5 and 10 mm have the compression center close to the beam flange, particularly for increasing values of rotation when buckling reduces the load bearing capacity of the compressed rib. The buckling of the plate occurs around 0.018rad which is clearly reflected as a drop in the curve. Conversely, for all the others thicknesses configurations, the results show a level of downwards shifting between 0.3 and 0.4 of the rib height and the position remains almost constant with the rotation. Moreover, it is important notice how for the unstiffened connection, according to the classical theory of the component method, the compression center is in the beam flange.

The same trend can be observed for the equal and partial strength joint configurations, but where, since the larger concentration of the damage in the connection, the compression center reaches higher value. Indeed, observing the Figure 4-6 c, it can be conclude that since the presence of the gap opening the compression center can reach higher value with respect to the full strength configuration, up to 0.6 the rib high in case of a rib thickness equal to 30mm.

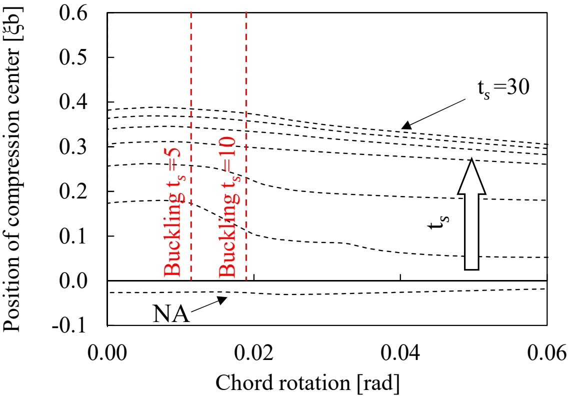

a)

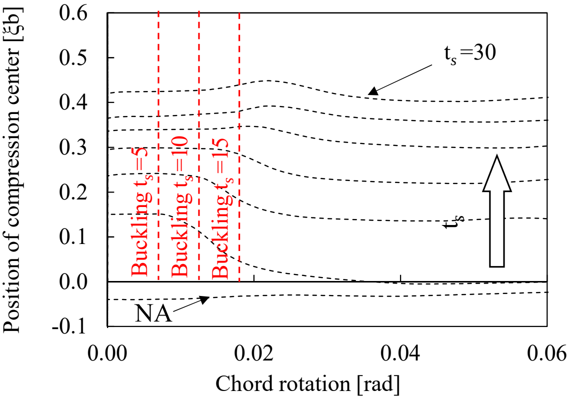

b)

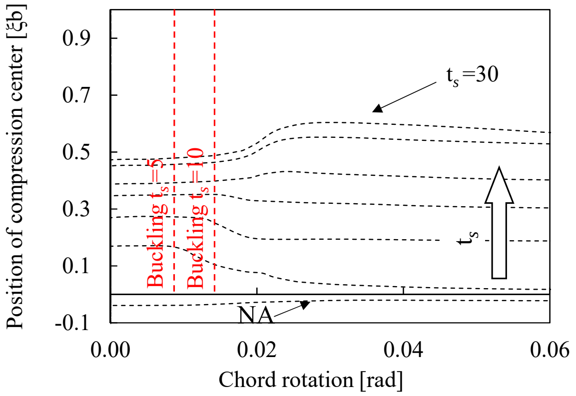

c)

Figure 4-6: Compression center evolution in function of the chord rotation for: a) ES-2 full strength, b) ES-2 equal strength and ES-2 partial strength.

Finally, it can be observed that for all the design criteria investigated, increasing the rib thickness increase the shifting of the compression center and if the buckling is avoided its position can be approximately considered constant with the chord rotation. Another approach that can confirm the shifting of the compression center and its variation respect the rib thickness could be investigate the repartition of the normal action between the beam and the rib on the compression side. For instance, the results of the ES2-P are investigated and discussed (see Figure 4-7).

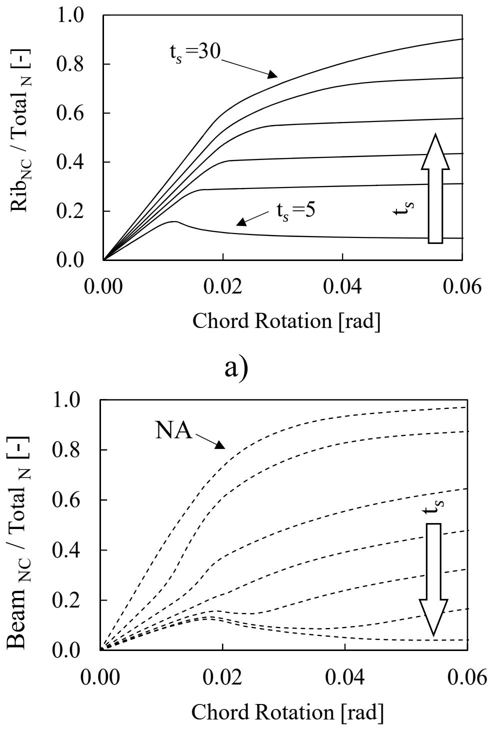

a)

b)

Figure 4-7: ES-2-P Normal action in the rib (a) and in the beam (b)normalized with respect the maximum normal action for all the rib thickness investigated.

In unstiffened configurations, the beam flange in compression carries all the compressive action, but by introducing the rib and increasing its thickness, the normal action transfers from the beam to the stiffener. When the rib dimension overcomes the beam web thickness, plastic deformation develops in the beam and localizes at the rib-beam flange interface. Particularly for stocky ribs, when the rotation level is around 2% the beam plasticize and a significant variation of the normal action in the beam flange can be observed. This phenomena explains the downwards shifting of the compression center for equal and partial strength joints observed in Figure 4-6.

In the case of slender ribs, a linear increase of the normal action can be observed for small values of rotation until the buckling of the rib occurs. On the other hand, stockier ribs lead to high plastic demand concentration in the beam and a sudden drop of normal action, which will inflict the change of the compression center position.

Moreover, the effectiveness of these observation i.e. the rib buckling, are confirmed by the results showed in Figure 4-8, where the PEEQ distribution (at 4% of rotation) are reported for all the rib thickness investigated.

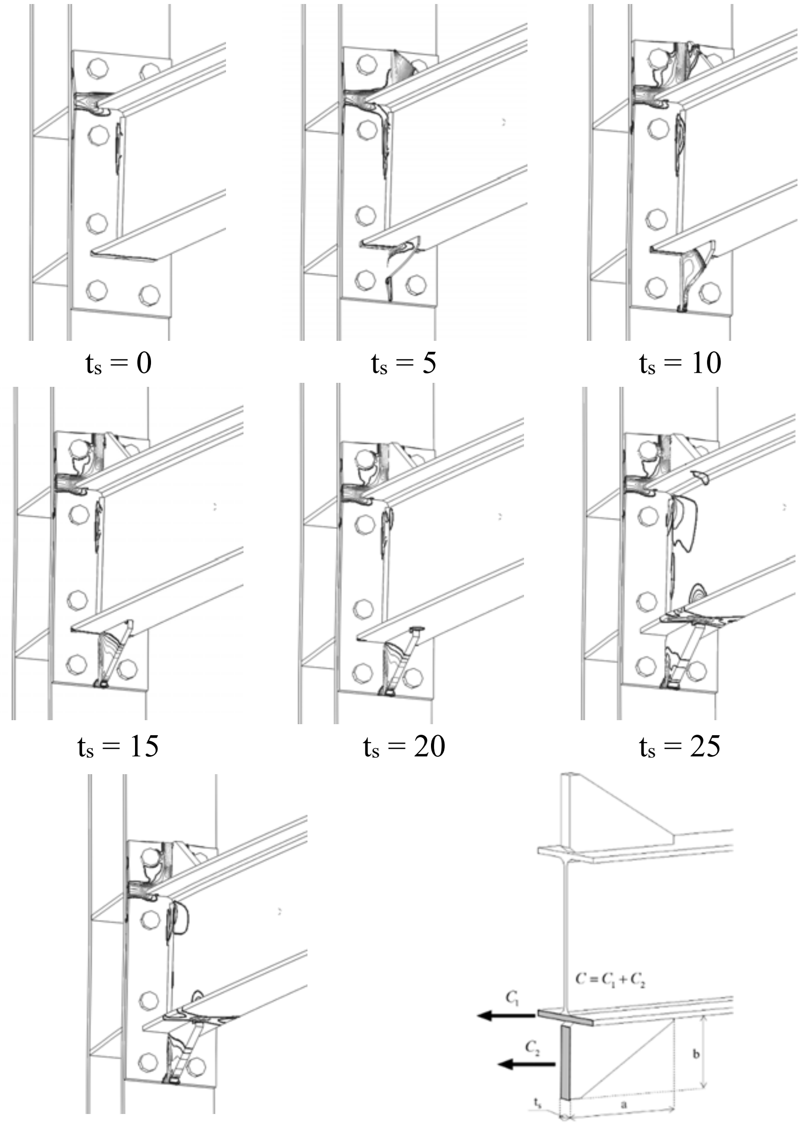

$t_s = 0$ $t_s = 5$ $t_s = 10$

$t_s = 15$ $t_s = 20$ $t_s = 25$

$t_s = 30$

Figure 4-8: PEEQ distribution on ES-2-P.

4.3 Slope of rib stiffener

The slope of the rib is another crucial parameter for the design process. Indeed, the rib slope changes the local distribution between the beam and the end-plate, the design action on the column face and the concentrated action in the beam web.

As anticipated in this paragraph two configurations for the rib are investigated: 30° and 40°. Using a smaller inclination for the stiffeners helps the tension distribution between the beam and the rib although it also increases the design moment on the connection. Indeed, introducing a rib with a larger base leads to an increase of shear force developed at the beam extremities. Based on these consideration, AISC358-16 [4] impose ribs with 30° in the prequalification procedure. Conversely, in this thesis as also find in same study in literature [3] the rib inclination was assumed equal to 40°.

Hereinafter, the influence of the rib inclination, also in function of the thickness is investigated; for reason of brevity, only the results of ES2 are reported and illustrated, while all the results are reported in the Annex.

Table 4.2: Comparison in terms of bending capacity between the 30° and 40° configuration for ES2 beam-to-column assembly.

Rib thickness	Full Strength joints			Equal Strength joints			Partial Strength joints		
	30° Conf.	40° Conf.	30°/40°	30° Conf.	40° Conf.	30°/40°	30° Conf.	40° Conf.	30°/40°
[mm]	[kN]	[kN]	[-]	[kN]	[kN]	[-]	[kN]	[kN]	[-]
NA	664.5		-	543.1		-	497.8		-
5	869.4	804.4	1.08	684.6	653.5	1.05	594.5	583.0	1.02
10	937.9	901.1	1.04	783.0	766.7	1.02	679.8	665.0	1.02
15	965.3	930.1	1.04	839.1	807.2	1.04	713.1	696.5	1.02
20	967.2	931.9	1.04	861.7	821.4	1.05	733.9	719.8	1.02
25	969.1	923.0	1.05	876.2	827.6	1.06	756.1	729.3	1.04
30	959.4	934.9	1.03	885.8	832.7	1.06	776.1	738.3	1.05

The aspect ratio was varied also for the models with different rib thickness and the response was evaluated in terms of both moment rotation curves and compression center position. The moment rotation curve reported in Figure 4-9 show a good agreement both in terms of elastic stiffness and in terms of resistance between the two joint configuration. Indeed, it can be notice that the rib inclination does not influence the joint stiffness, while some small differences can be observed in terms on bending capacity, where for all the design criteria investigated the 30° configuration show a larger value of resistance. Moreover, the differences in terms of bending capacity (at 4% of rotation) are also reported in Table 4.2 where it can be observed (for the three performance level and for all the thickness configuration) that the maximum difference between the 30° and 40° configuration is 6%.

ES2 – Full Strength

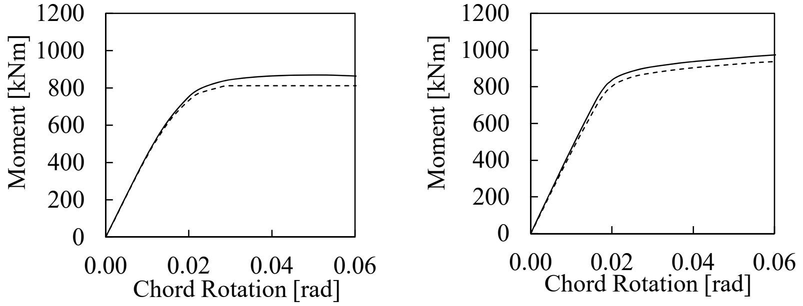

$t_s = 5$

$t_s = 10$

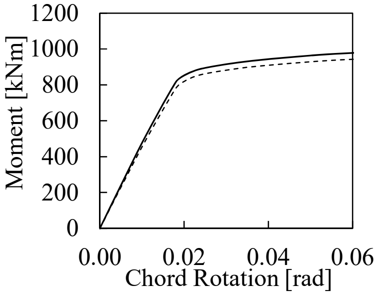

$t_s = 15$

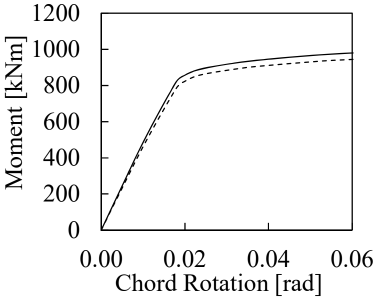

$t_s = 20$

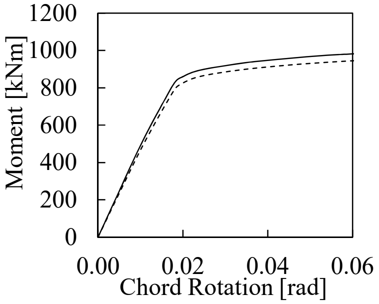

$t_s = 25$

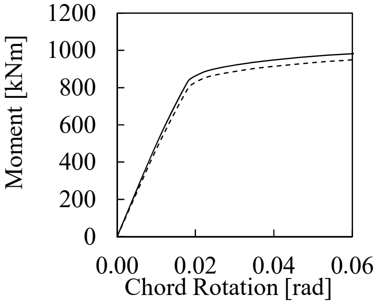

$t_s = 30$

ES2 – Equal Strength

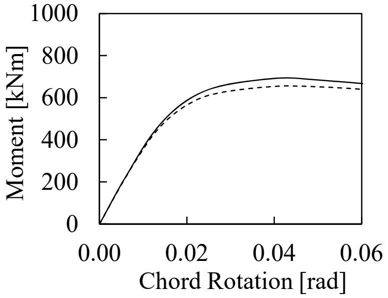

$t_s = 5$

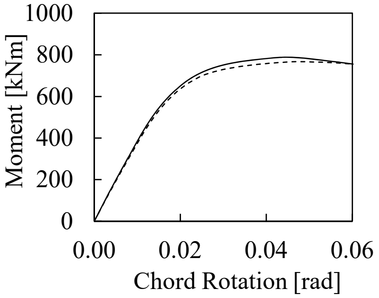

$t_s = 10$

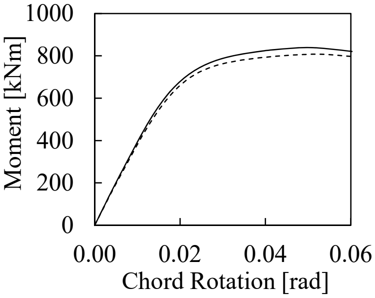

$t_s = 15$

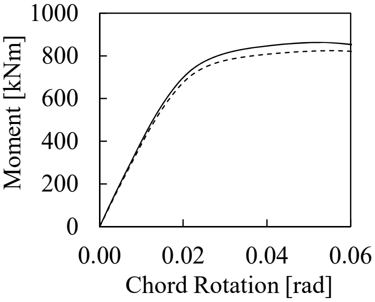

$t_s = 20$

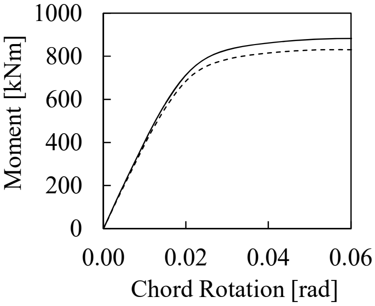

$t_s = 25$

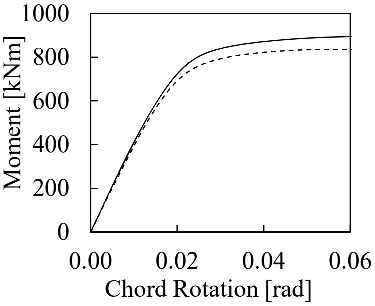

$t_s = 30$

ES2 – Partial Strength

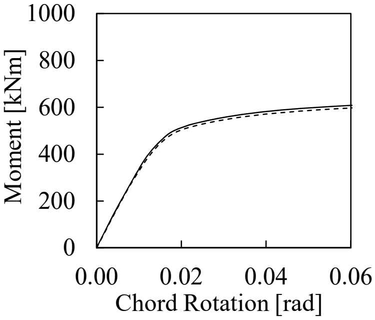

$t_s = 5$

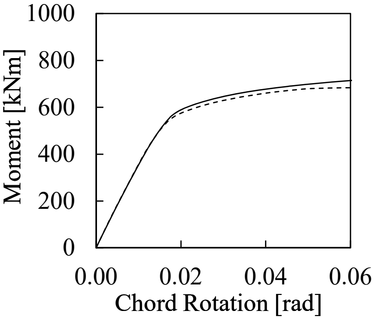

$t_s = 10$

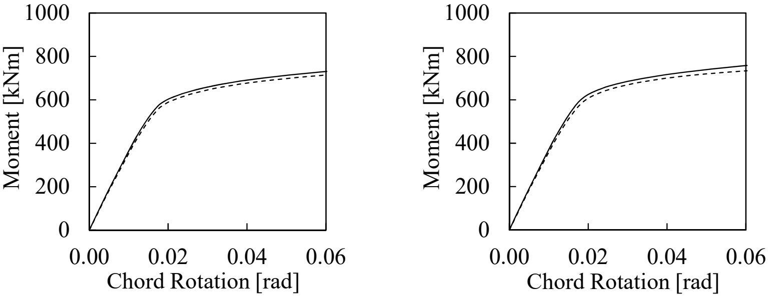

$t_s = 15$ $t_s = 20$

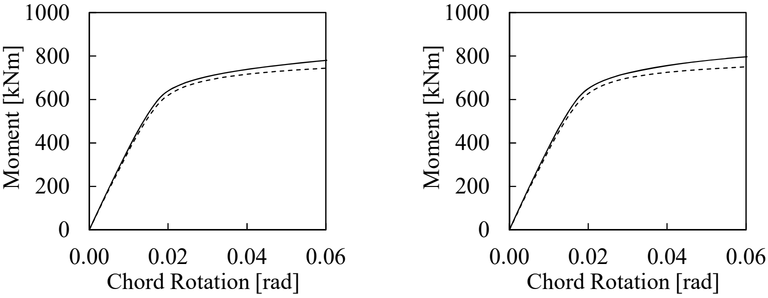

$t_s = 25$ $t_s = 30$

Figure 4-9: Comparison in terms of moment rotation curve between 30° and 40° joint configuration (ES-2) for all the rib thickness value introduced.

Another important difference between the two slope is the distribution of the internal actions and in particular the position of the compression center in function of the chord rotation. Figure 4-10 show, just for the Full strength configuration, the compression center difference from the two ribs configuration; it can be notice that the joints has approximately the same behavior just shifted deeper in the rib high in case of 30°configuration.

Contrariwise, the compression center for the 40° configurations is localized around the center of the equivalent T in compression. Therefore, when a 30° rib slope is use, the joint internal level arm increase with a correspondent increase of the joint capacity.

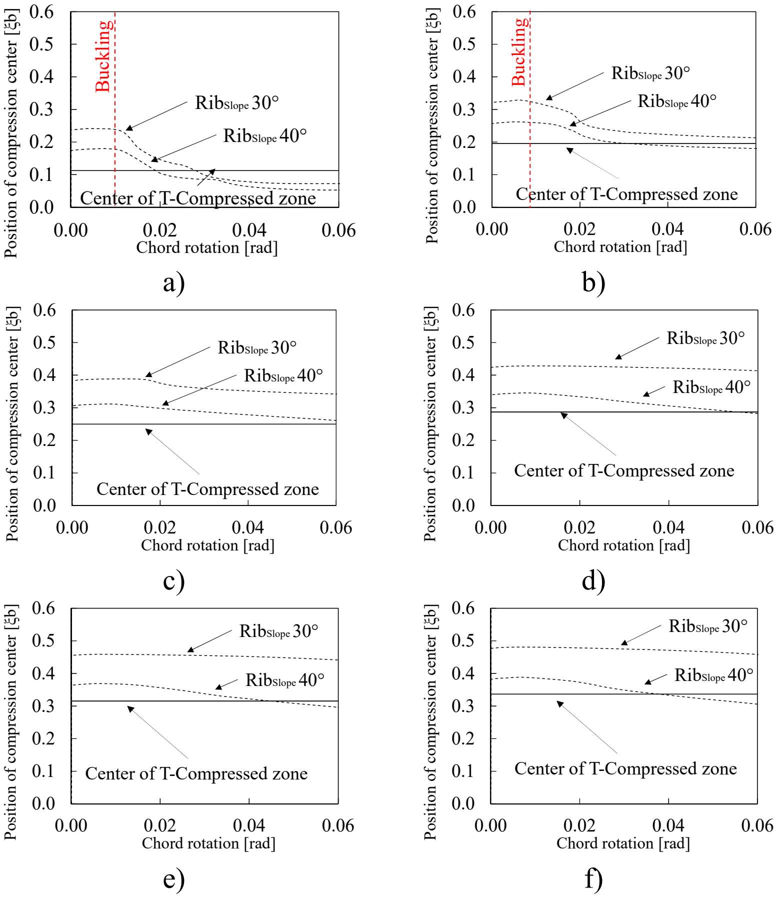

Figure 4-10: Comparison in terms of compression center position between 30° and 40° joint configuration for all the rib thickness value introduced.

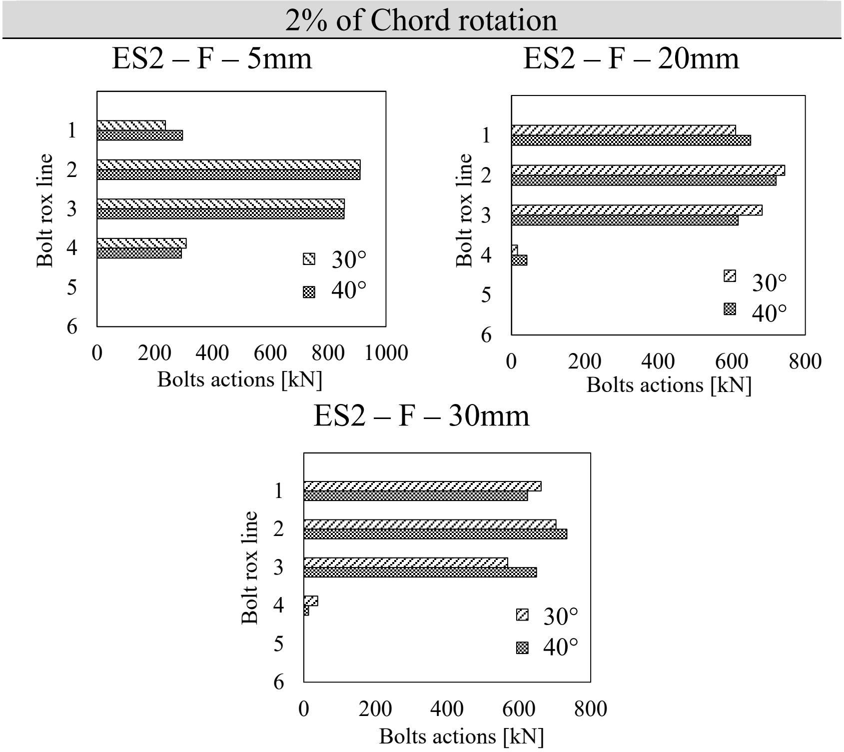

Figure 4-11: Normal action in the bolts row line for ES-2-F configuration at 2% of rotation for rib thickness equal to: 5mm, 20mm and 30mm.

Moreover, also the distribution of the bolt row forces were evaluated. As reported in Figure 4-12 and Figure 4-12, the tensile stress distribution on the 2% and 4% of rotation respectively for 5, 20 and 30mm of ribs thickness are given.

It can be observed that also in elastic range (2%) there is a difference between the two slope configuration; indeed, exception for the ES2-F-5mm, the other two configuration show a larger engage of the bolts in case of 30° rib.

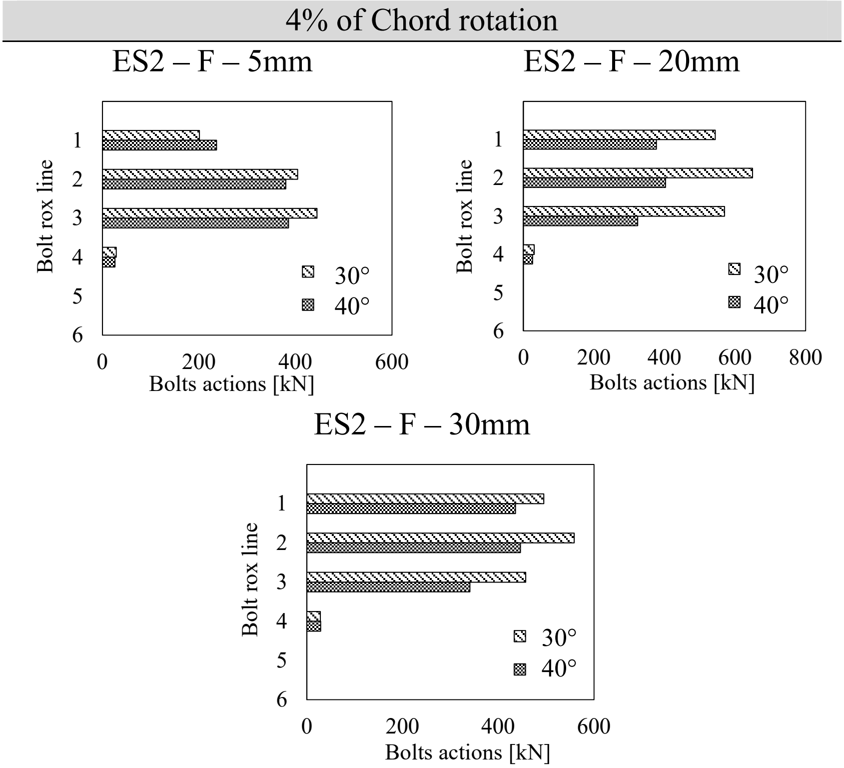
4% of Chord rotation

ES2 – F – 5mm

ES2 – F – 20mm

ES2 – F – 30mm

Figure 4-12: Normal action in the bolts row line for ES-2-F configuration at 4% of rotation for rib thickness equal to: 5mm, 20mm and 30mm.

The differences are also confirmed at larger value of rotation (4%), where in almost all the cases the 30° slope configuration carry a larger value of the tension action. These results are confirmed also from the evaluation of the bending moment reported in Table 4.3 where the bending joints bending capacity is compared considering also the real position of the compression center.

Finally, all these results are align with the differences observed in the moment-rotation curves.

Table 4.3: Bolts row action contribution to the moment considering the level arm coming from the evaluate compression center at 4% of rotation.

Bolt row line	ES -2-F-5				ES -2-F-20				ES -2-F-30			
	30°		40°		30°		40°		30°		40°	
	Normal action [kN]	Level arm [mm]	Normal action [kN]	Level arm [mm]	Normal action [kN]	Level arm [mm]	Normal action [kN]	Level arm [mm]	Normal action [kN]	Level arm [mm]	Normal action [kN]	Level arm [mm]
Line 1	296	626	236	623	651	698	610	672	661	708	624	678
Line 2	910	551	911	548	720	623	744	597	703	633	733	603
Line 3	855	371	856	368	617	443	682	417	569	453	649	423
Line 4	292	191	308	188	42	263	16	237	38	273	13	243
Moment [kNm]		1060		1020		1187		1143		1181		1142

CHAPTER VII

References

[1] Tsai K.C. and Popov EP. (1990). Cyclic behavior of end-plate moment connections. Journal of Structural Engineering.116:2917-2930.

[2] Guo, Q. Gu, F. Liu. (2006). Experimental behavior of stiffened and unstiffened end-plate connections under cyclic loading. Journal of Structural Engineering 132 (9)1352–1357.

[3] Abidelah A., Bouchaïr A., Kerdal D.E. (2012). Experimental and analytical behavior of bolted end-plate connections with or without stiffeners. Journal of Constructional Steel Research, 76, 13–27.

[4] ANSI/AISC 358-16 (2016). Prequalified Connections for Special and Intermediate Steel Moment Frames for Seismic Applications.

[5] Cermelj Blaz (2015). Seismic resistance of welded beam-to-column connections in hybrid moment and braced frames. Ph.D. University of Ljubljana.

[6] Dassault Systèmes. Abaqus analysis 6.16 user's manual. Simula Inc. 2016.

[7] EN 1993:1-8, Design of steel structures - Part 1-8: Design of joints. CEN 2005.

List of figures

Figure 1-1: Investigated Rib parameters................................ 443

Figure 2-1: Moment rotation curve of ES1 assembly designed as: full strength (a and b in terms of chord and joint rotation respectively), equal strength (c and d in terms of chord and joint rotation respectively) and partial strength e and f in terms of chord and joint rotation respectively)... 448

Figure 2-2: Moment rotation curve of ES2 assembly designed as: full strength (a and b in terms of chord and joint rotation respectively), equal strength (c and d in terms of chord and joint rotation respectively) and partial strength e and f in terms of chord and joint rotation respectively)... 449

Figure 2-3: Moment rotation curve of ES1 assembly designed as: full strength (a and b in terms of chord and joint rotation respectively), equal strength (c and d in terms of chord and joint rotation respectively) and partial strength e and f in terms of chord and joint rotation respectively)... 450

Figure 2-4: ES3-P PEEQ distribution changing the material yielding strength. 451

Figure 2-5: Joint bending capacity in function of the performance design and the end-plate material variability for: ES1 (a), ES2 (b) and ES3 (c) joint configurations. 453

Figure 2-6: ES2-Full strength moment rotation curve changing the end-plate material. 454

Figure 2-7: ES2-Full strength joints dissipated energy for component (a, c, e, and g) and PEEQ distribution (b, d, g and h) for increasing material strengthening. .456

Figure 2-8: ES2-Equal strength moment rotation curve changing the end-plate material. 458

Figure 2-9: ES2-Equal strength joints dissipated energy for component (a, c, e, and g) and PEEQ distribution (b, d, g and h) for increasing material strengthening. .459

Figure 2-10: ES2-Partial strength moment rotation curve changing the end-plate material. 461

Figure 2-11: ES2-Partail strength joints dissipated energy for component (a, c, e, and g) and PEEQ distribution (b, d, g and h) for increasing material strengthening. 463

Figure 2-12: Dissipated energy at 4% of rotation for: Full strength (a), equal strength (b) and Partial strength (c). 465

Figure 3-1: Comparison between the bending capacity of the RJ and MBRJ joints in terms of : bending capacity (a) and elastic stiffeness (b)... 467
Figure 3-2: ES1 comparison between RJ and MBRJ in terms of moment rotation curve and dissipated energy ration respectively for Full, equal and partiacl strength joints. 468
Figure 3-3: ES2 comparison between RJ and MBRJ in terms of moment rotation curve and dissipated energy ration respectively for Full, equal and partiacl strength joints. 469
Figure 3-4: ES3 comparison between RJ and MBRJ in terms of moment rotation curve and dissipated energy ration respectively for Full, equal and partiacl strength joints. 470
Figure 3-5: Cycles shape comparison between RJ and MBRJ at: 5% (a), 6% (b) and 7% (c) of chord rotation. 471
Figure 3-6: Column removal scenario. 472
Figure 3-7: ES2-F Comparison between RJ and MBRJ joint configuration in terms of: moment rotation curve (a), Normal action in the beam (b) and PEEQ distribution at 20% of rotation (c and d). 475

Figure 3-8: ES2-E Comparison between RJ and MBRJ joint configuration in terms of: moment rotation curve (a), Normal action in the beam (b) and PEEQ distribution at 20% of rotation (c and d). 475

Figure 3-9: ES2-P Comparison between RJ and MBRJ joint configuration in terms of: moment rotation curve (a), Normal action in the beam (b) and PEEQ distribution at 20% of rotation (c and d). 476

Figure 4-1: ES-2 Moment rotation curve: a) full strength, b) equal strength, c) partial strength and d) geometrical sketch. 478

Figure 4-2: Yielding line (PEEQ) and contact pressure (CPRESS) distribution. 482

Figure 4-3: Rib and beam geometrical parameters..................483

Figure 4-4: Moment joint rotation curves...............................487

Figure 4-5: Results for various rib thicknesses a) Yielding line distribution and b) CPRESS distribution..............489

Figure 4-6: Compression center evolution in function of the chord rotation for: a) ES-2 full strength, b) ES-2 equal strength and ES-2 partial strength. 493

Figure 4-7: ES-2-P Normal action in the rib (a) and in the beam (b)normalized with respect the maximum normal action for all the rib thickness investigated........... 494
Figure 4-8: PEEQ distribution on ES-2-P................................ 496
Figure 4-9: Comparison in terms of moment rotation curve between 30° and 40° joint configuration (ES-2) for all the rib thickness value introduced......................... 502
Figure 4-10: Comparison in terms of compression center position between 30° and 40° joint configuration for all the rib thickness value introduced.................................... 503
Figure 4-11: Normal action in the bolts row line for ES-2-F configuration at 2% of rotation for rib thickness equal to: 5mm, 20mm and 30mm.................................. 504
Figure 4-12: Normal action in the bolts row line for ES-2-F configuration at 4% of rotation for rib thickness equal to: 5mm, 20mm and 30mm.................................. 505

List of tables

Table 1.1: Investigated variability of steel strength of the end-plate material. 444
Table 1.2: Investigated rib parameters. 445
Table 4.1: AISC verifications for ribs thickness parametric analysis. 485
Table 4.2: Comparison in terms of bending capacity between the 30° and 40° configuration for ES2 beam-to-column assembly. 498
Table 4.3: Bolts row action contribution to the moment considering the level arm coming from the evaluate compression center at 4% of rotation. 507

CHAPTER VIII

EJ vs AISC358 design and performance approach

Introduction

Extended stiffened (ES) end-plate bolted joints are seismically pre-qualified according to AISC358-16 [1] in the United States (US) following the SAC joint venture project started in 1994 after Northridge earthquake. The design criteria and detailing rules proposed by European approach for extended stiffened end-plate joints (discussed up to here) differ in some aspects from US criteria. Therefore, the aim of this Chapter is verify and compare the effectiveness of both design procedures.

1 Differences between the Equaljoints design procedure and AISC 358

1.1 Codes differences

Several differences can be pointed out between the European and American design approach both form the structural and joint point of view. In the following, the attention is posed on the main differences from the seismic design approach, focusing on the MRF structures and on the extended stiffened (ES) joints.

1.2 Structural design differences

The design philosophy of both American and the European seismic codes is based on the concept of dissipating the earthquake energy by means of plastic hinges at the ends of the beams.

Both seismic codes use response spectra reduced by behavior or reduction (*q* for the European code and *R* for the American one) factor to define the seismic demand on the structures. Despite the general approach is similar, some substantial differences can be pointed out: (i) the value of the behavior factor, (ii) the inter-story drift limitations and (iii) the capacity design verification.

The behavior factor is defined as: “the factor used for design purposes to reduce the forces obtained from a linear analysis, in order to account for the non-linear response of a structure, associated with the material, the structural system and the design procedures" [EN1998-1-1 pr. 1.5.2 [2]]. In case of steel MRFs structures, the European code, recommends a maximum value of the behavior factor equal to 6.5, assuming the energy dissipation at the beam extremity by the formation of the plastic hinges and structural regularity in both plan and elevation. AISC360-16 [3] recommends a larger reduction factor R=8 for special moment resisting frame (SMF).

Despite that, as it will be show hereinafter this difference will not play a central role in the structures design since usually in the MRFs structures the internal actions will not govern the section assignments. Indeed in the most of the cases, both in the US and EU practices the design sections are governed by the inter-story drift limitation. As already anticipated in Chapter V, EN1998-1-1 [2] requires for steel structures, where the non-structural elements are considered as ductile, a maximum design displacement equal to:

$$d_r \nu \leq 0.0075h \tag{1}$$

where: d_r is the design inter-story drift, h is the story height and ν is the reduction factor. Contrariwise, the American codes impose that the design story drift (Δ) as determined in ASEC7-10 [7] Sections 12.8.6, 12.9.2, or 16.1 [7], should not exceed the allowable story drift (Δa) equal for SMF to 0.02 (ASCE7-10 Table 12.12-1 [7]) for any story (see Figure 1-1):

<table>
<tr><td rowspan="4">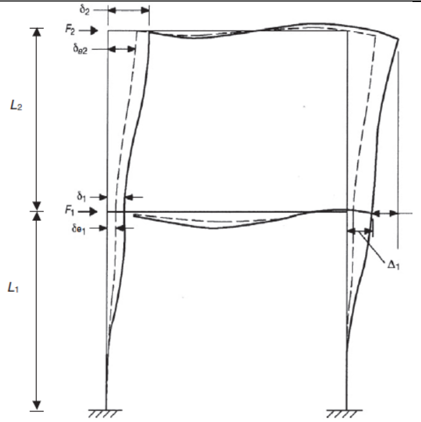
</td><td>$\frac{\Delta_x}{h_x} < \Delta_a = 0.02$</td></tr>
<tr><td>$\Delta_x = \delta_x - \delta_{x-1}$</td></tr>
<tr><td>$\delta_x = \frac{C_d \delta_{xe}}{I}$</td></tr>
<tr><td>δ_{xe} is the seismic elastic displacement</td></tr>
</table>

Figure 1-1: Story drift determination [7].

where: Δi is the story drift, is the total displacement, is the elastic displacement under the seismic force, C_d is the deflection amplification factor equal to 5.5 for SMF. The first aspect that should be noted is that the introduced European limit is more conservative (25%) than the one introduced in the ASEC7-10 [7]; indeed:

$$d_r v \le 0.0075h \rightarrow \frac{d_r}{h} \le \frac{0.0075}{v} = 0.015 \qquad (2)$$

$$\frac{\Delta_x}{h_x} < 0.02 \tag{3}$$

Despite these considerations, it should be notice that the EN1998-1-1 pr. 4.4.3.2 [2] allow also the use a less restrictive limitation if: (i) the non-structural elements does not have any interaction with the structural deformations, or (ii) there are not non-structural elements. In this case, both the codes suggest the same limitations:

$$d_r \nu \leq 0.01h \rightarrow \frac{d_r}{h} \leq \frac{0.01}{\nu} = 0.02 \tag{4}$$

Furthermore, the definition of the maximum displacements limits are not the only differences; indeed some distinctions can be also find in the design displacement definition. Indeed, from a simple calculation, it is possible to observe how, a single story structure with a height equal to 3.5m and subject to a seismic action, pass the American limitation but not the European one. Assuming for instance, a lateral displacement equal to 0.0127m, the ASEC7-10 [7] drift limitation is satisfy while the displacement does not met the European limit (see Figure 1-2).

Finally, from the comparison it is possible to observe that the EC verification is almost two time more recitative of the American practice.

European limitation	American limitation
$d_S = q \cdot d_e = 6.5 \cdot 0.0127 = 0.08255m$ $d_r = d_S - d_{S-1} = 0.08255 - 0 = 0.08255m$ $\frac{d_r}{h} = \frac{0.08255}{3.5} = 0.0236 \geq 0.015$ $\frac{0.0236}{0.015} = 1.576$	$\delta_x = \frac{C_d \cdot \delta_{xe}}{I_e} = \frac{5.5 \cdot 0.0127}{1} = 0.07m$ $\Delta_x = \delta_x - \delta_{x-1} = 0.07 - 0 = 0.07m$ $\frac{\Delta_x}{h_x} = \frac{0.07}{3.5} = 0.02 = 0.02$

a) b)

$$d_S = q \cdot d_e = 6.5 \cdot d_e$$

$$\delta_x = \frac{C_d \cdot \delta_{xe}}{I_e} = \frac{5.5 \cdot \delta_{xe}}{1}$$

$$\frac{d_S}{\delta_{xe}} = 1.18 \rightarrow 15.4\%$$

c)

Figure 1-2: European (a) and American (b) inter-story drift limitations and their comparison (c).

The strong column weak beam principal is adopted in both the codes to force the activation of the plastic hinge in the beam leaving the column free from damage.

However, the two codes follow different way to guide the design of the column cross section; in particular, EN1993-1-1 pr. 6.6.3 [2] prescribes to design the less ductile elements and force the plastic hinge in the beam, introducing an alternative loading combination, considering the hardening, the overstrength factor and the Omega coefficient, as reported hereinafter:

$$E_{Ed} = E_{Ed,G} + 1.1\gamma_{ov}\Omega E_{Ed,E} \tag{5}$$

where $E_{Ed,E}$ are the action due to the vertical loads, 1.1 is a coefficient to take into account the steel hardening, γ_{ov} is the overstrength factor equal to 1.25, omega (Ω) is the ratio between the beam bending capacity and its seismic demand and $E_{Ed,E}$ are the action due to the seismic loads.

On the other hand, the American codes define directly different loading combinations for the columns, increasing the demand by the introduction Ω_0 factor (which will be better explained in the following paragraph).

In line with the capacity design principles, and to verify also the local hierarchy, both the codes impose to verify the ratio between the column and the beam bending capacity. EN1998-1-1 [2] impose to amplify the beam capacity of the 30% as reported in the following equation:

$$\sum M_{Rc} \geq 1.3 \cdot \sum M_{Rb} \tag{6}$$

where M_{Rc} are the column bending capacity and M_{Rb} is the beam flexural capacity. On the other hand, AISC341 [4], impose to verify the same mechanism but introducing the following equation:

$$\frac{\sum M_{pc}^{*}}{\sum M_{pb}^{*}} \geq 1 \tag{7}$$

where the M^{*}_{pc} is the column capacity and M^{*}_{pb} is the beam resistance. Therefore, differently from the Eurocode, the American approach does not introduce any amplification factor that is already present in the M^{*}_{pb} definition; indeed it can be defined as:

$$M_{pb} = 1.1 \cdot R_y \cdot F_{yb} \cdot Z + M_{uv} \tag{8}$$

where: 1.1 is an amplification factor to take into account the material hardening, R_y is a coefficient equal to 1.2, F_y is the material yielding stress (corresponding the f_{yd} in the European nomenclature), Z is the plastic resistant modulus (corresponding to W_{pl} in the European nomenclature). Finally, M_{uv} is an additional moment that take into account the shear time the distance between the beam end and the column face.

Therefore, the two codes approaches show some differences, but at the same time follow a similar design philosophy.

1.3 Connection design differences

Both American (i.e. AISC 358-10 [1]) and European (i.e. Chapter V) design procedures for full strength joints aim at ensuring the formation of plastic hinges in the beam tips. This purpose is differently achieved and the main differences concern: (i) the allowed beam-to-column assemblies, (ii) the configuration of the connection (i.e. distribution of bolts and requirements on rib stiffeners), (iii) the calculation assumptions (i.e. hierarchy criterion, position of center of compression, active bolt rows, yield line pattern), and (iv) the ductility criteria (i.e. limitations on the diameter of bolts).

In the following the most important and effective differences between the two approaches are reported and discussed.

The first important aspect is that, as already showed in Chapter III, AISC 358-10 [1] procedure imposes limits of the allowed size for both beam and column, while EJ procedure does not impose any limitation once provided that the beam-to-column hierarchy (i.e. weak beam-strong column) is satisfied.

According to AISC 358-10 [1], either 4 bolt row or 8 bolt row joint configurations can be adopted (see Figure 1-3), but the selection should be based on geometrical limitations, e.g. the distance of bolts rows, the thickness of end-plate, the size of the connected beam, etc. On the contrary, only one joint configuration with 6 bolt rows (see Figure 1-3) is considered by the EJ procedure for full strength joints.

The design rules to avoid the rib stiffeners buckling are provided from both the approaches. However, they differ in the requirements: AISC 358-10 [1] imposes a rib slope equal to 30°, while EJ propose to relax this requirements and assuming a slope within 30° and 40° in order to reduce the design moment acting on the connection.

In addition, the EJ procedure accounts for the presence of the rib to estimate the center of compression, which is assumed in the centroid of the equivalent T section, made of the flange of the beam and the area of the rib connected to the end-plate in line with the findings obtained by Abidelah et al. [4]. On the contrary, AISC 358-10 [1], in line with the classical component method approach, assumes the center of compression at the centroid of the beam flange.

Another substantial difference between the two methods is the way to compute the resistance of the end-plate. The AISC procedure directly provides the length of the yield line and a calculation equation in closed form on the basis of the adopted joint configuration (i.e. for both 4 bolts and 8 bolts configuration).

On the contrary, EJ procedure adopts the equivalent T-Stub theory implemented in EN1993:1-8 [6], which allows calculating the resistance of an equivalent T-Stub at each active bolt row (namely the two bolt rows above and the one below the beam flange in tension).

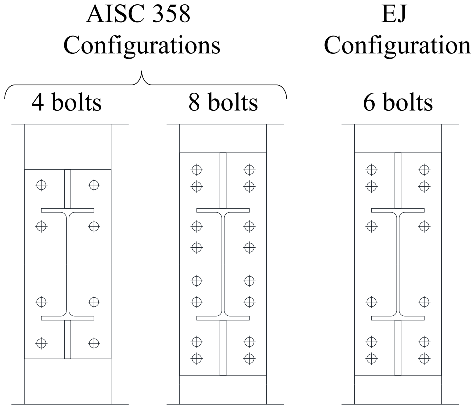

Figure 1-3: American and European joint configurations.

For what concerns the ductility of the connection, AISC 358-16 [1] impose that the joint has to reach a rotation at least of 4% without showing a capacity decrease larger than the 20%. However, despite this general requirement the code does not introduce any specific requirements in the design rules, considering that ES joints are conceived to be theoretically full strength, without experiencing plastic deformations.

The limitations on both minimum bolt diameter and thickness of end-plate are given separately and solely related to a strength verification against the design bending moment at the column face Mf. Indeed, AISC358 [1], does not provide any rules about the internal hierarchy of resistance between bolts and end-plate or column flange. Hereinafter, as already anticipated in Chapter III, the limitations on the minimum diameter for bolts are given:

$$d_{b,required} = \sqrt{\frac{2M_f}{\pi\phi_n F_{nt}\left(h_0 + h_1\right)}} \tag{9}$$

$$d_{b,required} = \sqrt{\frac{2M_f}{\pi\phi_n F_{nt}\left(h_1 + h_2 + h_3 + h_4\right)}} \tag{10}$$

Respectively for four bolts (4E and 4ES) and eight (8ES) bolts row configuration (all the dimension are reported in Chapter III).

The minimum thickness is obtained as follows:

$$t_{cf} \geq \sqrt{\frac{1.11M_f}{\phi_d F_{yc} Y_c}} \tag{11}$$

where all the dimensions are reported in Chapter III.

However, due to the variability of the yield strength of the material constituting both the end-plate and the bolts and the hardening that could be developed into the end-plate if activated, the AISC 358 [1] approach could not avoid mode 3 failure (i.e. failure of bolts). In light of these considerations, provided that the connection flexural strength should be larger than M_f, the EJ approach proposes the limitation of the minimum diameter of bolts on the basis of the maximum thickness between end-plate and column flange in order to avoid mode 3. Thus, to guarantee a ductile failure mode of the connection, even though the joint is theoretically designed to be full strength.

This requirement, applied at each line, is fulfilled if, the tensile strength of the bolts per line is larger than the strength of the entire line, accounting for both the random variability of its yield stress and its relevant strain hardening, which is expressed by the following inequality (as already reported in Chapter V):

$$F_{t,Rd} \geq \gamma \cdot F_{p,Rd} = \gamma_{ov} \cdot \gamma_{sh} \cdot F_{p,Rd} \tag{12}$$

2 MRF structures designed according to US codes

2.1 Designed structures

The effectiveness of the design criteria discussed in the previous paragraph is investigated by means of parametric monotonic and cyclic finite element analyses (FEAs) carried out on two sets of joints, namely one designed according to AISC 358-10 [1] and the full strength joints designed in Chapter V (ES1-F, ES2-F and ES3-F) according to the introduced European design procedure (EJ).

The first step is, as already shown for the EJ joints, extrapolate, from a set of MRFs structures properly designed according both to AISC 341 [4] and AISC360 [3], the beam-to-column assemblies.

The three American structures have the same geometry of the European from where the ES-1, ES-2 and ES-3 were extracted.

To be consistent with the European structures the US ones were designed considering the same geometry, the same vertical actions and the same seismic demand. Moreover a simplify procedure was conducted to evaluate the S_{DS} (design, 5% damping, spectrum response acceleration ASCE 7 [7]) value that represent a fundamental parameter to define the American seismic loading combination (ASCE 7-10 [7]). S_{DS} can be evaluated, according to ASCE 7 pr. 11.4.4 [7] as 2/3S_{MS}, but since a European elastic response spectrum was introduced to define the seismic demand, it was be evaluated as (see Figure 2-1):

$$S_{DS} = \frac{S_{de,Plateau}}{R \cdot I} \tag{13}$$

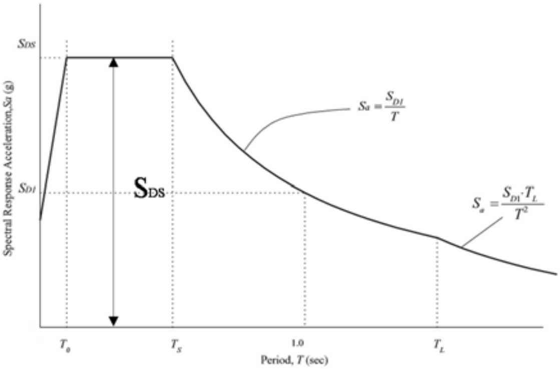

Figure 2-1: Design response spectrum[7].

Where S_{de} is the maximum elastic spectrum acceleration, *R* is the AISC341 behavior factor and *I* is a coefficient [7].

Once the S_{DS} is evaluated, also the E_v can be define:

$$E_V = 0.2 S_{SD} \tag{14}$$

Therefore, according to ASCE 7 pr. 2.3.2 [7], the loading combination introduced were defined and with particular regard to the seismic area the following combinations are the most conservative:

- For vertical loads: $Combo \quad 2 = 1.2D + 1.6L$
- For seismic loads: $$\begin{array}{l} Combo \quad 5 = 1.2D + 1.0E + L + 0.2S \\ Combo \quad 7 = 0.9D + 1.0E \end{array}$$

where: *D* are the dead load, *L* the live load, *E* the earthquake load and *S* the snow load. More in particular, the seismic loads *E* for the design of the dissipative elements can be evaluated as:

- For Combination 5: $E = E_h + E$
- For combination 7: $E = E_h - E_v$

where: E_h is the effect of the horizontal seismic force and E_v is the effect of the vertical load, and are defined as:

$$\begin{array}{l} E_h = \rho Q_E \\ E_v = 0.2 S_{DS} D \end{array}$$

where: ρ is the redundancy factor (section 12.3.4 ASCE7 [7]), Q_E is the effects of the horizontal seismic forces from V or F_p (Section 12.14.7.5)

In the design of the non-dissipative parts, where the elements will be designed to remains in elastic range (i.e. the columns in MRF structure) the earthquake actions can be defined as:

- For Combination 5: $E_m = E_{mh} + E_v$

- For combination 7: $E_m = E_{mh} - E_v$

where: E_{mh} is the effect of the horizontal seismic force including the overstrenght factor and E_v is the effect of the vertical load, in particular the coefficient can be evaluated as:

$$E_{mh} = \Omega_0 Q_E$$

where Ω_0 is the overstrength factor.

Both the structural imperfection, and stiffness adjustments, were taken into account; indeed according to AISC341 section C2.2 [4]; the geometrical imperfection were considered applying a notational loads as reported in C2.2b.

Moreover, according to AISC 341 [4] section C2.3 the structural stiffness was decreased to take into account the plastic degradation of the cross section.

Response spectrum analysis were introduced for the design phase and all the internal actions on the elements were verify according to AISC360 [3]. Moreover as prescribed form the AIS341 Chapter E also the hierarchy between the beam and the column was verified. The results, in terms of beam and column cross sections, are reported in Table 2.1.

The behavior of the designed structures was also investigated by means a pushover analyses to verify if, the global behavior, in terms of elastic stiffness, resistance and distribution of the plastic hinges between the American and European structures, are comparable.

Table 2.1: SMRF designed starting from the EC structures.

Floor	Structure	Column		Beam	
		External	Internal	External	Internal
I	M-3-3-6-0.25	W14x68	W14x132	W18x50	W18x50
II		W14x53	W14x82	W14x38	W14x38
III		W14x53	W14x82	W14x30	W14x30
I	M-3-3-6-0.35	W14x132	W18x158	W21x57	W21x57
II		W14x82	W18x158	W18x50	W18x50
III		W14x82	W18x130	W18x50	W18x50
I	M-3-3-8-0.25	W18x158	W24x207	W24x84	W24x84
II		W18x158	W24x162	W24x84	W24x84
III		W18x130	W24x162	W21x57	W21x57

According to EN1998-1-1 pr. 4.3.3.4.2.2 [2] two loading distribution were applied: (i) proportional to the mass distribution (uniform response acceleration) and (ii) consistent with the modal pattern, proportional to the lateral force distribution.

Plastic hinges were placed at the all the beams extremity, while brittle hinge at the columns in order to monitoring their stress concentration; the hinges behavior was modelled according to

FEM356 [8]. All the analysis were performed by means SAP2000 [9] software and the structures were pushed up to a top displacement equal to 0.5m.

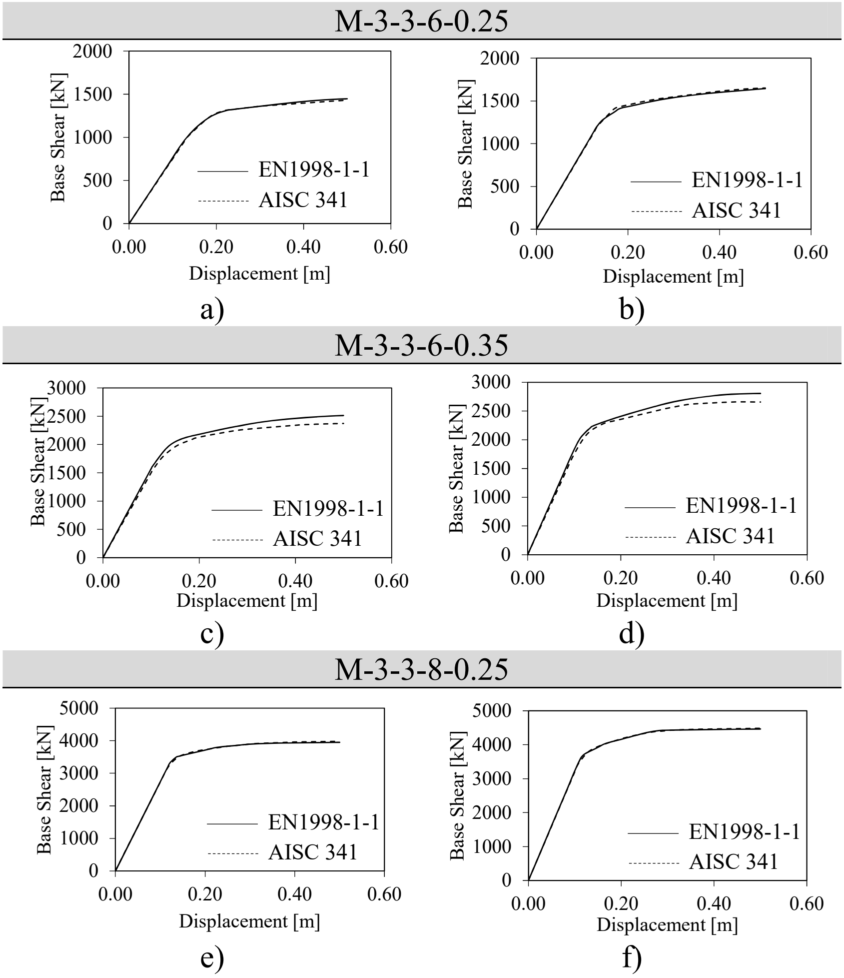

Figure 2-2: Pushover results: proportional to the lateral force distribution a), c) and e); proportional to a masses distribution b), d) and f).

The pushover results are represented just in terms of force displacement curves (see Figure 2-2).

For all the three structures, the results give a good agreement between the American and European approach; some differences can be highlight just in terms of ultimate resistance for the M-3-3-6-0.35 structures. In this case, the not perfect overlap of the curve is due to the distribution of the plastic hinge and their rotational level achieved. Indeed, since the European structure has a smaller beam dimension, the structure present a larger engage of the plastic hinge where the hardening play a central role in capacity definition.

It is important to highlight that American steel structures were designed in order to have the closest geometrical and mechanical features (i.e. second moment of area, shear area, plastic strength, etc.) in order to guarantee theoretically the mechanical equivalence of the beam-to-column assemblies, thus minimizing any influence or disturbance of the steel profile on the behavior of the joints. Therefore, from the designed structure the beam to column profiles were extracted and compared to the European profile in terms of the inertia (I) and the plastic module (W).

Indeed monitoring these two value is possible to control the elastic stiffness and the plastic resistance of the steel cross sections; an example of their comparison is reported in Table 2.2 and Table 2.3 respectively for the column and beam cross section regarding the M-3-3-6-0.35 structures.

Table 2.2: European and American columns cross section comparison.

Element	Type	Section	Ix/Ix	Z/Wpl
C_101	EC	HE300B	1	1
	AISC	W14X68	1.2	1.01
C_102	EC	HE280B	1	1
	AISC	W14X53	1.17	0.93
C_103	EC	HE280B	1	1
	AISC	W14X53	1.17	0.93
C_201	EC	HE400B	1	1
	AISC	W14X132	1.1	1.19
C_202	EC	HE340B	1	1
	AISC	W14X82	1	0.95
C_203	EC	HE340B	1	1
	AISC	W14X82	1	0.95

Table 2.3: European and American beams cross section comparison.

Element	Type	Section	Ix/Ix	Z/Wpl
B_101	EC	IPE450	1	1
	AISC	W18X50	0.99	0.98
B_102	EC	IPE450	1	1
	AISC	W18X50	0.99	0.98
B_201	EC	IPE360	1	1
	AISC	W14X38	0.98	0.99
B_202	EC	IPE360	1	1
	AISC	W14X38	0.98	0.99
B_301	EC	IPE330	1	1
	AISC	W14X30	1.03	0.96
B_302	EC	IPE330	1	1
	AISC	W14X30	1.03	0.96

2.2 American and European designed joints

From the structures designed in the previous paragraph, three beam-to-column assemblies were selected for the comparison with the European joints; Table 2.4 reports the configurations of both American and European assemblies that were analyzed by finite element simulations.

Table 2.4: Beam to column assembly extracted from reference MRFs.

Label	US Joints		EJ Joints	
	Column	Beam	Column	Beam
ES-1	W14×53	W14×38	HE 280 B	IPE 360
ES-2	W14×82	W18×50	HE 340 B	IPE 450
ES-3	W18×130	W24×84	HE 500 B	IPE 600

The steel grades of the profiles were selected among those from US market with the closest yield stress to European one. Namely ASTM 992 for profiles, while for bolts, high strength preloaded grade A325 bolts (A57 Gr.50 as steel grade) were used.

Moreover, each set of joints (i.e. both the US and EJ assemblies) was designed twice: (i) the first group was designed assuming continuity plates and supplementary web plates to strengthen the column, provided that the weak beam-strong column hierarchy is satisfied. (ii) The second was conceived keeping the same beam and the same geometry of the connections (i.e. bolt spacing, end-plate dimensions, rib stiffeners); but increasing the column size in order to satisfy the design strength verifications without using any continuity plate and supplementary web plates.

Indeed, even though this design solution leads selecting heavier profiles for columns, it becomes very popular because of the significant reduction of fabrication costs thanks to the limited use of welds.

The geometry of the designed joints is reported in Table 2.6, while the meaning of the adopted symbols and the definition of the joint components are clarified in Figure 2-4. In particular, each joint is identified by means of a new label code, given as follows:

Design rule (e.g. A stands for US and EJ for European design procedure)-Extended Stiffened joint (e.g. ES)-beam-to-column assembly (e.g. 1 for the shallow beam, 2 for intermediate and 3 for deep beam)-Column details (e.g. S stands for stiffened by continuity plates and supplementary web plates; NS stands for deeper column without strengthening plates)

It is also worth noting that the mechanical equivalence of the profiles is theoretically guaranteed by the nominal geometrical features. Indeed, the geometrical imperfections due to mill tolerances allowed by ASTM A6 / A6M **Error! Reference source ot found.** for US profiles and EN 10034 [10] for European profiles are different. As it can be recognized comparing the values reported in Table 2.5 for the maximum allowed out-of-square of the flange tips with respect to the nominal mid-axis of the flange, the US profiles can be affected by imperfections that are large than those accepted for EU profiles.

Therefore, the influence of constructional imperfections was investigated by means of finite element analyses [13] in order to examine and to quantify their influence on the mechanical behavior of the joint under both monotonic and cyclic loadings using both US and EU steel profiles.

As already show in Chapter V also for the American profile, a cantilever beam subject to a concentrated force imposing both coincident and not buckling waves, were investigated (see Figure 2-3).

The results show one again that no large differences can be pointed out between the two possible buckling configurations. In line with how already did for the European joint the coincident configuration were applied in the following analysis.

The nonlinear performance of the designed joints was investigated in terms of moment-rotation response curve, distribution of plastic deformation and dissipated energy.

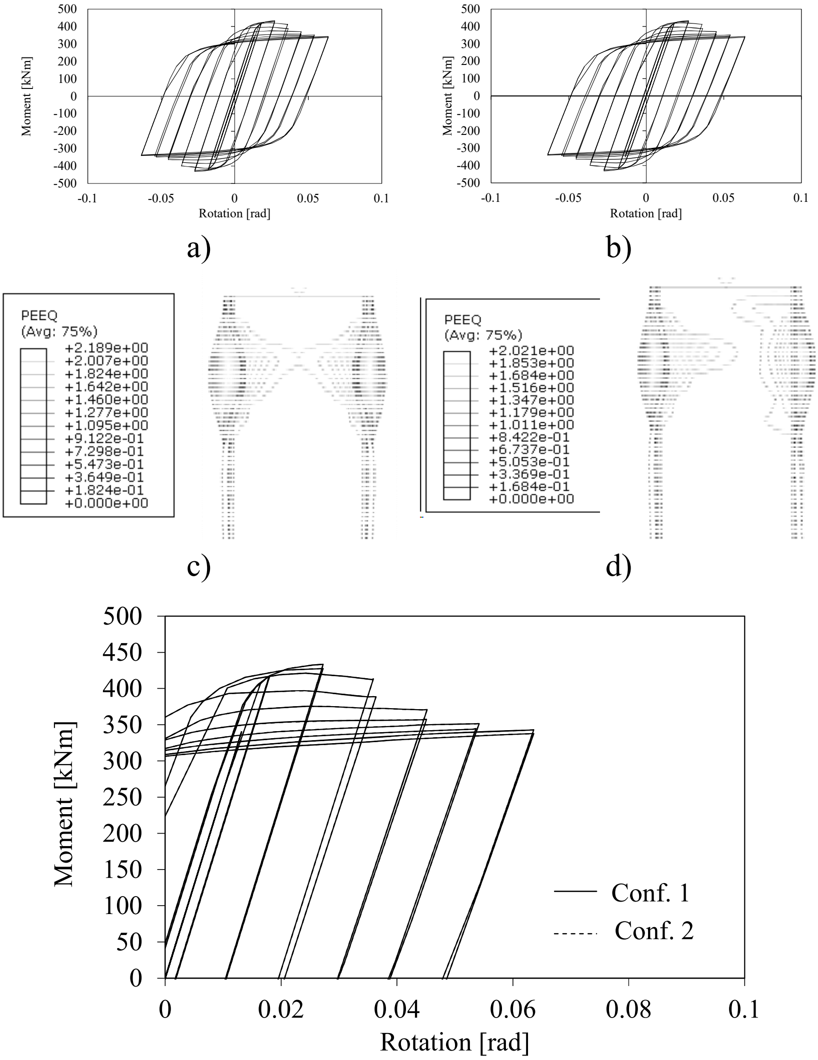

a) b) c) d) e)

Figure 2-3: Buckling sing influence investigation: a), b), e) in terms of moment rotation curve and c), d) in terms of PEEQ deformation.

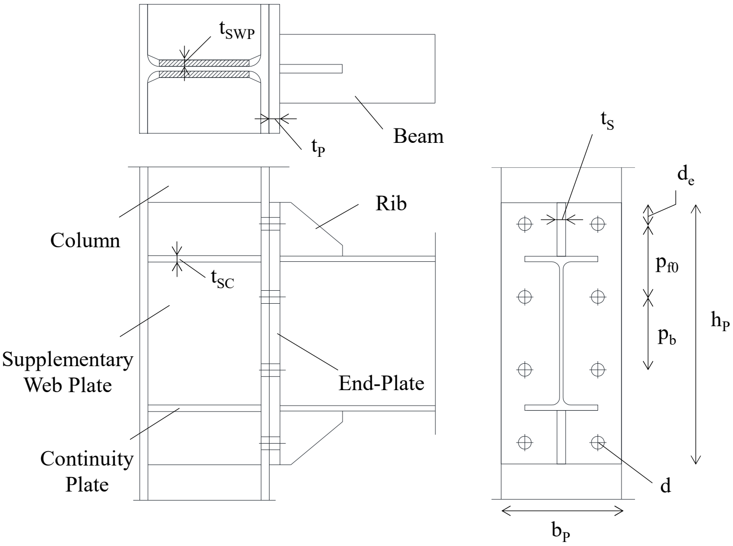

Figure 2-4: Joint geometrical dimension definition.

Table 2.5: Joints beam differences.

Joint labels	Code	Cross Section				Plastic modulus		Second moment of area		Mill tolerances	
		Profile	d	t_{bf}	b_{bf}	W_{pl}	$W_{pl,US/}W_{pl,EU}$	I	I_{US}/I_{EU}	δ_o	$\delta_{o,US}$ /$\delta_{o,EU}$
		[-]	[mm]	[mm]	[mm]	[mm^3]	[-]	[mm^4]	[-]	[mm]	[-]
A-ES_1	US	W14×38	358	13	172	1.01E+06	0.99	1.60E+08	0.99	3.97	2.33
E-ES_1	EJ	IPE 360	360	13	170	1.02E+06		1.63E+08		1.7	
A-ES_2	US	W18×50	457	14	191	1.66E+06	0.97	3.33E+08	0.99	3.97	2.10
E-ES_2	EJ	IPE 450	450	15	190	1.70E+06		3.37E+08		1.90	
A-ES_3	US	W24×84	612	20	229	3.67E+06	1.05	9.86E+08	1.07	3.97	1.80
E-ES_3	EJ	IPE 600	600	19	220	3.51E+06		9.21E+08		2.2	

Table 2.6: Joints geometrical characteristics.

Label	Column	Beam	Bolt Rows	EP							CP	SWP		Rib	
				Bolt	b_P	h_P	t_P	d_e	p_{f0}	p_b	t_{SC}	n	t_{SWP}	Slope	t_S
				[mm]	[mm]	[mm]	[mm]	[mm]	[mm]	[mm]	[mm]	[-]	[mm]	[-]	[mm]
A-ES_1_S	W14×53	W14×38	4	32	205	549	25	44	51	0	13	1	16	30°	12.7
A-ES_1_NS	W14×159	W14×38	4	32	205	549	25	44	51	0	0	0	0	30°	12.7
E-ES_1_S	HE 280 B	IPE 360	6	30	260	760	25	50	75	160	15	2	8	40°	20
E-ES_1_NS	HE 400 B	IPE 360	6	30	260	760	25	50	75	160	0	0	0	40°	20
A-ES_2_S	W14×82	W18×50	8	29	257	826	22	44	51	89	14	1	16	30°	15.9
A-ES_2_NS	W14×193	W18×50	8	29	257	826	22	44	51	89	0	0	0	30°	15.9
E-ES_2_S	HE 340 B	IPE 450	6	30	280	870	25	50	75	180	15	2	10	40°	20
E-ES_2_NS	HE 600 B	IPE 450	6	30	280	870	25	50	75	180	0	0	0	40°	20
A-ES_3_S	W18×130	W24×84	8	35	284	987	32	44	54	89	20	2	13	30°	15.2
A-ES_3_NS	W18×234	W24×84	8	35	284	987	32	44	54	89	0	0	0	30°	15.2
E-ES_3_S	HE 500 B	IPE 600	6	36	280	1100	30	55	95	210	20	2	15	40°	20
E-ES_3_NS	HE 800 B	IPE 600	6	36	280	1100	30	55	95	210	0	0	0	40°	20

CHAPTER VIII

---

3 Designed joint according to AISC 358

3.1 American vs European steel Profile

As previously discussed, the steel profiles of both beam and column assemblies were chosen to be mechanically equivalent (namely the closest as possible second moment of area, shear area, plastic modulus) in order to focus the study on the influence of the design criteria for extended stiffened joints.

With particular regard to the beams, the effectiveness of this design choice was validated by means of finite element analyses on all selected profiles that were schematized using a cantilever beam, as shown in Chapter V xx. Figure 3-1 show that both US and EU profiles at the same depth exhibit very similar plastic capacity evaluated by analytical procedure and the FEM results, considering the beam material as elastic perfectly plastic and without geometrical imperfections. The differences arise when mill tolerances are accounted for as it can be noted comparing the response curves depicted from Figure 3-2 to Figure 3-4.

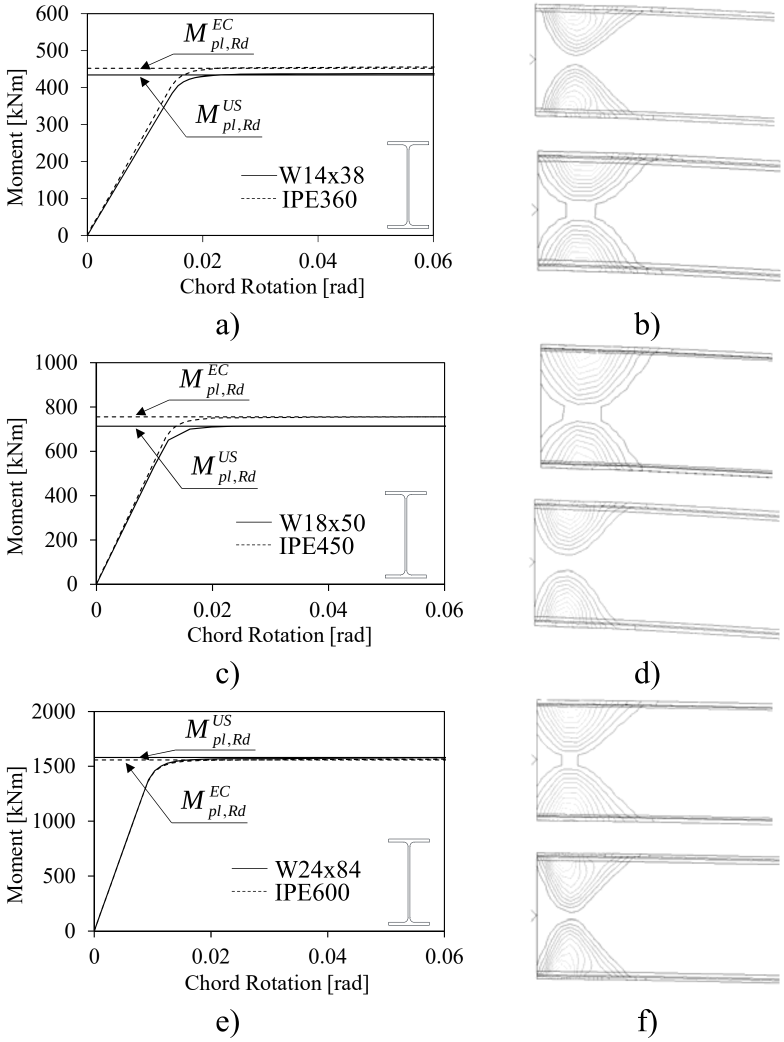

a) b)

c) d)

e) f)

Figure 3-1: Analytical vs FEM beam capacity prediction for: ES1 (a), ES2 (c) and ES3 (e) with the corresponding PEEQ deformation (b, d, f).

Indeed, the maximum tolerances (see Table 3.1) allowed by [4] for US profiles are almost twice those considered for corresponding European members [10]. This feature explains the reason of the deterioration of the beam flexural capacity for American shapes. It is worth noting that this detrimental effect is more significant under cyclic loading (see Figure 5).

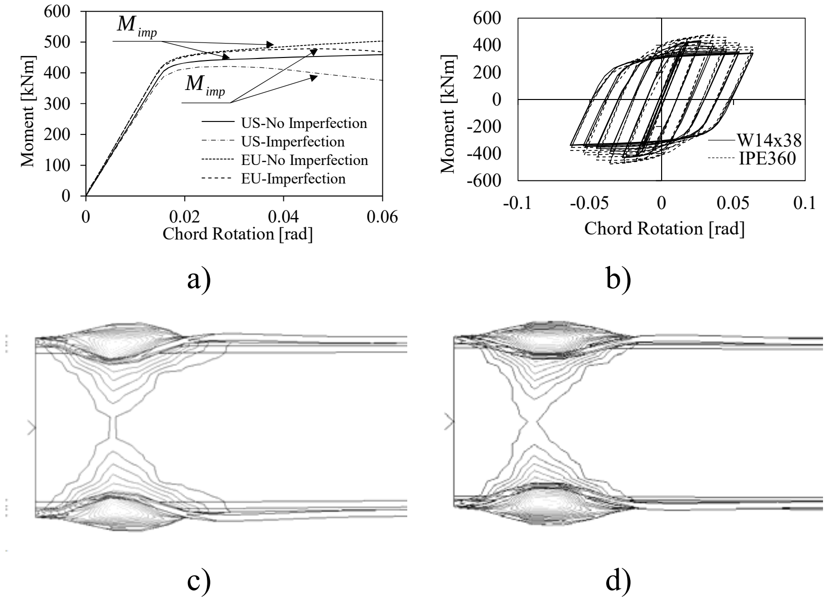

a) b)

c) d)

Figure 3-2: ES1 beam behavior in terms of moment rotation curve under monotonic (a) and cyclic (b) action and PEEQ distribution (c and d).

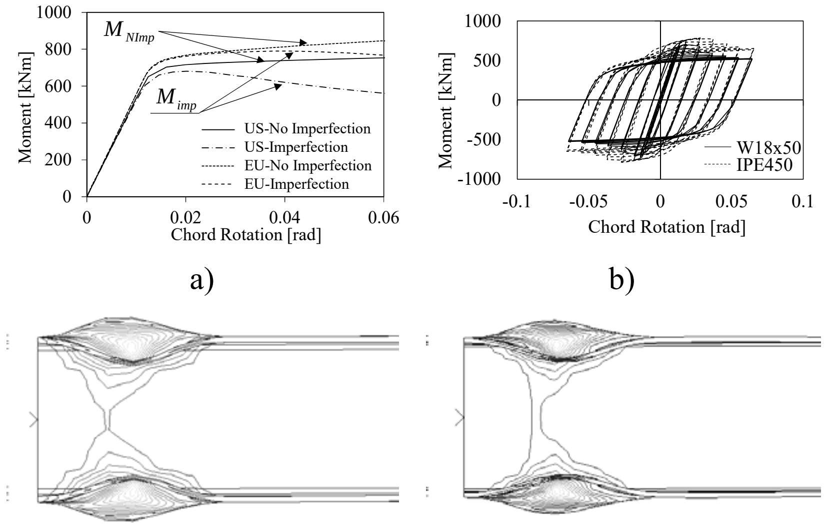

a) b)

c) d)

Figure 3-3:ES2 beam behavior in terms of moment rotation curve under monotonic (a) and cyclic (b) action and PEEQ distribution (c and d).

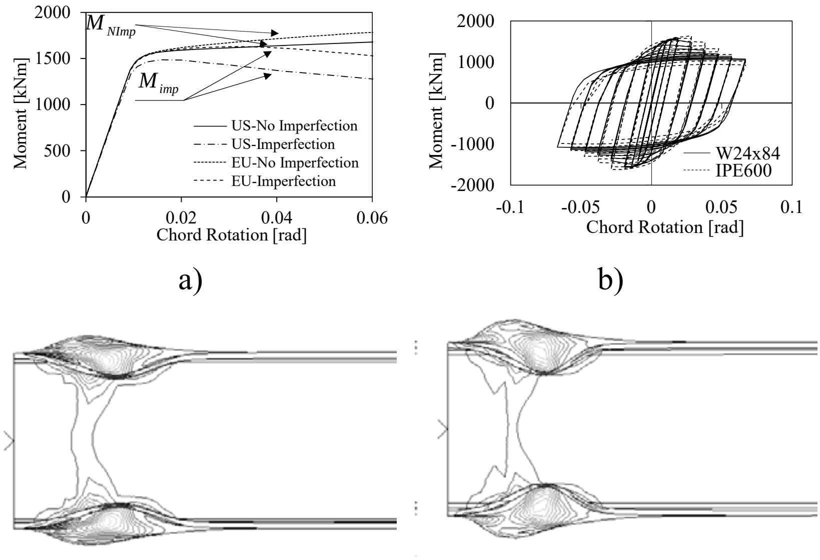

a) b)

c) d)

Figure 3-4: ES3 beam behavior in terms of moment rotation curve under monotonic (a) and cyclic (b) action and PEEQ distribution (c and d).

3.2 American vs European joints behavior

Monotonic and cyclic analyses were carried out both considering and disregarding mill imperfections in order to deepen the investigation on the effectiveness of the US and EJ design criteria. The results obtained from FEAs showed that all investigated joints ensure the formation of a plastic hinge at the end of the beam out of the protruding part of the connection (i.e. the rib tip), thus demonstrating that both US and EJ design criteria can satisfy the design objective.

The results for the ES1 (see Figure 3-5), ES2 (see Figure 3-6) and ES3 (see Figure 3-7) joints are hereinafter presented both for the models without geometrical imperfections and for those with imperfections.

The comparison highlights that the response curves of the nominally perfect model are very similar with slight differences in terms of elastic stiffness and yield resistance, which are mainly due to the geometrical differences of the chosen steel members.

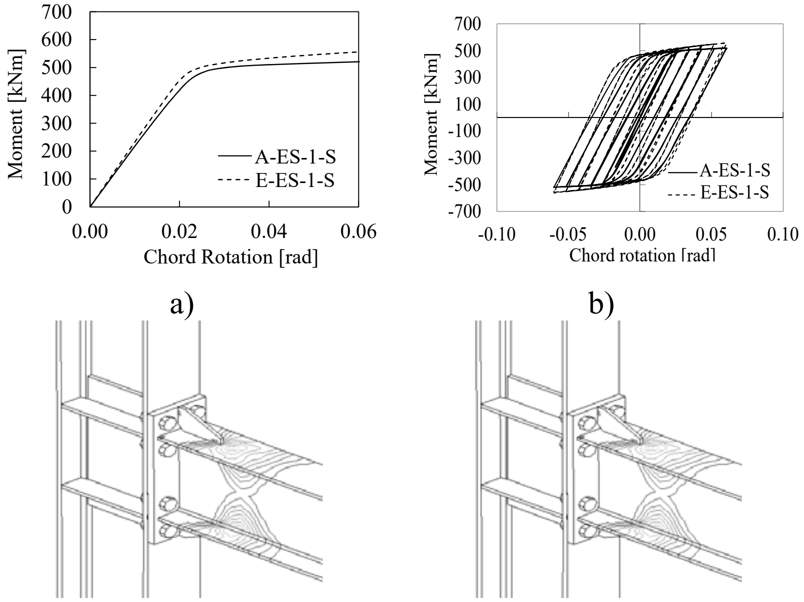

a) b)

c) d)

Figure 3-5: Comparison between A-ES-1-S and E-ES-1-S in terms of: monotonic (a) and cyclic (b) moment rotation and PEEQ distribution (c and d).

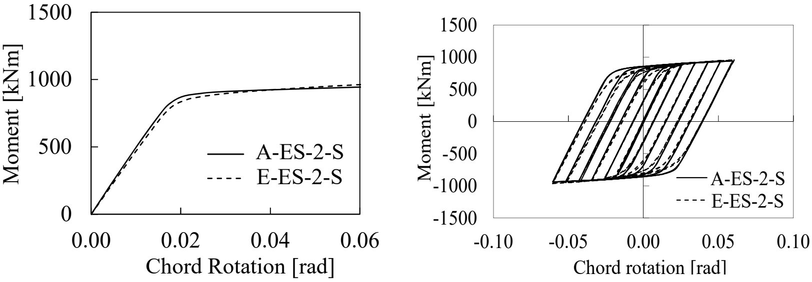

a) b)

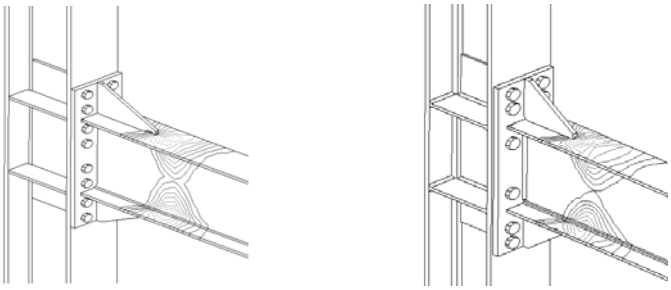

c) d)

Figure 3-6: Comparison between A-ES-2-S and E-ES-2-S in terms of: monotonic (a) and cyclic (b) moment rotation and PEEQ distribution (c and d).

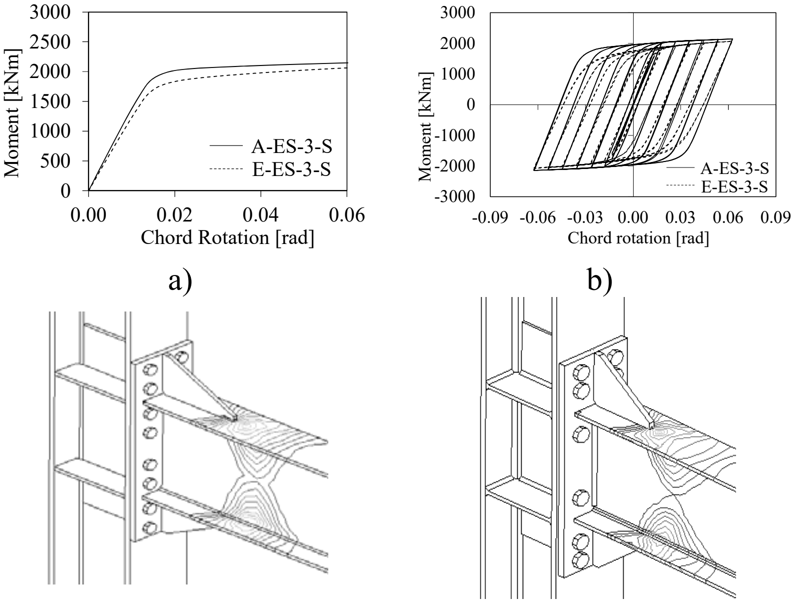

a) b)

c) d)

Figure 3-7: Comparison between A-ES-3-S and E-ES-3-S in terms of: monotonic (a) and cyclic (b) moment rotation and PEEQ distribution (c and d).

Even though the response curves of both US and EJ assemblies are similar, the joint failure mode can be different. In order to investigate this feature, FEAs were carried out on models in which the material of the beams was fictitiously assumed to be perfectly elastic.

This assumption was adopted in order to evaluate the plastic response of the connection and the column web panel, and to investigate the joint overstrength with respect to the beam flexural resistance.

For instance, with reference to the ES-1 (see Figure 3-8) beam-to-column assembly, US and EJ joints experience different failure modes. The American joint shows a less ductile behavior due to bolt failure, which occurred at a 4% of rotation. On the other hand, the ES1-EJ joint is characterized by a ductile failure mode with plastic deformations occurring into the plates and the column. In addition, no gap opening is observed resulting in a bending capacity increased by about 35% at a 0.04 radian chord rotation with respect to the corresponding US joint.

This difference can be explained considering that AISC 358-16 [1] does not enforce controlling the bolt diameter with respect to the thickness of the plate, in order to avoid mode 3. In addition, the four bolt rows configuration imposed by AISC 358-16 [1] is weaker than the 6 bolt rows configuration and the smaller lever arm induces a larger tension demand into the tensile bolt rows.

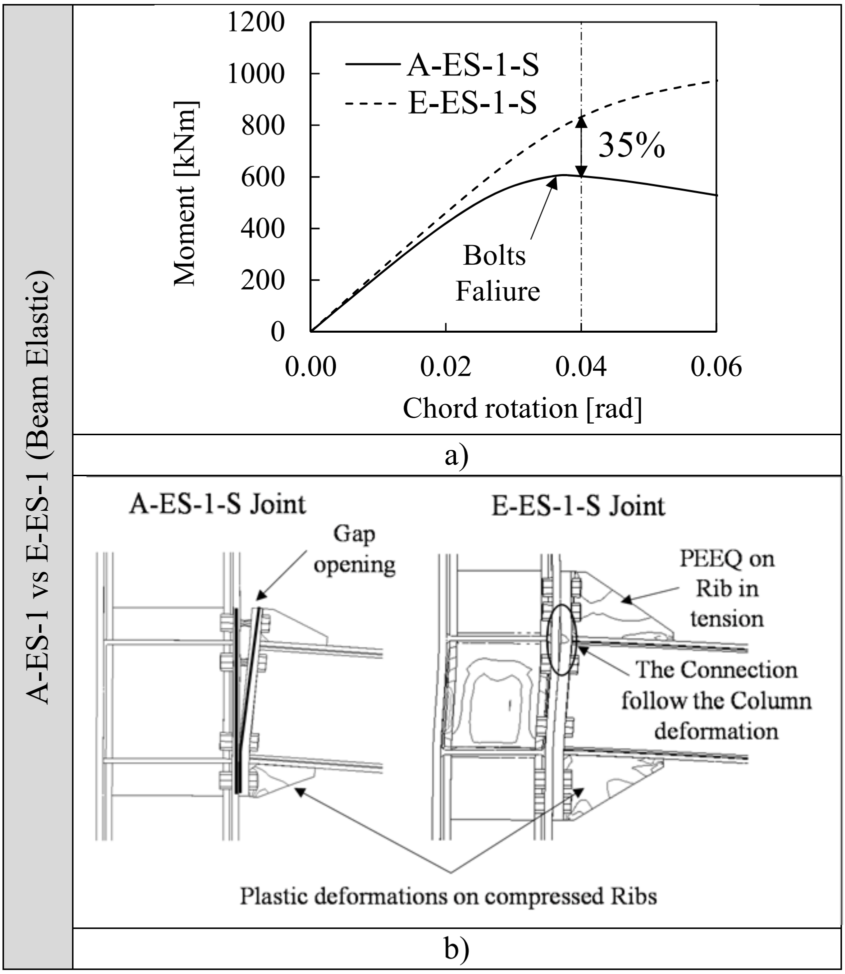

Figure 3-8: ES1 with elastic beam, moment rotation curve (a) and PEEQ distribution (b).

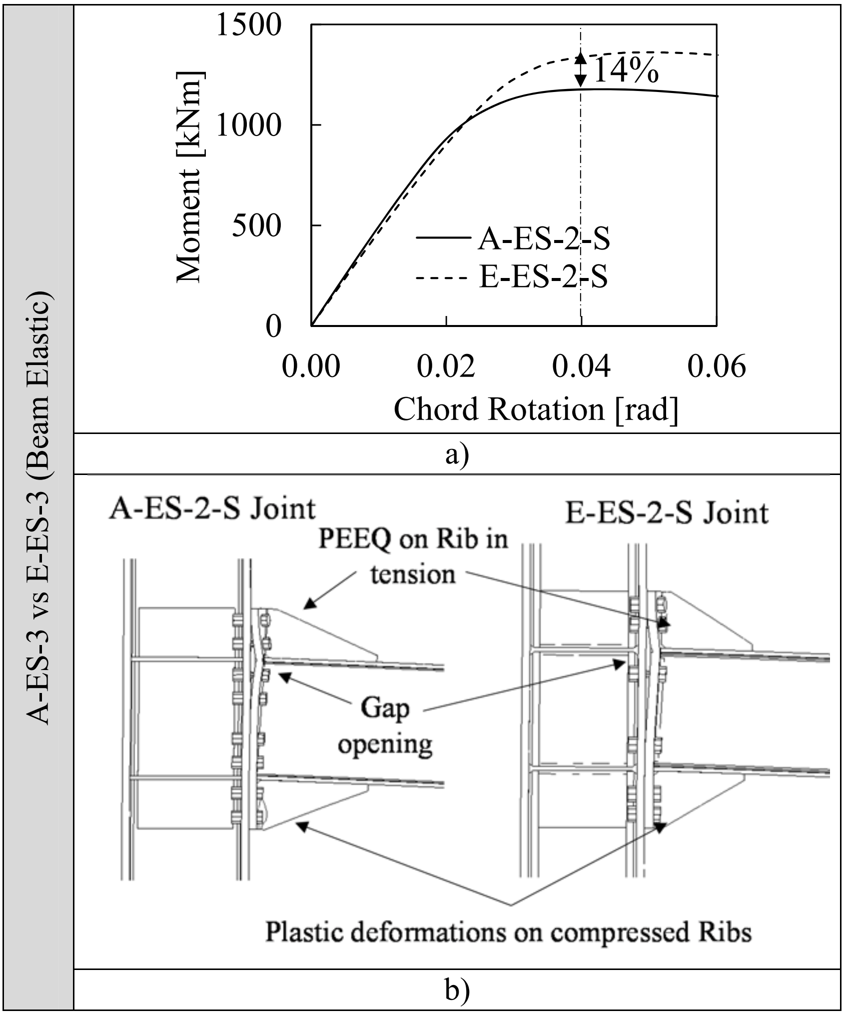

a)

b)

Figure 3-9: ES2 with elastic beam, moment rotation curve (a) and PEEQ distribution (b).

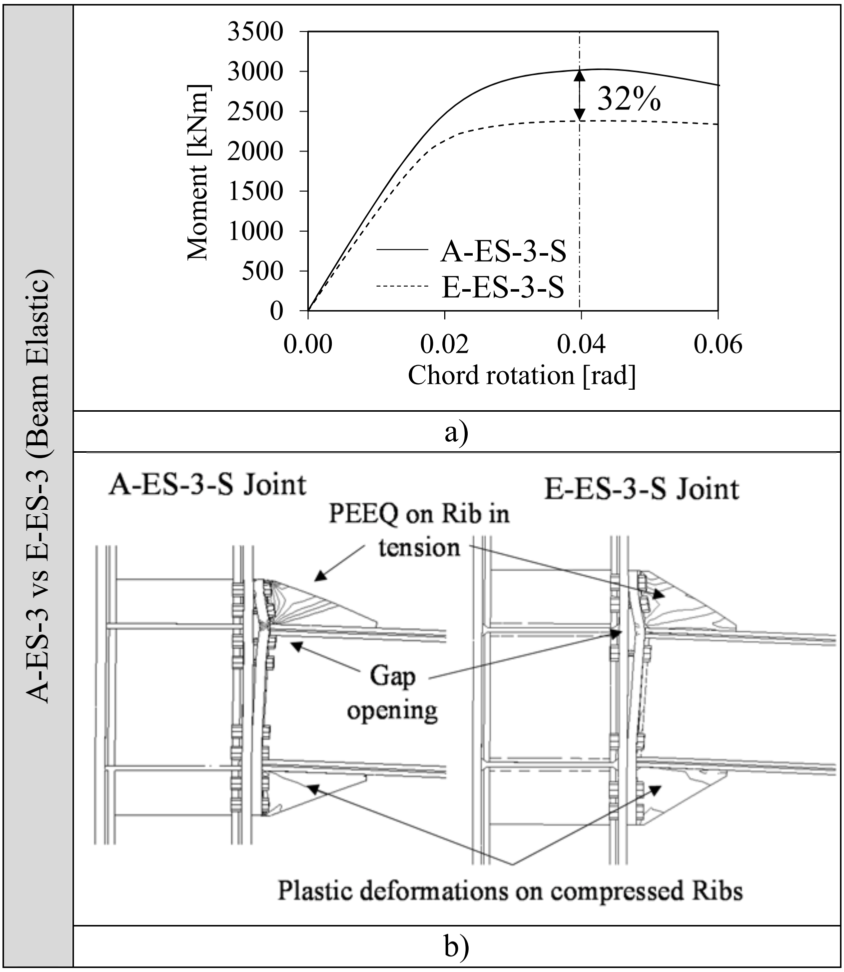

Figure 3-10: ES3 with elastic beam, moment rotation curve (a) and PEEQ distribution (b).

ES-3 joints (namely those with deep beams) exhibit similar failure modes. Indeed, in this case both joints show a failure mode 2 with a tendency to work mode 3 due to strain hardening occurring at rotations larger than 4% (see Figure 3-10). Despite the failure mode, substantial differences can be observed in terms of bending capacity (see Figure 3-10), which are mainly due to the different number of bolt rows in tension. In the US joints the presence of four bolt rows guarantees that both the ultimate strength and stiffness of the connection will be larger than that of EJ 6 bolt rows joint.

The comparison depicted in Figure 3-10 in terms of yield line pattern also highlights that the US 8-bolt rows joint allow concentrating the plastic strain into the end-plate at the beam flange level on the tension side, while the plastic strains on the compression side are slightly smaller than those shown by the corresponding EJ joint where plastic strain tends to concentrate into the rib tip. These findings are also confirmed by the comparison between the dissipated energy by each joint component (expressed in terms of percentage of the total amount) summarized in Table 3.1. Indeed, at a rotation equal to 0.04 rad both American and European joints with realistic steel material experience more than 90% of the plastic dissipated energy in the beam and a negligible percentage in the connection.

The plastic energy distribution was also monitored for the models with the elastic beam. Consistently with the observed failure mode, A-ES-1 shows that most of the plastic demand is in the bolts (85%), while the end-plate, the column and the ribs, dissipate the remaining 15%. On the other hand, E-ES-1 shows a large amount of energy concentrated into the column web panel (i.e. about 50%) and in the ribs (i.e. 20% considering both the rib in tension and that in compression). The plastic demand in the bolts is negligible (i.e. about 0.1%).

Similar considerations can be observed for the ES-3 assemblies. Indeed, the amount of dissipated energy by each component is consistent with the monitored failure mode as discussed previously.

Table 3.1: Dissipated energy per joint component at rotation equal to 0.04 rad (as percentage of the total).

Joint Configuration		Beam [%]	Column [%]	EP [%]	Bolts [%]	Ribs [%]	Others [%]
A-ES-1-S	Realistic Steel	95.81	1.15	0.13	2.19	0.72	0.00
	Elastic Beam	0.00	4.45	4.782	84.35	6.39	0.02
E-ES-1-S	Realistic Steel	99.48	0.07	0.00	0.10	0.33	0.02
	Elastic Beam	0.00	58.33	7.86	13.24	20.50	0.06
A-ES-3-S	Realistic Steel	93.15	0.02	0.60	3.14	3.06	0.03
	Elastic Beam	0.00	3.78	19.44	53.07	23.12	0.58
E-ES-3-S	Realistic Steel	95.45	0.04	0.55	1.89	2.01	0.06
	Elastic Beam	0.00	0.67	15.83	47.36	36.03	0.10

3.3 Influence of mill imperfections

The behavior of beam-to-column joints is influenced by the geometrical mill imperfections.

Indeed, considering the maximum permitted beam mill tolerances the cyclic response of the joints deteriorates for a chord rotation of about 0.03 rad due to beam flange plastic buckling followed by web out-of-plane deformations, as depicted in Figure 3-11, Figure 3-13, and Figure 3-16 for the ES-1, ES-2 and ES-3 assemblies respectively.

The comparison between A-ES1-S and E-ES1-S (see Figure 3-11) configurations highlights a very similar behavior in terms of: (i) elastic stiffness, (ii) flexural strength and (iii) the curve shape, while some differences can be highlighted from the PEEQ distribution and the dissipated energy point of view.

Indeed, Figure 3-11 *f)* shows that the American joints experience also plastic deformation at the welds between the beam flange and the end-plate, thus confirming the need to use full penetration welds for those details, while only the beam is plastically engaged in the European ES-1 joint. In addition, both cases show plastic strains developing at the rib tip on the beam side.

Moreover, comparing the dissipated energy (DE) accumulated per cycle (i.e. calculated as the sum of the areas enclosed by each hysteretic loop) normalized to the energy cumulated up to 0.04 rad of chord rotation by full strength joints ($DE_{0.04Full}$) the American joint show a slightly larger ductility respect to the European one (see Figure 3-11 *e*).

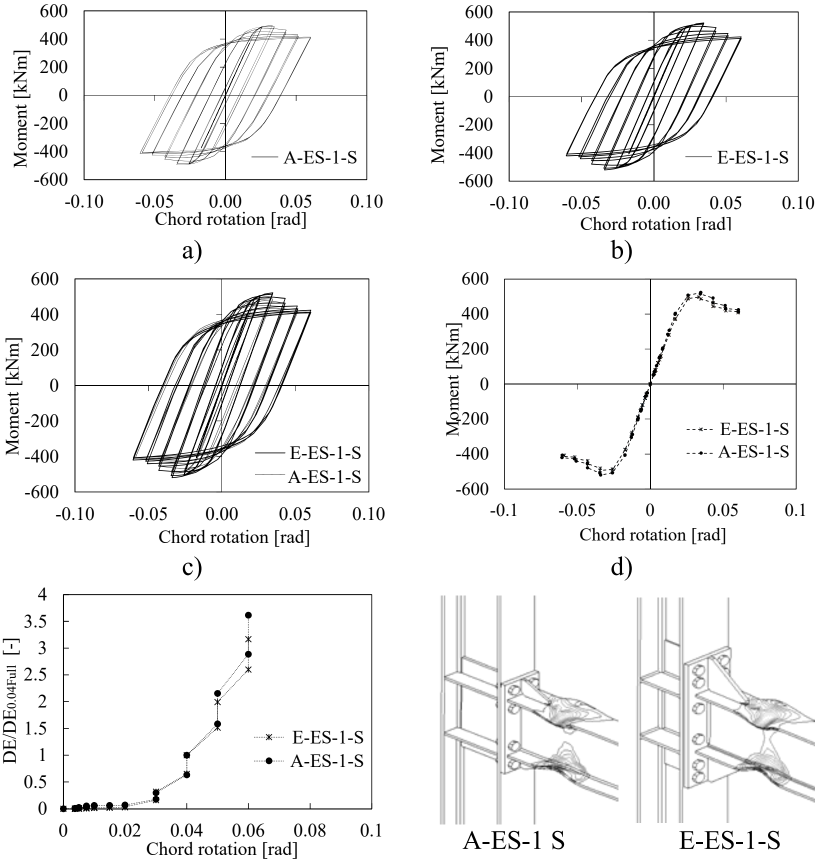

a) b)

c) d)

e) f)

Figure 3-11: ES-1-S joint assembly: Moment-rotation curve (a, b and c), back bone curves (d), PEEQ distribution (f) and cumulated dissipated (e).

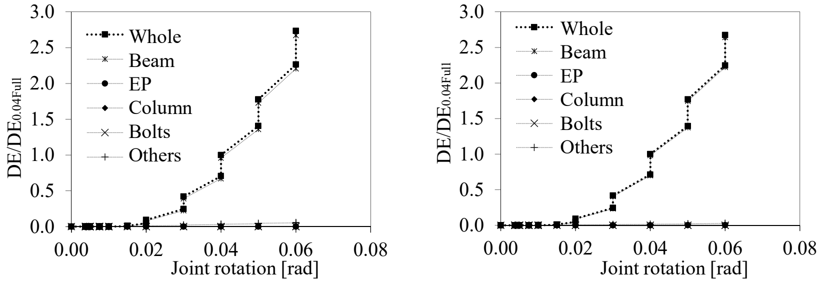

a) b)

Figure 3-12: American (a) and European (b) cumulated dissipated energy for each component.

On the other hand, looking at their global behavior (see Figure 3-12) it can be recognized for both US and EJ, most of the energy dissipation is taking place in the beam and no appreciable energy was dissipated by the other components.

No differences can be observed comparing the ES2 joints, where the PEEQ distribution and the relative internal dissipated energy are very similar for both American and European joints (see Figure 3-13).

It is interesting to observe that the shape of the cyclic moment-rotation response curves differs slightly for US and EJ assemblies, but the backbone curves are overlapped. This result highlights that even though the maximum constructional tolerances allowed for US profiles are larger than those permitted for European members, their effects are less significant on the overall performance of the joint assembly. Moreover, the perfect behavior of the ES2 joints is also confirmed by the distribution of the dissipated energy in the joints component (see Figure 3-14).

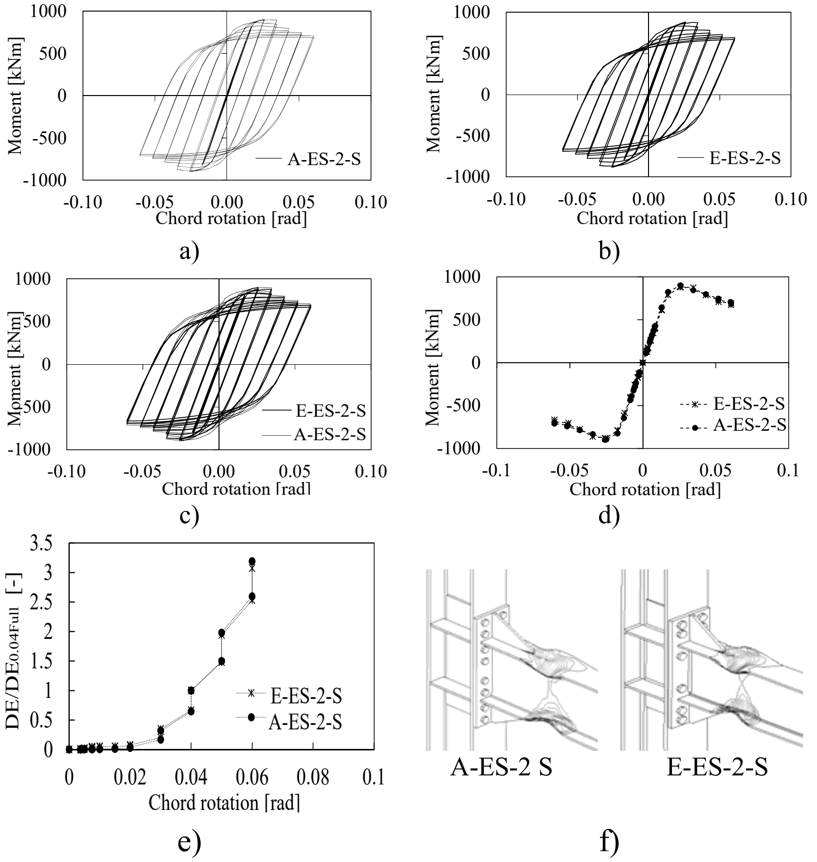

Figure 3-13: E S-2-S joint assembly: Moment-rotation curve (a, b and c), back bone curves (d), PEEQ distribution (f) and cumulated dissipated (e).

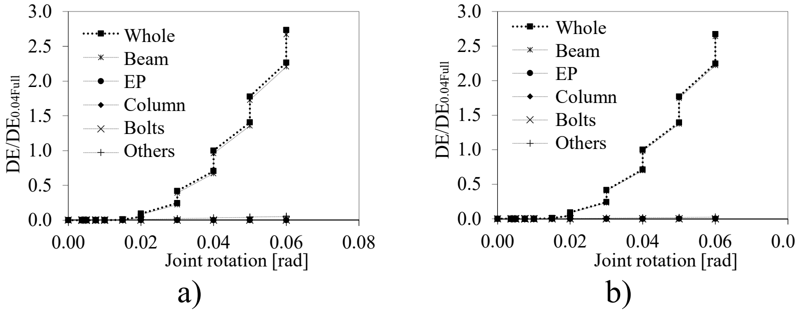

Figure 3-14: American (a) and European (b) cumulated dissipated energy for each component.

In the case of ES-3 assemblies (see Figure 3-16), the connections of both US and EJ joints are almost elastic with plastic deformations concentrated into the beam. However, the US joint experiences some plastic strains in the rib (see Figure 3-16 *f*) due to the out-of-plane bending induced by the flange buckling as well as plastic strain in the welds between the rib and the end-plate.

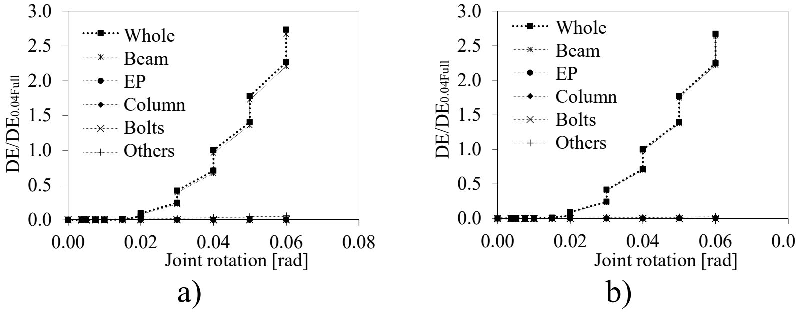

Figure 3-15: American (a) and European (b) cumulated dissipated energy for each component.

On the other hand, in the EJ joint the plastic strains are developed only at the rib tip on the beam side, as in the ES-1 joint.

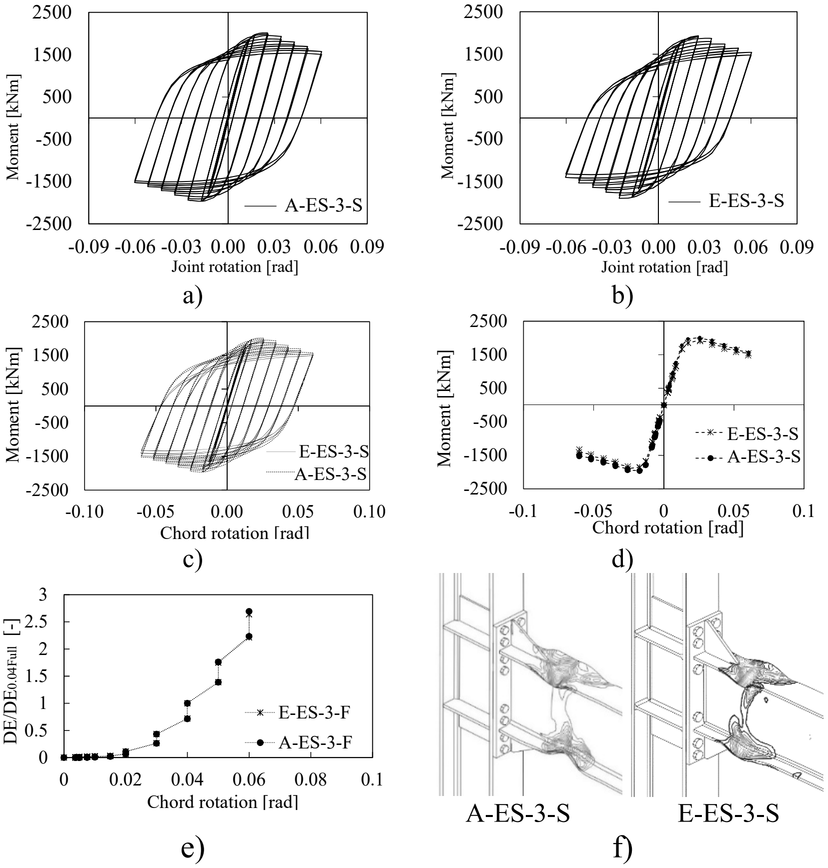

Figure 3-16: E S-3-S joint assembly: Moment-rotation curve (a, b and c), back bone curves (d), PEEQ distribution (f) and cumulated dissipated (e).

The analyzed cases confirm that both US and EJ joints exhibit similar performance. In particular, it should be noted that the differences in terms of degradation of bending strength is lower for the joint assemblies than for the beams taken alone (see from Figure 3-2 to Figure 3-4). This feature is due to the fact that at the same chord rotation the connection and the column also contribute to the overall deformation, thus the deflection of the beam as part of the joint assembly is smaller than in the cantilever configuration.

Moreover, it is important to highlight that both US and EJ joints exhibit similar performance notwithstanding the significant geometrical differences, namely the different number of bolts and their spacing, and the slope of the rib stiffener.

Therefore, as shown Figure 3-17, the distribution of bolt tensile forces was monitored in order to investigate the evolution of bolt reactions with the joint rotation. For low levels of rotation, the bolt normal action is equal to the initial clamping force. Increasing the rotation, the bolt force increases up to the formation of a plastic hinge in the beam, after which it remains constant.

Disregarding the value of the initial clamping force, in case of ES1 joints (see Figure 3-17 *a*, *b*) the imposed peak bolt tension force is approximately the same for the both US and EJ assemblies, even though in the former case the connection has only 4 bolts, while there are 6 bolts in the second connection.

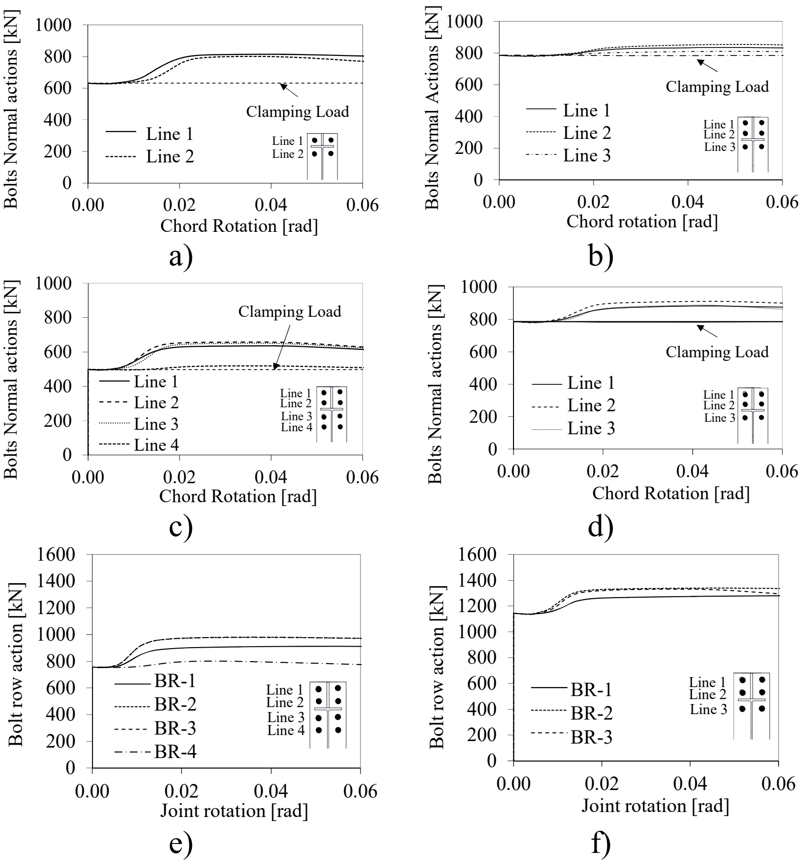

a) b)

c) d)

e) f)

Figure 3-17: American and European bolt force evolution in function of the chord rotation for: ES1 (a and b), ES-2 (c and d) and ES-3 (e and f).

ES-2 and ES-3 joints (i.e. configurations with medium and deep beams) do not show this feature. Indeed, the EJ connections are characterized by a larger bolts force demand than the corresponding US connection. In this case it is trivial to recognize that the larger demand in EJ joints depends on the lower number of resisting bolts, which are more engaged than those present in the US joint.

Another important difference is that the slope of the ribs in US joints is equal to 30°, while it can be increased up to 40° in the EJ joints. As it was demonstrated by [12] for welded rib stiffened joints, the smaller the rib slope is closer to the de Saint Venant beam theory is the transfer mechanism of internal stresses. On the contrary, with a larger rib slope the internal stresses are transferred by a strut-tie mechanism.

In line with this observation, the distribution of compression forces for ES-1 joints is depicted in Figure 3-18 *a* and *b*. As it can be noted, in A-ES1-S joint the compression force into the beam flange is three times larger than that imposed to the rib stiffener. On the contrary, in the EJ joint the compression resultants acting into the beam flange and the rib plate are very similar.

The results of ES-3 joints exhibit similar trend. Indeed, a large difference in the US assemblies and a more balance distribution in the European one can be recognized.

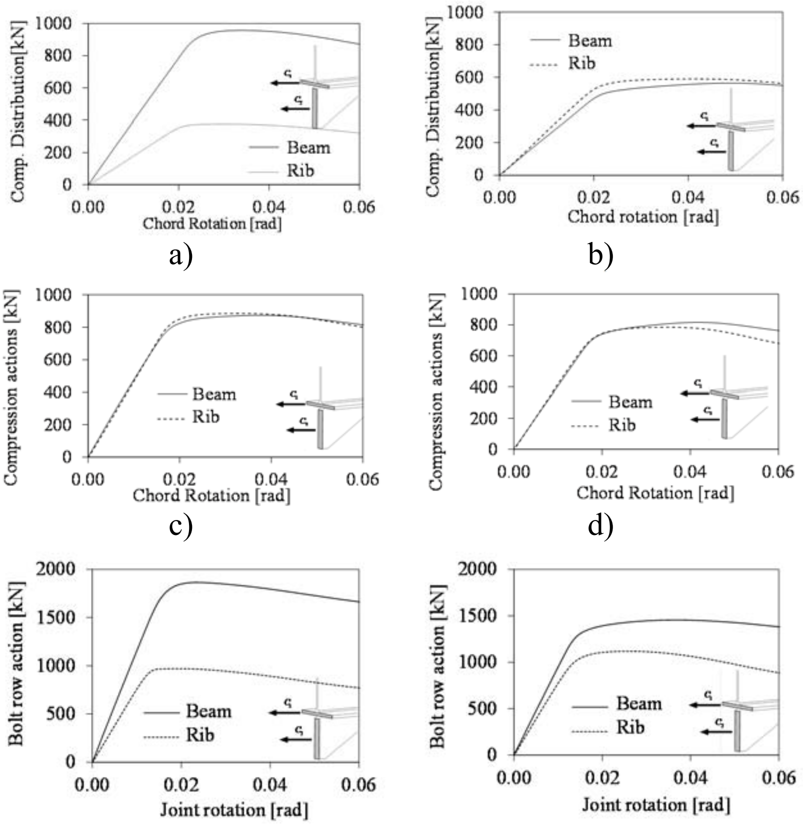

a) b)

c) d)

e) f)

Figure 3-18: Compression action distribution between the beam flange and the rib for: ES-1 (a and b), ES-2 (c and d) and ES-3 (e and f).

In contrast with the US joints, where the ratio between the compression force in the beam and in the rib is almost constant for all the investigated cases, the EJ joints show three different loading distribution corresponding to the three joints assemblies. These differences can be ascribed to the joint geometries, indeed the American joints have an increasing value of the rib thickness for each beam-to column joints (according to AISC358 [1]), while the European joints have a constant rib thickness for all the specimens.

Since the rib thickness is constant, increasing the beam dimensions means have three different ratio between the rib and the beam compressive flange dimensions. Therefore the in the first case where the beam (IPE360) is small, it is the rib that carry the most of the compression capacity (see Figure 3-18 *b*), while increasing the beam size (E-ES2) the ratio between the beam and the rib is almost the same and the compression is equally divided (see Figure 3-18 *d*).

In the last case, with the increase of the beam dimension (IPE600), most of the compression is transmitted by the beam (see Figure 3-18 *f*).

4 Influence of column details: presence of continuity plates and supplementary web plates

The presence of stiffeners and strengthening plates, e.g. continuity plate and supplementary web plates, improves the joint performance but requires the use of welds that could significantly increase the fabrication time and related costs. Moreover, the welds may represent a critical point in the joints, which should be properly verified and tested after manufacturing to avoid a premature brittle failure. Nowadays, it is a common practice to reduce the use of welds minimizing the use of web double plates. As a consequence larger column sizes are selected to satisfy the strength requirements and capacity design rules. In light of these considerations, all assemblies were designed keeping the same beam and connection but increasing the column size to avoid both continuity plate and supplementary web panel as previously discussed and reported in Table 2.6.

FEAs showed that this design choice does not affect the monotonic and cyclic moment rotation curves of both American and European joints.

For reason of brevity, in the following, just the results of the intermediate joints will be reported because all the other models (reported in the Annex) show the same results.

The cyclic moment rotation curves (see Figure 4-1 *a*) and the PEEQ distribution (see Figure 4-1 *b*) show a perfect full strength behavior allowing the plastic deformation only in the connected beam. This result is also confirmed by the internal energy distribution among the joints components, where it can be observed that, for both European and American assemblies investigated, more than the 90% of the internal energy is dissipated by the beam (see Figure 4-1 *c* and *d*).

The comparison against the stiffened joints is reported in terms of moment rotation curve, for both monotonic and cyclic actions. It can be noted (see Figure 4-2) that, since the column stiffness play a central role in the joint elastic stiffness definition, the unstiffened joint are characterized by slightly larger stiffness, without showing appreciable differences in terms of ultimate strength.

The comparison between the backbone curves obtained for joints with stiffened and unstiffened column are depicted in Figure 4-2 *c* and in Figure 4-2 *d* for US and EJ assemblies, respectively. As it can be noted, the differences of backbone curves are negligible.

Moreover, by the comparison of both American and European stiffened joints, against the un-stiffened configuration from the dissipated energy point of view, it is possible notice how the latter case the joints result more ductile.

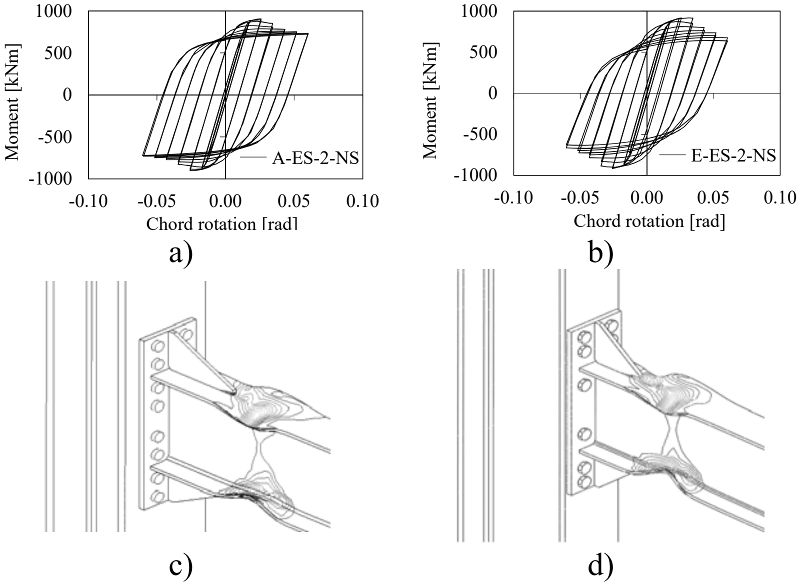

a) b)

c) d)

Figure 4-1: American and European ES-2 joints results in terms of: Cyclic moment rotation curve (a and b) and PEEQ distribution (c and d).

All cases with increased and unstiffened column show lesser plastic deformations into the beam web and a longer portion of the beam subjected to flange buckling.

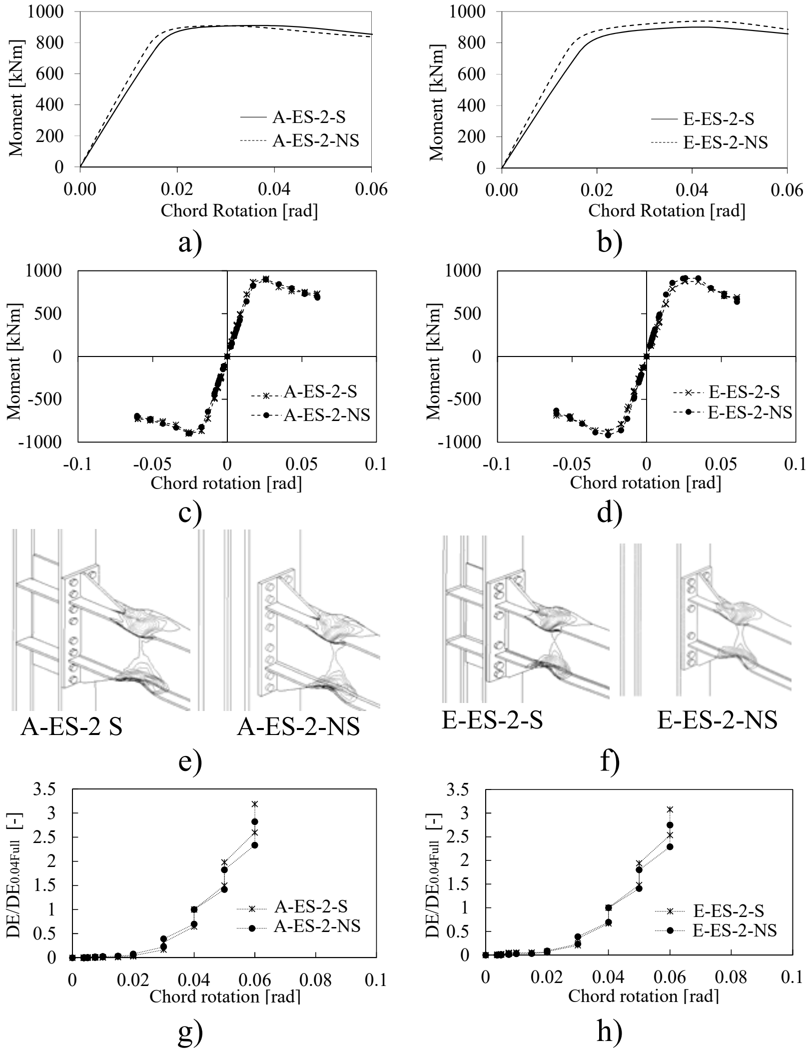

Figure 4-2: Comparison for both American and European ES-2 joints between the Stiffened and Unstiffened configuration in terms of: Monotonic moment rotation curve (a and b); Back bone curve (c and d), PEEQ distribution and backbone curve (e and f) and dissipated energy (g and h).

However, these findings suggest that changing the column size does not appreciably modify the local response of the joint assembly, while some differences can arise for the global structural response because a larger size of the column modifies the structural lateral stiffness, the internal force distribution and the seismic forces, as well. Therefore, if adopted, this design choice requires a re-analysis and re-verification of the structural system.

References

[1] ANSI/AISC 358-16 (2016). Prequalified Connections for Special and Intermediate Steel Moment Frames for Seismic Applications. American Institute of Steel Construction.

[2] EN 1998-1, Design of structures for earthquake resistance - Part 1: General rules, seismic actions and rules for buildings. CEN 2005.

[3] ANSI/AISC 360-16 (2016). Specification for Structural Steel Buildings. American Institute of Steel Construction.

[4] ANSI/AISC 341-16 (2016). Seismic Provisions for Structural Steel Buildings. American Institute of Steel Construction.

[5] Abidelah A., Bouchaïr A., Kerdal D.E. (2012). Experimental and analytical behavior of bolted end-plate connections with or without stiffeners. Journal of Constructional Steel Research, 76, 13–27

[6] EN 1993:1-8, Design of steel structures - Part 1-8: Design of joints. CEN 2005.

[7] ASTM A6 / A6M (2016). Standard Specification for General Requirements for Rolled Structural Steel Bars, Plates, Shapes, and Sheet Piling. West Conshohocken, PA.

[8] FEMA 356 (2001). Prestandard and Commentary for the Seismic Rehabilitation of Buildings. ASCE Standards Committee on Seismic Rehabilitation of Buildings.

[9] CSI, “SAP2000 Integrated Software for Structural Analysis and Design,” Computers and Structures Inc., Berkeley, California.

[10] ASTM (American Society for Testing and Materials International). (2016). “Standard Specification for General Requirements for Rolled Structural Steel Bars, Plates, Shapes, and Sheet Piling”. ASTM A6 / A6M, West Conshohocken, PA.

[11] EN 10034. Structural steel I and H sections: Tolerances on shape and dimensions. CEN 1993.

[12] Lee C.-H. Jung J.-H., Oh M.-H., Koo E-S. (2005). Experimental Study of Cyclic Seismic Behavior of Steel Moment Connections Reinforced with Ribs. Journal of Structural Engineering, ASCE, 131(1), 108-118

[13] Dassault Systèmes. Abaqus analysis 6.14 user’s manual. Simula Inc.; 2015

List of figures

Figure 1-1: Story drift determination [7]. 518
Figure 1-2: European (a) and American (b) inter-story drift limitations and their comparison (c). 520
Figure 1-3: American and European joint configurations. 525
Figure 2-1: Design response spectrum[7]. 529
Figure 2-2: Pushover results: proportional to the lateral force distribution a), c) and e); proportional to a masses distribution b), d) and f). 533
Figure 2-3: Buckling sing influence investigation: a), b), e) in terms of moment rotation curve and c), d) in terms of PEEQ deformation. 539
Figure 2-4: Joint geometrical dimension definition................ 540
Figure 3-1: Analytical vs FEM beam capacity prediction for: ES1 (a), ES2 (c) and ES3 (e) with the corresponding PEEQ deformation (b, d, f). 544
Figure 3-2: ES1 beam behavior in terms of moment rotation curve under monotonic (a) and cyclic (b) action and PEEQ distribution (c and d). 545

Figure 3-3:ES2 beam behavior in terms of moment rotation curve under monotonic (a) and cyclic (b) action and PEEQ distribution (c and d)..546
Figure 3-4: ES3 beam behavior in terms of moment rotation curve under monotonic (a) and cyclic (b) action and PEEQ distribution (c and d)..547
Figure 3-5: Comparison between A-ES-1-S and E-ES-1-S in terms of: monotonic (a) and cyclic (b) moment rotation and PEEQ distribution (c and d)..................................549
Figure 3-6: Comparison between A-ES-2-S and E-ES-2-S in terms of: monotonic (a) and cyclic (b) moment rotation and PEEQ distribution (c and d)..................................550
Figure 3-7: Comparison between A-ES-3-S and E-ES-3-S in terms of: monotonic (a) and cyclic (b) moment rotation and PEEQ distribution (c and d)..................................550
Figure 3-8: ES1 with elastic beam, moment rotation curve (a) and PEEQ distribution (b). 552
Figure 3-9: ES2 with elastic beam, moment rotation curve (a) and PEEQ distribution (b). 553
Figure 3-10: ES3 with elastic beam, moment rotation curve (a) and PEEQ distribution (b). 554

Figure 3-11: ES-1-S joint assembly: Moment-rotation curve (a, b and c), back bone curves (d), PEEQ distribution (f) and cumulated dissipated (e). 558

Figure 3-12: American (a) and European (b) cumulated dissipated energy for each component. 559

Figure 3-13: E S-2-S joint assembly: Moment-rotation curve (a, b and c), back bone curves (d), PEEQ distribution (f) and cumulated dissipated (e). 560

Figure 3-14: American (a) and European (b) cumulated dissipated energy for each component. 561

Figure 3-15: American (a) and European (b) cumulated dissipated energy for each component. 561

Figure 3-16: E S-3-S joint assembly: Moment-rotation curve (a, b and c), back bone curves (d), PEEQ distribution (f) and cumulated dissipated (e). 562

Figure 3-17: American and European bolt force evolution in function of the chord rotation for: ES1 (a and b), ES-2 (c and d) and ES-3 (e and f). 564

Figure 3-18: Compression action distribution between the beam flange and the rib for: ES-1 (a and b), ES-2 (c and d) and ES-3 (e and f). 566

Figure 4-1: American and European ES-2 joints results in terms of: Cyclic moment rotation curve (a and b) and PEEQ distribution (c and d)..570

Figure 4-2: Comparison for both American and European ES-2 joints between the Stiffened and Unstiffened configuration in terms of: Monotonic moment rotation curve (a and b); Back bone curve (c and d), PEEQ distribution and backbone curve (e and f) and dissipated energy (g and h)...................................571

List of tables

Table 2.1: SMRF designed starting from the EC structures.....532

Table 2.2: European and American columns cross section comparison..535

Table 2.3: European and American beams cross section comparison..535

Table 2.4: Beam to column assembly extracted from reference MRFs. 536

Table 2.5: Joints beam differences. 541

Table 2.6: Joints geometrical characteristics. 542

Table 3.1: Dissipated energy per joint component at rotation equal to 0.04 rad (as percentage of the total). 556

CHAPTER IX

Conclusions

The work presented in this thesis was aimed at investigating design rules for seismic resistant extended end-plate bolted (ES) joints by means of both numerical and experimental tests.

After the critical review of the relevant state of the art, the first part of the thesis was devoted to carry out experimental tests on T-stub connection to investigate the influence of the type of European pre-loadable bolts (i.e. HV and HR bolts) on the failure mode 2 and 3. The results showed that when the T-stubs are designed to exhibit the most of plastic deformation in the plate (mode 1 or mode 2 close to mode 1), the response of T-stub is insensitive to the type of pre-loadable bolt assembly.

Contrariwise, when the T-stub is designed for mode 3 (i.e. failure of bolts) the type of bolt significantly affect the response of the T-Stub and two different collapse mechanisms can be observed, namely nut stripping for HV and shank tearing for HR assemblies. Therefore, if the proposed ductility criteria (i.e. to avoid mode 3, see Chapter V) are respected, both types of bolts can be used without affecting the joints ductility.

Then starting from the component method approach [1] a mechanical model was adopted to design the joint under seismic load. The effectiveness of this mechanical model is confirmed by numerical analysis results, and in particular the following remarks can be pointed out:

- The design performance (full, equal and partial strength) can be easily obtained if the internal macro-component hierarchy is respected.
- The design overstrength factor recommended by EN1998-1 [1] is not effective to prevent plastic deformations in the joint. Conversely, the overstrength factor recommended by AISC341 [3] is satisfactory to enforce plastic engagement in the beam, preventing the joint from damage.

- The presence of rib stiffeners substantially increases the strength and the stiffness of end-plate joints. The yield line pattern is significantly affected by the rib and the adopted effective lengths are suitable to predict the yield strength of ES connections.
- Differently from extended unstiffened connections, the center of compression is not located into the mid-thickness of the beam flange in compression, but it is shifted into the rib depth, thus increasing the lever arm. Finite element simulations show that its position depends on both the joint performance level and the level of joint rotation . Therefore, investigating the assumptions proposed by both Lee [4], [5] and Abidelah [6] it was observed that: (i) the truss model proposed by Lee [4], [5] for welded rib stiffened joints, overestimates the position of the compression center, while (ii) the Abidelah et al. [6] assumptions gives the better prediction.
- The shifting of the compression center is beneficial for the design of the column web panel increasing its depth. Therefore, lower design shear forces can be conservatively assumed.

- The contribution of bolt rows below the symmetry axis of the connection can be neglected without affecting the prediction of strength. Whereas this approximation is not properly verified for partial strength joints but the error is negligible.

Moreover, from the pre-tests analysis it can be observed how, the cyclic behavior of full strength joints is significantly affected by the beam degradation, while equal and partial strength joints are mostly influenced by the connection response. Consistently with the design assumptions, partial strength joints dissipate more energy than equal strength joints because the plastic deformations occur into the end-plate that is bended in mode 1, while equal strength are characterized by mode 2 with plastic demand into the bolts. The effectiveness of these assumptions was also confirmed by the experimental tests conducted on both equal and full strength joints. Therefore, from the observed experimental campaign results the following remarks can be drawn:

- All tested joints are able to provide the 4% of rotation without a decrease of the 80% of the plastic resistance of the connected beam. Therefore all the joints can be considered qualified for seismic applications.

- Full strength joints are able to dissipate all the plastic deformation in the connected beam, leaving the column web panel and the connection in the elastic range as also confirmed by the bolts deformation after the tests.
- The failure mode of Equal strength joints is in accordance with the design assumptions, showing a plastic deformation both in the connection and in the beam. Moreover, the column web panel behave in elastic range in line with the hypothesis of equal connection strong web panel.
- All tested equal strength joints show a large ductility, slightly smaller than the one observed for the full strength joint, but large enough to be considered a ductile joints.
- The influence of the Shot peening on the welds (both for the ES2 and ES3 joints configurations) does not influence in significant way the joints performance.
- The EqualJoints loading protocol is able, in a less number of cycles (respect to the AISC341 [3]) to require the same plastic demand to the joint. Indeed not appreciable differences can be pointed out by comparing the ES2-TS-F-CA and ES2-TS-F-C2.
- The welds requirements are fundamental to exploit the joints ductility. Both the equal and full strength joints show a

concentration of the internal force between the rib and both the beam and the end-plate. Moreover, with particular regard to the equal strength joints also between beam flange and end-plate, full penetration weld should be introduced.

Once the design assumptions were validate against the numerical and experimental results, on the base of finite elements analysis properly calibrated, a large parametric analysis was conduced to extend the experimental tests results. In particular, as reported in Chapter VII, the influence of the material variability, the additional inner bolt row and the rib slope and thickness were investigated. In light of the numerical results the following remarks can be pointed out:

- The variability of end plate material does not influence the design failure mode. Only at high values of rotation (larger than 4%) equal strength joints reveal a change from a failure mode II to a mode III.
- Full strength joints are poorly affected by the variability of end plate material. The overstrength factor introduced in the design phase provides an adequate over-resistance to ensure that all the plastic demand is in beam. Therefore, the only

difference that could be noted is the contribution of the joint to the total rotation.

- The middle bolt row (MBR) in the symmetry axis does not inflict any differences in terms of moment-rotation response for both cyclic and monotonic analysis of the joint. Comparing the dissipated energy, some differences can be highlighted: Partial strength joints, in particular ES-2 and ES-3, show a slight increase of the dissipated energy for the MBR models. Indeed, the strong pinching effect observed in the case of cyclic analyses is slightly reduced by adding the middle bolt rows. However, the existing differences are negligible. This is also confirmed for full strength joints.
- The effectiveness of an additional bolt row can be find when the joint is subject to the column loss scenario that gives birth to severe normal actions in the beam. In the robustness scenario the benefit from the presence of an additional bolt row will increase the joint tensile resistance is important especially for equal and partial strength joints.
- The presence of the rib stiffeners in the tension side increases the strength and the stiffness of end-plate joints. In presence of additional transversal stiffeners, the yielding line distribution increases the resistance of the first or both

first and second bolt line – function of the joint configuration.

- The presence of the rib in the compression side increases the lever arm depth. Hence, both strength and stiffness increase.
- The AISC358-16 [7] recommendations for the rib geometry can be successfully used in order to avoid the buckling phenomena. Nevertheless, the regulations cannot ensure that the rib behaves in elastic range. The rib and beam web behavior represents a good application of the capacity design approach, where the beam buckling is preferred against the instability of the rib. The verification proposed by AISC358-16 [7] could be improved by introducing an additional factor that takes into account the randomness of the rib material. It is true that the geometrical imperfections are more effective on the beam profile but on the other hand the material variability on the cut plate is larger than the one on the profile.
- The joint moment rotation response curve is very sensitive to the rib thickness, up to the value that prevents the loss of stability in the rib. After this point the rib thickness does not strongly influence the global joint response but it may regulate the joint participation to the total rotation.

- For full strength joints, once the instability is avoided, the compression center remains virtually constant and could be assumed in the design phase equal to 0.3 the rib height.
- The discontinuities in the compression center position are caused by the incursions in plastic of the beam flange. This phenomena changes the regular force distribution between the rib and the beam flange taking its toll on the compression center position.
- Rib slope does not bring significant differences in terms of moment rotation curve, the maximum differences observed in this study amounting as much as 10%. Looking at the local behavior of the models, one can notice that the rib inclination changes the internal force distribution. The 30° joint configuration exhibits a larger internal lever arms.

The design criteria for extended stiffened end-plate bolted beam-to-column joints provided by AISC358-16 [7] are investigated and compared to those developed in this thesis.

The main differences of both American and European rules for full strength joints are critically discussed on the basis of parametric finite element analyses. Based on the results, the following remarks can be drawn:

- Both American and European design procedures guarantee the formation of a plastic hinge in the connected beam, preserving the joint (i.e. connection and column web panel) from damage.
- AISC358-16 [7]recommends 4 bolt row and 8 bolt row configurations depending on the type of connected beam. The European design criteria recommend solely one configuration with 6 bolt rows.
- Differently from AISC358-16 [7] the introduced procedure imposes ductility requirements to avoid failure of bolts even though the joints are designed to be full strength with respect to the connected beam. The results from FEAs confirm that European requirements are effective to guarantee ductile joint response in case of excessive strength of the connected beam. On the other hand, the AISC-compliant joints have a less ductile failure mode, especially the 4 bolt rows joint that showed a brittle failure mode (i.e. mode 3 with rupture of bolts).
- The distribution of the internal compression forces into the connections depends on the ratio between the rib and the beam web thickness. In the investigated case, the joints designed according to AISC358-16 [7] show that the

compression forces into the beam flange are almost twice those into the rib. Contrariwise, the joints designed in accordance with the proposed assumptions show resultants of compression forces into the beam and the rib stiffener are similar.

The analyses carried out considering the maximum allowed mill tolerances for the beams showed that geometrical imperfections largely affect the response of an isolated beam. In particular, American steel profiles are characterized by larger imperfections at the same depth of the corresponding European members and consequently subjected to more severe strength degradation under both monotonic and cyclic loadings. However, the effects induced by imperfections on both US and European joints are very similar.

The joint assemblies designed increasing the size of the column to avoid the use of continuity plates and supplementary web plates show very similar behavior to those designed with smaller columns but strengthened with welded stiffeners. However, even though the local behavior does not differ, the global structural response can be significantly modified because increasing the size of the column modifies the stiffness of the structural system.

References

[1] EN 1993:1-8, Design of steel structures - Part 1-8: Design of joints. CEN 2005.

[2] EN 1998-1, Design of structures for earthquake resistance - Part 1: General rules, seismic actions and rules for buildings. CEN 2005.

[3] ANSI/AISC 341-10 (2010). Seismic Provisions for Structural Steel Buildings. American Institute of Steel Construction.

[4] C.-H. Lee, J.-H. Jung, M.-H. Oh, E.-S. Koo (2005). Experimental study of cyclic seismic behavior of steel moment connections reinforced with ribs. Journal of Structural Engineering, ASCE 131 (1) 108–118.

[5] C.-H. Lee (2002). Seismic design of rib-reinforced steel moment connections based on Equivalent Strut Model, Journal of Structural Engineering, ASCE 128 (9), 1121–1129.

[6] A. Abidelah, A. Bouchaïr, D.E. Kerdal (2012). Experimental and analytical behavior of bolted end-plate connections with or without stiffeners. Journal of Constructional Steel Research, 76, 13–27.

[7] ANSI/AISC 358-16 (2016). Prequalified Connections for Special and Intermediate Steel Moment Frames for Seismic Applications.

Annex

Introduction

In the following annex the results of both the coupon tests and the parametric analyses are reported.

In the first two paragraphs all the coupon tests, for both the T-stub and Equaljoint experimental campaign are reported, while in the subsequent paragraphs depict the summary of the FEA results. In particular, in paragraph three all the material investigation results are pointed out, while the fourth paragraph reports the results of the Rib paramedic analysis.

Paragraph five and six show the results of the X investigating and the influence of the secondary beam, respectively.

Annex I Example of joint calculation

1.1 Theoretical approach

Chapter V presents the new assumptions on the design criteria which render the component method applicable also for extended stiffened joints in seismic areas. In the following, the complete procedure is analyzed and explained step by step for each component, with particular regard to the two joint configurations introduced: one (1br) and two (2br) bolt rows above the beam flange. As suggested also by the EN1993-1-8 [1], the first step is to evaluate the joint resistance and then, their stiffness.

1.2 Resistance definition

This paragraph reports and illustrates all the required steps for the evaluation of the two joint configurations (see Figure I-1) bending capacity (see Table I.1).

The first step is the definition of the column web panel in shear, where the only difference with respect to the classical component method [1] is the definition of the column web panel height (z_{wp}) that changes due to the change in the connection's compression center position. Moreover, the contribution of the continuity plate (in terms of additional resisting area) should be considered only in case the column web panel is designed to be the weaker component or to be equal to the dissipative one. Indeed, as already anticipated in Chapter V, if the column web panel is designed to remain elastic, its deformations are too small to activate the continuity plate contribution.

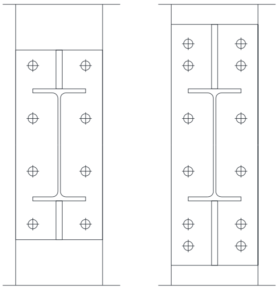

Figure I-1: Joints configurations investigated.

The following step is the definition of the resistance of the column web panel in compression, in order to avoid the local buckling of the column. However, since in the introduced design procedure the use of the continuity plate is strongly recommended, this verification can be neglected as also suggested by [1]. Indeed, the use of the continuity plates in seismic areas is important mainly due to their contribution to the resistance of the column flange in transversal bending. No additional prescriptions are introduced in the definition of the column web panel in tension (Step 3), where all the limitations are in line with the ones provided by EN1993-1-8 [1].

Table I.1: Component method considering the new assumptions.

Component	Details rules Step 1	References
Column web panel in shear	$V_{wp,Rd} = \frac{0.9 A_{vc} f_{y,\mathrm{wc}}}{\sqrt{3}\gamma_{M0}}^{*} + V_{wp,\mathrm{add},Rd}^{**}$ $V_{wp,\mathrm{add},Rd} = \frac{4\ \mathrm{M_{pl,fc,Rd}}}{d_s} \leq \frac{2\ \mathrm{M_{pl,fc,Rd}} + \mathrm{M_{pl,st,Rd}}}{d_s}$ where: $A_{vc} = A_c - 2b_c t_{fc} + (t_{wc} + 2r_c) t_{fc}$; $\mathrm{M_{pl,fc,Rd}}$ is the column design plastic moment resistance; $\mathrm{M_{pl,st,Rd}}$ is the continuity plate design plastic moment resistance; 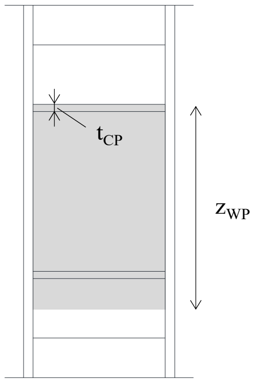 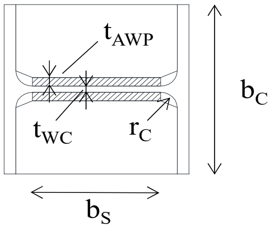 *The only contribution to take into account for Full and Equal strength joints **Additional contribution for Partial strength joints	EC3-1-8 pr.6.2.6.1

Component	Details rules Step 2	References
Column web in trasverse compression	The resistance of the column web and continuity plates may be computed by: $F_{wcc,Rd} = \frac{\omega k_{wc} b_{eff,c,cf} t_{wc} f_{y,wc}}{\gamma_{M0}} + \frac{A_{cp} f_{y,cp}}{\gamma_{M0}}$ where: $b_{eff,c,cf} = t_{fb} + \sqrt{2}(a_{w1} + a_{w2}) + 5(t_{fc} + r_c) + 2t_{ep}$ A_{cp} is the area of the continuity plates (both two sides); The reduction factor k_{wc} taking into account the axial stress in the column web, given in 6.2.6.2(2) of EC3-1-8. The reduction factor ω is given by Table 6.3 in EC3-1-8; 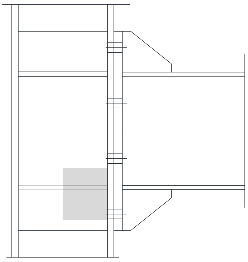 Note: when the continuity plates are used, the reduction due to buckling of the column web under transverse compression can be neglected	EC3-1-8 pr.6.2.6.2

Component	Details rules Step 3	References
Column web in tension	$F_{wct,Rd} = \frac{\omega b_{eff,t,wc} t_{wc} f_{y,wc}}{\gamma_{M0}}$ The effective width $b_{\mathrm{eff,t,wc}}$ of the column flange in tension should be taken as equal to the effective length of the equivalent T-stub representing the column flange in bending for an individual bolt-row or a bolt-group. 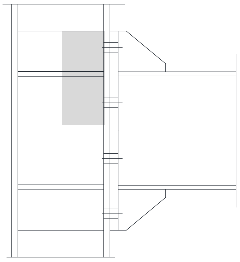 The reduction factor ω is given by Table 6.3 in EC3-1-8.	EC3-1-8: pr. 6.2.6.3

The definition of the column flange in transverse bending (step 4) is not influenced by the new assumption; indeed the seismic criteria introduced does not change the design procedure, but limits the failure mode of the equivalent T-stub. Hence, the procedure is the same as given by EN1993-1-8 [1] but with the integration of new limits on the ductility requirements.

Component	Details rules Step 4	References
Column flange in transversal bending	***Resistance of the equivalent T-stub:*** $F_{cfb,Rd} = \min[F_{T,1,Rd}; F_{T,2,Rd}; F_{T,3,Rd}]$ * or $F_{cfb,Rd} = \min[F_{T,1-2,Rd}; F_{T,3,Rd}]$ ** with: ● $F_{T,1,Rd} = \frac{4M_{pl,1,Rd}}{m}$ ● $F_{T,2,Rd} = \frac{2M_{pl,2,Rd} + n\Sigma F_{t,Rd}}{m+n}$ ● $F_{T,3,Rd} = \sum \frac{0.9 f_{ub} A_s}{\gamma_{M2}}$ ● $F_{T,1,Rd} = \frac{2M_{pl,1,Rd}}{m}$ where: $M_{pl,1,Rd} = 0,25\Sigma\ell_{eff,1} t_{fc}^{2} f_{y,fc} / \gamma_{M0}$ $M_{pl,2Rd} = 0,25\Sigma\ell_{eff,2} t_{fc}^{2} f_{y,fc} / \gamma_{M0}$ $m = (w/2 - t_{wc}/2 - 0.8r_c)$ $n = \min[e, 1.25m]$, with circular patterns n=∞ can be used. $e_w = d_w / 4$ d_W is the diameter of the washer, or the width across points of the bolt head or nut, as relevant *If the prying force will be developed ** If the prying force will not be developed NB EC1993-1-8 [1] allows considering prying forces in any case. For bolted connection. In light of the results described within this thesis this statement is not conservative and the prying force activation should be verified case by case.	EC3-1-8: pr. 6.2.6.3

<table>
<tr><th>Component</th><th colspan="2">Details rules
step 4</th><th>References</th></tr>
<tr><td rowspan="4">Column flange in transversal bending (1br)</td><td colspan="2">Equivalent T-stub dimensions</td><td rowspan="4">EC3-1-8: pr. 6.2.6.3</td></tr>
<tr><td>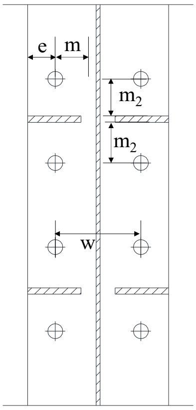 </td><td>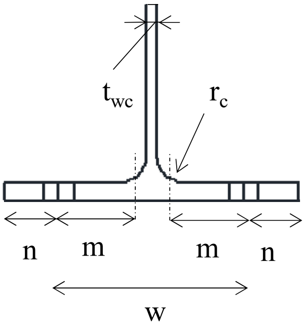 </td></tr>
<tr><td>First bolt row</td><td>Second bolt row</td></tr>
<tr><td>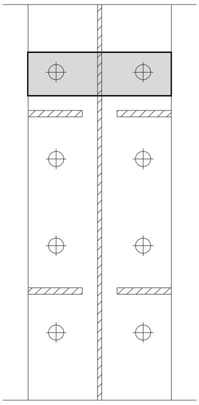</td><td>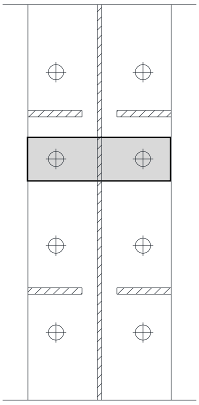</td></tr>
</table>

<table>
<tr><th>Component</th><th>Details rules
step 4</th><th>References</th></tr>
<tr><td>Column flange in transversal bending (1br)</td><td>

Effective lengths

<u>Bolt row 1 (bolt adjacent to a stiffeners)</u>:

$$l_{eff,1} = \min[2\pi m, \alpha m]$$

$$l_{eff,2} = \alpha m$$

<u>Bolt row 2 (bolt adjacent to a stiffeners)</u>:

$$l_{eff,1} = \min[2\pi m, \alpha m]$$

$$l_{eff,2} = \alpha m$$

α is given by figure 6.11 in EC3-1-8, depending on:

$$\lambda_1 = \frac{m}{m+e}\ ;\ \lambda_2 = \frac{m_2}{m+e}$$

Effective length introduced (for both first and second bolt rows line):

- Circular pattern (Circular yielding)

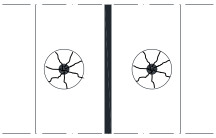

$$l_{eff,cp} = 2\pi m$$

- Non Circular pattern (Side yielding near to a stiffener)

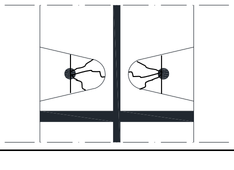

$$l_{eff,nc} = \alpha m$$

</td><td>EC3-1-8: pr. 6.2.6.4 table 6.5</td></tr>
</table>

<table>
<tr><th>Component</th><th>Details rules
step 4</th><th>References</th></tr>
<tr><td>Column flange in transversal bending (2br)</td><td>
<table>
<tr><th>Equivalent T-stub</th><th>First bolt row</th></tr>
<tr><td>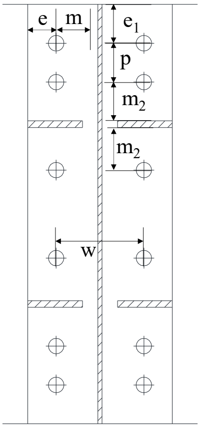
</td><td>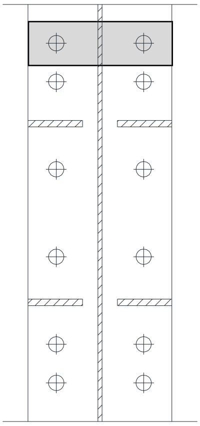</td></tr>
<tr><th>Second bolt row</th><th>Third bolt row</th></tr>
<tr><td>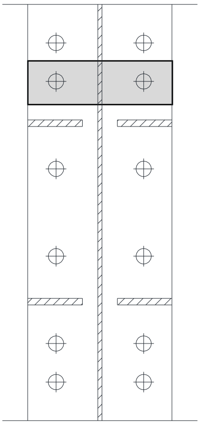</td><td>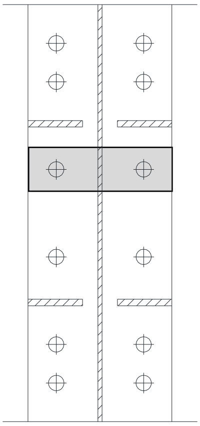</td></tr>
</table>
</td><td>EC3-1-8: pr. 6.2.6.3</td></tr>
</table>

Component	Details rules step 4	References
Column flange in transversal bending (2br)	***Effective lengths*** *Bolt row 1 (Other inner bolt row)*: $l_{eff,1} = \min[2\pi m; 4m + 1.25e]$ $l_{eff,2} = 4m + 1.25e$ *First row of the group 1+2* $l_{eff,1} = \min[2p; p]$ $l_{eff,nc} = p$ *Bolt row 2 (bolt adjacent to a stiffeners)*: $l_{eff,1} = \min[2\pi m, \alpha m]$ $l_{eff,2} = \alpha m$ *Second row of the group 1+2* $l_{eff,1} = \min[\pi m + p; 0.5p + \alpha m - (2m + 0.625e)]$ $l_{eff,1} = 0.5p + \alpha m - (2m + 0.625e)$ *Bolt row 3 (bolt adjacent to a stiffeners)*: $l_{eff,1} = \min[2\pi m, \alpha m]$ $l_{eff,2} = \alpha m$ α is given by figure 6.11 in EC3-1-8, depending on: $\lambda_1 = \frac{m}{m+e}$ $\lambda_2 = \frac{m_2}{m+e}$ N.B. Between the first and the second bolt row line the group effect can influence the line resistance; conversely, no group effect with the third bolt row line can be activated since the continuity plate are introduced.	EC3-1-8: pr. 6.2.6.4 table 6.5

Component	Details rules step 4	References
Column flange in transversal bending (2br)	Effective length introduced (first bolt row line): • Circular pattern (Circular yielding) 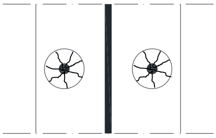 $l_{eff,cp} = 2\pi m$ • Non Circular pattern (Side yielding) 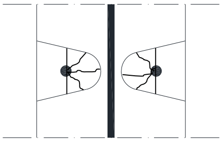 $l_{eff,cp} = 4m + 1.25e$ Effective length introduced (Second and third bolt rows lines): • Circular pattern (Circular yielding) 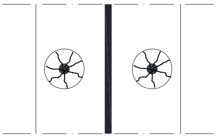 $l_{eff,cp} = 2\pi m$ • Non Circular pattern (Side yielding near to a stiffener) 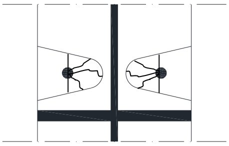 $l_{eff,nc} = \alpha m$	EC3-1-8: pr. 6.2.6.4 table 6.5

Component	Details rules step 4	References
Column flange in transversal bending (2br)	Effective length introduced (Group effect 1+2): - Circular pattern: 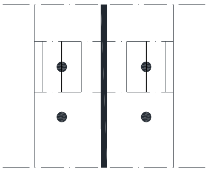 $l_{eff,cp} = 2p$ - Non Circular pattern 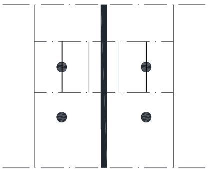 $l_{eff,nc} = p$ - Circular yielding 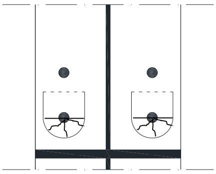 $l_{eff,cp} = \pi m + p$ - Circular yielding (Circular yielding) 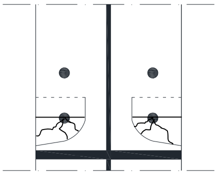 $l_{eff,nc} = 0.5p + \alpha m - (2m + 0.625e)$	EC3-1-8: pr. 6.2.6.4 table 6.5

Component	Details rules step 4	References
Ductile limitations	➢ T-stub verification: 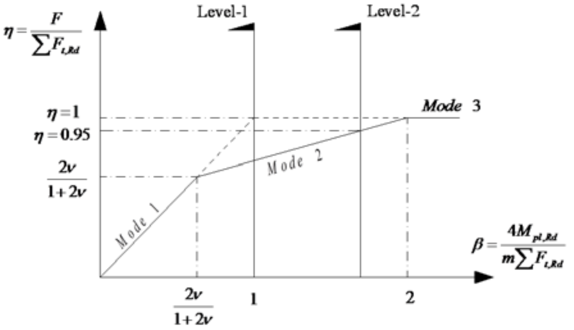 Level-1: $\beta \le 1$ Level-2: $\beta < 2$ and $\eta \le 0.95$ ➢ Bolt diameter verifications: $F_{t,Rd} \ge \gamma_{ov} \cdot F_{p,Rd}$ where: $F_{t,rd}$ is the bolts tension resistance; $F_{p,Rd}$ is the maximum relative line resistance γ_{ov} is the overstrenght factor	Chapter V

As anticipated, the ductility limitations have the aim of control the bolts behavior in order to avoid the failure mode three. Therefore, two limitations, reported in Table I.4, are introduced: (i) on the equivalent T-stub and (ii) on the resistance ratio between the bolts and the equivalent resistance line.

Component	Details rules step 5	References
End-plate in transversal bending	***Resistance of the equivalent T-stub:*** $F_{cfb,Rd} = \min[F_{T,1,Rd}; F_{T,2,Rd}; F_{T,3,Rd}]$ * or $F_{cfb,Rd} = \min[F_{T,1-2,Rd}; F_{T,3,Rd}]$ ** with: ● $F_{T,1,Rd} = \frac{4M_{pl,1,Rd}}{m}$ ● $F_{T,2,Rd} = \frac{2M_{pl,2,Rd} + n\Sigma F_{t,Rd}}{m+n}$ ● $F_{T,3,Rd} = \sum \frac{0.9 f_{ub} A_s}{\gamma_{M2}}$ ● $F_{T,1,Rd} = \frac{2M_{pl,1,Rd}}{m}$ where: $M_{pl,1,Rd} = 0,25 \Sigma \ell_{eff,1} t_{fc}^2 f_{y,fc} / \gamma_{M0}$ $M_{pl,2Rd} = 0,25 \Sigma \ell_{eff,2} t_{fc}^2 f_{y,fc} / \gamma_{M0}$ $m = (w/2 - t_{wc}/2 - 0.8r_c)$ $n = \min[e, 1.25m]$, with circular patterns n=∞ can be used. $e_w = d_w / 4$ d_W is the diameter of the washer, or the width across points of the bolt head or nut, as relevant *If the prying force will be developed ** If the prying force will not be developed NB EC1993-1-8 [1] allows considering prying forces in any case. For bolted connection. In light of the results described within this thesis this statement is not conservative and the prying force activation should be verified case by case.	EC3-1-8: pr. 6.2.6.4 table 6.5

Component	Details rules step 5	References
End-plate in transversal bending (1br)	Equivalent T-stub dimensions 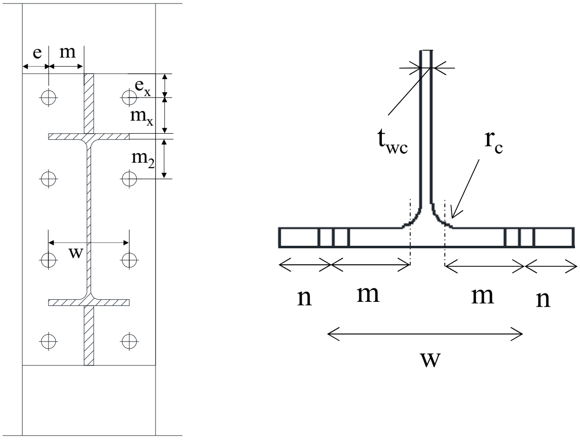 First bolt row 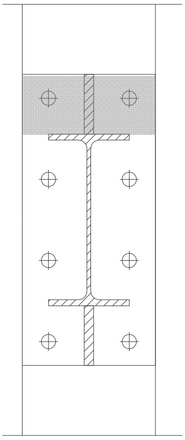 Second bolt row 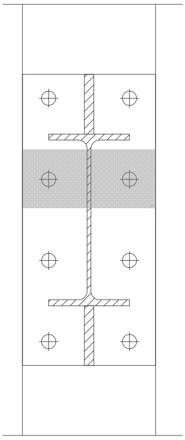	EC3-1-8: pr. 6.2.6.5

Component	Details rules step 5	References
End-plate in transversal bending (1br)	***Effective lengths*** *Bolt row 1 (Frist bolt row outside beam tension flange)*: $l_{eff,1} = \min\begin{cases}2\pi m\\ \pi m + 2e_x\\ \alpha m - (2m + 0.625e) + e_x\\ 2m + 0.625e + e_x\\ 4m + 1.25e\end{cases}$ $l_{eff,2} = \min\begin{cases}\alpha m - (2m + 0.625e) + e_x\\ 2m + 0.625e + e_x\\ 4m + 1.25e\end{cases}$ *Bolt row 2 (first bolt row below beam tension flange)*: $l_{eff,1} = \min[2\pi m, \alpha m]$ $l_{eff,2} = \alpha m$ α is given by figure 6.11 in EC1993-1-8, depending on: $\lambda_1 = \frac{m}{m+e}$ $\lambda_2 = \frac{m_2}{m+e}$	EC3-1-8: pr. 6.2.6.4 table 6.5

Component	Details rules step 5	References
End-plate in transversal bending (1br)	Effective length introduced (for first bolt row): - Circular pattern 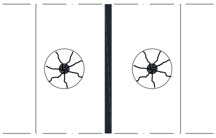 $l_{eff,cp} = 2\pi m$ 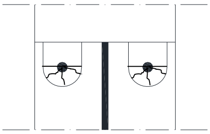 $l_{eff,\mathrm{cp}} = \pi m + 2e_x$ - Non Circular pattern 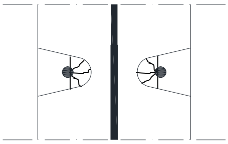 $l_{eff,\mathrm{nc}} = 4m + 1.25e$ 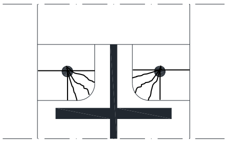 $l_{eff,\mathrm{nc}} = \alpha m - (2m + 0.625e) + e_x$ 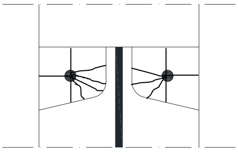 $l_{eff,\mathrm{nc}} = 2m + 0.625e + e_x$	Green Book 229

Component	Details rules step 5	References
End-plate in transversal bending (1br)	Effective length introduced (for second bolt row): • Circular pattern 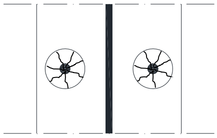 $l_{eff,cp} = 2\pi m$ • Non Circular pattern 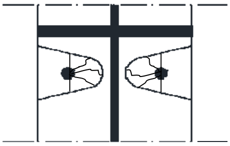 $l_{eff,\mathrm{nc}} = \alpha m$	EC3-1-8: pr. 6.2.6.5 table 6.6

Component	Details rules step 5	References
End-plate in transversal bending (2br)	Eqivalent T-stub 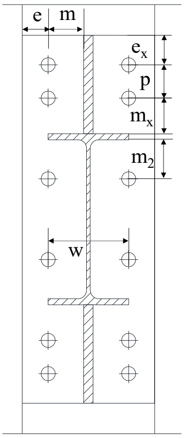 First bolt row 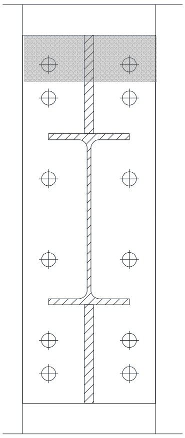 Second bolt row 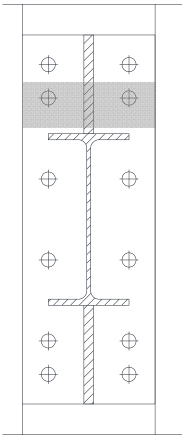 Third bolt row 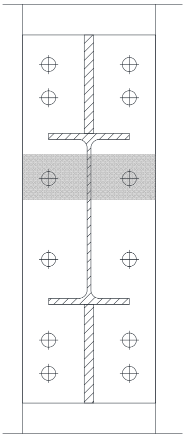	EC3-1-8: pr. 6.2.6.5

Component	Details rules step 5	References
End-plate in transversal bending (2br)	***Effective lengths*** *Bolt row 1 (Frist bolt row outside beam tension flange)*: $l_{eff,1} = \min\begin{cases}2\pi m\\ \pi m + 2e_x\\ 4m + 1.25e\\ 2m + 0.625e + e_x\end{cases}$ $l_{eff,2} = \min\begin{cases}4m + 1.25e\\ 2m + 0.625e + e_x\end{cases}$ *First row of the group 1+2* $l_{eff,1} = \min\begin{cases}\pi m + p\\ 2e_x + p\\ 2m + 0.625e + 0.5p\\ e_x + 0.5p\end{cases}$ $l_{eff,2} = \min\begin{cases}2m + 0.625e + 0.5p\\ e_x + 0.5p\end{cases}$ *Bolt row 2 (bolt adjacent to a stiffeners)*: $l_{eff,1} = \min[2\pi m, \alpha m]$ $l_{eff,2} = \alpha m$ *Second row of the group 1+2* $l_{eff,1} = \min[\pi m + p; 0.5p + \alpha m - (2m + 0.625e)]$ $l_{eff,2} = 0.5p + \alpha m - (2m + 0.625e)$ *Bolt row 3 (bolt adjacent to a stiffeners):* $l_{eff,1} = \min[2\pi m, \alpha m]$ $l_{eff,2} = \alpha m$ α is given by figure 6.11 in EC3-1-8 [1].	EC3-1-8: pr. 6.2.6.5

Component	Details rules step 5	References
End-plate in transversal bending (2br)	Effective length introduced (first bolt row line): - Circular pattern 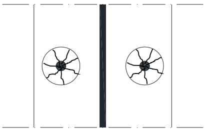 $l_{eff,cp} = 2\pi m$ 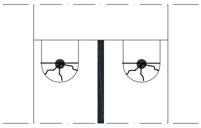 $l_{eff,cp} = \pi m + 2e_x$ - Non Circular pattern 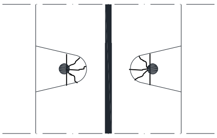 $l_{eff,nc} = 4m + 1.25e$ 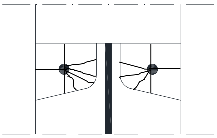 $l_{eff,nc} = 2m + 0.625e + e_x$ Effective length introduced (first bolt row line in group): - Circular pattern 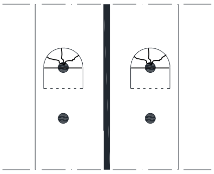 $l_{eff,cp} = \pi m + p$	EC3-1-8: pr. 6.2.6.4 table 6.5

Component	Details rules step 5	References
End-plate in transversal bending (2br)	Effective length introduced (first bolt row line in group): - Circular pattern 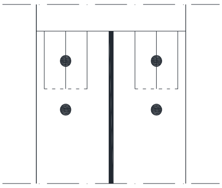 $l_{eff,\mathrm{cp}} = 2e_x + p$ - Non Circular pattern 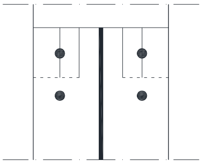 $l_{eff,\mathrm{nc}} = e_x + 0.5p$ 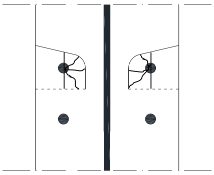 $l_{eff,\mathrm{nc}} = 2m + 0.625e + 0.5p$ Effective length introduced (second and third bolt row line): - Circular pattern 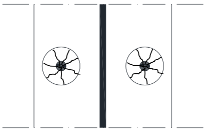 $l_{eff,cp} = 2\pi m$	EC3-1-8: pr. 6.2.6.4 table 6.5

Component	Details rules step 5	References
End-plate in transversal bending (2br)	Effective length introduced (second and third bolt row line): - Non Circular pattern 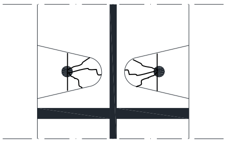 $l_{eff,nc} = \alpha m$ Effective length introduced (second and third bolt row line in group): - Circular pattern 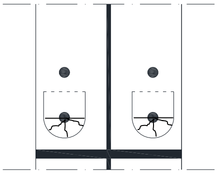 $l_{eff,cp} = \pi m + p$ - Non Circular pattern 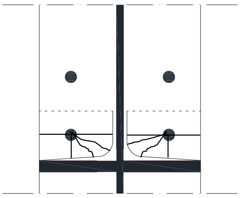 $l_{eff,nc} = 0.5 p_1 + \alpha m - (2m + 0.625e)$	EC3-1-8: pr. 6.2.6.4 table 6.5

Component	Details rules step 6	References
Beam flanges and web in compression	$F_{fbc,Rd} = M_{c,Rd}\, f_{y,b} \big/ (h + \xi b - 0.5 t_{fb})$ • h is the depth of the connected beam; • $M_{c,Rd}$ is the design moment resistance of the beam plus the rib cross-section, reduced if necessary to allow for shear, see EN 1993-1-1. • t_{fb} is the flange thickness of the connected beam. • ξ_b is the position of the compression center 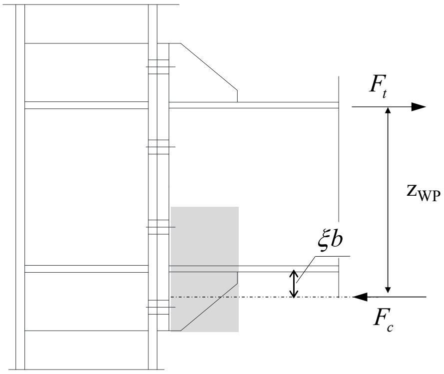	EC3-1-8 pr. 6.2.6.7

Component	Details rules step 7	References
Beam web in tension	$F_{wbt,Rd} = b_{eff,t,wb}\, t_{wb}\, f_{y,wb} / \gamma_{M0}$ The effective width $b_{eff,t,wb}$ of the beam web in tension should be taken as equal to the effective length of the equivalent T-stub representing the end-plate in bending for an individual bolt-row or a bolt-group. 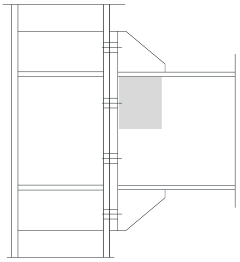	EC3-1-8 pr. 6.2.6.8

Component	Details rules Line Resistance	References
Joint bending resistance	***First bolt row line*** $F_{tr,Rd,r1} = min(F_{t,fc,Rd,r1}; F_{t,wc,Rd,r1}; F_{t,ep,Rd,r1};F_{c,fb,Rd})$ In the seismic application the continuity plate (CP) are recommended; therefore in the most of the case the column web in compression component could be neglected. ***Second bolt row line*** $F_{tr,Rd,r2} = min(F_{t,fc,Rd,r2}; F_{t,wc,Rd,r2}; F_{t,ep,Rd,r2}; F_{t,wb,Rd,r2};F_{c,}$ ***Column Bending Capacity*** $M_{wp,Rd} = \frac{V_{wp,Rd,Tot}}{z_{wp}} = 693.8kNm$ ***Connection Bending Capacity*** $M_{j,Rd} = \sum_r h_r F_{tr,Rd}$ $M_{j,Rd} = 535kN \cdot 603mm + 718kN \cdot 403mm = 612.2kNn$ ***Joint Demand*** $M_{j,Ed} = \alpha \cdot \left(M_{pl,Rd} + V_u \cdot s_h\right) = 619kNm$ ***Internal hierarchy Demand*** $M_{wp,Rd} \geq M_{j,Rd} = M_{j,Ed} \rightarrow 694 \geq 612 \cong 619kNm$ ***Equal strength with strong column web panel.***	EC3-1-8: pr. 6

Component	Details rules Step 8 – For both First and Second line	References
Ductile limitations	***T-stub verification:*** Bolt Row 1 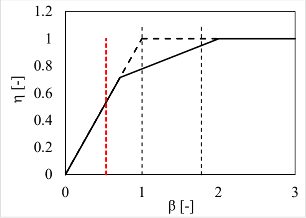 $\eta = \frac{F}{\sum F_{t,Rd}}$ =0.53 $\beta = \frac{4M_{pl,Rd}}{m\sum F_{t,Rd}}$ =0.53 Bolt Row 2 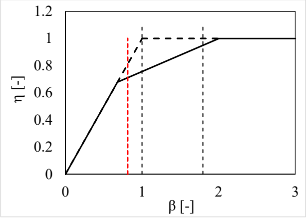 $\eta = \frac{F}{\sum F_{t,Rd}}$ =0.71 $\beta = \frac{4M_{pl,Rd}}{m\sum F_{t,Rd}}$ =0.81 ***Bolt diameter verifications:*** Bolt Row 1 $F_{c,Rd,1} = 669kN \le 1010kN$ Bolt Row 2 $F_{t,Rd,2} = 718kN \le 1010kN$	Chapter V

The shear verification of the joint should be made against three possible failure modes: the beam web buckling, the bolts shear resistance and the column flange/end-plate bearing capacity. In the following table the three contribution are described.

Table I.2: Joint shear resistance.

Component	Details rules Shear resistance	References
Beam web in shear	Beam web in shear (buckling verification): $V_{b,RD} = \chi_w A_{vb} f_{y,b} / \sqrt{3}$ where: $A_{vb} = A_b - 2b_b t_{fb} + (t_{wb} + 2r_b) t_{fb}$ $\chi_w = if \begin{cases} \overline{\lambda}_w \geq 0.83 \rightarrow 0.83 / \overline{\lambda}_w \\ \overline{\lambda}_w < 0.83 \rightarrow 1 \end{cases}$ $\overline{\lambda}_w = 0.3467(h_{wb} / t_{wb})\sqrt{f_{y,b} / E}$	EC3-1-5: pr. 5.3
Bolts in shear	$F_{b,Rd} = 2\dfrac{\alpha_v f_{ub} A_s}{\gamma_{M2}}$ where $\alpha_v = 0.5$ for 10.9 bolts	EC3-1-8: pr. 361

Component	Details rules Shear resistance	References
Column flange in bearing	The resistance of the column flange in bearing should be defined: $F_{b,Rd} = 2\frac{k_1 \alpha_b f_u d t_{fc}}{\gamma_{M2}}$ where: $k_1 = \min[2.8\frac{e}{d_0} - 1.7, \quad 2.5]$ α_b depending on the sear load direction and bolt row position. Column side 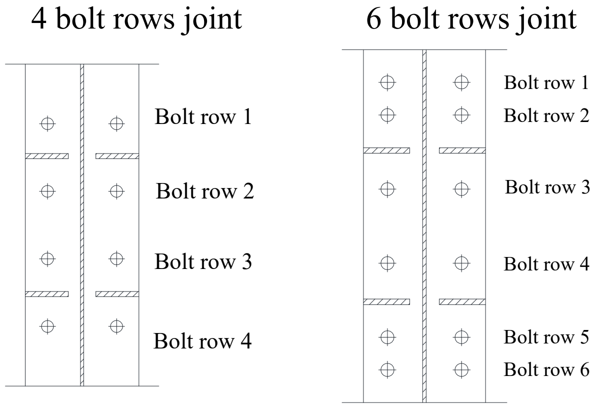 	EC3-1-8: pr. 3.6

Component	Details rules Shear resistance		References
Column flange in bearing	*Connection with 4 bolt rows*		EC3-1-8: pr. 3.6
	Shear load going down	Shear load going down	
	Bolt rows 1, 3 and 4: $\alpha_b = 1.0$	Bolt rows 1, 2 and 4: $\alpha_b = 1.0$	
	Bolt rows 2: $\alpha_b = \min[1.0, \quad \frac{p}{3d_0} - \frac{1}{4}]$	Bolt rows 3: $\alpha_b = \min[1.0, \quad \frac{p}{3d_0} - \frac{1}{4}]$	
	Connection with 6 bolt rows		
	Shear load going down	Shear load going down	
	Bolt rows 1, 3 and 5: $\alpha_b = 1.0$	Bolt rows 1, 3 and 5: $\alpha_b = \min[1.0, \quad \frac{p}{3d_0} - \frac{1}{4}]$	
	Bolt rows 2, 4 and 6: $\alpha_b = \min[1.0, \quad \frac{p}{3d_0} - \frac{1}{4}]$	Bolt rows 2, 4 and 6: $\alpha_b = 1.0$	

<table>
<tr><th>Component</th><th>Details rules
Shear resistance</th><th>References</th></tr>
<tr><td>End-plate in bearing</td><td>

Connection with 4 bolt rows

<table>
<tr><th>Shear load going down</th><th>Shear load going down</th></tr>
<tr><td>Bolt row 1:
$\alpha_b = \min[1.0, \frac{e_x}{3d_0}]$</td><td>Bolt rows 1 and 3:
$\alpha_b = 1.0$</td></tr>
<tr><td>Bolt rows 2 and 4:
$\alpha_b = 1.0$</td><td>Bolt row 2:
$\alpha_b = \min[1.0, \frac{p}{3d_0} - \frac{1}{4}]$</td></tr>
<tr><td>Bolt row 3:
$\alpha_b = \min[1.0, \frac{p}{3d_0} - \frac{1}{4}]$</td><td>Bolt row 4:
$\alpha_b = \min[1.0, \frac{e_x}{3d_0}]$</td></tr>
</table>

End-plate side

4 bolt rows joint 6 bolt rows joint

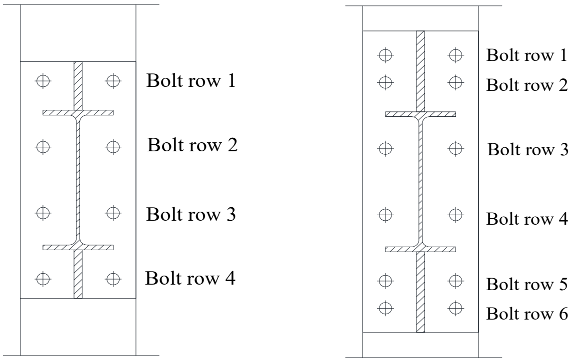

</td><td>EC3-1-8: pr. 3.6</td></tr>
</table>

Component	Details rules Shear resistance		References
End-plate in bearing	*Connection with 6 bolt rows*		EC3-1-8: pr. 3.6
	Shear load going down	Shear load going down	
	Bolt row 1: $\alpha_b = \min[1.0, \quad \frac{e_x}{3d_0}]$	Bolt rows 1 and 3: $\alpha_b = 1.0$	
	Bolt rows 2 and 4: $\alpha_b = 1.0$	Bolt row 2: $\alpha_b = \min[1.0, \quad \frac{p}{3d_0} - \frac{1}{4}]$	
	Bolt row 3: $\alpha_b = \min[1.0, \quad \frac{p}{3d_0} - \frac{1}{4}]$	Bolt row 4: $\alpha_b = \min[1.0, \quad \frac{e_x}{3d_0}]$	

1.3 Stiffness definition

The joint elastic stiffness should be evaluate as the resistance, starting from the definition of the equivalent stiffness for each component, as reported in the following (see Table I.3) for both investigated joint configurations.

Table I.3: Stiffness coefficient definition according to [1].

Component	Stiffness definition	References
Column web panel in shear	*Column web panel in shear* For the stiffened joint, k_1 contribution is equal to infinite, while if the joint is un-stiffened: $k_1 = \frac{0.38 \cdot A_{VC}}{\beta z}$ where: β is the transformation parameter defined in EN1993-1-8 pr. 5.3(7) [1], and z is the level arm.	EC3-1-8 pr.6.3.2
Column web in compression	*Colum web in compression* For the stiffened joint, k_2 contribution is equal to infinite, while if the joint is un-stiffened: $k_2 = \frac{0.7 \cdot b_{eff,c,wc} \cdot t_{wc}}{d_c}$ Where all the dimensions are already described in Table I.1.	

Component	Stiffness definition	References
Column web in tension	*Column web in tension* The column web in tension stiffness component should be evaluated for each bolt row line: $k_{3,i} = \frac{0.7 \cdot b_{eff,t,wc} \cdot t_{wc}}{d_c}$ Where all the dimensions are already described in Table I.1	EC3-1-8 pr.6.3.2
Column flange in bending	*Column flange in bending* The column flange in bending stiffness component should be evaluated for each bolt row line: $k_{4,i} = \frac{0.9 \cdot l_{eff} \cdot t_{fc}^2}{m^3}$ where is a geometrical parameter defined in Table I.1, t_{fc} is the column flange thickness and l_{eff} is the smallest of the effective lengths, individually or as part of a bolt group.	
End-plate in bending	*End-plate in bending* The end-plate in bending stiffness component should be evaluated for each bolt row line: $k_{5,i} = \frac{0.9 \cdot l_{eff} \cdot t_p^2}{m^3}$ where is a geometrical parameter defined in Table I.1, t_p is the connected plate thickness and l_{eff} is the smallest of the effective lengths, individually or as part of a bolt group.	

Component	Stiffness definition	References
Bolts in tension	*Bolts in tension* The bolts stiffness for each bolt row line is: $k_{10,i} = \frac{1.6 \cdot A_s}{L_b}$ where As is the bolt effective area and L_b is the bolt elongation length, taken as equal to the grip length plus half the sum of the height of the bolt head and the height of the nut.	EC3-1-8 pr.6.3.2
Rib on the compression side	*Rib in compression* $k_{RIB} = \frac{A_{eq}}{L_{Strut}} \cdot \cos(\alpha)$ where (as defined by Lee [2]): $A_e = \frac{\eta(ab - c^2)}{\sqrt{(a-c)^2 + (b-c)^2}}$ $L_e = (0.6)\sqrt{\left(a^2 + b^2\right)}$ where α is the rib strut inclination.	Chapter V

Once all the contribution k_i are defined, if the joint has more than one line on the tension side, the equivalent stiffness coefficient (k_{eq}) and the relative equivalent internal lever arm should be evaluate (z_{eq}). These coefficients, allow the definition of the joint initial stiffness ($S_{j,ini}$) as reported in Chapter III and summarized in the following table.

Component	Stiffness definition	References
Stiffness definition	Effective stiffness of the bolt rows $k_{ef,r1} = \frac{1}{(1/k_{3,r1} + 1/k_{4,r1} + 1/k_{5,r1} + 1/k_{10,r1})}$ $k_{ef,r2} = \frac{1}{(1/k_{3,r2} + 1/k_{4,r2} + 1/k_{5,r2} + 1/k_{10,r2})}$ Equivalent arm level and stiffness $z_{eq} = \frac{\sum k_{ef,i} z_i^2}{\sum k_{ef,i} z_i}$ $k_{eq} = \frac{\sum k_{ef,i} z_i}{z_{eq}}$ Joint Initial Stiffness $S_j = \frac{E \cdot z_{eq}^2}{(1/k_{wp} + 1/k_{Rib} + 1/k_{eq})^{-1}}$ Stiffnes classification $k_b = \frac{S_j}{EI_b / L_b} = \begin{cases} k_b \leq 0.5 \quad Pinned \\ 0.5 < k_b < 25 \quad Semi-Rigid \\ k_b \geq 25 \quad Full \quad Rigid \end{cases}$ where E is the steel elastic modulus, I_b is the beam inertia and L_b is the beam length	EC3-1-8 pr.6.3.2

1.4 Example of one bolt row joint configuration

In order to clarify the design procedure introduced, an example is hereinafter discussed for both configurations i.e. with one (4br) and two bolts (6br) row above the beam flange.

In particular, the joints showed are ES2-F and ES2-E designed following Abidelah's [3] hypothesis for the compression center definition. (all the geometry characteristics are showed in Chapter V and in Figure I-2).

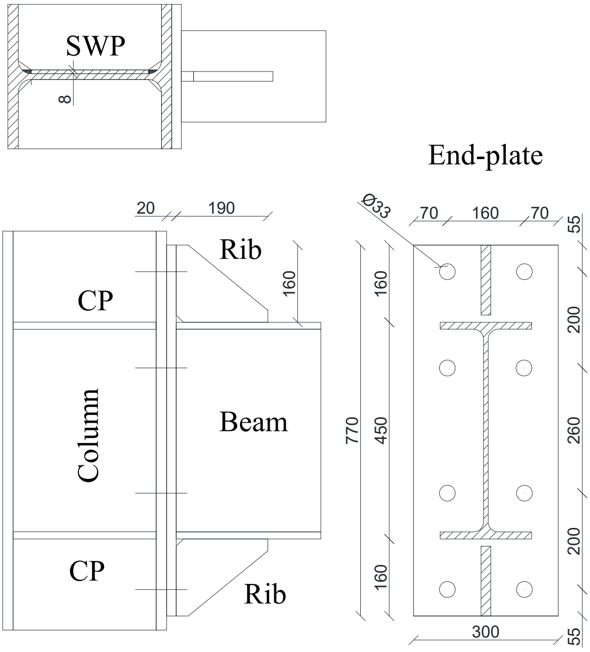

Figure I-2: Example 1: ES2-TS-E joint (4 bolts lines)

Table I.4: Component method considering the new assumptions.

Component	Details rules Step 1	References
Column web panel in shear	The column shear resistance is: $V_{wp,Rd} = \frac{0.9 A_{vc} f_{y,\mathrm{wc}}}{\sqrt{3}\gamma_{M0}} = 1034.6kN$ Moreover, an additional web panel was introduced with a thickness equal to 8mm: $V_{\mathrm{AWP},Rd} = \frac{0.9 A_{SWP} f_{y,\mathrm{wc}}}{\sqrt{3}\gamma_{M0}} = 358.6kN$ $V_{wp,Rd,Tot} = V_{wp,Rd,Tot} + V_{AWP,Rd} = 1393kN$ where: $A_{vc} = A_c - 2b_c t_{fc} + (t_{wc} + 2r_c)t_{fc} = 5609mm^2$ $A_{AWP} = 1 \cdot 8 \cdot 243 = 1944mm^2$ Therefore the column web panel bending capacity is: $M_{wp,Rd} = \frac{V_{wp,Rd,Tot}}{z_{wp}} = 693.8kNm$	EC3-1-8 pr.6.2.6.1

Component	Details rules Step 3 – For First and Second bolts row lines	References
Column web in tension	Bolt row 1 $F_{wct,Rd} = \frac{\omega b_{eff,t,wc} t_{wc} f_{y,wc}}{\gamma_{M0}} = 1911kN$ Where: $\omega = 0.87$ $l_{eff} = 308mm$ Bolt Row 2 $F_{wct,Rd} = \frac{\omega b_{eff,t,wc} t_{wc} f_{y,wc}}{\gamma_{M0}} = 1955kN$ =1954.6kN where: $\omega = 0.87$ $l_{eff} = 317.6mm$	EC3-1-8: pr. 6.2.6.3

Component	Details rules Step 4 – Frist line	References
Column flange in transversal bending	***Resistance of the equivalent T-stub:*** $L_b = 73mm \le L_b^* = 232mm$ - Prying force will develop $F_{cfb,Rd} = \min[F_{T,1,Rd}; F_{T,2,Rd}; F_{T,3,Rd}]$ with: • $F_{T,1,Rd} = \frac{4M_{pl,1,Rd}}{m} = 965.4kN$ • $F_{T,2,Rd} = \frac{2M_{pl,2,Rd} + n\Sigma F_{t,Rd}}{m+n} = 775.5kN$ • $F_{T,3,Rd} = \sum \frac{0.9 f_{ub} A_s}{\gamma_{M2}} = 1009.8kN$ where: $M_{pl,1,Rd} = 0,25\Sigma\ell_{eff,1} t_{fc}^2 f_{y,fc} / \gamma_{M0} = 12.65kNm$ $M_{pl,2Rd} = 0,25\Sigma\ell_{eff,2} t_{fc}^2 f_{y,fc} / \gamma_{M0} = 12.65kNm$ $m = (w/2 - t_{wc}/2 - 0.8r_c) = 52.4mm$ $n = \min[e, 1.25m] = 62.5mm$ $e_w = d_w / 4 = 14mm$ *Bolt row 1 (bolt adjacent to a stiffeners)*: $l_{eff,1} = \min[2\pi m, \alpha m] = 308.3$ $l_{eff,2} = \alpha m = 308.3$ $F_{ep,b,Rd} = 775.5kN$ $l_{eff} = 308mm$	EC3-1-8: pr. 6.2.6.3

Component	Details rules Step 4 – Second Line	References
Column flange in transversal bending	***Resistance of the equivalent T-stub:*** $L_b = 73mm \le L_b^* = 225mm$ - Prying force will develop $F_{cfb,Rd} = \min[F_{T,1,Rd}; F_{T,2,Rd}; F_{T,3,Rd}]$ with: • $F_{T,1,Rd} = \frac{4M_{pl,1,Rd}}{m} = 994.7kN$ • $F_{T,2,Rd} = \frac{2M_{pl,2,Rd} + n\Sigma F_{t,Rd}}{m+n} = 782.kN$ • $F_{T,3,Rd} = \sum \frac{0.9 f_{ub} A_s}{\gamma_{M2}} = 1009.8kN$ where: $M_{pl,1,Rd} = 0,25\Sigma\ell_{eff,1} t_{fc}^2 f_{y,fc} / \gamma_{M0} = 8.81kNm$ $M_{pl,2Rd} = 0,25\Sigma\ell_{eff,2} t_{fc}^2 f_{y,fc} / \gamma_{M0} = 8.81kNm$ $m = (w/2 - t_{wc}/2 - 0.8r_c) = 52.4$ $n = \min[e, 1.25m] = 62.5mm$ $e_w = d_w / 4 = 14mm$ *Bolt row 2 (bolt adjacent to a stiffeners)*: $l_{eff,1} = \min[2\pi m, \alpha m] = 317.6mm$ $l_{eff,2} = \alpha m = 317.6mm$ $F_{ep,b,Rd} = 782kN$ $l_{eff} = 318mm$	EC3-1-8: pr. 6.2.6.3

Component	Details rules Step 5 – First line	References
End-plate in transversal bending	***Resistance of the equivalent T-stub:*** $L_b = 73mm \le L_b^* = 509.7mm$ - Prying force will develop $F_{ep,b,Rd} = \min[F_{T,1,Rd}; F_{T,2,Rd}; F_{T,3,Rd}]$ with: • $F_{T,1,Rd} = \frac{4M_{pl,1,Rd}}{m} = 535.3kN$ • $F_{T,2,Rd} = \frac{2M_{pl,2,Rd} + n\Sigma F_{t,Rd}}{m+n} = 673.9kN$ • $F_{T,3,Rd} = \sum \frac{0.9 f_{ub} A_s}{\gamma_{M2}} = 1009.8kN$ where: $M_{pl,1,Rd} = 0,25\Sigma\ell_{eff,1} t_{fc}{}^2 f_{y,fc} / \gamma_{M0} = 7.47kNm$ $M_{pl,2Rd} = 0,25\Sigma\ell_{eff,2} t_{fc}{}^2 f_{y,fc} / \gamma_{M0} = 7.47kNm$ $m = (w/2 - t_{wc}/2 - 0.8r_c) = 55.8mm$ $n = \min[e, 1.25m] = 69.7mm$ $e_w = d_w / 4 = 14mm$ $l_{eff,1} = \min \begin{cases} 2\pi m \\ \pi m + 2e_x \\ \alpha m - (2m + 0.625e) + e_x \\ 2m + 0.625e + e_x \\ 4m + 1.25e \end{cases}$ =210.4mm $F_{ep,b,Rd} = 535.3kN$ $l_{eff} = 210.4mm$	EC3-1-8: pr. 6.2.6.4 table 6.5

Component	Details rules Step 5 – Second line	References
End-plate in transversal bending	***Resistance of the equivalent T-stub:*** $L_b = 73mm \le L_b^* = 509.7mm$ - Prying force will develop $F_{ep,\mathrm{b},Rd} = \min[F_{T,1,Rd} ; F_{T,2,Rd} ; F_{T,3,Rd}]$ with: • $F_{T,1,Rd} = \frac{4M_{pl,1,Rd}}{m} = 819.9kN$ • $F_{T,2,Rd} = \frac{2M_{pl,2,Rd} + n\Sigma F_{t,Rd}}{m+n} = 718.1kN$ • $F_{T,3,Rd} = \sum \frac{0.9 f_{ub} A_s}{\gamma_{M2}} = 1009.8kN$ where: $M_{pl,1,Rd} = 0,25\Sigma\ell_{eff,1} t_{fc}{}^2 f_{y,fc} / \gamma_{M0} = 13.6kNm$ $M_{pl,2Rd} = 0,25\Sigma\ell_{eff,2} t_{fc}{}^2 f_{y,fc} / \gamma_{M0} = 13.6kNm$ $m = (w/2 - t_{wc}/2 - 0.8r_c) = 66.2mm$ $n = \min[e, 1.25m] = 70mm$ $e_w = d_w / 4 = 14mm$ *Bolt row 2 (bolt adjacent to a stiffeners)*: $l_{eff,1} = \min[2\pi m, \alpha m] = 382.5mm$ $l_{eff,2} = \alpha m = 382.5mm$ $F_{ep,b,Rd} = 718.1kN$ $l_{eff} = 382.5mm$	EC3-1-8: pr. 6.2.6.4 table 6.5

Component	Details rules Step 6 and 7	References
Beam flanges and web in compression and Beam web in tension	Step 7 – Beam flanges and web in compression $F_{fbc,Rd} = \frac{M_{c,Rd}}{(h+\xi b-0.5t_{fb})} = 2829.9kN$ where: $\xi = 0.3$ Step 8 – Beam web in tension $F_{t,wb,Rd} = \frac{b_{eff,t,wb}t_{wp}f_{y,wp}}{\gamma_{M0}} = 1277kN$ where: $b_{eff,t,wb} = 382.5mm$	EC3-1-8 pr. 6.2.6.7 and 6.2.6.8

Component	Details rules Line Resistance	References
Bending capacity	***First bolt row line*** $F_{tr,Rd} = min(F_{t,fc,Rd}\,;\ F_{t,wc,Rd}\,;\ F_{t,ep,Rd}\ )$ $F_{tr,Rd} = min(1911;776;\ 535;\ 2830) = 535kN$ The First bolt row line is governed by the end-plate in transversal bending ***Second bolt row line*** $F_{tr,Rd} = min(F_{t,fc,Rd}\,;\ F_{t,wc,Rd}\,;\ F_{t,ep,Rd}\,;\ F_{t,wb,Rd}\ )$ $F_{tr,Rd} = min(1954;782;\ 718;\ 2830;1277) = 718kN$ The second bolt row line is governed by the end-plate in transversal bending ***Column Bending Capacity*** $M_{wp,Rd} = \frac{V_{wp,Rd,Tot}}{z_{wp}} = 693.8kNm$ ***Connection Bending Capacity*** $M_{j,Rd} = \sum_r h_r F_{tr,Rd}$ $M_{j,Rd} = 535kN \cdot 603mm + 718kN \cdot 403mm = 612.2kNm$ ***Joint Demand*** $M_{j,Ed} = \alpha \cdot \left(M_{pl,Rd} + V_u \cdot s_h\right) = 619kNm$ ***Internal hierarchy Demand*** $M_{wp,Rd} \geq M_{j,Rd} = M_{j,Ed} \rightarrow 694 \geq 612 \cong 619kNm$ ***Equal strength with strong column web panel.***	EC3-1-8: pr. 6

Once the joint capacity is defined the ductility of the connection should be verified:

Table I.5: The ductility limitation

Component	Details rules Step 8 – For both First and Second line	References
Ductile criteria	***T-stub verification:*** Bolt Row 1 Bolt Row 2 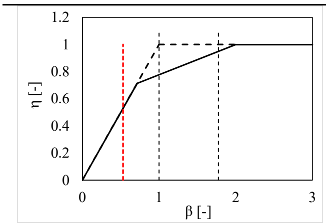 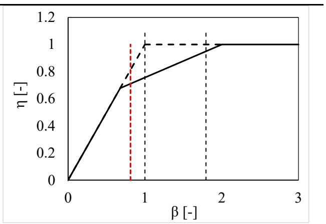 $\eta = \frac{F}{\sum F_{t,Rd}}$=0.53 $\eta = \frac{F}{\sum F_{t,Rd}}$=0.71 $\beta = \frac{4M_{pl,Rd}}{m\sum F_{t,Rd}}$=0.53 $\beta = \frac{4M_{pl,Rd}}{m\sum F_{t,Rd}}$=0.81 ***Bolt diameter verifications:*** Bolt Row 1 Bolt Row 2 $F_{c,Rd,1} = 669kN \le 1010kN$ $F_{t,Rd,2} = 718kN \le 1010kN$	Chapter V

As show in the previous paragraph, the joint shear resistance should be investigated:

Table I.6: Joint shear resistance.

Component	Details rules Shear resistance	References
Beam web in shear	Beam web in shear (buckling verification): $V_{b,Rd} = \chi_w A_{vb} f_{y,b} / \sqrt{3} = 1 \cdot 5084 \cdot 355 / \sqrt{3}$ $V_{b,Rd} = 1042kN$ where: $A_{vb} = A_b - 2b_b t_{fb} + (t_{wb} + 2r_b)t_{fb} = 5084.5mm^2$ $\chi_w = if \begin{cases} \overline{\lambda}_w \geq 0.83 \rightarrow 0.83 / \overline{\lambda}_w \\ \overline{\lambda}_w < 0.83 \rightarrow 1 \end{cases}$ $\overline{\lambda}_w = 0.3467(h_{wb} / t_{wb})\sqrt{f_{y,b} / E} = 0.638$	EC3-1-5: pr. 5.3
Bolts in shear	$F_{v,Rd} = 2\frac{\alpha_v f_{ub} A_s}{\gamma_{M2}} = 2 \cdot \frac{0.5 \cdot 1000 \cdot 561}{1.25} / 10^3$ $F_{v,Rd} = 561kN$ where $\alpha_v = 0.5$ for 10.9 bolts	EC3-1-8: pr. 361

Component	Details rules Shear resistance	References
Column flange in bearing	The resistance of the column flange in bearing should be defined: Bolt Row 1 $k_1 = \min[2.8\frac{70}{33}-1.7, \quad 2.5] = 2.5$ $\alpha_b = 1.0$ $F_{b,Rd,R1} = 2\frac{2.5\cdot 1\cdot 490\cdot 21.5\cdot 33}{1.25}/10^3$ $F_{b,Rd,R1} = 1391kN$ Bolt Row 2 $k_2 = \min[2.8\frac{70}{33}-1.7, \quad 2.5] = 2.5$ $\alpha_b = 1.0$ $F_{b,Rd,R2} = 2\frac{2.5\cdot 1\cdot 490\cdot 21.5\cdot 33}{1.25}/10^3$ $F_{b,Rd,R2} = 1391kN$	EC3-1-8: pr. 3.6

Component	Details rules Shear resistance	References
Column flange in bearing	The resistance of the column flange in bearing should be defined: Bolt Row 3 $k_1 = \min[2.8\frac{70}{33}-1.7, \quad 2.5] = 2.5$ $\alpha_b = 1.0$ $F_{b,Rd,R1} = 2\frac{2.5\cdot 1\cdot 490\cdot 21.5\cdot 33}{1.25}/10^3$ $F_{b,Rd,R1} = 1391kN$ Bolt Row 4 $k_2 = \min[2.8\frac{70}{33}-1.7, \quad 2.5] = 2.5$ $\alpha_b = 1.0$ $F_{b,Rd,R2} = 2\frac{2.5\cdot 1\cdot 490\cdot 21.5\cdot 33}{1.25}/10^3$ $F_{b,Rd,R2} = 1391kN$	EC3-1-8: pr. 3.6

Component	Details rules Shear resistance	References
End-plate in bearing	The resistance of the column flange in bearing should be defined: Bolt Row 1 $k_1 = \min[2.8\frac{70}{33} - 1.7, \quad 2.5] = 2.5$ $\alpha_b = \min[1.0, \quad \frac{55}{3 \cdot 33}] = 0.56$ $F_{b,Rd,R1} = 2\frac{2.5 \cdot 0.56 \cdot 490 \cdot 21.5 \cdot 33}{1.25} / 10^3$ $F_{b,Rd,R1} = 719kN$ Bolt Row 2 $k_2 = \min[2.8\frac{70}{33} - 1.7, \quad 2.5] = 2.5$ $\alpha_b = 1.0$ $F_{b,Rd,R2} = 2\frac{2.5 \cdot 1 \cdot 490 \cdot 20 \cdot 33}{1.25} / 10^3$ $F_{b,Rd,R2} = 1294kN$	EC3-1-8: pr. 3.6

Component	Details rules Shear resistance	References
End-plate in bearing	The resistance of the column flange in bearing should be defined: Bolt Row 3 $k_1 = \min[2.8\frac{70}{33} - 1.7, \quad 2.5] = 2.5$ $\alpha_b = \min[1.0, \quad \frac{260}{3 \cdot 33} - \frac{1}{4}] = 1$ $F_{b,Rd,R1} = 2\frac{2.5 \cdot 1 \cdot 490 \cdot 20 \cdot 33}{1.25} / 10^3$ $F_{b,Rd,R1} = 1294 kN$ Bolt Row 4 $k_2 = \min[2.8\frac{70}{33} - 1.7, \quad 2.5] = 2.5$ $\alpha_b = 1.0$ $F_{b,Rd,R2} = 2\frac{2.5 \cdot 1 \cdot 490 \cdot 20 \cdot 33}{1.25} / 10^3$ $F_{b,Rd,R2} = 1294 kN$	EC3-1-8: pr. 3.6

Component	Details rules Shear resistance	References
Shear capacity	Resistance shear for each bolt row: Bolt row 1 $V_{Rd,1} = \min[F_{b,cf,Rd,1}, \quad F_{b,ep,Rd,1}, \quad F_{v,Rd,1}]$ $V_{Rd,1} = \min[1391kN, 719kN, 561kN] = 561kN$ Bolt row 2 $V_{Rd,2} = \min[F_{b,cf,Rd,2}, \quad F_{b,ep,Rd,2}, \quad F_{v,Rd,2}]$ $V_{Rd,2} = \min[1391kN, 1294kN, 561kN] = 561kN$ Bolt row 3 $V_{Rd,3} = \min[F_{b,cf,Rd,2}, \quad F_{b,ep,Rd,2}, \quad F_{v,Rd,2}]$ $V_{Rd,3} = \min[1391kN, 1294kN, 561kN] = 561kN$ Bolt row 4 $V_{Rd,4} = \min[F_{b,cf,Rd,4}, \quad F_{b,ep,Rd,4}, \quad F_{v,Rd,4}]$ $V_{Rd,4} = \min[1391kN, 1294kN, 561kN] = 561kN$ Connection Shear resistance $V_{con,Rd} = \sum V_{Rd,i} = 561 \cdot 4 = 2244kN$ $V_{con,Rd} \geq V_{Rd,i} = 1042kN$ ***Full Strength***	EC3-1-5: pr. 5.3

Once the joint bending and shear capacity is defined, the initial stiffness value should be evaluate starting from the definition of all the k*i* described hereinafter (due to the presence of the continuity plate, the contribution of the column web in compression can be neglected by considering k2 infinite):

Table I.7: Joint stiffness definition

Component	Stiffness definition	References
Column web panel in shear	*Column web panel in shear* $k_1 = \frac{0.38 \cdot A_{VC}}{\beta z} = \frac{0.38 \cdot 7553}{1 \cdot 498} = 5.76mm$ where: β is the transformation parameter defined in EN1993-1-8 pr. 5.3(7), and z is the level arm.	EC3-1-8 pr.6.3.2
Rib in compression	*Rib in compression* $k_{RIB} = \frac{A_e}{L_e} \cdot \cos(\alpha) = \frac{4190}{149} \cos(0.70) = 21.5mm$ where (as defined by Lee [2]): $A_e = \frac{\eta(ab - c^2)}{\sqrt{(a-c)^2 + (b-c)^2}}$ $L_e = (0.6)\sqrt{\left(a^2 + b^2\right)}$ α is the rib strut inclination.	Chapter V

Component	Stiffness definition	References
Column web in tension	*Column web in tension* *Bolt row 1* $k_{3,r1}=\frac{0.7\cdot b_{eff,t,wc}\cdot t_{wc}}{d_c}=\frac{0.7\cdot 308.3\cdot 20}{297}=14.53mm$ *Bolt row 2* $k_{3,r2}=\frac{0.7\cdot b_{eff,t,wc}\cdot t_{wc}}{d_c}=\frac{0.7\cdot 317.6\cdot 20}{297}=14.97mm$	EC3-1-8 pr.6.3.2
Column flange in bending	*Column flange in bending* *Bolt row 1* $k_{4,r1}=\frac{0.9\cdot l_{eff}\cdot t_{fc}^2}{m^3}=\frac{0.9\cdot 308.3\cdot 21.5^2}{52.4^3}=19.16mm$ *Bolt row 2* $k_{4,r1}=\frac{0.9\cdot l_{eff}\cdot t_{fc}^2}{m^3}=\frac{0.9\cdot 317.6\cdot 21.5^2}{52.4^3}=19.74mm$	
End-plate in bending	*Bolt row 1* $k_{5,r1}=\frac{0.9\cdot l_{eff}\cdot t_p^2}{m^3}=\frac{0.9\cdot 210.4\cdot 20^2}{55.8^3}=8.72mm$ *Bolt row 2* $k_{5,r1}=\frac{0.9\cdot l_{eff}\cdot t_p^2}{m^3}=\frac{0.9\cdot 382.5\cdot 20^2}{66.25^3}=9.47mm$	
Bolts in tension	*Bolt row 1 and 2* $k_{10,r1/2}=\frac{1.6\cdot A_s}{L_b}=\frac{1.6\cdot 561}{73}=12.3mm$	

Component	Stiffness definition	References
Stiffness	Effective stiffness of the bolt rows $k_{ef,r1} = \frac{1}{(1/k_{3,r1} + 1/k_{4,r1} + 1/k_{5,r1} + 1/k_{10,r1})} = 3.15$ $k_{ef,r2} = \frac{1}{(1/k_{3,r2} + 1/k_{4,r2} + 1/k_{5,r2} + 1/k_{10,r2})} = 3.28$ Equivalent arm level and stiffness $z_{eq} = \frac{\sum k_{ef,i} z_i^2}{\sum k_{ef,i} z_i} = 521mm$ $k_{eq} = \frac{\sum k_{ef,i} z_i}{z_{eq}} = 6.19$ Joint Initial Stiffness $S_{j,ini} = \frac{E \cdot z_{eq}^2}{(1/k_{wp} + 1/k_{Rib} + 1/k_{eq})^{-1}} = 287588kNm$ Stiffnes classification $k_b = \frac{S_{j,ini}}{EI_b / L_b} = 16.23$ ***Semi-rigid joint***	EC3-1-8 pr.6.3.2

<table>
<tr><th>Component</th><th>Stiffness definition</th><th>References</th></tr>
<tr><td>Summary results</td><td>
BENDING CAPACITY
$M_{wp,Rd} \geq M_{j,Rd} = M_{j,Ed} \rightarrow 694 \geq 612 \cong 619kNm$
<i>Equal strength with strong column web panel</i>
DUCTILITY CRITERIA
<table>
<tr><th>Bolt Row 1</th><th>Bolt Row 2</th></tr>
<tr><td>$\eta = \frac{F}{\sum F_{t,Rd}}$ =0.53</td><td>$\eta = \frac{F}{\sum F_{t,Rd}}$ =0.71</td></tr>
<tr><td>$\beta = \frac{4M_{pl,Rd}}{m\sum F_{t,Rd}}$ =0.53</td><td>$\beta = \frac{4M_{pl,Rd}}{m\sum F_{t,Rd}}$ =0.81</td></tr>
<tr><td>$F_{c,Rd,1} = 669kN \leq 1010kN$</td><td>$F_{t,Rd,2} = 718kN \leq 1010kN$</td></tr>
</table>
SHEAR CAPACITY
$V_{con,Rd} \geq V_{Rd,i} = 1042kN$
<i>Full Strenght</i>
STIFFNESS
$k_b = \frac{S_j}{EI_b / L_b} = 16.23$
<i>Semi-Rigid joint</i>
</td><td>EC3-1-8 pr.6.3.2</td></tr>
</table>

1.5 Example of two bolt rows joint configuration

The same design procedure showed in the previous paragraph for ES2-E, is reported also for ES2-F (see Figure I-3), to show the design procedure also for the configuration with two bolt rows above the beam flange.

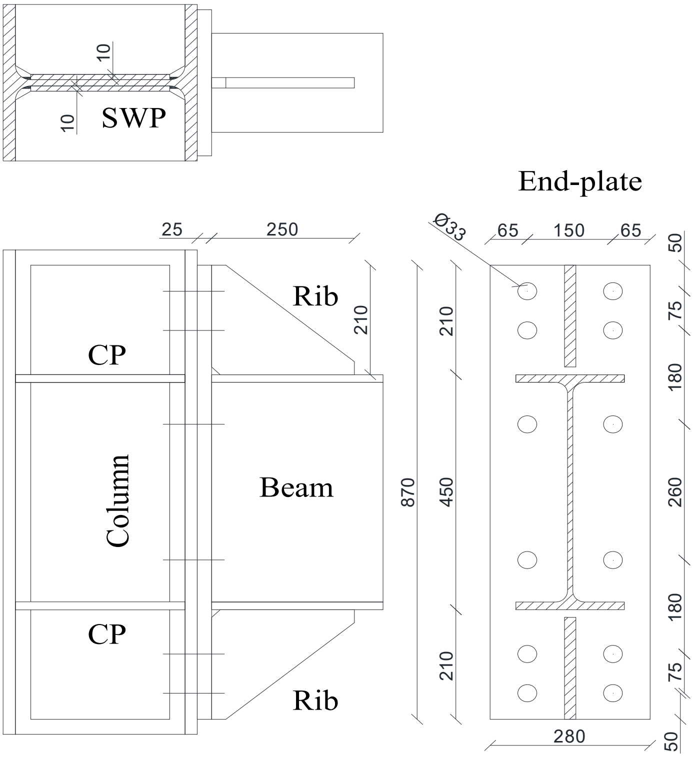

Figure I-3: Example 1: ES2-TS-F joint (6 bolts lines)

Component	Details rules Step 1	References
Column web panel in shear	The column shear resistance is: $V_{wp,Rd}=\dfrac{0.9A_{vb}f_{y,\mathrm{wc}}}{\sqrt{3}\gamma_{M0}}=103.5kN$ Moreover, an additional web panel was introduced with a thickness equal to 8mm: $V_{\mathrm{AWP},Rd}=\dfrac{0.9A_{AWP}f_{y,\mathrm{wc}}}{\sqrt{3}\gamma_{M0}}=936.3kN$ $V_{wp,Rd,Tot}=V_{wp,Rd,}+V_{AWP,Rd}=1971kN$ where: $A_{vb}=A_{b}-2b_{b}t_{fb}+(t_{wb}+2r_{b})t_{fb}=5609mm^{2}$ $A_{AWP}=2\cdot 10\cdot 254=5076mm^{2}$ Therefore the column web panel bending capacity is: $M_{wp,Rd}=\dfrac{V_{wp,Rd,Tot}}{z_{wp}}=1011.1kNm$	EC3-1-8 pr.6.2.6.1

Component	Details rules Step 3 – For First and Second bolts row lines	References
Column web in tension	Bolt row 1 $F_{wct,Rd} = \frac{\omega b_{eff,t,wc} t_{wc} f_{y,wc}}{\gamma_{M0}} = 2907kN$ Where: ω = 0.94 l_{eff}= 270.8mm Bolt row 2 $F_{wct,Rd} = \frac{\omega b_{eff,t,wc} t_{wc} f_{y,wc}}{\gamma_{M0}} = 3022.4kN$ where: ω = 0.94 l_{eff}= 282.9mm Group effect: 1+2 $F_{wct,Rd} = \frac{\omega b_{eff,t,wc} t_{wc} f_{y,wc}}{\gamma_{M0}} = 1051.1kN$ Where: ω = 0.95 l_{eff}= 260.1mm Bolt row 3 $F_{wct,Rd} = \frac{\omega b_{eff,t,wc} t_{wc} f_{y,wc}}{\gamma_{M0}} = 3037.1kN$ where: ω = 0.94 l_{eff}= 284.5mm	EC3-1-8: pr. 6.2.6.3

Component	Details rules Step 4 – First line	References
Column flange in transversal bending	***Resistance of the equivalent T-stub:*** $L_b = 78mm \le L_b^* = 195.3mm$ - Prying force will develop $F_{cfb,Rd} = \min[F_{T,1,Rd};F_{T,2,Rd};F_{T,3,Rd}]$ with: • $F_{T,1,Rd} = \frac{4M_{pl,1,Rd}}{m} = 937kN$ • $F_{T,2,Rd} = \frac{2M_{pl,2,Rd} + n\Sigma F_{t,Rd}}{m+n} = 769.4kN$ • $F_{T,3,Rd} = \sum \frac{0.9 f_{ub} A_s}{\gamma_{M2}} = 1009.8kN$ where: $M_{pl,1,Rd} = 0,25\Sigma\ell_{eff,1}\, t_{fc}{}^2 f_{y,fc} / \gamma_{M0} = 11.1kNm$ $M_{pl,2Rd} = 0,25\Sigma\ell_{eff,2}\, t_{fc}{}^2 f_{y,fc} / \gamma_{M0} = 11.1kNm$ $m = (w/2 - t_{wc}/2 - 0.8r_c) = 47.4mm$ $n = \min[e, 1.25m] = 59.25mm$ $e_w = d_w / 4 = 14mm$ *Bolt row 1 (Other inner bolt row):* $l_{eff,1} = \min[2\pi m; 4m + 1.25e] = 270.8\,\mathrm{mm}$ $l_{eff,2} = 4m + 1.25e = 270.8mm$ $F_{cfb,Rd} = 769.4kN$ $l_{eff} = 270.8mm$	EC3-1-8: pr. 6.2.6.3

Component	Details rules Step 4 – Second line	References
Column flange in transversal bending	***Resistance of the equivalent T-stub:*** $L_b = 78mm \le L_b^* = 186.9mm$ - Prying force will develop $F_{cfb,Rd} = \min[F_{T,1,Rd}; F_{T,2,Rd}; F_{T,3,Rd}]$ with: • $F_{T,1,Rd} = \frac{4M_{pl,1,Rd}}{m}$ =979.7kN • $F_{T,2,Rd} = \frac{2M_{pl,2,Rd} + n\Sigma F_{t,Rd}}{m+n}$ =778.7kN • $F_{T,3,Rd} = \sum \frac{0.9 f_{ub} A_s}{\gamma_{M2}}$ =1009.8kN where: $M_{pl,1,Rd} = 0,25\Sigma\ell_{eff,1} t_{fc}^2 f_{y,fc} / \gamma_{M0}$ =11.61kNm $M_{pl,2Rd} = 0,25\Sigma\ell_{eff,2} t_{fc}^2 f_{y,fc} / \gamma_{M0}$ =11.61kNm $m = (w/2 - t_{wc}/2 - 0.8r_c)$ =47.4mm $n = \min[e, 1.25m]$ =59.25mm $e_w = d_w / 4 = 14mm$ *Bolt row 2 (bolt adjacent to a stiffeners)*: $l_{eff,1} = \min[2\pi m, \alpha m] = 283$ mm $l_{eff,2} = \alpha m = 283$ $F_{cfb,Rd} = 778.7kN$ $l_{eff} = 283mm$	EC3-1-8: pr. 6.2.6.3

Component	Details rules Step 4 – Group effect: 1+2	References
Column flange in transversal bending	***Resistance of the equivalent T-stub:*** $L_b = 78mm \le L_b^* = 406.8mm$ - Prying force will develop $F_{cfb,Rd} = \min[F_{T,1,Rd}; F_{T,2,Rd}; F_{T,3,Rd}]$ with: • $F_{T,1,Rd} = \frac{4M_{pl,1,Rd}}{m} = 900.3kN$ • $F_{T,2,Rd} = \frac{2M_{pl,2,Rd} + n\Sigma F_{t,Rd}}{m+n} = 1322.1kN$ • $F_{T,3,Rd} = \sum \frac{0.9 f_{ub} A_s}{\gamma_{M2}} = 2019.6kN$ where: $M_{pl,1,Rd} = 0,25\Sigma\ell_{eff,1} t_{fc}^2 f_{y,fc} / \gamma_{M0} = 10.67kNm$ $M_{pl,2Rd} = 0,25\Sigma\ell_{eff,2} t_{fc}^2 f_{y,fc} / \gamma_{M0} = 10.67kNm$ $m = (w/2 - t_{wc}/2 - 0.8r_c) = 47.4mm$ $n = \min[e, 1.25m] = 59.25mm$ $e_w = d_w / 4 = 14mm$ *Bolt row 1+2 (bolt adjacent to a stiffeners)*: $l_{eff,1} = \min[2p, \mathrm{p}] + \min[\pi m + p; 0.5p + \alpha m - (2m + 0.625e)]$ $l_{eff,1} = 260.1mm$ $l_{eff,2} = [p] + [0.5p + \alpha m - (2m + 0.625e)] = 260.1mm$ $F_{cfb,Rd} = 900.3kN$ $l_{eff} = 260.1mm$	EC3-1-8: pr. 6.2.6.3

Component	Details rules Step 4 – Third line	References
Column flange in transversal bending	***Resistance of the equivalent T-stub:*** $L_b = 78mm \le L_b^* = 185.9mm$ - Prying force will develop $F_{cfb,Rd} = \min[F_{T,1,Rd};F_{T,2,Rd};F_{T,3,Rd}]$ with: • $F_{T,1,Rd} = \frac{4M_{pl,1,Rd}}{m} = 985.1kN$ • $F_{T,2,Rd} = \frac{2M_{pl,2,Rd} + n\Sigma F_{t,Rd}}{m+n} = 779.9kN$ • $F_{T,3,Rd} = \sum \frac{0.9 f_{ub} A_s}{\gamma_{M2}} = 1009.8kN$ where: $M_{pl,1,Rd} = 0,25\Sigma\ell_{eff,1} t_{fc}{}^2 f_{y,fc} / \gamma_{M0} = 11.67kNm$ $M_{pl,2Rd} = 0,25\Sigma\ell_{eff,2} t_{fc}{}^2 f_{y,fc} / \gamma_{M0} = 11.67kNm$ $m = (w/2 - t_{wc}/2 - 0.8r_c) = 47.4$ mm $n = \min[e, 1.25m] = 59.2mm$ $e_w = d_w / 4 = 14mm$ *Bolt row 3 (bolt adjacent to a stiffeners)*: $l_{eff,1} = \min[2\pi m, \alpha m] = 284$ mm $l_{eff,2} = \alpha m = 284$ $F_{cfb,Rd} = 779.9kN$ $l_{eff} = 284mm$	EC3-1-8: pr. 6.2.6.3

Component	Details rules Step 5 – First line	References
End-plate in transversal bending	***Resistance of the equivalent T-stub:*** $L_b = 78mm \le L_b^* = 221.5mm$ - Prying force will develop $F_{cfb,Rd} = \min[F_{T,1,Rd}; F_{T,2,Rd}; F_{T,3,Rd}]$ with: • $F_{T,1,Rd} = \frac{4M_{pl,1,Rd}}{m} = 835.2kN$ • $F_{T,2,Rd} = \frac{2M_{pl,2,Rd} + n\Sigma F_{t,Rd}}{m+n} = 746.6kN$ • $F_{T,3,Rd} = \sum \frac{0.9 f_{ub} A_s}{\gamma_{M2}} = 1009.8kN$ where: $M_{pl,1,Rd} = 0,25\Sigma\ell_{eff,1} t_{fc}^2 f_{y,fc} / \gamma_{M0} = 10.73kNm$ $M_{pl,2Rd} = 0,25\Sigma\ell_{eff,2} t_{fc}^2 f_{y,fc} / \gamma_{M0} = 10.73kNm$ $m = (w/2 - t_{wb}/2 - 0.8r_b) = 51.4\text{mm}$ $n = \min[e, 1.25m] = 64.2\text{mm}$ $e_w = d_w / 4 = 14mm$ *Bolt row 1 (Frist bolt row outside beam tension flange):* $l_{eff,1} = \min\begin{cases} 2\pi m \\ \pi m + 2e_x \\ 4m + 1.25e \\ 2m + 0.625e + e_x \end{cases} = 193.4\text{mm}$ $F_{cfb,Rd} = 746.6kN$ $l_{eff} = 193.4mm$	EC3-1-8: pr. 6.2.6.5

Component	Details rules Step 5 – Second line	References
End-plate in transversal bending	***Resistance of the equivalent T-stub:*** $L_b = 73mm \le L_b^* = 142mm$ - Prying force will develop $F_{cfb,Rd} = \min[F_{T,1,Rd}; F_{T,2,Rd}; F_{T,3,Rd}]$ with: • $F_{T,1,Rd} = \frac{4M_{pl,1,Rd}}{m} = 1302.3kN$ • $F_{T,2,Rd} = \frac{2M_{pl,2,Rd} + n\Sigma F_{t,Rd}}{m+n} = 850.4kN$ • $F_{T,3,Rd} = \sum \frac{0.9 f_{ub} A_s}{\gamma_{M2}} = 1009.8kN$ where: $M_{pl,1,Rd} = 0,25\Sigma\ell_{eff,1} t_{fc}{}^2 f_{y,fc} / \gamma_{M0} = 16.72kNm$ $M_{pl,2Rd} = 0,25\Sigma\ell_{eff,2} t_{fc}{}^2 f_{y,fc} / \gamma_{M0} = 16.72kNm$ $m = (w/2 - t_{wb}/2 - 0.8r_b) = 51.4\,\text{mm}$ $n = \min[e, 1.25m] = 64.2\,\text{mm}$ $e_w = d_w / 4 = 14mm$ *<u>Bolt row 2 (bolt adjacent to a stiffeners)</u>*: $l_{eff,1} = \min[2\pi m, \alpha m] = 301.5\,\text{mm}$ $l_{eff,2} = \alpha m = 301.5mm$ $F_{cfb,Rd} = 850.4kN$ $l_{eff} = 301.5mm$	EC3-1-8: pr. 6.2.6.3

Component	Details rules Step 5 – Group effect: 1+2	References
End-plate in transversal bending	***Resistance of the equivalent T-stub:*** $L_b = 73mm \le L_b^* = 302.5mm$ - Prying force will develop $F_{cfb,Rd} = \min[F_{T,1,Rd}; F_{T,2,Rd}; F_{T,3,Rd}]$ with: ● $F_{T,1,Rd} = \frac{4M_{pl,1,Rd}}{m} = 1223kN$ ● $F_{T,2,Rd} = \frac{2M_{pl,2,Rd} + n\Sigma F_{t,Rd}}{m+n} = 1394kN$ ● $F_{T,3,Rd} = \sum \frac{0.9 f_{ub} A_s}{\gamma_{M2}} = 1009.8kN$ where: $M_{pl,1,Rd} = 0,25\Sigma\ell_{eff,1}\, t_{fc}^{\ 2} f_{y,fc} / \gamma_{M0} = 15.71kNm$ $M_{pl,2Rd} = 0,25\Sigma\ell_{eff,2}\, t_{fc}^{\ 2} f_{y,fc} / \gamma_{M0} = 15.71kNm$ $m = (w/2 - t_{wb}/2 - 0.8r_b) = 51.4\,\text{mm}$ $n = \min[e, 1.25m] = 64.2\,\text{mm}$ $e_w = d_w / 4 = 14mm$ *Bolt row 1+2 (bolt adjacent to a stiffeners)*: $l_{eff,1} = \min[\pi m + p, 2e_x + p, 2m + 0.625e + 0.5p, e_x + 0.5p] +$ $+ \min[\pi m + p; 0.5p + \alpha m - (2m + 0.625e)] = 283.1mm$ $l_{eff,2} = \min[2m + 0.625e + 0.5p, e_x + 0.5p] +$ $+[0.5p + \alpha m - (2m + 0.625e)] = 283.1mm$ $F_{cfb,Rd} = 1223kN$ $l_{eff} = 283.1mm$	EC3-1-8: pr. 6.2.6.3

Component	Details rules Step 5 – Third line	References
End-plate in transversal bending	***Resistance of the equivalent T-stub:*** $L_b = 73mm \le L_b^* = 190.8mm$ - Prying force will develop $F_{cfb,Rd} = \min[F_{T,1,Rd}; F_{T,2,Rd}; F_{T,3,Rd}]$ with: • $F_{T,1,Rd} = \frac{4M_{pl,1,Rd}}{m} = 1278.1kN$ • $F_{T,2,Rd} = \frac{2M_{pl,2,Rd} + n\Sigma F_{t,Rd}}{m+n} = 833.4kN$ • $F_{T,3,Rd} = \sum \frac{0.9 f_{ub} A_s}{\gamma_{M2}} = 1009.8kN$ where: $M_{pl,1,Rd} = 0,25\Sigma\ell_{eff,1} t_{fc}^{\ 2} f_{y,fc} / \gamma_{M0} = 18.85kNm$ $M_{pl,2Rd} = 0,25\Sigma\ell_{eff,2} t_{fc}^{\ 2} f_{y,fc} / \gamma_{M0} = 18.85kNm$ $m = (w/2 - t_{wb}/2 - 0.8r_b) = 58.9$ mm $n = \min[e, 1.25m] = 65$ mm $e_w = d_w / 4 = 14mm$ *Bolt row 3 (bolt adjacent to a stiffeners)*: $l_{eff,1} = \min[2\pi m, \alpha m] = 339.8$ mm $l_{eff,2} = \alpha m = 339.8mm$ $F_{cfb,Rd} = 833.4kN$ $l_{eff} = 339.8mm$	EC3-1-8: pr. 6.2.6.3

Component	Details rules Step 6 and 7	References
Beam flanges and web in compression	Step 6 – Beam flanges and web in compression $$F_{fbc,Rd} = \frac{M_{c,Rd}}{(h + \xi b - 0.5t_{fb})} = 3647.7kN$$ where: $\xi b = 0.3$	EC3-1-8 pr. 6.2.6.7
Beam web in tension	Step 7 – Beam web in tension $$F_{t,wb,Rd} = \frac{b_{eff,t,wb} t_{wp} f_{y,wp}}{\gamma_{M0}} = 1134kN$$ where: $b_{eff,t,wb} = 339.8mm$	EC3-1-8 pr. 6.2.6.8

Component	Details rules Line Resistance	References
Joint bending resistance	***First bolt row line*** $F_{tr,Rd,1} = min(F_{t,wb,Rd};F_{t,fc,Rd};F_{t,ep,Rd}; F_{c,wb,Rd})$ $F_{tr,Rd,1} = min(2907;769; 746; 3648) =746kN$ The First bolt row line is governed by the end-plate in transversal bending ***Second bolt row line*** $F_{tr,Rd,2} = min(F_{t,wb,Rd};F_{t,fc,Rd};F_{t,ep,Rd}; F_{c,wb,Rd})$ $F_{tr,Rd,2} = min(3022;778; 850; 3648) =778kN$ The Second bolt row line is governed by the column flange in transversal bending ***First and Second bolt row in Group*** $F_{tr,Rd,1+2} = min(F_{t,wb,Rd};F_{t,fc,Rd}; F_{t,ep,Rd}; F_{c,wb,Rd})$ $F_{tr,Rd,1+2} = min(1051;900; 1223; 3648) =900kN$ $F_{tr,Rd,2} = min(F_{tr,Rd,2}; F_{tr,Rd,1+2} - F_{tr,Rd,1})$ $F_{tr,Rd,2} = min(778; 900 - 746) = 154kN$ The group effect reduce the resistance of the Second line ***Third bolt row line*** $F_{tr,Rd,3} = min(F_{t,wb,Rd};F_{t,fc,Rd};F_{t,ep,Rd}; F_{c,wb,Rd};F_{t,wb,Rd})$ $F_{tr,Rd,3} = min(3038;780; 833; 3648;1134) =780kN$ The Third bolt row line is governed by the column flange in transversal bending	EC3-1-8: pr. 6

Component	Details rules Line Resistance	References
Joint bending resistance	***Moment corresponding to column web shear Capacity*** $M_{wp,Rd} = \frac{V_{wp,Rd,Tot}}{z_{wp}} = 1011 kNm$ ***Connection Bending Capacity*** $M_{j,Rd} = \sum_r h_r F_{tr,Rd}$ $M_{j,Rd} = 746kN \cdot 673mm + 154kN \cdot 598mm +$ $+780kN \cdot 418mm = 920.4kNm$ ***Joint Demand*** $M_{j,Ed} = \alpha \cdot \left(M_{pl,Rd} + V_u \cdot s_h \right) = 908kNm$ ***Internal hierarchy Demand*** $M_{wp,Rd} \geq M_{j,Rd} = M_{j,Ed} \rightarrow 1011 \geq 920 \geq 908kNm$ ***Full strength with strong column web panel***	EC3-1-8: pr. 6

<table>
<tr><th>Component</th><th>Details rules
Step 8</th><th>References</th></tr>
<tr><td>Ductile limitations</td><td>

T-stub verification:

Bolt Row 1

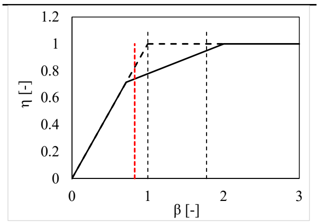

$$\eta = \frac{F}{\sum F_{t,Rd}} = 0.74$$

$$\beta = \frac{4M_{pl,Rd}}{m\sum F_{t,Rd}} = 0.83$$

Bolt Row 2

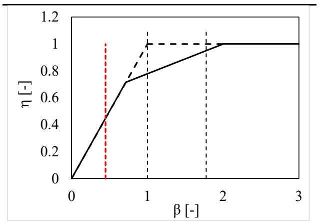

$$\eta = \frac{F}{\sum F_{t,Rd}} = 0.45$$

$$\beta = \frac{4M_{pl,Rd}}{m\sum F_{t,Rd}} = 0.45$$

Bolt Row 3

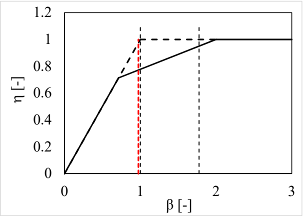

$$\eta = \frac{F}{\sum F_{t,Rd}} = 0.77$$

$$\beta = \frac{4M_{pl,Rd}}{m\sum F_{t,Rd}} = 0.98$$

Bolt diameter verifications:

Bolt Row 1

$F_{c,Rd,1} = 933kN \leq 1010kN$

Bolt Row 2

$F_{t,Rd,2} = 192kN \leq 1010kN$

Bolt Row 3

$F_{t,Rd,3} = 975kN \leq 1010kN$

</td><td>Chapter V</td></tr>
</table>

As shown in the previous paragraph, the joint shear resistance should be investigated:

Table I.8: Joint shear resistance.

Component	Details rules Shear resistance	References
Beam web in shear	Beam web in shear (buckling verification): $V_{b,Rd} = \chi_w A_{vb} f_{y,b} / \sqrt{3} = 1 \cdot 5084 \cdot 355 / \sqrt{3}$ $V_{b,Rd} = 1042kN$ where: $A_{vb} = A_b - 2b_b t_{fb} + (t_{wb} + 2r_b)t_{fb} = 5084.5mm^2$ $\chi_w = if \begin{cases} \overline{\lambda}_w \geq 0.83 \rightarrow 0.83 / \overline{\lambda}_w \\ \overline{\lambda}_w < 0.83 \rightarrow 1 \end{cases}$ $\overline{\lambda}_w = 0.3467(h_{wb} / t_{wb})\sqrt{f_{y,b} / E} = 0.638$	EC3-1-5: pr. 5.3
Bolts in shear	$F_{v,Rd} = 2\dfrac{\alpha_v f_{ub} A_s}{\gamma_{M2}} = 2 \cdot \dfrac{0.5 \cdot 1000 \cdot 561}{1.25} / 10^3$ $F_{v,Rd} = 561kN$ where $\alpha_v = 0.5$ for 10.9 bolts	EC3-1-8: pr. 361

Component	Details rules Shear resistance	References
Column flange in bearing	The resistance of the column flange in bearing should be defined: Bolt Row 1 $k_1 = \min[2.8\frac{70}{33} - 1.7, \quad 2.5] = 2.5$ $\alpha_b = \min[1.0, \frac{75}{3 \cdot 33} - \frac{1}{4}] = 0.51$ $F_{b,Rd,R1} = 2\frac{2.5 \cdot 0.51 \cdot 490 \cdot 21.5 \cdot 33}{1.25} / 10^3$ $F_{b,Rd,R1} = 706kN$ Bolt Row 2 $k_2 = \min[2.8\frac{70}{33} - 1.7, \quad 2.5] = 2.5$ $\alpha_b = 1.0$ $F_{b,Rd,R2} = 2\frac{2.5 \cdot 1 \cdot 490 \cdot 21.5 \cdot 33}{1.25} / 10^3$ $F_{b,Rd,R2} = 1391kN$	EC3-1-8: pr. 3.6

Component	Details rules Shear resistance	References
Column flange in bearing	The resistance of the column flange in bearing should be defined: Bolt Row 3 $k_3 = \min[2.8\frac{70}{33} - 1.7, \quad 2.5] = 2.5$ $\alpha_b = \min[1.0, \frac{260}{3 \cdot 33} - \frac{1}{4}] = 1$ $F_{b,Rd,R3} = 2\frac{2.5 \cdot 1 \cdot 490 \cdot 21.5 \cdot 33}{1.25} / 10^3$ $F_{b,Rd,R3} = 1391 kN$ Bolt Row 4 $k_4 = \min[2.8\frac{70}{33} - 1.7, \quad 2.5] = 2.5$ $\alpha_b = 1.0$ $F_{b,Rd,R4} = 2\frac{2.5 \cdot 1 \cdot 490 \cdot 21.5 \cdot 33}{1.25} / 10^3$ $F_{b,Rd,R4} = 1391 kN$	EC3-1-8: pr. 3.6

Component	Details rules Shear resistance	References
Column flange in bearing	The resistance of the column flange in bearing should be defined: Bolt Row 5 $k_5 = \min[2.8\frac{70}{33}-1.7, \quad 2.5] = 2.5$ $\alpha_b = \min[1.0, \frac{75}{3 \cdot 33} - \frac{1}{4}] = 0.51$ $F_{b,Rd,R5} = 2\frac{2.5 \cdot 0.51 \cdot 490 \cdot 21.5 \cdot 33}{1.25} / 10^3$ $F_{b,Rd,R5} = 706kN$ Bolt Row 6 $k_6 = \min[2.8\frac{70}{33}-1.7, \quad 2.5] = 2.5$ $\alpha_b = 1.0$ $F_{b,Rd,R6} = 2\frac{2.5 \cdot 1 \cdot 490 \cdot 21.5 \cdot 33}{1.25} / 10^3$ $F_{b,Rd,R6} = 1391kN$	EC3-1-8: pr. 3.6

Component	Details rules Shear resistance	References
End-plate in bearing	The resistance of the column flange in bearing should be defined: Bolt Row 1 $k_1 = \min[2.8\frac{70}{33}-1.7, \quad 2.5] = 2.5$ $\alpha_b = \min[1.0, \quad \frac{50}{3\cdot 33}] = 0.51$ $F_{b,Rd,R1} = 2\frac{2.5\cdot 0.51\cdot 490\cdot 25\cdot 33}{1.25}/10^3$ $F_{b,Rd,R1} = 817kN$ Bolt Row 2 $k_2 = \min[2.8\frac{70}{33}-1.7, \quad 2.5] = 2.5$ $\alpha_b = \min[1.0, \quad \frac{75}{3\cdot 33}-\frac{1}{4}] = 0.51$ $F_{b,Rd,R2} = 2\frac{2.5\cdot 0.51\cdot 490\cdot 25\cdot 33}{1.25}/10^3$ $F_{b,Rd,R2} = 821kN$	EC3-1-8: pr. 3.6

Component	Details rules Shear resistance	References
End-plate in bearing	The resistance of the column flange in bearing should be defined: Bolt Row 3 $k_3 = \min[2.8\frac{70}{33} - 1.7, \quad 2.5] = 2.5$ $\alpha_b = 1.0$ $F_{b,Rd,R3} = 2\frac{2.5 \cdot 1 \cdot 490 \cdot 25 \cdot 33}{1.25} / 10^3$ $F_{b,Rd,R3} = 1617 kN$ Bolt Row 4 $k_4 = \min[2.8\frac{70}{33} - 1.7, \quad 2.5] = 2.5$ $\alpha_b = \min[1.0, \quad \frac{260}{3 \cdot 33} - \frac{1}{4}] = 1$ $F_{b,Rd,R4} = 2\frac{2.5 \cdot 1 \cdot 490 \cdot 25 \cdot 33}{1.25} / 10^3$ $F_{b,Rd,R4} = 1617 kN$	EC3-1-8: pr. 3.6

Component	Details rules Shear resistance	References
End-plate in bearing	The resistance of the column flange in bearing should be defined: Bolt Row 5 $k_5 = \min[2.8\frac{70}{33}-1.7, \quad 2.5] = 2.5$ $\alpha_b = 1.0$ $F_{b,Rd,R5} = 2\frac{2.5\cdot 1\cdot 490\cdot 25\cdot 33}{1.25}/10^3$ $F_{b,Rd,R5} = 1617kN$ Bolt Row 6 $k_6 = \min[2.8\frac{70}{33}-1.7, \quad 2.5] = 2.5$ $\alpha_b = \min[1.0, \quad \frac{75}{3\cdot 33}-\frac{1}{4}] = 0.51$ $F_{b,Rd,R6} = 2\frac{2.5\cdot 0.51\cdot 490\cdot 25\cdot 33}{1.25}/10^3$ $F_{b,Rd,R6} = 821kN$	EC3-1-8: pr. 3.6

Component	Details rules Shear resistance	References
Shear capacity	Resistance shear for each bolt row: Bolt row 1 $V_{Rd,1} = \min[F_{b,cf,Rd,1}, \quad F_{b,ep,Rd,1}, \quad F_{v,Rd,1}]$ $V_{Rd,1} = \min[706kN, 817kN, 561kN] = 561kN$ Bolt row 2 $V_{Rd,2} = \min[F_{b,cf,Rd,2}, \quad F_{b,ep,Rd,2}, \quad F_{v,Rd,2}]$ $V_{Rd,2} = \min[1391kN, 821kN, 561kN] = 561kN$ Bolt row 3 $V_{Rd,3} = \min[F_{b,cf,Rd,3}, \quad F_{b,ep,Rd,3}, \quad F_{v,Rd,3}]$ $V_{Rd,3} = \min[1391kN, 1617kN, 561kN] = 561kN$ Bolt row 4 $V_{Rd,4} = \min[F_{b,cf,Rd,4}, \quad F_{b,ep,Rd,4}, \quad F_{v,Rd,4}]$ $V_{Rd,4} = \min[1391kN, 1617kN, 561kN] = 561kN$ Bolt row 5 $V_{Rd,5} = \min[F_{b,cf,Rd,4}, \quad F_{b,ep,Rd,4}, \quad F_{v,Rd,4}]$ $V_{Rd,5} = \min[1391kN, 1617kN, 561kN] = 561kN$	EC3-1-5: pr. 5.3

Component	Details rules Shear resistance	References
Shear capacity	Resistance shear for each bolt row: Bolt row 6 $V_{Rd,6} = \min[F_{b,cf,Rd,6}, \quad F_{b,ep,Rd,6}, \quad F_{v,Rd,6}]$ $V_{Rd,6} = \min[1391kN, 821kN, 561kN] = 561kN$ Connection Shear resistance $V_{con,Rd} = \sum V_{Rd,i} = 561 \cdot 6 = 3366kN$ $V_{con,Rd} \geq V_{Rd,i} = 1042kN$ ***Full Strength***	EC3-1-5: pr. 5.3

Once the joint bending capacity is defined, the initial stiffness value should be evaluate starting from the definition of all the k*ᵢ* coefficients described hereinafter (the contribution of the column web panel is negligible and therefore k*ᵢ* can be assumed infinite):

Table I.9: Stiffness definition

Component	Stiffness definition	References
Column web panel in shear	*Column web panel in shear* $k_1 = \frac{0.38 \cdot A_{VC}}{\beta z} = \frac{0.38 \cdot 10685}{1 \cdot 513} = 7.91 mm$ where: β is the transformation parameter defined in EN1993-1-8 pr. 5.3(7), and z is the level arm.	EC3-1-8 pr.6.3.2
Rib in compression	*Rib in compression* $k_{RIB} = \frac{A_e}{L_e} \cdot \cos(\alpha) = \frac{5343}{196} \cos(0.70) = 20.9 mm$ where (as defined by Lee [2]): $A_e = \frac{\eta(ab - c^2)}{\sqrt{(a-c)^2 + (b-c)^2}}$ $L_e = (0.6)\sqrt{\left(a^2 + b^2\right)}$ α is the rib strut inclination.	Chapter V

Component	Stiffness definition	References
Column web in tension	*Column web in tension* *Bolt row 1* $k_{3,r1} = \frac{0.7 \cdot b_{eff,t,wc} \cdot t_{wc}}{d_c} = \frac{0.7 \cdot 270.9 \cdot 32}{297} = 20.43mm$ *Bolt row 2* $k_{3,r2} = \frac{0.7 \cdot b_{eff,t,wc} \cdot t_{wc}}{d_c} = \frac{0.7 \cdot 260.1 \cdot 32}{297} = 19.61mm$ *Bolt row 3* $k_{3,r3} = \frac{0.7 \cdot b_{eff,t,wc} \cdot t_{wc}}{d_c} = \frac{0.7 \cdot 284.5 \cdot 32}{297} = 21.46mm$	EC3-1-8 pr.6.3.2
Column flange in bending	*Column flange in bending* *Bolt row 1* $k_{4,r1} = \frac{0.9 \cdot l_{eff} \cdot t_{fc}^2}{m^3} = \frac{0.9 \cdot 270.9 \cdot 21.5^2}{47.4^3} = 22.75mm$ *Bolt row 2* $k_{4,r2} = \frac{0.9 \cdot l_{eff} \cdot t_{fc}^2}{m^3} = \frac{0.9 \cdot 260.1 \cdot 21.5^2}{47.4^3} = 21.84mm$ *Bolt row 3* $k_{4,r3} = \frac{0.9 \cdot l_{eff} \cdot t_{fc}^2}{m^3} = \frac{0.9 \cdot 284.5 \cdot 21.5^2}{47.4^3} = 23.90mm$	

Component	Stiffness definition	References
End-plate in bending	*End-plate in bending* *Bolt row 1* $k_{5,\mathrm{r}1}=\frac{0.9\cdot l_{eff}\cdot t_p^2}{m^3}=\frac{0.9\cdot 193.4\cdot 25^2}{51.4^3}=20.06mm$ *Bolt row 2* $k_{5,\mathrm{r}2}=\frac{0.9\cdot l_{eff}\cdot t_p^2}{m^3}=\frac{0.9\cdot 283.1\cdot 25^2}{51.4^3}=29.38mm$ *Bolt row 3* $k_{5,\mathrm{r}3}=\frac{0.9\cdot l_{eff}\cdot t_p^2}{m^3}=\frac{0.9\cdot 339.8\cdot 25^2}{59.9^3}=23.28mm$	EC3-1-8 pr.6.3.2
Bolts in tension	*Bolts in tension 1-3* $k_{10,r1-3}=\frac{1.6\cdot A_s}{L_b}=\frac{1.6\cdot 561}{78}=11.5mm$	

Component	Stiffness definition	References
Stiffness	Effective stiffness of the bolt rows $k_{ef,r1} = \frac{1}{(1/k_{3,r1}+1/k_{4,r1}+1/k_{5,r1}+1/k_{10,r1})} = 4.35$ $k_{ef,r2} = \frac{1}{(1/k_{3,r2}+1/k_{4,r2}+1/k_{5,r2}+1/k_{10,r2})} = 4.59$ $k_{ef,r3} = \frac{1}{(1/k_{3,r3}+1/k_{4,r3}+1/k_{5,r3}+1/k_{10,r3})} = 4.58$ Equivalent arm level and stiffness $z_{eq} = \frac{\sum k_{ef,i} z_i^2}{\sum k_{ef,i} z_i} = 581mm$ $k_{eq} = \frac{\sum k_{ef,i} z_i}{z_{eq}} = 13.05$ Joint Initial Stiffness $S_{j,ini} = \frac{E \cdot z_{eq}^2}{(1/k_{wp}+1/k_{Rib}+1/k_{eq})^{-1}} = 637971kNm$ Stiffnes classification $k_b = \frac{S_{j,ini}}{EI_b/L_b} = 36.01$ ***Full-rigid joint***	EC3-1-8 pr.6.3.2

Component	Stiffness definition	References
Summary results	**BENDING CAPACITY** $M_{wp,Rd} \geq M_{j,Rd} = M_{j,Ed} \rightarrow 1011 \geq 920 \geq 908kNm$ ***Full strength with strong column web panel*** **DUCTILITY CRITERIA** Bolt Row 1 $\eta = \frac{F}{\sum F_{t,Rd}} = 0.53$ $\beta = \frac{4M_{pl,Rd}}{m\sum F_{t,Rd}} = 0.53$ Bolt Row 2 $\eta = \frac{F}{\sum F_{t,Rd}} = 0.71$ $\beta = \frac{4M_{pl,Rd}}{m\sum F_{t,Rd}} = 0.81$ Bolt Row 3 $\eta = \frac{F}{\sum F_{t,Rd}} = 0.77$ $\beta = \frac{4M_{pl,Rd}}{m\sum F_{t,Rd}} = 0.98$ $F_{c,Rd,1} = 669kN \leq 1010kN$ $F_{t,Rd,2} = 718kN \leq 1010kN$ $F_{t,Rd,3} = 975kN \leq 1010kN$	EC3-1-8 pr.6.3.2

Component	Stiffness definition	References
Summary results	**SHEAR CAPACITY** $V_{con,Rd} \geq V_{Rd,i} = 1042kN$ ***Full Strength*** **STIFFNESS** $k_b = \frac{S_j}{EI_b / L_b} = 36.01$ ***Full-Rigid joint***	EC3-1-8 pr.6.3.2

Annex II Coupon tests results

The results of all the coupon tests performed at University of Naples (white) and at University of Liege (in grey) are presented hereinafter (from Table II.1 to Table II.4) in terms of: (i) yielding strength (f_y), (ii) ultimate strength (f_u), (iii) elastic stiffness (E) and (iv) elongation at rapture (Elong). Moreover, some test pictures are reported in Figure II-1.

Table II.1: Coupon tests results (IPE 600 and IPE 450).

Coupons tests								
Specimen n°		a_0	b_0	S_0	f_y	f_u	E	Elong
Coupon		mm	mm	mm²	N/mm²	N/mm²	N/mm²	%
IPE 600	web-1	11.8	25.1	296	454.7	504.6	202558	33.1
	web-2	11.8	25.1	296	469.1	507.8	211711	32.9
	flange-1	19.3	25.1	485	472.5	542.5	203972	36.6
	flange-2	18.4	25.0	462	479.1	561.9	164334	34.4
IPE 450	web-1	8.9	25.0	223	449.0	536.5	202255	28.3
	web-2	8.9	25.0	223	483.4	540.9	205981	29.6
	web-3	9.8	32.0	313	379.7	493.7	205981	33.6
	web-4	9.8	32.4	318	390.3	493.8	205981	31.3
	flange-1	14.2	25.0	355	457.5	533.9	205981	32.9
	flange-2	14.0	25.0	350	433.8	526.9	205981	33.7
	flange-3	14.3	32.1	459	409.9	470.7	205981	36.6
	flange-4	14.2	32.1	454	353.3	414.3	205981	34.4

Table II.2: Coupon tests results (IPE 360 and HEB 280).

Coupons tests								
Specimen n°		a0	b0	S0	fy	fu	E	Elong
Coupon		mm	mm	mm^2	N/mm^2	N/mm^2	N/mm^2	%
IPE 360	web-1	8.3	32.4	268	388.7	495.7	194345	33.5
	web-2	8.2	32.0	262	397.8	513.2	198910	30.7
	web-3	9.4	32.1	303	423.3	538.0	211650	29.6
	web-4	8.2	32.1	262	388.4	505.5	194220	33.3
	web-5	8.0	32.1	258	386.0	506.3	193000	32.2
	web-6	8.0	32.2	257	389.9	507.1	194945	33.4
	web-7	8.0	32.0	258	389.9	513.4	194935	33.0
	flange-1	12.5	32.2	402	375.5	514.0	187755	30.9
	flange-2	12.0	32.0	385	397.8	513.2	198910	30.7
	flange-3	13.9	32.2	446	403.0	548.9	201490	29.8
	flange-4	12.3	32.2	396	368.7	509.2	184330	29.9
	flange-5	12.0	32.1	385	370.8	506.3	185420	32.2
	flange-6	12.3	32.3	398	377.2	516.5	188575	29.1
	flange-7	12.0	32.1	384	375.2	519.1	187585	29.3
HEB280	web-1	10.6	32.2	342	382.8	498.2	191380	25.1
	web-2	10.6	32.1	339	380.4	496.6	190205	29.1
	web-3	10.6	32.2	342	388.1	499.4	194060	26.2
	web-4	11.5	32.2	369	383.0	495.6	191495	27.6
	flange-1	17.8	32.1	572	355.2	483.9	177600	31.0
	flange-2	17.3	32.2	555	357.2	480.0	178585	33.0
	flange-3	17.8	32.2	572	368.5	491.1	184255	32.7
	flange-4	17.4	32.3	562	467.3	556.3	233640	27.5

Table II.3: Coupon tests results (HEB340, HEB500 and HEB650).

Coupons tests								
Specimen n°		a0	b0	S0	fy	fu	E	Elong
Coupon		mm	mm	mm²	N/mm²	N/mm²	N/mm²	%
HEB 340	web-1	12.9	25.0	322	459.6	497.3	219356	34.2
	web-2	12.8	25.0	321	450.9	500.8	197042	33.3
	web-3	12.6	32.4	409	401.3	491.7	200625	32.8
	web-4	12.6	32.2	406	405.0	499.6	202495	29.8
	web-5	12.5	32.1	401	395.0	496.0	197500	31.7
	web-6	12.8	32.2	411	409.7	501.1	204865	30.2
	flange-1	20.3	25.0	507	518.3	576.0	193992	33.4
	flange-2	20.4	25.0	512	499.7	569.4	213240	34.4
	flange-3	20.7	32.1	664	483.4	565.7	241700	28.9
	flange-4	20.8	32.1	666	472.2	565.6	236095	26.0
	flange-5	20.8	32.2	669	476.1	562.8	238065	26.8
	flange-6	21.6	32.1	694	467.7	555.1	233825	27.7
HEB 500	web-1	14.2	25.1	356	440.1	477.1	214140	36.1
	web-2	14.2	25.0	357	429.6	474.2	210821	36.2
	web-3	14.5	32.3	468	439.0	551.7	219490	31.5
	flange-1	27.7	25.0	693	451.6	555.9	218606	36.5
	flange-2	27.1	25.0	678	441.9	548.6	226792	38.0
	flange-3	27.1	32.1	869	411.7	552.7	205840	29.6
HEB 650	web-1	16.1	25.0	403	444.1	483.0	202423	36.4
	web-2	16.1	25.0	402	438.9	486.1	204016	36.1
	flange-1	29.9	25.0	748	435.4	533.5	206646	36.8
	flange-2	28.9	25.0	722	382.7	484.7	216500	40.8

Table II.4: Coupon tests results (plates of 15, 18, 20, 25 and 30mm).

Coupons tests								
Specimen n°		a0	b0	S0	fy	fu	E	Elong
Coupon		mm	mm	mm²	N/mm²	N/mm²	N/mm²	%
Plate 15	PL-1	15.2	25.1	381	459.8	567.7	208149	33.1
	PL-2	15.2	25.0	380	458.6	567.0	209855	34.4
Plate 18	PL-1	18.2	25.1	456	426.2	552.6	199897	33.8
	PL-2	18.2	25.0	456	409.7	550.8	192509	32.9
Plate 20	PL-1	20.2	25.0	505	520.0	570.5	210082	18.4
	PL-2	20.1	25.0	504	498.6	556.3	212425	22.8
Plate 25	PL-1	24.8	25.0	620	460.0	590.0	213304	33.2
	PL-2	24.8	25.0	620	459.6	589.6	218752	32.5
Plate 30	PL-1	29.4	25.0	735	365.9	485.5	215331	42.0
	PL-2	29.4	25.0	736	323.2	485.6	196368	40.6

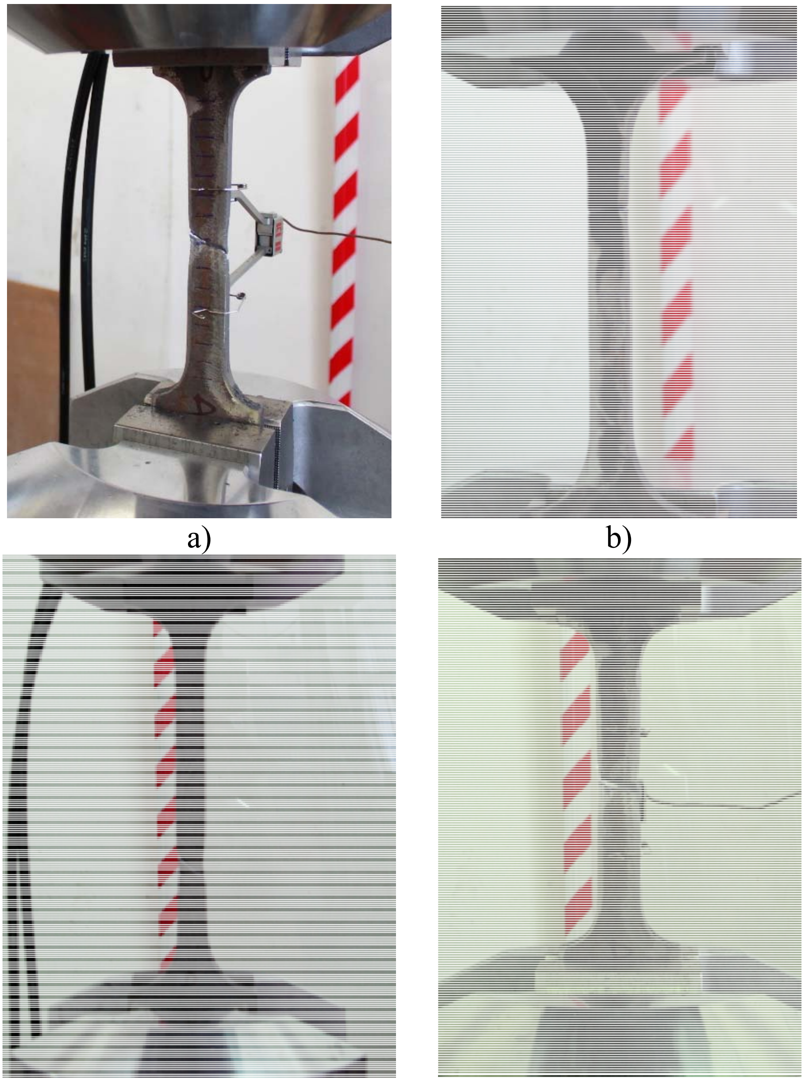

a) b)

e) f)

Figure II-1: Experimental test results performed at University of Naples: IPE450 flange and web (a and b respectively), HEB340 flange and web (c and d respectively).

Annex III Rib investigation

The results of the rib parametric investigation discussed in Chapter VII are hereinafter reported (Table III.1).

The rib inclinations (30° or 40°) and their thickness (starting from the unstiffened configuration and increasing their thickness with 5mm increments from 5mm, up to 30mm) influence were investigated for all the beam-to-column assemblies (ES1, ES2 and ES3) and considering full, equal and partial strength performance level.

For each parameter, FE monotonic analyses up to the 6% of rotation were performed. The results are reported in terms of: (i) moment-rotation curve, Von Misses stress distribution, (iii) PEEQ* distribution and (iv) CPRESS** distribution.

*PEEQ: equivalent plastic deformation [4]

**CPRESS: pressure on the elements coming from the integration on the element of the CFORCE [4]

Table III.1: Rib Investigation results.

ES1 – FULL – R-5		
A40	Moment-Rotation curve 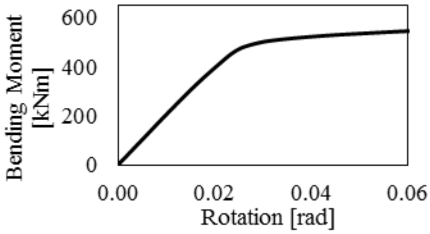	Von Mises stress 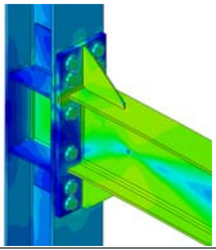
	Equivalent plastic deformation (PEEQ) 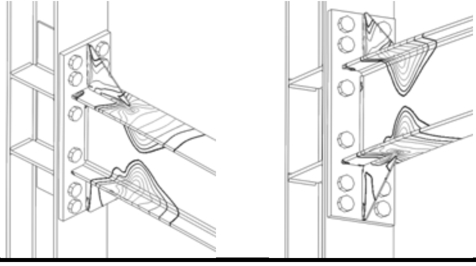	Contact pressure (CPRESS) 
A30	Moment-Rotation curve 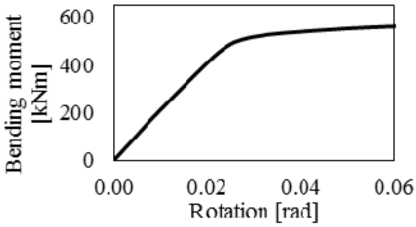	Von Mises stress 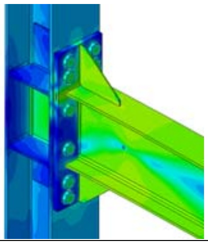
	Equivalent plastic deformation (PEEQ) 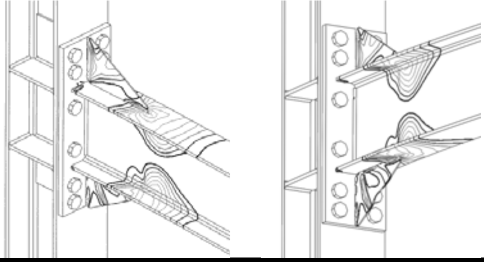	Contact pressure (CPRESS) 

	ES1 – FULL – R-10	
A40	Moment-Rotation curve 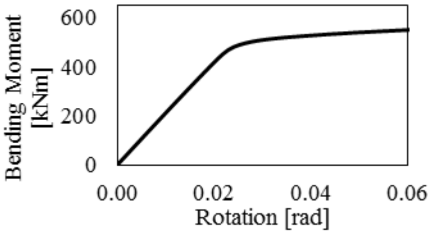	Von Mises stress 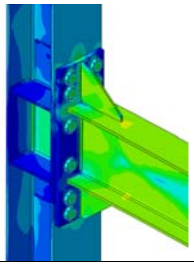
	Equivalent plastic deformation (PEEQ) 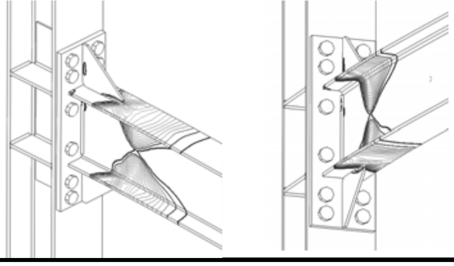	Contact pressure (CPRESS) 
A30	Moment-Rotation curve 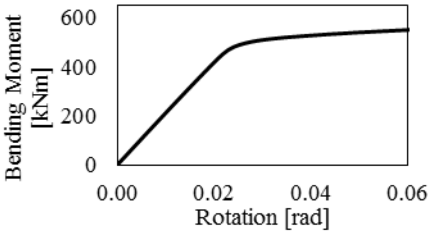	Von Mises stress 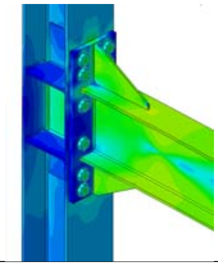
	Equivalent plastic deformation (PEEQ) 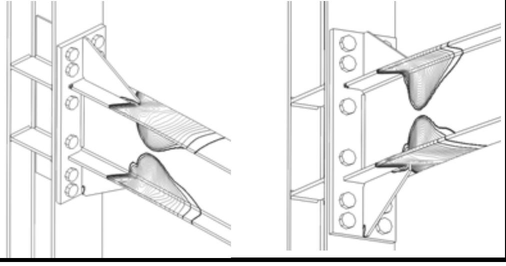	Contact pressure (CPRESS) 

ES1 – FULL – R-15

A40

Moment-Rotation curve

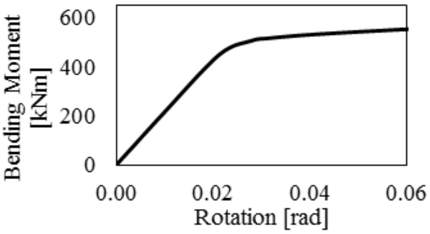

Von Mises stress

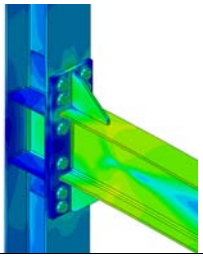

Equivalent plastic deformation (PEEQ)

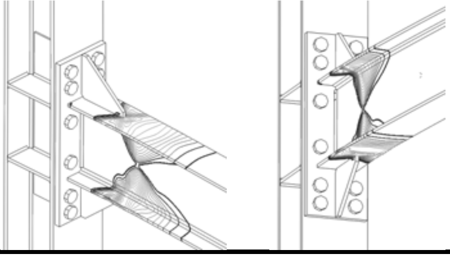

Contact pressure (CPRESS)

A30

Moment-Rotation curve

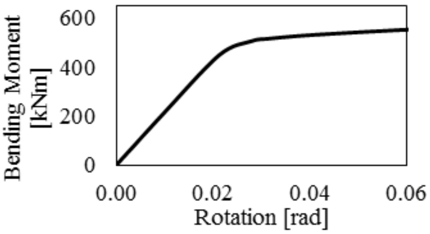

Von Mises stress

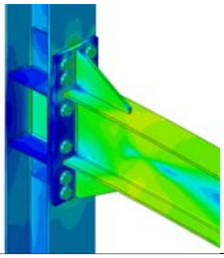

Equivalent plastic deformation (PEEQ)

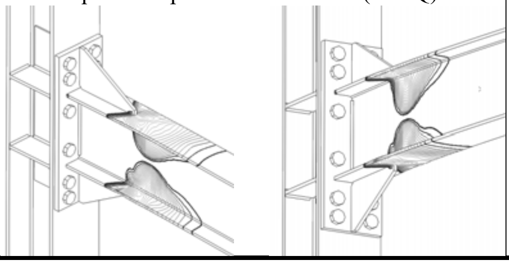

Contact pressure (CPRESS)

ES1 – FULL – R-20

A40

Moment-Rotation curve

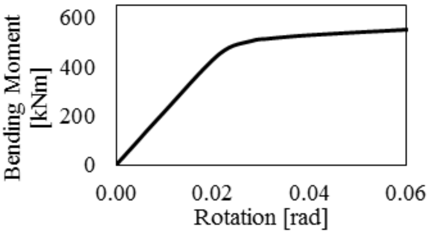

Von Mises stress

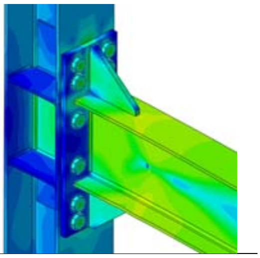

Equivalent plastic deformation (PEEQ)

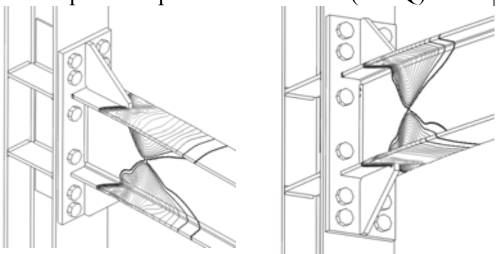

Contact pressure (CPRESS)

A30

Moment-Rotation curve

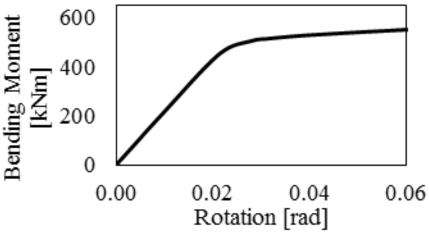

Von Mises stress

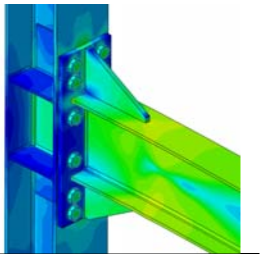

Equivalent plastic deformation (PEEQ)

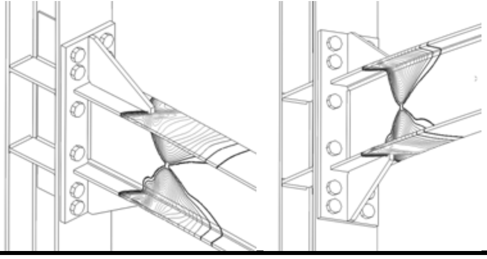

Contact pressure (CPRESS)

ES1 – FULL – R-25

A40

Moment-Rotation curve

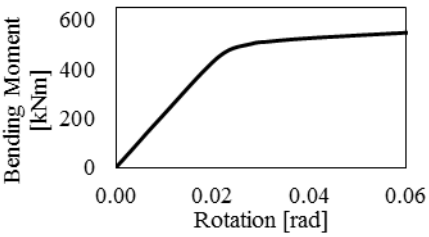

Von Mises stress

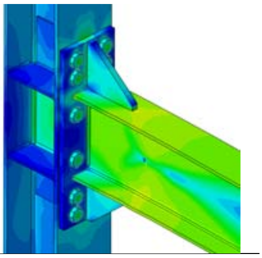

Equivalent plastic deformation (PEEQ)

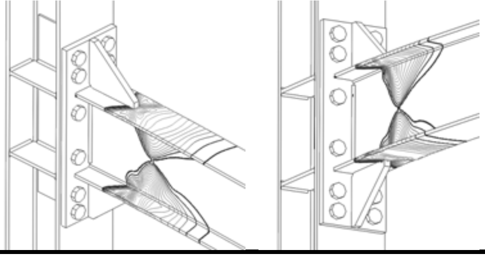

Contact pressure (CPRESS)

A30

Moment-Rotation curve

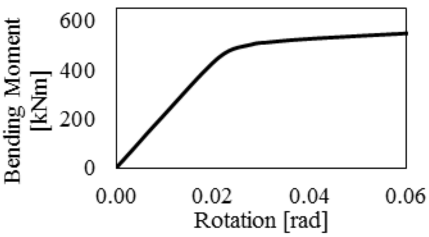

Von Mises stress

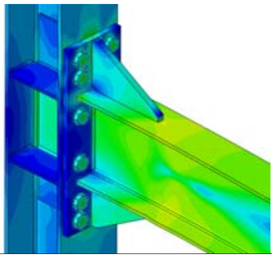

Equivalent plastic deformation (PEEQ)

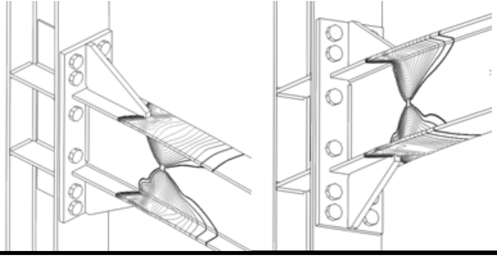

Contact pressure (CPRESS)

ES1 – FULL – R-30

A40

Moment-Rotation curve

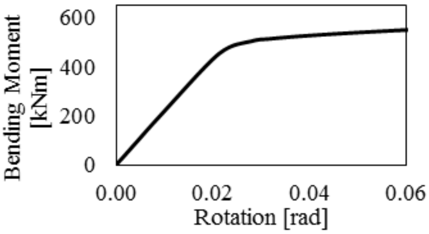

Von Mises stress

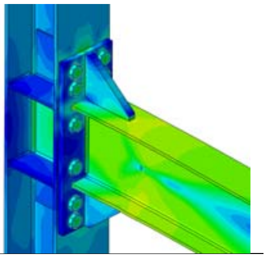

Equivalent plastic deformation (PEEQ)

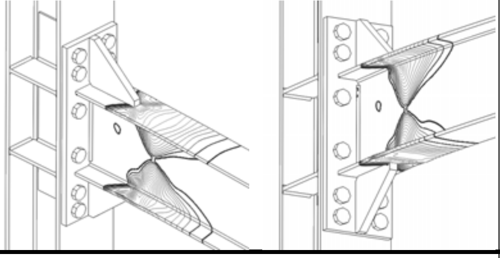

Contact pressure (CPRESS)

A30

Moment-Rotation curve

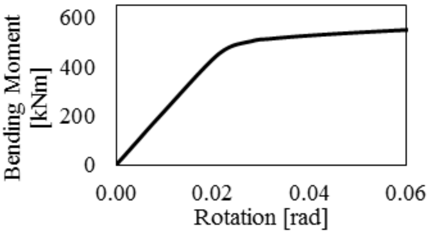

Von Mises stress

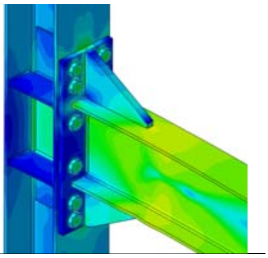

Equivalent plastic deformation (PEEQ)

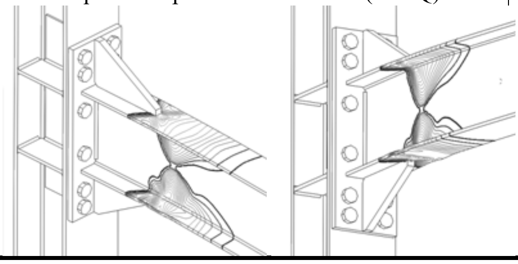

Contact pressure (CPRESS)

ES1 – EQUAL – R-5

A40

Moment-Rotation curve

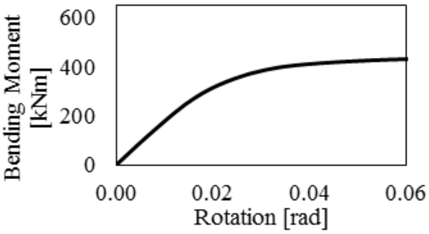

Von Mises stress

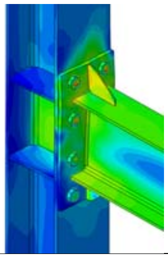

Equivalent plastic deformation (PEEQ)

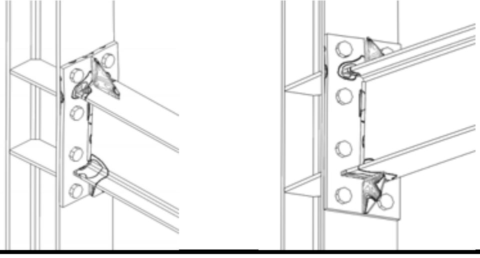

Contact pressure (CPRESS)

A30

Moment-Rotation curve

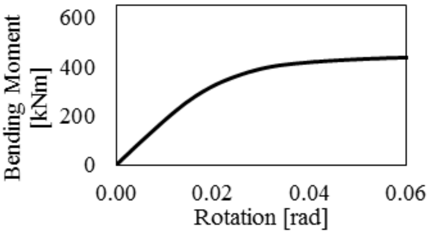

Von Mises stress

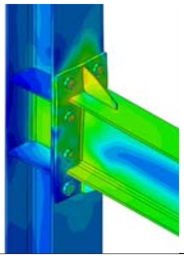

Equivalent plastic deformation (PEEQ)

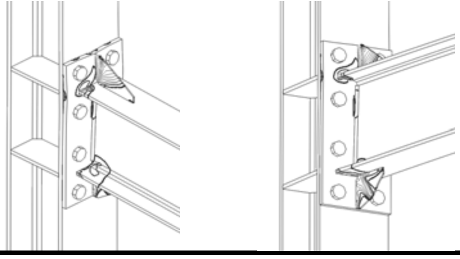

Contact pressure (CPRESS)

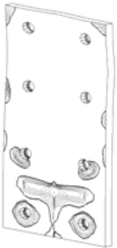

ES1 – EQUAL – R-10

A40

Moment-Rotation curve

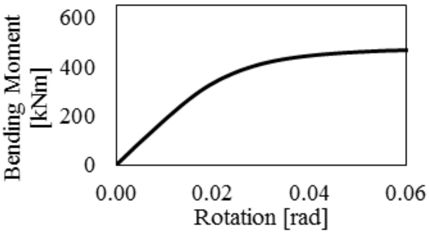

Von Mises stress

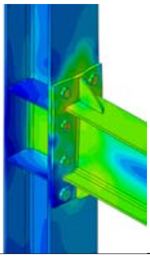

Equivalent plastic deformation (PEEQ)

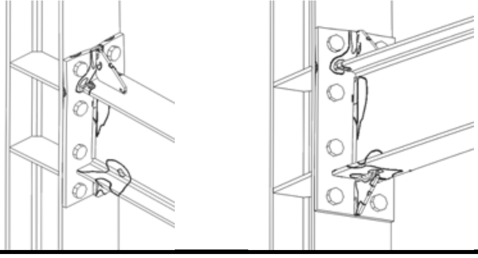

Contact pressure (CPRESS)

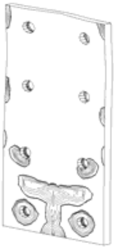

A30

Moment-Rotation curve

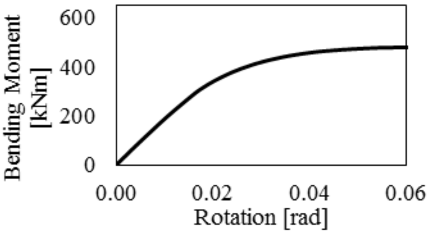

Von Mises stress

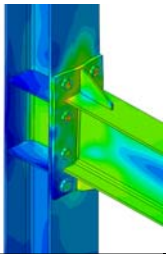

Equivalent plastic deformation (PEEQ)

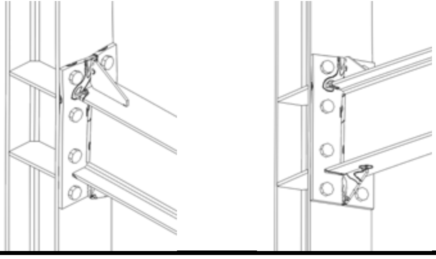

Contact pressure (CPRESS)

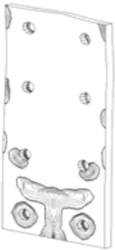

ES1 – EQUAL – R-15

A40

Moment-Rotation curve

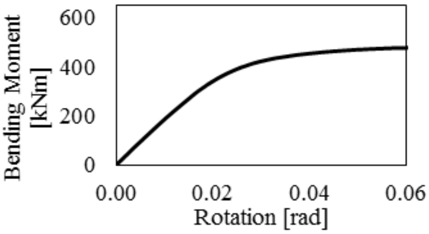

Von Mises stress

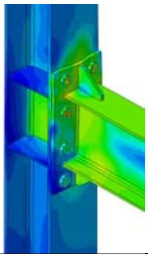

Equivalent plastic deformation (PEEQ)

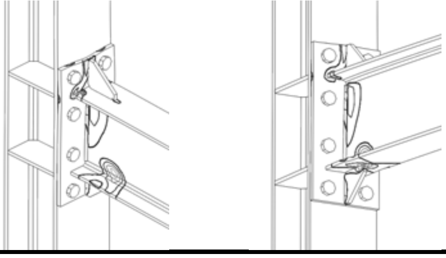

Contact pressure (CPRESS)

A30

Moment-Rotation curve

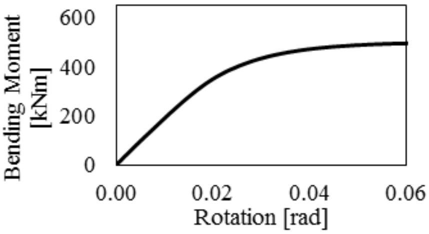

Von Mises stress

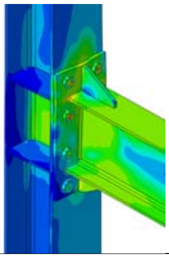

Equivalent plastic deformation (PEEQ)

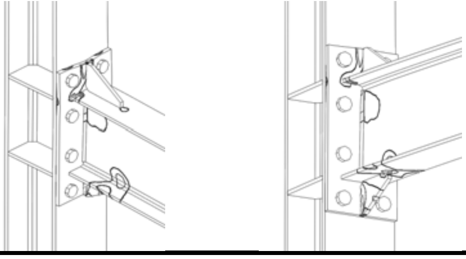

Contact pressure (CPRESS)

ES1 – EQUAL – R-20

A40

Moment-Rotation curve

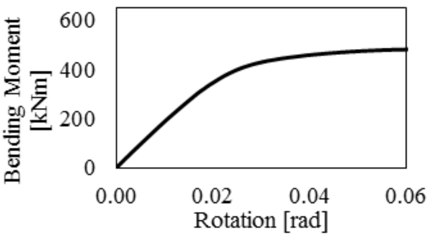

Von Mises stress

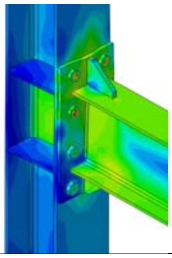

Equivalent plastic deformation (PEEQ)

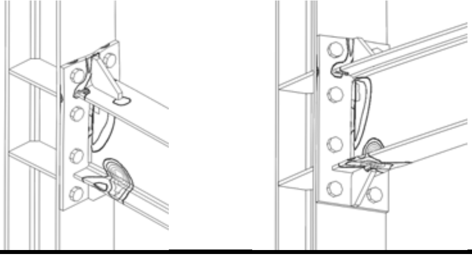

Contact pressure (CPRESS)

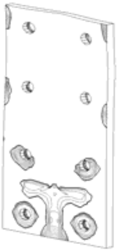

A30

Moment-Rotation curve

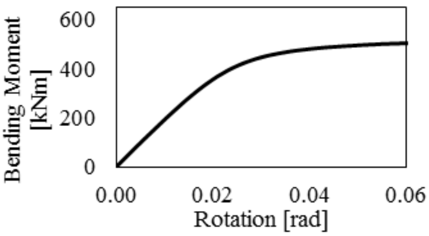

Von Mises stress

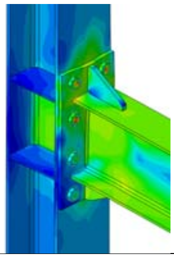

Equivalent plastic deformation (PEEQ)

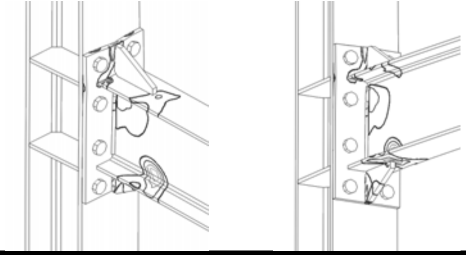

Contact pressure (CPRESS)

ES1 – EQUAL – R-25

A40

Moment-Rotation curve

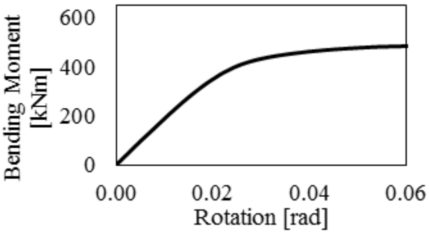

Von Mises stress

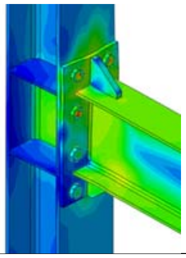

Equivalent plastic deformation (PEEQ)

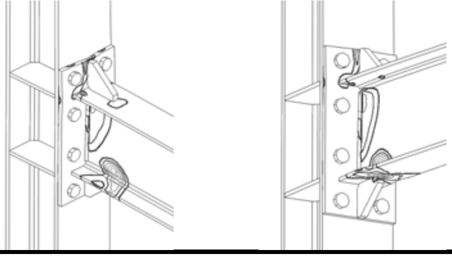

Contact pressure (CPRESS)

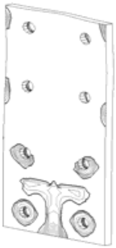

A30

Moment-Rotation curve

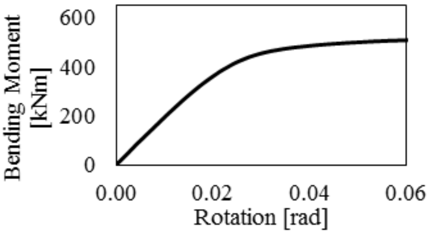

Von Mises stress

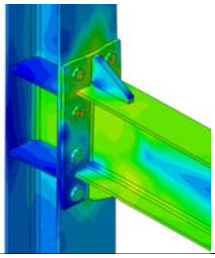

Equivalent plastic deformation (PEEQ)

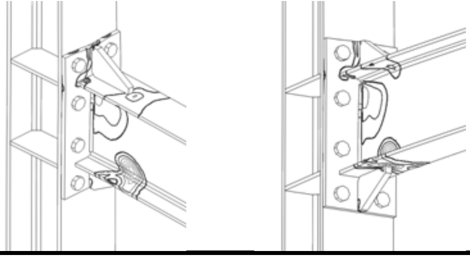

Contact pressure (CPRESS)

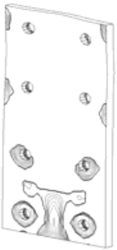

ES1 – EQUAL – R-30

A40

Moment-Rotation curve

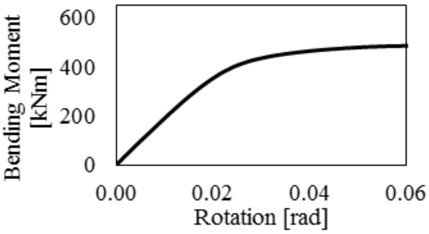

Von Mises stress

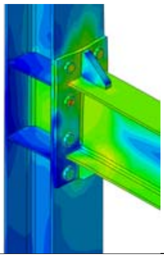

Equivalent plastic deformation (PEEQ)

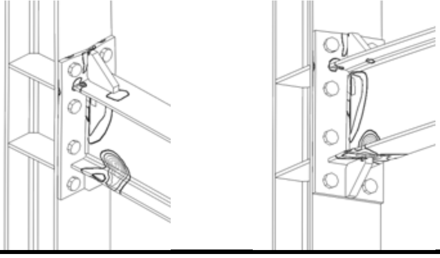

Contact pressure (CPRESS)

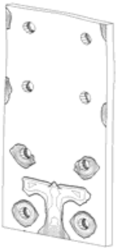

A30

Moment-Rotation curve

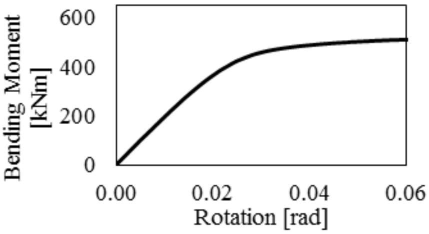

Von Mises stress

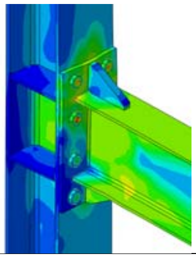

Equivalent plastic deformation (PEEQ)

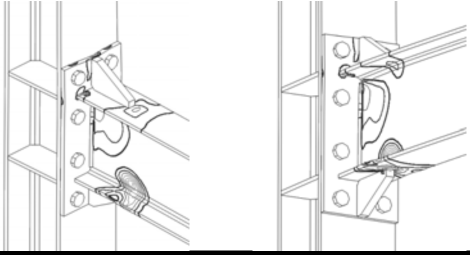

Contact pressure (CPRESS)

ES1 – PARTIAL – R-5

A40

Moment-Rotation curve

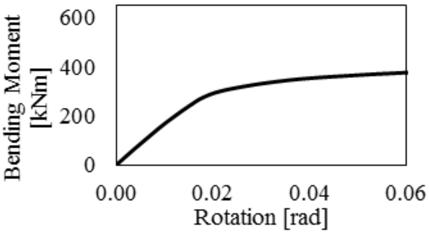

Von Mises stress

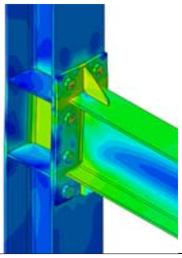

Equivalent plastic deformation (PEEQ)

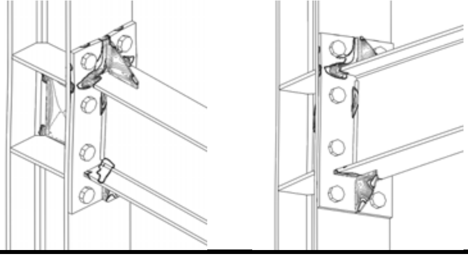

Contact pressure (CPRESS)

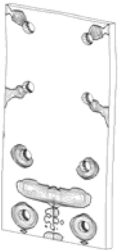

A30

Moment-Rotation curve

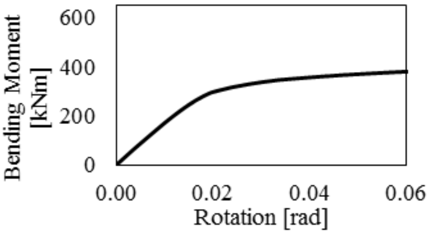

Von Mises stress

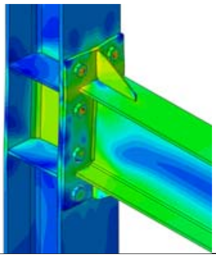

Equivalent plastic deformation (PEEQ)

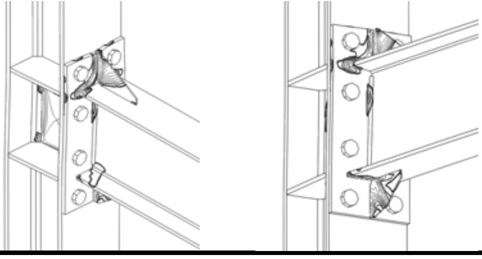

Contact pressure (CPRESS)

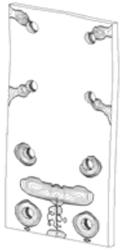

ES1 – PARTIAL – R-10

A40

Moment-Rotation curve

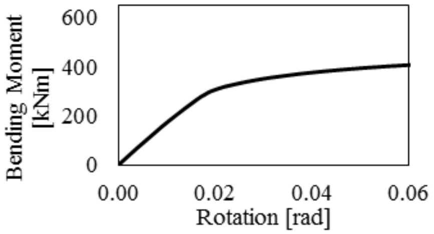

Von Mises stress

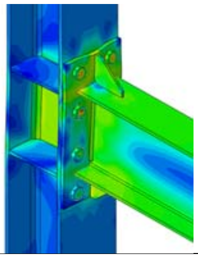

Equivalent plastic deformation (PEEQ)

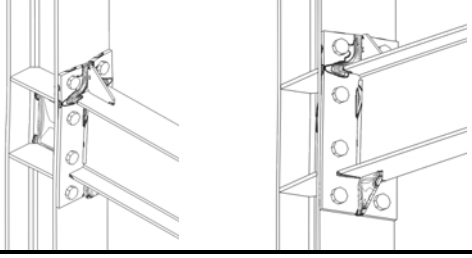

Contact pressure (CPRESS)

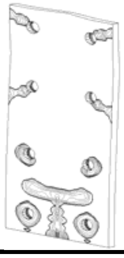

A30

Moment-Rotation curve

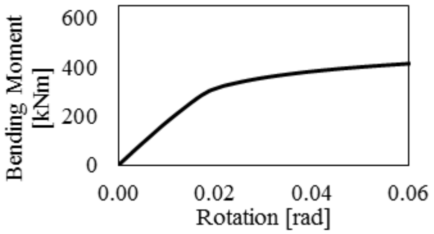

Von Mises stress

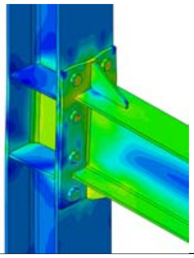

Equivalent plastic deformation (PEEQ)

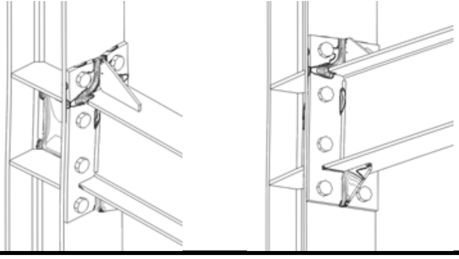

Contact pressure (CPRESS)

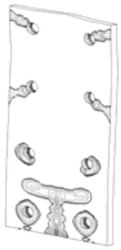

ES1 – PARTIAL – R-15

A40

Moment-Rotation curve

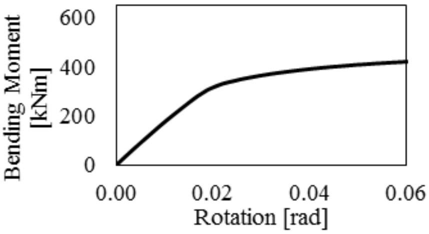

Von Mises stress

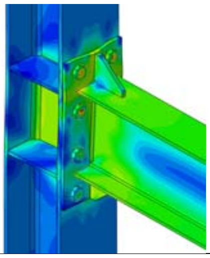

Equivalent plastic deformation (PEEQ)

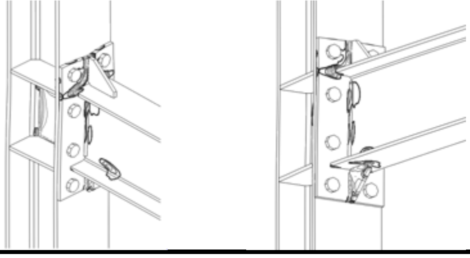

Contact pressure (CPRESS)

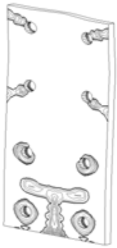

A30

Moment-Rotation curve

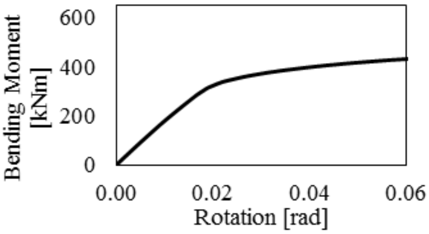

Von Mises stress

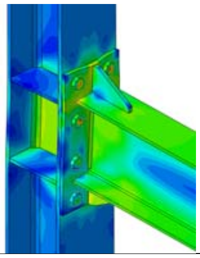

Equivalent plastic deformation (PEEQ)

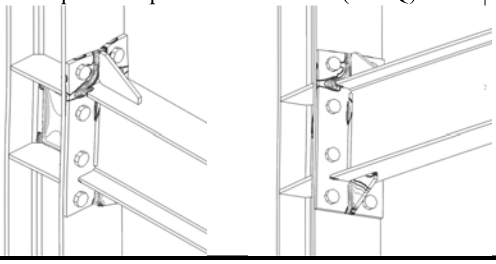

Contact pressure (CPRESS)

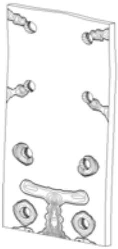

ES1 – PARTIAL – R-20

A40

Moment-Rotation curve

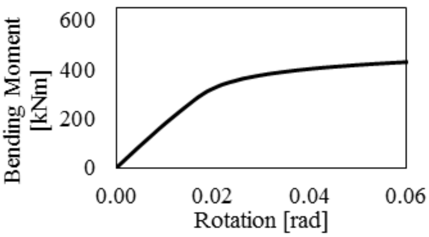

Von Mises stress

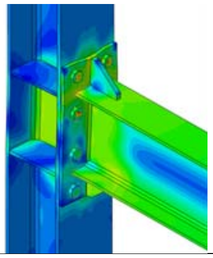

Equivalent plastic deformation (PEEQ)

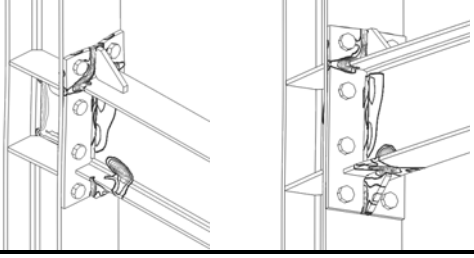

Contact pressure (CPRESS)

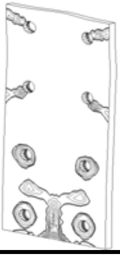

A30

Moment-Rotation curve

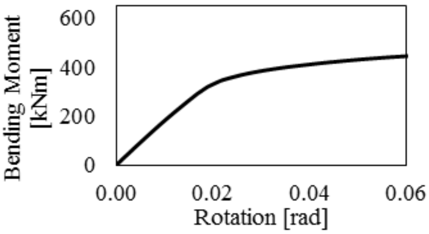

Von Mises stress

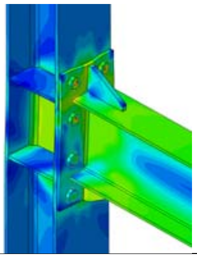

Equivalent plastic deformation (PEEQ)

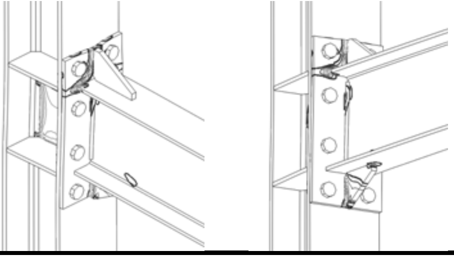

Contact pressure (CPRESS)

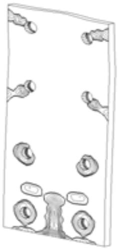

ES1 – PARTIAL – R-25

A40

Moment-Rotation curve

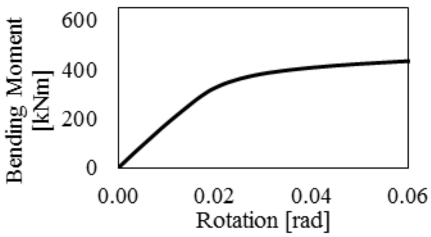

Von Mises stress

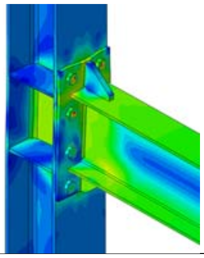

Equivalent plastic deformation (PEEQ)

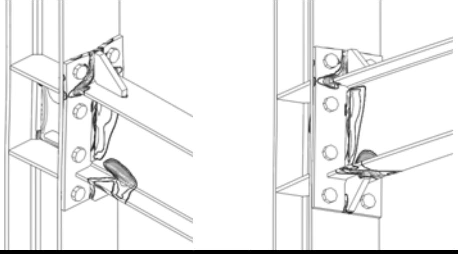

Contact pressure (CPRESS)

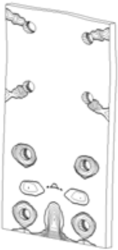

A30

Moment-Rotation curve

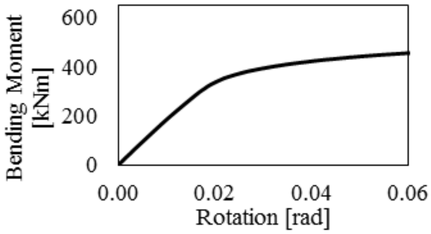

Von Mises stress

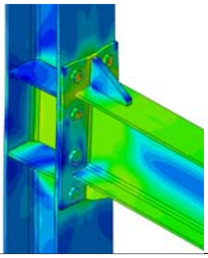

Equivalent plastic deformation (PEEQ)

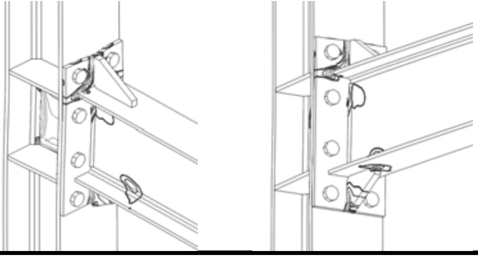

Contact pressure (CPRESS)

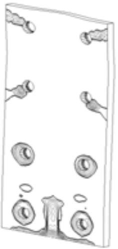

ES1 – PARTIAL – R-30

A40

Moment-Rotation curve

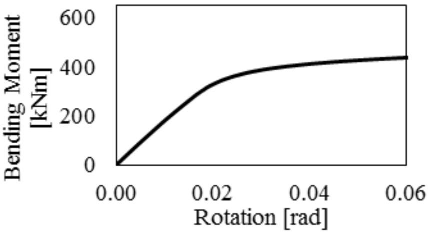

Von Mises stress

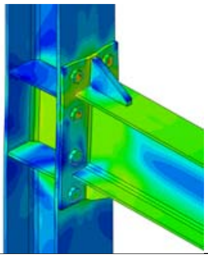

Equivalent plastic deformation (PEEQ)

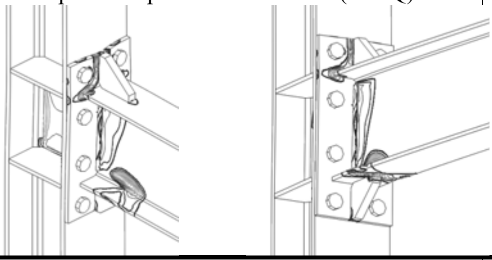

Contact pressure (CPRESS)

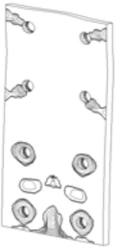

A30

Moment-Rotation curve

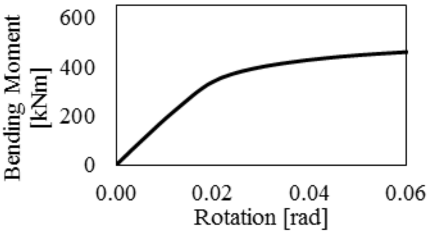

Von Mises stress

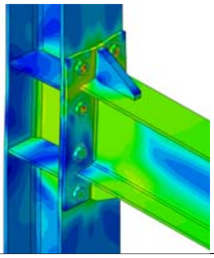

Equivalent plastic deformation (PEEQ)

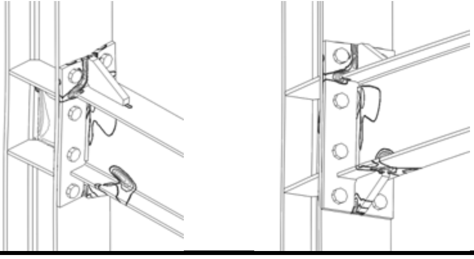

Contact pressure (CPRESS)

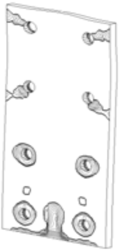

ES2 – FULL – R-5

A40

Moment-Rotation curve

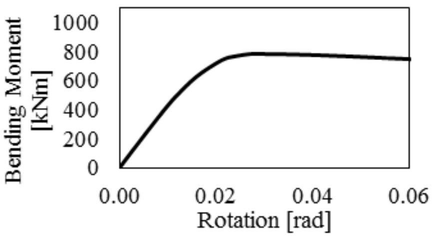

Von Mises stress

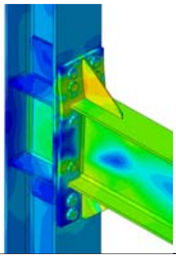

Equivalent plastic deformation (PEEQ)

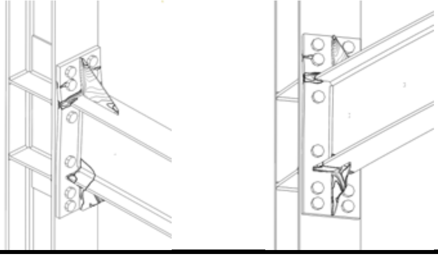

Contact pressure (CPRESS)

A30

Moment-Rotation curve

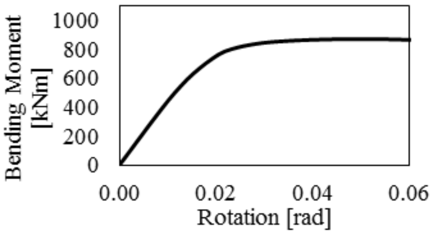

Von Mises stress

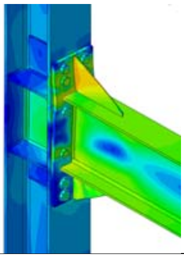

Equivalent plastic deformation (PEEQ)

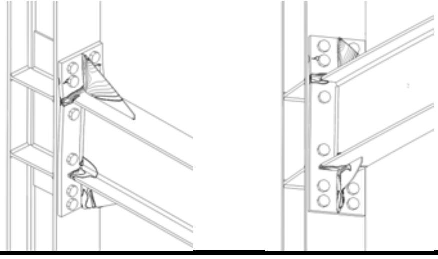

Contact pressure (CPRESS)

ES2 – FULL – R-10

A40

Moment-Rotation curve

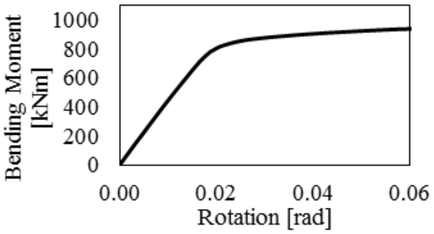

Von Mises stress

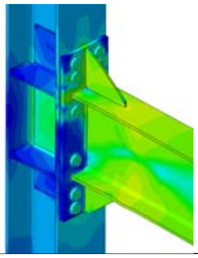

Equivalent plastic deformation (PEEQ)

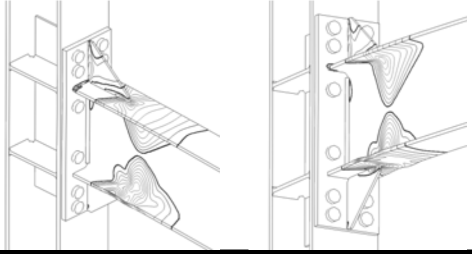

Contact pressure (CPRESS)

A30

Moment-Rotation curve

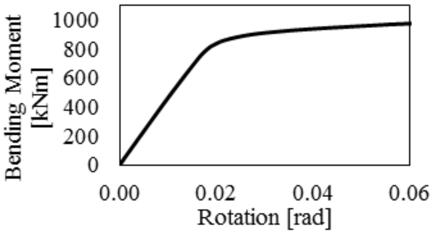

Von Mises stress

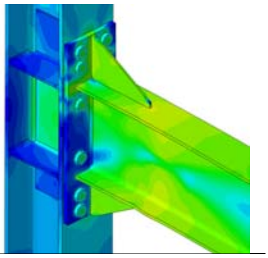

Equivalent plastic deformation (PEEQ)

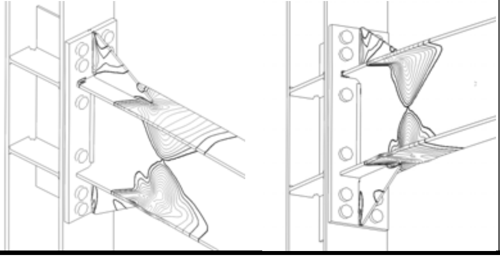

Contact pressure (CPRESS)

ES2 – FULL – R-15

A40

Moment-Rotation curve

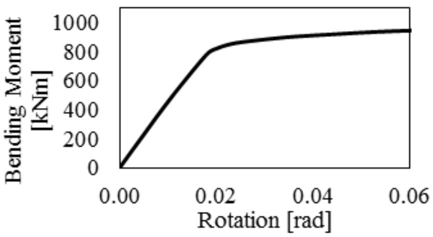

Von Mises stress

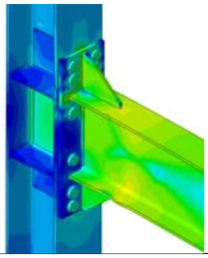

Equivalent plastic deformation (PEEQ)

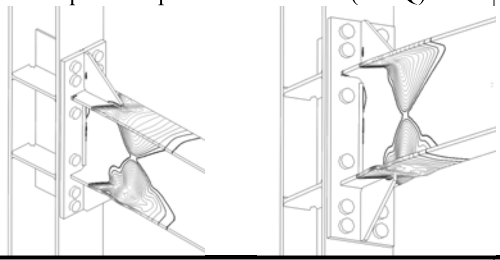

Contact pressure (CPRESS)

A30

Moment-Rotation curve

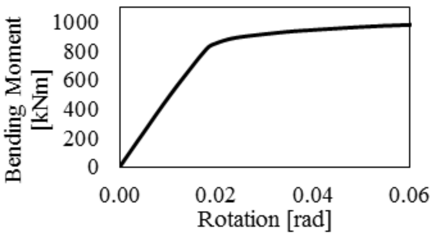

Von Mises stress

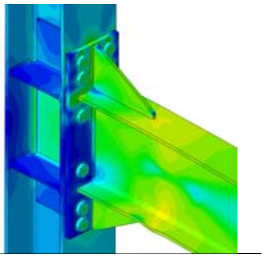

Equivalent plastic deformation (PEEQ)

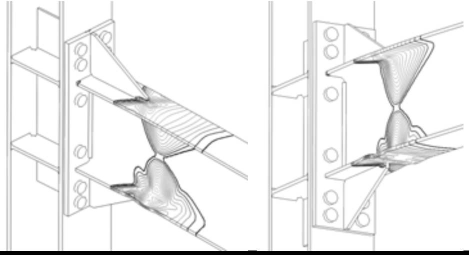

Contact pressure (CPRESS)

ES2 – FULL – R-20

A40

Moment-Rotation curve

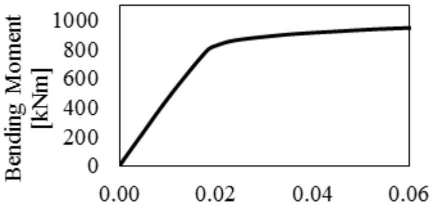

Von Mises stress

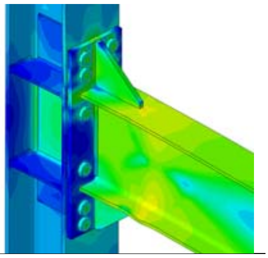

Equivalent plastic deformation (PEEQ)

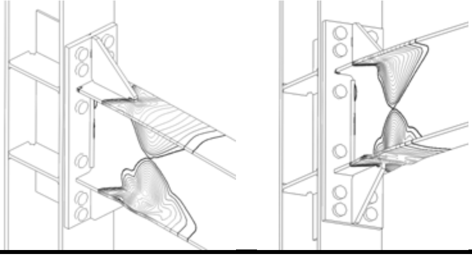

Contact pressure (CPRESS)

A30

Moment-Rotation curve

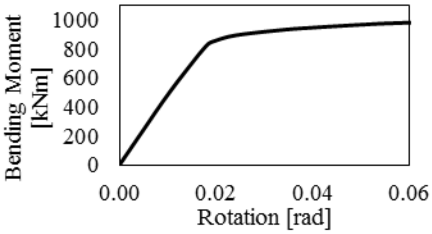

Von Mises stress

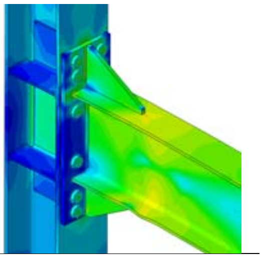

Equivalent plastic deformation (PEEQ)

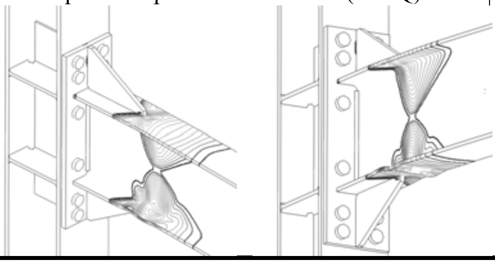

Contact pressure (CPRESS)

ES2 – FULL – R-25

A40

Moment-Rotation curve

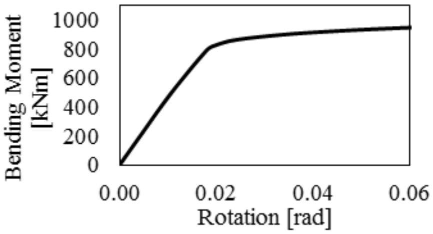

Von Mises stress

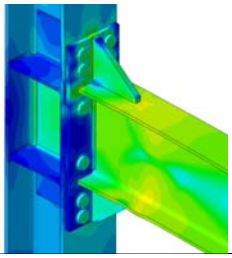

Equivalent plastic deformation (PEEQ)

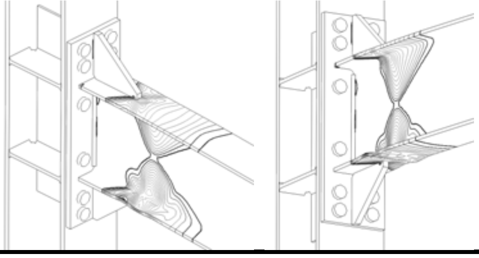

Contact pressure (CPRESS)

A30

Moment-Rotation curve

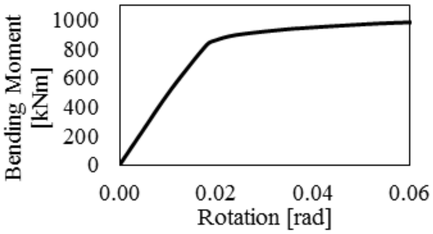

Von Mises stress

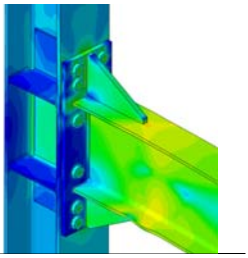

Equivalent plastic deformation (PEEQ)

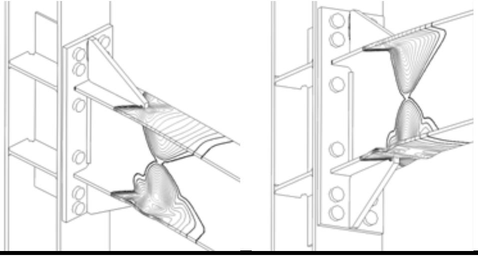

Contact pressure (CPRESS)

ES2 – FULL – R-30

A40

Moment-Rotation curve

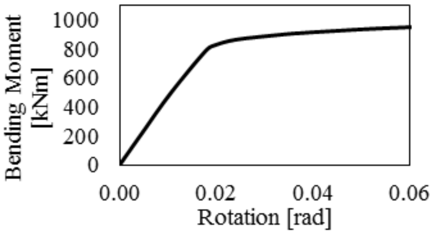

Von Mises stress

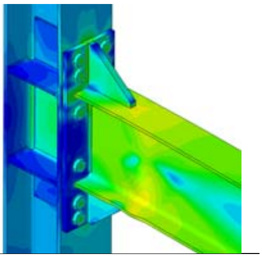

Equivalent plastic deformation (PEEQ)

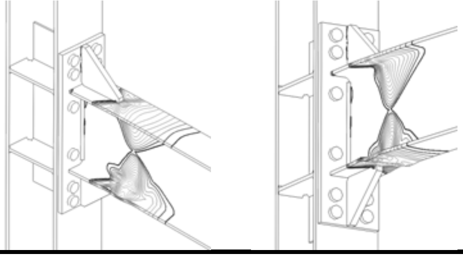

Contact pressure (CPRESS)

A30

Moment-Rotation curve

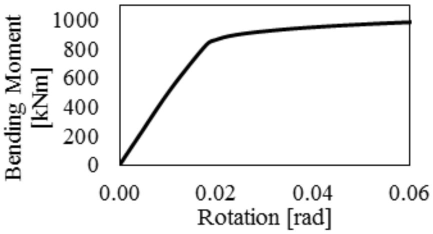

Von Mises stress

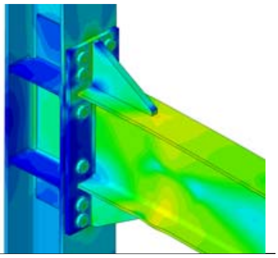

Equivalent plastic deformation (PEEQ)

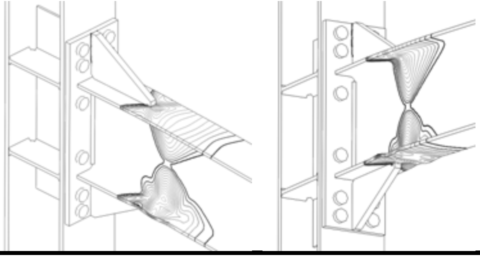

Contact pressure (CPRESS)

ES2 – EQUAL – R-5

A40

Moment-Rotation curve

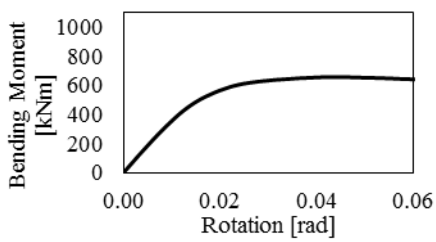

Von Mises stress

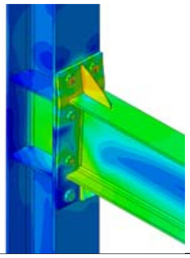

Equivalent plastic deformation (PEEQ)

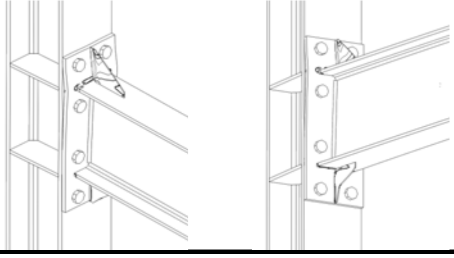

Contact pressure (CPRESS)

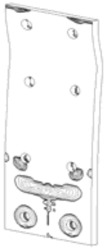

A30

Moment-Rotation curve

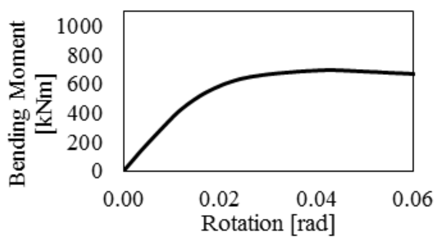

Von Mises stress

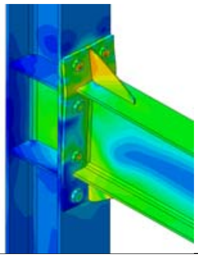

Equivalent plastic deformation (PEEQ)

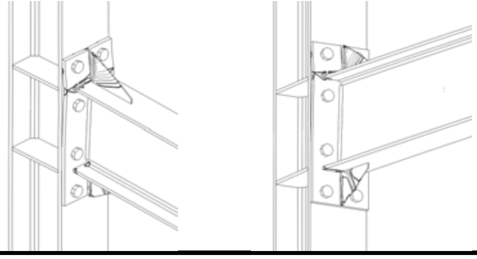

Contact pressure (CPRESS)

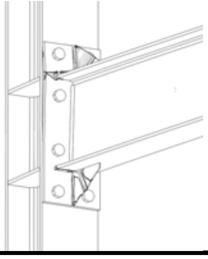

ES2 – EQUAL – R-10

A40

Moment-Rotation curve

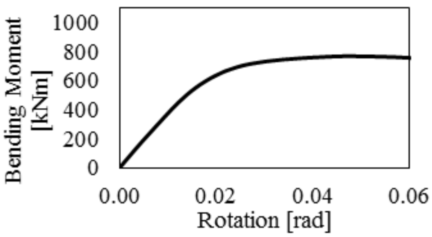

Von Mises stress

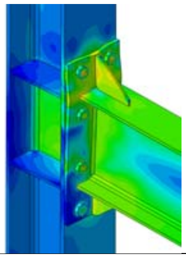

Equivalent plastic deformation (PEEQ)

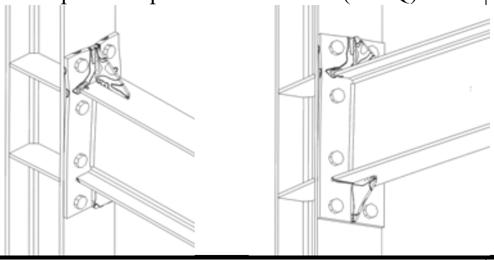

Contact pressure (CPRESS)

A30

Moment-Rotation curve

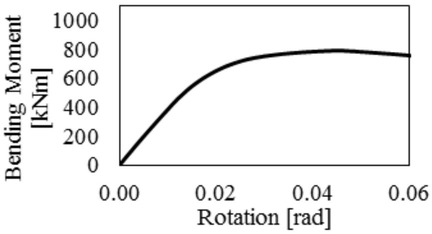

Von Mises stress

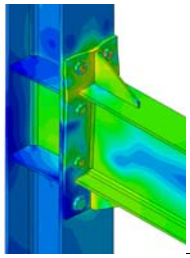

Equivalent plastic deformation (PEEQ)

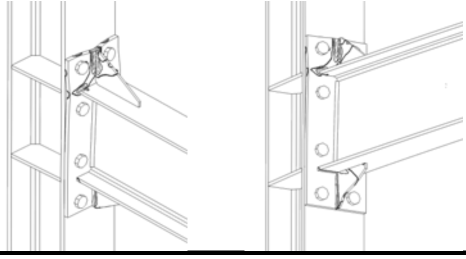

Contact pressure (CPRESS)

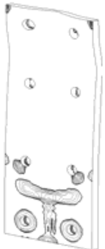

ES2 – EQUAL – R-15

A40

Moment-Rotation curve

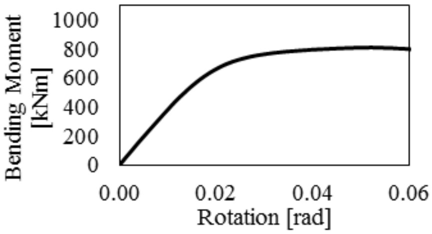

Von Mises stress

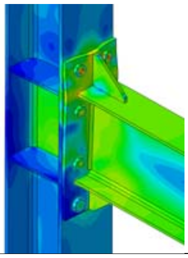

Equivalent plastic deformation (PEEQ)

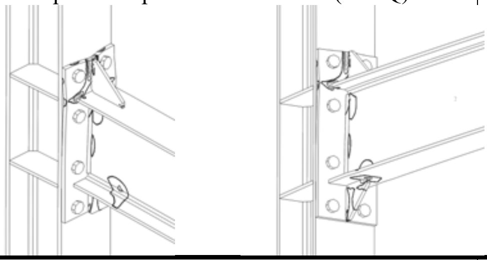

Contact pressure (CPRESS)

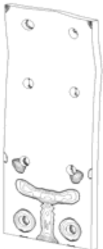

A30

Moment-Rotation curve

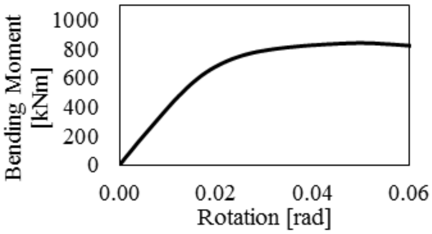

Von Mises stress

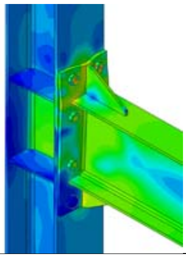

Equivalent plastic deformation (PEEQ)

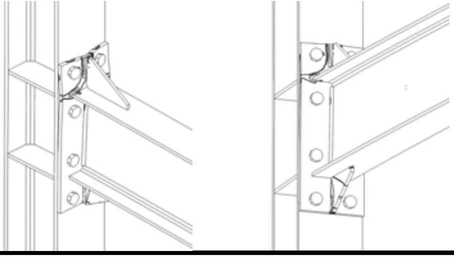

Contact pressure (CPRESS)

ES2 – EQUAL – R-20

A40

Moment-Rotation curve

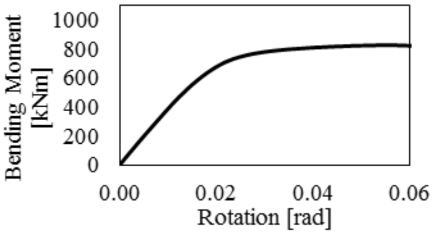

Von Mises stress

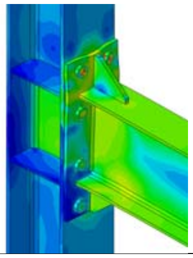

Equivalent plastic deformation (PEEQ)

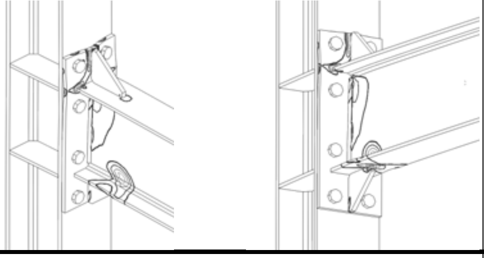

Contact pressure (CPRESS)

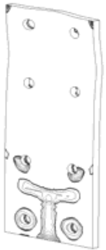

A30

Moment-Rotation curve

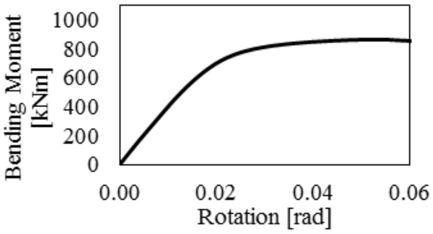

Von Mises stress

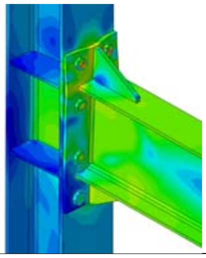

Equivalent plastic deformation (PEEQ)

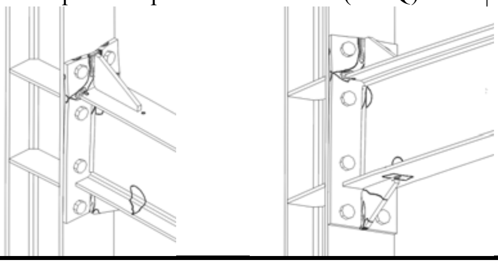

Contact pressure (CPRESS)

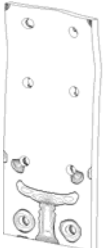

ES2 – EQUAL – R-25

A40

Moment-Rotation curve

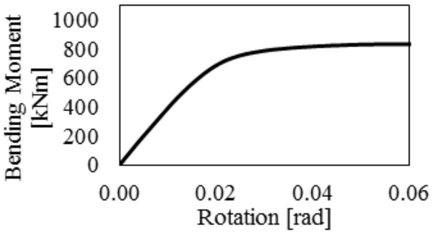

Von Mises stress

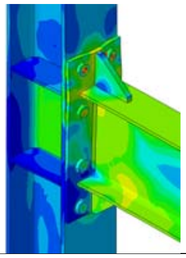

Equivalent plastic deformation (PEEQ)

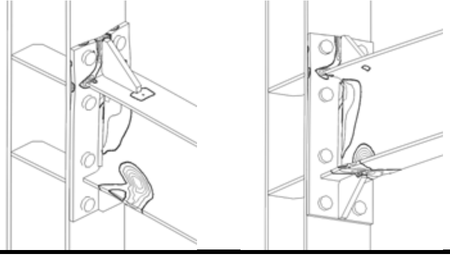

Contact pressure (CPRESS)

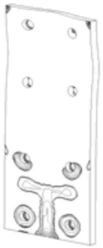

A30

Moment-Rotation curve

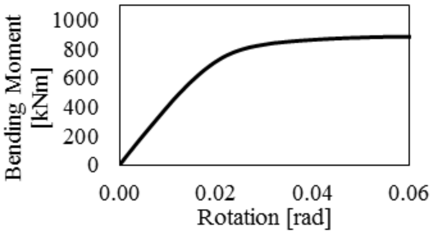

Von Mises stress

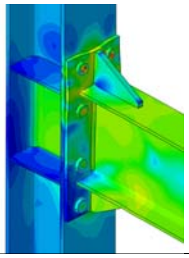

Equivalent plastic deformation (PEEQ)

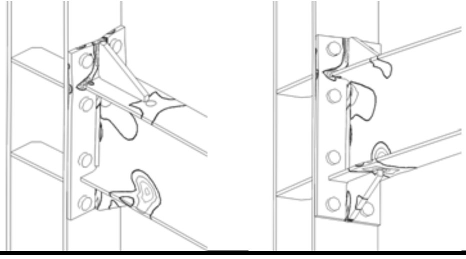

Contact pressure (CPRESS)

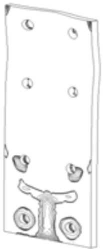

ES2 – EQUAL – R-30

A40

Moment-Rotation curve

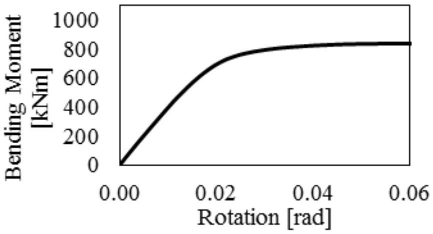

Von Mises stress

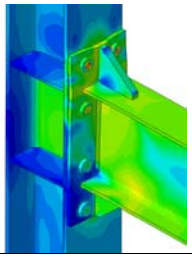

Equivalent plastic deformation (PEEQ)

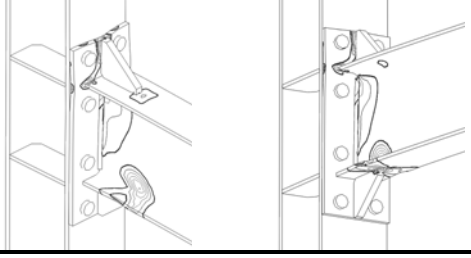

Contact pressure (CPRESS)

A30

Moment-Rotation curve

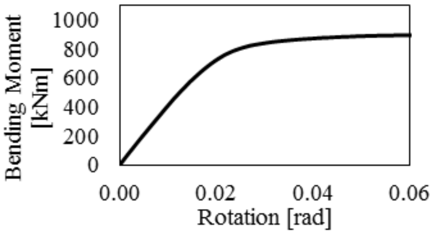

Von Mises stress

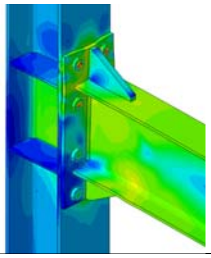

Equivalent plastic deformation (PEEQ)

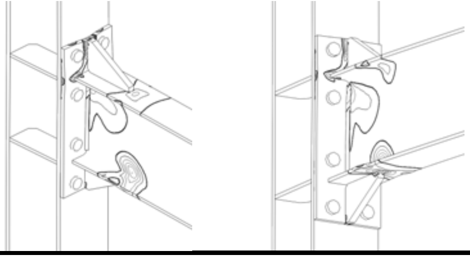

Contact pressure (CPRESS)

ES2 – PARTIAL – R-5

A40

Moment-Rotation curve

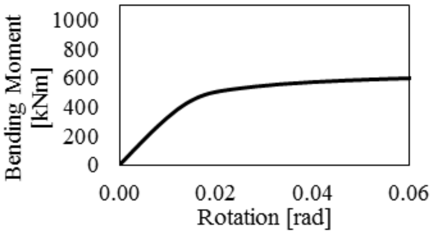

Von Mises stress

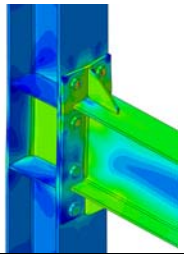

Equivalent plastic deformation (PEEQ)

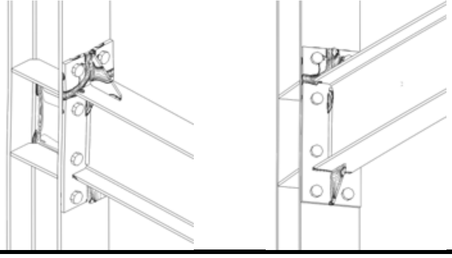

Contact pressure (CPRESS)

A30

Moment-Rotation curve

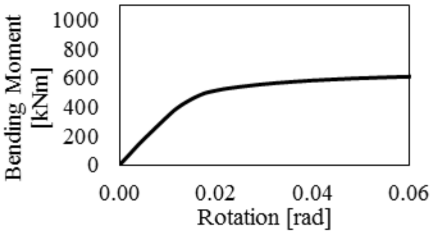

Von Mises stress

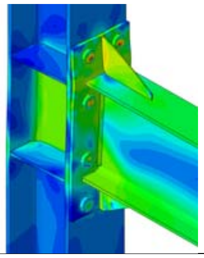

Equivalent plastic deformation (PEEQ)

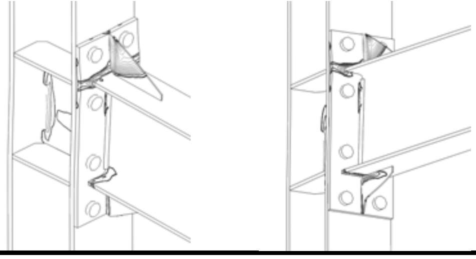

Contact pressure (CPRESS)

ES2 – PARTIAL – R-10

A40

Moment-Rotation curve

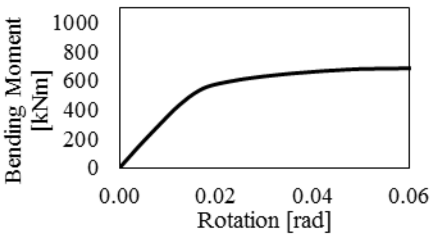

Von Mises stress

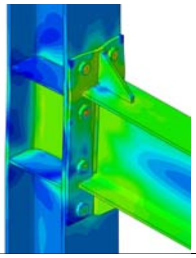

Equivalent plastic deformation (PEEQ)

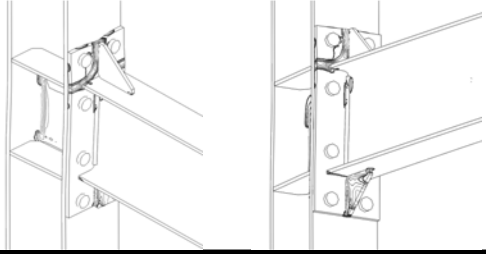

Contact pressure (CPRESS)

A30

Moment-Rotation curve

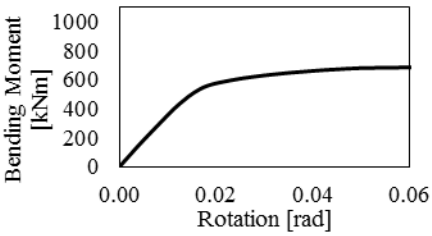

Von Mises stress

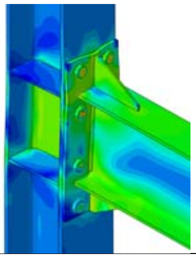

Equivalent plastic deformation (PEEQ)

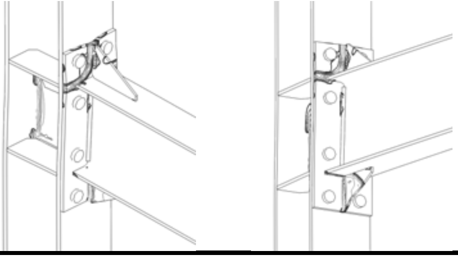

Contact pressure (CPRESS)

ES2 – PARTIAL – R-15

A40

Moment-Rotation curve

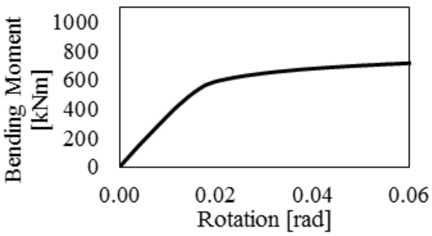

Von Mises stress

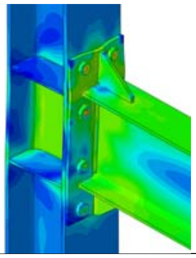

Equivalent plastic deformation (PEEQ)

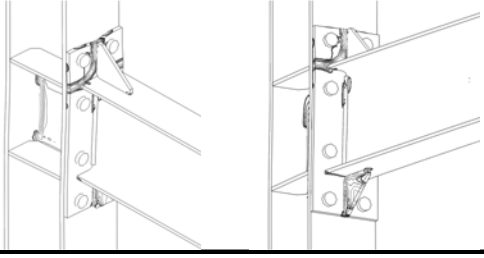

Contact pressure (CPRESS)

A30

Moment-Rotation curve

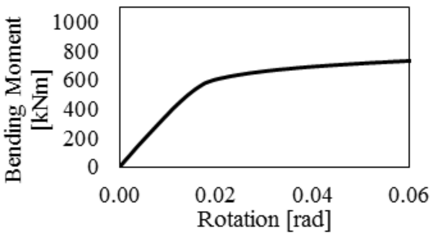

Von Mises stress

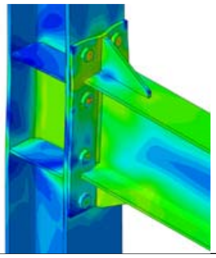

Equivalent plastic deformation (PEEQ)

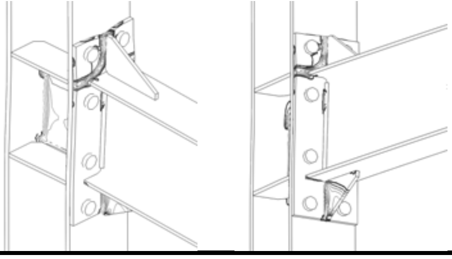

Contact pressure (CPRESS)

ES2 – PARTIAL – R-20

A40

Moment-Rotation curve

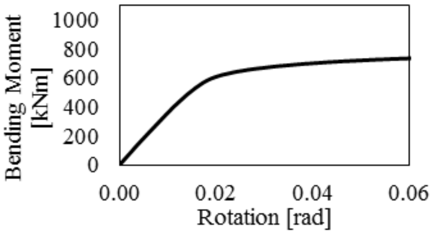

Von Mises stress

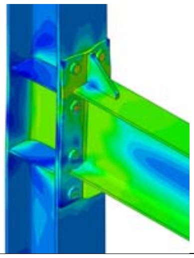

Equivalent plastic deformation (PEEQ)

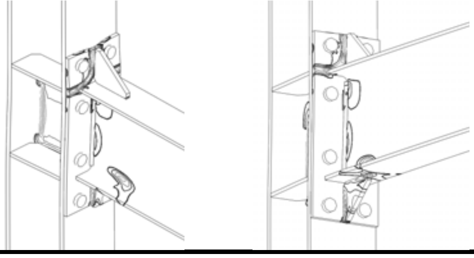

Contact pressure (CPRESS)

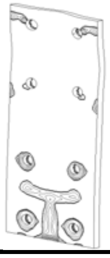

A30

Moment-Rotation curve

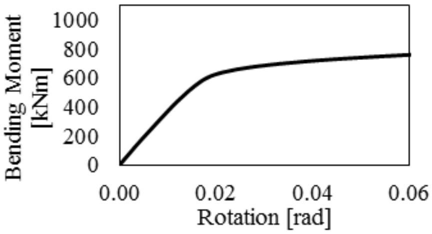

Von Mises stress

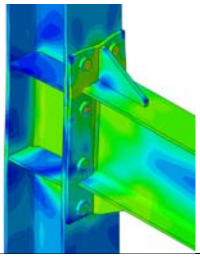

Equivalent plastic deformation (PEEQ)

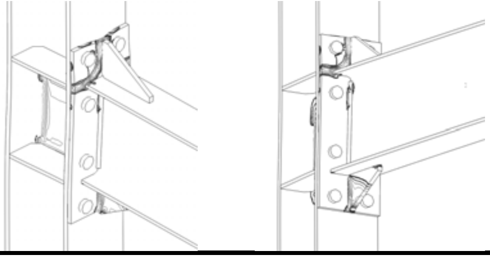

Contact pressure (CPRESS)

ES2 – PARTIAL – R-25

A40

Moment-Rotation curve

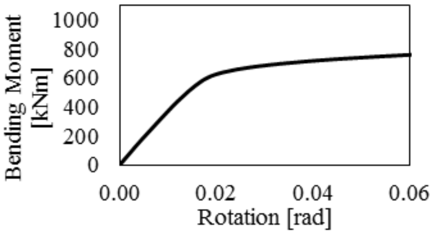

Von Mises stress

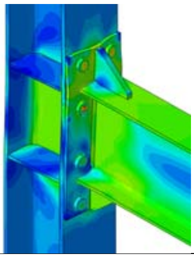

Equivalent plastic deformation (PEEQ)

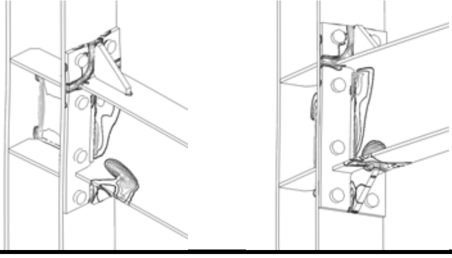

Contact pressure (CPRESS)

A30

Moment-Rotation curve

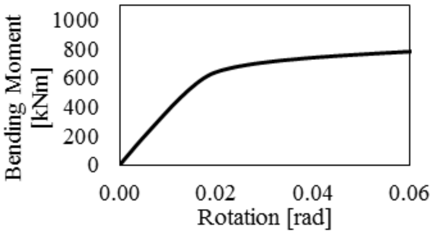

Von Mises stress

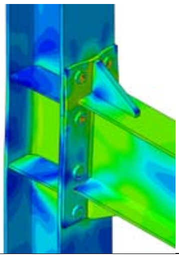

Equivalent plastic deformation (PEEQ)

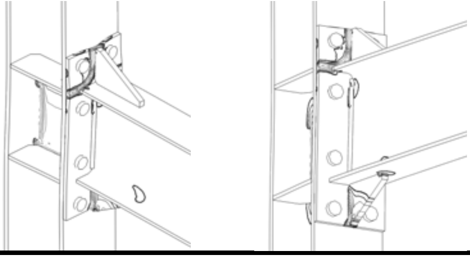

Contact pressure (CPRESS)

ES2 – PARTIAL – R-30

A40

Moment-Rotation curve

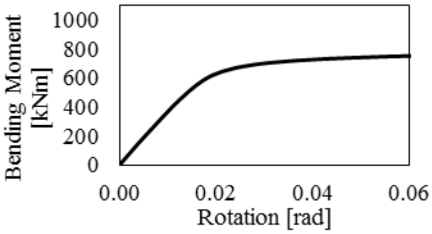

Von Mises stress

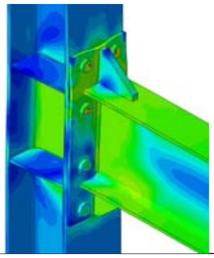

Equivalent plastic deformation (PEEQ)

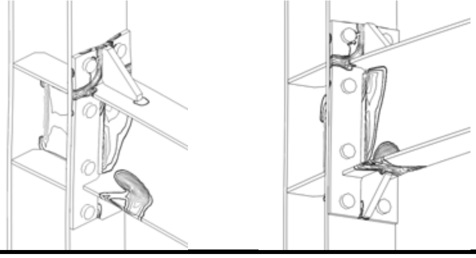

Contact pressure (CPRESS)

A30

Moment-Rotation curve

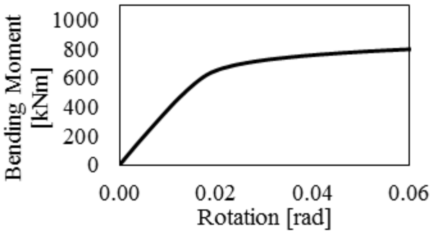

Von Mises stress

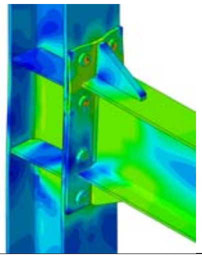

Equivalent plastic deformation (PEEQ)

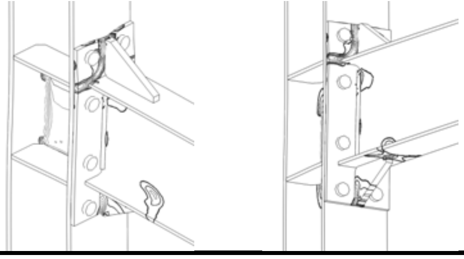

Contact pressure (CPRESS)

ES3 – FULL – R-5

A40

Moment-Rotation curve

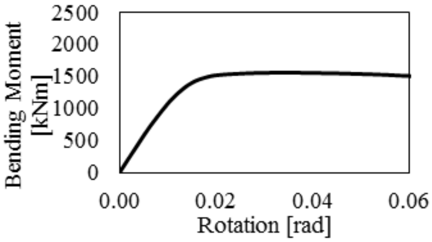

Von Mises stress

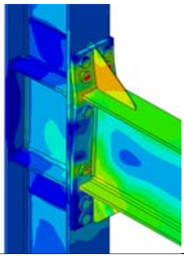

Equivalent plastic deformation (PEEQ)

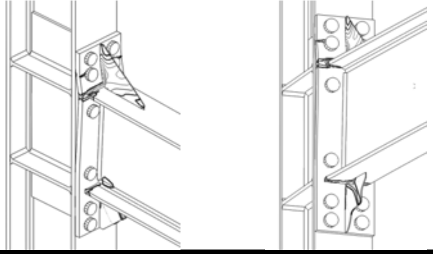

Contact pressure (CPRESS)

A30

Moment-Rotation curve

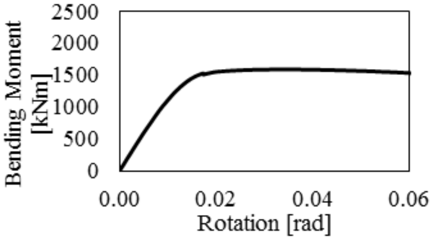

Von Mises stress

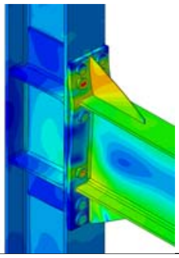

Equivalent plastic deformation (PEEQ)

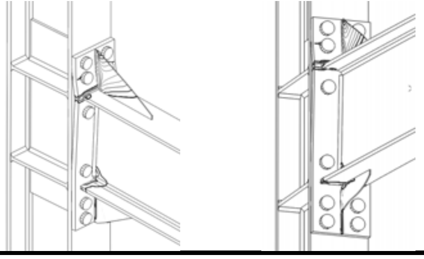

Contact pressure (CPRESS)

ES3 – FULL – R-10

A40

Moment-Rotation curve

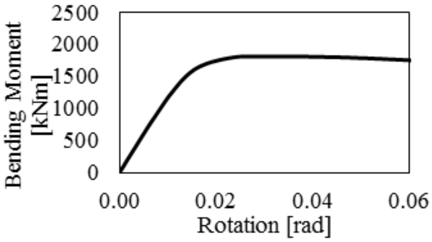

Von Mises stress

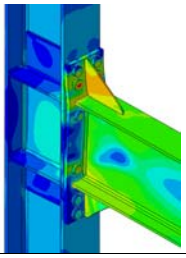

Equivalent plastic deformation (PEEQ)

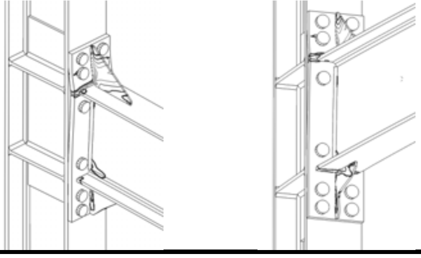

Contact pressure (CPRESS)

A30

Moment-Rotation curve

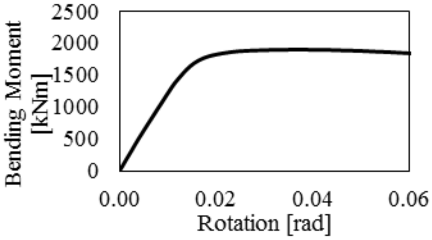

Von Mises stress

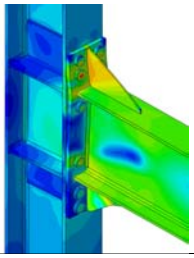

Equivalent plastic deformation (PEEQ)

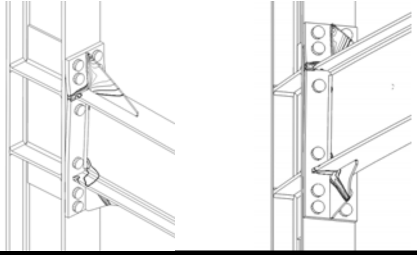

Contact pressure (CPRESS)

ES3 – FULL – R-15

A40

Moment-Rotation curve

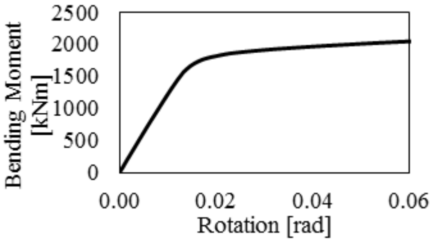

Von Mises stress

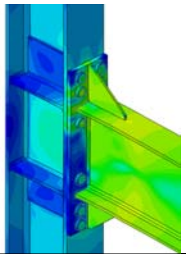

Equivalent plastic deformation (PEEQ)

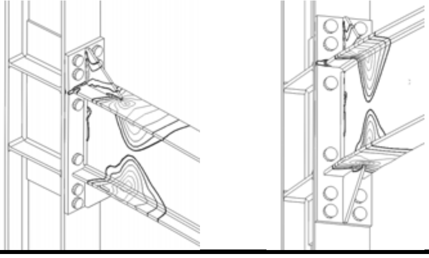

Contact pressure (CPRESS)

A30

Moment-Rotation curve

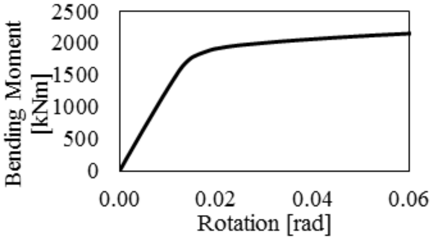

Von Mises stress

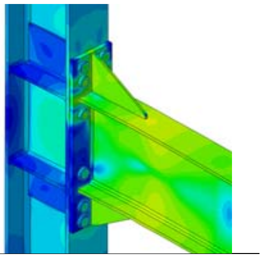

Equivalent plastic deformation (PEEQ)

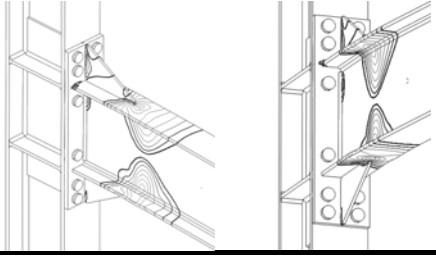

Contact pressure (CPRESS)

<table>
<tr><th colspan="3">ES3 – FULL – R-20</th></tr>
<tr><td rowspan="2">A40</td><td>Moment-Rotation curve
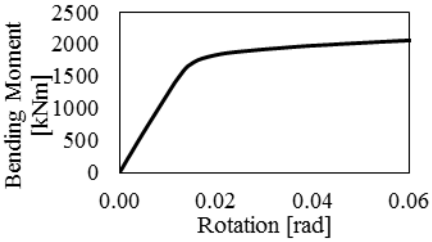 </td><td>Von Mises stress
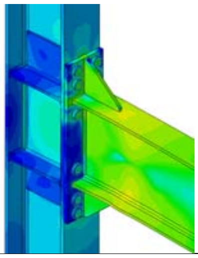</td></tr>
<tr><td>Equivalent plastic deformation (PEEQ)
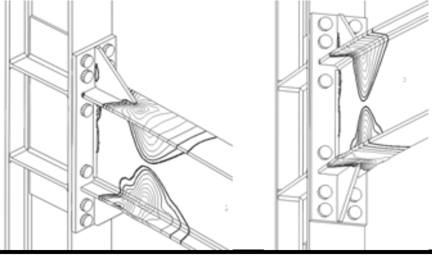</td><td>Contact pressure (CPRESS)
</td></tr>
<tr><td rowspan="2">A30</td><td>Moment-Rotation curve
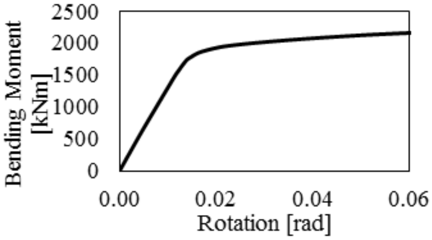 </td><td>Von Mises stress
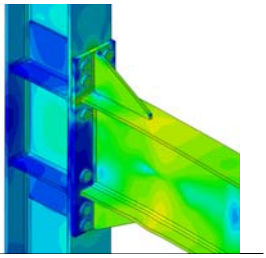</td></tr>
<tr><td>Equivalent plastic deformation (PEEQ)
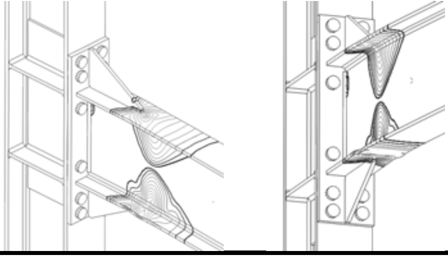</td><td>Contact pressure (CPRESS)
</td></tr>
</table>

ES3 – FULL – R-25

A40

Moment-Rotation curve

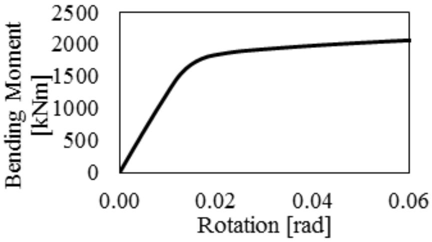

Von Mises stress

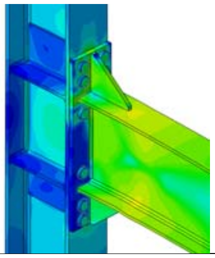

Equivalent plastic deformation (PEEQ)

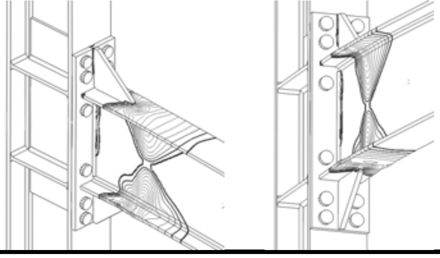

Contact pressure (CPRESS)

A30

Moment-Rotation curve

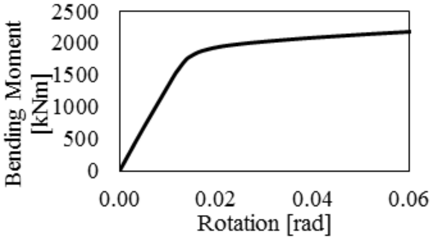

Von Mises stress

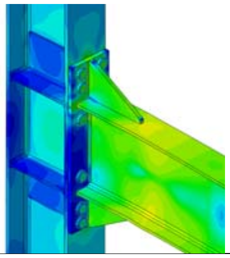

Equivalent plastic deformation (PEEQ)

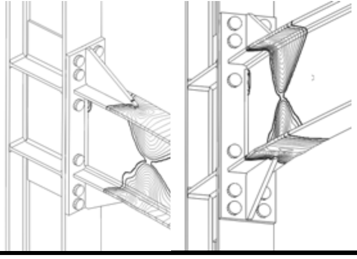

Contact pressure (CPRESS)

ES3 – FULL – R-30

A40

Moment-Rotation curve

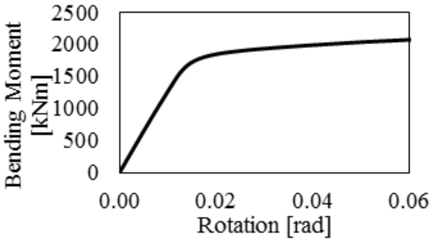

Von Mises stress

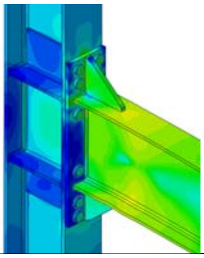

Equivalent plastic deformation (PEEQ)

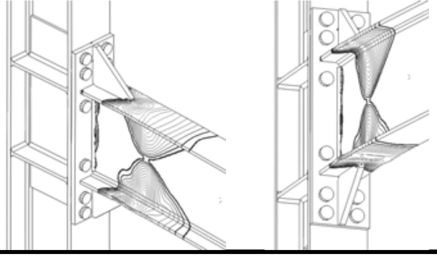

Contact pressure (CPRESS)

A30

Moment-Rotation curve

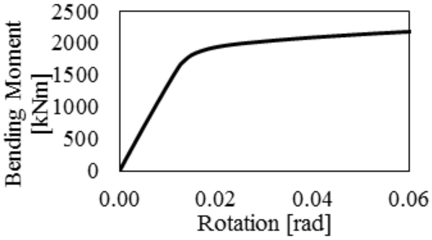

Von Mises stress

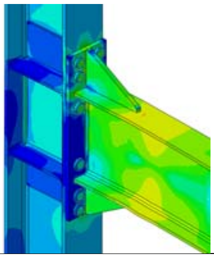

Equivalent plastic deformation (PEEQ)

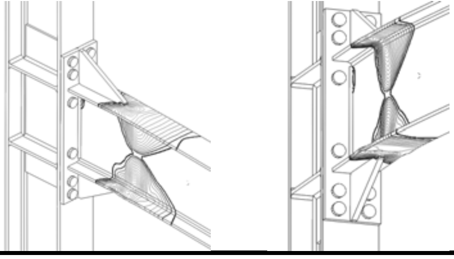

Contact pressure (CPRESS)

ES3 – EQUAL – R-5

A40

Moment-Rotation curve

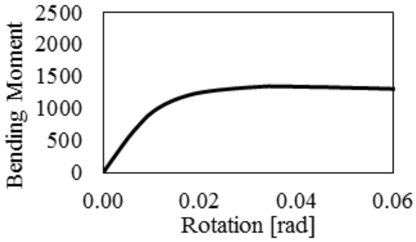

Von Mises stress

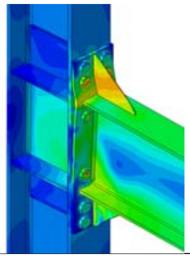

Equivalent plastic deformation (PEEQ)

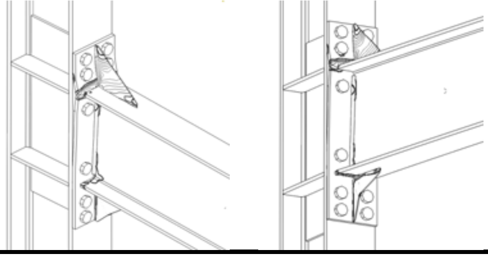

Contact pressure (CPRESS)

A30

Moment-Rotation curve

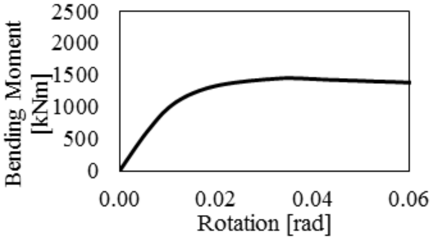

Von Mises stress

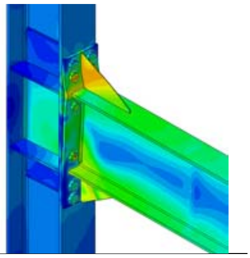

Equivalent plastic deformation (PEEQ)

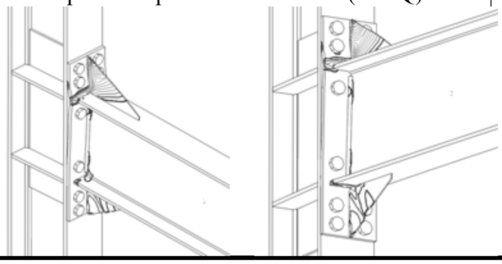

Contact pressure (CPRESS)

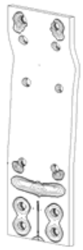

ES3 – EQUAL – R-10

A40

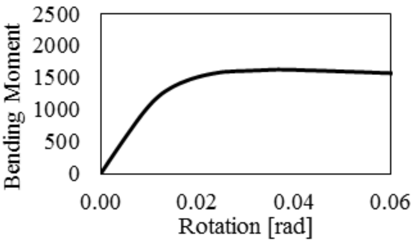
Moment-Rotation curve

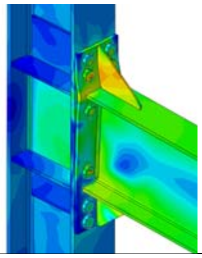
Von Mises stress

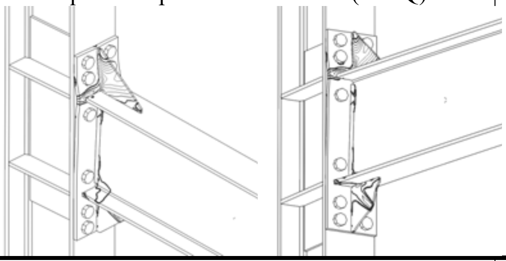
Equivalent plastic deformation (PEEQ)


Contact pressure (CPRESS)

A30

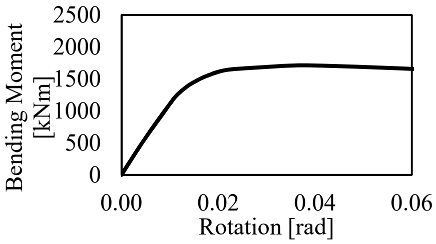
Moment-Rotation curve

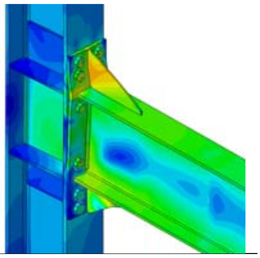
Von Mises stress

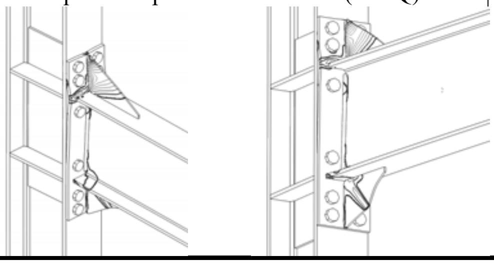
Equivalent plastic deformation (PEEQ)

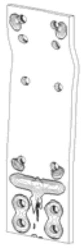
Contact pressure (CPRESS)

ES3 – EQUAL – R-15

A40

Moment-Rotation curve

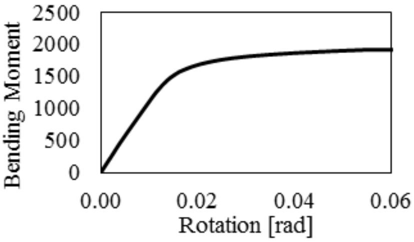

Von Mises stress

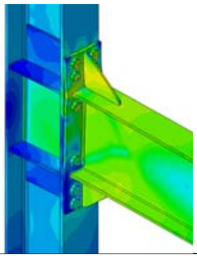

Equivalent plastic deformation (PEEQ)

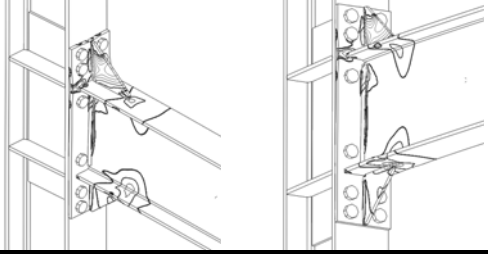

Contact pressure (CPRESS)

A30

Moment-Rotation curve

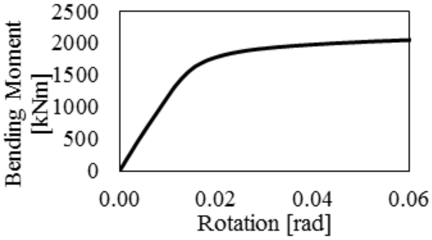

Von Mises stress

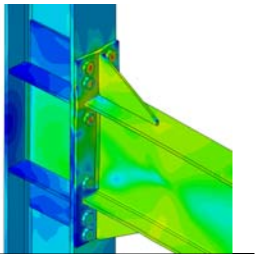

Equivalent plastic deformation (PEEQ)

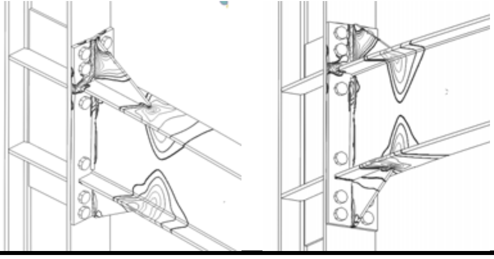

Contact pressure (CPRESS)

ES3 – EQUAL – R-20

A40

Moment-Rotation curve

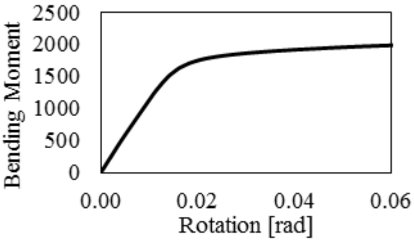

Von Mises stress

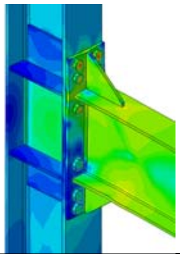

Equivalent plastic deformation (PEEQ)

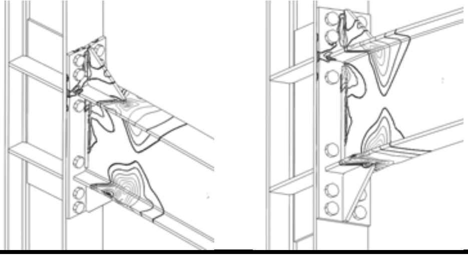

Contact pressure (CPRESS)

A30

Moment-Rotation curve

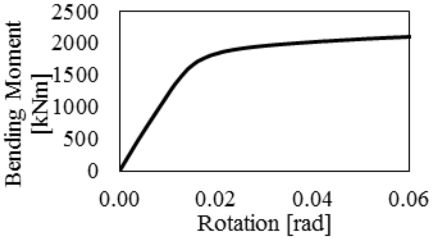

Von Mises stress

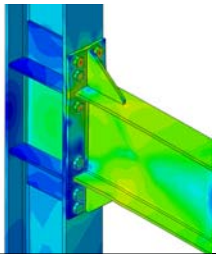

Equivalent plastic deformation (PEEQ)

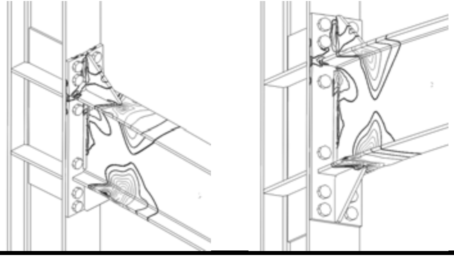

Contact pressure (CPRESS)

ES3 – EQUAL – R-25

A40

Moment-Rotation curve

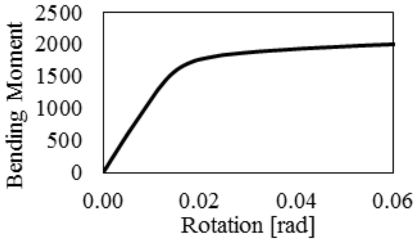

Von Mises stress

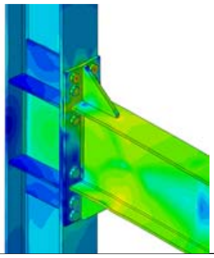

Equivalent plastic deformation (PEEQ)

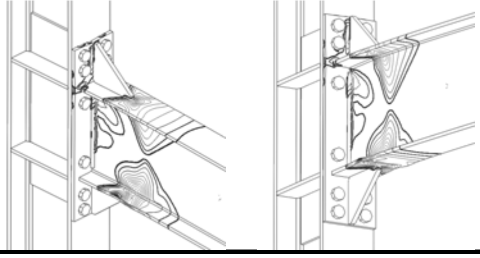

Contact pressure (CPRESS)

A30

Moment-Rotation curve

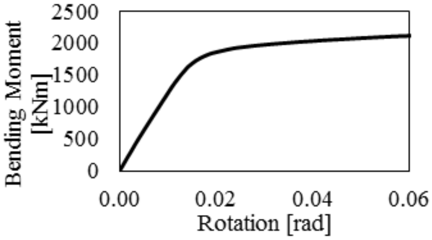

Von Mises stress

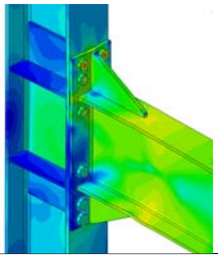

Equivalent plastic deformation (PEEQ)

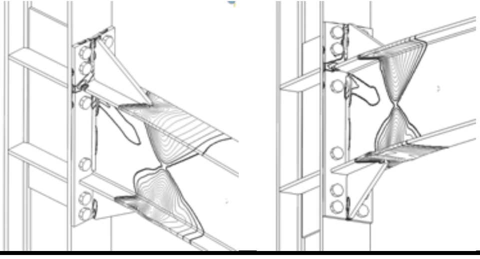

Contact pressure (CPRESS)

ES3 – EQUAL – R-30

A40

Moment-Rotation curve

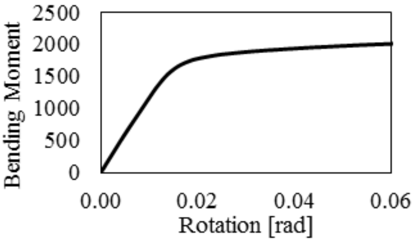

Von Mises stress

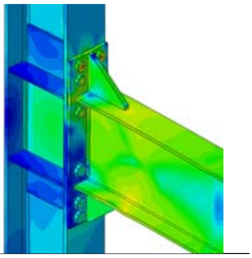

Equivalent plastic deformation (PEEQ)

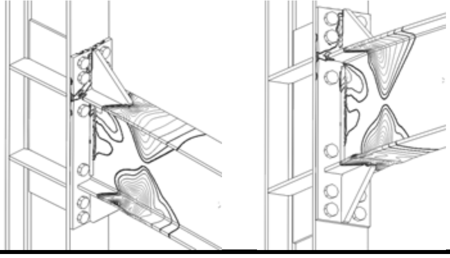

Contact pressure (CPRESS)

A30

Moment-Rotation curve

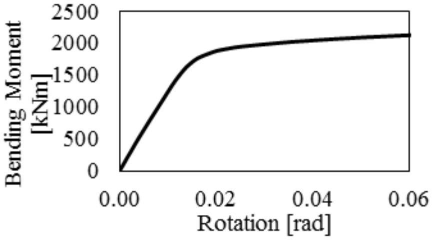

Von Mises stress

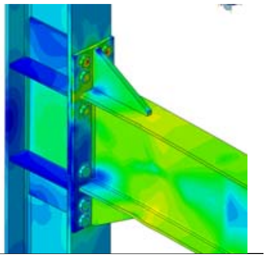

Equivalent plastic deformation (PEEQ)

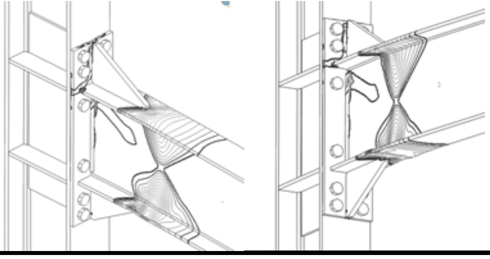

Contact pressure (CPRESS)

ES3 – PARTIAL – R-5

A40

Moment-Rotation curve

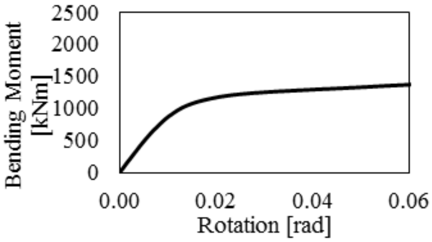

Von Mises stress

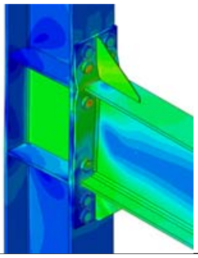

Equivalent plastic deformation (PEEQ)

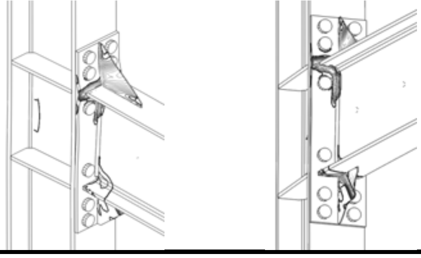

Contact pressure (CPRESS)

A30

Moment-Rotation curve

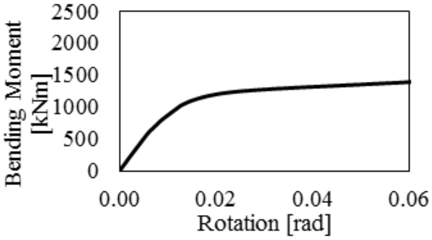

Von Mises stress

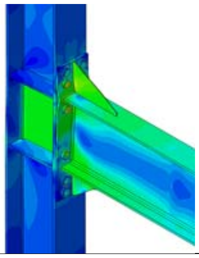

Equivalent plastic deformation (PEEQ)

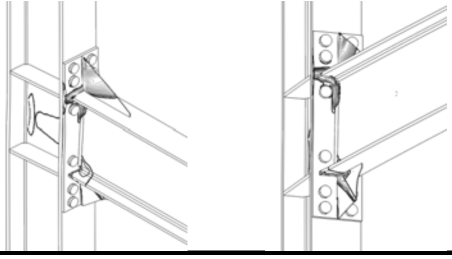

Contact pressure (CPRESS)

ES3 – PARTIAL – R-10

A40

Moment-Rotation curve

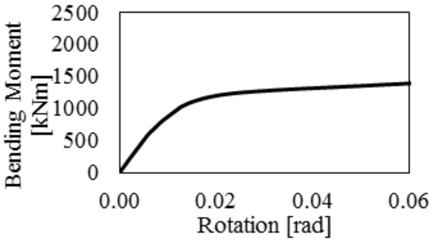

Von Mises stress

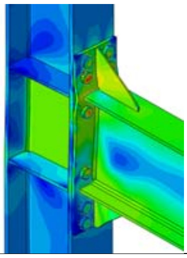

Equivalent plastic deformation (PEEQ)

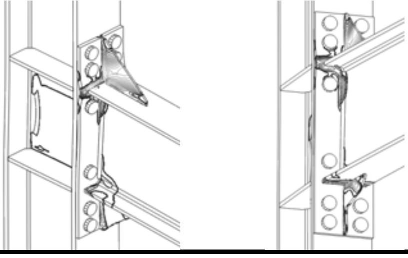

Contact pressure (CPRESS)

A30

Moment-Rotation curve

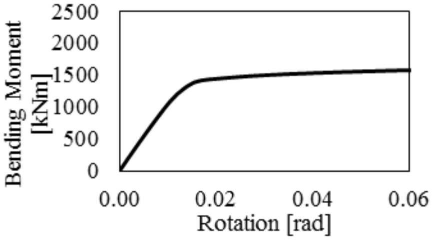

Von Mises stress

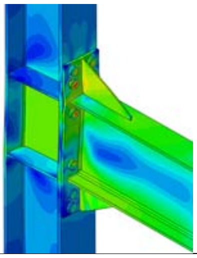

Equivalent plastic deformation (PEEQ)

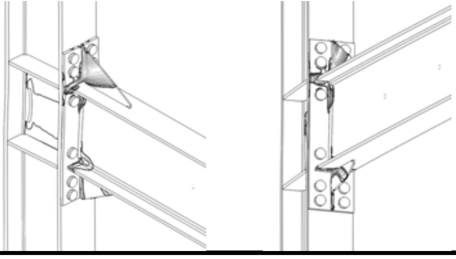

Contact pressure (CPRESS)

ES3 – PARTIAL – R-15

A40

Moment-Rotation curve

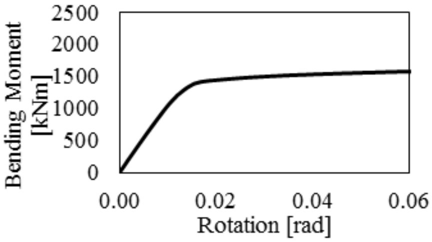

Von Mises stress

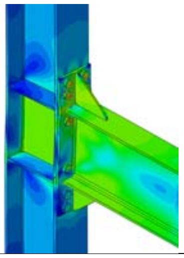

Equivalent plastic deformation (PEEQ)

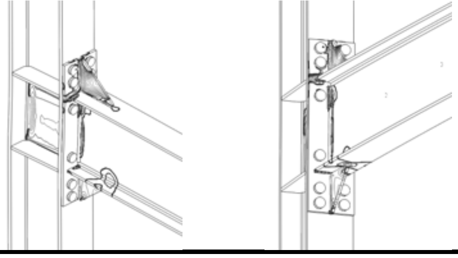

Contact pressure (CPRESS)

A30

Moment-Rotation curve

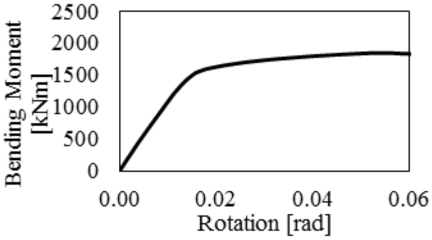

Von Mises stress

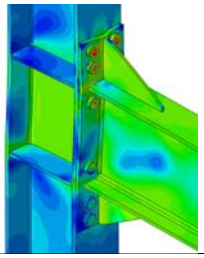

Equivalent plastic deformation (PEEQ)

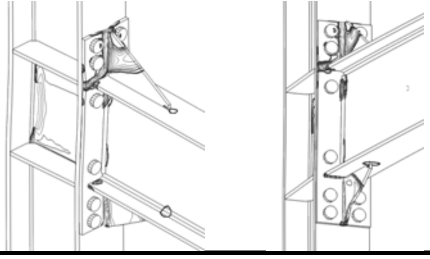

Contact pressure (CPRESS)

ES3 – PARTIAL – R-20

A40

Moment-Rotation curve

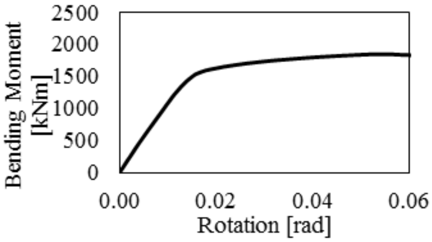

Von Mises stress

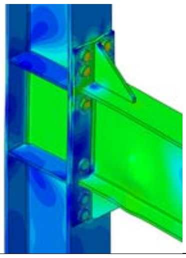

Equivalent plastic deformation (PEEQ)

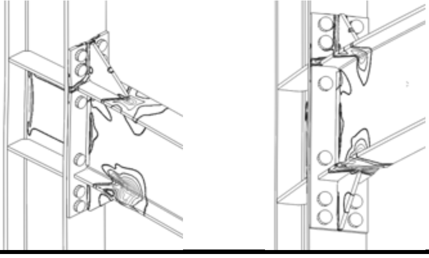

Contact pressure (CPRESS)

A30

Moment-Rotation curve

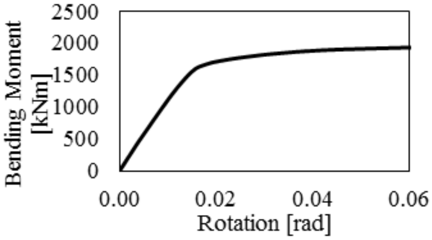

Von Mises stress

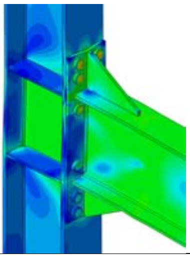

Equivalent plastic deformation (PEEQ)

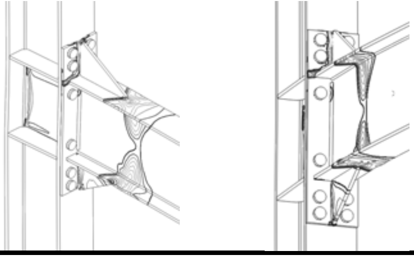

Contact pressure (CPRESS)

ES3 – PARTIAL – R-25

A40

Moment-Rotation curve

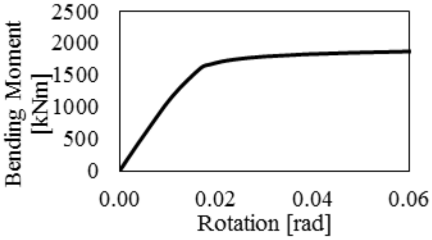

Von Mises stress

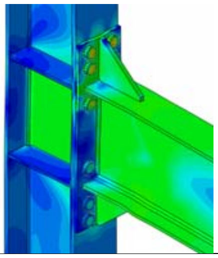

Equivalent plastic deformation (PEEQ)

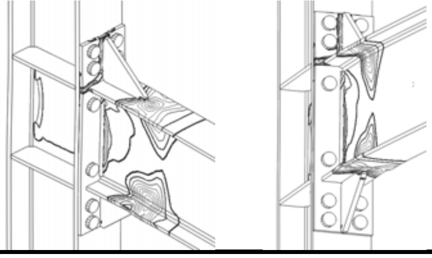

Contact pressure (CPRESS)

A30

Moment-Rotation curve

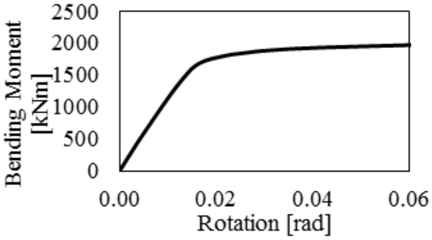

Von Mises stress

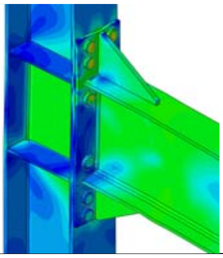

Equivalent plastic deformation (PEEQ)

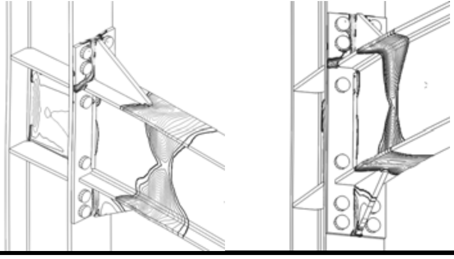

Contact pressure (CPRESS)

ES3 – PARTIAL – R-30

A40

Moment-Rotation curve

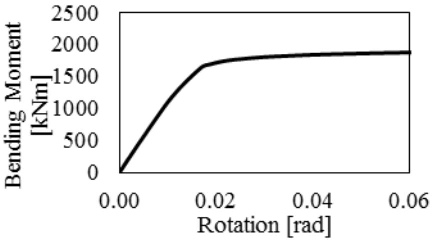

Von Mises stress

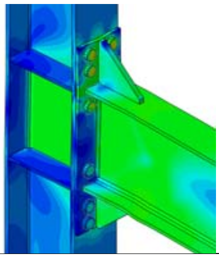

Equivalent plastic deformation (PEEQ)

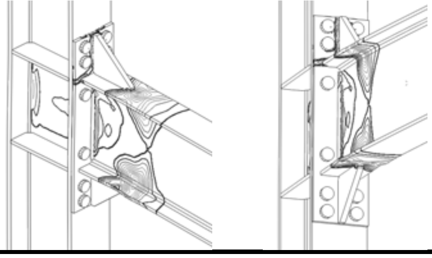

Contact pressure (CPRESS)

A30

Moment-Rotation curve

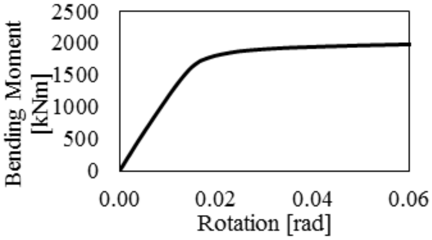

Von Mises stress

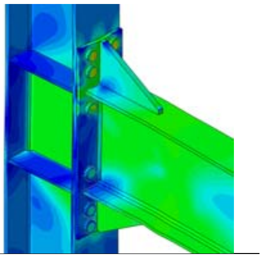

Equivalent plastic deformation (PEEQ)

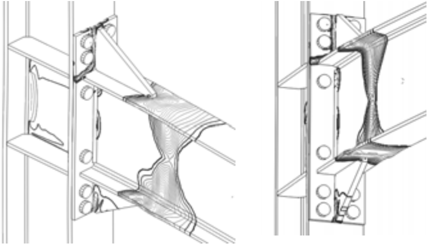

Contact pressure (CPRESS)

Annex IV Material investigation

The results of the material investigation are hereinafter presented (Table IV.1). As already anticipated in Chapter VII, only the end-plate material was changed and both monotonic and cyclic analysis were performed for each of the material introduced (M1 to M5).

As already done for the rib investigation, also in this investigation the analyses were performed for the three beam-to-column assemblies (ES1, ES2 and ES3) considering all the design criteria introduced in Chapter V (full, equal and partial strength).

The results are reported in terms of: (i) moment rotation curve, (ii) Von Misses stress distribution and (iii) in terms of PEEQ*.

*PEEQ: equivalent plastic deformation [4].

Table IV.1: Material investigation.

<table>
<tr><td rowspan="5">ES1 – FULL – M1</td><td colspan="3">Moment Rotation Curves</td></tr>
<tr><td colspan="3">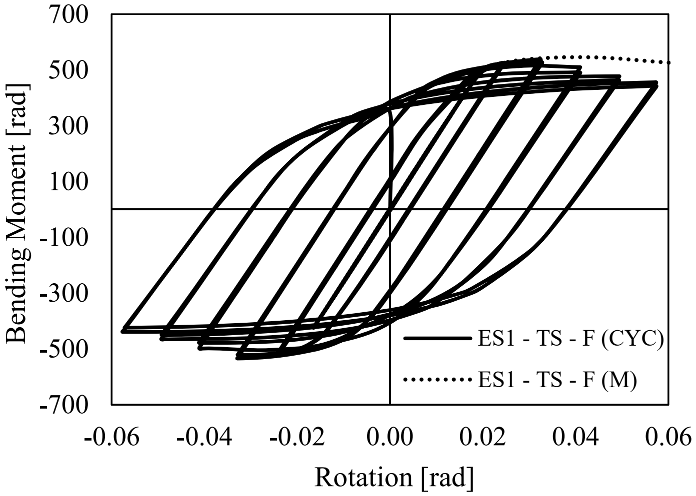
</td></tr>
<tr><td></td><td>Von Mises Stress</td><td>Equivalent plastic deformation (PEEQ)</td></tr>
<tr><td>Monotonic</td><td>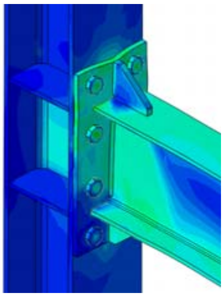</td><td>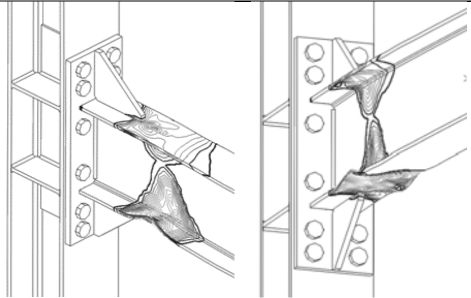</td></tr>
<tr><td>Cyclic</td><td>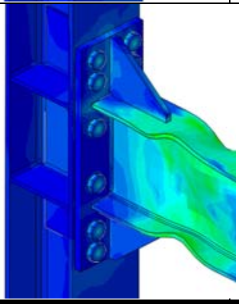</td><td>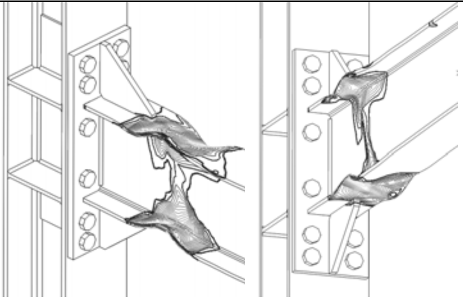</td></tr>
</table>

ES1 – FULL – M2

Moment Rotation Curves

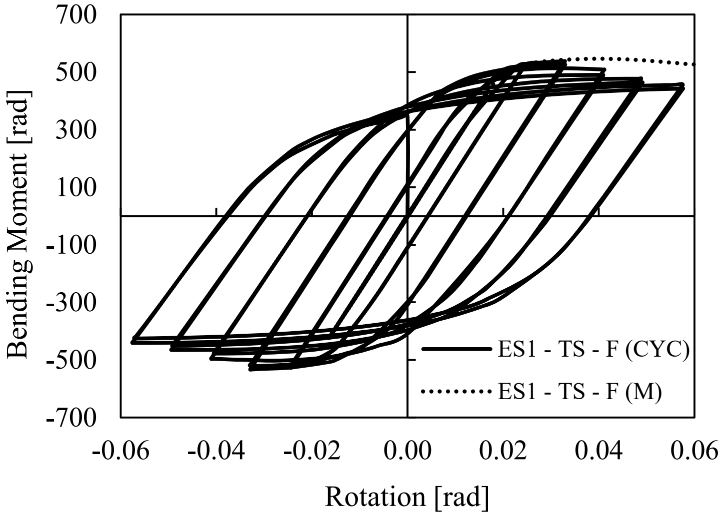

	Von Mises Stress	Equivalent plastic deformation (PEEQ)
Monotonic	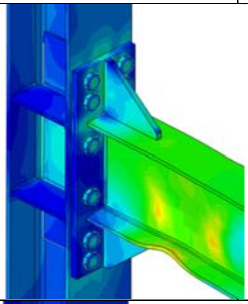	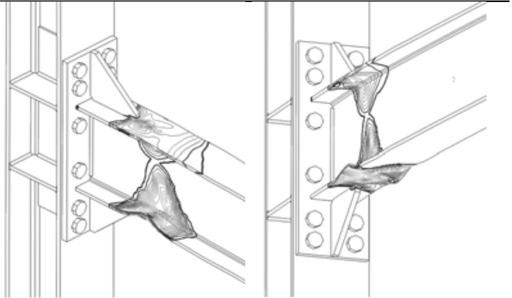
Cyclic	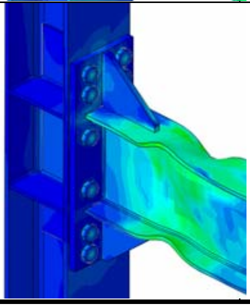	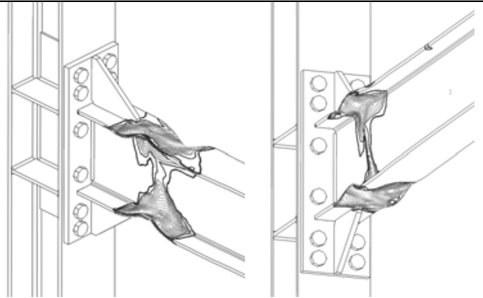

ES1 – FULL – M3

Moment Rotation Curves

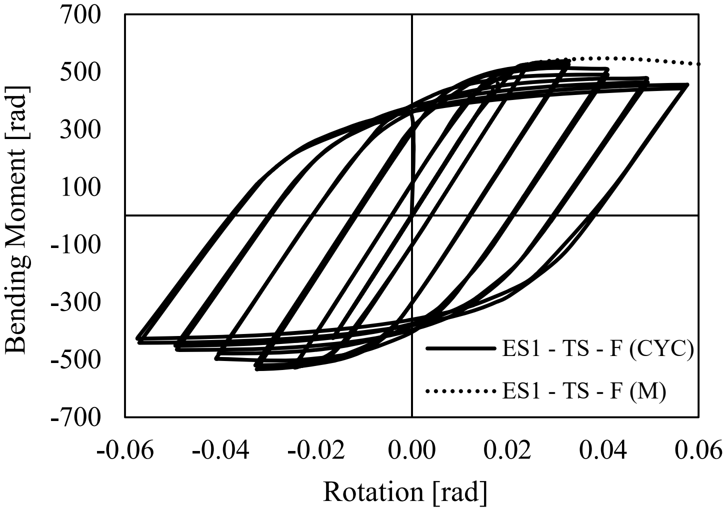

	Von Mises Stress	Equivalent plastic deformation (PEEQ)
Monotonic	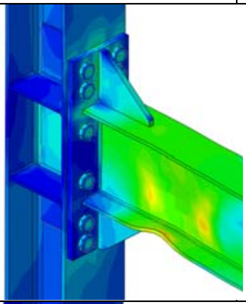	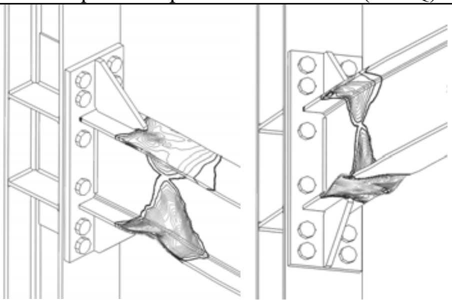
Cyclic	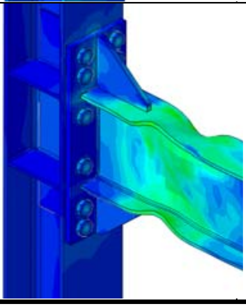	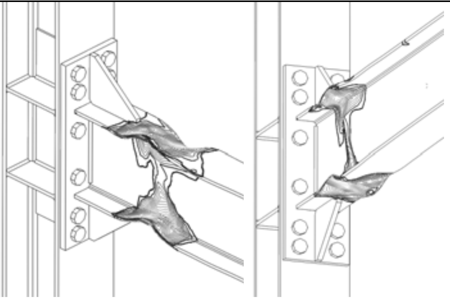

ES1 – FULL – M4

Moment Rotation Curves

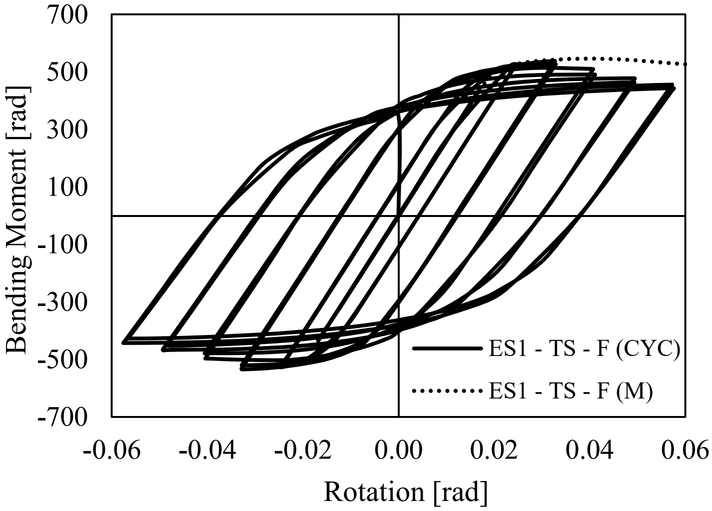

	Von Mises Stress	Equivalent plastic deformation (PEEQ)
Monotonic	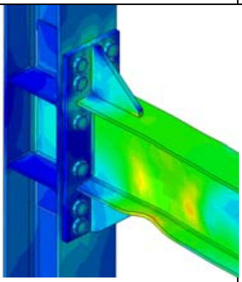	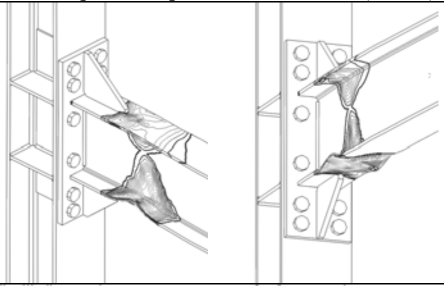
Cyclic	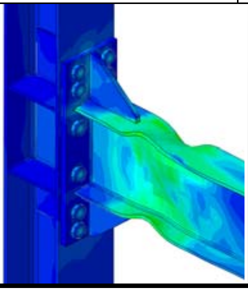	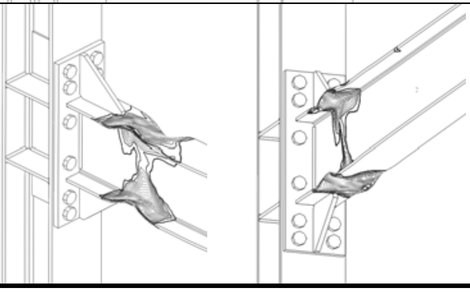

ES1 – EQUAL – M1

Moment Rotation Curves

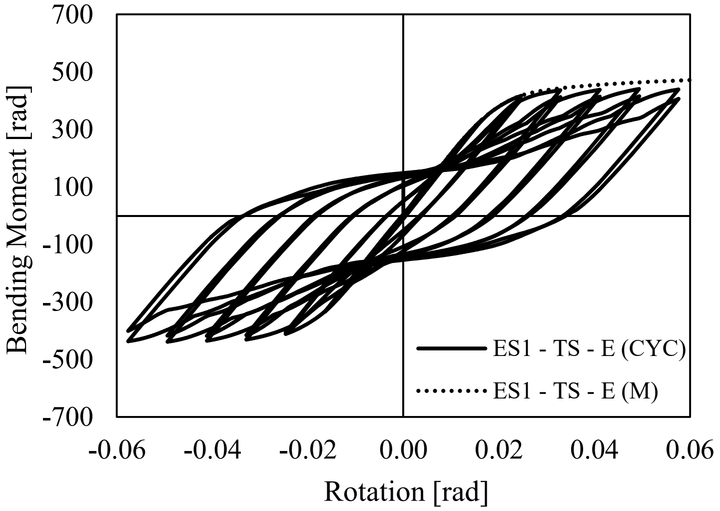

	Von Mises Stress	Equivalent plastic deformation (PEEQ)
Monotonic	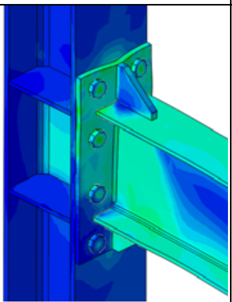	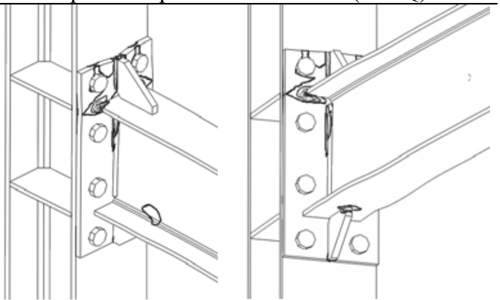
Cyclic	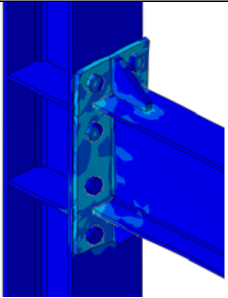	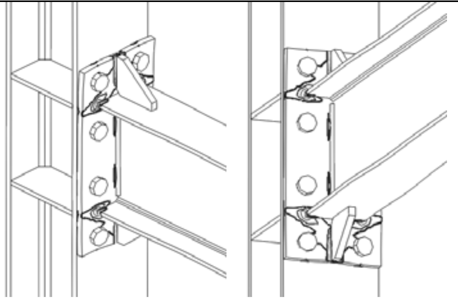

ES1 – EQUAL – M2

Moment Rotation Curves

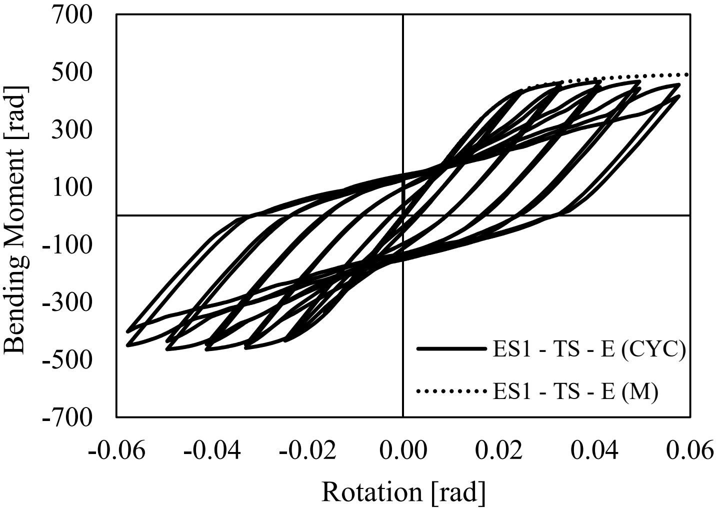

	Von Mises Stress	Equivalent plastic deformation (PEEQ)
Monotonic	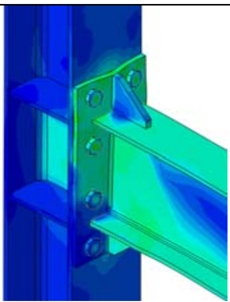	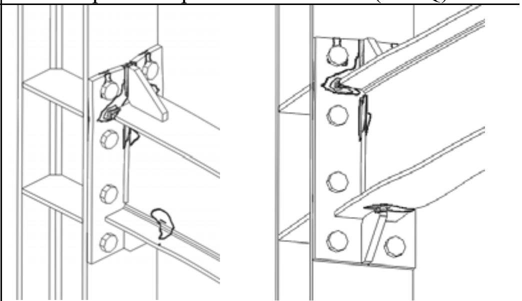
Cyclic	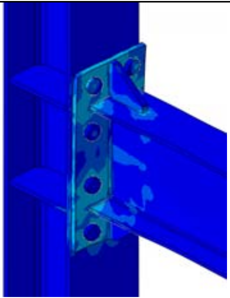	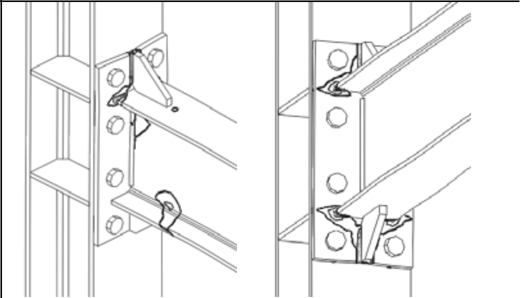

ES1 – EQUAL – M3

Moment Rotation Curves

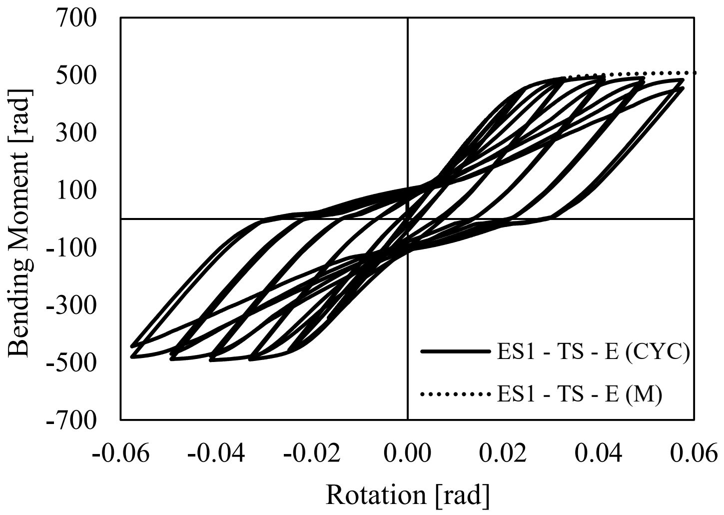

	Von Mises Stress	Equivalent plastic deformation (PEEQ)
Monotonic	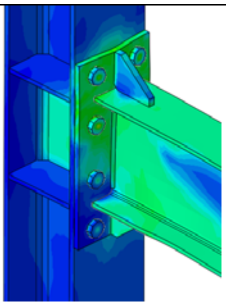	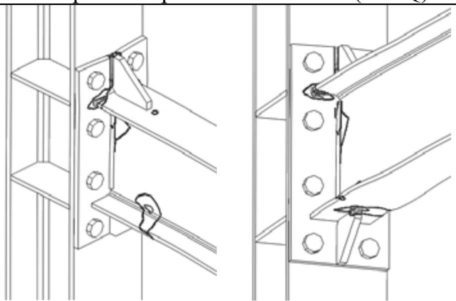
Cyclic	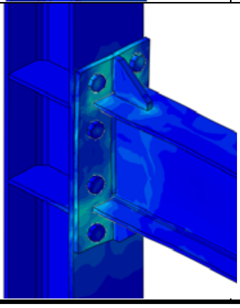	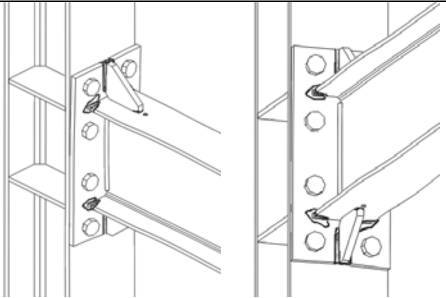

ES1 – EQUAL – M4

Moment Rotation Curves

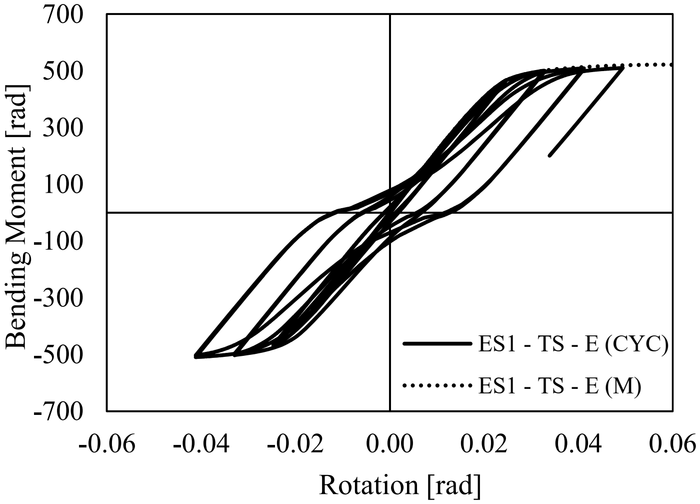

	Von Mises Stress	Equivalent plastic deformation (PEEQ)
Monotonic	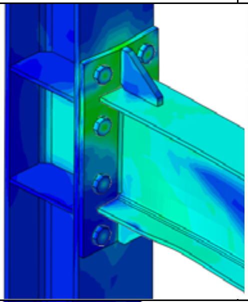	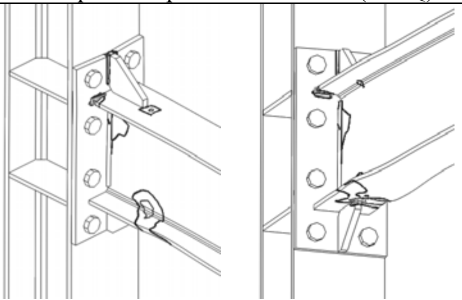
Cyclic	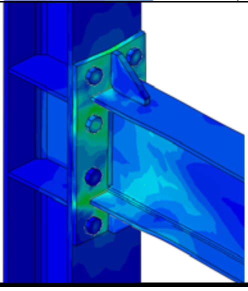	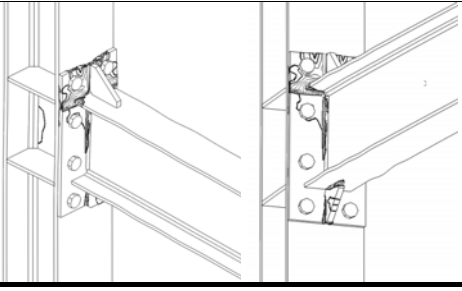

ES1 – PARTIAL – M1

Moment Rotation Curves

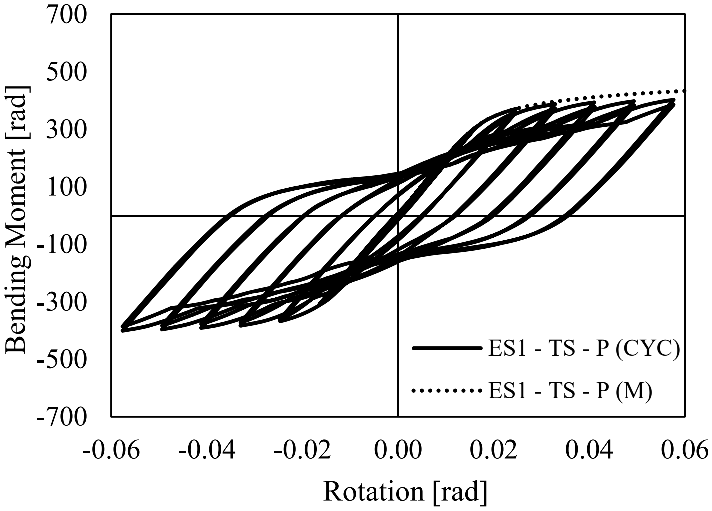

	Von Mises Stress	Equivalent plastic deformation (PEEQ)
Monotonic	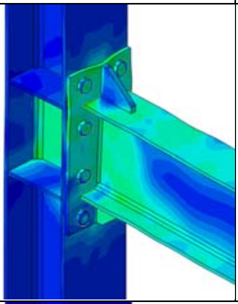	
Cyclic	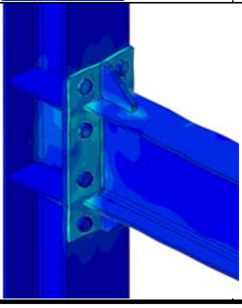	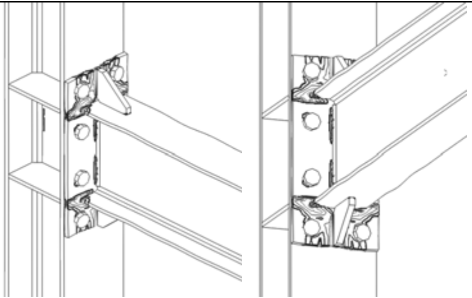

ES1 – PARTIAL – M2

Moment Rotation Curves

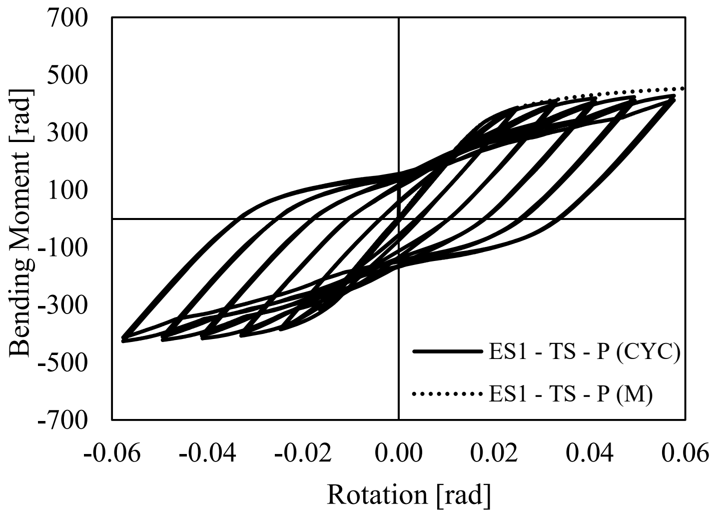

	Von Mises Stress	Equivalent plastic deformation (PEEQ)
Monotonic	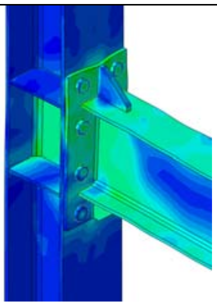	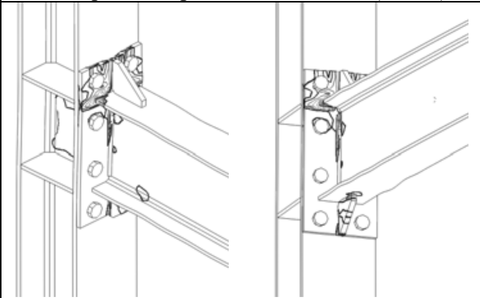
Cyclic	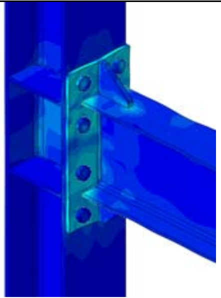	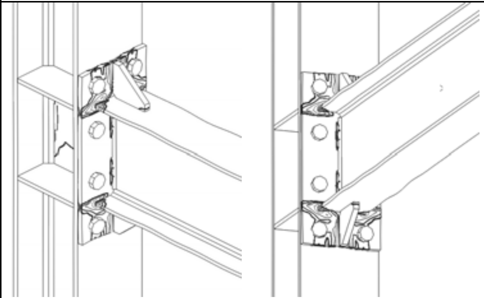

ES1 – PARTIAL – M3

Moment Rotation Curves

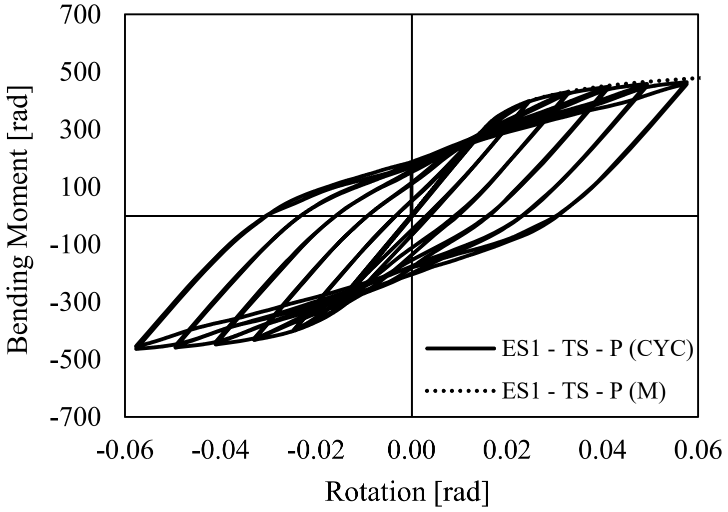

	Von Mises Stress	Equivalent plastic deformation (PEEQ)
Monotonic	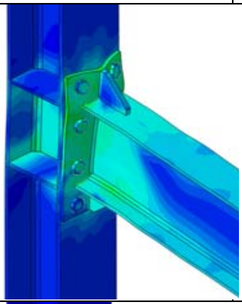	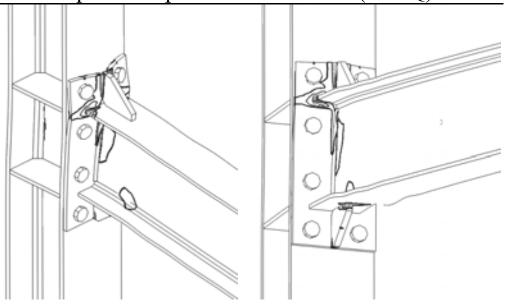
Cyclic	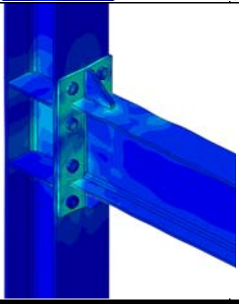	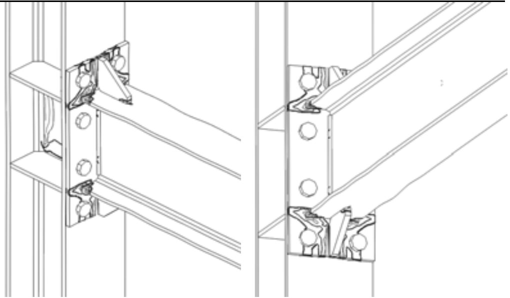

ES1 – PARTIAL – M4

Moment Rotation Curves

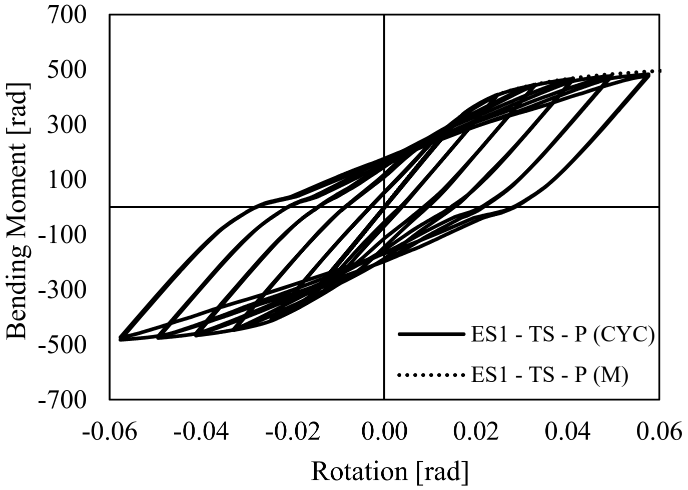

	Von Mises Stress	Equivalent plastic deformation (PEEQ)
Monotonic	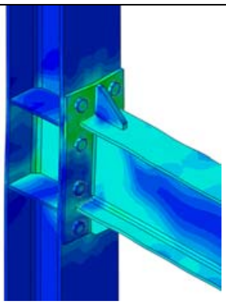	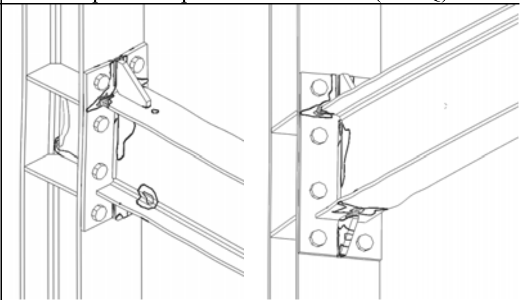
Cyclic	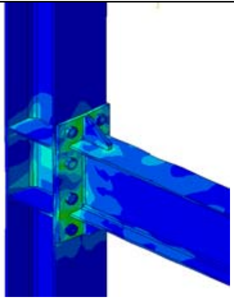	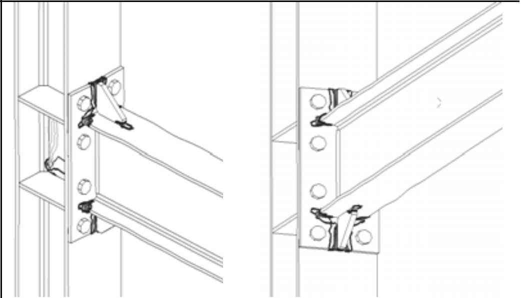

ES2 – FULL – M1

Moment Rotation Curves

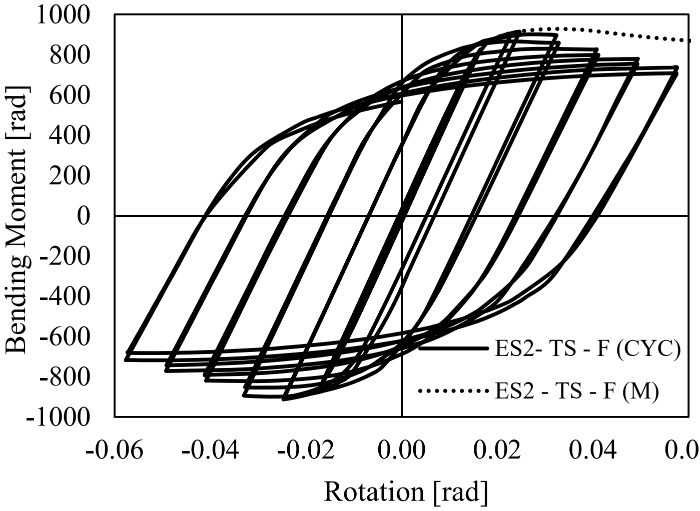

Von Mises Stress

Equivalent plastic deformation (PEEQ)

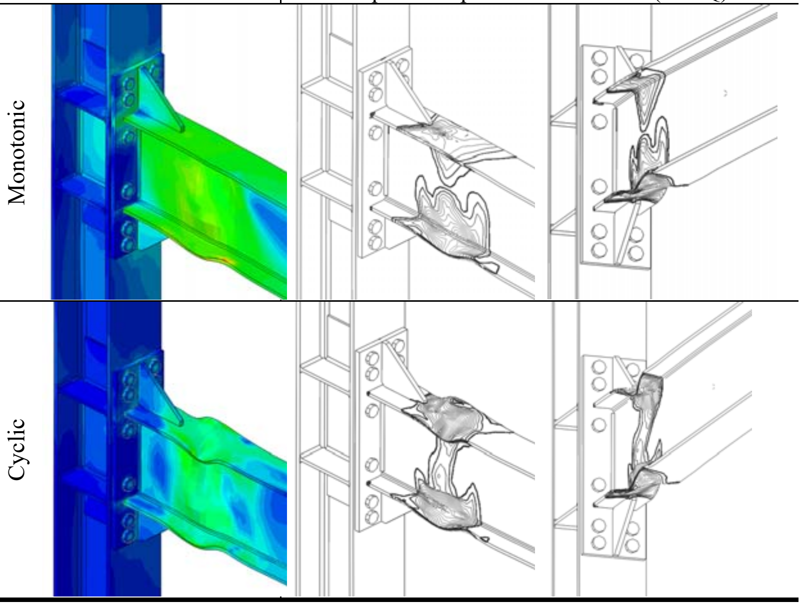

ES2 – FULL – M2

Moment Rotation Curves

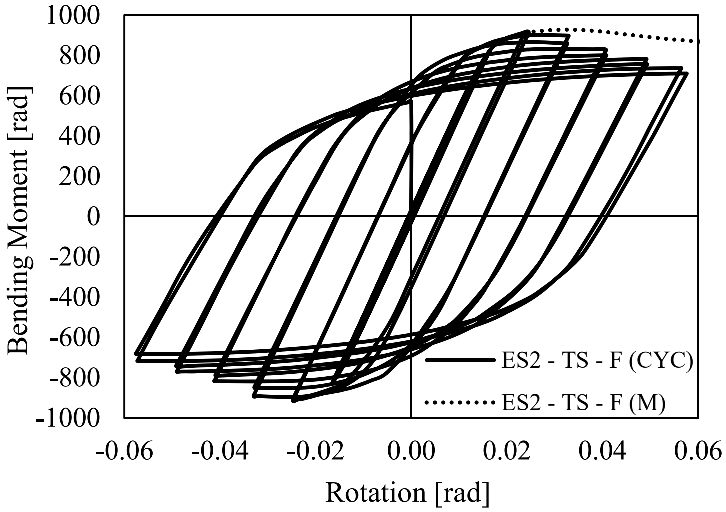

	Von Mises Stress	Equivalent plastic deformation (PEEQ)
Monotonic	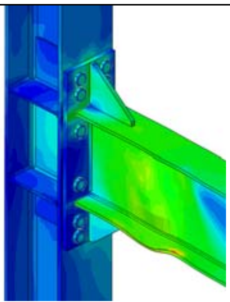	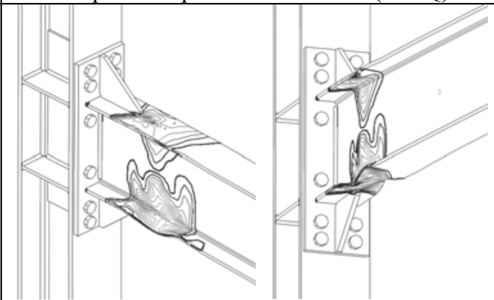
Cyclic	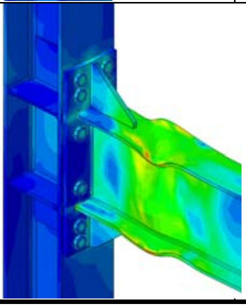	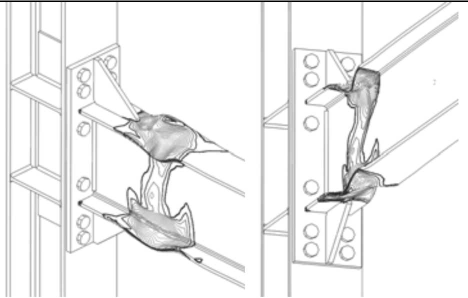

ES2 – FULL – M3

Moment Rotation Curves

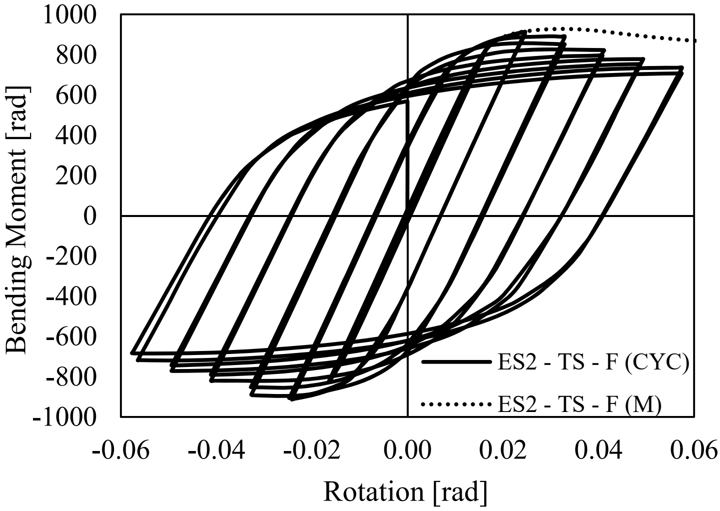

	Von Mises Stress	Equivalent plastic deformation (PEEQ)
Monotonic	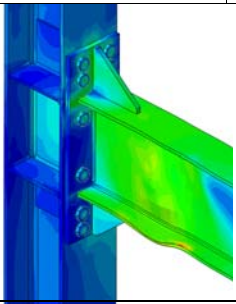	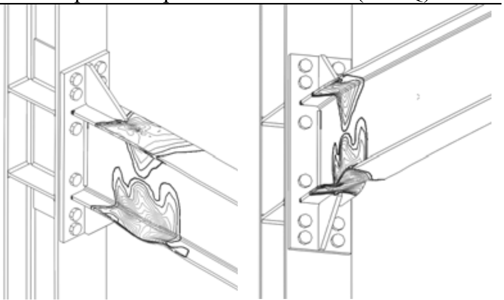
Cyclic	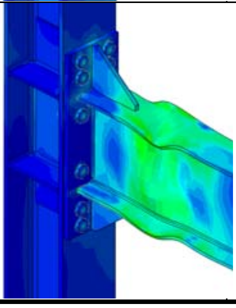	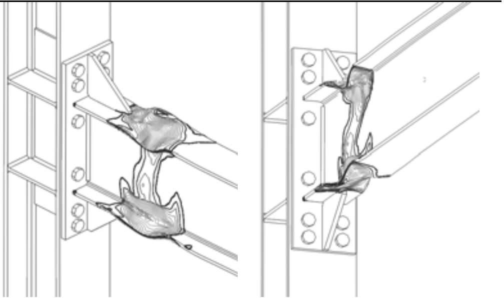

ES2 – FULL – M4

Moment Rotation Curves

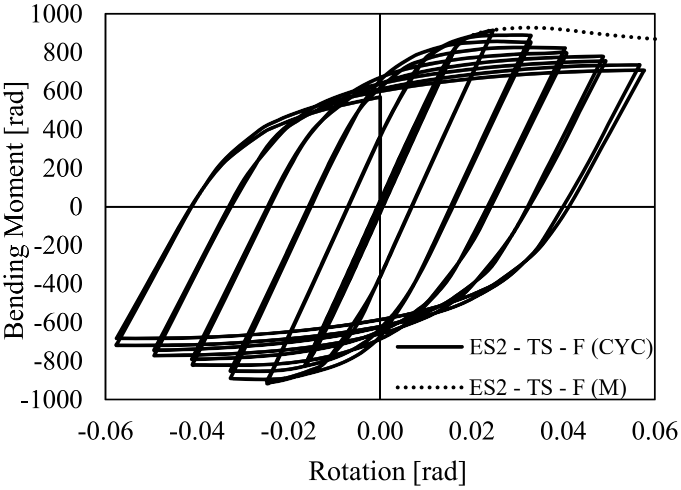

	Von Mises Stress	Equivalent plastic deformation (PEEQ)
Monotonic	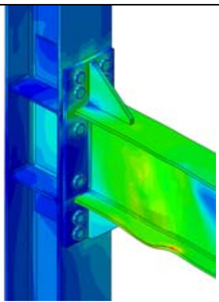	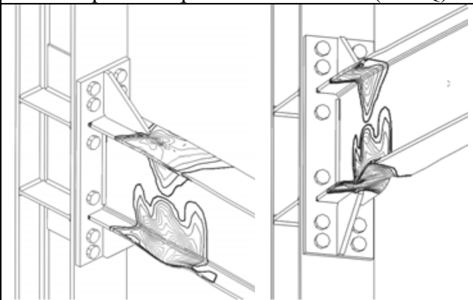
Cyclic	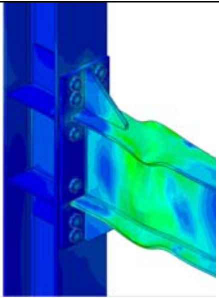	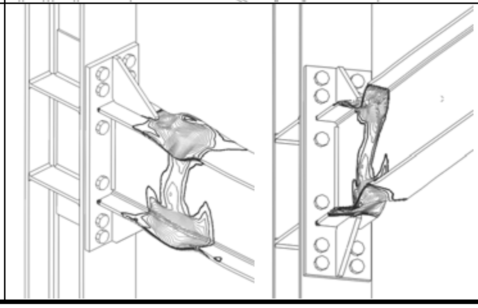

ES2 – EQUAL – M1

Moment Rotation Curves

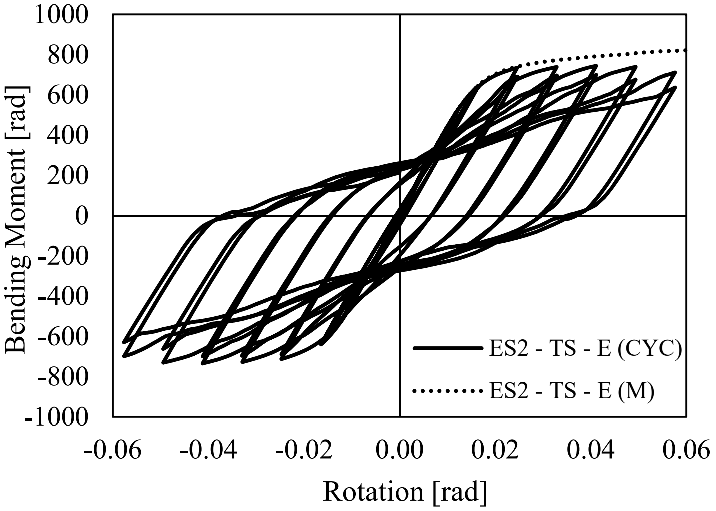

	Von Mises Stress	Equivalent plastic deformation (PEEQ)
Monotonic		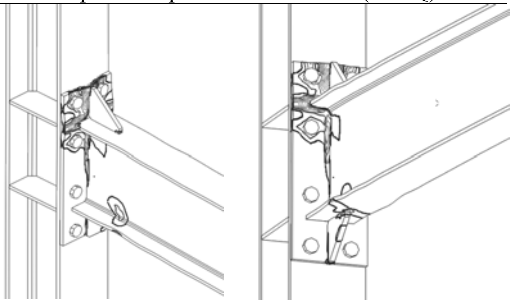
Cyclic	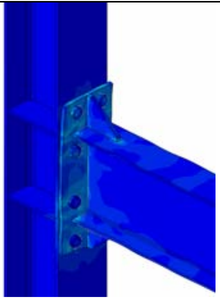	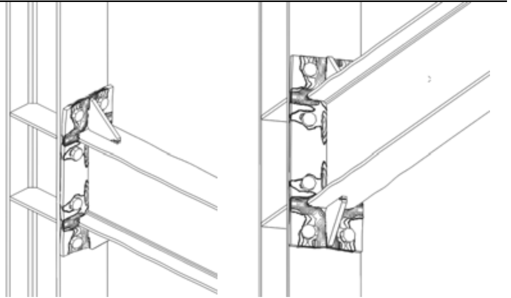

ES2 – EQUAL – M2

Moment Rotation Curves

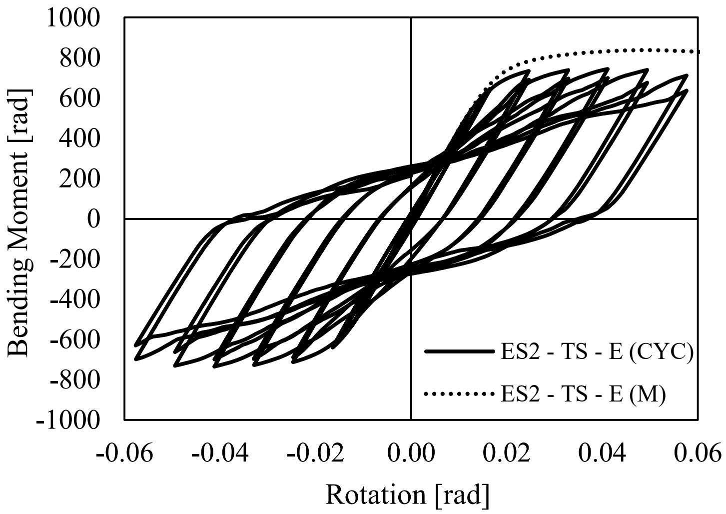

Von Mises Stress

Equivalent plastic deformation (PEEQ)

Monotonic

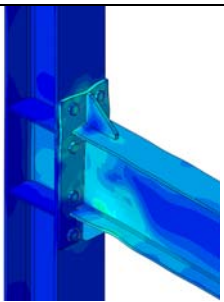

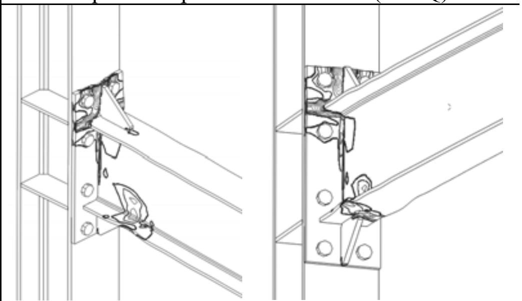

Cyclic

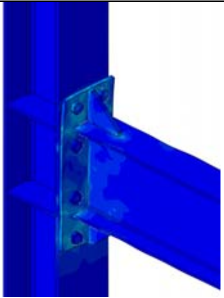

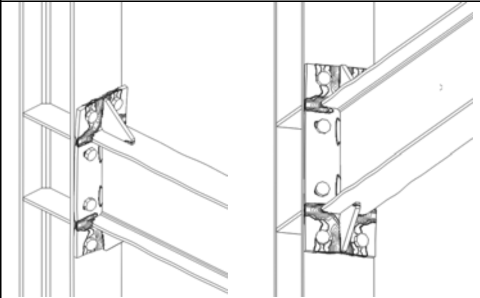

ES2 – EQUAL – M3

Moment Rotation Curves

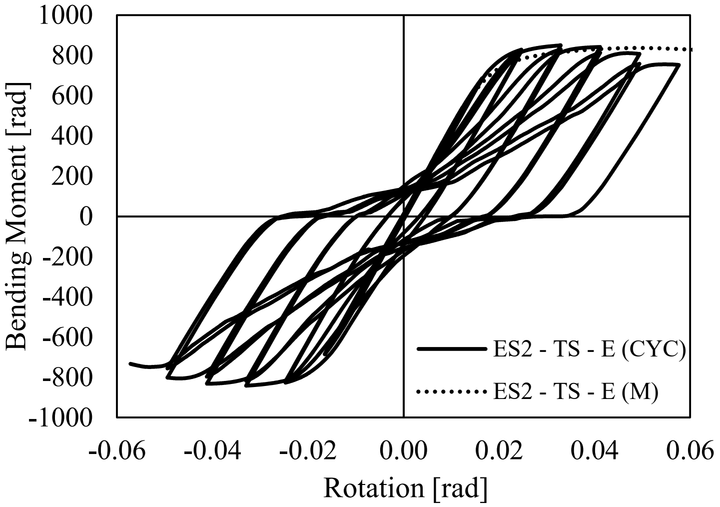

Von Mises Stress

Equivalent plastic deformation (PEEQ)

Monotonic

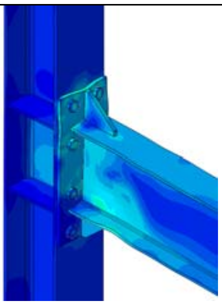

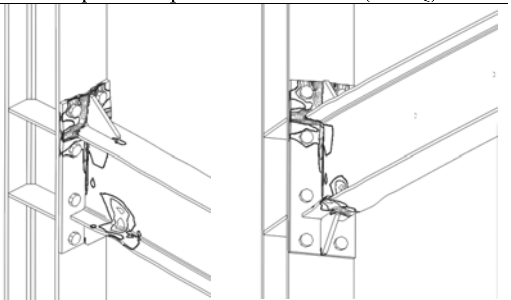

Cyclic

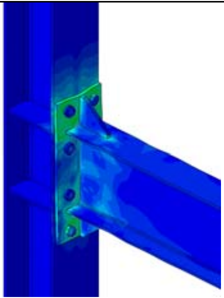

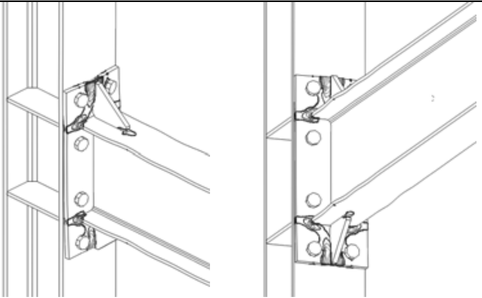

ES2 – EQUAL – M4

Moment Rotation Curves

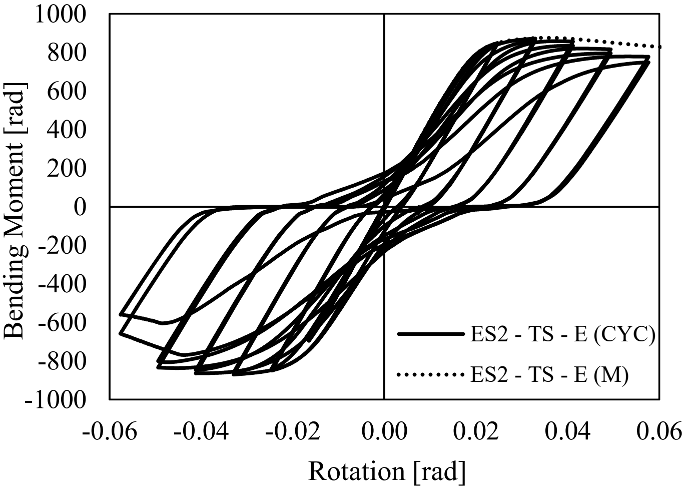

	Von Mises Stress	Equivalent plastic deformation (PEEQ)
Monotonic	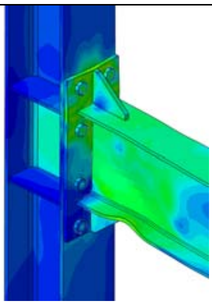	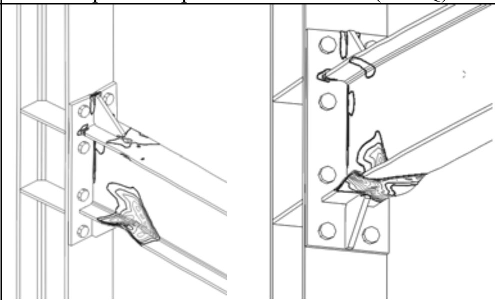
Cyclic	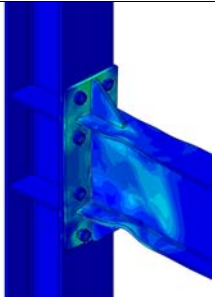	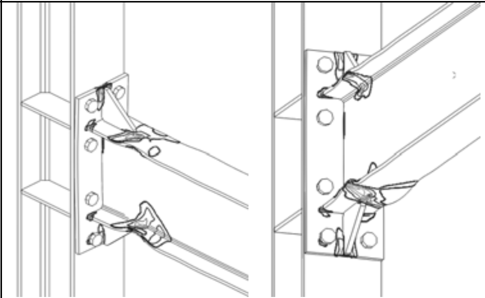

ES2 – PARTIAL – M1

Moment Rotation Curves

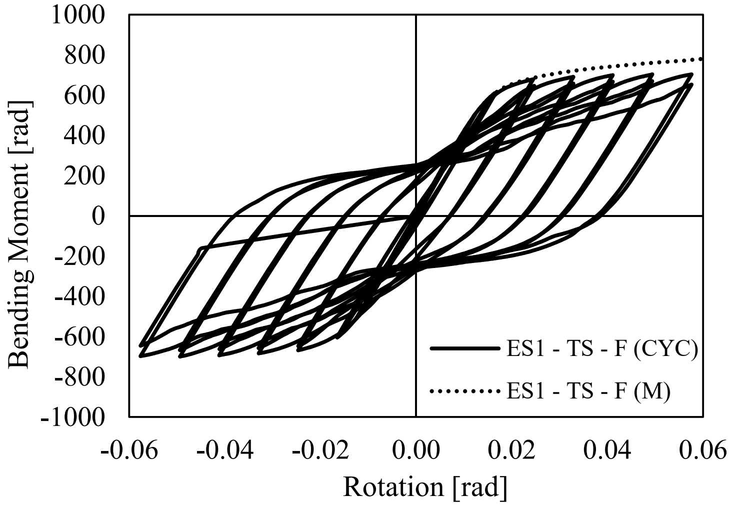

	Von Mises Stress	Equivalent plastic deformation (PEEQ)	
Monotonic	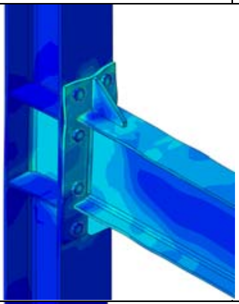	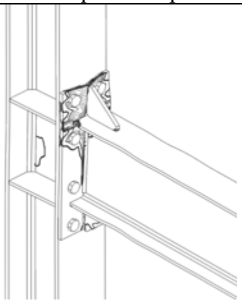	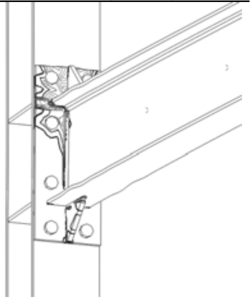
Cyclic	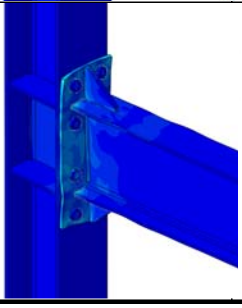	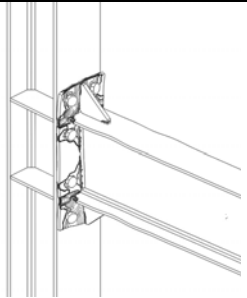	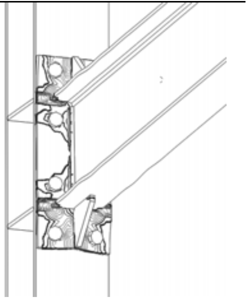

ES2 – PARTIAL – M2

Moment Rotation Curves

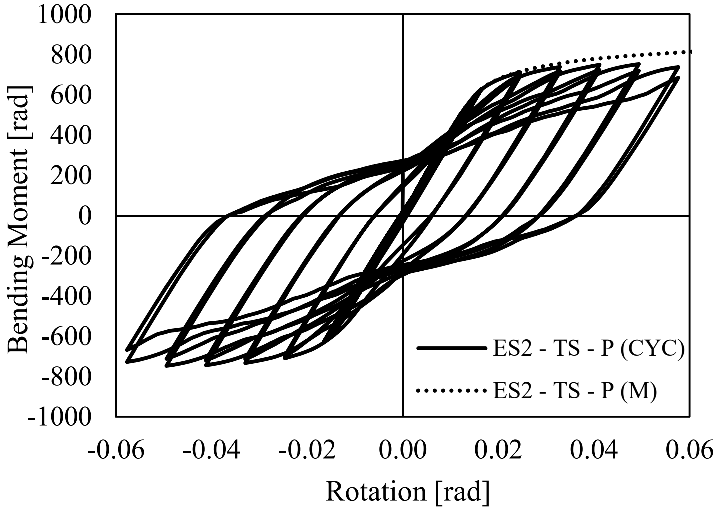

	Von Mises Stress	Equivalent plastic deformation (PEEQ)
Monotonic	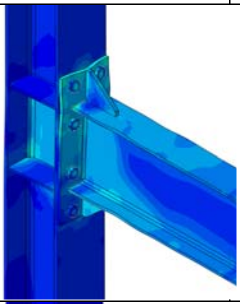	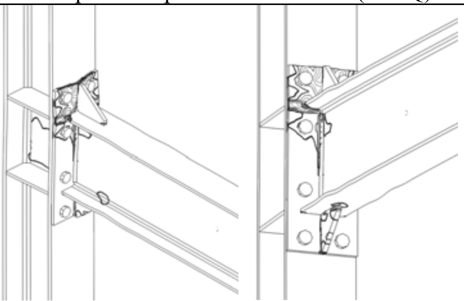
Cyclic	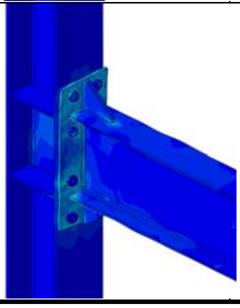	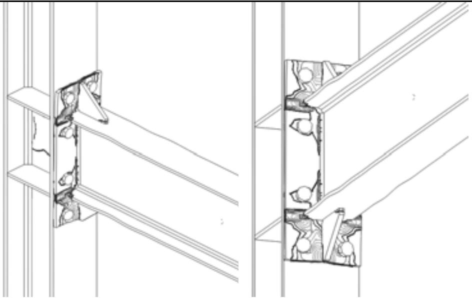

ES2 – PARTIAL – M3

Moment Rotation Curves

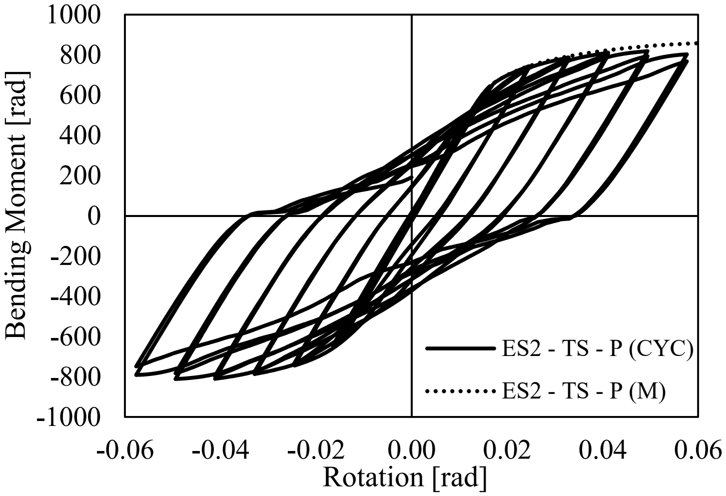

Von Mises Stress

Equivalent plastic deformation (PEEQ)

Monotonic

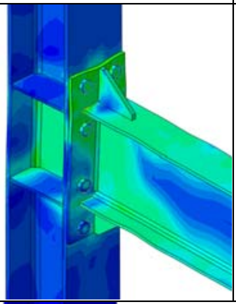

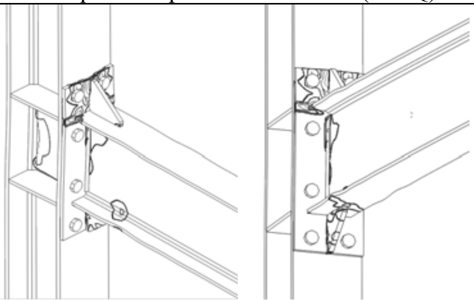

Cyclic

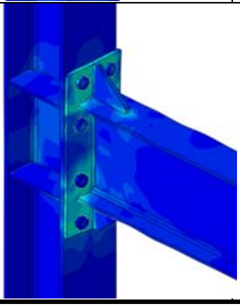

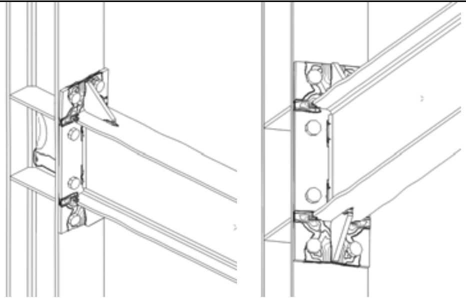

ES2 – PARTIAL – M4

Moment Rotation Curves

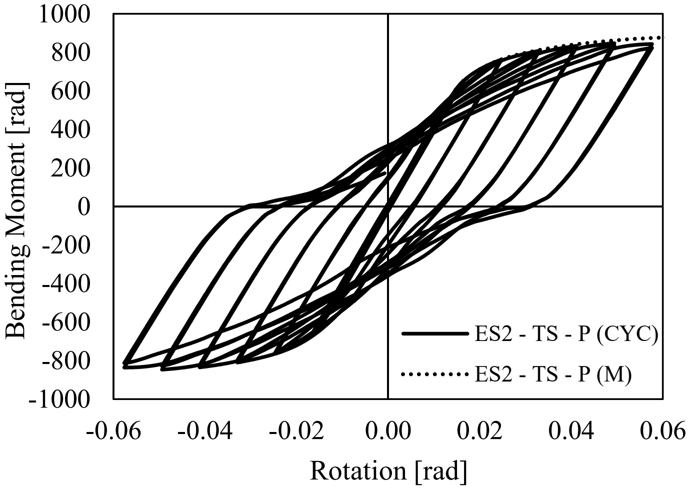

Von Mises Stress | Equivalent plastic deformation (PEEQ)

Monotonic

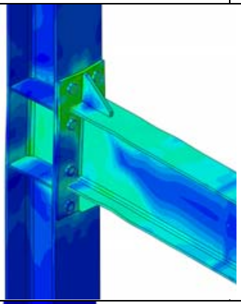

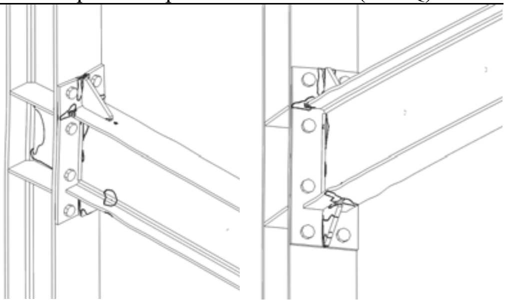

Cyclic

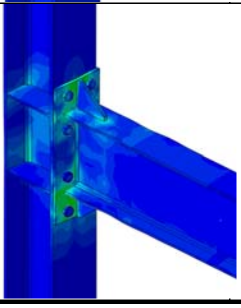

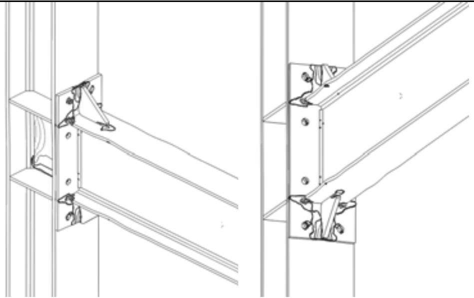

ES3 – FULL – M1

Moment Rotation Curves

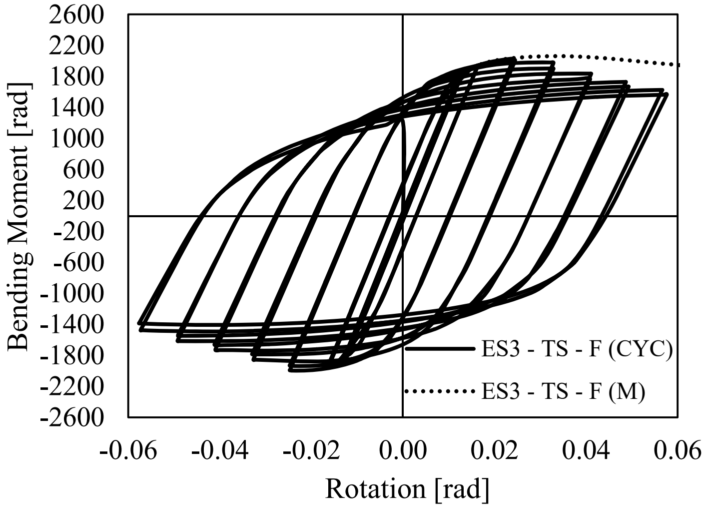

	Von Mises Stress	Equivalent plastic deformation (PEEQ)
Monotonic	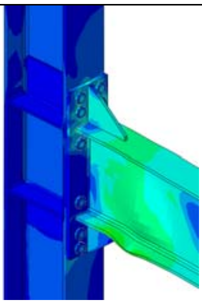	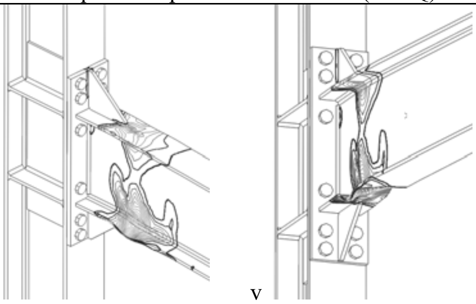
Cyclic	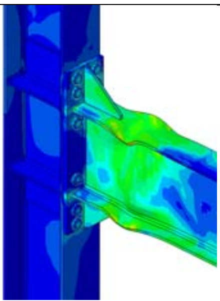	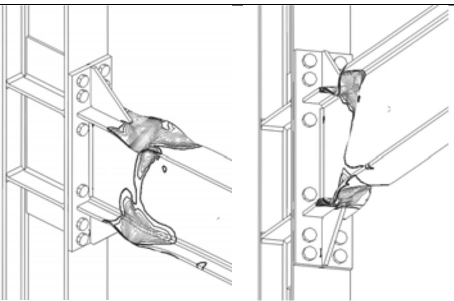

ES3 – FULL – M2

Moment Rotation Curves

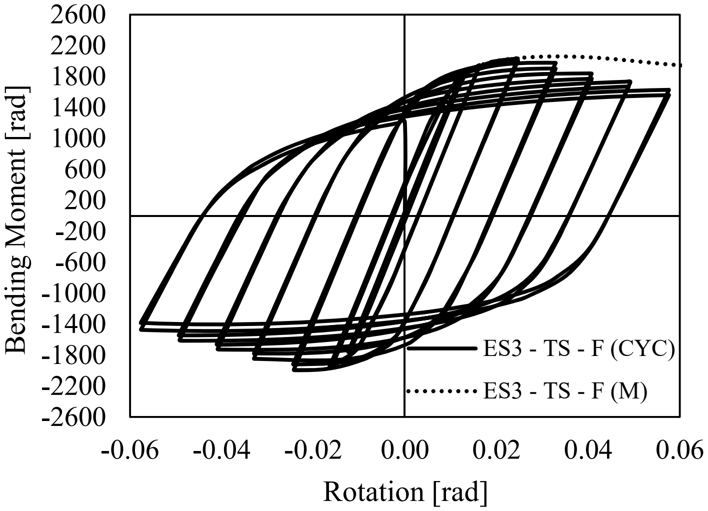

	Von Mises Stress	Equivalent plastic deformation (PEEQ)
Monotonic	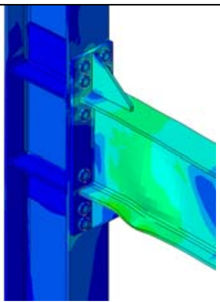	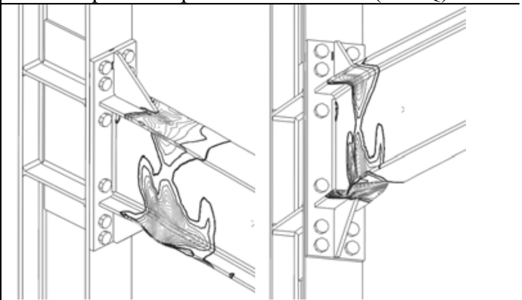
Cyclic	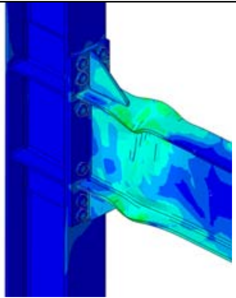	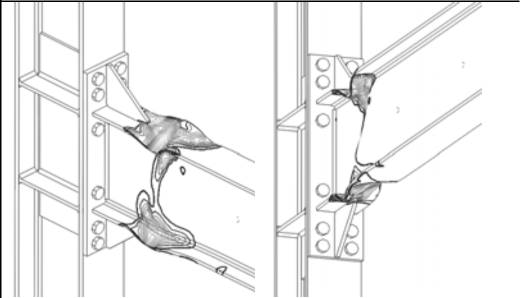

ES3 – FULL – M3

Moment Rotation Curves

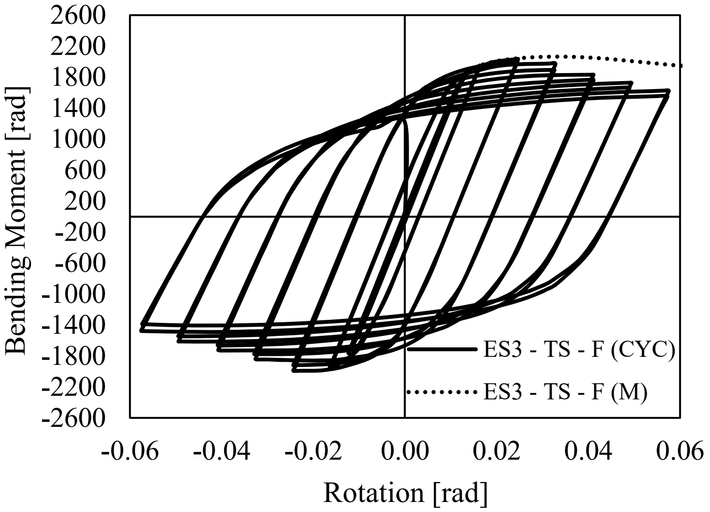

	Von Mises Stress	Equivalent plastic deformation (PEEQ)
Monotonic	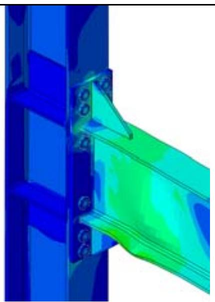	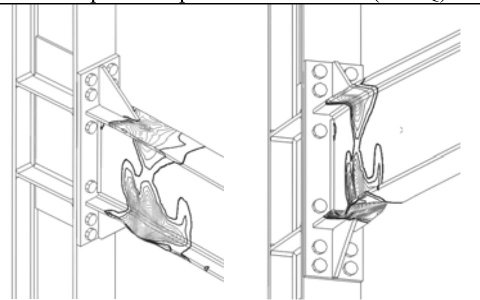
Cyclic	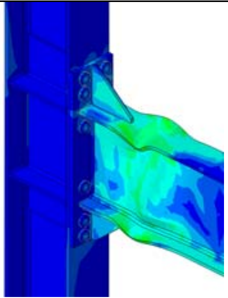	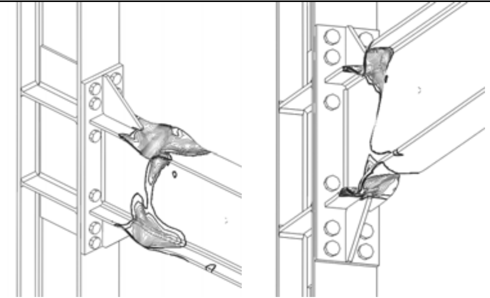

ES3 – FULL – M4

Moment Rotation Curves

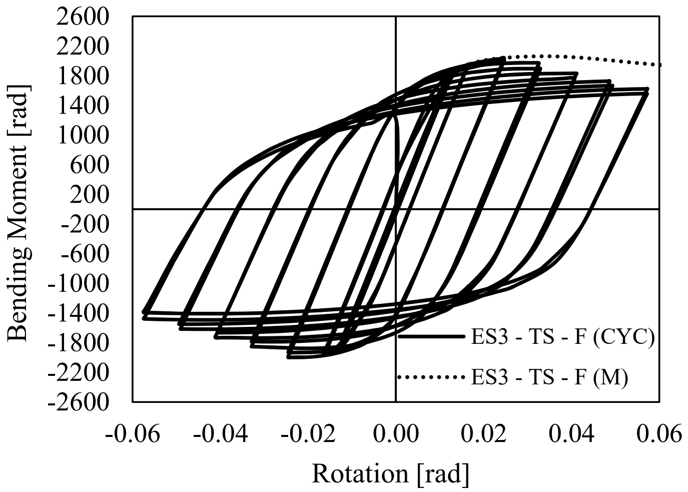

	Von Mises Stress	Equivalent plastic deformation (PEEQ)
Monotonic	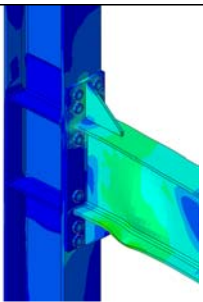	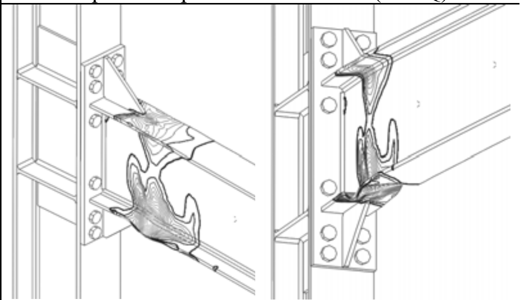
Cyclic	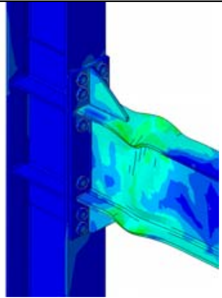	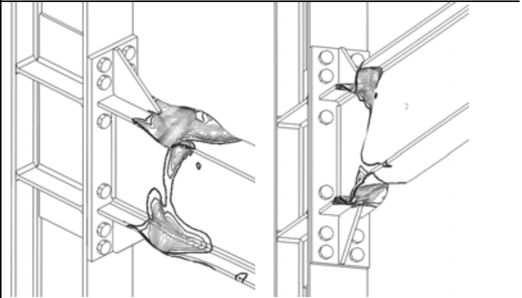

ES3 – EQUAL – M1

Moment Rotation Curves

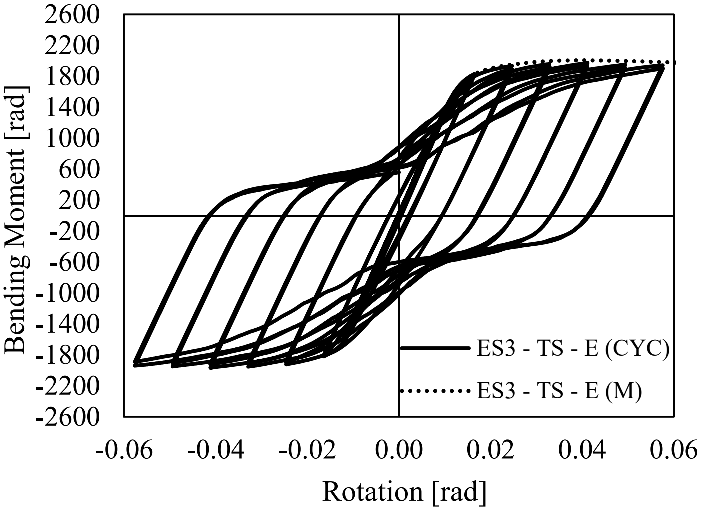

Von Mises Stress

Equivalent plastic deformation (PEEQ)

Monotonic

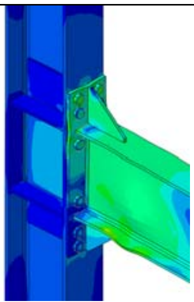

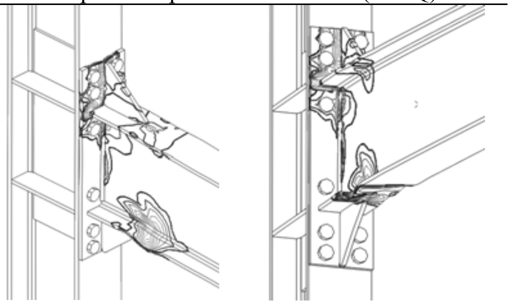

Cyclic

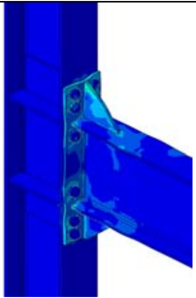

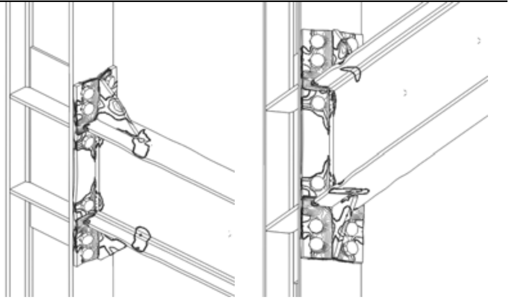

ES3 – EQUAL – M2

Moment Rotation Curves

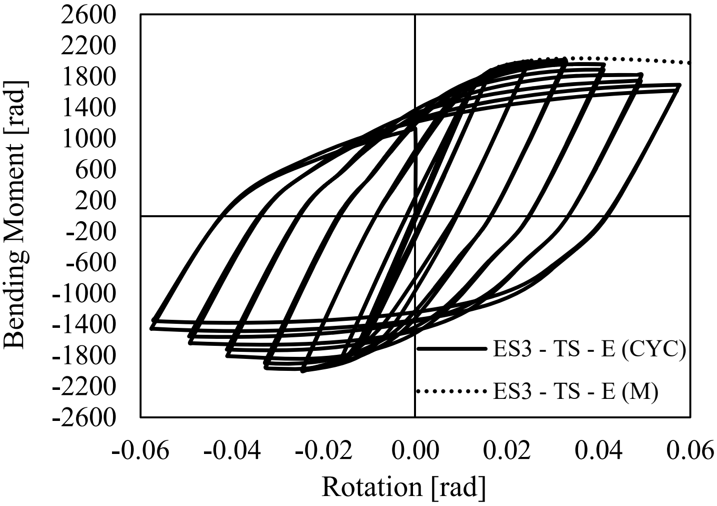

	Von Mises Stress	Equivalent plastic deformation (PEEQ)	
Monotonic	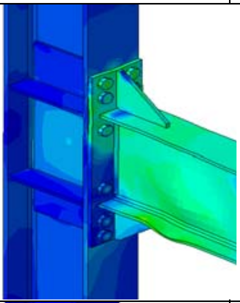		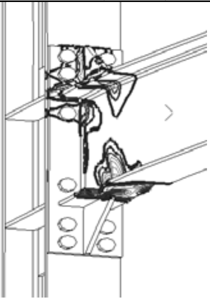
Cyclic	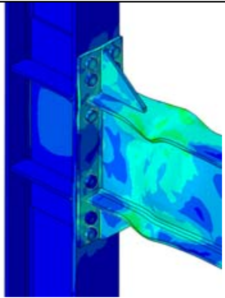	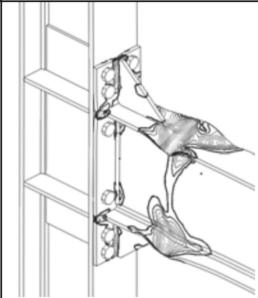	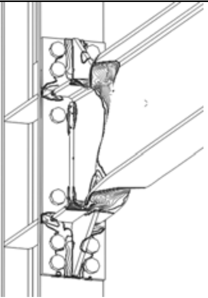

ES3 – EQUAL – M3

Moment Rotation Curves

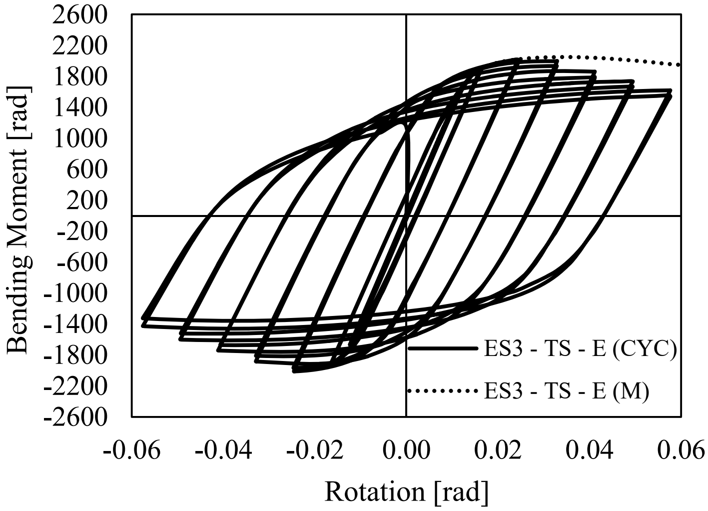

	Von Mises Stress	Equivalent plastic deformation (PEEQ)
Monotonic	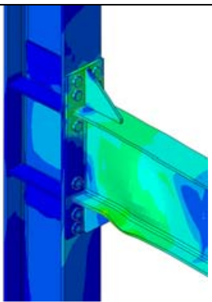	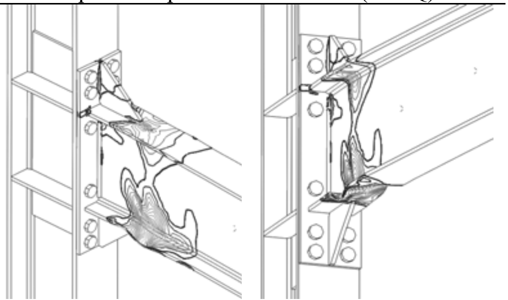
Cyclic	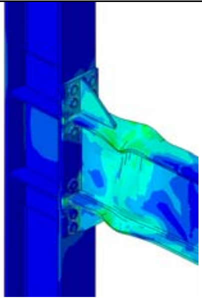	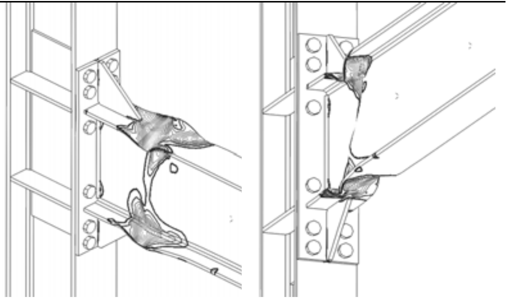

ES3 – EQUAL – M4

Moment Rotation Curves

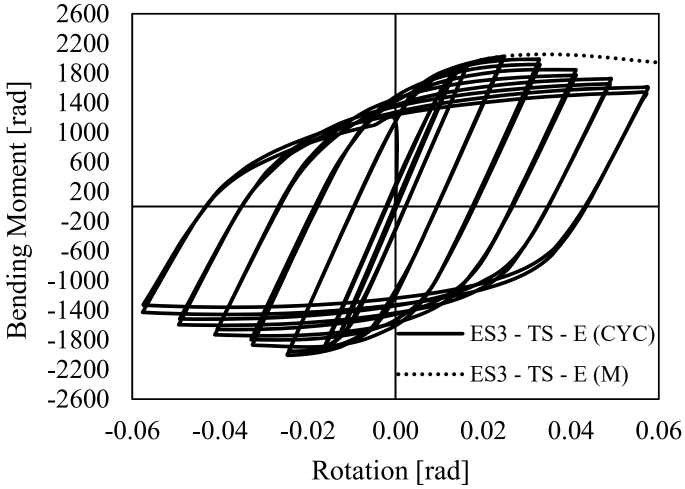

	Von Mises Stress	Equivalent plastic deformation (PEEQ)
Monotonic	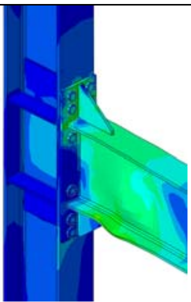	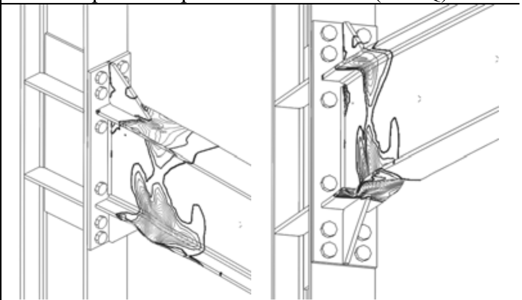
Cyclic	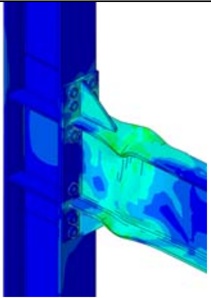	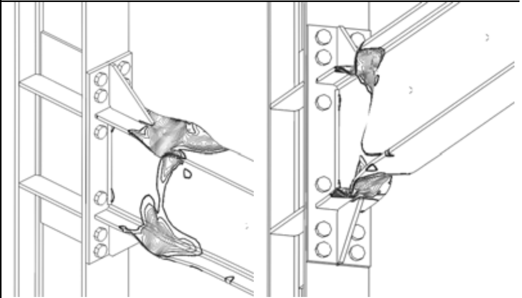

ES3 – PARTIAL – M1

Moment Rotation Curves

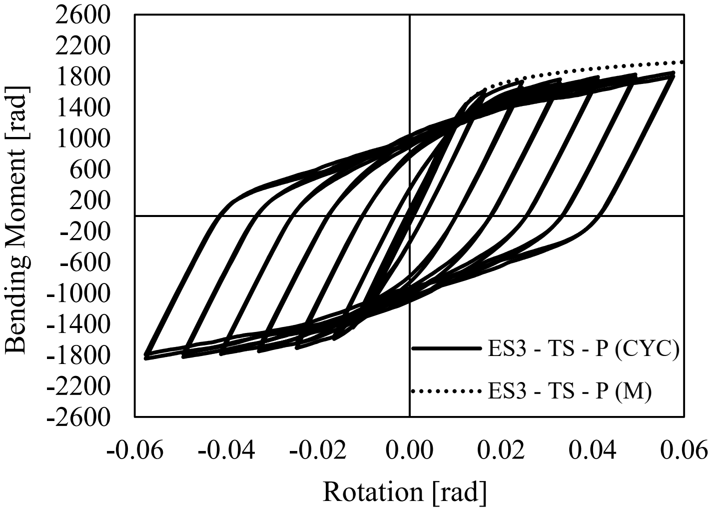

	Von Mises Stress	Equivalent plastic deformation (PEEQ)
Monotonic	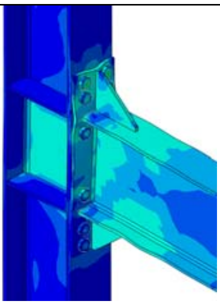	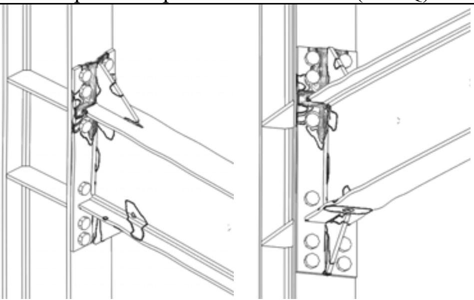
Cyclic	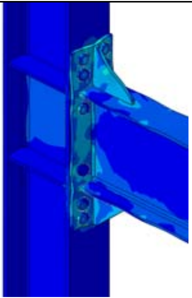	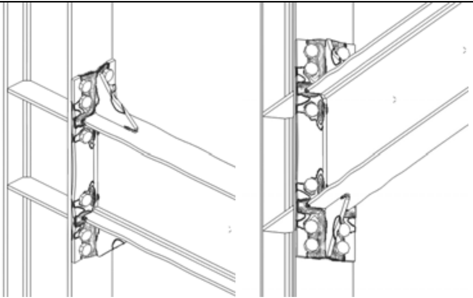

ES3 – PARTIAL – M2

Moment Rotation Curves

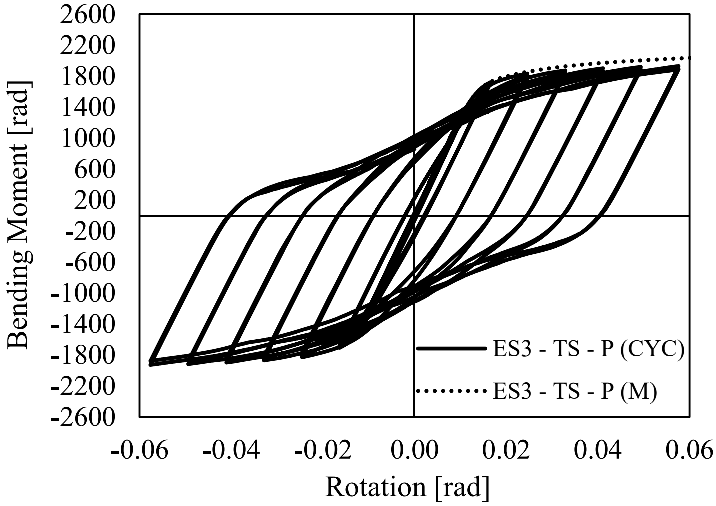

	Von Mises Stress	Equivalent plastic deformation (PEEQ)
Monotonic	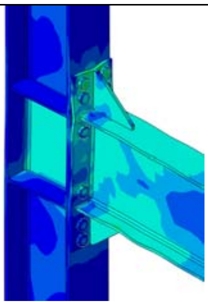	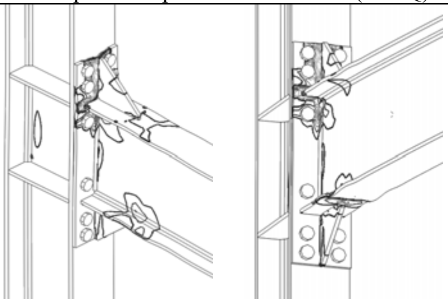
Cyclic	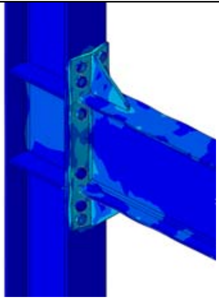	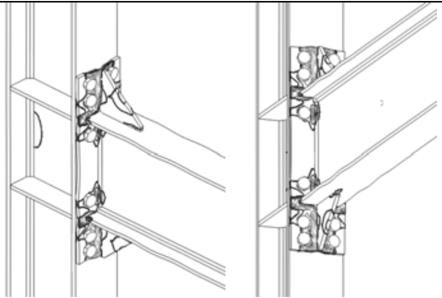

ES3 – PARTIAL – M3

Moment Rotation Curves

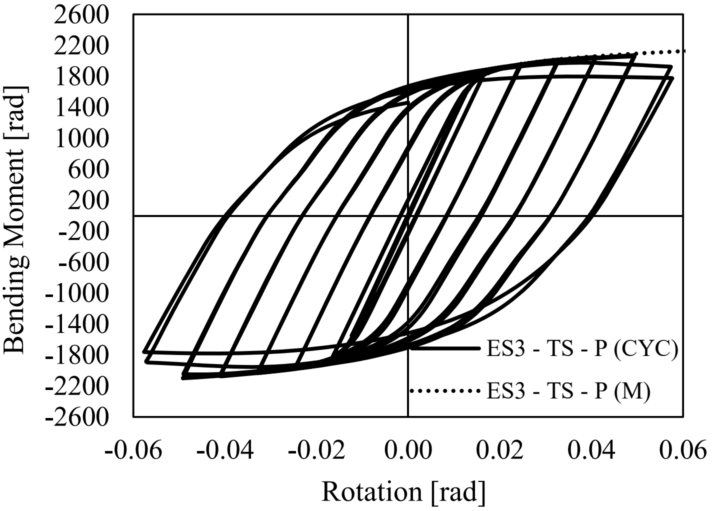

	Von Mises Stress	Equivalent plastic deformation (PEEQ)
Monotonic	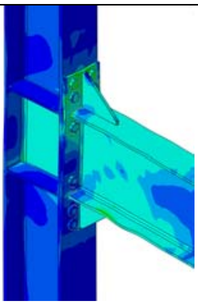	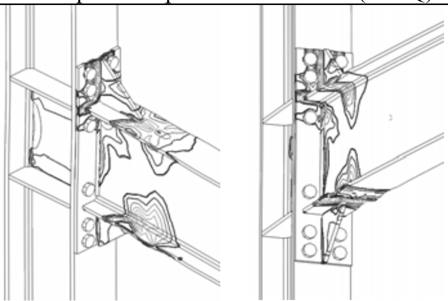
Cyclic	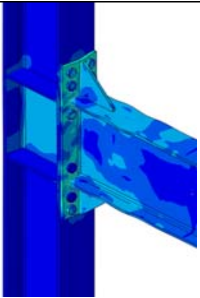	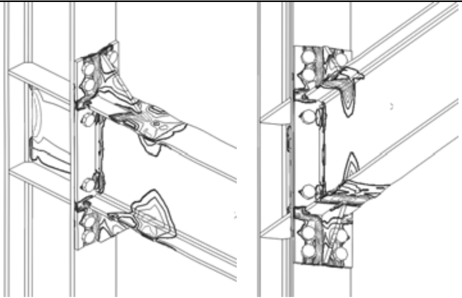

ES3 – PARTIAL – M4

Moment Rotation Curves

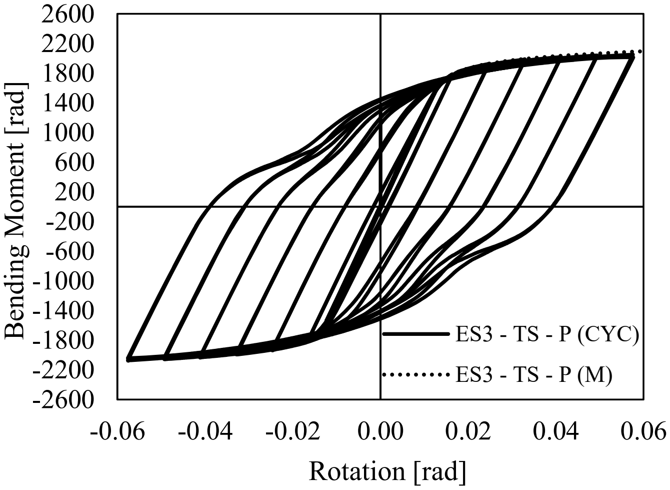

	Von Mises Stress	Equivalent plastic deformation (PEEQ)
Monotonic	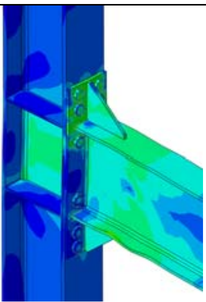	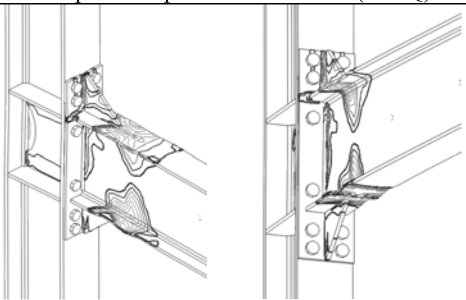
Cyclic	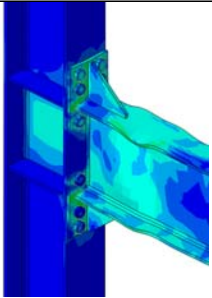	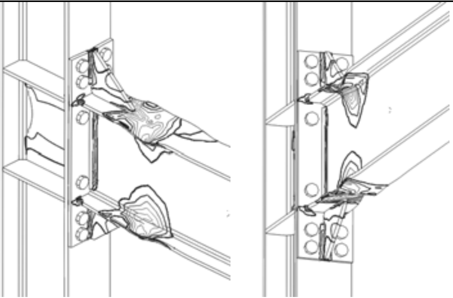

Annex V EJ vs AISC 358: additional results

In chapter IX the differences between the American (US) design procedure for the extended stiffened joint in seismic areas [6] was compared against the proposed method (EJ) described in Chapter V. With particular regard to the comparison between the stiffened and unstiffened column connections (configurations S and NS), assemblies ES1 and ES3 are hereinafter plotted.

In Figure V-1, the ES1-NS behavior is reported in terms of both moment rotation curve and PEEQ distribution. The differences between the two joint configurations, both for the European and American joints is showed in Figure V-3.

The same results are reported in Figure V-2 and in Figure V-4 for the ES3 beam-to-column assembly.

Finally, as already discussed in Chapter IX, from local point of view, no appreciable differences can be observed between the two joint configurations.

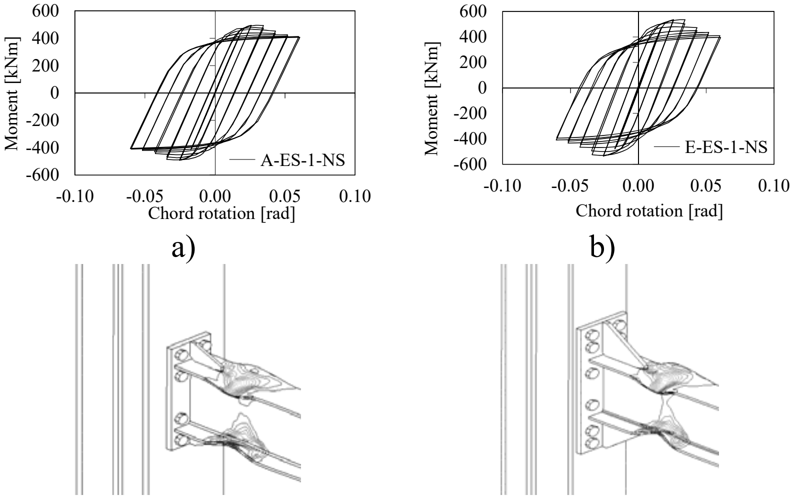

a) b)

c) d)

Figure V-1: American and European ES-1 joints results in terms of: Cyclic moment rotation curve (a and b) and PEEQ distribution (c and d).

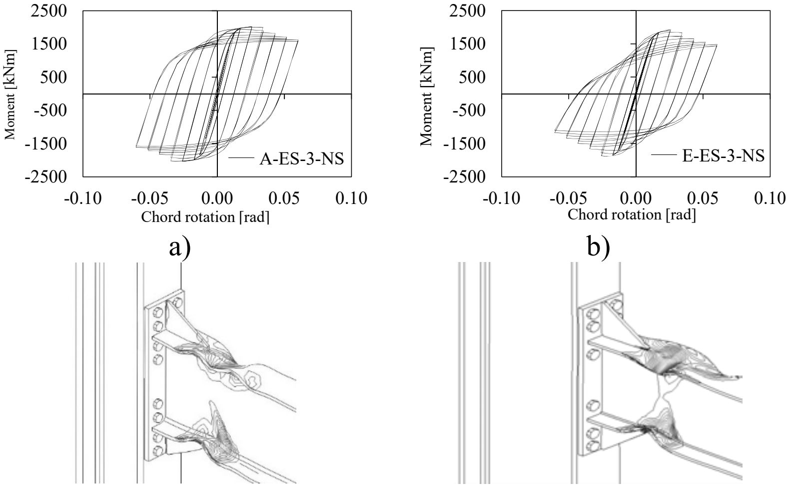

a) b)

c) d)

Figure V-2: American and European ES-3 joints results in terms of cyclic moment rotation curve (a and b) and PEEQ distribution (c and d).

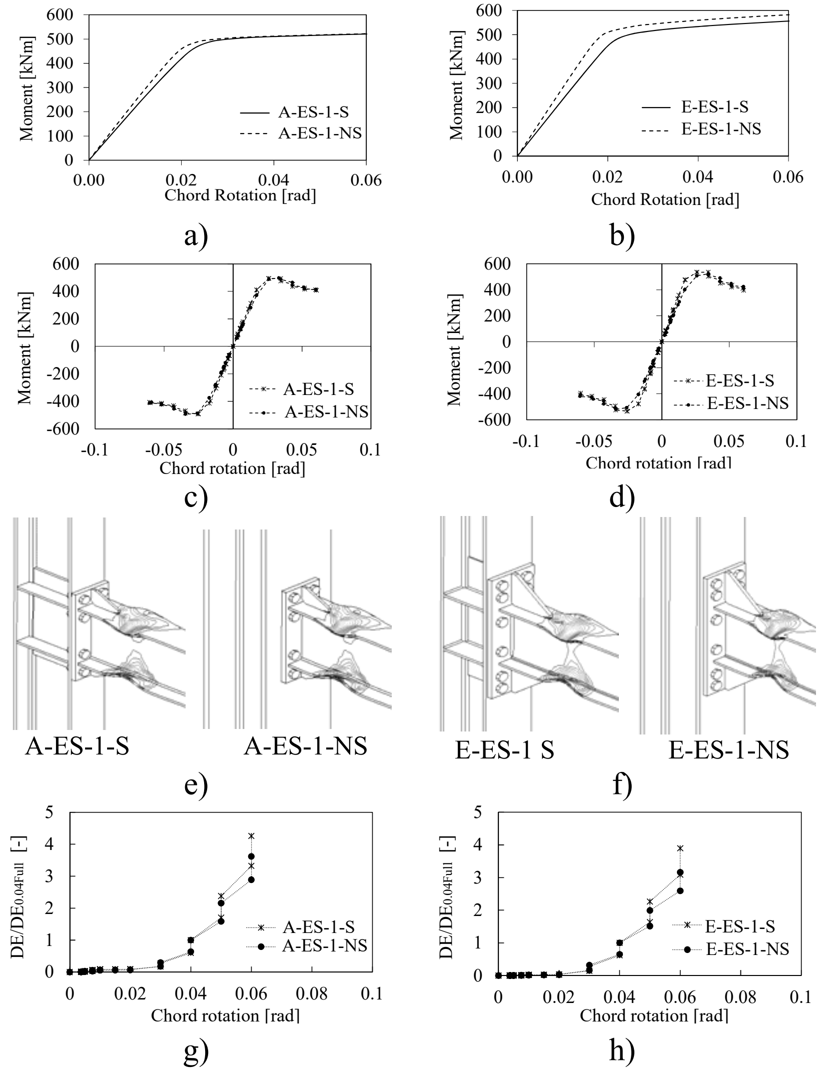

a) b)

c) d)

e) f)

g) h)

Figure V-3: Comparison for both American and European ES-1 joints between the Stiffened and Unstiffened configuration in terms of: Monotonic moment rotation curve (a and b); Back bone curve (c and d), PEEQ distribution and backbone curve (e and f) and dissipated energy (g and h).

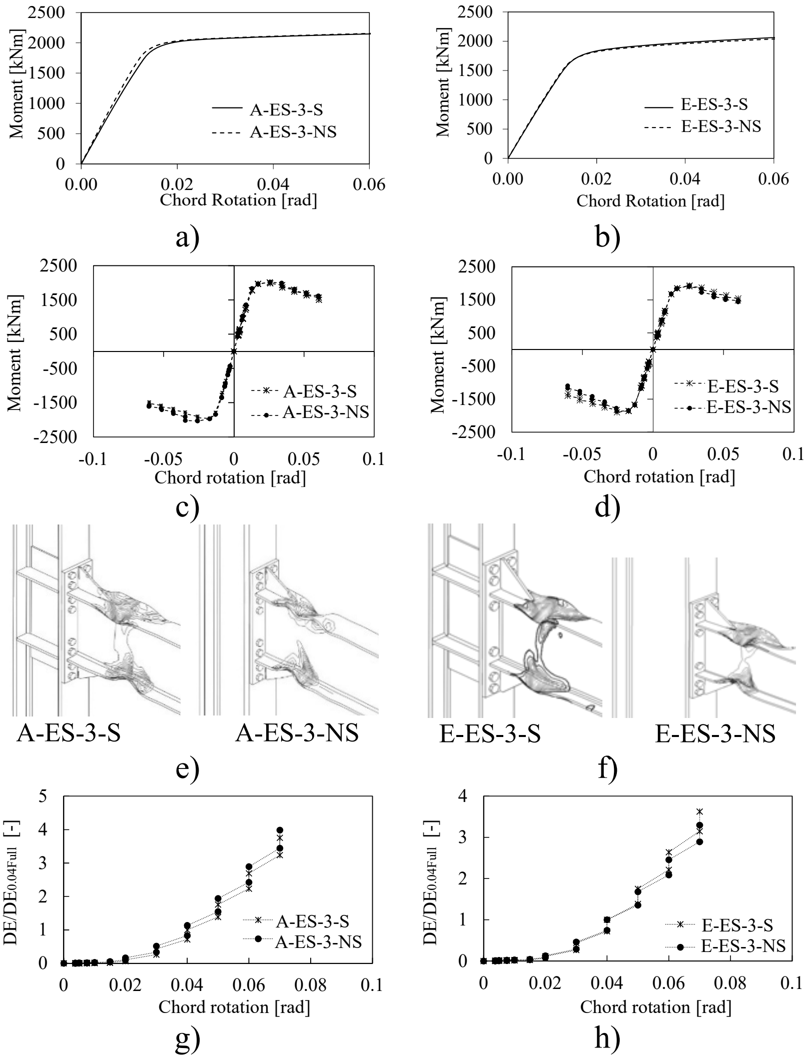

Figure V-4: Comparison for both American and European ES-3 joints between the Stiffened and Unstiffened configuration in terms of: Monotonic moment rotation curve (a and b); Back bone curve (c and d), PEEQ distribution and backbone curve (e and f) and dissipated energy (g and h).

References

[1] EN 1993:1-8, Design of steel structures - Part 1-8: Design of joints. CEN 2005.

[2] Lee C.-H. Jung J.-H., Oh M.-H., Koo E-S. (2005). Experimental Study of Cyclic Seismic Behavior of Steel Moment Connections Reinforced with Ribs. Journal of Structural Engineering, ASCE, 131(1), 108-118.

[3] Abidelah A., Bouchaïr A., Kerdal D.E. (2012). Experimental and analytical behavior of bolted end-plate connections with or without stiffeners. Journal of Constructional Steel Research, 76, 13–27.

[4] Dassault Systèmes. Abaqus analysis 6.14 user's manual. Simula Inc.; 2015

[5] EN 1998-1, Design of structures for earthquake resistance - Part 1: General rules, seismic actions and rules for buildings. CEN 2005.

[6] ANSI/AISC 341-16 (2016). Seismic Provisions for Structural Steel Buildings. American Institute of Steel Construction.

[7] ANSI/AISC 358-16 (2016). Prequalified Connections for Special and Intermediate Steel Moment Frames for Seismic Applications.

List of figures

Figure I-1: Joints configurations investigated. 593

Figure II-1: Experimental test results performed at University of Naples: IPE450 flange and web (a and b respectively), HEB340 flange and web (c and d respectively). ...682

Figure I-1: American and European ES-1 joints results in terms of: Cyclic moment rotation curve (a and b) and PEEQ distribution (c and d)..776

Figure I-2: American and European ES-3 joints results in terms of cyclic moment rotation curve (a and b) and PEEQ distribution (c and d)..776

Figure I-3: Comparison for both American and European ES-1 joints between the Stiffened and Unstiffened configuration in terms of: Monotonic moment rotation curve (a and b); Back bone curve (c and d), PEEQ distribution and backbone curve (e and f) and dissipated energy (g and h). 777

Figure I-4: Comparison for both American and European ES-3 joints between the Stiffened and Unstiffened configuration in terms of: Monotonic moment rotation curve (a and b); Back bone curve (c and d), PEEQ distribution and backbone curve (e and f) and dissipated energy (g and h). 778

List of tables

Table I.1: Component method considering the new assumptions. 594
Table I.2: Stiffness coefficient definition according to [1]...... 624
Table I.3: Component method considering the new assumptions. 629
Table II.1: Coupon tests results (IPE 600 and IPE 450).......... 678
Table II.2: Coupon tests results (IPE 360 and HEB 280)........ 679
Table II.3: Coupon tests results (HEB340, HEB500 and HEB650). 680
Table II.4: Coupon tests results (plates of 15, 18, 20, 25 and 30mm)... 681
Table III.1: Rib Investigation results....................................... 684
Table IV.1: Material investigation.. 739